

VOLUME 77

MARCH 1, 1973

✓ NUMBER 5

JPCA X

THE JOURNAL OF

PHYSICAL

CHEMISTRY

PUBLISHED BIWEEKLY BY THE AMERICAN CHEMICAL SOCIETY

THE JOURNAL OF PHYSICAL CHEMISTRY

BRYCE CRAWFORD, Jr., *Editor*
STEPHEN PRAGER, *Associate Editor*
ROBERT W. CARR, Jr., **FREDERIC A. VAN-CATLEDGE,** *Assistant Editors*

EDITORIAL BOARD: A. O. ALLEN (1970-1974), C. A. ANGELL (1973-1977), J. R. BOLTON (1971-1975), F. S. DANTON (1972-1976), M. FIXMAN (1970-1974), H. S. FRANK (1970-1974), R. R. HENTZ (1972-1976), J. R. HUIZENGA (1969-1973), W. J. KAUZMANN (1969-1973), R. L. KAY (1972-1976), W. R. KRIGBAUM (1969-1973), W. J. MOORE (1969-1973), R. M. NOYES (1973-1977), J. A. POPLER (1971-1975), B. S. RABINOVITCH (1971-1975), H. REISS (1970-1974), S. A. RICE (1969-1975), F. S. ROWLAND (1973-1977), R. L. SCOTT (1973-1977); W. A. ZISMAN (1972-1976)

AMERICAN CHEMICAL SOCIETY, 1155 Sixteenth St., N.W., Washington, D. C. 20036

Books and Journals Division

JOHN K CRUM *Director*
RUTH REYNARD *Assistant to the Director*

CHARLES R. BERTSCH *Head, Editorial Processing Department*
D. H. MICHAEL BOWEN *Head, Journals Department*
BACIL GUILEY *Head, Graphics and Production Department*
SELDON W. TERRANT *Head, Research and Development Department*

©Copyright, 1973, by the American Chemical Society. Published biweekly by the American Chemical Society at 20th and Northampton Sts., Easton, Pa. 18042. Second-class postage paid at Washington, D. C., and at additional mailing offices.

All manuscripts should be sent to *The Journal of Physical Chemistry*, Department of Chemistry, University of Minnesota, Minneapolis, Minn. 55455.

Additions and Corrections are published once yearly in the final issue. See Volume 76, Number 26 for the proper form.

Extensive or unusual alterations in an article after it has been set in type are made at the author's expense, and it is understood that by requesting such alterations the author agrees to defray the cost thereof.

The American Chemical Society and the Editor of *The Journal of Physical Chemistry* assume no responsibility for the statements and opinions advanced by contributors.

Correspondence regarding accepted copy, proofs, and reprints should be directed to Editorial Processing Department, American Chemical Society, 20th and Northampton Sts., Easton, Pa. 18042. Head: CHARLES R. BERTSCH. Assistant Editor: EDWARD A. BORGER. Editorial Assistant: JOSEPH E. YURVATI.

Advertising Office: Centcom, Ltd., 142 East Avenue, Norwalk, Conn. 06851.

Business and Subscription Information

Remittances and orders for subscriptions and for single copies,

notices of changes of address and new professional connections, and claims for missing numbers should be sent to the Subscription Service Department, American Chemical Society, 1155 Sixteenth St., N.W., Washington, D. C. 20036. Allow 4 weeks for change of address. Please include an old address label with the notification.

Claims for missing numbers will not be allowed (1) if received more than sixty days from date of issue, (2) if loss was due to failure of notice of change of address to be received before the date specified in the preceding paragraph, or (3) if the reason for the claim is "missing from files."

Subscription rates (1973): members of the American Chemical Society, \$20.00 for 1 year; to nonmembers, \$60.00 for 1 year. Those interested in becoming members should write to the Admissions Department, American Chemical Society, 1155 Sixteenth St., N.W., Washington, D. C. 20036. Postage to Canada and countries in the Pan-American Union, \$5.00; all other countries, \$6.00. Single copies for current year: \$3.00. Rates for back issues from Volume 56 to date are available from the Special Issues Sales Department, 1155 Sixteenth St., N.W., Washington, D. C. 20036.

This publication and the other ACS periodical publications are now available on microfilm. For information write to MICROFILM, Special Issues Sales Department, 1155 Sixteenth St., N.W., Washington, D. C. 20036.

THE JOURNAL OF
PHYSICAL CHEMISTRY

Volume 77, Number 5 March 1, 1973

JPCHAx 77(5) 569-724 (1973)

- Crossed-Beams Reactions of Barium, Strontium, and Calcium with Some Halides of Methane
Shen-Maw Lin, Charles A. Mims, and Ronald R. Herm* 569
- Bimolecular Dissociation of Cyanogen behind Incident Shock Waves
T. Fueno,* K. Tabayashi, and O. Kajimoto 575
- A Thermal Desorption Study of the Surface Interactions between Water and Plutonium Dioxide
J. L. Stakebake 581
- Formation of Oxygen-Containing Products in the Radiolysis of Cyclohexane Solutions of Nitrous Oxide
Yoshihiko Hatano,* Ken-ichi Takeuchi, and Satoshi Takao 586
- Radiation-Induced Homolytic Aromatic Substitution. I. Hydroxylation of Nitrobenzene, Chlorobenzene, and Toluene
Manfred K. Eberhardt* and Massayoshi Yoshida 589
- Ionic Yields in Methanol Measured by Conductometric Pulse Radiolysis
J. Lilie, Shamim A. Chaudhri, A. Mamou, M. Grätzel, and J. Rabani* 597
- Excited State Reactivity of Aza Aromatics. I. Basicity of 3-Styrylpyridines in the First Excited Singlet State
G. Favaro, U. Mazzucato,* and F. Masetti 601
- Excited State Reactivity of Aza Aromatics. II. Solvent and Protonation Effects on Photoisomerization and Luminescence of Styrylpyridines
G. Bartocci, P. Bortolus, and U. Mazzucato* 605
- An Electron Spin Resonance Study of Nitrosamine Anion Radicals
Gerald R. Stevenson,* Jesus Gilberto Concepción, and Jorge Castillo 611
- Reduction of Mercuric Chloride by Hydrated Electrons and Reducing Radicals in Aqueous Solutions. Formation and Reactions of HgCl
N. B. Nazhat and K.-D. Asmus* 614
- Electron Spin Resonance Study of Radical Anions from Aromatic Carboxylic Acids
P. Neta* and Richard W. Fessenden 620
- Electron Spin Resonance Studies of Heisenberg Spin Exchange. The Effect of Macrocyclic Polyethers on the Spin Exchange Rate for Ion Pairs
M. T. Watts, Ming Liang Lu, and M. P. Eastman* 625
- Electron-Electron Double Resonance of Irradiated Single Crystals of Zinc Acetate and Malonic Acid. The Influence of Nuclear Spin Exchange
Lowell D. Kispert,* Kichoon Chang, and Carolyn M. Bogan 629
- Nitrogen-14 Contact Shifts and Line Broadening Studies for Acetonitrile Complexes of Copper(II), Nickel(II), Cobalt(II), and Titanium(III)
V. K. Kapur and B. B. Wayland* 634
- Outer Sphere Complex between Trisethylenediaminecobalt(III) and Phosphate
Thomas H. Martin and B. M. Fung* 637
- Raman Studies of Molten Salt Hydrates. The Magnesium Chlorate-Water System
D. J. Gardiner,* R. B. Girling, and R. E. Hester 640
- Conformational Effects on the Nitrogen-Hydrogen Stretching Frequencies of Lactams
Charles A. Swenson* and Catherine Y. S. Chen 645

ห้องสมุด กรมวิทยาศาสตร์
23 พ.ค. 2516

American Chemical Society

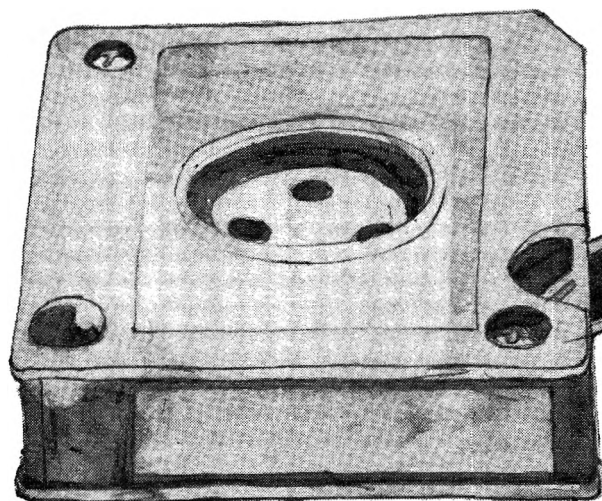
"Primary Publications on Microfilm"

Your Key to—

■ Dramatic savings in archival space and dollars . . . over 1,000,000 pages of chemical literature contained in a carousel measuring only 17" x 17" x 39".

■ Faster access to needed data. Slash costly search and retrieval time required of your scientists and librarians.

■ Unlimited distribution of copyrighted scientific data. "ACS Primary Publications on Microfilm" are available under a unique licensing agreement permitting you to make as many enlarged photocopies per page as desired . . . for distribution throughout your company.



American Chemical Society Primary Publications included in this microfilm program:

JOURNAL OF THE AMERICAN CHEMICAL SOCIETY
INDUSTRIAL & ENGINEERING CHEMISTRY
CHEMICAL TECHNOLOGY
CHEMICAL & ENGINEERING NEWS
CHEMICAL & ENGINEERING NEWS ANNUAL INDEXES
ANALYTICAL CHEMISTRY
JOURNAL OF PHYSICAL CHEMISTRY
JOURNAL OF AGRICULTURAL AND FOOD CHEMISTRY
JOURNAL OF ORGANIC CHEMISTRY
JOURNAL OF CHEMICAL AND ENGINEERING DATA
CHEMICAL REVIEWS
JOURNAL OF CHEMICAL DOCUMENTATION
I&EC FUNDAMENTALS
I&EC PROCESS DESIGN AND DEVELOPMENT
I&EC PRODUCT RESEARCH AND DEVELOPMENT
BIOCHEMISTRY
INORGANIC CHEMISTRY
JOURNAL OF MEDICINAL CHEMISTRY
CHEMISTRY
ENVIRONMENTAL SCIENCE & TECHNOLOGY
ACCOUNTS OF CHEMICAL RESEARCH
MACROMOLECULES

For information on "ACS Primary Publications on Microfilm", write or call:

**Special Issues Sales
American Chemical Society
1155 16th Street, N.W.
Washington, D.C. 20036
(202-872-4364)**

Hydrophobic Fluorescence Probe Studies with Poly-L-lysine Gisela Witz and Benjamin L. Van Duuren*	648
Location of Nickel Ions in Y Zeolites. I. Influence of Thermal Treatment and Exchange Level on Nickel Positions P. Gallezot and B. Imelik*	652
Calculated Potential Energies for the Adsorption of Rare Gases on Graphite C. Pisani, F. Ricca,* and C. Roetti	657
Adsorption of Ammonia in Copper(II) Y Zeolites Yun-yang Huang* and E. F. Vansant	663
Viscous Liquids and the Glass Transition. IV. Thermodynamic Equations and the Transition Martin Goldstein	667
An Alternating Current Conductivity Method for Studies of Pulse Radiolysis in Aqueous Solutions. Determination of the State of Ionization of Several e_{aq}^- Adducts J. Lilie and Richard W. Fessenden*	674
Effect of Water on the Titanium Complexes in Methanolic Solutions Containing Hydrogen Chloride E. P. Parry,* I. B. Goldberg,* D. H. Hern, and W. F. Goepfinger	678
Self-Diffusion in Normal and Heavy Water in the Range 1–45° R. Mills	685
The Limiting Equivalent Conductance of Perchloric Acid in 0.9914 Mole Fraction N-Methylacetamide (NMA) at 40° Jerry F. Casteel and Edward S. Amis*	688
High-Temperature Kinetics of Pyrolytic Graphite Gasification by Fluorine Atoms and Molecules Daniel E. Rosner* and Joseph P. Strakey	690
Dissociation Energies and Heats of Formation of the Gaseous Eu_2 and $EuAg$ Molecules J. Kordis and K. A. Gingerich*	700
Binary Diffusion Coefficients for the System Helium–Chlorotrifluoromethane at 300°K and 1 Atmosphere. A Test of the Chapman–Enskog Theory M. A. Yabsley, P. J. Carson, and Peter J. Dunlop*	703
Relative Bond Dissociation Energies of Silicon–Hydrogen Bonds in Methylsilanes as Estimated from Recoil Tritium Abstraction Yields Akio Hosaka and F. S. Rowland*	705
Electron Paramagnetic Resonance Studies of the Kinetics of the Intramolecular Cation Migration Process in Alkali Metal Anthraquinone Kuang S. Chen, Takuo Takeshita, Kazuo Nakamura, and Noboru Hirota*	708
Dielectric Studies. XXXIII. Establishment of Acetyl Group Relaxation in Mono- and Para-Substituted Benzene Compounds D. B. Farmer, P. F. Mountain, and S. Walker*	714
Conductance of 1–1 Electrolytes in Sulfolane and 3-Methylsulfolane at 30.0° Arden P. Zipp	718

COMMUNICATIONS TO THE EDITOR

An Interpretation of the $K\beta$ X-Ray Emission Spectra of Dibenzyl Sulfide and S_8 H. C. Whitehead and G. Andermann*	721
On the Electron Spin Resonance Measurement of Radical Termination Rates E. J. Hamilton, Jr., and H. Fischer*	722

AUTHOR INDEX

- | | | | |
|--|--|--|--|
| <p>Amis, E. S., 688
 Andermann, G., 721
 Asmus, K.-D., 614</p> | <p>Fischer, H., 722
 Fueno, T., 575
 Fung, B. M., 637</p> | <p>Kapur, V. K., 634
 Kispert, L. D., 629
 Kordis, J., 700</p> | <p>Roetti, C., 657
 Rosner, D. E., 690
 Rowland, F. S., 705</p> |
| <p>Bartocci, G., 605
 Bogan, C. M., 629
 Bortolus, P., 605</p> | <p>Gallezot, P., 652
 Gardiner, D. J., 640
 Gingerich, K. A., 700
 Girling, R. B., 640
 Goeppinger, W. F., 678
 Goldberg, I. B., 678
 Goldstein, M., 667
 Grätzel, M., 597</p> | <p>Lilie, J., 597, 674
 Lin, S.-M., 569
 Lu, M. L., 625</p> | <p>Stakebake, J. L., 581
 Stevenson, G. R., 611
 Strakey, J. P., 690
 Swenson, C. A., 645</p> |
| <p>Carson, P. J., 703
 Casteel, J. F., 688
 Castillo, J., 611
 Chang, K., 629
 Chaudhri, S. A., 597
 Chen, C. Y. S., 645
 Chen, K. S., 708
 Concepción, J. G., 611</p> | <p>Hamilton, E. J., Jr., 722
 Hatano, Y., 586
 Herm, R. R., 569
 Hern, D. H., 678
 Hester, R. E., 640
 Hirota, N., 708
 Hosaka, A., 705
 Huang, Y., 663</p> | <p>Mamou, A., 597
 Martin, T. H., 637
 Masetti, F., 601
 Mazzucato, U., 601, 605
 Mills, R., 685
 Mims, C. A., 569
 Mountain, P. F., 714</p> | <p>Tabayashi, K., 575
 Takao, S., 586
 Takeshita, T., 708
 Takeuchi, K., 586</p> |
| <p>Dunlop, P. J., 703</p> | <p>Imelik, B., 652</p> | <p>Nakamura, K., 708
 Nazhat, N. B., 614
 Neta, P., 620</p> | <p>Van Durren, B. L., 648
 Vansant, E. F., 663</p> |
| <p>Eastman, M. P., 625
 Eberhardt, M. K., 589</p> | <p>Kajimoto, O., 575</p> | <p>Parry, E. P., 678
 Pisani, C., 657</p> | <p>Walker, S., 714
 Watts, M. T., 625
 Wayland, B. B., 634
 Whitehead, H. C., 721
 Witz, G., 648</p> |
| <p>Farmer, D. B., 714
 Favaro, G., 601
 Fessenden, R. W., 620,
 674</p> | | <p>Rabani, J., 597
 Ricca, F., 657</p> | <p>Yabsley, M. A., 703
 Yoshida, M., 569
 Zipp, A. P., 718</p> |

In papers with more than one author the name of the author to whom inquiries about the paper should be addressed is marked with an asterisk in the by-line.

THE JOURNAL OF PHYSICAL CHEMISTRY

Registered in U. S. Patent Office © Copyright, 1973, by the American Chemical Society

VOLUME 77, NUMBER 5 MARCH 1, 1973

Crossed-Beams Reactions of Barium, Strontium, and Calcium with Some Halides of Methane

Shen-Maw Lin, Charles A. Mims, and Ronald R. Herm*

Inorganic Materials Research Division, Lawrence Berkeley Laboratory and Department of Chemistry, University of California, Berkeley, California 94720 (Received December 4, 1972)

Publication costs assisted by the Lawrence Berkeley Laboratory, Berkeley, California

A crossed-beams apparatus, equipped with an electron bombardment ionizer-massfilter detector unit, has been employed to measure scattered angular distributions of: MI^+ from Ba, Sr, and Ca + CH_3I and CH_2I_2 ; BaI^+ from Ba + CF_3I ; and $BaCl^+$ from Ba + CCl_4 . Product center-of-mass (CM) recoil angle and energy distributions have been fit to the measured laboratory (LAB) data by averaging the CM \rightarrow LAB transformation over the (nonthermal) beam speed distributions. The $MI + CH_3$ products from $M + CH_3I$ scatter predominately backward in the CM system (*i.e.*, MI scatters in the direction defined by the CH_3I reactant) with substantial recoil energy (average value ≈ 10 – 15 kcal/mol); the BaI product angular distribution is broader than is that of SrI or CaI . All of the other reactions preferentially scatter products into the forward CM hemisphere. For these reactions, the MX^+ massfilter signals might arise from ionization of MX or MX_2 products. Features of the derived CM distributions, as well as other indirect evidence, suggest (but do not confirm) that MI and MI_2 are formed from $M + CH_2I_2$ and BaI and $BaIF$ are formed from Ba + CF_3I .

This paper reports measurements of angular distributions of reactive scattering from crossed beams of alkaline earth atoms (M) and CH_3I , CH_2I_2 , CF_3I , and CCl_4 . The reactions of alkali atoms (A) with these halides of methane are known to span a wide range of dynamical behaviors, and this present study was undertaken in order to further compare the chemical behaviors of gaseous alkaline earth and alkali atoms. Reference 1 cites the variety of crossed-beams studies of the $A + CH_3I$ reactions. Studies with Li,² Na,³ and K⁴⁻⁶ indicate that the $A + CH_3I$ reactions provide classic examples of a "rebound" mechanism wherein the products scatter backward in the center-of-mass (CM) coordinate system (*i.e.*, A scatters preferentially in the direction defined by the CH_3I reactant) with a relatively large product recoil energy, E' . A recent study⁷ showed that the Cs + CH_2I_2 reaction was an example of the opposite extreme direct reaction mechanism wherein the products recoil forward with a relatively small E' value; K + CH_2I_2 also exhibited⁷ somewhat similar behavior, although the KI was less sharply forward peaked. The intermediate case between these extreme direct reaction mechanisms is provided by the A + CCl_4 reactions;^{2,5,8} here, the product CM angular distributions peak at intermediate angles and are especially sensitive to

the identity of the alkali atom. There are no published product angular distributions for $A + CF_3I$. However, electric deflection experiments with spatially orientated CF_3I ⁹ and CH_3I ^{10,11} indicate quite different steric effects for reactions of these molecules with alkali atoms.

Experimental Procedure

The apparatus is the same as that which was used to study the reactions of Ba, Sr, Ca, and Mg with Cl_2 and

- (1) M. E. Gersh and R. B. Bernstein, *J. Chem. Phys.*, **56**, 6131 (1972).
- (2) D. D. Parrish and R. R. Herm, *J. Chem. Phys.*, **54**, 2518 (1971).
- (3) J. H. Birely, E. A. Entemann, R. R. Herm, and K. R. Wilson, *J. Chem. Phys.*, **51**, 5461 (1969).
- (4) G. H. Kwei, J. A. Norris, and D. R. Herschbach, *J. Chem. Phys.*, **52**, 1317 (1970).
- (5) J. C. Whitehead, D. R. Hardin, and R. Grice, *Mol. Phys.*, **23**, 787 (1972).
- (6) A. M. Rulis and R. B. Bernstein, *J. Chem. Phys.*, **57**, 5497 (1972).
- (7) E. A. Entemann, *J. Chem. Phys.*, **55**, 4872 (1971).
- (8) K. R. Wilson and D. R. Herschbach, *J. Chem. Phys.*, **49**, 2676 (1968).
- (9) P. R. Brooks, *J. Chem. Phys.*, **50**, 5031 (1969).
- (10) P. R. Brooks and E. M. Jones, *J. Chem. Phys.*, **45**, 3449 (1966).
- (11) R. J. Beuhler, Jr., R. B. Bernstein, and K. H. Kramer, *J. Amer. Chem. Soc.*, **88**, 5331 (1966); R. J. Beuhler, Jr., and R. B. Bernstein, *Chem. Phys. Lett.*, **2**, 166 (1968); **3**, 118 (1969); *J. Chem. Phys.*, **51**, 5305 (1969).

TABLE I: Experimental Beam Conditions^a

Collision partners	Alkaline earth atom beam				Halogenated methane beam			
	Source conditions		Speed distribution ^b		Source conditions		Speed distribution ^c	
	Temp	Pressure	α_1	a_1	Temp	Pressure	α_2	a_2
CH ₃ I + Ba	1030	0.3	3.1	1.1	360	3.6	2.1	1.7
CH ₃ I + Sr	980	0.6	3.7	1.3	330	3.3	2.0	1.7
CH ₃ I + Ca	1050	0.6	5.8	1.9	370	3.4	2.1	1.7
CH ₂ I ₂ + Ba	1050	0.3	3.1	1.1	330	0.6	1.4	0.7
CH ₂ I ₂ + Sr	970	0.5	3.7	1.3	340	0.5	1.5	0.6
CH ₂ I ₂ + Ca	1030	0.4	5.8	1.9	330	0.4	1.4	0.4
CF ₃ I + Ba	1060	0.4	3.1	1.1	330	3.8	1.7	1.4
CCl ₄ + Ba	1040	0.3	3.1	1.1	370	3.0	2.0	1.6

^a Temperatures are given in °K, pressures in Torr, and speeds in 100 m/sec. ^b These are parameters of eq 1. Parameters for Ba are from measurements reported in ref 13b; parameters for Sr and Ca are from an extrapolation discussed in ref 13b. ^c These are parameters of eq 1. Parameters for CH₃I, CH₂I₂, and CCl₄ are from measurements reported in ref 13b; parameters for CF₃I are from an extrapolation discussed in ref 13b. Note that this beam is much more "nonthermal" than is the alkaline earth atom beam.

Br₂;¹² it is described in detail in ref 13. The two beams cross at right angles, resulting in a 1–5% attenuation of the M beam (beam 1) and negligible attenuation of the halide beam (beam 2). The laboratory (LAB) scattering angle, θ , is measured from the M beam; the halide beam direction defines $\theta = 90^\circ$. The number density speed probability distributions of beams 1 and 2 are nonthermal and are given by

$$\rho_i(v_i) = N_i(v_i - a_i)^2 \exp[-(v_i - a_i)^2/\alpha_i^2] u(v_i - a_i) \quad (1)$$

Here, $u(t)$ is the unit step function ($u(t) = 0$ for $t \leq 0$, $u(t) = 1$ for $t > 0$); a_i and α_i are parameters which depend on the source temperature and pressure of beam i ; and $N_i = 4\pi^{-1/2}\alpha_i^{-3}$. Table I gives beam operating conditions.

The scattered species are ionized by ~150-eV electrons and mass analyzed. The detector unit rotates about the beam collision zone in the plane defined by the two beams. The speeds of the scattered species are not measured; only product LAB angular distributions are determined. All reactive scattering angular distributions which are reported here were measured with the massfilter tuned to the alkaline earth monohalide (MX) ion peak. Interference from fragment ions due to methyl halide reactants precluded angular distribution measurements of the methyl and halogenated methyl products. No alkaline earth dihalide signals were observed for scattering of M from CH₂I₂, CF₃I, or CCl₄. However, alkaline earth dihalides formed in these reactions would probably be vibrationally excited and would be expected to fragment into MX⁺ upon electron bombardment ionization.

As Table II indicates, a number of reactions were examined in this study. Although uncertain and changing detector response factors precluded determinations of total reaction cross sections (Q_R), we estimate that our detection sensitivity is such that: $Q_R < 1 \text{ \AA}^2$ for those reactions which failed to produce any detectable product (NR in Table II); $Q_R \approx 1\text{--}5 \text{ \AA}^2$ for those reactions which provided only a fragmentary product signal (F in Table II); and $Q_R > \sim 5 \text{ \AA}^2$ for the eight reactions for which product angular distributions are reported.

Results and Data Analysis

The data analysis procedure, described in more detail in ref 12 and 13, consists in assuming a form for the CM

cross section, $\sigma(\theta, u)$, and calculating the resultant LAB number density angular distribution by

$$I_{\text{LAB}}(\theta) = \int_0^{v^*} \int_0^\infty \int_0^\infty V \sigma(\theta, u) (v/u^2) \rho_1(v_1) \rho_2(v_2) dv_1 dv_2 dv \quad (2)$$

the procedure is repeated until the calculated $I_{\text{LAB}}(\theta)$ fits the measured data. In eq 2, \bar{V} is the initial relative velocity, and \bar{u} and \bar{v} are, respectively, the CM and LAB recoil velocities of the species which is detected; the CM scattering angle, θ , is defined as 0° when \bar{u} lies along \bar{V} in the direction defined by the M velocity; v^* , the upper limit on v , is calculated from the reaction exoergicity, ΔD_0 . Table III lists values of ΔD_0 as well as the relative collision energy, E , and average thermal reactant internal excitation, W .

The derived CM cross sections which are presented here are of the simple functional form

$$\sigma(\theta, u) = T(\theta)U(u) \quad (3)$$

the limited information content of the data do not warrant use of a more sophisticated form. For convenience, $T(\theta)$ and $U(u)$ are also often expressed as

$$T(\theta) = (1 - C_1) \exp[-\ln 2((\theta - \theta_1)/H_1)^2] + C_1 \quad (\theta > \theta_1)$$

$$T(\theta) = 1 \quad (\theta_1 > \theta > \theta_2) \quad (4a)$$

$$T(\theta) = (1 - C_2) \exp[-\ln 2((\theta - \theta_2)/H_2)^2] + C_2 \quad (\theta < \theta_2)$$

$$U(u) = (u/u_1)^{n_1} \exp[(n_1/m_1)(1 - (u/u_1)^{m_1})] \quad (u < u_1) \quad (4b)$$

$$U(u) = (u/u_1)^{n_2} \exp[(n_2/m_2)(1 - (u/u_1)^{m_2})] \quad (u > u_1)$$

where all subscripted variables serve as adjustable parameters. Three $T(\theta) - U(u)$ functions are presented for each CH₃I reaction in order to provide insight into the range of possible CM cross sections which will provide fits to the measured LAB data. One of these, termed the "single recoil energy" (SRE) result, should provide an upper limit on the breadth of the true CM product angular distribution because it unrealistically treats the product recoil speed distribution as a delta function.

$M + \text{CH}_3\text{I}$. Figures 1–3 show that the measured MI⁺ angular distributions from $M + \text{CH}_3\text{I}$ all peak at larger

(12) S.-M. Lin, C. A. Mims, and R. R. Herm, submitted for publication in *J. Chem. Phys.*

(13) (a) S.-M. Lin, Ph.D. Thesis, University of California, Berkeley, Calif., 1972; (b) G. A. Mims, Ph.D. Thesis, University of California, Berkeley, Calif., 1973.

TABLE II: Summary of Reactions Studied^a

	Alkaline earth atom				Mass peak detected
	Ba	Sr	Ca	Mg	
CH ₃ I	R	R	R	NR	MI ⁺
CH ₂ I ₂	R	R	R	NS	MI ⁺
CF ₃ I	R	NS	NS	NS	MI ⁺
CF ₃ I	F ^b	NS	NS	NS	MF ⁺
CH ₂ Br ₂	NS	NS	F	NS	MBr ⁺
CH ₂ ClBr	F	NS	NS	NS	MBr ⁺
CH ₂ ClBr	NR	NS	NS	NS	MCl ⁺
CCl ₃ Br	NS	NS	NR	NS	MCl ⁺ ; MBr ⁺
CCl ₄	R	I	NR	NS	MCl ⁺
(CH ₃) ₃ C-OH	NR	NS	NS	NS	MO ⁺ ; MOH ⁺ ; MOC(CH ₃) ₃ ⁺

^a R, product angular distribution is reported here; NR, no product signal was observed; F, a product signal was observed which was too weak to permit measurement of a reliable angular distribution; I, it proved impossible to draw any conclusion about this reaction because of an interfering reactant mass peak; NS, this reaction was not studied. ^b The mass spectrometer cannot actually distinguish between BaF⁺ and ClF⁺. However, this mass peak clearly corresponded to a scattered product because it was confined to a narrow range of LAB angles (~10°–30°).

TABLE III: M + X - R → MX + R Reaction Energetics^a

Reaction	Relative collision energy, E ^b	Reactant internal excitation, W ^c	Reactive exoergicity, ΔD ₀ ^{d,e}
Ba + I-CH ₃	2.6	1.4	34
Sr + I-CH ₃	2.5	1.4	26
Ca + I-CH ₃	2.8	1.4	23
Ba + I-ICH ₂	2.4	1.9	34
Sr + I-ICH ₂	2.3	1.9	26
Ca + I-ICH ₂	2.6	1.9	23
Ba + I-CF ₃	2.6	2.8	34
Ba + Cl-CCl ₃	2.7	3.5	37

^a All energies are given in kcal/mol. ^b Calculated for the most probable (number density distributions) beam speeds. ^c The average thermal rotational and vibrational reactant excitation which is given here will be too large if the internal degrees of freedom relax somewhat in the expansion process. ^d ΔD₀ = D₀(M-X) - D₀(R-X); D₀ taken from: for MCl, ref 21; for MI, A. G. Gaydon, "Dissociation Energies and Spectra of Diatomic Molecules," 3rd ed. Chapman and Hall, London, 1968; for CH₃I and CCl₄, B. de B. Darwent, "Bond Dissociation Energies in Simple Molecules," U. S. National Bureau of Standards Report NSRDS-NBS 31 (1970); for CH₂I₂ and CF₃I, value taken as the same as in CH₃I. ^e In the event that two halogen atoms are transferred in the last five reactions, the estimated ΔD₀ values become: 70 (BaI₂ + CH₂); 59 (SrI₂ + CH₂); 54 (CaI₂ + CH₂); 46 (BaIF + CF₂); and 80 (BaCl₂ + CCl₂).

LAB scattering angles than do the calculated (assuming an energy independent collision cross section) angular distributions of the LAB velocity of the center-of-mass, \bar{C} , indicating that the MI products rebound predominately into the backward CM hemisphere (i.e., 90° ≤ θ ≤ 180°). Examples of CM cross sections, of the form of eq 3, which provide fits to the data for each reaction are given in Figures 1–3 as well as Table IV; the product recoil energy distributions plotted in these figures are calculated from $P(E') dE' = U(u) du$. The fits to the data which were provided by the A CM cross sections are also shown in Figures 1–3; the SRE and B CM cross sections provided fits of comparable or only slightly poorer quality. A recent study¹ of the K + CH₃I reaction indicated that $Q_R(E)$ exhibits a maximum for E = 4 kcal/mol. In order to investigate the significance of this to the data analysis presented here, LAB MI angular distributions were calculated for the Ba, Sr, and Ca + CH₃I reactions using a CM cross section of the form: $\sigma(\theta, u) = T(\theta)U(u)Q_R(E)$. Here, $T(\theta)$ and $U(u)$ were taken as the A functions given in Table IV. Although the true form of $Q_R(E)$ for CH₃I reactions is undoubtedly dependent on the metal atom reactant,¹⁴ the

form of $Q_R(E)$ reported¹ for K + CH₃I was employed in the calculation. The resulting calculated MI LAB angular distributions were practically indistinguishable from those shown in Figures 1–3. Thus, although the true form of $\sigma(\theta, u)$ for these reactions is undoubtedly more complex, this calculation supports the reliability of the product angle and energy distributions which are derived here by use of eq 3.

The rather wide range of CM cross sections which can be fit to the data presented for any one reaction prevents a detailed comparison of the features of the Ba, Sr, and Ca + CH₃I reactions; however, some features are clearly established. The CM MI product angular distributions clearly peak in the backward direction, at or near 180°. Moreover, the Ba reaction leads to a broader product angular distribution than do the Sr and Ca reactions; this is shown in Figures 1–3 and in the entries in Table IV for the fraction of the products which scatter backwards

$$Q_B = \frac{\int_{\pi/2}^{\pi} T(\theta) \sin \theta d\theta}{\int_0^{\pi} T(\theta) \sin \theta d\theta} \quad (5)$$

Figures 1–3 also show that, for a given reaction, the derived form of the product angular distribution is relatively insensitive to the assumed form of the recoil energy distribution (except for fit B for the Ca reaction). The approximate constancy of the average product recoil energy

$$\langle E' \rangle = \frac{\int_0^{\Delta D_0} E' P(E') dE'}{\int_0^{\Delta D_0} P(E') dE'} \quad (6)$$

for very different assumed forms of $P(E')$ which is shown in Table IV also clearly establishes that the products separate with a recoil energy which is relatively large and is rather insensitive to the identity of the attacking atom. The SRE and B fits represent two extremes for the breadth of the true $P(E')$ function; thus, the true $T(\theta)$ and $P(E')$ should lie within the ranges provided by these fits. The A fits are obtained for a more likely form of $P(E')$ and are likely to closely approximate the true CM cross sections. Recent product velocity measurements of the KI scattered from a beam of CH₃I crossed by a velocity selected K beam have determined⁶ a $P(E')$ function for this reaction which is of roughly the same breadth (although peaking at a somewhat higher E') as the $P(E')$ A fits shown in Figures 1–3.

(14) D. L. Bunker and E. A. Goring, *Chem. Phys. Lett.*, **15**, 521 (1972).

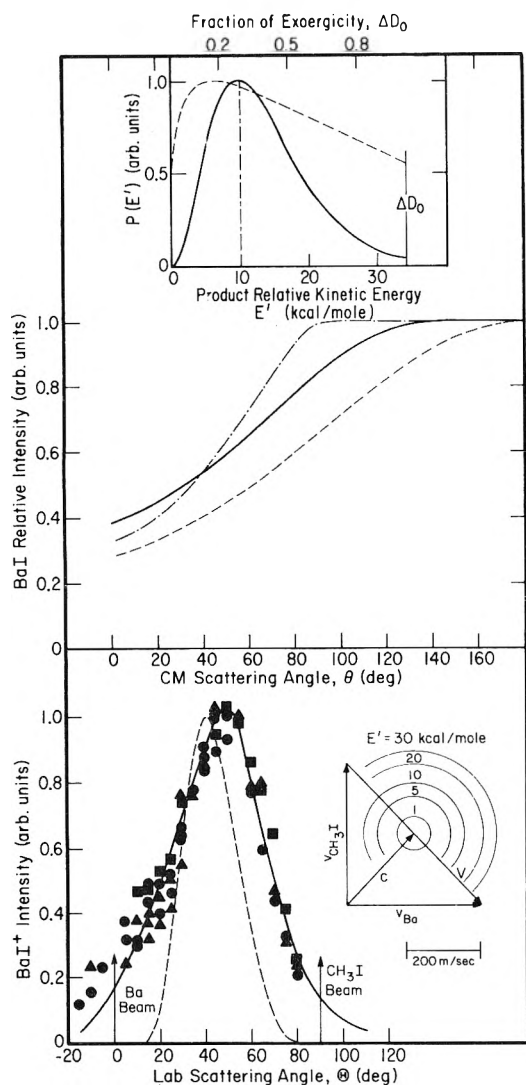


Figure 1. Data points show measured BaI^+ LAB angular distribution from $\text{Ba} + \text{CH}_3\text{I}$; different data symbols show results measured on different apparatus pumpdowns. The upper panel shows three derived CM cross sections ($T(\theta)$) and associated $P(E')$; parameters for these are given in Table IV as SRE (dot-dashed), A (solid), and B (dashed); the corresponding fit to the LAB data provided by the A CM cross section is shown as the solid curve in the lower panel. Also shown in the lower panel are: (1) a calculated angular distribution for the LAB velocity of the center-of-mass, \bar{C} (dashed curve); and (2) a LAB \leftrightarrow CM transformation diagram for $\text{Ba} + \text{CH}_3\text{I} \rightarrow \text{BaI} + \text{CH}_3$. This latter was drawn for most probable beam speeds; the circles show loci of BaI recoil velocities for some possible product recoil energies, E' .

$M + \text{CH}_2\text{I}_2$, CF_3I , and CCl_4 . Figures 4 and 5 show that the measured angular distributions of MX^+ for the CH_2I_2 , CF_3I , and CCl_4 reactions are skewed to smaller LAB angles than the calculated angular distributions of \bar{C} , indicating that the products are preferentially scattered into the forward CM hemisphere. All of these reactions share the property that the MX^+ signal observed might have arisen from ionization of product MX , MX_2 (MIF for the CF_3I reaction), or a combination of the two. Indeed, if both MX and MX_2 products are formed the data analysis provided here, using a cross section of the form of eq 3, could be misleading because the two products might scatter with quite different angle and recoil energy distributions. Because of this possibility, derived CM cross sections are not presented graphically. For each reaction, how-

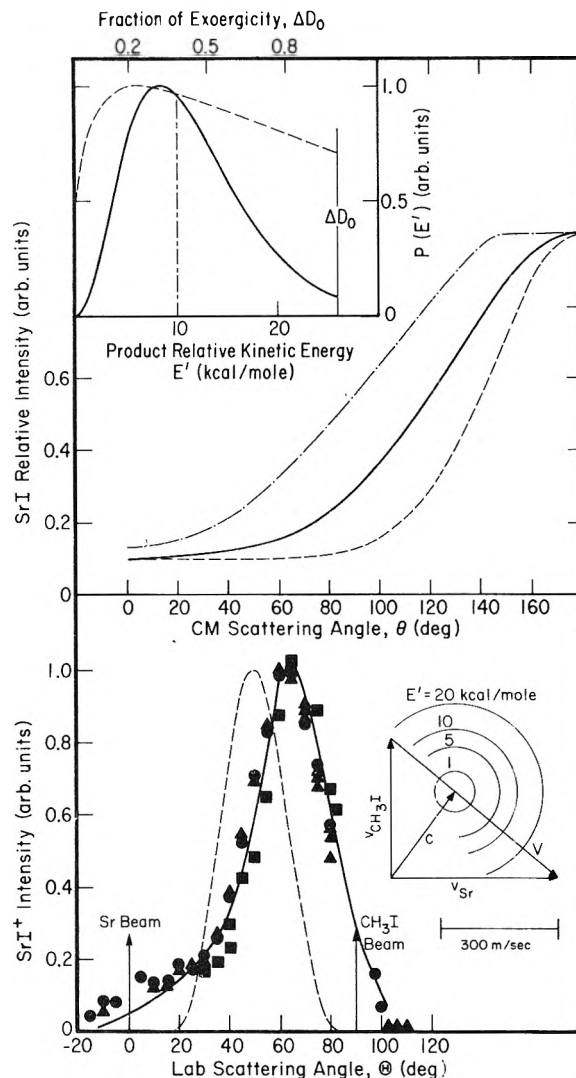


Figure 2. Measured SrI^+ LAB angular distribution and derived product CM cross sections for $\text{Sr} + \text{CH}_3\text{I} \rightarrow \text{SrI} + \text{CH}_3$. Conventions as described for Figure 1.

ever, an example of a CM cross section of the form of eq 3 is given in Table IV, and Figures 4 and 5 show the corresponding fits to the measured data. A number of other calculations, also based on eq 3, which are discussed in ref 13a indicate that $T(\theta)$ must peak within the ranges of 0° – 70° for $M + \text{CH}_2\text{I}_2$ and $\text{Ba} + \text{CCl}_4$ and $\sim 50^\circ$ – $\sim 90^\circ$ for $\text{Ba} + \text{CF}_3\text{I}$.

Discussion

Reactions of metal atoms of the type studied here involve the rupture of a covalent reactant bond to form an ionic product bond. Since this involves the transfer of an electron from the metal atom, it is natural to discuss the observed dynamical features in terms of the reactant attraction and product repulsion which are suggested by the known (or estimated) electron attachment behavior of the halogen containing reactant.

$M + \text{CH}_3\text{I}$. Herschbach¹⁵ discusses the dynamics of the $\text{A} + \text{CH}_3\text{I}$ reactions in terms of the known electronic absorption spectrum of CH_3I and the likely structure of CH_3I^- ; he estimates the vertical electron affinity of CH_3I as $\sim -20 \pm 20$ kcal/mol. Thus, reaction of CH_3I with a metal atom is not expected to proceed *via* a long-range (15) D. R. Herschbach, *Advan. Chem. Phys.*, **10**, 319 (1966).

TABLE IV: $M + X - R \rightarrow MX + R$ Derived CM Reaction Cross Sections^a

Reaction	Legend	Angular distribution ^b							Speed distribution ^c					Recoil energy ^d	
		θ_1	θ_2	H_1	H_2	C_1	C_2	Q_B	u_1	n_1	m_1	n_2	m_2	E'	$\langle E' \rangle$
Ba + I-CH ₃	SRE							0.58						10	10
	A	180	140	80	80	0.3	0.3	0.59	1.4	6	2	6	2	9.6	13
	B	180	180	100	100	0.2	0.2	0.62	2.0	2	1	2	2	5.9	16
Sr + I-CH ₃	SRE							0.70						10	10
	A	180	180	60	60	0.1	0.1	0.77	1.6	6	2	6	2	8.3	11
	B	180	180	40	40	0.1	0.1	0.78	2.5	2	1	2	2	6.1	13
Ca + I-CH ₃	SRE							0.74						8.0	8.0
	A	180	180	40	40	0.1	0.1	0.78	1.9	6	2	6	2	7.3	9.7
	B	180	180	20	20	0.0	0.0	1.00	2.5	2	1	2	2	3.8	11
Ba + I-CH ₂ I		0	0	100	100	0.3	0.3	0.39	1.2	2	2	2	2	0.7	2.0
Sr + I-CH ₂ I		0	0	100	100	0.3	0.3	0.39	1.2	2	2	2	2	0.5	1.4
Ca + I-CH ₂ I		0	0	100	100	0.5	0.5	0.43	1.0	2	2	2	2	0.2	0.7
Ba + I-CF ₃		90	70	45	15	0.0	0.8	0.42	2.5	6	6	6	6	9.0	9.0
Ba + Cl-CCl ₃		30	30	60	30	0.2	0.5	0.31	4.0	2	2	2	2	4.0	11

^a Energies are given in kcal/mol, speeds in 100 m/sec, and angles in degrees. ^b θ_1 , θ_2 , H_1 , H_2 , C_1 , and C_2 are parameters of eq 4a; if no entries are given, $T(\theta)$ was not restricted to the form of eq 4a. Q_B is the fraction scattered backwards (eq 5). ^c These are parameters of eq 4b. ^d (E') is the average product recoil energy (eq 6); \bar{E}' , the most probable E' value is obtained from $dP(E')/dE'|_{E'=\bar{E}'} = 0$. Values are given for formation of an alkaline earth monohalide product. If the dihalide product were formed in the last five reactions, the corresponding E' , $\langle E' \rangle$ entries would be: 9.7, 25 (BaI₂ + CH₂); 7.5, 20 (SrI₂ + CH₂); 3.8, 11 (CaI₂ + CH₂); 3, 13 (BaI + CF₂); and 7.0, 20 (BaCl₂ + CCl₂).

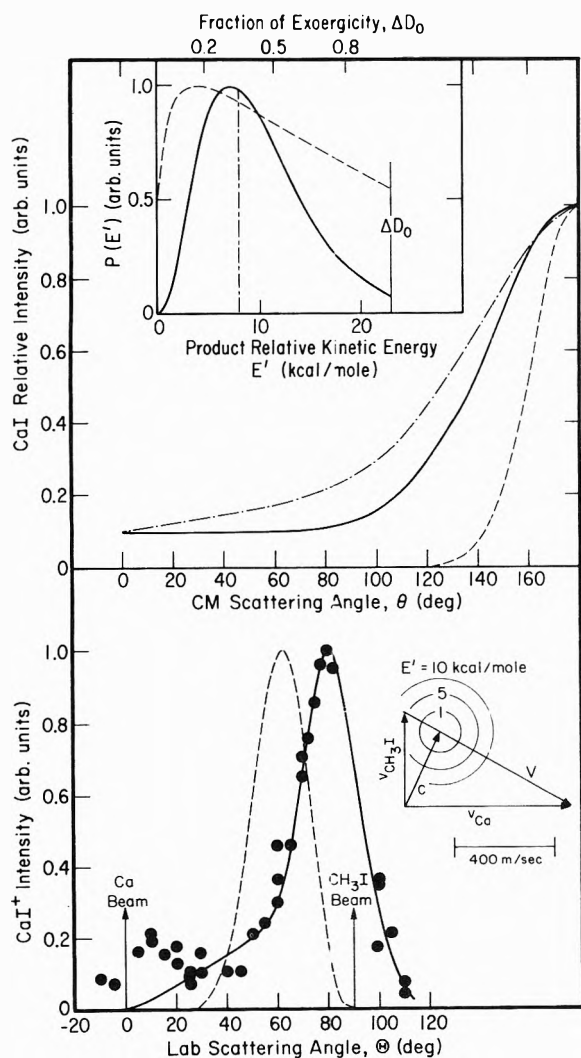


Figure 3. Measured CaI⁺ LAB angular distribution and derived product CM cross sections for Ca + CH₃I → CaI + CH₃. Conventions as described for Figure 1.

electron transfer and is likely to take place only for smaller impact parameters which permit appreciable overlap of

the A (or M) and I electron distributions. This is consistent with the backward product scattering which is observed with both the alkali and alkaline earth atoms. Moreover, the observation that both the A and M + CH₃I reactions channel a considerable fraction of ΔD_0 into product recoil energy is consistent with the picture¹⁵ of considerable C-I repulsion in CH₃I⁻. The M + CH₃I reaction dynamics might have differed somewhat from those of A + CH₃I because of a possible substantial attraction between the departing MI and CH₃ free radical products. However, the observed similarities of the A and M + CH₃I reactions indicate that this effect is not important, possibly because of an unfavorable combination of appreciable C-I repulsion, which leads to rapid product separation, and a steric effect which, for the K¹⁰ and Rb¹¹ reactions, has been shown to favor approach of the metal atom along the I end of the C-I bond. The trend toward narrower product angular distributions on proceeding to lighter and less readily ionizable atoms which is observed in this work runs counter to that observed for K, Na, and Li.² However, this could simply be a consequence of decreasing ΔD_0 's in the alkaline earth family which might restrict reaction to a decreasing range of impact parameters.¹⁶

Ba + CF₃I. For the Ba + CF₃I reaction, four exothermic reaction channels are possible, corresponding to formation of BaI, BaF, BaF, and BaF₂ products. Table IV indicates that the measured BaI⁺ angular distribution, which might arise from ionization of BaI and/or BaF, can be fit, using eq 3, to a CM angular distribution which peaks at $\theta = 70$ – 90° . However, the bimodal structure of this measured distribution is striking and is suggestive of contributions from two reaction mechanisms. Table II shows that a weak BaF⁺ signal was observed as well, with a peak magnitude about 5–10% of that seen for BaI⁺; this might arise from ionization of BaF, BaF₂, or BaF. Berkowitz and Marguait¹⁷ have reported that fragmentation into MgF⁺ upon electron bombardment ionization of MgF₂ is much more likely than is fragmentation into MgI⁺ upon ioniza-

(16) D. D. Parrish and R. R. Herm, *J. Chem. Phys.*, **53**, 2431 (1970).

(17) J. Berkowitz and J. R. Marguait, *J. Chem. Phys.*, **37**, 1853 (1962).

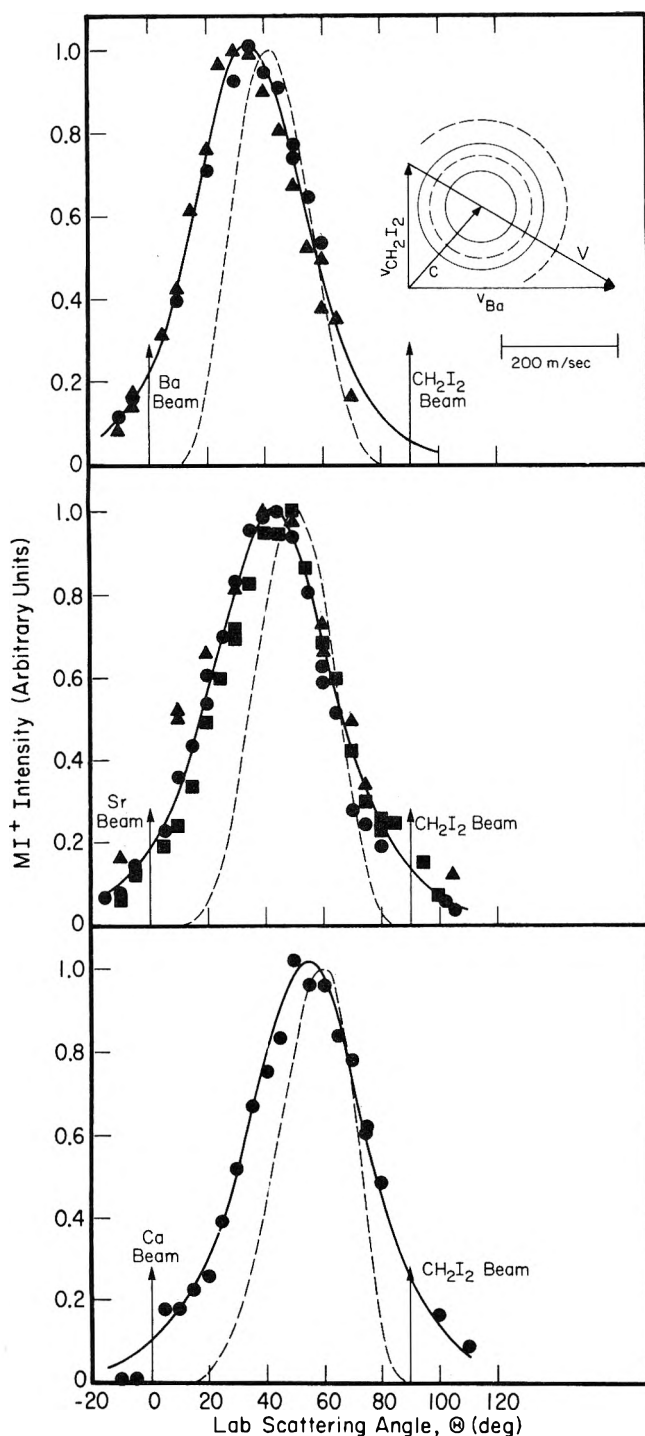


Figure 4. Data points show measured MI^+ LAB angular distributions from the Ba, Sr, and Ca + CH_2I_2 reactions. Solid curves show fits to the data provided by CM cross section functions given in Table IV; dashed curves show calculated distributions in \bar{C} . On the LAB \leftrightarrow CM transformation diagram, solid circles correspond to BaI^+ CM recoil velocities (for $E' = 0.3$ and 1) whereas dashed circles correspond to BaI_2^+ CM recoil velocities (for $E' = 10$ and 30).

tion of MgI_2 . This suggests that ionization of BaI would likely involve a vertical transition to a repulsive BaF bond in BaFI^+ , leading one to expect formation of BaI^+ to be favored over formation of BaF^+ . Thus, the magnitudes of the BaF^+ and BaI^+ signals which are observed here are consistent with formation of BaIF , and possibly some BaI as well.

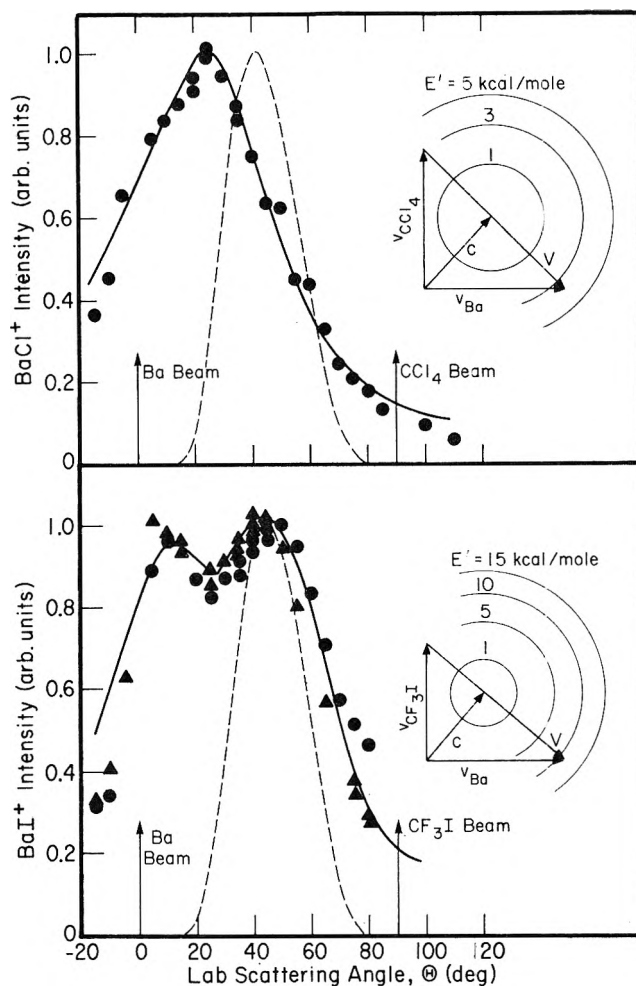


Figure 5. Data points show measured BaI^+ (from Ba + CF_3I) and BaCl^+ (from Ba + CCl_4) angular distributions. Solid curves show fits to the data provided by CM cross sections given in Table IV; dashed curves show calculated distributions in \bar{C} . Circles on the LAB \leftrightarrow CM transformation diagrams show loci of possible CM recoil velocities of alkaline earth monohalide products.

Diffusion flame studies^{18,19} of the reactions of Na with CF_3I , CF_3Br , and CF_3Cl have been analyzed in terms of primary reactions giving only $\text{NaX} + \text{CF}_3$. In his classic diffusion flame study, Polanyi²⁰ found that the rate constants for the Na + CH_3X reactions followed the sequence $k_{\text{I}} > k_{\text{Br}} > k_{\text{Cl}} > k_{\text{F}}$, with $k_{\text{I}} > 10^6 k_{\text{F}}$. Presumably this trend arises because the Na atom must transfer an electron into the σ^* antibonding C-X orbital which becomes progressively more repulsive on going from I to F. Although $D_0^0(\text{BaF}) > D_0^0(\text{NaF})$, these trends are likely to hold, at least qualitatively, for Ba reactions as well; evidence of this is provided by entries in Table II. This suggests that it is unlikely that the observed BaF^+ signal arose from ionization of BaF or BaF_2 . The reaction of CF_3 with a metal atom, on the other hand, might well be quite fast because the metal atom can initially transfer its electron into a nonbonding orbital on CF_3 . Moreover, BaI might react in much the same way as Ba because the ionization potentials of the two species are comparable;²¹ thus, it is reasonable to expect some decomposition of an

(18) J. W. Hodgins and R. L. Haines, *Can. J. Chem.*, **30**, 473 (1952).

(19) E. D. Kaufman and J. F. Reed, *J. Phys. Chem.*, **67**, 896 (1963).

(20) M. Polanyi, "Atomic Reactions," Williams and Norgate, London, 1932.

(21) D. L. Hildebrand, *J. Chem. Phys.*, **52**, 5751 (1970).

F_3C -IBa reaction intermediate into BaIF and CF_2 . Although bimolecular reactions which involve the transfer of two groups are rare in conventional kinetics literature, these considerations suggest that the observed BaI^+ and BaF^+ signals indicate formation of BaIF, and possibly BaI, from $Ba + CF_3I$.

$M + CH_2I_2$. A previous study⁷ of K and Cs + CH_2I_2 indicated that the AI + CH_2I products scattered, *via* a direct reaction mechanism, with SRE E' values of about 3 and 2 kcal/mol, respectively. The MI^+ signals observed in the present study might have arisen from ionization of product MI and/or MI_2 . However, analyses of the MI^+ data assuming no MI_2 product result in surprisingly small values for the product recoil energies. This is illustrated by the \bar{E}' values listed in Table IV and by the fact that SRE fits (not shown here) are obtained^{13a} for E' values of 0.7 (Ba), 0.6 (Sr), and 0.3 (Ca) kcal/mol. Thus, these comparisons suggest that these alkaline earth reactions do not produce exclusively the MI + CH_2I products *via* the mechanism characteristic of the K and Cs reactions. These low \bar{E}' values might be understandable²² in terms of a mechanism which proceeded *via* an intermediate complex whose lifetime was long enough to statistically partition the reaction energy and still short enough to be consistent with the anisotropic angular distribution given in Table IV; the divalency of the alkaline earth atoms could give rise to such a difference in the M and A reactions. In view of the ideas developed in discussing the $Ba + CF_3I$

reaction, however, it seems likely that such a statistical complex would produce some MI_2 product as well. Because of the mass differences, the measured angular distributions shown in Figure 4 can be fit to CM cross sections with more reasonable E' values for $MI_2 + CH_2$ products; Table IV gives the recoil energies obtained in this case. Thus, as for $Ba + CF_3I$, the data are inconclusive but suggest formation of MI_2 product, and possibly some MI as well. Interestingly, rupture of both C-I bonds has also been observed²³ in the uv photodissociation of CH_2I_2 , yielding CH_2 and an electronically excited I_2 .

$Ba + CCl_4$. Here again, the observed $BaCl^+$ signal might have arisen from ionization of product BaCl and/or $BaCl_2$; the measured $BaCl^+$ LAB distribution provides no basis for estimating which is formed. In analogy with CH_2I_2 and CF_3I , both products might form; this would also be consistent with dissociative electron attachment results for CCl_4 , where both Cl^- and Cl_2^- are observed.²⁴

Acknowledgment. This work was supported by the U.S. Atomic Energy Commission through the Lawrence Berkeley Laboratory. Partial support from the Committee on Research of the University of California at Berkeley is also gratefully acknowledged.

(22) S. A. Safran, N. D. Weinstein, D. R. Herschbach, and J. C. Tully, *Chem. Phys. Lett.*, **12**, 564 (1972).

(23) D. W. G. Style and J. C. Ward, *J. Chem. Soc. London*, 2125 (1952).

(24) J. J. DeCorpo, D. A. Bafus, and J. L. Franklin, *J. Chem. Phys.*, **54**, 1592 (1971).

Bimolecular Dissociation of Cyanogen behind Incident Shock Waves

T. Fueno,* K. Tabayashi, and O. Kajimoto

Department of Chemistry, Faculty of Engineering Science, Osaka University, Toyonaka, Osaka, Japan

(Received September 15, 1972)

The kinetics and thermodynamics of the dissociation of cyanogen behind an incident shock wave have been studied in the temperature range 2200–3700°K. The course of the dissociation was followed by monitoring the CN (0-1) $B^2\Sigma^+ - X^2\Sigma^+$ absorption and emission centered at 4216 Å. Analysis of the absorption coefficients at equilibrium resulted in $\Delta H_f^\circ(\text{CN}) = 99.5 \pm 0.5$ kcal/mol [$D_0(\text{NC-CN}) = 125.5 \pm 1.0$ kcal/mol]. The bimolecular rate constants k_D for the reaction, $C_2N_2 + \text{Ar} \rightarrow 2\text{CN} + \text{Ar}$, obtained from the initial slopes of absorption were best fitted by $k_D = [3.51 \times 10^{12}/5!] T^{1/2}(E/RT)^5 \exp(-E/RT)$ $\text{cm}^3 \text{mol}^{-1} \text{sec}^{-1}$, with $E = 125.5$ kcal/mol. Emission studies gave essentially the same kinetic results. These findings permit critical assessment of the kinetic data which were reported for the same reaction by previous workers.

I. Introduction

The bimolecular dissociation of cyanogen in argon behind shock waves



is of fundamental importance to the studies of the chemistry of CN radicals. Tsang, *et al.*,¹ followed the dissociation process by monitoring the CN $X^2\Sigma^+ \rightarrow B^2\Sigma^+$ absorption in the temperature range 1700–2500°K. They showed that the second-order rate constant is fitted by

$$k_D = [3.3 \times 10^{12}/5.5!] T^{1/2}(E/RT)^{5.5} \times \exp(-E/RT) \text{ cm}^3 \text{ mol}^{-1} \text{ sec}^{-1} \quad (2)$$

with $E = 125$ kcal/mol, which is the NC-CN bond dissociation energy determined from the absorption intensities at equilibrium. Recently, Slack, *et al.*,² measured the rates of the same reaction by monitoring the time-dependent CN $B^2\Sigma^+ \rightarrow X^2\Sigma^+$ emission over the temperature range 2700–4000°K. The results were best fitted by the Arrhenius expression

$$k_D = 4.58 \times 10^{14} \exp(-69,000/RT) \text{ cm}^3 \text{ mol}^{-1} \text{ sec}^{-1} \quad (3)$$

(1) W. Tsang, S. H. Bauer, and M. Cowperthwaite, *J. Chem. Phys.*, **36**, 1768 (1962).

(2) M. W. Slack, E. S. Fishburne, and A. R. Johnson, *J. Chem. Phys.*, **54**, 1652 (1971).

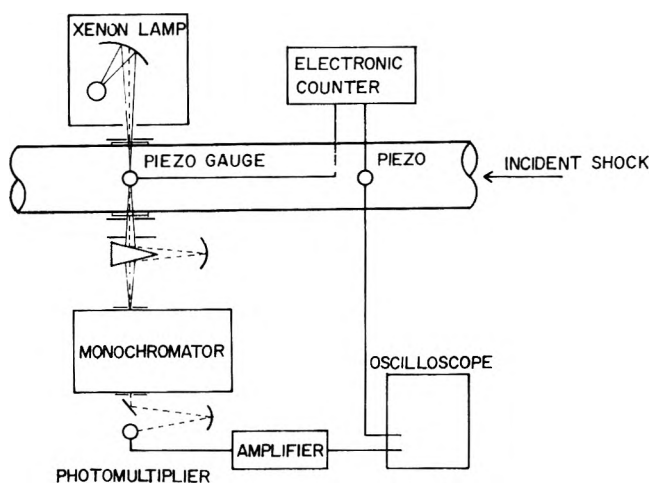


Figure 1. Schematic diagram of the optical and electrical systems of the shock-tube apparatus used.

These two expressions, eq 2 and 3, differ greatly in temperature variation. Thus, the emission data obtained at "high" temperatures show an experimental activation energy considerably smaller than $E - 5RT$ which is to be expected from the absorption results obtained at "low" temperatures. A question now arises as to whether the above apparent discrepancy indeed reflects the true mechanistic character of the reaction at varying temperature or is due to inadequacy of either the absorption or emission spectroscopy used.

We have thus undertaken to reinvestigate kinetics and thermochemistry of the C_2N_2 dissociation in the "middle" temperature range 2200–3700°K, using both the absorption and emission techniques. Special precautions were taken to conduct precise measurements. The two techniques gave essentially the same results, if perturbation of the thermal equilibrium $CN + Ar \rightleftharpoons CN^* + Ar$ by the electronic quenching of CN^* was duly taken into consideration. The results obtained were found to be in good agreement with the rate data of Tsang, *et al.*, except for a constant factor of *ca.* 2.

II. Experimental Section

(A) *Apparatus.* A stainless-steel cylindrical shock tube of 10.4-cm diameter was used. The driver section was 1.0 m in length, while the driven section was 4.0 m in length. The two sections, separated by a Mylar diaphragm, had flange ends to be bolted together. A dump tank of 21.2 l. capacity was fitted to the downstream end of the driven section.

Figure 1 is a schematic diagram of the test section. The detection system had two piezoelectric detector stations, one being located about 300 cm downstream from the diaphragm and the other 60 cm further downstream. The optical station consisted of two diametrically opposed quartz windows which were sealed with O-rings and held in compression by close-tolerance steel collets.

The light source used for the absorption measurements was an Ushio 300 D (300 W) xenon lamp. The light was focused with a mirror on the radial center of the shock tube, collimated with a 1-mm slit, and refocused on the entrance slit of a Rikotsusho MG-50 grating (Bausch and Lomb) monochromator. The violet light, whether transmitted or emitted, was collected on an RCA-1P28 photomultiplier, whose output signal was amplified and displayed on the beams of a Sony/Tektronix 564B storage oscilloscope. The collimating slit width of 1 mm gave a

reaction volume with a gas passage time less than 1 μ sec over the range of the incident shock velocities adopted. The response time of the photomultiplier and its associated electronics was no greater than 2 μ sec.

The time intervals for the incident shock to traverse the distance between the two stations were measured with an Iwatsu UC-6131 universal counter to *ca.* $\pm 1 \mu$ sec. This uncertainty (about 0.3%) in shock velocity resulted in a $\pm 30^\circ$ K uncertainty in the calculated incident shock temperature.

(B) *Material.* Cyanogen was generated by pouring an aqueous solution of sodium cyanide onto cupric sulfate at 50° and was dried by passing through phosphorus pentoxide.³ Mass spectrometric analysis revealed slight amounts of HCN and CO_2 as impurities. In order to remove volatile impurities, the material was solidified and degassed at the temperature of a Dry Ice-acetone bath (-78°). It was further purified by trap-to-trap distillations using a carefully controlled acetone bath (-78 to -40°). Mass spectrometric analysis of the purified samples showed no indication of impurities. High-purity (99.999%) argon was used without further purification.

(C) *Procedure.* Mixtures of 0.1, 0.2, and 0.5% C_2N_2 in Ar were prepared. They were kept in 10-l. glass flasks for more than 12 hr before use.

The driven section was evacuated with a trapped-oil diffusion pump, prior to introducing the test gas. To minimize impurities due to the residue of air, the driven tube was purged with argon after the evacuation down to 10^{-4} Torr, and then re-evacuated to a pressure less than 5×10^{-6} Torr before each run. The leak rate was less than 10×10^{-6} Torr/min.

Shocks were driven with hydrogen gas. Mylar diaphragms of 0.05-, 0.1-, and 0.188-mm thickness, which corresponded to the driver bursting pressures of 2, 4, and 7.5 kg/cm², respectively, were used. Diaphragm rupture was initiated with a stainless plunger.

The temperature, pressure, and density of the shocked gas were calculated from the measured shock velocity. Boundary layer effects⁴ on gas properties were estimated to be small under our experimental conditions and hence were neglected throughout. Further, since low concentration mixtures of cyanogen were used for the present measurements, we also neglected possible temperature drops due to the enthalpy effect of the dissociation reaction.

Specific absorption and emission of the P branch of the (0–1) band (head at 4216 Å) of the $B^2\Sigma^+ - X^2\Sigma^+$ system was used to determine the concentrations of the CN radicals. The grating monochromator with 300- μ entrance and exit slits was set to isolate the spectral bandwidth 4212.9–4217.1 Å. This region encompasses the overlapping rotational lines $J = 9-36$ of the ground state CN ($X^2\Sigma^+$, $v = 1$) and $J' = 8-35$ of CN ($B^2\Sigma^+$, $v' = 0$).

III. Absorption Studies

(A) *Dissociation Equilibrium.* Figure 2 shows a typical oscillogram of the CN ($X^2\Sigma^+ \rightarrow B^2\Sigma^+$) light absorption with time behind the shock front. At temperatures below 3200°K, a rise to the final constant value was observed. This constancy in absorption suggests that the equilibrium



holds behind the incident shock waves and that side reac-

- (3) G. J. Janz, "Inorganic Syntheses," Vol. 5, McGraw-Hill New York, N. Y., 1957, p 43.
- (4) R. L. Belford and R. A. Strehlow, *Ann. Rev. Phys. Chem.*, **20**, 247 (1969).

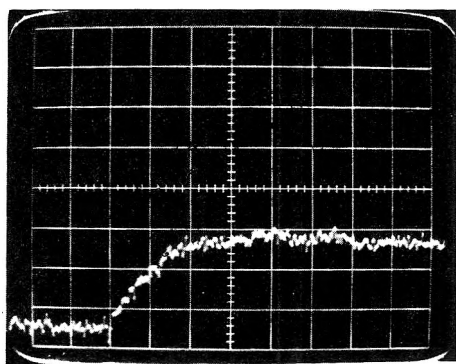


Figure 2. Typical experimental oscillogram showing the variation of CN(0-1) violet absorption with time. $C_2N_2 = 0.501$ mol %; $P_1 = 11.1$ Torr; $T_2 = 2950^\circ\text{K}$; ordinate, 0.2 V/division; abscissa, $20 \mu\text{sec/division}$.

tions of CN would not affect the equilibrium appreciably during the time intervals recorded.

In analyzing the equilibrium records, we basically followed the method of Tsang, *et al.*¹ The observed absorbance at equilibrium is related to the equilibrium concentration of CN radicals through

$$\ln(I_0/I)_e = \beta l F_{ab}(T)[CN]_e \quad (5)$$

where β is the effective absorption for the CN radicals in the absorbing levels, l is the optical path length, and $F_{ab}(T)$ is the fractional population of the absorbing CN($X^2\Sigma^+$) radicals. The $F_{ab}(T)$ is given in our present instance by

$$F_{ab}(T) = \frac{\sum_{J=9}^{36} (2J+1) \exp\left(-\frac{J(J+1)\epsilon_{rot}}{kT} - \frac{\epsilon_{vib}}{kT}\right)}{Q_{rot}Q_{vib}} \quad (6)$$

where ϵ_{rot} and ϵ_{vib} respectively denote the rotational and vibrational quanta of CN radicals and where Q_{rot} and Q_{vib} stand for the corresponding partition functions. The absorption coefficient β thus related with $(I_0/I)_e$ should be least temperature-dependent.

The magnitudes of β could be determined from the observed absorbance, given the equilibrium concentration $[CN]_e$. The $[CN]_e$ in turn could readily be calculated if the appropriate heat and entropy of reaction were available as the functions of temperature. Because our ultimate purpose here was to evaluate the heat of formation of CN radicals $\Delta H_f^\circ(\text{CN})$, we treated this particular heat as the only unknown quantity. The remaining thermodynamic quantities, *i.e.* the entropy change ΔS° and the specific heat change ΔC_p° of the reaction and the heat of formation of C_2N_2 [$\Delta H_f^\circ(C_2N_2) = 73.4$ kcal/mol], were all evaluated according to the JANAF tables.⁵ Under these conditions, both the magnitude and temperature dependence of the β value calculated from eq 5 should eventually hinge on the value of $\Delta H_f^\circ(\text{CN})$ selected. Thus, we sought a value for $\Delta H_f^\circ(\text{CN})$ such that the resulting β values would be invariant over the temperature range studied. Adoption of $\Delta H_f^\circ(\text{CN}) = 99.5 \pm 0.5$ kcal/mol, which corresponded to $D_0(\text{NC-CN}) = 125.5 \pm 1.0$ kcal/mol, was found to give statistically the best results. The experimental β values obtained in this best case are plotted against the reaction temperatures in Figure 3. Although the plotted points are somewhat scattered, they show no apparent temperature dependence. The average β value was $(9.16 \pm 0.76) \times 10^6 \text{ cm}^2/\text{mol}$.

(B) *Dissociation Kinetics.* The bimolecular dissociation rate constants k_D were determined from the initial slopes

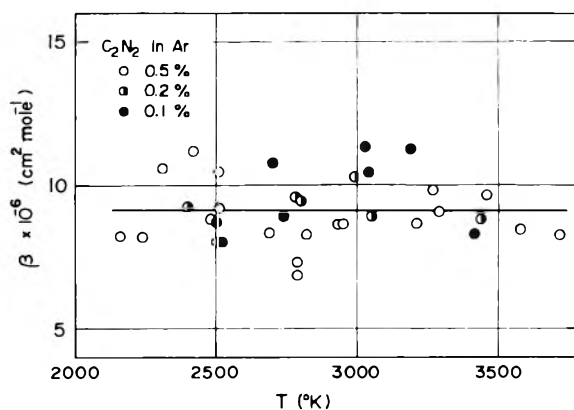


Figure 3. Temperature variation of CN absorption coefficient at 4216 \AA .

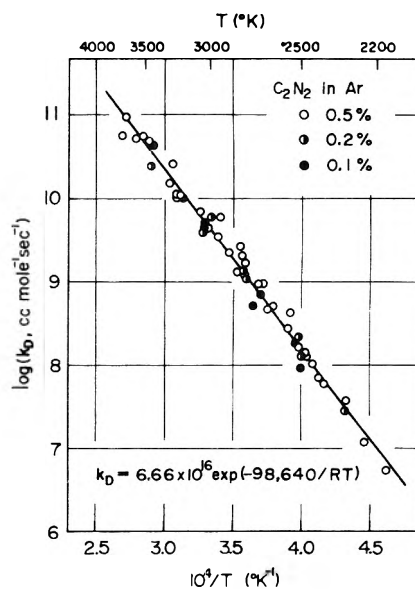


Figure 4. Arrhenius plots of k_D .

of the absorption records, corresponding to the first 10-20% rise in the CN concentrations. Guided by eq 5, we may write

$$\begin{aligned} k_D &= \frac{1}{2} \frac{d[\text{CN}(X^2\Sigma^+)]}{dt} / [C_2N_2]_0 [Ar]_0 \\ &= \frac{1}{2} r_0 / \beta l F_{ab}(T) / [C_2N_2]_0 [Ar]_0 \end{aligned} \quad (7)$$

where r_0 is the initial slope of absorbance defined as

$$r_0 = \left(\frac{d \ln(I_0/I)}{dt}\right)_0 \simeq - \left(\frac{dI}{dt}\right)_0 / I_0 \quad (8)$$

and where $[C_2N_2]_0$ and $[Ar]_0$ are the concentrations of cyanogen and argon at zero time, immediately behind the shock. We set $\beta = 9.16 \times 10^6 \text{ cm}^2/\text{mol}$ as determined in the preceding section.

Kinetic data were taken for the 0.1, 0.2, and 0.5% C_2N_2 -Ar mixtures at the total pressures between 0.21 and 1.35 atm. The temperature range was limited by immeasurably weak light absorption below 2200°K and by significant influence of CN emission on the absorption intensity above 3700°K . Experimental data and the values of k_D obtained for some representative runs are listed in Table I.

Figure 4 shows the Arrhenius plots of k_D obtained for a total of 52 experiments. A single straight line fits the plots, irrespective of the C_2N_2 /Ar ratio and the total gas

(5) D. R. Stull, Ed., "JANAF Thermochemical Tables," Dow Chemical Co., Midland, Mich., 1965.

TABLE I: Absorption Rate Data

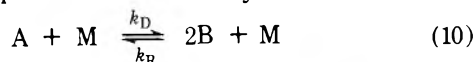
C ₂ N ₂ , mol %	P ₁ , Torr	U _s , mm/μsec	ρ ₂₁	T ₂ , °K	[Ar] ₀ , 10 ⁻⁶ mol/cm ³	x _e	τ _{1/2} , μsec	k _D ^a , cm ³ mol ⁻¹ sec ⁻¹
0.105	29.0	1.58	3.57	2498	5.71	0.379	106.9	9.23 × 10 ⁷
0.105	23.6	1.66	3.60	2742	4.69	0.753	42.9	5.12 × 10 ⁸
0.112	18.8	1.76	3.64	3041	3.79	0.958	11.2	4.46 × 10 ⁹
0.105	8.41	1.88	3.68	3422	1.70	0.998	1.54	4.58 × 10 ¹⁰
0.217	32.4	1.54	3.55	2397	6.29	0.176	81.5	5.99 × 10 ⁷
0.217	28.9	1.58	3.57	2499	5.67	0.285	55.0	1.34 × 10 ⁸
0.232	13.2	1.68	3.61	2801	2.59	0.789	40.8	1.38 × 10 ⁹
0.232	8.28	1.98	3.68	3445	1.65	0.996	3.76	2.38 × 10 ¹⁰
0.501	36.4	1.46	3.50	2163	7.04	0.0311	126.3	5.42 × 10 ⁶
0.501	19.1	1.51	3.53	2312	3.68	0.100	107.2	3.90 × 10 ⁷
0.501	16.6	1.57	3.56	2477	3.23	0.231	83.0	1.29 × 10 ⁸
0.501	13.8	1.64	3.59	2690	2.69	0.517	37.4	9.58 × 10 ⁸
0.501	23.4	1.68	3.61	2787	4.57	0.556	14.2	1.16 × 10 ⁹
0.501	11.1	1.73	3.63	2950	2.18	0.847	15.6	3.51 × 10 ⁹
0.512	8.70	1.83	3.67	3287	1.75	0.978	5.79	1.51 × 10 ¹⁰
0.512	3.47	1.96	3.70	3720	0.698	0.999	2.84	5.67 × 10 ¹⁰

^a Determined by the initial slope method (eq 7).

pressure. Least-squares treatment of the linearity led to the Arrhenius expression

$$k_D = 6.66(\pm 1.25) \times 10^{16} \exp\left(-\frac{98,640 \pm 1210}{RT}\right) \text{ cm}^3 \text{ mol}^{-1} \text{ sec}^{-1} \quad (9)$$

The rate constants were also evaluated by the half-time method. For the reversible dissociation-recombination reactions in the presence of a third body



one can write

$$-\frac{dA}{dt} = \frac{1}{2} \frac{dB}{dt} = k_D M \left(A - \frac{1}{K_e} B^2 \right) \quad (11)$$

where K_e is the equilibrium constant

$$K_e = k_D / K_R = B_e^2 / A_e \quad (12)$$

We may express the reactant concentrations by use of the initial concentration A_0 and the degree of dissociation x

$$A = A_0(1 - x); \quad B = 2A_0x \quad (13)$$

Equation 11 is now rewritten into

$$\frac{dx}{dt} = -\left(\frac{1-x_e}{x_e^2}\right) k_D M \left(x + \frac{x_e}{1-x_e}\right) (x - x_e) \quad (14)$$

x_e being the degree of dissociation at equilibrium. Integrating eq 14 from $x = 0$ to $x = x_e/2$, we obtain

$$k_D = \frac{x_e \ln(3 - x_e)}{(2 - x_e) M t_{1/2}} \quad (15)$$

where $t_{1/2}$ is the relevant half time. Incidentally, for the case where $x_e \ll 1$, eq 15 reduces to

$$k_D = (B_e \ln 3) / (4A_0 M t_{1/2}) \quad (16)$$

a form which was derived and used by Tsang, *et al.*,¹ for the lower-temperature dissociation of C₂N₂.

The half-time $t_{1/2}$ appearing in eq 15 and 16 is equal to the laboratory half-time $\tau_{1/2}$ times the gas density ratio across the shock front ρ_{21} . In determining the $\tau_{1/2}$, we expediently assumed that the laboratory time corresponding to one-half the absorbance at equilibrium, $(1/2) \ln(I_0/I_e)$, can be approximated to the time corresponding to the half-height of the equilibrium absorption record, $(1/2)(I_0 - I_e)$. In reality, this expedience introduced no serious error into the final results, because $(I_0 - I_e)/I_0 < 0.1$ in the majority of our runs.

The dissociation rate constants evaluated from eq 15

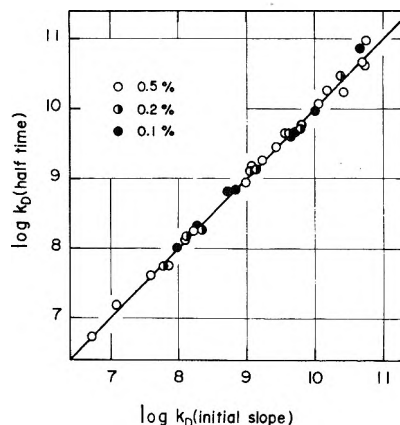


Figure 5. Agreement of the k_D values determined by the half-time method with those obtained by the initial-slope method.

were compared with those obtained by the initial slope method. The good agreement found between the two sets of data (Figure 5) provides confidence in the assumptions which were involved in the estimations of β and $\Delta H_f^\circ(\text{CN})$.

The experimental activation energy $E_a = 98.6$ kcal/mole is considerably smaller than $D_0(\text{NC-CN}) = 125.5$ kcal/mole, indicative of the participation of the internal degrees of freedom in the activation process. In cases like the present, the Fowler-Guggenheim expression⁶ is applicable.

$$k_D = \lambda(Z/n!)(E/RT)^n \exp(-E/RT) \quad (17)$$

If 3000°K is taken as the average temperature at which data were taken, and if E is assumed to be equal to $D_0(\text{NC-CN})$, then the temperature variation of eq 9 is best fitted to that of eq 17 when n is assigned a value of 5. The least-squares fit of eq 17 with $n = 5$ to the experimental values led to the expression

$$k_D = [3.51(\pm 1.06) \times 10^{12}/5!] T^{1/2} (E/RT)^5 \exp(-E/RT) \text{ cm}^3 \text{ mol}^{-1} \text{ sec}^{-1} \quad (18)$$

Assuming a collision diameter of 3.9 Å, we deduce the steric factor $\lambda = 0.40$, a value which seems to be reasonable.

(6) R. Fowler and E. A. Guggenheim, "Statistical Thermodynamics," Cambridge University Press, Cambridge, 1952, pp 495-499.

TABLE II: Emission Rate Data

C ₂ N ₂ , mol %	P ₁ , Torr	U _s , mm/μsec	ρ ₂₁	T ₂ , °K	[Ar] ₀ , 10 ⁻⁶ mol/cm ³	x _e	γ	k _{D'} ^a , cm ³ mol ⁻¹ sec ⁻¹
0.232	17.5	1.55	3.55	2419	3.41	0.247	0.239	1.44 × 10 ⁸
0.232	11.0	1.74	3.63	2981	2.17	0.931	0.181	4.98 × 10 ⁹
0.232	8.42	1.87	3.68	3403	1.69	0.995	0.156	2.77 × 10 ¹⁰
0.232	6.05	1.97	3.71	3743	1.22	0.999	0.123	9.16 × 10 ¹⁰
0.503	31.9	1.53	3.54	2374	6.20	0.107	0.361	4.64 × 10 ⁷
0.507	16.5	1.57	3.56	2476	3.21	0.230	0.230	9.86 × 10 ⁷
0.507	9.60	1.58	3.56	2500	1.87	0.319	0.149	2.89 × 10 ⁸
0.485	13.8	1.63	3.59	2649	2.70	0.465	0.206	7.08 × 10 ⁸
0.485	12.8	1.68	3.61	2785	2.52	0.660	0.199	1.35 × 10 ⁹
0.507	7.17	1.69	3.62	2843	1.41	0.807	0.123	2.18 × 10 ⁹
0.507	4.97	1.82	3.66	3234	0.991	0.983	0.0954	1.08 × 10 ¹⁰
0.507	4.05	1.92	3.69	3566	0.813	0.997	0.0833	3.55 × 10 ¹⁰

^a Determined by the initial slope method (eq 21).

IV. Emission Studies

(A) *Emission Profile.* The CN B²Σ⁺ → X²Σ⁺ emission intensities were monitored in mixtures of 0.2 and 0.5% C₂N₂ in Ar over the temperature range 2300–3800°K. A typical oscillographic record is shown in Figure 6.

If all internal modes of the CN(B²Σ⁺) are relaxed instantaneously and if the effect of induced absorption can be neglected, the emission intensity *H* (measured in volts) from CN(B²Σ⁺) radicals may be written as

$$H = c[\text{CN}(\text{B}^2\Sigma^+)]_{\Delta v} = cF_{em}(T)[\text{CN}(\text{B}^2\Sigma^+)] \quad (19)$$

where *c* is an instrumental constant depending on the bandpass chosen; [CN(B²Σ⁺)]_{Δv} is the concentration of the radiating radicals in the observed states (B²Σ⁺, *v*' = 0, *J*' = 8–35); and *F*_{em}(*T*) is the fractional population of the [CN(B²Σ⁺)]_{Δv} in the CN(B²Σ⁺) radicals, as was defined in eq 6. Further, if electronic relaxation is assumed to be so rapid that the thermal equilibrium between the CN(B²Σ⁺) and CN(X²Σ⁺) species is maintained, then

$$[\text{CN}(\text{B}^2\Sigma^+)]/[\text{CN}(\text{X}^2\Sigma^+)] = \exp(-E^*/RT) \quad (20)$$

where *E** = 73.58 kcal/mol is the electronic excitation energy of the B²Σ⁺ state.

If the assumptions underlying eq 19 and 20 are acceptable at all, the threshold height *H*_e of the emission profile divided by *F*_{em} should be proportional to equilibrium concentrations of CN(B²Σ⁺) calculated from [CN(X²Σ⁺)]_e and eq 20. The proportionality held roughly over a [CN(B²Σ⁺)] range of ca. 300 (Figure 7). The proportionality constant *c* came out to be 1.0 × 10¹³ cm³ mol⁻¹.

(B) *Dissociation Rates.* With the instrumental constant in hand, we can evaluate the dissociation rate constants from the initial slopes *s*₀ ≡ (d*H*/d*t*)₀ of the emission records.

$$k_{D'} = \frac{1}{2} \{s_0/cF_{em}(T)\} \exp(E^*/RT)/[C_2N_2]_0[Ar]_0 \quad (21)$$

experimental results for some representative runs are given in Table II.

The values of *k*_{D'} so obtained for a total of 27 runs are plotted as a function of temperature in Figure 8. Although in general the plotted points are found to lie in the vicinity of the absorption results (dotted line), those for the higher-temperature region systematically show a downward deviation. As a consequence, a least-squares fit of the plots to the Arrhenius equation (full line) has led to

$$k_{D'} = 9.32(\pm 135) \times$$

$$10^{15} \exp\left(-\frac{87,440 \pm 2580}{RT}\right) \text{ cm}^3 \text{ mol}^{-1} \text{ sec}^{-1} \quad (22)$$

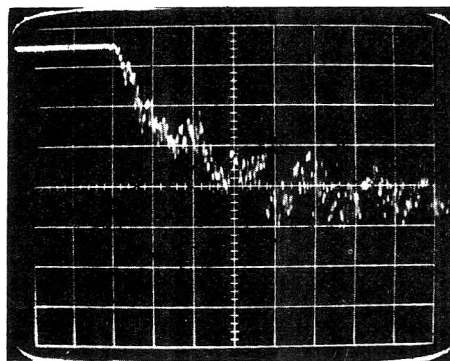


Figure 6. Typical experimental oscillogram showing CN(0-1) emission profile. C₂N₂ = 0.232 mol %; P₁ = 11.0 Torr; T₂ = 2981°K; ordinate, 0.05 V/division; abscissa, 20 μsec/division.

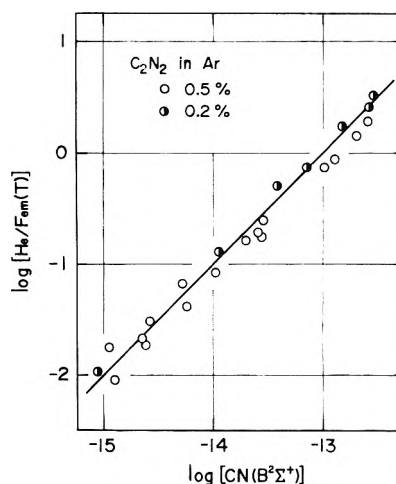
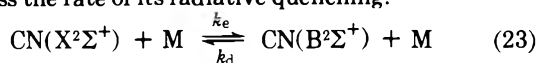
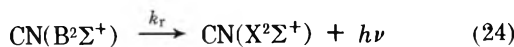


Figure 7. Variation of the emission intensities with calculated concentration of CN(B²Σ⁺) at equilibrium. Solid line; *H*_e/*F*_{em}(*T*) = 1.0 × 10¹³[CN(B²Σ⁺)]_e.

which has an apparent activation energy *E*_a = 87.4 kcal/mol, about 11 kcal smaller than that obtained from the absorption studies.

We suspect that the apparently smaller temperature coefficient of *k*_{D'} (eq 22) as compared with *k*_D (eq 9) is at least partly ascribable to inadequacy of the assumption of the thermal equilibrium between CN(B²Σ⁺) and CN(X²Σ⁺). Obviously, the equilibrium should be affected if the rate of the collisional deexcitation of CN(B²Σ⁺) does not surpass the rate of its radiative quenching.





The steady-state assumption leads, instead of eq 20, to

$$[\text{CN}(\text{B}^2\Sigma^+)]/[\text{CN}(\text{X}^2\Sigma^+)] = \gamma \exp(-E^*/RT) \quad (25)$$

where

$$\gamma = (1 + k_r/k_d[M])^{-1} \quad (26)$$

Fairbairn⁷ has already noted this departure from equilibrium and estimated the collisional deexcitation cross section to be as small as *ca.* 0.1 Å². The significance of the nonequilibrium character of the CN(B²Σ⁺) emission has recently been emphasized by Jackson and Faris.⁸

Adopting Fairbairn's cross section 0.1 Å² for *k_d* and the radiative quenching rate constant *k_r* = 1.2 × 10⁷ sec⁻¹ obtained by Bennett and Dalby,⁹ we find that under our experimental conditions the *γ* takes on values ranging from 0.08 to 0.36, depending on [M]. Our rate data need to be corrected accordingly. Corrections proceed as follows. Calculate [CN(B²Σ⁺)] from eq 25 and determine a new instrumental constant *c'* which satisfies the proportionality between *H/F_{em}(T)* and [CN(B²Σ⁺)]. Evaluate *k_D'* for each run from eq 21 by replacing *c* with *c'*.

The *c'* value thus obtained was 5.5 × 10¹³ V cm³ mol⁻¹. Arrhenius plots of the *k_D'* thus corrected (Figure 9) gave

$$k_{D' \text{ cor}} = 7.59(\pm 1.56) \times$$

$$10^{16} \exp\left(-\frac{98,970 \pm 2540}{RT}\right) \text{ cm}^3 \text{ mol}^{-1} \text{ sec}^{-1} \quad (27)$$

which is in essential agreement with *k_D* obtained by the absorption studies (eq 9). The improved agreement between *k_D* and *k_D'* has resulted from relatively smaller values of *γ* at higher temperatures; experimentally, higher temperatures were attained by reducing the initial gas pressure in the driven section and hence by lowering [M] in the reaction zone.

V. Discussion

The heat of formation Δ*H_f*⁰(CN) = 99.5 ± 0.5 kcal/mol deduced from the present work is in excellent agreement with 99.0 ± 4 kcal/mol found by Tsang, *et al.*,¹ and 100.0 ± 1 kcal/mol reported recently by Dibeler and Liston.¹⁰ Further, it also compares well with 100 ± 3 kcal/mol obtained by Boden and Thrush¹¹ from a kinetic study of the reaction, CN + H₂ → HCN + H, by means of elec-

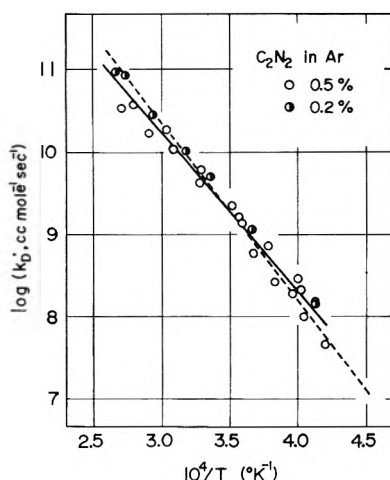


Figure 8. Arrhenius plots of the second-order rate constant *k_D'* determined by the emission technique. The least-squares fit to the data is shown by the solid line (eq 22). The dashed line is from the absorption data (eq 9).

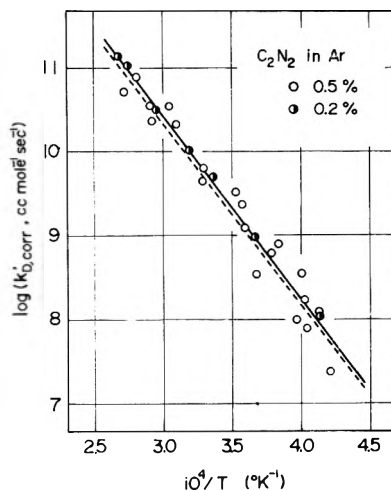


Figure 9. Arrhenius plots of *k_D' cor*. The least-squares fit to the data is shown by the solid line (eq 27). The dashed line is from the absorption data (eq 9).

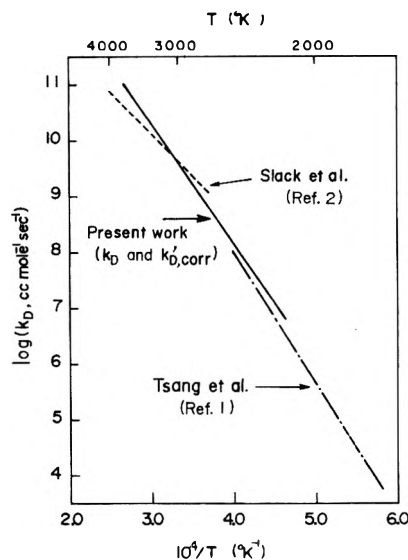


Figure 10. Comparison of the shock wave measurements of the rate of dissociation of C₂N₂ in Ar.

tronic absorption spectroscopy. Kinetic data for the flow-tube study of H + C₂N₂ → HCN + CN by Dunn, *et al.*,¹² require Δ*H_f*⁰(CN) ≤ 100 kcal/mol, which is also compatible with the present result.

Figure 10 compares the bimolecular dissociation rate constants obtained in this work with those reported by previous workers. Our results (eq 9 and 27) agree closely with the low-temperature absorption results (eq 2)¹³ of Tsang, *et al.*¹ However, the high-temperature emission results (eq 3) obtained by Slack, *et al.*,² do not agree with

- (7) A. R. Fairbairn, *J. Chem. Phys.*, **51**, 972 (1969).
- (8) W. M. Jackson and J. L. Faris, *J. Chem. Phys.*, **56**, 95 (1972).
- (9) R. G. Bennett and F. W. Dalby, *J. Chem. Phys.*, **36**, 399 (1962).
- (10) V. H. Dibeler and S. K. Liston, *J. Chem. Phys.*, **48**, 4765 (1968).
- (11) J. C. Boden and B. A. Thrush, *Proc. Roy. Soc., Ser. A*, **305**, 107 (1968).
- (12) M. R. Dunn, C. G. Freeman, M. J. McEwan, and L. F. Phillips, *J. Phys. Chem.*, **75**, 2662 (1971).
- (13) Tsang, *et al.*,¹ defined the rate constant *k_D* by $d[\text{CN}]/dt = k_D([\text{C}_2\text{N}_2] - [\text{CN}]^2/K_e)[\text{M}]$, instead of eq 11. Thus, by definition, their *k_D* is twice as large as ours. Their rate results shown in Figure 10 are those obtained by dividing eq 2 by 2.

ours in the temperature dependence, their value of E_a being anomalously low (69.0 kcal/mol). The discrepancy is not likely to be eliminated by the nonequilibrium corrections of their k_D' values. It appears that their rate data involve some technical errors which tend to lower the k_D' values at high temperatures.

In this connection, it should be noted that emission experiments appear to necessitate far greater technical precautions than absorption studies. In preliminary studies, we observed that both peak intensities and initial slopes of emission strongly depended on the cleanliness of the vacuum system. Only after most stringent precautions to avoid contamination could reliable values of k_D' be obtained.

Slack, *et al.*, combined their high-temperature data with the low-temperature results of Tsang, *et al.*, and ob-

tained a Fowler-Guggenheim expression with $n = 8$ and $E = 128.7$ kcal/mol. It is now evident that there was no physical ground for doing this. In fact, $n = 8$ requires that all the vibrational degrees of freedom for C_2N_2 be involved in the activation process, a situation which is highly unlikely to occur. Further, $n = 8$ gives the steric factor $\lambda = 0.017$, which is somewhat too small for reactions of the type studied here. Their interpretation of the kinetic data is thus hardly justifiable.

Acknowledgments. The authors wish to express gratitude to Professor G. Kamimoto and Dr. H. Matsui of Kyoto University for helpful advices on the experimental work. They are also indebted to Mr. K. Murakami, presently at the Dainippon Ink Co. Ltd., for assistance in the construction of the apparatus.

A Thermal Desorption Study of the Surface Interactions between Water and Plutonium Dioxide¹

J. L. Stakebake

Dow Chemical U. S. A., Rocky Flats Division, Golden, Colorado 80401 (Received September 18, 1972)

Publication costs assisted by The Dow Chemical Company

The interactions between water vapor and plutonium dioxide have been investigated using a mass spectrometric thermal desorption technique. Chemisorbed water vapor was found to be desorbed in two temperature ranges: one between 100 and 150° and the second between 300 and 350°. In terms of adsorption, these results are attributed to the hydroxylation of the oxide followed by the double hydrogen bonding of water molecules to the hydroxyl groups. The heat of adsorption was calculated to be 68 kcal/mol for hydroxylation and 20 kcal/mol for the hydrogen bonding.

Introduction

Following exposure to the atmosphere the surfaces of metal oxides are usually covered with adsorbed water. This contamination can significantly affect oxide sintering characteristics and other surface properties such as catalytic activity and selective adsorbability. A knowledge of the mechanism of water adsorption including adsorbed species, bond strengths, and the temperature required for desorption could provide valuable criteria for powder conditioning.

The interaction between water and several metal oxides has been studied fairly extensively by a number of workers.²⁻⁶ It is generally agreed that oxide surfaces become hydroxylated upon exposure to water vapor. The exact conditions under which this occurs, however, have not been agreed upon and may in fact depend on the nature of the oxide. In addition to the dissociative adsorption forming a hydroxylated surface, water may also be adsorbed in two molecular forms.

Little has been done to investigate the plutonium dioxide-water system because of the toxic nature of plutonium. An earlier study showed water vapor to be irreversibly adsorbed on plutonium dioxide.⁷ Thermogravimetric desorption measurements further revealed that this irre-

versibly adsorbed water consisted of two different adsorbed phases or species. To provide additional information on the characteristics of these two species the desorption of water from plutonium dioxide was investigated by a "thermal desorption" technique.

Thermal desorption is the removal of adsorbed species by heating the sample under vacuum. During the linear heating cycle different species are desorbed at different temperatures depending upon their binding energy. This technique provides information on several adsorption parameters including (a) the number of adsorbed phases or species, (b) the adsorbed population in each phase, (c) the activation energy of desorption reactions, and (e) the

- (1) (a) Work performed under the auspices of the U. S. Atomic Energy Commission, Contract No. AT(29-1)-1106. (b) Presented, in part, at the 163rd National Meeting of The American Chemical Society, Boston, Mass., April 9-14, 1972.
- (2) P. J. Anderson, R. F. Horiack, and J. F. Oliver, *Trans. Faraday Soc.*, **61**, 2754 (1965).
- (3) (a) P. T. Dawson, *J. Phys. Chem.*, **71**, 838 (1967); (b) A. Zecchina, S. Coluccia, E. Guglielminotti, and G. Ghiotti, *ibid.*, **75**, 2774 (1971).
- (4) R. C. Day and G. D. Parfitt, *Trans. Faraday Soc.*, **63**, 708 (1967).
- (5) J. B. Peri and R. B. Hannan, *J. Phys. Chem.*, **64**, 1526 (1960).
- (6) J. H. deBoer, J. M. H. Fortuin, B. C. Lippens, and W. H. Meijs, *J. Catal.*, **2**, 1 (1963).
- (7) J. L. Stakebake and L. M. Steward, *J. Colloid Interface Sci.*, in press.

preexponential kinetic factor for the desorption of each phase.

The desorption process was followed with a time-of-flight mass spectrometer.⁸ This instrument provided a simultaneous measurement of desorption rates and an identification of the desorbed species. This paper is a discussion of the results obtained from the thermal desorption of water from plutonium dioxide and proposes a mechanism for water adsorption.

Theory

When plutonium dioxide is heated at a linear rate under vacuum, the amount of surface coverage by water molecules varies as a function of time (t) and temperature (T). The rate of desorption of a chemisorbed gas has been found to be governed by the Arrhenius equation

$$d\sigma/dt = -\nu_x \sigma^x \exp(-E_d/RT) \quad (1)$$

where σ is the surface coverage at temperature, T ; ν the preexponential kinetic factor; E_d the activation energy of desorption; and x the order of the reaction. During the thermal desorption process the sample temperature is increased at a linear rate, β ; hence, $T = T_0 + \beta t$ where T_0 is the initial temperature and T is the temperature at time t . At some temperature T_m in the desorption process the rate of desorption from the sample will reach a maximum value and $d^2\sigma/dt^2 = 0$. Imposing this condition on eq 1 the following relations between E_d and T_m have been derived.⁹⁻¹²

$$\beta E_d/RT_m^2 \nu_1 = \exp(-E_d/RT_m) \quad (\text{for } x = 1) \quad (2)$$

$$\beta E_d/RT_m^2 \sigma_0 \nu_2 = \exp(-E_d/RT_m) \quad (\text{for } x = 2)$$

where σ_0 is the initial surface coverage.

When the desorption reaction is first order with a first activation energy of desorption, the peak which appears at T_m in the desorption spectrum is not altered by a change in the surface coverage. For a first-order reaction, eq 2 can be further simplified to

$$2 \ln T_m - \ln \beta = E_d/RT_m + \ln E_d/R\nu \quad (4)$$

which is the equation used by several workers.^{10,11} A plot of the left side of eq 4 vs. $1/T_m$ will yield a straight line from which E_d and ν may be calculated. If a value for the preexponential factor is assumed, an estimate of the activation energy of desorption can be obtained from eq 2. The theoretical value of the preexponential factor ν , at some absolute temperature T , can be calculated from transition state theory by

$$\nu = kT/h \quad (5)$$

where k is the Boltzmann constant and h is Planck's constant. For the desorption of water ν is approximately equal to 10^{13} sec^{-1} . Redhead has numerically evaluated E_d as a function of T_m using various values of β^9 and ν .¹³ This relationship was very nearly linear. A change in ν of 10^3 was found to produce a change of only 20% in E_d calculated from measured T_m .

Experimental Section

Sample Preparation. Plutonium dioxide used for this study was prepared by the air oxidation of plutonium metal. This oxide was conditioned by exposure to oxygen at 800° for 2 hr. The physical properties of the plutonium dioxide prepared in this manner are shown in Table I.

TABLE I: Physical Properties of Plutonium Dioxide

Composition	PuO _{2.0}
Surface area, m ² /g	1.3
Crystallite size, Å	260
Particle size, μ	1-5
Lattice parameter, Å	5.394 ± 0.001

In preparation for thermal desorption, samples of oxide were placed in the adsorption system shown in Figure 1. This system contains an electromagnetic recording microbalance for measuring adsorption. The samples were out-gassed to a constant weight at 1000°. Water was then introduced into the system from sulfuric acid solutions. The water was adsorbed on the oxide and partly removed by evacuation at 30°. The water remaining after evacuation was irreversibly adsorbed and was of primary interest. Samples containing approximately three monolayers of irreversibly adsorbed water were used for the thermal desorption studies. The amount of water adsorbed on the individual samples was determined by measuring the total water desorbed during the thermal desorption cycle.

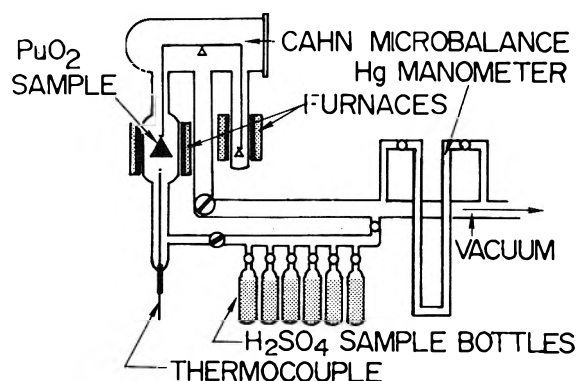


Figure 1. Gravimetric adsorption system.

Apparatus. The thermal desorption process was followed with a Bendix Model 12-107 time-of-flight mass spectrometer. This instrument provided simultaneous qualitative analyses of the desorption products and a quantitative measure of the desorption rates. The m/e range of 1 to 100 may be scanned at approximately 5-sec intervals or any given peak can be monitored continuously. For this study the water peak (m/e 18) was monitored continuously and recorded at 30-sec intervals.

Prior to beginning a run the sample desorption cell was connected to a short inlet tube leading directly into the ionizing region of the spectrometer (Figure 2). During desorption the sample was pumped on continuously with all of the desorbed gases being pumped through the spectrometer source and detected. The temperature of the sample was continuously recorded using the thermocouple at the bottom of the sample tube. This thermocouple had previously been calibrated with a second thermocouple buried in the sample.

- (8) J. L. Stakebake, R. W. Loser, and C. A. Chambers, *Appl. Spectrosc.*, **25**, 70 (1971).
- (9) P. A. Redhead, *Trans. Faraday Soc.*, **57**, 641 (1961).
- (10) Y. Amenomiya and R. J. Cvetanovic, *J. Phys. Chem.*, **67**, 144 (1963).
- (11) I. V. Krylova, A. P. Filonenko, and Yu. P. Sitonite, *Zh. Fiz. Khim.*, **41**, 2839 (1967).
- (12) P. A. Redhead, *Vacuum*, **12**, 203 (1962).
- (13) P. A. Redhead, *Amer. Vacuum Soc. Symp.*, **12**, (1959).

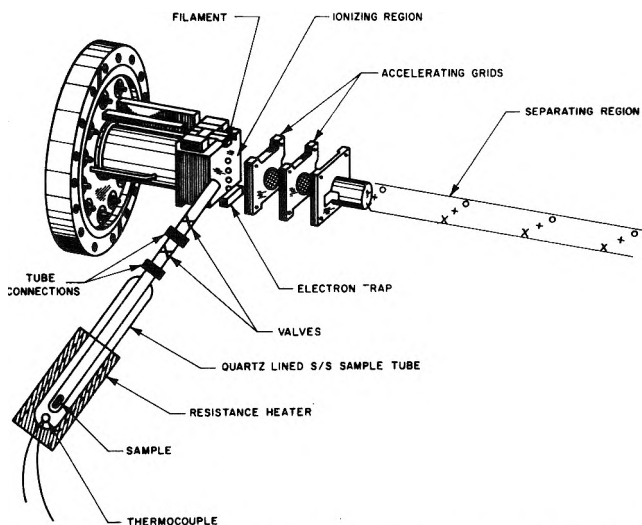


Figure 2. Inlet section of the mass spectrometer as used for thermal desorption.

Procedure. For each run a sample weighing approximately 50 mg was loaded into the sample tube which was in turn attached to the mass spectrometer. It was found that when samples larger than 50 mg were used the amount of water desorbed during a run would overload the instrument. The sample tube was evacuated at room temperature until the pressure in the ionization region of the spectrometer reached the 10^{-7} Torr range. Actual pressures in the sample chamber were slightly higher due to the location of the ionization gauge tube. During each run a temperature programmer was used to increase the temperature of the sample at a linear rate from 25 to 900°. The inertia of the system required the use of fairly slow heating rates. For this study approximate heating rates of 5, 10, 20, and 30°/min were chosen. The exact heating rate was measured for each individual run. The temperature of that portion of the desorption cell above the furnace was maintained at about 135° to minimize readsorption of the gases before they reached the mass spectrometer source.

The spectra obtained from the spectrometer during a desorption run were processed *via* a time-sharing Fortran computer program.¹⁴ This program converted measured peak height into outgassing rates in standard cm^3 per sec. The program also provided a summation of the water desorbed during a run.

Results and Discussion

Gravimetric Desorption. The initial water desorption studies had previously been carried out gravimetrically.⁷ Water was first adsorbed on a sample of plutonium dioxide at 27°. Following adsorption the surface was saturated with adsorbed water. While the sample was still in the microbalance, the water was desorbed by heating the sample under vacuum at successively higher temperatures. The results of this study are summarized in Figure 3. The desorption curve contains two discontinuities indicating three different modes of adsorption. The first type of desorption results from the physical adsorption of water. Approximately 67% of the water was adsorbed in this manner and could be removed under vacuum without the application of heat. The remaining 33% of the water was present as two chemisorbed phases which could only be removed by heating up to 1000°.

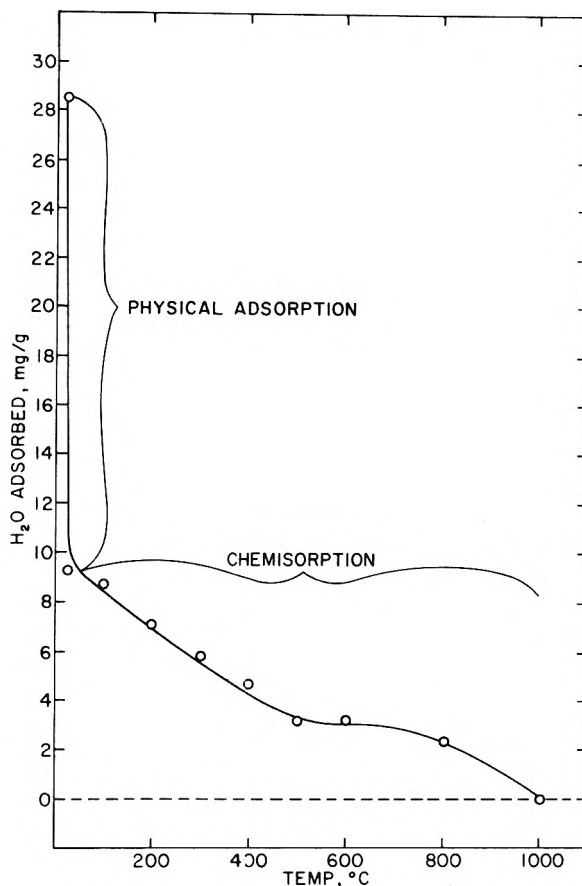


Figure 3. Gravimetric desorption of water from plutonium dioxide.

The first chemisorbed phase to be desorbed is believed to consist of water molecules hydrogen bonded to the surface. Molecules in this phase were removed by heating under vacuum to 500°. The second chemisorbed phase encountered during desorption was the result of what is believed to be a dehydroxylation process. As mentioned earlier the initial adsorbed layer of water is believed to consist of hydroxyl groups. When these hydroxyl groups are desorbed from metal oxides, they reassociate to form water molecules. Temperatures of 1000° were required to remove this second chemisorbed phase.

Thermal Desorption. Results from the thermal desorption of water vapor are presented as thermal desorption spectra which indicate a two-phase chemisorption of water on plutonium dioxide (Figure 4). Samples used for these spectra contained from 0.72 to 1.1 mg of chemisorbed water per gram of oxide. Similar spectra were obtained from samples containing various amounts of chemisorbed water.

Table II summarizes the results of this study and shows the location of the water desorption peaks. All of the desorption results show one species to be desorbed in the temperature range from 100 to 150° while a second species was removed between 300 and 350°.

The total chemisorbed water removed from these samples varied from about 0.72 to 1.15 mg/g and was associated with both adsorbed species. Since the peak height of each species is proportional to the total water removed

(14) R. W. Loser, C. A. Chambers, and E. D. Ruby, RFP-1400, "Time-Sharing Fortran Program for the Dynamic Analysis of Gases by TOF Mass Spectrometry," The Dow Chemical Co., Rocky Flats Division, Golden, Colorado, 1969.

TABLE II: Analysis of Thermal Desorption Spectra for H₂O Adsorbed on PuO₂

Run	σ_0 , mg/g	β , °C/sec	Maximum desorption			
			Species I		Species II	
			T_m , °K	Rate, cm ³ /sec	T_m , °K	Rate, cm ³ /sec
FD-A	0.72	0.073	371	1.5×10^{-3}	598	1.2×10^{-3}
FD-B	1.15	0.161	378	4.5×10^{-3}	601	3.5×10^{-3}
FD-C	0.99	0.363	393	8.0×10^{-3}	613	6.9×10^{-3}
FD-D	0.72	0.498	398	7.5×10^{-3}	618	7.4×10^{-3}

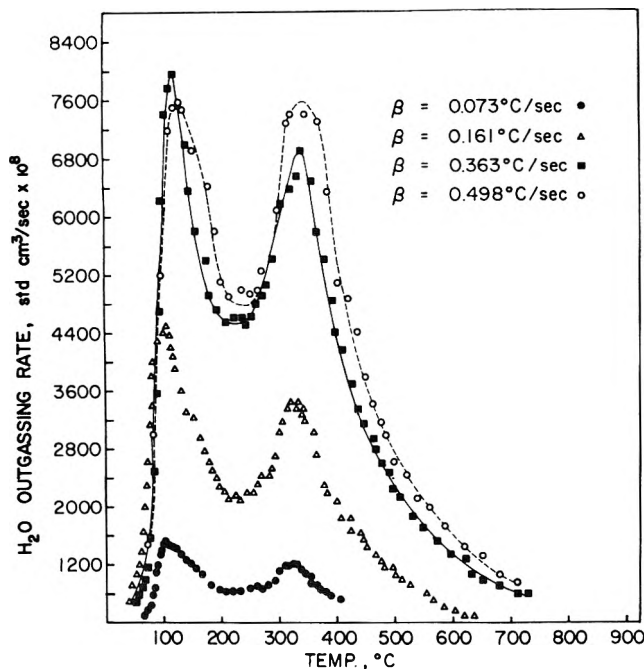


Figure 4. Thermal desorption spectra of water chemisorbed on plutonium dioxide.

during the run, the approximate amount of water adsorbed in each phase can be calculated. Table III shows the approximate amounts of water adsorbed as species I and II and the relative surface coverage for each species. The ratio of the water adsorbed as species I to that adsorbed as species II varied from 1 to 1.3. The fact that the relative surface coverages were greater than 1.0 for each species is attributed to two probable causes: (1) some of the water was being adsorbed in the next molecular layer, and (2) variations in the surface area of the individual samples due to the surface area being measured on the bulk sample.

Another illustration of the two-phase adsorption of water is shown in Figure 5. These spectra were obtained by thermally desorbing water from a sample over the temperature range from 100 to 900° and then cooling the sample to room temperature while still under vacuum. The desorption process was then repeated a second time over the same temperature range. Both adsorbed species appear to be desorbed at a higher temperature than the comparable ones shown in Figure 4. This is the result of a 1- μ particulate filter which was used to contain the radioactive contamination. This filter retarded the flow into the mass spectrometer thus producing T_m values which were abnormally high and decreasing the spectral resolution. Nevertheless, these data still provide qualitative comparisons.

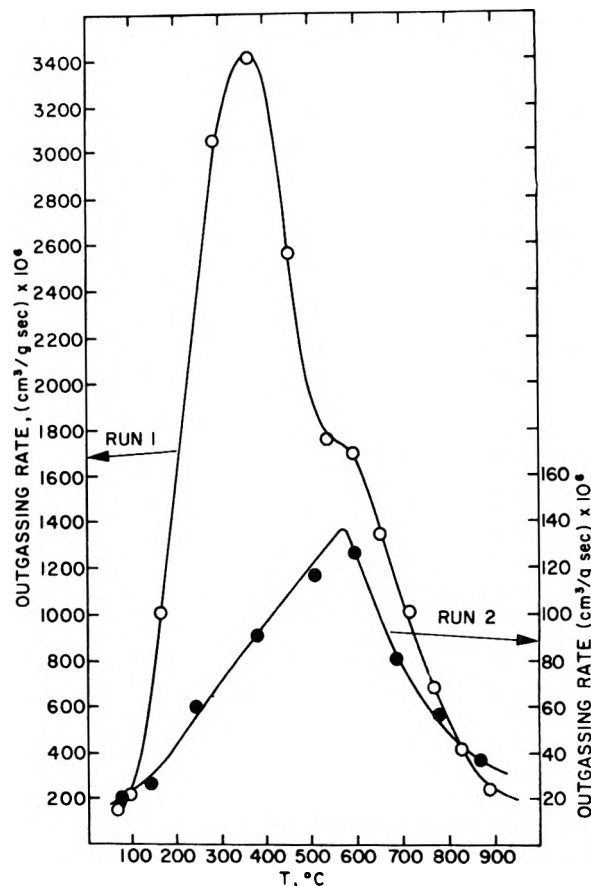


Figure 5. Run 1, thermal desorption spectrum of water chemisorbed on plutonium dioxide. Run 2, thermal desorption spectrum of water re-adsorbed on plutonium dioxide which had been heated under vacuum to 900°.

All of the water adsorbed as species I was removed during the first desorption run. The strongly bound water adsorbed as species II also appeared to be completely removed during the first run. However, when the second run was made, desorption spectrum 2 shown in Figure 5 was obtained indicating some re-adsorption of species II. This is indicative of a very reactive plutonium dioxide surface being formed during the high-temperature evacuation. When the sample was cooled traces of water in the residual gas were re-adsorbed as species II. Such adsorption under vacuum has also been observed in the case of thorium oxide.¹⁵

The activation energy of desorption for each of the two chemisorbed species shown in Figure 4 was calculated

(15) E. L. Fuller, Jr., H. F. Holmes, and C. H. Secoy, *J. Phys. Chem.*, **70**, 1633 (1966).

TABLE III: Surface Coverage of Chemisorbed Species

Run	Total chemisorbed water, mg/g	Species I		Species II	
		Adsorbed water, mg/g	Relative surface coverage	Adsorbed water, mg/g	Relative surface coverage
FD-A	0.72	0.41	1.3	0.31	1.0
FD-B	1.15	0.66	2.1	0.49	1.6
FD-C	0.99	0.53	1.7	0.46	1.5
FD-D	0.72	0.36	1.2	0.36	1.2

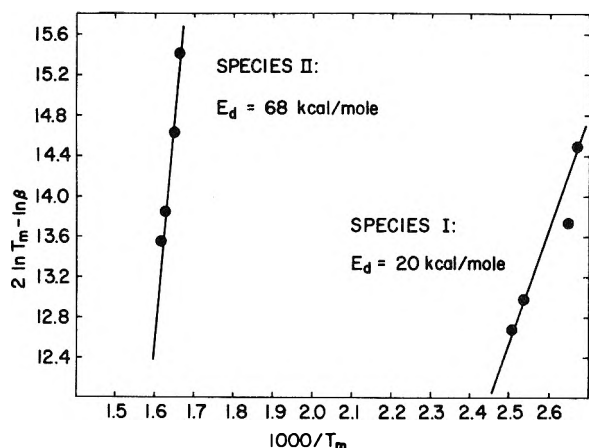


Figure 6. Activation energies for the desorption of chemisorbed water from plutonium dioxide.

using eq 4 for a first-order reaction and eq 3 for a second-order reaction. The best fit of the data was obtained from the first-order equation. A plot of eq 4 for the two species is shown in Figure 6. For the first desorbed species the activation energy of desorption was calculated from a least-squares fit of the data and found to be 20 kcal/mol and the preexponential kinetic factor was equal to $4 \times 10^9 \text{ sec}^{-1}$. This observed value is somewhat less than that calculated from transition state theory. However, it is probably more realistic since it was determined from experimental data. This also tends to suggest that this species is not chemisorbed in the strictest sense of the word.

In the case of the second desorbed species the activation energy of desorption was calculated to be 68 kcal/mol. The preexponential kinetic factor was equal to $4 \times 10^{12} \text{ sec}^{-1}$. Both of these values are typical of a chemisorbed species.

Mechanism of Water Adsorption. Results from the gravimetric and thermal desorption studies have shown water to be desorbed from plutonium dioxide in three different steps. This is interpreted as being indicative of three adsorbed species involving two or three different types of bonds. Adsorption of these species is the result of a combination of physical and chemical adsorption processes. Positive identification of each species has not been made. However, on the basis of this investigation and the conclusions reached by other workers^{7,16,17} the three-step adsorption mechanism shown in Figure 7 can be proposed.

Step I. Chemisorption. The initial step (in terms of desorption this is species II) involves the adsorption and dissociation of the water molecule to form two adsorbed hydroxyl groups. This process occurs very rapidly on a clean plutonium dioxide surface which is typical of nonactivated chemisorption. The heat of adsorption can be assumed

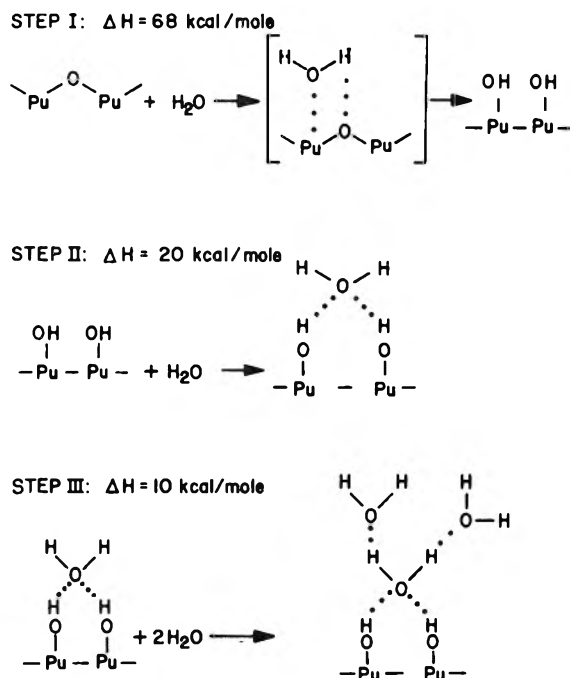


Figure 7. Proposed mechanism for the adsorption of water on plutonium dioxide.

to be equal to the activation energy of desorption for species II. For this hydroxylation step this is 68 kcal/mol. This value is comparable to the 60 kcal/mol observed by Ustinov and Ionov¹⁸ for their β_2 adsorbed phase of water on tungsten.

Step II. Quasi-Chemisorption. The second step in the chemisorption process involves a species which is not too strongly bound. The most likely candidate for this type of adsorption is a water molecule held by a hydrogen bond between the oxygen of the water molecule and the hydrogen atoms of the surface hydroxyl groups. Water adsorbed in this manner may either be singly or doubly hydrogen bonded to underlying surface hydroxyls. If the molecules are doubly bonded, the maximum number which could be adsorbed in this manner would equal the number of molecules actually chemisorbed. Single hydrogen bonds would allow twice as many water molecules to be quasi-chemisorbed.

A rough comparison of the amount of water adsorbed as species I and II indicates that the ratio of chemisorbed water molecules to hydrogen bonded molecules is 1:1 as

- (16) T. Morimoto, M. Nagao, and F. Tokuda, *J. Phys. Chem.*, **73**, 243 (1969).
 (17) H. F. Holmes, E. L. Fuller, Jr., and C. H. Secoy, *J. Phys. Chem.*, **72**, 2095 (1968).
 (18) Yu. K. Ustinov and N. I. Ionov, *Phenomena Ioniz. Gases, Int. Conf., Contrib. Pap.*, 8th, 1967, 2, 6, 4 (1967).

required for double hydrogen bonding. The heat of adsorption for this step can be approximated by the activation energy of desorption of species II of about 20 kcal/mol. This value is the same as that reported by Ustinov and Ionov¹⁸ for their β_1 water species adsorbed on tungsten. It is also similar to the 19 kcal/mol reported by Holmes, et al.,¹⁷ for the heat of adsorption encountered in the hydroxylation of thorium dioxide.

Step III. Physisorption. The final step in the adsorption of water vapor is the actual physisorption of water molecules on a water covered plutonium dioxide surface. Interactions in this step are primarily between water molecules. The heat of adsorption for this step was not determined, however, it should approximate the heat of liquefaction of water.

Summary and Conclusions

Gravimetric and thermal desorption studies have illustrated the complexity of the water adsorption process. Thermal desorption spectra showed water to be chemisorbed as two different species with different binding energies. Hydroxylation of the oxide surface took place with a heat of adsorption of 68 kcal/mol while chemisorption on the hydroxylated surface took place with a heat of adsorption of 20 kcal/mol. A single physisorption process accompanied the two chemisorption processes.

Acknowledgment. The author gratefully acknowledges the assistance of T. L. McFeters and D. I. Hunter in making some of the experimental measurements and processing the data.

Formation of Oxygen-Containing Products in the Radiolysis of Cyclohexane Solutions of Nitrous Oxide

Yoshihiko Hatano,* Ken-ichi Takeuchi, and Satoshi Takao

Laboratory of Physical Chemistry, Tokyo Institute of Technology, Meguro-ku, Tokyo, Japan (Received July 13, 1972)

Oxygen-containing products in the radiolysis of cyclohexane solutions of N_2O have been quantitatively measured and found to be H_2O and $c-C_6H_{11}OH$, denoted by ROH. The yield of ROH, most of which is H_2O , is in good agreement with that of N_2 . This finding shows that the decomposition of N_2O in liquid cyclohexane finally leads to N_2 and ROH with the ratio of one to one. A further study of the correlation of the nitrogen yield with the decrement in the hydrogen yield has been made in order to estimate the nitrogen yield per electron captured by N_2O . Possible processes on the decomposition mechanism of N_2O in the radiolysis of cyclohexane solutions are discussed.

Introduction

Nitrous oxide has received more attention than any other solute among electron scavengers, particularly because of the comparative ease with which the nitrogen formed can be measured. The formation of N_2 from cyclohexane solutions of N_2O has been studied by many groups.¹ The results, however, cannot always be interpreted solely in terms of electron capture. The difficulty in interpreting the results arises from the fact that the observed yield of N_2 is much greater than the expected yield of electron in the radiolysis of liquid cyclohexane and also from the fact that the overall study on the formation of oxygen-containing products after the decomposition of N_2O has not been established yet.

As the oxygen-containing products, thus far, the formations of $c-C_6H_{11}OH^{2-4}$ and H_2O^5 were reported in the cyclohexane- N_2O system.⁶⁻⁸ The yield of $c-C_6H_{11}OH$, which occupied only a few per cent of the expected yield of oxygen-containing products, was measured quantitatively.³ The yield of H_2O , however, has scarcely been known. In the present study, the measurements of H_2O and other oxygen-containing products in the radiolysis of cyclohexane solutions of N_2O have been accurately carried out.^{9,10}

Further, an attempt has been made on the correlation of the nitrogen yield with the decrement of the hydrogen yield upon the addition of N_2O in the radiolysis of liquid cyclohexane. Assuming that electron scavengers depress the hydrogen yield from liquid cyclohexane by an amount approximately equivalent to the yield of scavenged electrons,¹¹ one can estimate the nitrogen yield per electron captured by N_2O .

- (1) J. M. Warman, K.-D. Asmus, and R. H. Schuler, *Advan. Chem. Ser.*, **No. 82**, 52 (1968), and the references cited therein.
- (2) R. Blackburn and A. Charlesby, *Nature (London)*, **210**, 1036 (1966).
- (3) N. H. Sagert and A. S. Blair, *Can. J. Chem.*, **45**, 1351 (1967).
- (4) R. A. Holroyd, *Advan. Chem. Ser.*, **No. 82**, 488 (1968).
- (5) S. Sato, R. Yugeta, K. Shinsaka, and T. Terao, *Bull. Chem. Soc. Jap.*, **39**, 156 (1966).
- (6) In hydrocarbon- N_2O systems other than cyclohexane^{7,8} the formation of H_2O and alcohols was also detected.
- (7) A. Menger and T. Gümman, *Helv. Chim. Acta*, **52**, 2477 (1969).
- (8) R. C. Koch, J. P. Houtman, and W. A. Cramer, *J. Amer. Chem. Soc.*, **90**, 3326 (1968).
- (9) Recently in our laboratory the quantitative analysis of H_2O in the gas-phase radiolysis of N_2O -hydrocarbon mixtures has also been carried out gas chromatographically.¹⁰
- (10) S. Takao, Y. Hatano, and S. Shida, *Bull. Chem. Soc. Jap.*, **44**, 873 (1971).
- (11) K.-D. Asmus, J. M. Warman, and R. H. Schuler, *J. Phys. Chem.*, **74**, 246 (1970).

The results will be useful for the understanding of the decomposition mechanism of N_2O in the radiolysis of cyclohexane solutions.

Experimental Section

Phillips Research grade cyclohexane was used as supplied. Since the G value of hydrogen did not change within experimental errors by the chromatographed treatment of the cyclohexane on silica gel, further purification was not made. Impurities of less than 0.01% in the cyclohexane, about half of which was 2,4-dimethylpentane, were detected by gas chromatography with a flame ionization detector. Cyclohexene and other olefins were not detected. Nitrous oxide supplied by Takachiho-Shoji Co. was thoroughly degassed and stored under vacuum through a -120° cold trap.

The cyclohexane was completely dehydrated before irradiation by using liquid Na-K alloy under vacuum. In the cyclohexane, cyclohexene and other olefins were again absent. The gas chromatogram showed the same impurities as in the case of nondehydrated cyclohexane.

The dehydrated cyclohexane solution of N_2O was sealed *in vacuo* into a small sampling glass tube (about 2.5 ml) with a breakable seal. The concentration of N_2O at room temperature was calculated by using the Ostwald absorption coefficient of 2.62.⁵ Special caution was used in order to avoid the contamination of the samples with H_2O .

The samples, 2 ml of the cyclohexane with various concentrations of N_2O , were irradiated by ^{60}Co γ rays to a total dose of 8.8 – 9.2×10^{19} eV/g at room temperature. In calculating the dose, $G(Fe^{3+}) = 15.6$ was used in Fricke dosimetry.

The products not condensable at the temperature of liquid nitrogen were measured by a gas buret attached to a Toepler pump and a copper oxide furnace kept at 250° . The composition of the noncondensable gases after the removal of H_2 through the furnace was mass spectrometrically confirmed to be nitrogen and a trace of methane. Nitrogen could not be detected in the radiolysis of cyclohexane samples not containing N_2O .

After the measurements of N_2 and H_2 yields and the removal of remaining N_2O using a -120° cold trap, all the mixture condensable at -120° was collected and sealed into the prepared glass tube with a clean liquid Na-K alloy. The total yields of H_2O and alcohols, denoted by ROH, were calculated stoichiometrically on the basis of the hydrogen yield produced by the reaction with Na-K alloy. Great caution was again used for the analysis of ROH containing the main product, H_2O , by the method described elsewhere.¹²

Other products in the solution were analyzed by a gas chromatograph with a flame ionization detector using a 6.0-m dimethylsulfolane column at 30° and a 0.75-m polyethylene glycol 600 column at 100° .

Results and Discussion

Figure 1 shows the yield of oxygen-containing products together with the yields of H_2 and N_2 in the radiolysis of cyclohexane solutions of N_2O . The yield of ROH, the total yield of H_2O and alcohol, is estimated to be twice the yield of H_2 produced by the reaction with Na-K alloy. The reaction has been justified stoichiometrically by the prepared cyclohexane solutions of $c-C_6H_{11}OH$ or H_2O . The yield of H_2O is calculated from the difference between the yield of ROH and that of $c-C_6H_{11}OH$ which is

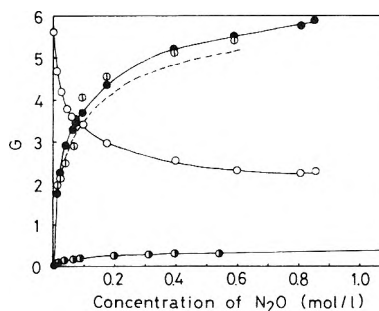


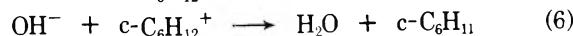
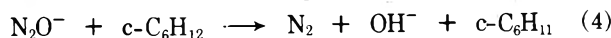
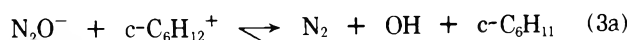
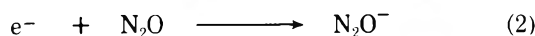
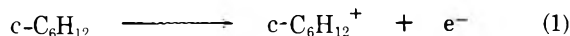
Figure 1. Yields of H_2 (○), N_2 (●), ROH (◼), $c-C_6H_{11}OH$ (◐), and H_2O (---) from the cyclohexane solutions of N_2O . The yield of H_2O is estimated by the difference between the yield of ROH and that of $c-C_6H_{11}OH$.

measured by gas chromatography. H_2O was not detected before and after irradiation in the dehydrated pure cyclohexane. The gas chromatogram did not reveal other oxygen-containing products, such as aldehydes, ketones, etc.

The hydrogen yield for pure cyclohexane is 5.57 ± 0.05 by the average of 5.52, 5.55, and 5.63 at a dose of 8.8×10^{19} eV/g. In a recent paper,¹¹ the observed hydrogen yield of 5.60 was reported at a dose of about 1×10^{19} eV/g and the effect of CO_2 as an impurity in cyclohexane on the hydrogen yield was pointed out. Since cyclohexane in the present experiment has been purified by using Na-K alloy, impurities such as CO_2 , O_2 , and H_2O initially dissolved in the cyclohexane may be eliminated.¹³ The initial yield of hydrogen should be taken 5.77 ± 0.05 by the correction¹¹ for the dose dependence of hydrogen yield. This value is a little larger than that reported earlier, 5.67 ± 0.05 .¹¹

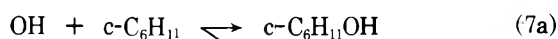
The yield of ROH is surprisingly in good agreement with nitrogen yield at all concentrations from 0.6 to 0.01 mol/l. The yield of $c-C_6H_{11}OH$ at 0.4 mol/l. of N_2O is about 0.3, which is only a few per cent of the total yield of oxygen-containing products. The yield of $c-C_6H_{11}OH$ approximately agrees with that previously reported.³ The yield of H_2O was measured as an oxygen-containing product in the radiolysis of *n*-hexane solution of N_2O ,⁷ in which the method using $LiAlH_4$ was applied. The result, however, involves large experimental errors and the method itself remains a problem of stoichiometrical reactivity.

As described above, the yield of ROH, most of which is H_2O , is in good agreement with that of N_2 . This finding shows that the decomposition of N_2O in liquid cyclohexane finally leads to N_2 and ROH with the ratio of one to one. Possible schemes of ROH formation through ionic processes may be deduced as follows.

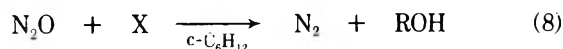


(12) K. Takeuchi, K. Shinsaka, S. Takao, Y. Hatano, and S. Shida, *Bull. Chem. Soc. Jap.*, **44**, 2004 (1971).

(13) K. Ueno, K. Hayashi, and S. Okamura, *J. Polym. Sci., Part B*, **3**, 363 (1965); K. Tsuji, H. Yoshida, and K. Hayashi, *J. Chem. Phys.*, **46**, 810 (1967); K. Funabashi, C. Hebert, and J. L. Magee, *J. Phys. Chem.*, **75**, 3221 (1971).

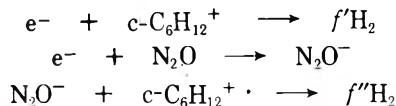


The ion-molecule reaction (4) is not established conclusively, since the electron affinity of N_2O is not yet known accurately. At present, however, this reaction seems to be possible.¹⁴ If both the neutralization (3a) or (3b) and the ion-molecule reaction (4) are possible, it may be rather difficult to decide which process is more important. The above scheme may explain the yields of N_2 and ROH, at least arising from the electron scavenging, but not their yields in excess of the expected yield of electron. The excess yields of N_2 and ROH will be interpreted effectively as



where X might be intermediates other than N_2O^- or an electron which is captured by N_2O as shown in reaction 2. The intermediate X is not determined here, but it must finally lead to the formation of N_2 and ROH with the ratio of one to one.

A following attempt has been made in order to realize the relative importance of reactions 2 and 8. The decrease in the hydrogen yield by the addition of N_2O to cyclohexane has been considered,^{1,11} at least at lower concentrations, as a result of electron capture by N_2O with subsequent interference in the normal ion-electron recombination.



where f' and f'' are the efficiencies of H_2 formation. If hydrogen is formed with unit efficiency ($f' - f'' = 1$),¹¹ $\gamma = G(\text{N}_2)/(G(\text{H}_2)_0 - G(\text{H}_2))$ gives approximately the ratio of nitrogen and electron contributing to the electron scavenging of N_2O . $G(\text{N}_2)$ is obtained by the correction for the direct radiolysis of N_2O using $G(\text{N}_2) = 12.9$,¹⁵ although its adequacy has not yet been certified. $G(\text{H}_2)_0$ is estimated to be 5.73 ± 0.05 by the correction¹¹ for the ionic part of dose effect on the hydrogen yield from pure cyclohexane at a dose of 8.8×10^{19} eV/g, and $G(\text{H}_2)$ is the observed hydrogen yield at this dose from the cyclohexane containing N_2O .

The ratio γ in Figure 3 can be estimated by using the experimental results in Figure 2 where the yields of N_2 and H_2 are shown as a function of $N_S(\text{N}_2\text{O})$, the mole fraction of N_2O . The ratio γ is larger than unity, which indicates, as is now generally recognized at least at the higher N_2O concentrations, more than one N_2 is formed per electron captured. The ratio γ seems to be approximately constant, 1.6, at all N_2O concentrations, although it is not so clear at $N_S(\text{N}_2\text{O}) < 10^{-3}$. Even in the lower concentration region it appears to be evident that γ is larger than unity, which seems to be different from the previous suggestion.^{1,11} Because of the following reason, however, this conclusion in the lower concentration region might be unwarranted. The value of $G(\text{H}_2)_0$ may be reduced by the unknown impurities in the cyclohexane if they had high reactivities for electrons or other precursors for hydrogen formation *via* neutralization. Assuming the ratio γ at the lower N_2O concentrations to be unity, one can estimate the value of $G(\text{H}_2)_0$ to be more than about 5.9.

Various species will be considered as possible sources of

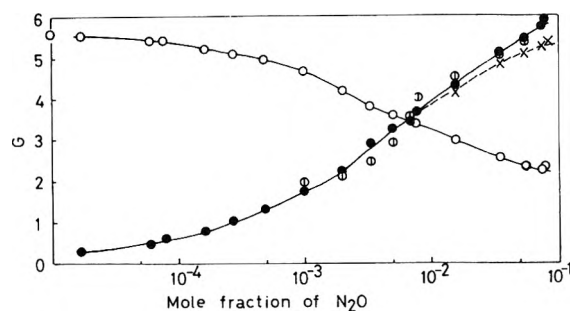


Figure 2. Yields of H_2O (\circ), N_2 (\bullet), and ROH (\times) as a function of N_2O mole fraction. The corrected yield of N_2 for the direct radiolysis of N_2O is also shown, taking $G(\text{N}_2)_0 = 12.9$ ¹⁵ for pure N_2O .

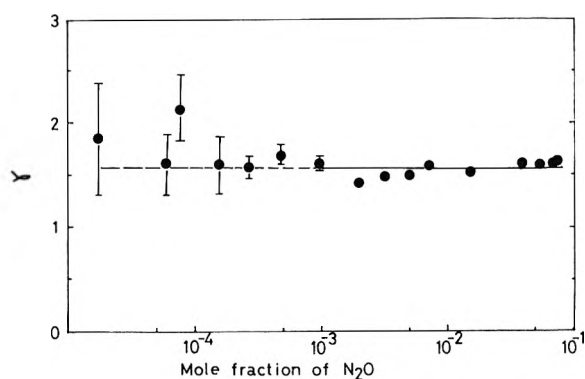
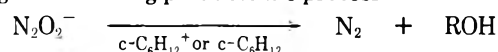


Figure 3. The γ values, $\gamma = G(\text{N}_2)/(G(\text{H}_2)_0 - G(\text{H}_2))$, as a function of N_2O mole fraction.

the excess nitrogen in the radiolysis of cyclohexane solutions of N_2O , that is, the intermediates X in reaction 8. Nitrous oxide has been generally recognized to be inert with respect to reactions with thermal hydrogen or alkyl radicals.¹ The reaction with OH radical to produce N_2 may also be excluded, because this reaction seems to be very slow compared with reaction 5.¹⁶ Excited cyclohexane may not be directly responsible for the formation of the excess nitrogen at least at lower concentrations of N_2O .

Secondary reactions with N_2O of negative ion formed on electron capture by N_2O have frequently been proposed to explain the excess nitrogen at higher N_2O concentrations.¹ The secondary reaction of negative ion, however, could not easily explain the experimental results in the present study on the oxygen-containing products. The reaction of N_2O^- with N_2O would be expected to produce N_2O_2^- ,¹ which is the precursor of the excess nitrogen at higher concentrations of N_2O . To explain the experimental result of oxygen-containing products the process



must be provided, and N_2O_2^- must exclusively give ROH as the oxygen-containing products. It seems rather difficult to expect such a process. In the case of the secondary reaction of O^- , it also seems difficult to expect that the reaction of O_2^- with $\text{c-C}_6\text{H}_{12}^+$ or $\text{c-C}_6\text{H}_{12}$ exclusively

(14) S. Takao, Y. Hatano, and S. Shida, *J. Phys. Chem.*, **75**, 3178 (1971).

(15) M. G. Robinson and G. R. Freeman, *J. Phys. Chem.*, **72**, 1394 (1968).

(16) N. R. Greiner, *J. Chem. Phys.*, **53**, 1070 (1970); R. Simonaitis, J. Hecklen, M. M. Maguire, and R. A. Bernheim, *J. Phys. Chem.*, **75**, 3205 (1971).

gives ROH as oxygen-containing products. Ketones or other oxygen-containing products might be produced in such a process. Especially at lower concentrations it also seems difficult to assume that N_2O^- or O^- reacts predominantly with N_2O itself. The rate of the reaction between O^- and $n-C_4H_{10}$ in the gas-phase is $1.2 \times 10^{-9} \text{ cm}^3 \text{ molecule}^{-1} \text{ sec}^{-1}$.¹⁷ If we take this value for the rate of reaction 4 and assume the excess nitrogen at lower concentrations of N_2O to be due to the secondary reaction of N_2O^- with N_2O , the rate of this secondary reaction should be at least about 10^4 times as large as that of reaction 4. Thus the possibility of the excess nitrogen forma-

tion *via* secondary reactions of negative ions with N_2O may be excluded at least at lower concentration of N_2O .

Other possibilities for the formation of the excess nitrogen, such as the role of positive ions, electrons which cannot be captured by N_2O , etc., should also be examined in detail.

Acknowledgment. The authors wish to thank Professor S. Shida and Dr. S. Sato for valuable suggestions.

(17) D. K. Bohme and F. C. Fehsenfeld, *Can. J. Chem.*, **47**, 2717 (1969).

Radiation-Induced Homolytic Aromatic Substitution. I. Hydroxylation of Nitrobenzene, Chlorobenzene, and Toluene^{1a}

Manfred K. Eberhardt* and Massayoshi Yoshida

Puerto Rico Nuclear Center,^{1b} Caparra Heights Station, San Juan, Puerto Rico 00924 (Received May 15, 1972)

Publication costs assisted by the University of Puerto Rico

The radiolysis of aqueous solutions of nitrobenzene, chlorobenzene, and toluene was investigated. The effect of O_2 and N_2O on the isomer distribution was studied. In presence of O_2 a substantial increase in the yield of phenols was observed as expected for a homolytic substitution. Our results indicate a selectivity in the disproportionation step. Evidence is presented for the formation of *p*-nitrophenol by a mechanism involving the nitrobenzene anion radical. A change in isomer distribution of nitrophenols in presence of N_2O as compared to deaerated or oxygenated solutions indicates the involvement of a more nucleophilic species like O^- or N_2O^- in the hydroxylation reaction. In the case of chlorobenzene phenol was formed in addition to the chlorophenols. In deaerated toluene solutions N_2O produced a three- to fourfold increase in the total yield of substituted phenols, but no change in isomer distribution was observed. On the other hand, O_2 produced a significant change in isomer distribution particularly in the case of toluene. The ratio of $G(\text{bibenzyl}):G(\text{total cresols})$ was found to increase in going from an argon-saturated to N_2O -saturated solution of toluene. This indicates the involvement of a nucleophilic species like O^- or N_2O^- . Evidence for a direct displacement of chlorine by OH radical is presented. The experimental results are interpreted on the basis of SCF-MO (CNDO-2 and INDO) calculations.

A large amount of work on radiation-induced hydroxylation of aromatic compounds has appeared in the literature.² Several workers have recently investigated the hydroxylation of nitrobenzene,³ but no quantitative work on the hydroxylation of chlorobenzene and toluene has been carried out.

We have started a program on radiation-induced hydroxylation of a series of aromatic compounds, and we are trying to interpret our results on the basis of SCF-MO theory.

Experimental Section

Materials. All solutions were prepared using triply distilled water as solvent. Nitrobenzene, chlorobenzene, and toluene analytical reagent grade were redistilled prior to use. Argon, nitrogen, oxygen, and nitrous oxide saturated solutions were prepared by bubbling the gas through 1 l. of triply distilled water for about 1 hr. The gas was introduced by means of a hypodermic needle inserted through

a silicone stopper. The saturation was enhanced by frequent shaking. After saturation the aromatic solute was introduced with a Hamilton syringe and dissolved by vigorous shaking.

Irradiations. Irradiations were carried out with a ⁶⁰Co room source. The dose rate was determined by Fricke dosimetry using a value of 15.6 for $G(\text{Fe}^{3+})$. The dose rate was 0.875×10^3 rads/min unless otherwise indicated in the tables. Samples (1 l.) were usually irradiated for 30 min or a maximum of 1 hr. All irradiations were carried out in unbuffered solutions and a solute concentration of

- (1) (a) Presented at the Metrochem Meeting, April 30–May 3, 1971, San Juan, Puerto Rico. This work was part of a Ph.D. Thesis presented by M. Yoshida, at the University of Sao Paulo, Brazil, 1971. (b) The Puerto Rico Nuclear Center is operated by the University of Puerto Rico for the U. S. Atomic Energy Commission under Contract No. AT-(40-1)-1833.
- (2) E. J. Fendler and J. H. Fendler, *Progr. Phys. Org. Chem.*, **8**, (1970).
- (3) (a) R. W. Matthews and D. F. Sangster, *J. Phys. Chem.*, **71**, 4056 (1967); (b) J. H. Fendler and G. L. Gasowski, *J. Org. Chem.*, **33**, 1965 (1968).

TABLE I: Yields of Nitrophenols in $4.9 \times 10^{-3} M$ Unbuffered Aqueous Nitrobenzene

Conditions ^a	G (total O ₂ NC ₆ H ₄ OH)	G (ortho)	G (meta)	G (para)
Ar sat., 1 hr	0.65	0.16 (25.3%)	0.12 (18.9%)	0.37 (56.7%)
N ₂ sat., 1 hr	0.77	0.18 (23.4%)	0.14 (18.8%)	0.45 (57.8%)
O ₂ sat., ^b 30 min	1.52	0.70 (46.0%)	0.36 (23.6%)	0.46 (30.4%)
O ₂ sat., 30 min ^c	1.33	0.59 (44.4%)	0.36 (27.4%)	0.38 (28.2%)
O ₂ sat., 1 hr	1.69	0.82 (48.5%)	0.38 (22.6%)	0.49 (28.9%)
N ₂ O sat., ^d 30 min ^e	1.49	0.70 (46.8%)	0.22 (14.5%)	0.58 (38.6%)
N ₂ O sat., ^d 1 hr ^e	1.56	0.69 (44.3%)	0.28 (18.1%)	0.59 (37.6%)
N ₂ O sat., ^d 30 min ^f	1.36	0.64 (46.7%)	0.15 (11.3%)	0.57 (42.0%)
N ₂ O sat., ^d 30 min ^g	1.17	0.50 (42.5%)	0.13 (12.5%)	0.53 (45.0%)

^a Dose rate 0.875×10^3 rads/min. ^b $1 \times 10^{-3} M$. ^c Solution extracted after 1 day. ^d $2.0 \times 10^{-2} M$. ^e Extracted immediately after irradiation. ^f Irradiated solution left 1 day with NaOH. ^g Extracted 1 day after irradiation.

$4.9 \times 10^{-3} M$ for nitrobenzene and chlorobenzene and $4.7 \times 10^{-3} M$ for toluene.

Analysis of Irradiated Nitrobenzene Solutions. The irradiated solutions were separated in two portions of 500 ml each. Each part was made alkaline by addition of NaOH, and then the solution was extracted with 100 ml of ether and two times with 50 ml of ether. The aqueous solution was then acidified with H₂SO₄ and extracted five times with 50 ml of ether. The ether extracts were then dried over Na₂SO₄ and subsequently concentrated to about 30 ml. Then 30 ml of ethereal diazomethane solutions (prepared from Diazald, Aldrich Chemical Co.) was added and the reaction mixture was allowed to stand for about 48 hr. The solution was then concentrated to 10 ml and analyzed by vapor-phase chromatography using a hydrogen flame detector. The column was a 6 ft by $\frac{1}{8}$ in. stainless steel column packed with diethylene glycol succinate (10%) on Chromosorb W-AW DMCS 100-120 mesh (Varian Aerograph). The temperature was 175° and the flow rate was 35 ml of N₂/min. Under these conditions good separation of the isomers was obtained. The sequence of elution was meta, ortho, and para. The analytical technique was checked several times with standard aqueous solutions of nitrophenols and was found to give quantitative recovery of the nitrophenols.

Analysis of Irradiated Chlorobenzene and Toluene Solutions. The irradiated solutions were separated into two 500-ml portions. Each portion was extracted once with 100 ml of ether and four times with 50 ml of ether. The ether extracts were dried over Na₂SO₄ and concentrated to 10 ml. The analysis was carried out by vapor-phase chromatography using a hydrogen flame detector. The column was a 6-ft by $\frac{1}{8}$ in. stainless steel column packed with diethylene glycol succinate (10%) on Chromosorb W-AW DMCS 100-120 mesh (Varian Aerograph). The temperature was 160° and the flow-rate was 22 ml of N₂/min. Under these conditions the meta and para isomers could not be separated. In order to separate the *m*- and *p*-chlorophenol the ether extract was allowed to react with an ethereal diazomethane solution (prepared from Diazald, Aldrich Chemical Co.). The diazotized solution was concentrated and analyzed by vapor-phase chromatography using a 150-ft capillary column (0.01-in. diameter) coated with Silicone SF-96 (Perkin-Elmer Corp.). The temperature was 90° and the splitting was such that only 3% of the injected 1- μ l sample passed through the detector. The detector was a hydrogen flame detector and the carrier gas was nitrogen. The *m*- and *p*-cresol could not be separated by this capillary column, nor could the methoxy derivatives. The ratio *m*-cresol:*p*-cresol was determined by the

isotope dilution technique. ¹⁴C-labeled toluene (0.5 mCi) was diluted with 50 μ l of unlabeled toluene and dissolved in 100 ml of deaerated or oxygenated water and irradiated for 1 hr at 2×10^3 rads/min. After irradiation the solution was separated into two parts of 50 ml each. To one portion 3 g of *m*-cresol and to the other portion 3 g of *p*-cresol was added. The solutions were made alkaline with NaOH and extracted four times with 25 ml of ether. Then the aqueous phase was acidified with H₂SO₄ and extracted eight times with 25 ml of ether. The ether extract was dried over Na₂SO₄ and concentrated. Then 3.75 ml of phenylisocyanate, 0.75 ml of pyridine, and 22.5 ml of petroleum ether (37.5-46.8°) were added. The phenylurethane precipitates and was recrystallized eight times from CCl₄, after which the activity of the sample remained constant. The ratio meta:para in argon saturated solution was found to be 62% meta and 38% para. In the oxygenated solution the ratio was 66.6% meta and 33.4% para.

Results

The main products which we measured were the isomeric phenols. The samples were irradiated with a total dose of 26.2×10^3 rads (30 min) or a maximum of 52.4×10^3 rads (1 hr). This dose is low enough to render secondary reactions insignificant. The *G* values of the nitrophenols in the absence and presence of oxygen and in N₂O-saturated solutions are summarized in Table I. All our experiments were carried out in duplicate and triplicate and were found to be reproducible within the limits of the analytical method ($\pm 5\%$). The results at the lower dose are somewhat less accurate. In the experiments with argon-saturated solutions of nitrobenzene a careful search was made for phenol, but none was found. This is in agreement with the results of Fendler and Gasowski^{3b} who found phenol only at very high doses of 10^6 rads. In general our results are in fair agreement with those of Matthews and Sangster^{3a} although we find considerably higher *G* value for *p*-nitrophenol in the absence of air in agreement with the results of Fendler and Gasowski.^{3b} Our *G*(*o*-nitrophenol) is in all cases higher than those reported by Fendler and Gasowski. This is probably due to our lower dose rate, which was found^{3a} to increase the amount of ortho isomer. The general trends are however in good agreement with previous results.

The *G* values for chlorophenols and phenol are shown in Table II. All our results are the average of at least two and many times three or four determinations. The results were found to be reproducible within an accuracy of $\pm 5\%$.

TABLE II: Radiation-Induced Hydroxylation of Chlorobenzene^a

Conditions	G(C ₆ H ₅ OH)	G(total ClC ₆ H ₄ OH)	G(ortho)	G(meta)	G(para)
Ar sat., 30 min	0.107	0.23	0.10 (44.6%)	0.05 (23.1%)	0.07 (32.3%)
Ar sat., 1 hr	0.083	0.18	0.08	0.04	0.06
N ₂ O sat., 30 min ^b	0.050	0.88	0.40 (45.4%)	0.18 (20.3%)	0.30 (34.2%)
N ₂ O sat., 1 hr ^b	0.039	0.69	0.31	0.14	0.24
O ₂ sat., 30 min ^c	0.050	0.86	0.32 (37.1%)	0.19 (21.8%)	0.35 (41.1%)
O ₂ sat., 1 hr ^c	0.044	0.80	0.30	0.17	0.33
H ₂ O ₂ , 30 min ^d	0.070	0.84	0.36 (42.9%)	0.16 (19.3%)	0.32 (37.8%)

^a Dose rate 0.875×10^3 rads/min. ^b 2.0×10^{-2} M. ^c 1.0×10^{-3} M. ^d 1.4×10^{-2} M.

TABLE III: Radiation-Induced Hydroxylation of Toluene^a

Conditions	G(ortho)	G(meta)	G(para)	G(H ₅ C ₆ CH ₂ CH ₂ C ₆ H ₅)	G(H ₅ C ₆ CH ₂ OH)	G(H ₅ C ₆ CH ₂ CH ₂ C ₆ H ₅)/ G (total phenols)
Ar sat., 30 min	0.24 (73%)	0.059 (18%)	0.030 (9%)	0.115		0.35
Ar sat., 1 hr	0.26 (72%)	0.066 (18.5%)	0.034 (9.5%)	0.15	0.08	0.42
N ₂ O sat., 30 min	0.68 (74%)	0.24 (26%)		0.50		0.54
N ₂ O sat., 1 hr	0.74 (75%)	0.24 (25%)		0.55	0.065	0.56
O ₂ sat., 30 min	0.21 (37%)	0.24 (42%)	0.12 (21%)	None		
O ₂ sat., 1 hr	0.22 (35.5%)	0.27 (43%)	0.13 (21.5%)	None		

^a Dose rate 0.875×10^3 rads/min g.

The results for toluene are summarized in Table III. In addition to cresols, bibenzyl and benzyl alcohol were formed in deaerated solution. In the oxygenated solution benzaldehyde was detected. In the deaerated toluene solution some probably dimeric product was formed. This peak however was absent in the oxygenated solution. We have checked the retention times of 4,4'-ditolyl- and *p*-benzyltoluene, but we found that these compounds, although very close, were different from the unknown peak. We had hoped that the detection of these compounds would imply the presence of *p*-tolyl radicals which could react with O₂ to give *p*-cresol and explain the increase of *p*-cresol in the oxygenated solution.

Most of the SCF-MO calculations were carried out using the complete neglect of differential overlap (CNDO-2) approximation.⁴ This type of calculation includes all valence orbitals (π and σ) in a self-consistent field approach. The HOMO (highest occupied molecular orbital) and LUMO (lowest unoccupied molecular orbital) coefficients of nitrobenzene, chlorobenzene, and toluene are shown in Figure 1. The HOMO and LUMO of these aromatic compounds are pure π -molecular orbitals. Their HOMO and LUMO energy levels and SOMO (singly occupied molecular orbital) of some attacking species (OH, O⁻, and N₂O⁻) are schematically represented in Figure 2. Figure 3 shows the spin densities in the nitrobenzene radical anion. In addition we have calculated the different hydroxycyclohexadienyl radicals, whose total energies and energy levels of the SOMO's are shown in Tables IV-VI. For the calculation of nitrobenzene and the *o*-, *m*-, and *p*-hydroxynitrocyclohexadienyl radicals the NO₂ group was assumed to be in the plane of the aromatic ring. Owing to the difference in bond length between N → O and N=O, the molecular orbitals are slightly asymmetric. The following bond distances were used: C-C, 1.40 Å; C-H, 1.085 Å; C-N, 1.46 Å; N=O, 1.10 Å; N → O, 1.18 Å;

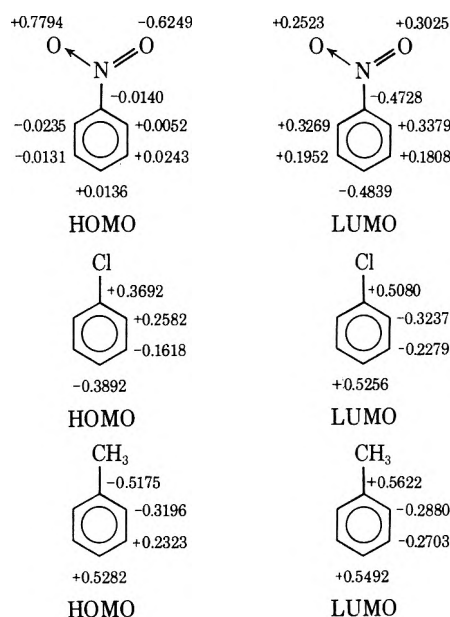


Figure 1. HOMO and LUMO coefficients.

C_{ali}-H, 1.09 Å; C_{ar}-CH₃, 1.52 Å; C_{ar}-Cl, 1.70 Å. Dihedral angles were 120° and tetrahedral angles 109°. In the calculation of the hydroxycyclohexadienyl radicals the aromatic skeleton was left undisturbed and the attacking OH radical was assumed to form a tetrahedral angle with the C-H bond: bond distance C-O, 1.42 Å; O-H, 0.97 Å; C-O-H angle, 109°.

The complete neglect of differential overlap (CNDO) approximation does not make adequate allowances for the different interactions between two electrons with parallel or antiparallel spins. This difference is to some extent

TABLE IV: CNDO-2 Calculations on Hydroxynitrocyclohexadienyl Radicals^{a,b}

	1,1	1,2	1,3	1,4	1,5	1,6
<i>E</i> (total),	-113.9726	-113.9934	-113.9890	-113.9926	-113.9891	-113.9937
au	(-109.4238)	(-109.4466)	(-109.4419)	(-109.4448)	(-109.4419)	(-109.4463)
ΔE ,						
kcal	12.9	2.8	2.2	2.2	2.9	
	(14.1)	(2.9)	(1.8)	(1.8)	(2.7)	
<i>E</i> (SOMO),	-0.3667	-0.3686	-0.3618	-0.3679	-0.3616	-0.3673
au	(-0.3626)	(-0.3660)	(-0.3603)	(-0.3668)	(-0.3606)	(-0.3669)

^a Results of INDO calculations are given in parentheses. ^b The numbers in the column headings indicate the position of the hydroxy and nitro group, respectively.

taken into consideration in the intermediate neglect of differential overlap (INDO) approximation,⁴ which includes one-center exchange integrals. The INDO method therefore gives better results for open-shell systems. We have used the INDO approximation for the calculation of the hydroxynitrocyclohexadienyl radicals, the hydroxy-methylcyclohexadienyl radicals, and the nitrobenzene radical anion. The results are given in parentheses in Tables IV and VI and Figure 3, respectively. All our calculations on open-shell systems were carried out in the spin-unrestricted formalism.⁴ For the calculation of the spin densities of the nitrobenzene radical anion no spin projection was carried out. Comparing the results of INDO and CNDO-2 calculations we can see that the SOMO energy levels change very little, and the relative stability of the radicals is the same in both approximations. Therefore our conclusions do not change through the use of the less-approximate INDO calculations. We have also carried out INDO calculations assuming an equal bond length (1.2 Å) for the two N-O bonds of the nitro group without observing any significant difference.

	C ₆ H ₅ NO ₂	C ₆ H ₅ Cl	C ₆ H ₅ CH ₃	·OH	·O ⁻	N ₂ O ⁻
LUMO	-0.0719	-0.1024	-0.1404	↑0.0784	↑0.1092	
				(SOMO)	(SOMO)	
HOMO	↑↓-0.4741	↑↓-0.4677	↑↓-0.4730			
				↑-0.6943		
				(SOMO)		

Figure 2. HOMO-LUMO and SOMO energy levels.

Discussion

In the radiolysis of liquid water the important intermediate species are H·, ·OH and e_{aq}⁻. All of these species can react with an aromatic compound present at a low concentration. For the convenience of the reader, the rate constants for the reaction of these species with nitrobenzene, chlorobenzene, toluene, and some additives used in our work are summarized in Table VII. The most reliable and recent determinations of the *G* values of these species at pH 7 gave the following results:⁵ *G*(·OH) = 2.74 ± 0.08; *G*(e_{aq}⁻) = 2.71 ± 0.05; *G*(H·) = 0.6.

A considerable amount of work on the mechanism of radiation-induced aromatic hydroxylation has been carried out on benzene,² and the correct mechanism was finally established through the work of Dorfman, Taub, and Bühler.⁶ These authors detected the hydroxycyclohexadienyl radical as an intermediate in the pulse radiolysis of an

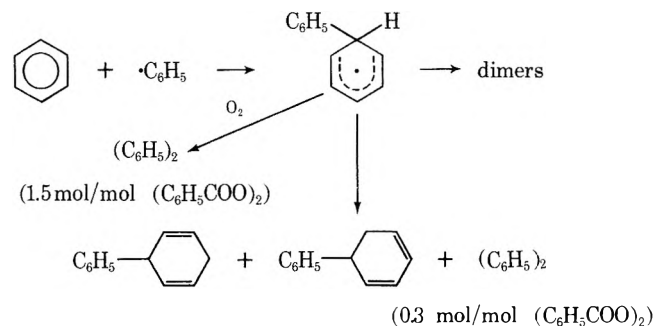
TABLE V: CNDO-2 Calculations on Hydroxychlorocyclohexadienyl Radicals^a

	1,1	1,2	1,3	1,4
<i>E</i> (total),	-81.6989	-81.6829	-81.6781	-81.6823
au				
ΔE ,				
kcal	10.0	3.0	2.6	
<i>E</i> (SOMO),	-0.3427	-0.3423	-0.3470	-0.3411
au				

^a The numbers in the column headings indicate the position of the chloro and hydroxy group, respectively.

aqueous benzene solution. Through studies on homolytic aromatic phenylation by thermal decomposition of benzoyl peroxide, the mechanism of homolytic substitution is well established,⁷ and is summarized in Scheme I.

Scheme I



This reaction sequence explains the low yields of bi-phenyl in the absence of oxygen. The same low yield of product is also observed in radiation-induced hydroxylations (*G* values of 0.07-0.65). The maximum *G* value for total phenol formation would be ca. 2.7 if all hydroxyl radicals are converted to phenol. Oxygen increases the yields considerably. Since oxygen is known to scavenge e_{aq}⁻ and H atoms the increase might be due to substitution by O₂⁻ or HO₂ radicals, which would eventually lead to phenols. The discovery of the oxygen effect⁸ in the ben-

- (4) For a detailed description of this method see J. A. Pople and D. L. Beveridge, "Approximate Molecular Orbital Methods," McGraw-Hill, New York, N. Y., 1970. The computer program was obtained from the Quantum Chemistry Program Exchange, Bloomington, Ind.
- (5) B. H. J. Bielski and A. O. Allen, *Int. J. Radiat. Phys. Chem.*, **1**(2), 153 (1969). For a review see G. V. Buxton, *Radiat. Res. Rev.*, **1**, 209 (1968).
- (6) L. M. Dorfman, I. A. Taub, and R. E. Bühler, *J. Chem. Phys.*, **36**, 3051 (1962).
- (7) D. H. Hey, *Advan. Free-Radical Chem.*, **2**, 59 (1967).
- (8) M. K. Eberhardt and E. L. Eliel, *J. Org. Chem.*, **27**, 2289 (1962).

TABLE VI: CNDO-2 Calculations on Hydroxymethylcyclohexadienyl Radicals^{a,b}

	1,1	1,2	1,3	1,4
$E(\text{total})$, au	-74.9332 (-72.3041)	-74.9518 (-72.3216)	-74.9477 (-72.3175)	-74.9509 (-72.3205)
ΔE , kcal	10.8 (10.8)	2.5 (2.5)	2.0 (1.9)	
$E(\text{SOMO})$, au	-0.3155 (-0.3134)	-0.3197 (-0.3201)	-0.3320 (-0.3310)	-0.3168 (-0.3169)

^a See footnote a, Table IV. ^b The numbers in the column headings indicate the position of the methyl and hydroxy group, respectively.

zoyl peroxide induced thermal phenylation of benzene, however, demonstrates that O_2 can oxidize intermediate cyclohexadienyl radicals. Evidence for a peroxy radical intermediate in the oxidation of cyclohexadienyl radicals has been presented by Howard and Ingold in the chain oxidation of 1,4-dihydronaphthalene.⁹ Additional evidence against a substitution by $HO_2\cdot$ or O_2^- radicals has been presented by Matthews and Sangster^{3a} in the hydroxylation of nitrobenzene.

Several theoretical approaches to the problem of aromatic substitution have appeared in the literature.¹⁰ One of the most successful ones has been the "frontier electron theory" developed by Fukui and coworkers.^{10,11} The frontier electron theory states that in electrophilic aromatic substitution the point of attack should be at the position of greatest electron density in the highest occupied molecular orbital (HOMO), and in nucleophilic substitution attack is expected where the lowest unoccupied molecular orbital (LUMO) has the maximum electron density. For homolytic attack the overlap between the SOMO of the radical and both the HOMO and LUMO of the substrate has to be considered. In cases of highly electrophilic radicals the interaction between the SOMO and HOMO predominates. An extension of Fukui's frontier electron theory was developed by Klopman and Hudson.¹² This theory however leads to the same conclusions as outlined above, especially for radical reactions. Another theory which has been quite successful is the "localization approach" originally proposed by Wheland.¹³ According to this theory the position of attack is determined by the energy of the intermediate localized σ complex, often referred to as Wheland intermediate. The results of CNDO-2 and INDO calculations of these intermediates are summarized in Tables IV-VI. In the case of nitrobenzene the frontier orbital theory and the localization approach do not give the same predictions. However, we have to realize that although the frontier orbital theory correctly predicts the position of initial interaction this may not be reflected in the isomer distribution of the final stable products.

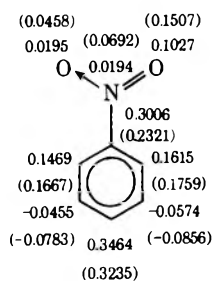


Figure 3. Total spin densities of nitrobenzene radical anion (CNDO-2). Numbers in parentheses are results of INDO calculation.

TABLE VII: Rate Constants for Reaction of e_{aq}^- and $\cdot OH$ with Solutes ($M^{-1} \text{ sec}^{-1}$)

Solute (pH 7.0)	e_{aq}^-	Ref	$\cdot OH$	Ref
$C_6H_5NO_2$	3.0×10^{10}	a	2.0×10^9	c
			3.2×10^9	d
			4.7×10^9	e
C_6H_5Cl	5.0×10^8	a	4.2×10^9	a
$C_6H_5CH_3$	1.2×10^7	a	3.0×10^9	a
O_2	2.0×10^{10}	b		
N_2O	8.7×10^9	a		
H_2O_2	1.3×10^{10}	a, b	4.5×10^7	a, b

^a M. Anbar and P. Neta, *Int. J. Appl. Radiat. Isotopes*, **16**, 227 (1965).
^b J. H. Baxendale, "Pulse Radiolysis," Academic Press, London, 1965, p 15. ^c M. Anbar, D. Meyerstein, and P. Neta, *J. Phys. Chem.*, **70**, 2660 (1966). ^d Reference 16. ^e Reference 17.

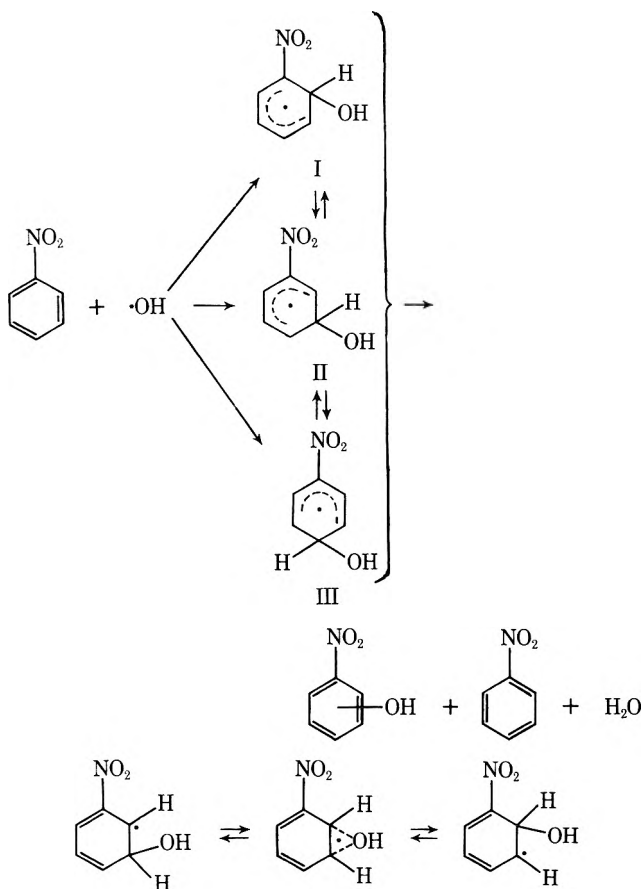
In our example of homolytic hydroxylation of nitrobenzene, chlorobenzene, and toluene, the interaction of the singly occupied MO of the OH radical with the HOMO of the aromatic predominates, since the OH radical has a very low-lying SOMO, i.e., it is highly electrophilic (see Figure 2). The transfer of an electron from the OH radical to the LUMO of the aromatic would require a high activation energy. If the attacking species, however, is the O^- or N_2O^- radical the interaction between the SOMO of these radicals and the LUMO of the aromatic becomes predominant due to the high-lying SOMO energy level of these species (Figure 2). A change in substitution pattern is to be expected, if the HOMO and LUMO of the aromatic have different coefficients. The HOMO and LUMO coefficients are shown in Figure 1. The HOMO coefficients of nitrobenzene at the ring positions are all very small in agreement with the resistance of nitrobenzene toward electrophilic substitution. The HOMO coefficients indicate a slight preference for meta substitution, whereas the LUMO coefficients are considerably greater and indicate a preference for ortho-para substitution. On the other hand, the HOMO and LUMO coefficients of chlorobenzene and toluene are of equal magnitude and show a preference for ortho-para substitution. An interesting observation are

- (9) J. A. Howard and K. U. Ingold, *Can. J. Chem.*, **45**, 785 (1967).
 (10) For a review of the older literature see A. Streitwieser, Jr., "Molecular Orbital Theory for Organic Chemists," Wiley, New York, N. Y., 1961, p 307 ff. For a more recent review see F. Fukui, *Top. Current Chem.*, **15**, 1 (1970).
 (11) K. Fukui, T. Yonezawa, and H. Shingu, *J. Chem. Phys.*, **20**, 722 (1952); K. Fukui, T. Yonezawa, C. Nagata, and H. Shingu, *ibid.*, **22**, 1433 (1954); F. Fukui, T. Yonezawa, and C. Nagata, *Bull. Chem. Soc. Jap.*, **27**, 423 (1954); *J. Chem. Phys.*, **27**, 1247 (1957).
 (12) G. Klopman and R. F. Hudson, *Theor. Chim. Acta*, **8**, 165 (1967); G. Klopman, *J. Amer. Chem. Soc.*, **90**, 223 (1968).
 (13) G. W. Wheland, *J. Amer. Chem. Soc.*, **64**, 900 (1942).

the high HOMO coefficients at the oxygen atoms of nitrobenzene. This would lead one to postulate attack at the oxygen atoms, followed by a rearrangement to the ring-substituted hydroxynitrocyclohexadienyl radical. This type of mechanism has been proposed in homolytic phenylation in order to explain the high percentage of ortho substitution.¹⁴ More recently attack by α -alkoxy radicals at the nitro group has been observed by means of esr spectroscopy.¹⁵ On the other hand, pulse radiolysis studies on aqueous nitrobenzene solution have clearly shown attack at the nucleus. This discrepancy between theory and experiment may be due to a solvation shell surrounding the nitro group in aqueous solution.

The hydroxylation of nitrobenzene has been studied by several workers using the technique^{16,17} of pulse radiolysis. From this work it follows that OH radicals attack nitrobenzene at the ring positions and not at the nitro group (Scheme II). The frontier orbital theory predicts the posi-

Scheme II



tion of initial interaction, but we can not be sure that these predictions will be reflected in the final product distribution. One possibility is that the primarily formed hydroxynitrocyclohexadienyl radicals rearrange to form the more stable Wheland intermediate (I, II, and III). Many 1,2 radical rearrangements are described in the literature.¹⁸ An important factor causing 1,2 shifts is the tendency of a less stable radical to rearrange forming a radical of greater stability. Under given conditions the mean lifetime of the radical markedly affects the rearrangement. Volkert and Schulte-Frohlinde¹⁹ have studied the hydroxylation of benzoic acid in presence of N_2O and $K_3[Fe(CN)_6]$. They were able to convert all the OH radicals ($G(OH) = 5.4$) into hydroxybenzoic acids, but they find a change in iso-

TABLE VIII: Isomer Distribution in Homolytic Substitution of Some Aromatic Compounds

Reaction	Ref	Ortho	Meta	Para	Ortho:meta
$C_6H_5Cl + CH_3\cdot$	<i>b</i>	64.0	25.0	11.0	2.60
$C_6H_5Cl + \cdot C_6H_5$	<i>c</i>	50.1	31.6	18.3	1.59
$C_6H_5Cl + \cdot OH$	This work	44.6	23.1	32.3	1.93
$C_6H_5CH_3 + CH_3\cdot$	<i>b</i>	56.5	26.5	17.0	2.13
$C_6H_5CH_3 + \cdot C_6H_5$	<i>c</i>	66.5	19.3	14.2	3.45
$C_6H_5CH_3 + \cdot OH$	This work	72.5	17.0	10.5	4.26
$C_6H_5NO_2 + CH_3\cdot$	<i>b</i>	65.5	6.0	28.5	10.90
$C_6H_5NO_2 + \cdot C_6H_5$	<i>c</i>	62.5	9.8	27.7	6.38
$C_6H_5NO_2 + \cdot OH^a$	This work	48.5	22.6	28.9	2.15

^a In the presence of $1 \times 10^{-3} M O_2$. ^b G. H. Williams, "Homolytic Aromatic Substitution," Pergamon Press, New York, N.Y., 1960, p 106. ^c D. H. Hey, *Advan. Free Radical Chem.*, 3, 60 (1967).

mer composition with changing concentration of $K_3[Fe(CN)_6]$. They explained this effect by a reversible addition step. A reversible addition step in the case of nitrobenzene appears highly unlikely, due to the fact that the addition reaction is exothermic by about 106 kcal/mol. The results of Volkert and Schulte-Frohlinde can be equally well explained by 1,2 shifts. A greater stability of the *o*- and *p*-hydroxynitrocyclohexadienyl radicals as compared to meta was found by SCF-MO calculations (Table III).

Another reaction which may contribute in forming a different ratio of nitrophenols than the initial ratio of I:II:III is the disproportionation reaction. If radical I and II (see Scheme II) undergo a disproportionation, which acts as oxidizing and which as reducing radical? In presence of oxygen the disproportionation reaction is suppressed because the cyclohexadienyl radicals are oxidized to the corresponding phenols. The change in isomer distribution in going from an argon-saturated to an oxygen-saturated solution (ortho:meta ratio changes from 1.3:1 to about 2:1) shows a selectivity in the disproportionation step, i.e., if *m*- and *o*-hydroxynitrocyclohexadienyl radicals disproportionate the meta acts as reducing and the ortho as oxidizing radical. This behavior is in agreement with the SCF-MO calculations (Table IV), which show that the meta adduct has a higher SOMO energy level than the ortho and para radicals. The oxidation of the hydroxynitrocyclohexadienyl radicals by oxygen as compared to disproportionation should of course be favored by a low dose rate, an effect which was observed in the work of Matthews and Sangster.^{3a}

A very interesting result is the high percentage of *p*-nitrophenol in argon-saturated solutions. This high reactivity at the para position is not observed in other homolytic substitution reactions. Phenylation and methylation give 27.7 and 28.5%, respectively, of para-substituted nitrobenzene. The percentage of *p*-nitrophenol, however, decreases in presence of O_2 and N_2O . These compounds are good electron scavengers. The decrease in para substitution must therefore be related to the high reactivity of nitro-

(14) C. S. Rondstedt and H. S. Blanchard, *J. Org. Chem.*, 21, 229 (1956).

(15) E. G. Janzen and J. L. Gerlock, *J. Amer. Chem. Soc.*, 91, 3108 (1969).

(16) P. Neta and L. M. Dorfman, *Advan. Chem. Ser.*, No. 81, 222 (1968).

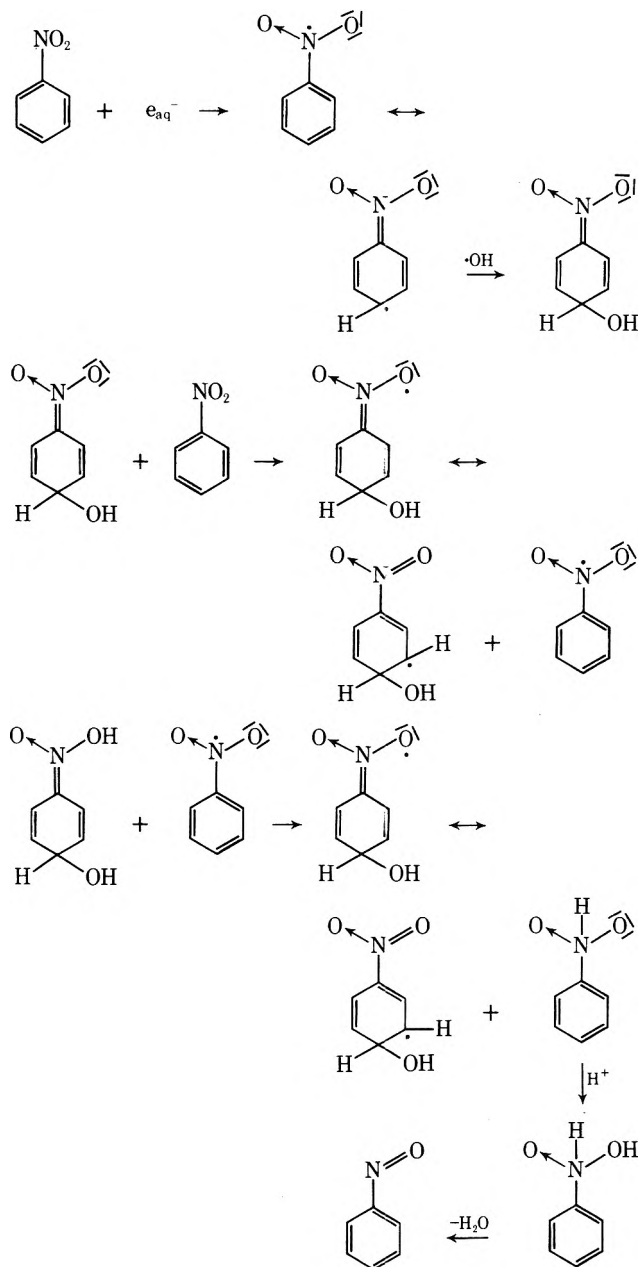
(17) K. D. Asmus, B. Cercek, M. Ebert, A. Henglein, and A. Wigger, *Trans. Faraday Soc.*, 63, 2435 (1967).

(18) R. K. H. Freidlina, *Advan. Free-Radical Chem.*, 1, 211 (1965).

(19) O. Volkert and D. Schulte-Frohlinde, *Tetrahedron Lett.*, No. 17, 2151 (1968).

benzene with solvated electrons ($3 \times 10^{10} M^{-1} \text{ sec}^{-1}$) (see the mechanism proposed in Scheme III).

Scheme III

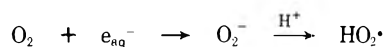


known to be an effective oxidizing agent in homolytic aromatic substitution.⁷ Schulte-Frohlinde and co-workers²⁰ have found in the hydroxylation of *p*-nitrophenol that the *p*-hydroxynitrobenzene radical anion can oxidize the intermediate cyclohexadienyl type radicals. The reaction of OH radicals with the nitrobenzene radical anion at the para position appears reasonable on the basis of SCF-MO (CNDO-2 and INDO) calculations. The nitrobenzene radical anion has the highest spin density at the para position (see Figure 3).

The only work on chlorobenzene solutions was reported by Johnson, Stein, and Weiss²¹ who carried out the X-ray irradiation of chlorobenzene in aerated aqueous solutions and found the following isomer distribution at pH 6: 15–20% ortho, 20–25% meta, and 50–50% para. They also reported the formation of unspecified amounts of phenol. Our results (Table II) show a much greater percentage of

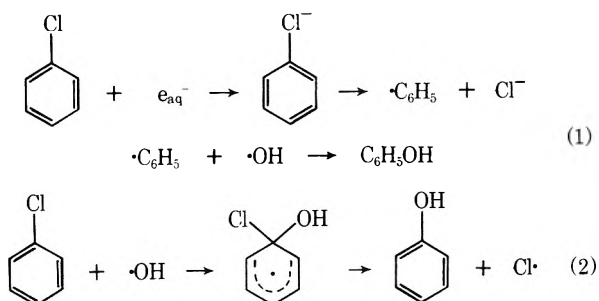
o-chlorophenol, more in agreement with theoretical expectations for a homolytic aromatic substitution by an electrophilic radical. All the additives studied increased the total yield of chlorophenol about fourfold. Oxygen not only causes an increase in total chlorophenol, but also changes the isomer distribution slightly. The percentage of ortho decreases and para increases. The decrease in the ortho:meta ratio could be explained by a selectivity in the disproportionation step, *i.e.*, the meta adduct acts preferentially as oxidizing species in disproportionation reactions, and therefore in presence of O_2 which suppresses the disproportionation reaction the ortho:meta ratio should decrease. This is in agreement with CNDO-2 calculations (Table V) which show that the meta adduct has a lower-lying SOMO energy level than the ortho and para adducts.

According to this mechanism, however, the percentage yield of *p*-chlorophenol should also decrease. In addition to OH radical attack another mechanism for *p*-chlorophenol formation must be involved. O_2 scavenges 89% of the e_{aq}^-



Previously evidence was presented against substitution of nitrobenzene by $\text{HO}_2\cdot$ or $\text{O}_2\cdot$ radicals.^{3a} This, however, does not preclude reaction of these radicals with chlorobenzene or toluene, which have much greater coefficients in the HOMO's and are therefore more reactive toward electrophilic substitution. The lower reactivity of $\text{HO}_2\cdot$ radical compared to OH radicals will make $\text{HO}_2\cdot$ more selective and it might therefore preferentially attack at the para position, which has the highest HOMO coefficient.

Another interesting problem is the mechanism of phenol formation. Phenol was reported in the radiolysis of fluorobenzene²² and anisole²³ solutions. The formation of phenol in nitrobenzene could not be confirmed. Two of the most obvious mechanisms are shown in eq 1 and 2.



The effect of electron scavengers will decrease the amount of phenol formed according to mechanism 1. This has indeed been found. In O_2 - or N_2O -saturated solution or in presence of H_2O_2 ($1.4 \times 10^{-2} M$) the $G(\text{phenol})$ is lowered to about one-half the value in argon-saturated solutions (Table II). A decrease of $G(\text{phenol})$ by O_2 or N_2O was also reported for anisole.²³ Mechanism 1 could explain the absence of phenol in the case of nitrobenzene. The nitrobenzene radical anion is quite stable, unlike the chlorobenzene radical anion.

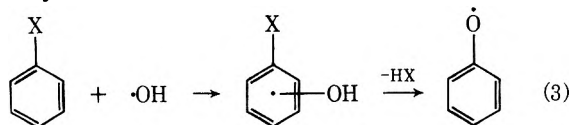
(20) D. Grässlin, F. Merger, D. Schulte-Frohlinde, and O. Volkert, *Z. Phys. Chem. (Frankfurt am Main)*, **51**, 84 (1966); O. Volkert, G. Thernens, and D. Schulte-Frohlinde, *ibid.*, **56**, 261 (1967).

(21) G. R. A. Johnson, G. Stein, and J. Weiss, *J. Chem. Soc.*, 3275 (1951).

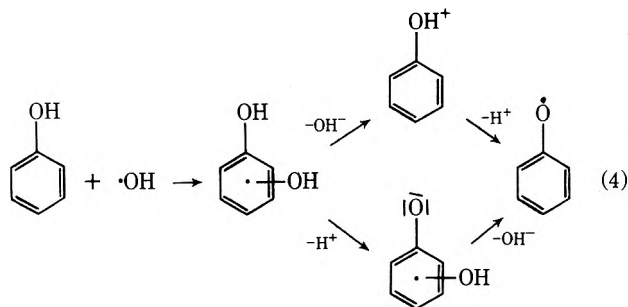
(22) J. H. Fendler, unpublished results, reported by F. J. Fendler and J. H. Fendler, *Progr. Phys. Org. Chem.*, **7**, 282 (1970).

(23) J. H. Fendler and G. L. Gasowski, *J. Org. Chem.*, **33**, 2755 (1968).

However, mechanism 1 cannot be the only one, otherwise no phenol should be formed in presence of N_2O or H_2O_2 , since 99% of the e_{aq}^- are scavenged. The residual $G(\text{phenol})$ must be due to a different mechanism for which we suggest a direct displacement of chlorine by OH radical (mechanism 2). Another mechanism (eq 3) was proposed by Fendler and Gasowski.^{3b}

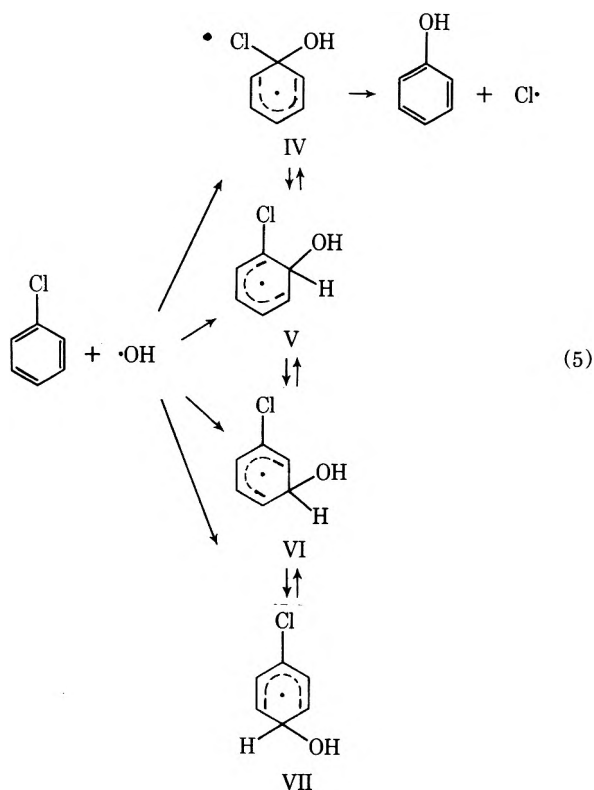


This mechanism was suggested on the basis of pulse radiolysis results of the hydroxylation of phenols (eq 4).²⁴



The elimination of water from the dihydroxycyclohexadienyl radical was found to be acid-base catalyzed. In the mechanism proposed by Land and Ebert the H^+ comes from the substituent and the OH^- from the attacking OH radical. An elimination of HX, where X is NO_2 , halogen, or OCH_3 from the corresponding hydroxycyclohexadienyl radicals is much more difficult to visualize.

The direct displacement mechanism appears more attractive since CNDO-2 calculations have shown that the intermediate α -hydroxychlorocyclohexadienyl radical has a considerable greater stability than the other hydroxychlorocyclohexadienyl radicals (see Table V). This re-

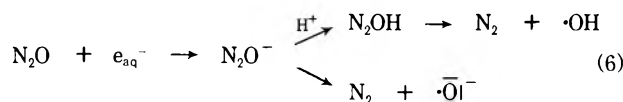


sult could explain the relatively small percentage of ortho substitution (eq 5).

The most striking result in the hydroxylation of toluene as compared to chlorobenzene is the high percentage of ortho substitution. This big difference between chlorobenzene and toluene is unexpected on the basis of frontier orbital theory (see HOMO coefficients of chlorobenzene and toluene). The frontier orbital theory predicts the position of initial interaction, but this ratio of hydroxycyclohexadienyl radicals may change due to 1,2 radical shifts leading to the more stable intermediate. In the case of chlorobenzene the formation of IV is favored over V, due to the greater stability of IV (Table V). On the other hand, for toluene the situation is reversed (Table VI) and we obtain a high percentage of o-cresol.

Oxygen considerably increases the G value for m - and p -cresol. The decrease of the ortho:meta ratio may be due to selectivity in the disproportionation step, *i.e.*, the meta adduct acts preferentially as an oxidizing radical in agreement with the CNDO-2 calculations. The increase in p -cresol cannot be explained this way. Besides homolytic substitution by OH radical, other reactions must be involved, possibly attack by HO_2 radical. The detailed mechanism involved in the radiolysis of aqueous toluene in presence of oxygen requires further study.

Effect of N_2O . N_2O has been extensively used in the radiolysis of aqueous systems since it is a very effective e_{aq}^- scavenger. It is usually assumed that N_2O is completely converted to OH radicals.²⁵ However, other possible intermediates may be able to react before being transformed into OH radicals (eq 6).



Evidence for species other than OH radicals has been presented by Nakken, *et al.*,²⁶ in the hydroxylation of benzoic and anthranilic acid.

From our theoretical results (Figure 2) we can see that the SOMO level of OH radical is very low, *i.e.*, the OH radical is electrophilic. On the other hand, O^- or N_2O^- radicals have high-lying SOMO levels which are close in energy to the LUMO level of nitrobenzene, and will therefore interact strongly with the LUMO; in other words they are nucleophilic. We can therefore expect more ortho-para and less meta substitution. The experimental results show an increase in the ortho:meta ratio as compared with argon- or oxygen-saturated solutions (Table I). In N_2O -saturated solution of chlorobenzene or toluene no change in isomer distribution was observed. Since the HOMO and LUMO of chlorobenzene do not differ substantially from each other one would not expect a drastic change in going from attack by an electrophilic radical like OH to a more nucleophilic radical like O^- or N_2O^- . Therefore we

(24) E. J. Land and M. Ebert, *Trans. Faraday Soc.*, **63**, 1181 (1967).

(25) G. E. Adams, J. W. Boag, J. Current, and B. D. Michael, "Pulse Radiolysis," M. Ebert, J. P. Keene, A. J. Swallow, and J. H. Baxendale, Ed., Academic Press, London, 1965, p 117; F. S. Dainton, and D. B. Peterson, *Nature (London)*, **186**, 878 (1960); *Proc. Roy. Soc., Ser. A*, **267**, 443 (1962); F. S. Dainton and W. S. Watt, *Nature (London)*, **195**, 1294 (1962); *Proc. Roy. Soc., Ser. A*, **275**, 447 (1963); S. Gordon, E. J. Hart, M. S. Mattheson, J. Rabani, and J. K. Thomas, *Discuss. Faraday Soc.*, **36**, 193 (1963); J. K. Thomas, *Trans. Faraday Soc.*, **61**, 702 (1965).

(26) K. F. Nakken, T. Brustad, and A. Karthum Hansen, *Advan. Chem. Ser.*, **No. 81**, 251 (1968).

do not expect to obtain any evidence for the presence of O^- or N_2O^- in the reaction with chlorobenzene. The same argument holds for toluene. In the radiolysis of N_2O -saturated solutions of nitrobenzene a significant change in isomer distribution was found due to the fact that HOMO and LUMO of nitrobenzene differ greatly. The much greater sensitivity of nitrobenzene toward changes in the electrophilicity of the attacking species compared with chlorobenzene or toluene is evident in looking at the substitution pattern of these compounds with methyl, phenyl, and hydroxyl radicals (see Table VIII). The ortho:meta ratios for nitrobenzene vary over a much larger range than those for chlorobenzene and toluene. In the radiolysis of aqueous solutions of toluene we observed in addition to aromatic substitution a large amount of side-chain attack, whose relative importance is changing in the presence of N_2O . The results in Table III show that the ratio of $G(\text{bibenzyl}):G(\text{total cresols})$ is increasing in N_2O -saturated solutions. Since side-chain attack is favored by a nucleophilic species our results indicate the involvement of a species like O^- or N_2O^- which is more nucleophilic than the OH radical.

Conclusion

The application of SCF-MO theory to radiation-induced aromatic hydroxylation gives a better understanding of the observed isomer distribution. The results show that a variety of factors play an important role in determining the isomer distribution. The HOMO-LUMO overlap, the total SCF energies, and the energy levels of the singly occupied molecular orbital (SOMO) of the intermediate cyclohexadienyl radicals have to be considered. The experimental and theoretical results show further the electrophilic character of the hydroxyl radical and the nucleophilic character of O^- . The electrophilic hydroxyl radical interacts primarily with the highest occupied molecular orbital (HOMO) whereas the nucleophilic O^- radical interacts mainly with the lowest unoccupied molecular orbital (LUMO).

Acknowledgment. We wish to thank the Organization of American States (OAS) and the Fundacao de Amparo de Pesquisa do Estado de Sao Paulo (F.A.P.E.S.P.), Sao Paulo, Brazil, for granting financial support to Dr. Yoshida.

Ionic Yields in Methanol Measured by Conductometric Pulse Radiolysis

J. Lilie, Shamim A. Chaudhri,¹ A. Mamou,² M. Grätzel, and J. Rabani*³

Hahn-Meitner-Institut für Kernforschung Berlin GmbH, Sektor Strahlenchemie, 1 Berlin 39, West Germany
(Received September 27, 1972)

Publication costs assisted by the Hahn-Meitner-Institut für Kernforschung Berlin GmbH

Radiation yields of ions have been measured by pulse radiolysis in methanol solutions containing benzyl chloride, using an ac conductometric method. For the solvated electron a yield of $G(e_{s01}^-) = 1.8 \pm 0.2$ has been measured with benzyl chloride concentrations of 1 to 10 mM. Water has no effect on the electron yield. For the CH_3O^- a yield of $G = 0.35 \pm 0.15$ has been measured.

Introduction

When radiation is absorbed by material, ionization and excitation processes take place. The primary effects of radiation have been a matter for many discussions.⁴ Despite the extensive work which has been carried out in the past two decades, the role of ionizations and excitations is not yet fully known. Only a fraction of the radiation energy is used in the formation of radical and ionic species. In water, the net yield for water decomposition is about 4 molecules/100 eV, while 100 eV energy is sufficient to dissociate about 10 water molecules. According to the spur diffusion model, originally developed by Samuel and Magee⁵ and later refined by many others, part of the ions and radicals produced primarily react in the spurs rather than diffuse into the bulk of the solution. Schwarz⁶ estimated that actually between 5 and 6 water molecules are decomposed by 100 eV of radiation. Of those, a substantial fraction recombines in the spurs.

Less is known on media other than water. Alcohols are among the most extensively studied media, next to water.⁷ However, in addition to insufficient data, there is often disagreement concerning the nature and the yields of products in alcohols.

The purpose of this article is to report the yields of solvated electrons (e_{s01}^-) and methoxide ions (CH_3O^-) in methanol. Similar work has been carried out previously in

- (1) Postdoctoral Fellow from the Pakistan Atomic Energy Commission Karachi, with a grant from the Alexander von Humboldt-Stiftung, Bad Godesberg.
- (2) On leave from The Accelerator, The Hebrew University, Jerusalem 91 000, Israel.
- (3) Visiting professor from the Department of Physical Chemistry, The Hebrew University, Jerusalem 91 000, Israel.
- (4) See, e.g., U. L. Parsegian and H. M. Clark, Vol. 4, "Survey of Progress in Chemistry," Academic Press, New York, N. Y., 1968.
- (5) A. H. Samuel and J. L. Magee, *J. Chem. Phys.*, **21**, 1080 (1953).
- (6) H. A. Schwarz, *J. Phys. Chem.*, **73**, 1928 (1969).
- (7) See, e.g., J. Tepley, *Radiation Res. Rev.*, **1**, 361 (1969).

ethanol.⁸ A long-range purpose of such work is to understand the factors which determine the ionic yields (e.g., dielectric constant and viscosity of the media) so that the primary yields in previously not measured media can be predicted. In the present article we will provide data concerning the methanol system which adds to previous investigations⁸⁻¹¹ to yield information on media with a great variety of physical and chemical properties. In addition, the measurements of the radiation yields in various media are essential for a cross check of diffusion models. At present, there are too many parameters which are freely chosen, and the significance of a fit with a diffusion model is questionable. Any accurate measurements of the yields of products reduces the number of adjustable parameters.

Experimental Section

The pulse radiolysis apparatus and cell filling technique¹² have been described previously. The 10-MHz ac conductivity setup has been reported previously.¹³ Under our conditions, the time resolution of the measurements was about 3 μ sec in addition to the pulse duration. Electron pulses of 0.3–3 μ sec from a Van de Graaff machine, 1.5 MeV, were used. The cell consisted of two approximately matched pairs of electrodes in one quartz cell. The cell constant was ~ 0.5 cm⁻¹. The bridge works linearly only for small changes in the conductivity (<5%); therefore we always added 10^{-5} M NaClO₄ to the solution.

Since benzyl chloride decomposes in methanol at room temperature, the solutions were kept at -40° under helium and warmed up to 17° immediately (several seconds) before irradiation. (This was carried out when the solution was flowing from a cooled storage flask to the irradiation cell.)

The thermal decomposition of benzyl chloride in methanol produces products which have electrical conductivity, apparently H⁺ and Cl⁻. Conductivity measurements showed that practically no thermal decomposition of benzyl chloride took place at -40° . The conductivity observed after 1 hr was small compared with the conductivities produced by the electron pulses.

Dosimetry was carried out using a tetranitromethane saturated, deaerated aqueous solution containing 0.1 M isopropyl alcohol. Both conductivity and absorbance measurements were carried out simultaneously. The only products which contribute to the conductivity and optical absorbance at 350 nm in the microsecond time range are H⁺ and C(NO₂)₃⁻ (ϵ 14,800 M⁻¹ cm⁻¹ at 350 nm). $G = 6$ was assumed for the nitroform. The dose in methanol was assumed to be 0.8 of the dose in water. All measurements were done at 17° .

Materials. Perchloric acid, H₂SO₄, NaClO₄·H₂O, I₂, and dinitrophenylhydrazine were Merck's Analytical reagents; Mg powder was Riedel's reagent. They were used as received. Methanol of Merck ("for analysis") was purified from carbonyl compounds by refluxing for 12 hr with 3 ml of H₂SO₄ and 1.5 g of dinitrophenylhydrazine per liter.¹⁴ After distillation through a column, part of which was heated to prevent ion migration, it was refluxed with 2 g of Mg and 0.2 g of I₂ for at least 10 hr. It was subsequently distilled six times through a column. The whole process of cleaning of the methanol was carried out under dried argon (Linde, extra pure). An absorber (Linde's) for the elimination of water and oxygen was used. The purified methanol was further deaerated by bubbling for 20 min with dry purified argon. Even after this procedure,

the conductivity of the methanol was much higher than the theoretical value. We assume that some magnesium methoxide was transferred despite our repeated distillations. This is supported by the fact that very low conductivities were observed, when methanol from the bottle was distilled without the addition of Mg. After the introduction of Mg, this was the main impurity, all other ions being present in much smaller concentrations. In addition, the conducting impurity was a base, as demonstrated by a conductometric titration with perchloric acid. Checks for conductivity were always carried out and they showed 0.5 to 1 μ M magnesium methoxide to be present. Unless otherwise stated, a sufficient amount of perchloric acid was added to neutralize the methoxide and obtain a slightly acidic pH (in the range 6–7 for most of the experiments). In some cases, the CH₃O⁻ ions were neutralized by H⁺ generated by pulse irradiation. More details about these will be given later. Conductometric titrations were always carried out to confirm the presence of excess of acid. Benzyl chloride, Merck's (for analysis) was distilled five times *in vacuo* through a column.

The purity of the methanol with respect to the lifetime of e_{sol}⁻ was checked in each of the solutions just before the addition of the benzyl chloride.

Results

The effect of radiation on methanol can be represented by



where R represents neutral free radicals. When benzyl chloride is added, reaction 2 takes place.



Reaction 2 is in agreement with the disappearance of the e_{sol}⁻ absorption upon the addition of benzyl chloride. Reactions similar to (2) have been reported previously.¹⁵ In all our experiments, sufficient amounts of benzyl chloride were added so that e_{sol}⁻ reacted exclusively with it as was controlled by observing the decay of the optical absorption of the electron. The half-life always was shortened by more than a factor of 10 by the addition of the benzyl chloride. Any CH₃O⁻ which is formed by the irradiation is expected to be neutralized by the excess of ROH₂⁺. When the solution contains initially a large excess of CH₃OH₂⁺ ions, the neutralization reaction takes place during the pulse. At the end of the pulse a net conductivity change is expected due to the permanent products CH₃OH₂⁺ and Cl⁻ ($\Lambda_0 = 195$ ohm⁻¹ cm² mol⁻¹ at 25°). This is in accordance with our observations. There was no further conductivity change indicating no additional reactions involving ions. (Measurements were carried out in the time range 4–500 μ sec.) From such experi-

- (8) J. Rabani, M. Grätzel, and S. A. Chaudhri, *J. Phys. Chem.*, **75**, 3893 (1971).
- (9) (a) J. Rabani, M. Grätzel, S. A. Chaudhri, G. Beck, and A. Henglein, *J. Phys. Chem.*, **75**, 1759 (1971); (b) G. C. Barker, P. Fowles, D. C. Sammon, and B. Stringer, *Trans. Faraday Soc.*, **66**, 1498 (1970); (c) G. C. Barker, and P. Fowles, *ibid.*, **66**, 1661 (1970).
- (10) D. A. Head and D. C. Walker, *Can. J. Chem.*, **48**, 1657 (1970).
- (11) (a) W. F. Schmidt and A. O. Allen, *J. Phys. Chem.*, **72**, 3730 (1968); (b) W. F. Schmidt and A. O. Allen, *J. Chem. Phys.*, **52**, 2345 (1970).
- (12) G. Beck, *Int. J. Radiat. Phys. Chem.*, **1**, 361 (1969).
- (13) J. Lilie and R. W. Fessenden, *J. Phys. Chem.*, in press.
- (14) D. D. Perrin, W. L. F. Armarego, and D. R. Perrin, "Purification of Laboratory Chemicals," Pergamon Press, Oxford, 1966.
- (15) R. J. Hagemann and H. A. Schwarz, *J. Phys. Chem.*, **71**, 2694 (1967).

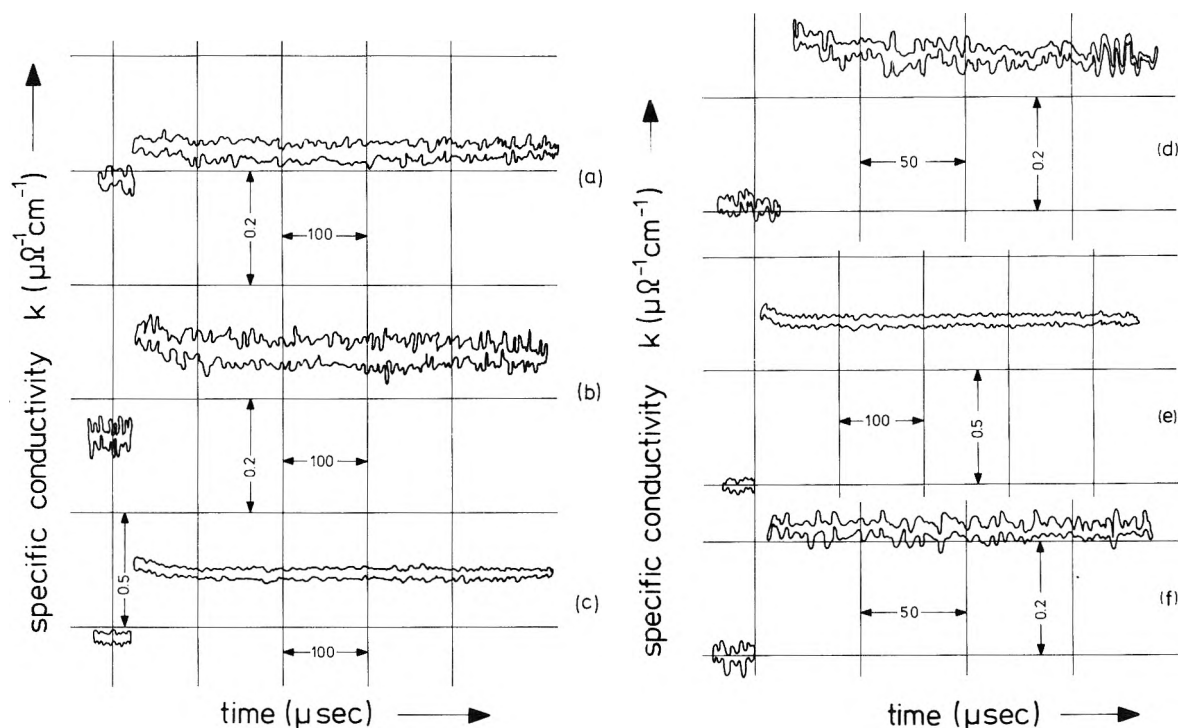
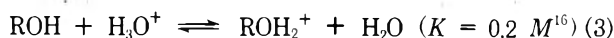


Figure 1. Oscilloscope traces (various pulse intensities) in $10^{-5} M$ NaClO_4 deaerated methanol solutions containing 5 mM benzyl chloride: (a)–(e), excess of $0.2 \mu M$ HClO_4 initially present, dose 60–1000 rads; (f), solution containing $0.2 \mu M$ HClO_4 has been previously pulse-irradiated until $2 \mu M$ HCl has been accumulated.

ments, $G(e_{\text{sol}^-})$ was calculated. The results at several benzyl chloride and CH_3OH_2^+ concentrations are presented in Table I.

In the presence of water, equilibrium 3 exists.



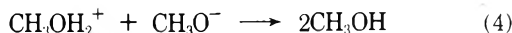
The equivalent conductivity of H_3O^+ at 25° is 50 compared with $144 \text{ ohm}^{-1} \text{ cm}^2 \text{ mol}^{-1}$ for CH_3OH_2^+ .¹⁷

The results of Table I show that the electron yield in methanol is similar to that reported for ethanol⁸ and depends only slightly, if at all, on the benzyl chloride and CH_3OH_2^+ concentrations in the range of our measurements. Our results agree with those reported by Freeman.¹⁸

The electron yields which are determined from the conductivity changes at long times, are the same with and without water, taking into account the different mobilities of the ions, but the behavior a short time after the pulse is different since CH_3OH_2^+ and CH_3O^- react with H_2O forming H_3O^+ and OH^- . Therefore for the subsequent measurements dry methanol was always used.

Measurements at Very Low Acid Concentrations. When a solution containing benzyl chloride and a relatively low acid concentration was pulse-irradiated, the initial conductivity change was higher by roughly 15% than in the stronger acidic solutions (Table I). The increase in conductivity which took place during the pulse partially decayed away within the first 30–100 μsec . Typical oscilloscope traces are presented in Figure 1. Under the conditions of Figure 1, the concentrations of CH_3OH_2^+ , produced by a single electron pulse, ranged between 0.1 and $1.5 \mu M$. The decaying fraction is in all cases (Figure 1a–e) about 15%, but the rate of the decay increases nearly proportional with pulse intensity. After several pulses have been given to the same solution, no decay is observed (Figure 1f). We interpret the decay as being due to the

neutralization reaction



Upon repetitive pulse irradiation of the same solution, CH_3OH_2^+ builds up. Reaction 4 is enhanced, and at sufficiently high CH_3OH_2^+ concentration the decay of conductivity takes place during the pulse and cannot be observed. The plateaus observed in Figure 1 correspond to $G(e_{\text{sol}^-}) = 1.9 \pm 0.1$. This agrees well with $G(e_{\text{sol}^-})$ measured at higher HClO_4 concentrations. The yield of CH_3O^- ions can be calculated using eq 5.

$$G(\text{CH}_3\text{O}^-) = G(e_{\text{sol}^-}) \times \frac{[\lambda(\text{Cl}^-) + \lambda(\text{CH}_3\text{OH}_2^+)]}{[\lambda(\text{CH}_3\text{O}^-) + \lambda(\text{CH}_3\text{OH}_2^+)]} \times \frac{K_0 - K_\infty}{K_\infty} \quad (5)$$

K_0 and K_∞ are the specific conductivities extrapolated back to the middle of the pulse and at the plateau, respectively. Extrapolation to the middle of the pulse was normally carried out from the linear plots of $\ln(K - K_\infty)$ vs. time.

In Table II we present values of $G(\text{CH}_3\text{O}^-)$ obtained in various benzyl chloride and CH_3OH_2^+ concentrations. A ratio $[\lambda(\text{Cl}^-) + \lambda(\text{CH}_3\text{OH}_2^+)]/[\lambda(\text{CH}_3\text{O}^-) + \lambda(\text{CH}_3\text{OH}_2^+)] = 0.98^{19}$ has been used for these calculations.

From the results of Figure 1 and Table II we conclude that $G(\text{CH}_3\text{O}^-) = 0.35 \pm 0.15$ as an average of all values. The values at higher doses are more reliable because of the better signal to noise ratio.

(16) L. S. Guss and I. M. Kolthoff, *J. Amer. Chem. Soc.*, **62**, 1494 (1940).

(17) B. E. Conway, J. O'M Eockris, and H. Linton, *J. Chem. Phys.*, **24**, 834 (1956).

(18) K. N. Jha and G. R. Freeman, *J. Chem. Phys.*, **48**, 5480 (1968).

(19) Landolt-Börnstein, "Zahlenwerte und Funktionen," Vol. II, Part 7, Springer-Verlag, Berlin, 1960.

TABLE I: $G(e_{\text{sol}}^-)$ in Acidic Benzyl Chloride Solutions^a

$[\text{C}_6\text{H}_5\text{CH}_2\text{Cl}]$, M	$[\text{CH}_3\text{OH}_2^+]$, ^b M	$[\text{H}_2\text{O}]$, M	$G(e_{\text{sol}}^-)$
1.4×10^{-3}	3×10^{-6}	...	1.6
3.2×10^{-3}	8.5×10^{-6}	...	1.6
5.0×10^{-3}	2×10^{-6}	...	1.8
5.0×10^{-3}	1.5×10^{-6}	0.18	2.0
5.0×10^{-3}	1.5×10^{-6}	1.9	1.9
1.3×10^{-2}	8.5×10^{-6}	...	1.8
1.3×10^{-2}	1.0×10^{-2}	0.025	1.9

^a The solution contained 10^{-5} M NaClO₄ in order to increase the initial (before pulse) conductivity. Pulse intensity varied between 6×10^{18} and 1.8×10^{19} eV l.⁻¹ per pulse. The above results represent averages of five measurements per G value. ^b HClO₄ (from a 70% aqueous solution) added.

It might be argued that the partial decay of conductivity is due to a reaction with an alkali or a buffer present initially and not due to the reaction with the radiation product CH₃O⁻. From our method of preparation one might suspect traces of water and of untitrated magnesium methoxide as possible impurities. The methoxide ions were neutralized by titration with HClO₄. Although an error in the determination of the end point is possible, when the excess of acid is so small, our results which show that $G(\text{CH}_3\text{O}^-)$ is independent of the pulse intensity rule out any significant alkalinity in our solutions before pulsing. If $G(\text{CH}_3\text{O}^-)$ was zero and the decay was entirely due to neutralization of alkali already present in the solutions before, one would expect the magnitude of the conductivity which decays away to be independent of CH₃OH₂⁺ formed by the pulse. Our observations (Figure 1 and Table II) show that the relative fraction which decayed away was constant within experimental error, although the pulse intensity has been varied by 15-fold.

To demonstrate the effect of initially present alkali, pulse experiments were carried out in solutions containing initially 7–15 μM magnesium methoxide and 5×10^{-3} M benzyl chloride. The conductivity produced upon pulse irradiation decayed away to zero as long as the solution contained an excess of alkali which was sufficient to neutralize all the H⁺ produced by the pulse. Under such conditions, process 1 is followed by reactions 2 and 4, and the net effect is to substitute CH₃O⁻ by Cl⁻. These two ions possess nearly the same conductances and therefore no net conductivity change is observed. The decay rate of the conductivity corresponds to $k_4 \cong 5 \times 10^{10} \text{ M}^{-1} \text{ sec}^{-1}$, in agreement with previous measurements²⁰ and with our experiments in the acid pH range, where rough estimates of k_4 could be made. When the same solution is again pulse irradiated, the decay of the conductivity becomes slower, since part of the methoxide ions have been neutralized by the previous pulse. Pulses were repeated until all of the CH₃O⁻ ions were neutralized and an excess of CH₃OH₂⁺ was obtained. A partial decay of the conductivity could be observed under such conditions, corresponding to $G(\text{CH}_3\text{O}^-)$ and $G(e_{\text{sol}}^-)$ 0.3 and 1.8, respectively. These experiments support the mechanism and values of $G(\text{CH}_3\text{O}^-)$ and $G(e_{\text{sol}}^-)$ proposed. The total ion yield can

TABLE II: $G(e_{\text{sol}}^-)$ and $G(\text{CH}_3\text{O}^-)$ in Benzyl Chloride Solutions

$[\text{HClO}_4]$, μM	$[\text{CH}_3\text{OH}_2^+]$, ^a μM	$[\text{C}_6\text{H}_5\text{CH}_2\text{Cl}]$, mM	$G(e_{\text{sol}}^-)$ ^b	$G(\text{CH}_3\text{O}^-)$ ^b
0.6	1.0	1.4	1.7	0.25
0.20	0.3	5.0	1.9	0.4
0.20	0.4	5.0	1.6	0.6
0.20	0.5	5.0	1.7	0.5
0.20	0.65	5.0	1.8	0.35
0.20	0.80	5.0	1.9	0.35
0.20	1.2	5.0	1.9	0.35
0.20	1.7	5.0	1.9	0.35

^a Average concentration during the decay of conductivity (including the HClO₄ initially added). ^b Average values of two runs.

be determined from the initial (extrapolated) conductivity produced in both alkaline and acidic solutions. The results yield $[G(e_{\text{sol}}^-) + G(\text{CH}_3\text{O}^-)] = 2.2 \pm 0.3$ (5×10^{-3} M benzyl chloride) in agreement with the value which can be calculated from previous experiments in the slightly acid range (Table II). Our results agree with those of Fowles, who reported a total yield of free ions in methanol 2.0 ± 0.2 .²⁰

The yield of free ions decreases from 3.5 in water and formamide¹⁰ to values below 1 in liquid hydrocarbons.¹¹ Methanol with an intermediate dielectric constant, yields an intermediate value for $G(\text{free ions})$. The yield of free ions is expected to increase with the dielectric constant.²¹ The intermediate value $G(\text{free ions})$ for methanol is in qualitative agreement with this conclusion.

Higher yields were reported in ethanol.⁸ Although the dielectric constant is not the only factor which is expected to determine the yield of free ions, it is difficult to rationalize a remarkable increased yield in ethanol, as compared with methanol. The work in ethanol was carried out using a different technique, in which some uncertainty exists with respect to the short-time range (10–20 μsec). In these measurements because of the extremely low conductance of the solution, the disturbances from the beam took a longer time to settle down than normal and on the other hand the signals were much smaller than in water or methanol, due to the low mobility of the ions in ethanol. Therefore, we feel that the previous ethanol results are reliable with respect to $G(e_{\text{sol}}^-)$, but $G(\text{C}_2\text{H}_5\text{O}^-)$ cannot be used safely before further experiments confirm the previously reported value. In fact, the work by Fowles,²⁰ combined with $G(e_{\text{sol}}^-) = 1.8 \pm 0.1$ ⁸ suggests that $G(\text{C}_2\text{H}_5\text{O}^-)$ is less than 0.7. Unfortunately, the project had to be terminated before further experiments in ethanol solutions could be carried out. From preliminary work it seems probable that the yields of both RO⁻ and e_{sol}^- may be similar in both methanol and ethanol.

Acknowledgment. We wish to thank A. Henglein and W. F. Schmidt for valuable discussions during the course of this work.

(20) P. Fowles, *Trans. Faraday Soc.*, **67**, 428 (1971).

(21) P. G. Fuochi and G. R. Freeman, *J. Chem. Phys.*, **56**, 2333 (1972).

Excited State Reactivity of Aza Aromatics. I. Basicity of 3-Styrylpyridines in the First Excited Singlet State

G. Favaro, U. Mazzucato,* and F. Masetti

Instituto di Chimica Fisica, University of Perugia, 1-06100 Perugia, Italy (Received August 8, 1972)

Publication costs assisted by the Consiglio Nazionale della Ricerche (Roma)

The basicities of the three isomeric *trans*-styrylpyridines in the first excited singlet state have been calculated from their absorption and fluorescence spectra. For 3-styrylpyridine and some of its 4'-substituted derivatives the pK^* has also been directly measured by fluorimetric titration. The basicity increases strongly on excitation, with the exception of the 4'-NO₂ derivative which becomes a stronger acid in the excited state. The substituent effect on the basicity of 3-styrylpyridine is larger in the excited than in the ground-state molecule. Kinetic parameters for the protolytic equilibration in the excited state have been evaluated from fluorescence-pH curves and fluorescence lifetimes.

Introduction

Calculations of the basicities of styrylpyridines (StP's) by applying the Förster cycle¹ to the absorption spectra showed that 2- and 4-StP become much stronger bases in the excited singlet state.^{2,3} The pK^* of 3-StP, roughly evaluated from absorption maxima, seemed close to the ground state pK . However, molecular orbital calculations indicated a noticeable migration of charge toward the heteroatom for all three isomers on excitation.² The pK^* values have now been recalculated using the more reliable method of averaging the absorption and fluorescence frequencies⁴ and they indicate a strong increase of basicity for the excited 3-StP also. This result has been confirmed directly by measurements of fluorescence intensity as a function of pH (obviously restricted to the fluorescent *trans* isomer, which attains a partial equilibrium with the proton during the lifetime of the fluorescent state). The investigation has been extended to include some 4'-substituted 3-StP's. The data obtained, together with fluorescence lifetimes, are important in the interpretation of the photochemical behavior of these compounds.⁵

Experimental Section

The styrylpyridines were prepared by standard procedures.⁶ Ground-state pK values were determined by both absorption and fluorescence spectrometry. As the precision of the absorption measurements cannot be high for 3-StP's, due to the small changes of the spectra with pH,⁷ the dissociation constants were also measured by fluorimetry, where the spectral shift due to protonation is much larger.⁸

Excited state ionization constants were directly determined by fluorimetry, when partial establishment of the excited state equilibrium was detected in a plot of the relative fluorescence intensity as a function of pH. Values in the tables are means of three independent experiments with a mean deviation of 0.05. All pK^* values were also calculated by the Förster cycle using the average of the absorption and fluorescence maximum frequencies (if detectable, the long-wavelength shoulder of the absorption spectra was used). Uncertainty from frequency determination can introduce errors of 0.3–0.4 pK units. The low solubility of these compounds did not allow us to take absorption spectra at high concentrations and so to get accu-

rate band onsets for these measurements. That calculated pK^* values are reliable is in any case confirmed by the very good agreement with those fluorimetrically measured.

Absorption spectra were taken with both single- and double-beam grating Optica CF4 spectrophotometers. For fluorescence spectra a CGA DC-3000/1 spectrofluorimeter was used. Some corrected spectra were run on a Perkin-Elmer MPF-3 fluorescence spectrophotometer with an accessory for spectral correction which uses Rhodamine B as a quantum counter. Fluorescence-pH curves were obtained exciting the compounds at the isosbestic point between the absorption bands of the free base and its conjugate acid.

All measurements were made at room temperature in water containing 10% (v/v) ethanol. Solutions were freshly prepared and kept in the dark before use to avoid *trans*-*cis* photoisomerization. Britton buffers were used in the pH interval 2 to 12; NaOH solutions were used for higher pH's.

A Sargent PXB pH meter with a glass electrode was employed. High pH's were corrected for the alkaline error. Solute concentration was of the order of 2×10^{-5} M. The ionic strength was kept constant at 0.01 for the measurements of ground-state equilibria and at 1 in the region of the excited state pK^* . In the latter case, Na₂SO₄ was used as added salt because of its very low quenching power on the luminescence. Under these conditions the emission intensity was proportional to concentration and the fluorescence-pH curves showed a regular trend.

Apparent pK^* values (K^* is the dissociation constant of the styrylpyridinium acid) were corrected (−0.3) to the thermodynamic values in Table II by the approximate formula for the activity coefficients (see *e.g.*, ref 8).

- (1) See *e.g.*, A. Weller, *Progr. React. Kinet.*, **1**, 187 (1961), and references cited therein.
- (2) P. Bortolus, G. Cauzzo, U. Mazzucato, and G. Galiazzo, *Z. Phys. Chem. (Frankfurt am Main)*, **51**, 264 (1966).
- (3) J. C. Doty, J. L. R. Williams, and P. J. Grisdale, *Can. J. Chem.*, **47**, 2355 (1969).
- (4) (a) E. L. Wehry and L. B. Rogers, *Spectrochim. Acta*, **21**, 1976 (1965); (b) *J. Amer. Chem. Soc.*, **87**, 4234 (1965).
- (5) G. Bartocci, P. Bortolus, and U. Mazzucato, *J. Phys. Chem.*, **77**, 605 (1973).
- (6) G. Galiazzo, *Gazz. Chim. Ital.*, **95**, 1322 (1965).
- (7) G. Cauzzo, G. Galiazzo, U. Mazzucato, and N. Mongiat, *Tetrahedron*, **22**, 589 (1966).
- (8) G. Beqqiatio, G. Favaro, and U. Mazzucato, *J. Heterocycl. Chem.*, **7**, 583 (1970).

TABLE I: Assumed 0-0 Frequencies (10^3 cm^{-1}) and Basicity of *trans*-Styrylpyridines in the Ground and Excited States in 90/10 (v/v) Water-Ethanol at 25°

Compd	$\bar{\nu}_{\text{StP}}$	$\bar{\nu}_{\text{StPH}^+}$	pK	pK^* (calcd)
2-StP	29.22	26.22	4.98 ^a	11.4
3-StP	29.45	25.87	4.76	12.4
4-StP	29.57	26.02	5.73 ^a	13.3

^a From ref 7.

TABLE II: Assumed 0-0 Frequencies (10^3 cm^{-1}), Basicity, and Percentage of Excited Molecules in Acidic Form at pH ~8 for Some *trans*-4'-X-3-Styrylpyridines in 90/10 (v/v) Water-Ethanol at Room Temperature

X	$\bar{\nu}_{\text{StP}}$	$\bar{\nu}_{\text{StPH}^+}$	pK	pK^* (calcd)	pK^* (fluor)	% StPH ⁺⁺
H	29.45	25.87	4.76	12.4	12.3	17
CH ₃	28.50	24.82	4.77	12.6	12.5	34
OCH ₃	27.17	23.32	4.73	12.9	13.0	20
Cl	29.25	25.68	4.74	12.4	12.3	9
Br	29.10	25.45	4.74	12.5	12.4	6.5
I	28.35	24.80	4.73	12.3		<1
NO ₂	23.07	24.42	4.44	1.6		

The fluorescence lifetimes were measured by the pulse sampling technique with an apparatus described elsewhere.⁹

Results and Discussion

Calculated ionization constants for the three isomeric styrylpyridinium cations in the first excited singlet state are reported in Table I together with the experimental parameters used for their calculation through the Förster cycle. It appears that 3-StP, which has the lowest pK in the ground state, displays a pK increase of about 8 units on excitation, similar to the 4 isomer and a little higher than the 2 isomer. The position of nitrogen has only a small effect on the pK*.

3-Styrylpyridine. The fluorescence maximum of *trans*-3-styrylpyridine is, at 350 nm in *n*-hexane, noticeably displaced toward longer wavelengths with respect to the absorption (~300 nm). A further red shift of about 10 nm (a little higher than for the isomeric 2- and 4-StP) is observed on going from *n*-hexane to polar solvents, while the absorption spectrum remains practically unchanged.

Protonation broadens the absorption spectrum toward the red (approximate onset shift 3000 cm^{-1}) leaving the maximum practically unchanged. On the other hand, the proton addition produces a much larger bathochromic shift of emission, the fluorescence maxima of the basic and acidic forms being at 360 and 460 nm ($\Delta\bar{\nu} \approx 6000 \text{ cm}^{-1}$), respectively, in buffered solutions (Figure 1). The much larger Stokes shift for the cation is rather surprising, because the S_0 and S_1 states are not expected to be much different in structure and polarity. However, the importance of solvent relaxation effects becomes evident from the larger fluorescence blue shift observed for the acidic than for the basic form in rigid matrix at 77°K, relative to solution spectra. Further work on the luminescence of this compound is in progress in order also to clarify better this point.

Solvent and protonation effects on emission spectra indicate π, π^* fluorescent states; a comparison between absorption¹⁰ and corrected excitation spectra confirms this assignment.

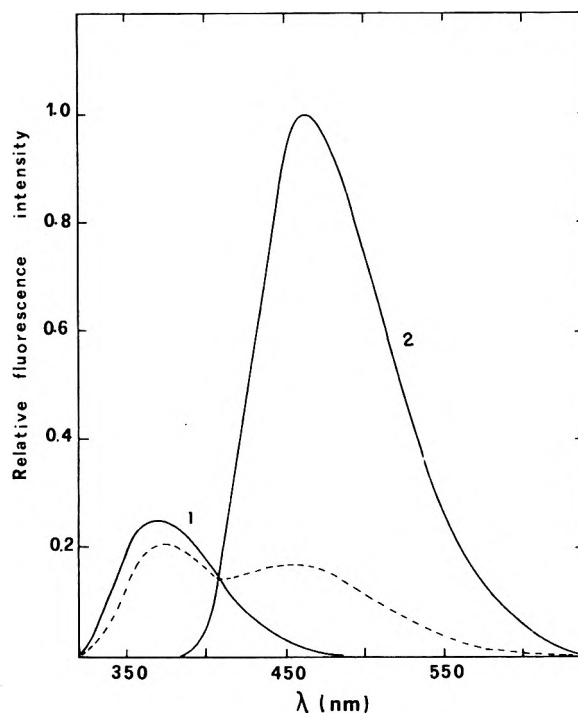


Figure 1. Corrected fluorescence spectra of *trans*-3-styrylpyridine in 90/10 (v/v) water-ethanol: (1) neutral form at pH 13.7; (2) protonated form at pH 2; dotted line shows spectrum of a solution at pH 8, when 17% of 3-StP is protonated in the excited state ($\lambda_{\text{exc}} = 280 \text{ nm}$, absorbance 0.1).

An investigation of the change in the fluorescence spectrum as a function of pH shows that it yields two maxima (Figure 1) over a wide range of pH (3.5–13.5). The emission maximum at 460 nm, characteristic of the cation, does not completely disappear with increasing pH above the ground state pK (4.76). Although its intensity is lowered on going from pH 3.5 to 6.5, the band is still present at the latter pH, when the absorption is due only to the neutral molecule. Its intensity remains practically the same up to pH 11, then it begins to decrease again, being completely quenched by further increase in pH. The band at 360 nm, characterizing the emission of the free base, correspondingly increases above pH 11. An experimental pK* of 12.6 was thus obtained for the first excited singlet state; the corresponding thermodynamic value is reported in Table II. There is a fairly good agreement with the calculated value, confirming the applicability of the Förster cycle to the observed spectra, despite change of the configuration on excitation. This is probably due to a partial cancellation of the solvent relaxation effects in the averaging of the absorption and fluorescence frequencies.^{4a}

From the emission intensities of the cationic and neutral forms at pH 8, relative to those in acidic and basic solutions (pH 2 and 13.5, respectively), the fraction of excited molecules equilibrated with the proton is found to be about 17% in 90/10 (v/v) water-ethanol (rapidly decreasing with increase in alcohol percentage). The acid-base equilibration of the excited singlet state, even if partial, indicates a longer lifetime of this isomer compared with 2- and 4-StP. τ_b is, however, shorter (<1 nsec) than the time resolution of our apparatus for fluorescence lifetimes. It must also be stressed that, of the isomers, 3-StP

(9) F. Masetti and U. Mazzucato, *Ann. Chim. (Roma)*, in press.

(10) G. Favini, S. Fasone, and M. Raimondi, *Gazz. Chim. Ital.*, **97**, 1434 (1967).

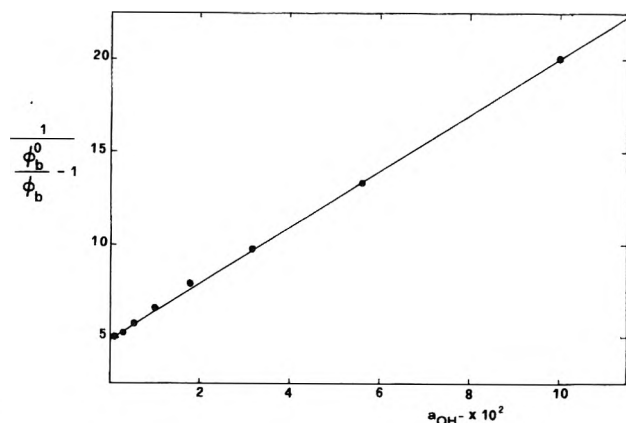
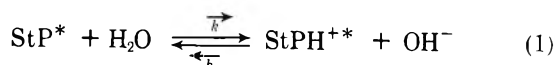


Figure 2. Plot of $1/(\phi_b^0/\phi_b - 1)$ against OH^- activity, according to eq 2.

has the highest fluorescence efficiency ($\phi_b = 0.04$).^{2,5,11,12} The fluorescence quantum yield and radiative lifetime become even higher for the cation ($\phi_a = 0.2$, $\tau_a = 5.5$ nsec).

From the fluorescence quantum yields and lifetimes of the two conjugate species



the kinetic parameters of the hydrolytic equilibrium can be calculated, following the usual kinetic procedure,^{1,13} utilizing the equation

$$[1/(\phi_b^0/\phi_b) - 1] = (1/k\tau_b) + (\overleftarrow{k}\tau_a/\overrightarrow{k}\tau_b)a_{\text{OH}^-} \quad (2)$$

The linear plot (Figure 2) of $1/(\phi_b^0/\phi_b - 1)$ against the OH^- activity (where ϕ_b^0 is the emission quantum yield of 100% base and ϕ_b that in solutions where StPH^{*+} coexists with StP^*) gives a slope = 150, an intercept = 5, and slope/intercept = $\overleftarrow{k}\tau_a = 30$

From the observed fluorescence lifetime of the cation, the rate constants of the pseudo-first-order and second-order protolytic reactions (eq 1) can be evaluated (see first row in Table III). Both rate constants, mainly that of protonation, are smaller than the diffusional rate constant ($k_d \sim 3 \times 10^{10} \text{ M}^{-1} \text{ sec}^{-1}$), calculated from the theory of diffusion-controlled reactions.¹ Also τ_b can be calculated from the slope

$$\tau_a/\tau_b = \text{slope}(\overleftarrow{k}/\overrightarrow{k}) = \text{slope}(K_w/K^*) \quad (3)$$

A calculation of τ values from the luminescence quantum yields and the natural lifetimes, τ^0 values, obtained from the absorption and fluorescence spectra by the integration formula of Strickler and Berg,¹⁴ leads to rather lower values (1 and 0.1 nsec for 3-StPH⁺ and 3-StP, respectively). The lack of quantitative agreement (found also for the 4'-substituted derivatives) between calculated and measured lifetimes is not unexpected as the considerable configurational distortion on going from the ground to the excited state, mainly for the cation, invalidates the application of Strickler and Berg's formula.

4'-Substituted 3-Styrylpyridines. Absorption and fluorescence spectra of 4'-substituted 3-StP follow a trend with pH analogous to that of the unsubstituted compound. Differences between the fluorescence maxima of the neutral and cationic forms are more noticeably dependent on the substituents than those between the absorption maxima. This indicates that the charge distribution

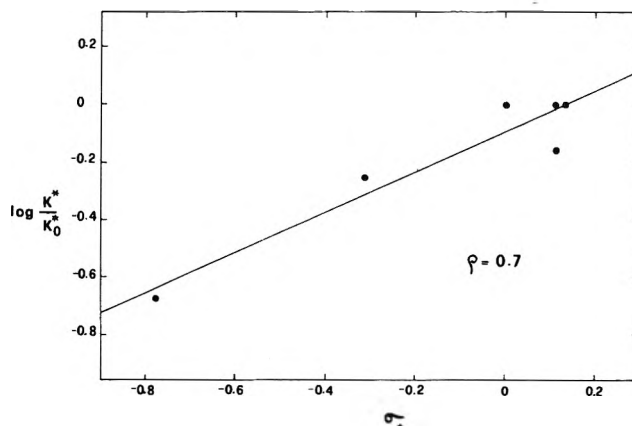


Figure 3. Hammett plot for the ionization constants of 3-styrylpyridines in their excited singlet state in 90/10 (v/v) water-ethanol.

in the electronically excited singlet state is significantly different from that in the ground state, and more sensitive to substitution, leading to a different orientation of the solvent cage. The frequencies reported in Table II refer to the assumed 0-0 bands, used for the pK^* calculations. A general bathochromic shift is observed for the cations with respect to the bases, the only exception being the nitro derivative for which an opposite shift is found. Moreover, this derivative displays a lower emission intensity in the acidic than in the basic form. The hypsochromic effect of both solvent polarity and protonation on the spectra seems to indicate a n, π^* nature (probably involving the NO_2 group) of the fluorescent level of this derivative.

Table II shows the ionization constants obtained, when possible, by both the Förster cycle and direct fluorimetric titration, together with the ground-state pK values and the percentages of acidic form still present in the excited state at about 3 pH units above the ground-state pK . Inspection of the table shows a significant heavy atom effect, which makes the direct fluorimetric measurement of pK^* for 4'-I-3-StP impossible, due to the low fraction of molecules which attain acid-base equilibrium during the excited state lifetime. The emission intensity of 4'- NO_2 -3-StP is so low that there is some doubt as to whether such equilibration is ever attained by this compound. The calculated decrease of its pK on excitation (about 3 units) is, however, in agreement with that found for the other isomeric 4'- NO_2 -StP's.³ Experimental and calculated pK^* values are in fairly good agreement in the other cases, where direct fluorimetric measurements were possible.

The main effect produced by excitation, with the exception of the NO_2 derivative, is a large increase in basicity (about 8 pK units) and a second-order effect is induced by substituent perturbation.

Table III reports the fluorescence lifetimes and kinetic parameters of the hydrolytic reaction 1, calculated in the way described for the unsubstituted compound. The lifetime of the 4'- CH_3O derivative is too short to be measured in both neutral and acidic solutions and the calcu-

(11) G. Favaro and G. Beggiato, *Gazz. Chim. Ital.*, **100**, 326 (1970).

(12) D. G. Whitten and M. T. McCall, *J. Amer. Chem. Soc.*, **91**, 5097, (1969).

(13) The equation used is derived by application of stationary state kinetics¹ and does not take into account the effect of transients on reaction rates. The results are, therefore, approximate but still significant because the corrections would be small (see also R. M. Noyes, *Progr. React. Kinet.*, **1**, 129 (1961)).

(14) S. J. Strickler and R. A. Berg, *J. Chem. Phys.*, **37**, 814 (1962).

TABLE III: Fluorescence Lifetimes for Some Neutral and Protonated 4'-Substituted 3-Styrylpyridines and Kinetic Parameters of Equilibrium 1 as Obtained from the Experimental τ_a Values and the Plots of Figure 2 in 90/10 (v/v) Water-Ethanol at Room Temperature

4'-X	τ_a (exptl), nsec	Slope/inter- cept = $k\tau_a$	τ_b , nsec	$\bar{k} \times 10^{-8}$, sec ⁻¹	$\bar{k} \times 10^{-9}$, M ⁻¹ sec ⁻¹
H	5.5	30.0	0.91	2.2	5.5
CH ₃	6.0	33.0	1.70	3.5	5.5
OCH ₃	(1.6) ^a	8.9	(0.31)	(10.0)	(5.5)
Cl	5.3	29.0	0.46	2.2	5.5
Br	3.2	17.5	0.24	3.1	5.5

^a Value obtained from the plot, assuming $\bar{k} = 5.5 \times 10^9 \text{ M}^{-1} \text{ sec}^{-1}$. For comparison, $\tau_a = \phi_a \tau_a^0 = 0.1 \text{ nsec}$.

lated value (from the integrated spectra) cannot be utilized, due to the poor agreement found between the experimental and calculated lifetimes of the other 3-StP's. The parameters reported on Table III for this compound are obtained assuming for \bar{k} the same constant value ($5.5 \times 10^9 \text{ M}^{-1} \text{ sec}^{-1}$) as found for the other 3-StP's. The results indicate that lifetimes of the excited species are the major factor in determining the percentage of equilibrated molecules in the pH range 6-11. At pH ~ 8 the back reaction of eq 1 can be neglected, so the equilibrium percentage depends only on the product $k\tau_b$. As the rate constant for hydrolysis of the base is scarcely influenced by substitution, the base lifetimes appear to determine the extent of equilibration. They are in fact almost in the same ratio as the respective percentages of excited equilibrated molecules in this pH range. Because of the approximations involved in their calculation, the values of τ_b reported in Table III may only be considered as approximate.

The possibility of applying the Hammett equation to the acid-base equilibrium constants in electronically excited states has been tested for certain series of aromatic compounds.^{4b,15} Not very precise correlations were found,

probably due to the great uncertainty in the pK^* values and also to the fact that the substituent constants reflect electronic distribution in the ground state.

Calculated pK^* values for 2- and 4-StP were found to fit better on σ_{\pm} than on σ plots because of the high polarity of the excited substrate.³ Our pK^* values for 4'-substituted 3-StP's also show a satisfactory Hammett correlation if σ_+ for para substituents are used (Table III and Figure 3). The reaction constant ($\rho = 0.7$; $r = 0.948$) is significantly larger than that for the reaction in the ground state ($\rho \sim 0.3$).⁷ The nitro derivative has not been considered, because of the probable nonequivalence of its electronic transitions.¹⁵ Insertion of the 4'-NO₂ derivative in the Hammett plot would lead to a much greater reaction constant (6-7), but to a very poor correlation.

Taking into account that the basic center is distant from, and unconjugated with, the substituted ring, the substituent effect on pK^* of 3-StP's is considerable. This behavior emphasizes the importance of resonance effects and supports the suggestion that ground state σ_m values do not apply in the excited states.^{15,16}

Further evidence of the greater importance of resonance effects in electronically excited molecules is given by the pK^* values obtained from the absorption spectra of *cis*-2-StP's.³ While direct measurements are not possible for *cis*-azastilbenes, due to their lack of fluorescence at room temperature, calculated pK^* values lead to ρ^* even higher than those of *trans* isomers,³ thus indicating a relevant resonance contribution by styryl part of the molecule also in compounds which noticeably deviate from planarity in the ground state.

Acknowledgment. This study was supported by the Consiglio Nazionale delle Ricerche under contract No. 70.00082.03. It is also part of the programs of the "Laboratorio di Fotochimica e Radiazioni di Alta Energia" of the C.N.R. (Bologna).

- (15) H. H. Jaffé and H. L. Jones, *J. Org. Chem.*, **30**, 964 (1965).
 (16) H. E. Zimmerman, *Tetrahedron Suppl.*, **2**, 393 (1963).

Excited State Reactivity of Aza Aromatics. II. Solvent and Protonation Effects on Photoisomerization and Luminescence of Styrylpyridines

G. Bartocci, P. Bortolus, and U. Mazzucato*

Instituto di Chimica Fisica, Università di Perugia, I-06100, Italy (Received August 8, 1972)

Publication costs assisted by the Consiglio Nazionale delle Ricerche (Roma)

The fluorescence and *cis-trans* photoisomerization of the three isomeric 2-, 3-, and 4-styrylpyridines and some 4' derivatives of the 3 isomer, have been investigated in *n*-hexane and in water-alcohol solutions, in the basic and acidic forms. While ϕ_t of the 2 and 4 isomers increases on going from nonpolar to polar solvent and from neutral to acidic solutions, ϕ_t of 3-styrylpyridine shifts in the opposite direction. The reaction and luminescence yields have been compared to extract information on the nature of the excited state responsible. Data on photostationary states, temperature dependence of ϕ_t , fluorescence quantum yields, and lifetimes, as well as a comparison with reaction photosensitized by triplet donors, allow the reaction mechanism to be discussed, also in terms of available information on MO calculations. A relation has been found between the photoreaction yield of 3-styrylpyridines in the pH range 0-14 and acid-base equilibria in the ground and first excited singlet state. A simultaneous singlet and triplet mechanism, with a prevalence of the former, seems to account reasonably for the experimental results. The relative importance of either pathway may depend on the nitrogen position, substituents, solvents, and protonation.

Introduction

Introduction of a nitrogen atom in the ring noticeably affects the photophysical and photochemical behavior of stilbene^{1,2} probably because of the involvement of n, π^* states in the reaction mechanism. There is general agreement that the sensitized isomerization occurs at the triplet level,¹⁻⁴ although the question of the mechanism of isomerization following direct excitation remains open. The similarity between the sensitized and direct photostationary compositions (the latter corrected for different extinction coefficients of the two isomers at the wavelength of direct excitation) seemed to imply the same mechanism for the direct and sensitized processes, at least for 2- and 4-styrylpyridines (StP's) in aprotic solvent.¹ By extension of this result, a comparison of direct and sensitized yields in benzene has shown that the maximum intersystem crossing (ISC) probability should be higher for 3-styrylpyridine (3-StP) compared to its two isomers.³ The behavior of *trans*-3-StP is noteworthy in that, *inter alia*, both fluorescence and photoisomerization quantum yields are higher than the other isomers.^{1,2}

The differences in the photochemical behavior of StP's and stilbene are enhanced in acidic medium.¹ Qualitative observations on photocyclization of *cis* isomers have shown an especially strong effect of protonation in lowering the reaction rate.

The effect of solvent and protonation on the geometrical conversion and fluorescent properties of StP's and some of their derivatives in water-alcohol solutions is now investigated in more detail, with the aim, also, of obtaining information on the excited state responsible for isomerization. The possible relation of photoisomerization of azastilbenes to the acid-base equilibria in the ground⁵ and excited state has already been considered¹ and is now studied on the basis of recently available information on the dissociation constants of styrylpyridinium ions in the first excited singlet state.⁶

Experimental Section

trans- and *cis*-styrylpyridines were prepared for previous research by methods described elsewhere.⁷ The *cis* isomers were purified by distillation under reduced pressure followed by chromatography on alumina. Their purity was checked by gas chromatographic analysis, the only impurity being a small quantity of *trans* isomers which did not exceed 1% (2% for 2-StP).

The *trans* \rightarrow *cis* (ϕ_t) and *cis* \rightarrow *trans* (ϕ_c) quantum yield determinations at low ionic strength ($\mu = 0.01$) were performed in Britton buffers containing 50% ethanol, which is the same medium in which the photosensitized reaction was studied.⁸ For the study of the dependence of ϕ_t and ϕ_r (fluorescence quantum yield) on excited state acid-base equilibrium of 3-StP's, Britton buffers or NaOH solutions of high ionic strength ($\mu = 1$) with 10% ethanol were used due to the necessity of carrying measurements up to pH 14. Ionic strength was in this case buffered with NaCl or Na₂SO₄. The strong quenching effect of chloride ion on the $^1\pi, \pi^*$ state of 3-StPH⁺ helped to magnify the change of ϕ_t as a function of pH (Figure 1). However, the fluorescence-pH curves were obtained buffering the ionic strength with Na₂SO₄, the quenching efficiency of which is negligible.

- (1) (a) P. Bortolus, G. Cauzzo, U. Mazzucato, and G. Galiazzo, *Z. Phys. Chem. (Frankfurt am Main)*, **51**, 264 (1966); **63**, 29 (1969); (b) G. Favaro, F. Masetti, and U. Mazzucato; *ibid.*, **66**, 206 (1969).
- (2) D. G. Whitten and M. T. McCall, *J. Amer. Chem. Soc.*, **91**, 5097 (1969).
- (3) P. Bortolus, G. Favaro and U. Mazzucato, *Mol. Photochem.*, **2**, 311 (1970).
- (4) G. Cauzzo, M. Casagrande, and G. Galiazzo, *Mol. Photochem.*, **3**, 59 (1971).
- (5) G. Cauzzo, G. Galiazzo, U. Mazzucato, and N. Mongiat, *Tetrahedron*, **22**, 589 (1966).
- (6) G. Favaro, U. Mazzucato, and F. Masetti, *J. Phys. Chem.*, **77**, 601 (1973).
- (7) G. Galiazzo, *Gazz. Chim. Ital.*, **95**, 1322 (1965).
- (8) G. Bartocci, thesis for the degree of "dottore in Chimica," Università di Perugia, 1969-1970.

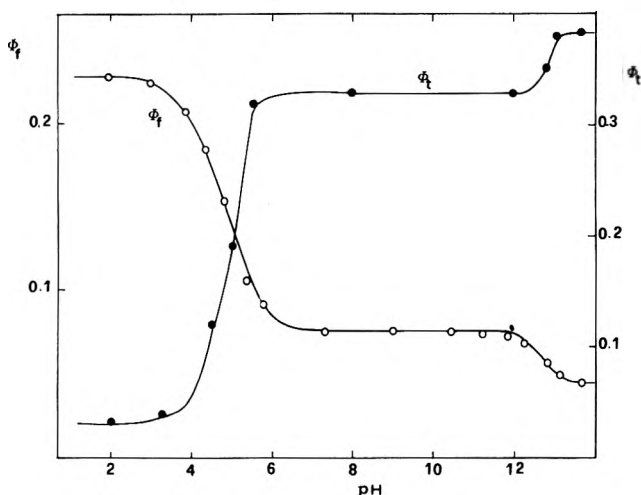


Figure 1. Photoisomerization and fluorescence quantum yields ($\mu = 1$, by NaCl and Na₂SO₄, respectively) of *trans*-3-styrylpyridine as a function of pH in 90/10 (v/v) water-ethanol at room temperature.

Excitation was by 313-nm radiation, isolated from a stabilized Osram HBO 200-W high-pressure mercury lamp by a Hilger-Watts D292 grating monochromator (reciprocal dispersion 66 Å/mm).

Irradiation was performed in deaerated solutions (by bubbling pure nitrogen) in conditions of total absorption of incident light (concentrations were about 2×10^{-4} M for the *trans* isomers and 1×10^{-3} M for the *cis* isomers). After dilution, the extent of isomerization was measured by uv spectrophotometry in the 290–320-nm region, using Unicam SP500/2 single-beam and Optica CF4 double-beam spectrophotometers. Conversions ranged from 2 to 3% for *cis* → *trans* and from 10 to 12% for *trans* → *cis* reaction. Control experiments were run to verify the absence of side reactions; except for two doubtful cases (4'-NO₂- and 4'-I-StP at pH 8) good *cis*-*trans* isosbestic points were obtained for more than 50% conversion. The isomerization quantum yields were corrected for the back reaction, by utilizing the photostationary compositions, and, in the case of the *cis* → *trans* process, for the light absorbed by the *trans* form produced. Values in the table are means of three–five independent experiments with a mean deviation of 1.5–2%. The photostationary compositions were determined approximately in preliminary experiments by irradiation of pure isomers and then reached from both sides by irradiation of solutions of composition near to the photostationary state. Ferrioxalate actinometry was used.⁹

Fluorescence measurements were made with a CGA DC-3000/1 spectrophotofluorimeter. For the ϕ_f determinations (three–four independent experiments; mean deviation 1 and 5% for yields of the order 10^{-1} and 10^{-3} , respectively), the following standards were used: quinine sulfate in 0.1 N H₂SO₄ ($\phi_f = 0.55$) for 3-StPH⁺ and its derivatives; 9,10-diphenylanthracene ($\phi_f = 0.83$) for 2- and 4-StPH⁺; α -naphthylamine ($\phi_f = 0.38$) and α -NPD ($\phi_f = 0.58$) for all StP's in basic form. Except for quinine sulfate, the values of fluorescence quantum yields of standards are referred to cyclohexane solutions.¹⁰ Some ϕ_f were also checked on a Perkin-Elmer MPF-3 spectrofluorimeter with an accessory for spectrum correction which uses Rhodamine B as a quantum counter (for 4'-OCH₃-3-StPH⁺, this was the only method employed). Good agree-

ment was always found between ϕ_f values obtained by the two methods.

Preliminary experiments on ϕ_f at 77°K were carried out in EPA using stilbene ($\phi_f = 0.75$)¹¹ as a standard.

Results

The *cis*-*trans* photoisomerization and fluorescence quantum yields of the three isomeric StP's in neutral and cationic forms are reported in Table I, together with the photostationary compositions. The yields in water-ethanol are a little higher than those previously reported,¹ because of the smaller ionic strength of the solutions and the correction for reversibility.

trans-2- and 4-Styrylpyridines. Both isomers are characterized by very low emission intensity in all media, which accounts for only a small fraction of the absorbed quanta. Only in EPA at liquid nitrogen temperature does ϕ_f increase to somewhat more than 0.6.

While the emission yield remains practically unchanged for 4-StP and increases for 2-StP on going from *n*-hexane to water, the isomerization yield increases for both isomers in polar solvents. No detectable temperature effect on ϕ_t was observed in the range 15–70°. It will be of interest to reach much lower temperatures and investigate this effect in more detail, although the solvent nature does not allow us to explore a wide temperature range below 0°.

Protonation affects isomerization in the same direction as solvent polarity: ϕ_t becomes still larger while ϕ_f decreases for the cationic species. Even in this case, ϕ_t is independent of temperature in the above range.

The α -methyl derivative of 4-StP was found to behave like the unsubstituted compound (at pH 8, $\phi_t = 0.43$, $\phi_c = 0.29$; at pH 2, $\phi_t = 0.51$, $\phi_c = 0.26$).

Lifetimes are too short to be measured (resolution time of our apparatus 1 nsec). Approximate evaluation⁶ from the integrated absorption spectra and emission yields of the basic and acidic forms gives lifetimes of the order of 0.01 nsec for both isomers. The short lifetimes, even for the cations, are confirmed by the negligible quenching of their emission by anions of added salts, such as Cl⁻ and Br⁻.

trans-3-Styrylpyridine. As already noted, this isomer displays a low yield of deactivating radiationless processes in *n*-hexane, its efficiency of isomerization and fluorescence being noticeably greatest in the series. The situation becomes different when the solvent is changed from the hydrocarbon to acetonitrile¹ or to water-ethanol, and from basic to acidic solutions. Both ϕ_t and ϕ_f decrease in the mixed polar solvent; the conversion rate of 3-StP at pH 8 has a 35% increase with temperature between 15 and 70°, while the luminescence yield correspondingly decreases, but at different rate ($|\Delta\phi_t| > |\Delta\phi_f|$ in the same temperature range).

Protonation also affects isomerization in the opposite direction than the two other isomers: ϕ_t becomes still smaller while ϕ_f increases. No temperature effect on ϕ_t was observed for the cationic species in the above range.

The emission lifetimes are longer for this isomer both in neutral and acidic forms ($\tau_a = 5.5$ nsec, $\tau_b \sim 1$ nsec⁶). The longer lifetime is reflected in the fluorescence quenching of 3-StPH⁺ by the counter ion X⁻ of alkali

(9) G. G. Hatchard and C. A. Parker, *Proc. Roy. Soc., Ser. A*, **235**, 518 (1956).

(10) J. B. Birks, "Photophysics of Aromatic Molecules," Wiley, London, 1970, pp 98, 123, 124.

TABLE I: Quantum Yields of Cis-Trans Photoisomerization and Fluorescence (Trans), and Photostationary Compositions of Styrylpyridines in *n*-Hexane and in 50/50 (v/v) Water-Ethanol ($\mu = 0.01$) at pH 2 and 8^a

Isomers	Medium											
	<i>n</i> -Hexane				Water-ethanol (pH 8)				Water-ethanol (pH 2)			
	ϕ_t	ϕ_c	ϕ_r	% cis	ϕ_t	ϕ_c	ϕ_r	% cis	ϕ_t	ϕ_c	ϕ_r	% cis
2-StP	0.23	0.24	0.002	90	0.39	0.35	0.004	90	0.55	0.28	0.003	73
3-StP	0.52	0.22	0.065	90	0.39	0.17	0.042	92	0.27	0.18	0.205	77
4-StP	0.39	0.34	0.003	90	0.44	0.25	0.003	91	0.53	0.25	0.002	76

^a At this alcohol percentage, the acid-base equilibration of the excited 3-StP at pH 8 is practically negligible.

halides, an effect which is negligible for the two other cationic isomers and for all the neutral molecules. This deactivation, which is strongly dependent on the nature of the anion, is under study from a mechanistic point of view in this laboratory.

As a consequence of this quenching, in the experiments at high ionic strength ($\mu = 1$), a large decrease of ϕ_t (of about one order of magnitude with respect to the value measured at $\mu = 0.01$, in the absence of NaCl) was observed in acidic medium when NaCl was used to buffer the ionic strength. The Stern-Volmer plots of ϕ_t and ϕ_r against [NaCl] for 3-StPH⁺ have practically the same slopes ($k_q\tau_a \sim 14 M^{-1}$ in 90/10 (v/v) water-ethanol).

Table II shows the 4'-substituent effect on the fluorescence and isomerization rate of 3-StP. Methyl and methoxy substitution leads to a considerable effect in acidic medium. The latter derivative, in particular, has a very low conversion yield when protonated. This cationic derivative is characterized by a low emission yield and lifetime⁶ and by an emission unquenched by added NaCl. Its ϕ_t increases markedly with temperature (more than one order of magnitude in the range 15–70°). The halogen effect is also interesting; while the 4'-Cl changes the rate little, the 4'-Br substitution leads to a rather faster isomerization. The interpretation of data for the iodine derivative is less clear but in this case a competitive photolysis of the C-I bond may be operative. In any case, the result, in acidic medium, shows a large increase in isomerization rate. The 4'-NO₂ group effect was only investigated at high ionic strength and is described later. As for 2 and 4 isomers, 3-StP and its 4'-derivatives display high ϕ_r (0.6–0.7) in EPA at 77°K, with the exception of the Br (~0.15), I, and NO₂ derivative (<0.01).

Cis to Trans Photoisomerization and Photostationary States. Cis → trans yields are all lower than the corresponding trans → cis ones and always lower for 3-StP than the other isomers. There is no clear trend for the effect of solvent and protonation in this case. In contrast to ϕ_t , ϕ_c is practically constant at different pH values. Here the singlet lifetime is very short, as indicated by the absence of fluorescence; the importance of solvation may consequently be reduced. As for the sum $\phi_t + \phi_r$, ϕ_c is also far from unity for both the free base and its conjugate acid, indicating important radiationless deactivations.

Photostationary state composition at 313 nm shifts toward the trans form in acid, in agreement with a marked decrease of the extinction coefficient ratio ϵ_t/ϵ_c in this medium.

Photoisomerization and Acid-Base Equilibria. A detailed comparison between the photoreaction and the fluorescence yields, both as a function of pH, is revealing, and should allow conclusions to be drawn concerning in-

TABLE II: Photoisomerization and Fluorescence Quantum Yields of *trans*-4'-X-3-Styrylpyridines and Their Conjugate Acids in 50/50 (v/v) Water-Ethanol at Low Ionic Strength ($\mu = 0.01$)

4'-X	pH 8		pH 2	
	ϕ_t	ϕ_r	ϕ_t	ϕ_r
H	0.39	0.042	0.27	0.21
CH ₃	0.40	0.034	0.20	0.22
OCH ₃	0.45	0.018	~0.0006	0.01 ₄
Cl	0.43	0.071	0.26	0.28
Br	0.48	0.048	0.37	0.20
I	0.34	0.005	0.42	0.03 ₅

volvement of the acid-base equilibrium in the excited state, particularly for 3-StP's the pK* values of which have recently been determined by fluorimetric titration.⁶ This comparison, necessarily carried out up to pH ~14 at a higher constant ionic strength ($\mu = 1$), could supply information on the role played by the excited singlet state in the isomerization. The emission maximum characteristic of the protonated 3-StPH⁺ at 460 nm is still present, although much reduced in intensity, in a rather large pH range over the ground state pK and disappears only in alkaline solution (pK* = 12.5). The fluorescence *vs.* pH plot runs parallel to that of absorption *vs.* pH in the region of the ground state pK (4.7), but displays a second inflection at higher pH values, which indicates a partial hydrolytic equilibrium of 3-StP* with the proton.⁶ The proton donor strength of water is weak, but still effective enough to protonate a fraction of molecules when the alcohol percentage is low. The weaker band at 360 nm, characteristic of the free base, behaves in the opposite manner. From the intensity ratio of the two emission bands the fraction of excited molecules equilibrated with the proton is 17% at 10% ethanol.⁶

If ϕ_t is now plotted against pH at constant ionic strength, two points of inflection are again observed, as for the fluorescence *vs.* pH curves. In particular, the trend of the photoreaction yield is opposite to that of the overall fluorescence yield (Figure 1). The ϕ_t for 3-StP increases from 0.03₁ at pH 2 to 0.33₁ at pH 8 (where the free base is 100% in the ground and 83% in the excited state) and again to 0.38₄ at pH 14 (100% of free base in both ground and excited state). The experimental reaction yield at a pH near 8, where only the free base is present in the ground state, is nearly the same as that calculated from the limiting yields for 3-StP and 3-StPH⁺, taking into account the percentage of equilibrated molecules

$$\phi_{t, \text{pH } 8} = 0.17\phi_{t, \text{pH } 2} + 0.83\phi_{t, \text{pH } 14} = 0.32_5$$

Similar behavior was observed for some 4' derivatives.

TABLE III: Photoisomerization Quantum Yields (Uncorrected for Photostationary State) of *trans*-3-Styrylpyridine and Some 4'-Substituted Derivatives in 90/10 (v/v) Water-Ethanol at Different pH's ($\mu = 1$, by NaCl)^a

4'-X	ϕ_t			
	pH 0	pH 2	pH 8	pH 14
H		0.03	0.33 (17)	0.38 ₄
CH ₃		0.04 ₅	0.32 ₆ (34)	0.37
OCH ₃		~0.0006	0.29 (20)	0.42
Cl		0.02	0.38 ₆ (9)	0.44
NO ₂	0.37	0.33	0.20 ₄	0.20 ₄ (pH 10)

^a Percentages of excited acidic molecules at pH 8 are reported in parentheses.

Table III shows their ϕ_t values at low and high pH, where they are present in solution as 100% acidic and 100% basic forms, respectively, and at the intermediate pH 8, where a certain amount of excited acid was detected by fluorimetric measurements. A change of ϕ_t was always found on passing from lower to higher pH's of the corresponding pK^* values. Also for these derivatives the yields at intermediate pH are approximately equal to those calculated from the limiting yields and the measured equilibrium percentage.⁶

We have investigated in more detail the 4'-NO₂ derivative, for which a base-weakening effect on excitation was observed.⁶ While for electron-donating substituents the yield increases, if any, with pH, for 4'-NO₂ derivative an opposite trend was observed (see Figure 2). The low fluorescence efficiency, which is a well-known characteristic of aromatic nitro derivatives (for the corresponding hydrocarbon, 4-nitrostilbene, no detectable emission has been found¹¹), and the blue shift with polarity and protonation, could indicate a significant n, π^* character of the fluorescent state.⁶ It may also be noted that in this case the cation displays less intense emission than the neutral molecule.

Discussion

The results of Table I indicate an important role of the medium and nitrogen position in affecting ϕ_t and ϕ_f , possibly through a change of the relative position of the excited energy levels, so as to favor the geometrical conversion for 2- and 4-StP in polar and acidic solutions, but in the opposite direction for 3-StP. The 2 and 4 isomers display in all media fluorescence yields too small to compete with isomerization. The quite larger effect of polar solvent and protonation on the photoreaction could mean that isomerization originates from a different nonemitting excited state. The fluorescence of 3-StP is one to two orders of magnitude more intense, so in this case, possible relations (coupling or competition) between photoreaction and emission appear more significant. The reaction yields in the tables can be discussed in term of two different mechanisms, which consider the isomerization as taking place in the singlet or in the triplet manifold, respectively. Correspondingly, activated processes in the reaction pathway may be variously assigned to ISC or to conversion to a twisted form in the singlet or triplet states.

As the sensitized isomerization at the triplet level is characterized by rather high yields for all three isomers,²⁻⁴ both as free bases and as their conjugate acids,⁸ it may be inferred that radiative or radiationless deactivation at

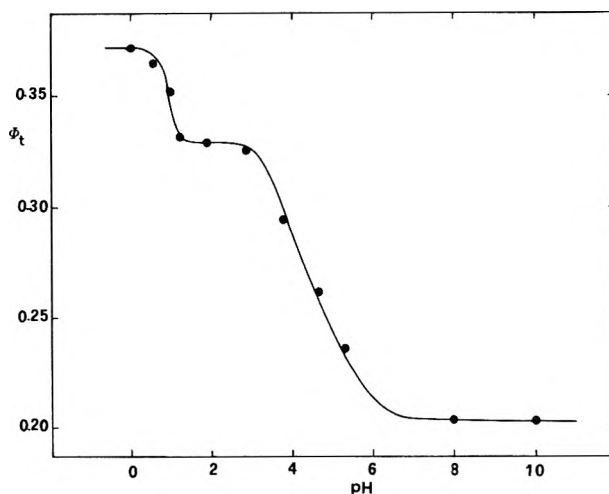


Figure 2. Photoisomerization quantum yield of *trans*-4'-nitro-3-styrylpyridine as a function of pH ($\mu = 1$, by NaCl) in 90/10 (v/v) water-ethanol at room temperature.

the singlet levels is the factor which mainly determines the photoreactivity of azastilbenes on direct excitation.

Before considering in detail the evidence in favor of the singlet or triplet mechanism, it seems thus interesting to examine the possible role of deactivating processes in the singlet manifold. Molecular orbital calculations have suggested the existence of low-lying non-fluorescent and non-isomerizable n, π^* singlets.¹² The weak n, π^* transitions could be masked by the much more intense π, π^* ones, to which the long-wavelength absorption bands are assigned. The fluorescence emission of the *trans* isomers (with the exception of 4'-NO₂-3-StP) shifts to longer wavelengths with increasing solvent polarity and with protonation, indicating a π, π^* nature also for their lowest emitting singlets. These hidden n, π^* states should be very easily available through internal conversion from $^1\pi, \pi^*$ for the 2 and 4 isomers, while the conversion should be improbable for the 3 isomer, because the heteroatom is located at a near node in the π and π^* MO.¹³ This theoretical prediction may be very important in explaining the different photochemical and photophysical behavior of the 3 isomer compared to the other two isomers. In particular, more probable intercombinational transitions are expected for the 2 and 4 isomers which do not possess nodes in the position occupied by the heteroatom in either the π or π^* MO.

From these n, π^* states, it is possible to have either internal conversion to the ground state or to a twisted $^1\pi, \pi^*$ (activated step), either ISC to a triplet level, probably $^3\pi, \pi^*$. In fact, according to the El-Sayed selection rules for radiationless transitions of heteroaromatics,¹⁴ efficient ISC can take place when it is accompanied by a change of configuration ($^1\pi, \pi^* \rightarrow ^3n, \pi^*$ or $^1\pi, \pi^* \rightarrow ^1n, \pi^* \rightarrow ^3\pi, \pi^*$, depending on the relative position of these levels, which can be influenced by solvents, nitrogen position, and substituents).

To account for the experimental results, we try now to

- (11) D. Gegiou, K. A. Muszkat, and E. Fischer, *J. Amer. Chem. Soc.*, **90**, 3907 (1968).
- (12) L. Pedersen, D. G. Whitten, and M. T. McCall, *Chem. Phys. Lett.*, **3**, 569 (1969).
- (13) Y. J. Lee, D. G. Whitten, and L. Pedersen, *J. Amer. Chem. Soc.*, **93**, 6330 (1971).
- (14) M. A. El-Sayed, *J. Chem. Phys.*, **38**, 2834 (1963); S. K. Lower and M. A. El-Sayed, *Chem. Rev.*, **66**, 199 (1966).

accommodate them in turn to the singlet and triplet mechanism.

Singlet Mechanism. It has been postulated, on the basis of MO calculations and of results on quenching by azulene of the direct and sensitized isomerization of other azastilbenes,¹³ that 2- and 4-StP isomerize *via* internal conversion to a $^1n,\pi^*$ state and subsequent activated conversion to a twisted $^1\pi,\pi^*$ state which decays with isomerization. The hypothesis of a fast deactivation of the fluorescent state is in agreement with the very low emission efficiency in both nonpolar and polar solvents. The latter increases the energy of $^1n,\pi^*$ levels, thus lowering the energy barrier to the twisted $^1\pi,\pi^*$ state, favoring isomerization. The absence of a temperature effect on ϕ_t in the range investigated could be due to a too low activation energy which should become detectable only at lower temperatures.

On the other hand, the internal conversion to $^1n,\pi^*$ should take place at a much reduced rate in 3-StP because of the near node at the 3 position. This could explain both the higher rate of isomerization and fluorescence for this isomer, assuming that the chemical process occurs in *n*-hexane at the fluorescent singlet by-passing the $^1n,\pi^*$ state. Polar solvent may reduce the energy of $^1\pi,\pi^*$ and increase that of $^1n,\pi^*$ level, so the internal conversion to $^1n,\pi^*$ could become less forbidden for reasons of energy, leading to a decrease of both chemical and physical photoprocesses. There is a positive temperature effect on ϕ_t , higher than the negative one on ϕ_f , because the photoreaction at the twisted $^1\pi,\pi^*$ state can originate from both $^1\pi,\pi^*$ and $^1n,\pi^*$ levels.

The $^1\pi,\pi^*$ state remains the only precursor of isomerization in the unsubstituted protonated molecules. Deactivation by internal conversion to the ground state is now much reduced in the 2 and 4 isomers which may isomerize in the twisted $^1\pi,\pi^*$ state at a faster rate, in competition with fluorescence and mainly with ISC. Unfortunately this scheme does not convincingly explain why their fluorescence remains so low, even more than for the neutral molecules. Deactivating processes remain practically the same for the 3 isomer which now isomerizes with a reduced yield compensated by the increase of fluorescence. That these two processes of 3-StPH⁺ originate in the same excited state may be shown by their competition at the various pH's and by the same k_q obtained in the quenching experiments by NaCl in acidic solutions. On the other hand, this behavior might also imply that quenching of the fluorescent state reduces ISC and isomerization at the $^3\pi,\pi^*$ state, and so cannot be taken as a proof for the singlet scheme. The quenching experiments should allow these two alternatives to be distinguished, if the triplet 3-StPH⁺ were also quenched. However, the Cl⁻ ions have no effect both on the energy transfer (k_q) from biacetyl to 3-StPH⁺ and on the photosensitized ϕ_t of the same compound. These results confirm that only $^1\pi,\pi^*$ is quenched.

The effect of methyl, chlorine, and methoxy groups on the photochemical behavior of 3-StP can be satisfactorily explained by the singlet mechanism. The drop in ϕ_t for the protonated methoxy derivative, in which the combined effect of donor (-OCH₃) and acceptor (-N=) groups probably increases the dipole moment of the excited molecule leading to strongly solvent-dependent energy levels, is attributed to a predominance of internal conversion processes, probably through n,π^* states of the substituent, in analogy with 4-nitro-4'-methoxy stilbene in polar sol-

vent.¹¹ The large increase in ϕ_t with temperature for this derivative indicates a high endothermic path to the isomerizable state in the protonated molecule.

For the nitro derivative, important radiationless decay occurs, mainly in basic solution, probably because n,π^* levels become more accessible than in 3-StP or because they are provided by the substituent group. In acid, ϕ_t increases for this compound and a marked quenching effect by oxygen was found, which is not easily explained by this mechanism.

This scheme fails to account for the effect of heavy atoms also.

Triplet Mechanism. Intersystem crossing to the triplet manifold could also be a pathway for isomerization. For the 2 and 4 isomers, the excited molecules rapidly reach the $^1n,\pi^*$ state, then some cross to an almost isoenergetic $^3\pi,\pi^*$, a process which should be favored in polar solvents, where it could become exothermic. The absence of possibly deactivating $^1n,\pi^*$ states in acidic solutions also agrees with the increase of ϕ_t accompanied by a slight decrease of fluorescence, which competes with ISC.

For 3-StP, ISC should start from $^1\pi,\pi^*$. The high values for both ϕ_t and ϕ_f in *n*-hexane could again be explained by the inaccessibility of the deactivating $^1n,\pi^*$ state for this isomer. The effect of polar solvent can be interpreted as for the singlet mechanism, implying a partial deactivating role of the $^1n,\pi^*$ but assuming here an activated ISC, directly from $^1\pi,\pi^*$ or through n,π^* states. Protonation greatly increases the energy of $^3n,\pi^*$ state and the ISC to $^3\pi,\pi^*$ remains the only path for isomerization in this scheme; the decrease in ϕ_t and increase in ϕ_f are so justified. The relatively longer fluorescence lifetime observed for 3-StPH⁺ is in agreement with a smaller ISC yield and the consequent lower isomerization yield of this cationic isomer. It is also to be noted that preliminary quenching experiments of the photoreaction of 3-StPH⁺ by Br⁻ seem to indicate a smaller slope than in the fluorescence Stern-Volmer plots.

The triplet mechanism accounts for the results obtained with the 4'-substituted 3-StP's likewise for the unsubstituted compound. In addition, the 4' halogen substitution (with the exception of 4'-I at pH 8)¹⁵ has an effect which is good evidence for a process going through the triplet manifold. In fact, it can reasonably be ascribed to a heavy-atom enhanced ISC. Moreover, the oxygen effect on ϕ_t of the 4'-NO₂ derivative in acidic solution could also indicate an involvement of the triplet path.

Using biacetyl,³ benzophenone,² and anthraquinone⁴ as triplet donors and assuming that the direct isomerization proceeds by way of triplets, 3-StP has been found to have the highest, and 2-StP the lowest, value of the calculated maximum ϕ_{ISC} in benzene. It is remarkable that the situation is reversed in water-alcohol solutions, where ϕ_{ISC} of 3-StP is about 0.6 and decreases again to about 0.5 in acid, while it reaches almost unity for the other isomers.⁸ This change of ISC with medium is unusual and could be justified only by admitting a solvent-dependent energy barrier. This seems to be confirmed by the luminescence yields at liquid nitrogen temperature, which also have high values for those isomers displaying very low luminescence in fluid solutions.

Conclusions

It is difficult to accommodate all the experimental results in a unique mechanistic scheme, because the presence of

the heteroatom complicates the situation with respect to the hydrocarbon analog. Neither of the two mechanisms examined, which consider isomerization to take place in only one manifold, singlet or triplet, is completely satisfactory. On the other hand, the dispute about the stilbene photoisomerization occurring in one or the other manifold is still not completely resolved;¹⁶ so it is not surprising that recently available evidence for azastilbenes in favor of the triplet^{1,2,17} or the singlet¹³ mechanism appears to be far from a definite conclusion. In particular, it seems that conclusions reached for a certain azastilbene cannot be generalized to other isomeric compounds, since the nitrogen position can force the pathway in one sense or the other.

Although the assumption of two concurrent mechanisms seems the best compromise to accommodate the available experimental results, the evidence in favor of the singlet mechanism outweighs that for the triplet, especially in the case of 3-StP. Important arguments indicating that the same state is responsible for both fluorescence and isomerization of 3-StP, are (1) the coupling between ϕ_t and ϕ_f on going from *n*-hexane to water and (2) the same percentage of molecules which fluoresce in acidic form at pH 8 as obtained from the ϕ_f vs. pH curve and calculated from the ϕ_t vs. pH curve. This also implies that the protonation of the excited base by water ($k \approx 10^8 \text{ sec}^{-1}$)⁶ is competitive with both emission and photoreaction. However, the singlet mechanism is not the only one operative, at least for the halogen-substituted 3-StP's, as demonstrated by the results obtained in fluid solutions as well as by the low-temperature ϕ_f 's.

Turning to the 2 and 4 isomers, some support for a triplet mechanism comes from (1) the relation between direct and sensitized photostationary state ratios found in non-polar solvent, using high-energy triplet donors^{1,18} and, but less important; (2) the low fluorescence lifetimes and

quantum yields for these isomers in acidic form, when the deactivating role of $^1n, \pi^*$ levels should be no longer operative; (3) the result of MO calculations for these two isomers, which predicts a higher rate of ISC for both neutral and protonated forms.¹⁹ It appears, however, that most of these arguments in favor of the triplet mechanism for 2- and 4-StP are rather weak and that, also for these isomers, a singlet mechanism accounts better for the experimental results, considering also that the direct ϕ_t for 2-StPH⁺ is a little higher than that sensitized by biacetyl.⁸

It is concluded, therefore, that, although both singlet and triplet states may be involved in the direct trans-cis photoisomerization of azastilbenes, the singlet mechanism prevails for the unsubstituted StP's. The effect of the medium and of substituents enhancing ISC efficiency may alter the mechanism changing the relative importance of the two paths. Further work is in progress on the temperature effects and on theoretical calculations.

Acknowledgment. This study was supported by the Consiglio Nazionale delle Ricerche under contract No. 70.00082.03. It is also part of the programs of the "Laboratorio di Fotochimica e Radiazioni d'Alta Energia" of the C.N.R. (Bologna). The authors would like to acknowledge the assistance of V. Rossetto in the determination of fluorescence yields.

- (15) The low ϕ_t for 4'-1-3-StP at pH 8 may not be significant, both because of the above-mentioned possibility of photolysis of the C-I bond and because the triplet deactivation may be important for this derivative. Unfortunately, we cannot compare ϕ_t for direct and sensitized reaction because of the insufficient solubility for sensitized experiments.
- (16) For a review of stilbene photoisomerization, see J. Sattiel *et al.* *Org. Photochem.*, in press.
- (17) D. G. Whitten and Y. J. Lee, *J. Amer. Chem. Soc.*, **92**, 415 (1970).
- (18) The relationship is not easy to establish in aqueous ethanol,⁸ mainly because of low solubility of the most commonly used high-energy triplet donors in this medium.
- (19) Unpublished results; see also ref 1.

An Electron Spin Resonance Study of Nitrosamine Anion Radicals

Gerald R. Stevenson,* Jesus Gilberto Concepción, and Jorge Castillo

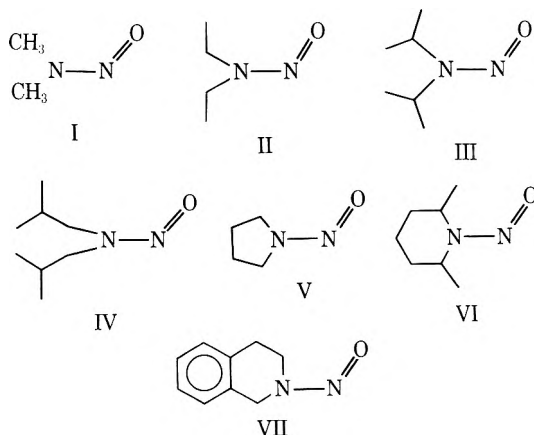
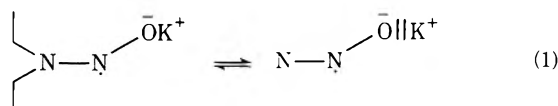
Chemistry Department, University of Puerto Rico, Rio Piedras, Puerto Rico 00931 (Received September 1, 1972)

Publication costs assisted by the University of Puerto Rico

The anion radicals of a series of nitrosamines have been generated by alkali metal reduction. In tetrahydrofuran and in a mixture of tetrahydrofuran and hexamethylphosphoramide three different ion pairs were observed simultaneously in solution. For all of the nitrosamine anion radicals studied, the majority of the spin density was found on the nitroso nitrogen, and this spin density increases when the N-N bond is twisted by steric interaction of the alkyl groups with the oxygen atom. Low-temperature esr spectra of the nitrosamine anion radical solutions exhibited a single broad line superimposed upon the spectrum of the monomer radical. This single line is attributed to a "living" polymer produced from the anionic polymerization of the nitrosamine monomer anion radicals.

Much of the recent interest in the chemistry of nitrosamines can be attributed to the fact that these compounds have been characterized as powerful carcinogens that occur in tobacco smoke and may be formed in the human stomach from the interaction of nitrites, used as food preservative, with the natural amines in the body.¹

In a preliminary communication we reported the reduction of *N*-methyl-*N*-nitrosoaniline, *N*-nitrosodiisopropylamine, and *N*-nitrosodiethylamine in 1,2-dimethoxyethane (DME) and tetrahydrofuran (THF).² For the case of *N*-nitrosodiethylamine reduced by potassium metal in DME, two different ion pairs of the nitrosamine anion radical were found to exist simultaneously in solution. The two ion pairs were proposed to be the tight ion pair and the solvent separated ion pair as shown in equation 1. We now propose a number of *N*-nitrosamine anion radicals including those from I-VII together with some of the solution equilibria in which these anion radicals are involved.



Experimental Section

The *N*-nitrosamines were prepared by the method described by Vogel.³ THF, DME, and hexamethylphosphoramide (HMPA) were distilled directly into the reaction vessel from the solvated electron under high vacuum (10^{-4} mm pressure).

Solutions of the *N*-nitrosamines (10^{-2} – 10^{-3} M) were shaken on an alkali metal mirror to yield the yellow-colored anion radical solutions.

The esr spectra were recorded on an X-band Varian E-3 esr spectrometer equipped with a Varian V-4557 temperature controller.

Results

Under low-resolution conditions (high modulation amplitude) all of the nitrosamine anion radicals, except for those of I and VI, gave esr patterns of nine lines due to two nonequivalent nitrogens. Upon high resolution more lines were observed. These extra lines are interpreted in terms of ion pairing. None of the nitrosamine anion radicals were stable enough in pure HMPA to afford esr spectra. A stable anion radical solution of *N*-nitrosodimethylamine could not be generated under any solvent metal conditions.

The experimental s orbital spin densities were determined from spectral data using the standard equation $\rho_i = A_N/510$, where $A_N = 12.6$ and 2.4 G (see Table I). Calculated s orbital spin densities obtained using an INDO treatment show good agreement with the experimental values. Experimental π -electron spin densities are also shown in Table I. The results show that the odd electron resides predominantly on the nitroso nitrogen.

Diethyl-N-nitrosamine (II). The system II-DME-K upon esr analysis yields an eleven-line pattern apparently resulting from the expected nine-line pattern, but with the end lines split (Figure 1).

These results can be nicely interpreted in terms of two different radical anions in solution (α and β), both having identical g values, but β having slightly larger coupling constants for both nitrogens (Table II). This results in the $m = 0, 0$ lines superimposing, thus yielding a sharp center line. However, due to the small differences in the coupling constants, the $m = 0 \pm 1$ lines do not exactly overlap. The result is that these lines become broadened and less intense. The coupling constants differ by less than the line width. The large nitrogen coupling constants also differ by less than the line width, which results in slightly broader $m = \pm 1, 0$ lines. Since the β anion radical has the

- (1) (a) M. F. Argus, J. C. Arcos, A. Alam, and J. H. Mathison, *J. Med. Chem.*, **7**, 460 (1964); (b) *Chem. Eng. News*, **49** No. 50, 15 (1971).
- (2) G. R. Stevenson and C. J. Colón, *J. Phys. Chem.*, **75**, 2704 (1971).
- (3) A. I. Vogel, "Practical Organic Chemistry," 3rd ed., Wiley, New York, N. Y., p 426.

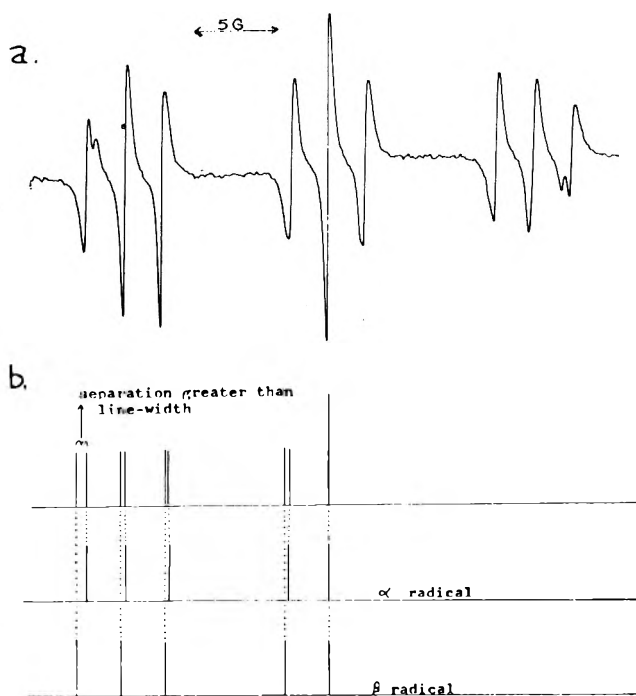
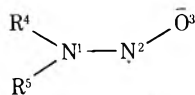


Figure 1. ESR spectrum (upper tracing) of II reduced by potassium in DME and recorded at room temperature. The line width of the center line is 0.28 G. The high-field lines are broader than the low-field lines due to g tensor anisotropy. The reduction in THF gives a similar spectrum, but with less obvious separation of the end lines. Lower tracing shows stick diagram for the low-field half of radicals α and β .

TABLE I: Calculated and Experimental Spin Densities



Position	Calculated s orbital spin density	Experimental s orbital spin density	Experimental π -electron spin density
1	+0.0002	0.0047	0.16
2	+0.0210	0.0247	0.84
3	+0.0067	0.0000	0.00
4	-0.0051		
5	-0.0030		

larger coupling constants for both nitrogens, the differences are additive in the end lines, and the resulting difference in line positions becomes slightly larger than the line width. The coupling constants for the β radical are 12.60 and 2.40 G. Those for the α radical are 12.45 and 2.23 G.

As the temperature is lowered a third radical appears. This new radical exhibits only a single broad line which narrows as the temperature is lowered (see Figure 2). At about -70° only the single broad line can be observed. The line width is 15 G.

When II is reduced by potassium metal in a 1:1 mixture of HMPA and THF, the resulting ESR spectrum consists of 17 lines. This spectrum can be interpreted in terms of three radicals which are shown in eq 2, with the same g value, but with different coupling constants. The three radicals in this case and the two radicals exhibited for the system II-THF-K can result from either different

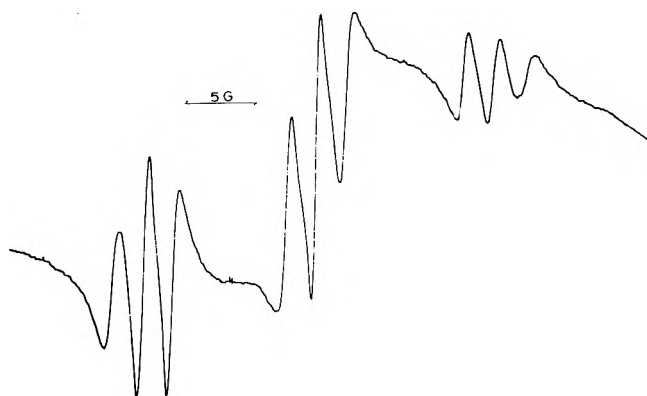
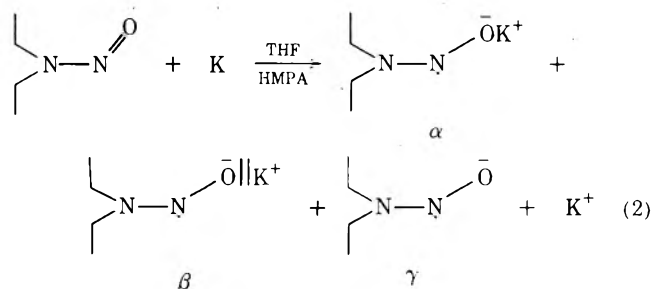


Figure 2. ESR spectrum of the system II-THF-K at -20° .

TABLE II: Coupling Constants for Nitrosamine Anion Radicals at Room Temperature

System	$A_{N(\text{nitroso})}$	$A_{N(\text{alkalated})}$	Ion pair
II-THF-K	12.56 ± 0.05	2.26 ± 0.02	β
	12.5 ± 0.05	2.1 ± 0.02	α
	12.4	1.8	β
II-THF:HMPA-K	12.56 ± 0.05	2.29 ± 0.02	γ
	12.1	1.7	α
	12.9	2.8	β
III-THF-K	13.0	3.1	γ
	12.8	2.3	α
	12.9	2.54 ± 0.02	β
IV-THF-K	12.7	2.7	α
V-THF-K	12.8	1.29 ± 0.02	β
VI-THF-K	12.9		γ

geometrical isomers or from different ion pairs. If the two or three radicals were due to a hindered internal rotation as observed by McKinney and Geske⁴ or some other intra-



molecular process, an increase in the temperature should time average the two spectra. Experimentally this is not the case for at $+60^\circ$ no coalescing of the lines is observed. In fact the lines narrow as the temperature increases and better separation of the lines due to the different radicals is observed. At $+60^\circ$ the line width is 0.19 G and at $+25^\circ$ the line width is 0.28 G. This leads us to believe that for both systems the different anion radicals seen simultaneously are due to different ion pairs, a tight ion pair (α), a loose ion pair (β), and an essentially free ion (γ). Table II gives the coupling constants for α , β , and γ (Figure 3).

N-Nitrosodiisopropylamine (III). The III-THF-K system exhibits 17 lines at room temperature just as for the

(4) T. M. McKinney and D. H. Geske, *J. Chem. Phys.*, **44**, 2277 (1966).

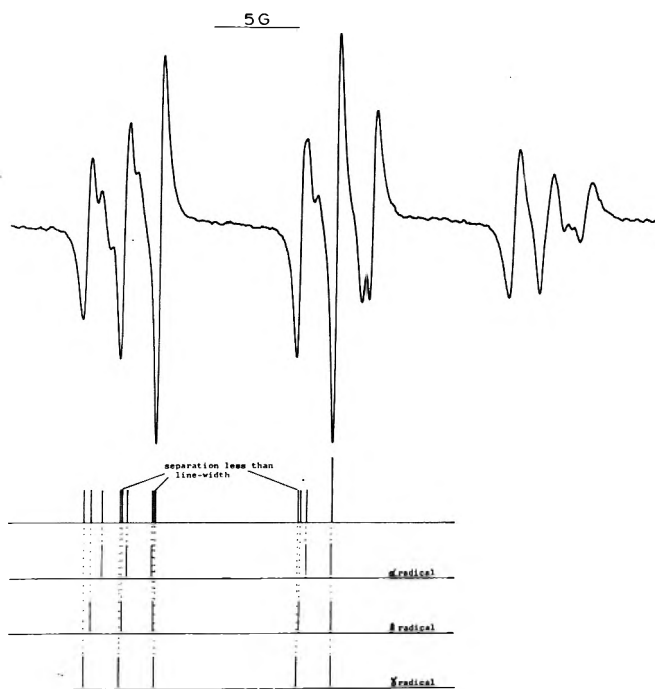


Figure 3. ESR spectrum (upper tracing) of II reduced by potassium in THF:HMPA and recorded at room temperature. The line width of the center line is 0.27 G. Lower tracing shows stick diagram for the low-field half of radicals α , β , and γ .

system II-THF:HMPA-K. At -40° the spectrum consists of nine equally intense hyperfine lines due to two nonequivalent nitrogens. Only a single broad line can be observed at -80° . For the system III-THF-Cs the spectrum consists of 36 lines due to $A_N = 12.70$ G, $A_N = 2.73$ G, and $A_{Cs} = 0.89$ G. When III is reduced in THF by Na an uninterpretable complex esr signal results with obvious metal splitting.

N-Nitrosodiisobutylamine (IV). The esr spectrum of IV yields nine lines of about equal intensity at room temperature. Only the $m = -1, -1$ line has a slightly lower intensity. At -40° only a single broad line is observed.

N-Nitrosopyrrolidine (V). At room temperature the system V-THF-K gives triplets of triplets superimposed upon a single broad line. The coupling constants are shown in Table II. At 20° only a single broad line can be observed upon esr analysis of this system. The anion radical of V is too short lived in a mixture of THF and HMPA to observe an esr signal.

N-Nitroso-cis-2,6-dimethylpiperidine (VI). As shown in Table II, the anion radical of VI gives an esr spectrum resulting from two nonequivalent nitrogens, but the alkylated nitrogen gives a much smaller hyperfine splitting (1.29 G) than all of the other nitrosamine anion radicals (Table II).

1,2,3,4-Tetrahydroisoquinoline-N-nitrosamine (VII). All methods of reduction of this compound lead to solutions that yield very complex uninterpretable esr spectra. This is probably due to the fact that there are two possible rotomers of this anion radical to add further complexity to the already existing ion pairs.

Discussion

The ion pairing interpretation of the three radicals obtained for the II-THF:HMPA-K system is supported by the fact that sodium reduction of II leads to metal split-

ting in THF. Three different ion pairs have been previously observed simultaneously for hydrocarbon anion radicals by Hirota⁵ and more recently by Allendoerfer and Papez.⁶

All of the nitrosamine anion radicals gave a single broad esr line superimposed upon the spectrum for the monomer anion radical at low temperature. This broad line is reminiscent of the single broad line obtained for living polymers produced during anionic polymerization.⁷⁻⁹ Since lowering the temperature increases the polymer concentration at the expense of the monomer, and raising the temperature diminishes the concentration of the polymer radical with a subsequent increase in the monomer anion radical concentration, the enthalpy of the reaction forming the living polymer from the monomer anion radical must be less than zero. This temperature effect is completely reversible for the compounds studied except for pyrrolidine. The nine-line esr signal from the *N*-nitrosopyrrolidine anion radical reduces to a single line at low temperature, but upon warming the signal irreversibly disappears. The apparent narrowing of the esr lines upon increasing the temperature is due to the disappearance of the living polymer and the decreasing of the dielectric constant of the solvent. This latter effect affords better separation of the different ion pairs.

The temperature region, where the ion pairs can be observed simultaneously, is very small. For this reason, it is impossible to obtain esr temperature data for the various ion pairs. Over the range available (about 20°) the coupling constants are invariant with temperature.

All attempts to reduce *N*-nitrosodimethylamine to its anion radical resulted in the immediate formation of a polymeric precipitate, which can be seen forming on the metal surface. The anion radical of *N*-nitrosopyrrolidine is also very unstable toward anionic polymerization. At room temperature the monomeric anion radical could be observed by esr, but a lowering of the temperature to 20° led to the observation of just the single esr line. The nitrosamine anion radicals tend toward anionic polymerization in the order $I > V > II > IV > III$. Further, the temperature at which the single line becomes predominant follows the same order. We notice that the order shown is the same order that one would write for the acidity of the α protons. The acidity of the α protons of V is greater than those of II due to the presence of the small five-member ring. If steric interaction were the only consideration in the polymerization, IV would be slower to polymerize than III. Just the opposite is observed.

The anion radical of VII exhibits a coupling constant for the alkylated nitrogen of only about half of the magnitude of that for the other nitrosamine anion radicals (1.29 G). *cis*-1,3-Dimethylcyclohexane must assume the diequatorial position for the methyl groups due to the steric interaction of the methyl groups when they are in the diaxial position.¹⁰ The anion radical of VI assumes the configuration shown below in order to maintain the methyl groups in the diequatorial position. However, this introduces a steric interaction between the oxygen and one of the

(5) N. Hirota, *J. Phys. Chem.*, **71**, 127 (1967).

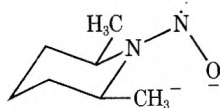
(6) R. D. Allendoerfer and R. J. Papez, *J. Phys. Chem.*, **76**, 1012 (1972).

(7) F. J. Smentowski and G. R. Stevenson, *J. Phys. Chem.*, **74**, 2525 (1970).

(8) K. Hirota and K. Kiwata, *J. Polym. Sci.*, **60**, S52 (1962).

(9) H. P. Leftin and W. K. Hall, *J. Phys. Chem.*, **64**, 382 (1960).

(10) J. B. Hendrichson, D. J. Cram, and G. S. Hammond, "Organic Chemistry," McGraw-Hill, New York, N. Y., 1970, p 214.



methyl groups. This interaction twists the N-O group out of the plane of the N-N bond. This has the effect of increasing the nitroso nitrogen coupling constant and decreasing that for the alkylated nitrogen. A good analogy to this effect lies with the anion radicals of di-ortho-substituted nitrobenzenes. Both calculation and experiment show that for hindered nitrobenzene anion radicals the ni-

trogen coupling constant increases and the ring proton coupling constants decrease as the NO₂ group is twisted by steric interaction from the plane of the ring.^{11,12}

Acknowledgments. The authors are indebted to the Research Corporation for the financial support of this work. We also wish to thank Dr. Carlos Colón for helpful discussion. We are grateful to Loctite of Puerto Rico for the financial support of G. Concepción.

- (11) P. H. Rieger and G. K. Fraenkel, *J. Chem. Phys.*, **39**, 609 (1961).
 (12) D. H. Geske, J. L. Ragle, M. A. Bambenek, and A. L. Balch, *J. Amer. Chem. Soc.*, **86**, 987 (1964).

Reduction of Mercuric Chloride by Hydrated Electrons and Reducing Radicals in Aqueous Solutions. Formation and Reactions of HgCl¹

N. B. Nazhat and K. -D. Asmus*

Hahn-Meitner-Institut für Kernforschung, Berlin GmbH, Sektor Strahlenchemie, 1 Berlin 39, West Germany
 (Received September 28, 1972)

Publication costs assisted by Hahn-Meitner-Institut für Kernforschung Berlin GmbH

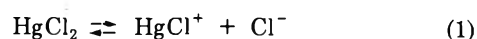
The reduction of HgCl₂ to Hg₂Cl₂ in aqueous solutions has been investigated by optical absorption and conductivity pulse radiolysis. The first step is a dissociative electron capture yielding Cl⁻ and HgCl. The following rate constants were obtained: $k(e_{aq}^- + HgCl_2) = (4.0 \pm 0.3) \times 10^{10} M^{-1} sec^{-1}$; $k(H \cdot + HgCl_2) = (1.0 \pm 0.5) \times 10^{10} M^{-1} sec^{-1}$; $k((CH_3)_2COH + HgCl_2) = (2.0 \pm 0.2) \times 10^9 M^{-1} sec^{-1}$. HgCl absorbs in the uv with absorption maxima at 330 ($\epsilon_{330} 2.3 \times 10^3 M^{-1} cm^{-1}$) and 245 nm ($\epsilon_{245} 7.5 \times 10^3 M^{-1} cm^{-1}$). HgCl dimerizes to Hg₂Cl₂ with $2k = (8.0 \pm 0.5) \times 10^9 M^{-1} sec^{-1}$, reacts with oxygen with $k = (1.0 \pm 0.3) \times 10^9 M^{-1} sec^{-1}$, transfers an electron to tetranitromethane with $k = (4.5 \pm 0.3) \times 10^9 M^{-1} sec^{-1}$, and undergoes a fast reaction with the hydroxyl radical, $k \approx 10^{10} M^{-1} sec^{-1}$. The yield of Hg₂Cl₂ precipitate has been measured in γ -irradiated solutions of mercuric chloride. In the presence of OH radical scavengers $G(Hg_2Cl_2) = \frac{1}{2}G(HgCl)$. Much less precipitate is formed in the absence of OH radical scavengers. This is explained in terms of a reoxidation of Hg₂Cl₂ (formed by dimerization of HgCl) by hydroxyl radicals. Mechanistic details of HgCl₂ reduction are discussed. Information has also been obtained on the hydrolysis and dissociation equilibrium of mercuric chloride.

Introduction

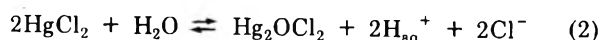
The reduction of mercuric chloride in aqueous solution by γ -irradiation leads to the formation of Hg₂Cl₂ precipitate as a final product.¹ The mechanism of this radiation chemical reduction has not yet been studied. Flash photolysis of HgCl₂ solutions has been carried out, however, and the Cl₂⁻ radical anion has been detected as an intermediate.² In studies of the reduction of HgCl₂ vapor by sodium atoms HgCl could be identified as a short-lived intermediate with a half-life of about 10⁻⁵ sec.³ This species was found to have optical absorption bands in the uv.

Mercuric chloride is known to be essentially undissociated in polar solvents. In aqueous solutions of 2×10^{-3}

M mercuric chloride, for example, only ca. 0.5% of the HgCl₂ is dissociated and ca. 1-2% is hydrolyzed according to the equilibria



and



respectively (at 20°). These two equilibria are only the two most important ones. Others also exist, they are con-

- (1) G. Stein, R. Watt, and J. Weiss, *Trans. Faraday Soc.*, **48**, 1030 (1952).
 (2) M. E. Langmuir and E. Hayon, *J. Phys. Chem.*, **71**, 3808 (1967).
 (3) D. Maeder, *Helv. Phys. Acta*, **16**, 503, 520 (1943).

tributing, however, only to a minor extent to the overall concentration of ions and molecules in aqueous solutions of mercuric chloride.^{4,5} It, therefore, can be expected that the HgCl₂ molecule is the main reaction partner of the reactive species (e_{aq}⁻, H·, etc.) formed in the radiolysis of the solvent.

The present study was undertaken to investigate the mechanism of the reduction of mercuric chloride by hydrated electrons and reducing radicals. Particular interest was focussed on the possible formation of HgCl, and the chemical properties of this radical species.

Experimental Section

The experimental details of optical and conductivity pulse radiolysis measurements have already been described.^{6,7} The pulse experiments were done with a 1.5-MeV Van de Graaff (10 mA) at pulse lengths of ca. 0.5–2 μsec and an absorbed dose of ca. 350–1400 rads. A ⁶⁰Co source of ca. 1500 Ci and an absorbed dose rate of ca. 3 × 10⁴ rads/hr was used for the γ irradiations. The experiments were carried out under commonly used radiation chemical conditions.⁶ Solutions were prepared from reagent grade compounds and triply distilled water, deaerated with either argon or N₂O, the latter being used if reactions of OH radicals were to be investigated.

Dosimetry was based on optical measurements of C(NO₂)₃⁻ ions (ε₃₅₀ 1.5 × 10⁴ M⁻¹ cm⁻¹) from the reduction of tetranitromethane by e_{aq}⁻ and (CH₃)₂CHOH in solutions of 10⁻³ M C(NO₂)₄ and 10⁻¹ M (CH₃)₂CHOH (G(C(NO₂)₃⁻) = 6.0.^{7,8} First- and second-order rate constants generally were obtained from log c vs. time and 1/c vs. time plots, respectively. Pure first or second order means no obvious deviation from the order over at least four half-lives.

Quantitative analysis of the conductivity data was based on eq I which describes the observed voltage signal, ΔV_s, due to the conductivity changes in the pulse irradiated solutions.⁷

$$\Delta V_s = (V_b R_a / 10^3 k_z) \sum_i \Delta c_i |z_i| \Lambda_i \quad (I)$$

where V_b is the voltage between the electrodes (30 V), R_a (1 kΩ) is an operating resistance in series with the cell, k_z is the cell constant in reciprocal centimeters, Δc_i is the concentration of the charged species produced as a result of the irradiation, z_i is the charge number, and Λ_i is the equivalent conductivity in Ω⁻¹ cm² equiv⁻¹. The cell constant was determined for each set of experiments using the dosimetry solution (average value k_z = 0.7 cm⁻¹) and the known equivalent conductivity of C(NO₂)₃⁻ of 40 Ω⁻¹ cm² equiv⁻¹.⁷ Hg₂Cl₂ formed during the irradiation was measured gravimetrically. The precipitate was filtered, washed with acetone, and dried in a vacuum desiccator. All data refer to room temperature.

Results and Discussion

Reaction of HgCl₂ with Reducing Species. The reaction of HgCl₂ with hydrated electrons was investigated by pulse irradiation of argon-saturated solutions of mercuric chloride. To remove OH radicals and H· atoms which are produced simultaneously with e_{aq}⁻ as primary species from the radiolysis of water, 5 × 10⁻¹ M *tert*-butyl alcohol was added to the solutions.⁹ From the kinetic analysis of the decay of the e_{aq}⁻ absorption at 720 nm and various HgCl₂ concentrations (3 × 10⁻⁶–2 × 10⁻⁵ M) the bimole-

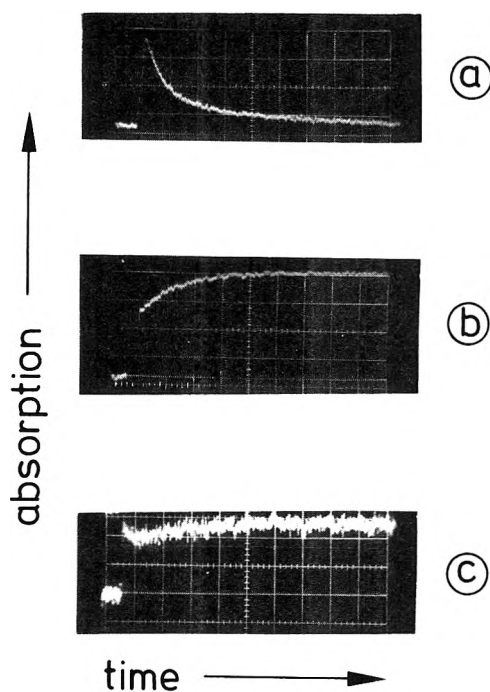


Figure 1. Absorption-time curves: (a) 2 × 10⁻⁴ M HgCl₂ and 5 × 10⁻¹ M *tert*-butyl alcohol in Ar-degassed aqueous solution, λ 330 nm, time scale 10 μsec/large division, dose ca. 5000 rads; (b) 2 × 10⁻⁴ M HgCl₂ and 10⁻¹ M isopropyl alcohol in Ar-degassed aqueous solution, λ 235 nm, time scale 20 μsec/large division, dose ca. 2500 rads; (c) 2 × 10⁻⁴ M HgCl₂ in Ar-degassed aqueous solution, λ 235 nm, time scale 50 μsec/large division, dose ca. 900 rads.

cular rate constant $k(e_{aq}^- + HgCl_2) = (4.0 \pm 0.3) \times 10^{10} M^{-1} sec^{-1}$ was obtained.

The reduction of HgCl₂ by hydrated electrons leads to the immediate formation of a transient species with strong absorption in the near uv. Figure 1a shows the absorption-time curve traced at 330 nm from a pulsed solution of 2 × 10⁻⁴ M HgCl₂ and 5 × 10⁻¹ M *tert*-butyl alcohol. At this HgCl₂ concentration the reduction process is complete within the 1-μsec pulse. The half-life of the transient decreases with increasing dose, i.e., with increasing concentration of the species, and the decay process was found to be of pure second-order kinetics. From the proportionality between the first half-life of the transient and its reciprocal concentration (calculated from $G(\text{transient}) = G(e_{aq}^-)$) at various doses the bimolecular decay rate constant $2k = (8.0 \pm 0.5) \times 10^9 M^{-1} sec^{-1}$ was derived.

The same reduction product of mercuric chloride is produced in pulsed N₂O-saturated solutions of HgCl₂ and isopropyl alcohol (10⁻¹ M). In such a solution all primary species (e_{aq}⁻, OH·, and H·) are converted into

- (4) "Gmelin's Handbuch der anorganischen Chemie," Part B, Vol. 2, Verlag Chemie, Weinheim, 1967.
- (5) H. Remy, "Lehrbuch der anorganischen Chemie," Vol. 2, 9th ed, Akademische Verlagsgesellschaft Geest und Portig KG, Leipzig, 1959.
- (6) A. Henglein, *Allg. Prakt. Chem.*, **17**, 296 (1966).
- (7) G. Beck, *Int. J. Rad. Phys. Chem.*, **1**, 361 (1969).
- (8) K.-D. Asmus, A. Henglein, M. Ebert, and J. P. Keene, *Ber. Bunsenges. Phys. Chem.*, **68**, 657 (1964).
- (9) (a) Primary reactive species in the radiolysis of aqueous solutions are e_{aq}⁻, OH·, and H· which are produced with $G = 2.7, 2.8, \text{ and } 0.6$, respectively,¹⁰ (G represents the number of species per 100 eV absorbed energy). (b) In solutions containing N₂O, *tert*-butyl alcohol, and HgCl₂, where all e_{aq}⁻, H·, and OH· are converted to *t*-BuOH radicals no HgCl₂ reduction product can be observed.
- (10) M. S. Matheson and L. M. Dorfman, "Pulsed Radiolysis," The M.I.T. Press, Cambridge, Mass., 1969.

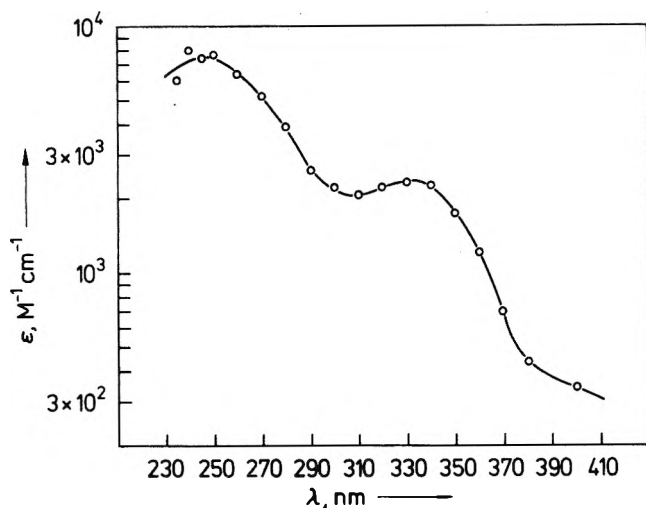
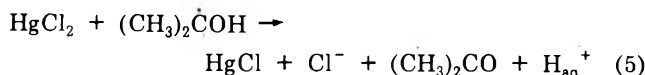
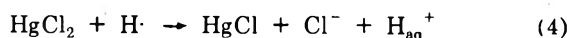
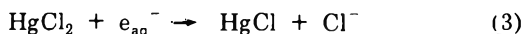


Figure 2. Absorption spectrum of HgCl.

($\text{CH}_3)_2\dot{\text{C}}\text{OH}$ radicals¹¹) which then act as reducing species. The rate constant for the reduction of HgCl_2 by *i*-PrOH radicals was calculated from the pseudo-first-order buildup of the transient absorption to be $k((\text{CH}_3)_2\dot{\text{C}}\text{OH} + \text{HgCl}_2) = (2.0 \pm 0.2) \times 10^9 \text{ M}^{-1} \text{ sec}^{-1}$.

The transient absorbing species is also formed in acid solutions (10^{-1} M HClO_4) of mercuric chloride. Since hydrated electrons are "converted" into $\text{H}\cdot$ atoms in such solutions this implies a reduction of HgCl_2 by hydrogen atoms. The bimolecular rate constant for this reaction has also been derived from the kinetic analysis of the buildup of the 330-nm absorption at various HgCl_2 concentrations and found to be $k(\text{H}\cdot + \text{HgCl}_2) = (1.0 \pm 0.5) \times 10^{10} \text{ M}^{-1} \text{ sec}^{-1}$.

Identification of the Transient Species. The transient could be one of the species from the following reaction paths: (a) electron capture would lead to the molecular anion HgCl_2^- ; (b) dissociative electron capture would yield either $\text{HgCl} + \text{Cl}^-$, (c) $\text{Hg}^+ + 2 \text{Cl}^-$, (d) or $\text{Hg} + \text{Cl}_2^-$. The transient absorption accordingly could be due to one of the following species: HgCl_2^- , HgCl , Hg^+ , Cl_2^- , or Hg . The second-order decay of the transient was found not to be affected by the ionic strength of the solution. This excludes all ionic species mentioned above. Furthermore, the known absorption spectra of both Hg^+ ¹² and Cl_2^- ¹³ are different from that of our transient. Also, no specific reaction of Cl_2^- as, for example, with isopropyl alcohol,² could be observed. Reaction path b is the only one in agreement with all experimental results. The transient optical absorption, therefore, is attributed to the HgCl radical molecule resulting from the processes



Spectrum of HgCl. Figure 2 shows the spectrum of the HgCl radical molecule. It has been obtained from the maximum absorption immediately after the pulse of argon-saturated solutions of $5 \times 10^{-4} \text{ M HgCl}_2$ and $2 \times 10^{-1} \text{ M}$ isopropyl alcohol. $G(\text{HgCl})$ in such solutions is 6.0 [$= G(e_{\text{aq}}^- + (\text{CH}_3)_2\dot{\text{C}}\text{OH}) = G(e_{\text{aq}}^- + \cdot\text{OH} + \cdot\text{H})$]. Identical spectra within the experimental limits of error

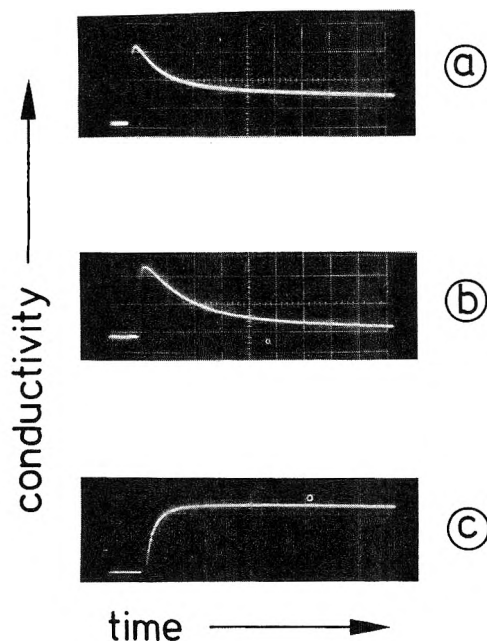


Figure 3. Conductivity-time curves: (a) $2 \times 10^{-4} \text{ M HgCl}_2$ and $2 \times 10^{-1} \text{ M}$ isopropyl alcohol in Ar-degassed aqueous solution, time scale 50 μsec /large division, dose ca. 300 rads; (b) $2 \times 10^{-4} \text{ M HgCl}_2$ in Ar-degassed aqueous solution, time scale 50 μsec /large division, dose ca. 850 rads; (c) 10^{-3} M HgCl_2 in Ar-degassed ethanol, time scale 50 μsec /large division, dose ca. 600 rads.

were obtained from solutions at pH 5 and 1 without alcohol and taking $G(\text{HgCl}) = G(e_{\text{aq}}^- + \text{H}\cdot) = 3.4$, and also from N_2O -saturated solutions of HgCl_2 (where e_{aq}^- are converted to the unreactive $\text{OH}\cdot$) taking $G(\text{HgCl}) = G(\text{H}\cdot) = 0.6$. The absorption spectrum shows a maximum at ca. 245 nm ($\epsilon 7.5 \times 10^3 \text{ M}^{-1} \text{ cm}^{-1}$) and another peak at 330 nm ($\epsilon 2.3 \times 10^3 \text{ M}^{-1} \text{ cm}^{-1}$).

Conductivity Measurements. The conductivity-time curve obtained from a pulse-irradiated saturated solution of $2 \times 10^{-4} \text{ M HgCl}_2$ and $2 \times 10^{-1} \text{ M}$ isopropyl alcohol is shown in Figure 3a. The initial increase in conductivity results from the reduction reactions 3 and 5 which under the experimental conditions are complete within the pulse. From the observed signal ΔV_s and taking $G(\text{reduction}) = 6.0$ the change in equivalent conductivity is calculated to be $\Delta\Lambda = 370 \Omega^{-1} \text{ cm}^2$. This is equivalent to the formation of six $\text{Cl}^- + \text{H}_{\text{aq}}^+$ ion pairs per 100 eV absorbed energy since $\Lambda(\text{Cl}^- + \text{H}_{\text{aq}}^+) = 380 \Omega^{-1} \text{ cm}^2 \text{ equiv}^{-1}$,¹⁴ i.e., the result is in agreement with the stoichiometry of the reactions 3 and 5 (the H_{aq}^+ yield includes the original counter ion of e_{aq}^-). The result also indicates that the HgCl is not dissociated since this would lead to a higher initial conductivity signal.

After the initial increase, the conductivity signal is seen to decrease by ca. 60%. Analysis of the partial decay shows that its kinetics are of mixed order and different to that of the disappearance of the optical HgCl absorption. It has been mentioned already in the Introduction that

(11) $e_{\text{aq}}^- + \text{H}_2\text{O} \rightarrow \text{OH}\cdot + \text{OH}^- + \text{N}_2$; $\text{OH}/\text{H} + (\text{CH}_3)_2\text{CHOH} \rightarrow \text{H}_2\text{O}/\text{H}_2 + (\text{CH}_3)_2\dot{\text{C}}\text{OH}$.

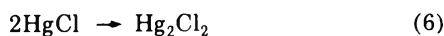
(12) M. Faraggi and A. Amozig, *Int. J. Rad. Phys. Chem.*, **4**, 353 (1972).

(13) (a) L. I. Grossweiner and M. S. Matheson, *J. Phys. Chem.*, **61**, 1089 (1957); (b) F. H. C. Edgecombe and R. G. W. Norrish, *Proc. Roy. Soc., Ser. A*, **253**, 154 (1959); (c) M. Anbar and J. K. Thomas, *J. Phys. Chem.*, **68**, 3829 (1964).

(14) Landolt-Bornstein, "Zahlenwerte und Funktionen," Vol. 11/7, Springer-Verlag, Berlin, 1970.

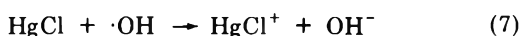
HgCl₂ to a small extent is dissociated and hydrolyzed in aqueous solutions.^{4,5} At a total concentration of 2×10^{-4} M mercuric chloride *ca.* 10^{-6} M HgCl⁺ ions are present in the solution. Since Cl⁻ ions are produced at *ca.* 2×10^{-6} M, during the 0.5- μ sec pulse they will be partially neutralized according to the dissociation equilibrium (eq 1). The back reaction of the hydrolysis equilibrium (eq 2) will also contribute to the decay of the conductivity signal.

Reactions of HgCl. Formation of Hg₂Cl₂. The insoluble precipitate Hg₂Cl₂ is one of the final reaction products from the reduction of mercuric chloride as is known from γ -radiolysis experiments¹ and classical reduction processes. Since saturated aqueous solutions of Hg₂Cl₂ (solubility product 2×10^{-18} M³ at 25^o) show strong absorption below 250 nm, optical measurements were also carried out at these wavelengths during the pulse radiolysis experiments. Figure 1b shows the absorption-time curve from a pulsed solution of 2×10^{-4} M HgCl₂ and 10^{-1} M isopropyl alcohol traced at 235 nm. A two-step increase of the signal is observed. The initial step is complete within the pulse and is attributed to the absorption of HgCl ($G(\text{HgCl}) = 6.0$). The slow secondary increase is of second-order kinetics and occurs simultaneously with the decay of HgCl shown in Figure 1a. The final absorption at 235 nm remains stable and is attributed to mercurous chloride formed in the dimerization process



which occurs with $2k = (8.0 \pm 0.5) \times 10^9 \text{ M}^{-1} \text{ sec}^{-1}$ (see Results and Discussion section). With $G(\text{Hg}_2\text{Cl}_2) = \frac{1}{2}G(\text{HgCl}) = 3.0$ the extinction coefficient of Hg₂Cl₂ at 235 nm is calculated to be $2.45 \times 10^4 \text{ M}^{-1} \text{ cm}^{-1}$. The spectrum of Hg₂Cl₂ which could be measured from 270 nm to *ca.* 232 nm in the pulse experiments is quite similar to that of saturated solutions of mercurous chloride.

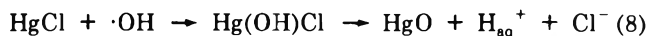
Reaction of HgCl with Hydroxyl Radicals. Figure 1c shows the absorption-time curve traced at 235 nm for a solution of 2×10^{-4} M HgCl₂ in the absence of isopropyl alcohol as an OH \cdot radical scavenger. The signal immediately after the pulse is smaller than in solutions with isopropyl alcohol since HgCl is now formed only by hydrated electrons and hydrogen atoms with $G = G(e_{\text{aq}}^- + \text{H}\cdot) = 3.4$. After the pulse a slight decrease in absorption is followed by a slight increase. The final stable signal which is again attributed to Hg₂Cl₂ is just as strong as the initial HgCl signal. If all of the HgCl had dimerized, as in the experiment shown in Figure 1b, a much larger increase in the stable 235-nm absorption would have been expected in Figure 1c. The decrease in Hg₂Cl₂ formation by almost a factor of 2 compared with isopropyl alcohol containing solutions is explained by an oxidation of part of the HgCl *via* hydroxyl radicals



The HgCl⁺ formed in this reaction is expected to be neutralized by Cl⁻ formed during the pulse *via* reactions 3 and 4, and the OH⁻ will be neutralized by the protons produced during the pulse. The conductivity experiment carried out simultaneously with the optical measurement confirms this mechanism as can be seen from Figure 3b. The conductivity signal increases immediately after the pulse owing to the formation of H_{aq}⁺ and Cl⁻ with $G = 3.4$. It then decreases much more than the signal in Figure 3a leaving almost no permanent change in conductivity. Since OH \cdot radicals are present in nearly the same con-

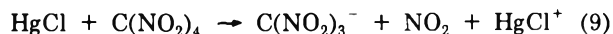
centration as HgCl after the pulse ($G(\text{OH}) = 2.7$ and $G(\text{HgCl}) = 3.4$) and since the two processes competing with reaction 7, *i.e.*, $\text{OH} + \text{OH} \rightarrow \text{H}_2\text{O}_2$ ¹⁰ and $\text{HgCl} + \text{HgCl} \rightarrow \text{Hg}_2\text{Cl}_2$, occur with diffusion-controlled rate constants, a similarly high rate constant must be attributed to the reaction of HgCl with hydroxyl radicals. A value of $k(\text{OH} + \text{HgCl}) \approx 10^{10} \text{ M}^{-1} \text{ sec}^{-1}$ best explains the results given in Figure 1c according to which *ca.* 40-50% of the HgCl formed initially is oxidized by OH \cdot radicals.

According to the conductivity results an alternative reaction



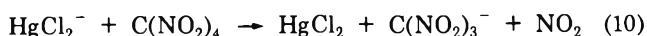
is less likely since it would lead to the formation of only H_{aq}⁺ and Cl⁻ ions, *i.e.*, to essentially the same situation as in solutions where alcohols are present. In such a case a conductivity curve of the type shown in Figure 3a would be expected. Though HgCl appears to be readily oxidized by hydroxyl radicals no reaction has been observed between HgCl and H₂O₂. Addition of hydrogen peroxide to solutions of mercuric chloride did not affect the decay of the HgCl absorption signal.

Reaction of HgCl with Tetranitromethane. Tetranitromethane which is known to be a good electron acceptor^{6,8} is reduced by HgCl. In solutions of 10^{-3} M HgCl₂, 2×10^{-1} M isopropyl alcohol, and small concentrations of C(NO₂)₄ [(1.2-8.8) $\times 10^{-5}$ M] the rate of disappearance of the initially produced HgCl (reactions 3 and 5) increases with the C(NO₂)₄ concentration. The decay of the HgCl absorption is accompanied by a simultaneous buildup of the nitroform ion absorption. From the kinetic analysis of the absorption-time curves traced at 270 (HgCl decay) or 370 nm (C(NO₂)₃⁻ formation) the bimolecular rate constant for the reaction



is calculated to be $k_9 = (4.5 \pm 0.3) \times 10^9 \text{ M}^{-1} \text{ sec}^{-1}$.

Conductivity experiments have been carried out with solutions containing 2×10^{-2} M HgCl₂, 2×10^{-4} M C(NO₂)₄, and 2×10^{-1} M isopropyl alcohol. Under these conditions the reduction of HgCl₂ to HgCl and the electron transfer reaction to tetranitromethane (eq 9) occur during the time of the pulse itself. The conductivity-time signal which is obtained is of the type given in Figure 3a, *i.e.*, the initial signal does not remain stable and decays with a half-life of *ca.* 20-30 μ sec to approximately one-half of its maximum value. This is, of course, expected since both Cl⁻ ions (from reactions 3 and 5) and HgCl⁺ ions (from reaction 9) will undergo, at least partial, neutralization. This conductivity experiment may also serve as a further argument against the existence of a relatively long-lived molecular anion HgCl₂⁻. If such species were formed as a result of the reduction of HgCl₂, and thus the electron transfer reaction to tetranitromethane was



no Cl⁻ and HgCl⁺ ions would be produced during the reaction. Consequently, the conductivity signal which would then be due to C(NO₂)₃⁻ and H_{aq}⁺ ions alone should not decay since nitroform is known to be stable and completely dissociated under the experimental conditions.^{8,16}

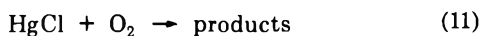
(15) R. C. Weast, Ed., Handbook of Chemistry and Physics, 51st ed., The Chemical Rubber Publishing Co., Cleveland, Ohio, 1970-1971.

(16) S. A. Chaudhri and K.-C. Asmus, *J. Chem. Soc., Faraday Trans. 1*, **68**, 385 (1972).

TABLE I: Yields of Hg_2Cl_2 from γ -Irradiated Argon-Saturated Solutions of $2 \times 10^{-1} M \text{HgCl}_2$

Dose, rads	OH scavenger, M	pH	$G(\text{Hg}_2\text{Cl}_2)$
2.9×10^6	Isopropyl alcohol 5×10^{-1}	5.0	3.1
1.0×10^6	Isopropyl alcohol 5×10^{-1}	0 (1 M HClO_4)	2.7
0.75×10^6	No scavenger	5.0	0.16
2.9×10^6	No scavenger	5.0	0.05
5.8×10^6	No scavenger	5.0	0.02
1.0×10^6	No scavenger	0 (1 M HClO_4)	0.05

Reaction of HgCl with Oxygen. In air-saturated solutions (O_2 ca. $2 \times 10^{-4} M$) of $5 \times 10^{-3} M \text{HgCl}_2$ the optical absorption of HgCl disappears by a first-order process. This indicates a reaction



From the observed half-life of 3.5 μsec the bimolecular rate constant $k_{11} = 10^9 M^{-1} \text{sec}^{-1}$ is derived.

γ -Irradiation Experiments on the Reduction of HgCl_2 . The formation of the stable reduction product, Hg_2Cl_2 , was also investigated by γ irradiation of mercuric chloride solutions. The results are presented in Table I and Figure 4. In solutions of $2 \times 10^{-1} M \text{HgCl}_2$ and $5 \times 10^{-1} M$ isopropyl alcohol $G(\text{Hg}_2\text{Cl}_2)$ is found to be 3.1 and 2.7 at pH 5 and 0, respectively. $G(\text{HgCl}) = 6.0$ in such solutions and dimerization of HgCl , therefore, should yield $G(\text{Hg}_2\text{Cl}_2) = 3.0$ which is in good agreement with the experimental results.

Only small yields of Hg_2Cl_2 are produced in the absence of OH radical scavengers, though HgCl is formed with $G = G(e_{\text{aq}}^- + \text{H}\cdot)$. Furthermore, $G(\text{Hg}_2\text{Cl}_2)$ was found to decrease with increasing dose. If *tert*-butyl alcohol which scavenges OH radicals is added to the solutions $G(\text{Hg}_2\text{Cl}_2)$ increases from almost zero to ca. 2 at high alcohol concentrations (Figure 4). (Under the experimental conditions *tert*-butyl alcohol will not compete for H atoms with HgCl_2 ; the radical produced from the reaction of *tert*-butyl alcohol and OH apparently does not reduce HgCl_2 .)

These results imply, as already indicated by the single pulse experiments, that reactions of HgCl with OH radicals are responsible for the lower Hg_2Cl_2 yields. Thus, the reaction of HgCl with the hydroxyl radical (eq 7) which competes with the dimerization of HgCl (eq 6) reduces $G(\text{Hg}_2\text{Cl}_2)$ by a factor of ca. 2 on account of the similar rate constants of these two reactions. The competition of these two reactions cannot, however, quantitatively explain the low Hg_2Cl_2 yields in the γ -irradiation experiments. Furthermore, the results presented in Figure 4 show that ca. $10^{-3} M$ *tert*-butyl alcohol is needed to obtain $G(\text{Hg}_2\text{Cl}_2) \approx 1$, i.e., half of the maximum yield which is found when all hydroxyl radicals are removed. If only the competitive reactions $\text{HgCl} + \text{HgCl}$, $\text{HgCl} + \text{OH}$, $\text{OH} + \text{OH}$, and $\text{OH} + \text{tert-butyl alcohol}$ ¹⁷ occurred analysis of the data from Figure 4 would lead to an unrealistic high value for $k(\text{OH} + \text{HgCl})$.

It is, therefore, assumed that, under γ -irradiation conditions, Hg_2Cl_2 can also be attacked by hydroxyl radicals leading to the reoxidation of the mercurous chloride. Such a reaction could also explain the observed dose dependence of $G(\text{Hg}_2\text{Cl}_2)$. Further experimental evidence for

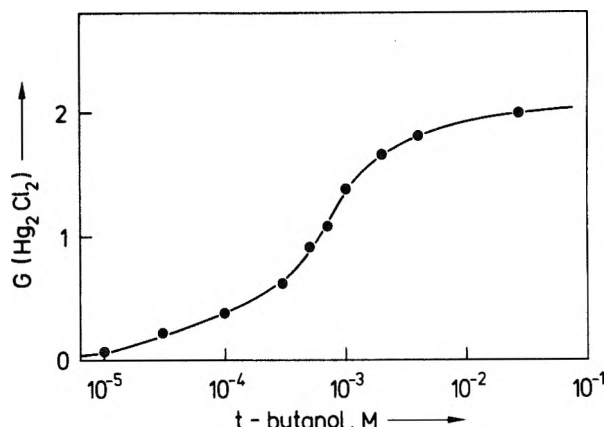
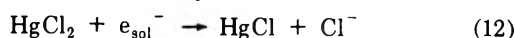


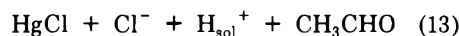
Figure 4. Yield of Hg_2Cl_2 as a function of *tert*-butyl alcohol concentration from γ -irradiated aqueous solutions of $2 \times 10^{-1} M \text{HgCl}_2$.

the attack of Hg_2Cl_2 by OH \cdot radicals is provided by the following experiment. A suspension of Hg_2Cl_2 (ca. 100 mg) in N_2O -saturated water was γ irradiated with occasional shaking of the sample. Between 2 and 10% of the Hg_2Cl_2 was found to go into solution at doses of 10^6 – 10^7 rads. Possibly OH \cdot radicals attack the suspended Hg_2Cl_2 directly or react with Hg_2^{2+} ions which are also present in the solutions (although only in small concentrations according to the solubility product¹⁵ of Hg_2Cl_2).

Experiments on the Dissociation and Hydrolysis Equilibrium of HgCl_2 . The partial decay of the conductivity signal obtained for a pulsed aqueous solution of mercuric chloride (Figure 3a) has been attributed to the neutralization of chloride ions (which were produced during the pulse) via the back reactions of the equilibria given in eq 1 and 2. This interpretation is also supported by the following experiments. In solutions of mercuric chloride in ethanol the solute is reduced by solvated electrons



and ethanol radicals

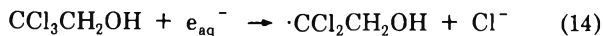


The transient absorption spectrum of HgCl is identical with that in aqueous solution. The conductivity signal obtained from a pulsed solution of $10^{-3} M \text{HgCl}_2$ in ethanol is shown in Figure 3c. It is seen to remain stable after its initial formation (owing to reactions 12 and 13). This means that the Cl^- ions produced during the pulse do not undergo any neutralization reaction as in the aqueous system. This, however, is expected since HgCl_2 is practically undissociated and not solvolyzed in ethanol.⁴

From the optical measurements the total reduction yield of HgCl_2 in the $10^{-3} M \text{HgCl}_2$ solution in ethanol is found to be $G = 4.3$, if the extinction coefficient of HgCl is assumed to be the same as in water. The change in conductivity (Figure 3c) calculated from this yield and eq 1 corresponds to $\Delta\Lambda = 85 \Omega^{-1} \text{cm}^2$. This is in good agreement with the theoretical value of $\Lambda = 87.7 \Omega^{-1} \text{cm}^2$ ¹⁴ (in ethanol at 25°) expected for the formation of one Cl^- ion plus the associated solvated proton per reducing species.

(17) $k(\text{OH} + \text{tert-butyl alcohol}) = 2.5 \times 10^8 M^{-1} \text{sec}^{-1}$; G. E. Adams, J. W. Boag, J. Currant, and B. D. Michael, "Pulse Radiolysis," J. H. Baxendale, M. Ebert, J. P. Keene, and A. J. Swallow, Ed., Academic Press, New York, N. Y., 1965.

Pulse experiments have also been carried out with aqueous solutions containing 2,2,2-trichloroethanol and mercuric chloride. In argon-saturated solutions containing $10^{-2} M$ CCl₃CH₂OH alone, the reaction



yields chloride ions which together with H_{aq}⁺ give a stable conductivity signal of the type shown in Figure 3c. Upon addition of $1.5 \times 10^{-4} M$ mercuric chloride to this solution all hydrated electrons are still scavenged by the 2,2,2-trichloroethanol and accordingly no HgCl formation can be observed. Nevertheless, the conductivity signal partially decays from its initial maximum value in a manner similar to the curve shown in Figure 3a. This finding is explained by the neutralization of the Cl⁻ ions produced from the 2,2,2-trichloroethanol *via* the back reactions of the mercuric chloride equilibria given in eq 1 and 2.

The decay of the conductivity signal to its final value can be described by an almost pseudo-first-order process with a half-life of 49 and 19 μsec at HgCl₂ concentrations of 1.5×10^{-4} and $6.2 \times 10^{-4} M$, respectively. In both solutions the HgCl⁺ and H_{aq}⁺ concentrations (resulting from the equilibria 1 and 2) are larger (estimated at $(2-6) \times 10^{-6} M$) than the Cl⁻ ion concentrations produced from reaction 14 during the pulse ($10^{-6} M$). From the observed half-lives and the HgCl⁺/H_{aq}⁺ concentrations the rate constant for the overall neutralization process is calculated to some $10^{10} M^{-1} \text{sec}^{-1}$, *i.e.*, to be in the range of diffusion-controlled reactions.

The equilibria given in eq 1 and 2 will, of course, be affected by changes in the concentration of any of the ionic species involved, *i.e.*, by HgCl⁺, H_{aq}⁺, and Cl⁻ ions. In pulsed solutions of $2 \times 10^{-4} M$ HgCl₂ and $2 \times 10^{-1} M$ isopropyl alcohol, for example, the conductivity signal (see Figure 3a) was found to decay from its initial value, ΔΛ_{max}, to a final permanent value, ΔΛ_{perm}, with a ratio ΔΛ_{perm}/ΔΛ_{max} = 0.38 (Λ values calculated from eq I). If chloride ions (NaCl) are added to the solution prior to the pulse higher yields of the permanent conductivity change, ΔΛ_{perm}, are found, *i.e.*, less neutralization occurs. This is shown in Figure 5 where the ratio ΔΛ_{perm}/ΔΛ_{max} is plotted against the Cl⁻ ion concentration of the solution. The increasing curve is seen to level off at a ratio of 0.7 at high chloride concentrations. The addition of Cl⁻ ions to the mercuric chloride solutions will, of course, reduce the HgCl⁺ and H_{aq}⁺ concentrations according to the equilibrium conditions of eq 1 and 2. As a result much less of the Cl⁻ ions produced from the reduction of HgCl₂ (reactions 3 and 5) will be neutralized and ΔΛ_{perm} is expected to be larger. The decay of the conductivity curve cannot, however, be entirely suppressed even at the highest Cl⁻ ion concentration.

For the same reasons the addition of H_{aq}⁺ ions (HClO₄) to solutions of HgCl₂ and isopropyl alcohol leads to an increase in ΔΛ_{perm}. But again the ratio ΔΛ_{perm}/ΔΛ_{max} does not reach the value of 1.0 at high H_{aq}⁺ concentrations. The half-lives of the decay are found to decrease with both increasing Cl⁻ and H_{aq}⁺ concentration.

The effect of increasing mercuric chloride, *i.e.*, HgCl⁺ ion concentration, on the conductivity signal can be seen from the results listed in Table II. Both the half-life of the conductivity and the ΔΛ_{perm}/ΔΛ_{max} ratio are found to decrease with increasing mercuric chloride concentration. This is expected since in the presence of higher HgCl⁺

TABLE II: Effect of HgCl₂ Concentration on the Decay of the Conductivity Signal^a

HgCl ₂ , M	ΔΛ _{perm} /ΔΛ _{max}	t _{1/2} , μsec
2×10^{-4}	0.40	35
1×10^{-3}	0.33	25
1×10^{-2}	0.22	20

^a Dose ca. 300 rads; ΔΛ_{max} = 370 Ω⁻¹ cm²; isopropyl alcohol $2 \times 10^{-1} M$.

TABLE III: Effect of Dose on the Decay of the Conductivity Signal^a

Dose, rads	ΔΛ _{perm} /ΔΛ _{max}
300	0.38
700	0.40
1400	0.43
1800	0.49
3000	0.54

^a ΔΛ_{max} = 370 Ω⁻¹ cm².

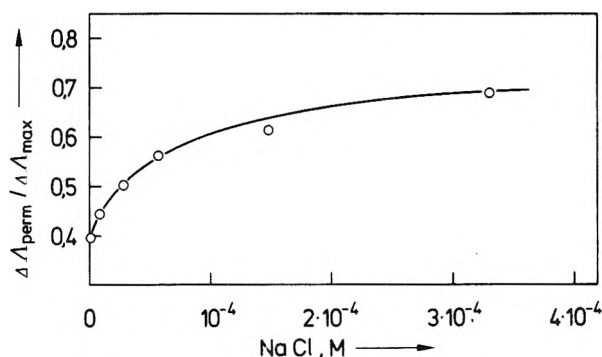


Figure 5. Ratio ΔΛ_{perm}/ΔΛ_{max} as a function of chloride ion concentration in pulsed aqueous solutions of $2 \times 10^{-4} M$ HgCl₂ and $2 \times 10^{-1} M$ isopropyl alcohol; dose ca. 300 rads.

concentrations neutralization of the Cl⁻ ions (produced during the pulse) should occur faster and more completely. Table III finally shows the effect of dose on the conductivity signal from a pulsed solution of $2 \times 10^{-4} M$ HgCl₂ and $2 \times 10^{-1} M$ isopropyl alcohol. The ratio ΔΛ_{perm}/ΔΛ_{max} is seen to increase with dose, *i.e.*, the yield of neutralization decreases. With increasing dose Cl⁻ ions will be produced during the pulse at concentrations which to an increasingly larger extent exceed the HgCl⁺ concentration available from the dissociation of the mercuric chloride. Thus a decreasing fraction of the Cl⁻ ions will be neutralized and an increasing yield of conductivity after the neutralization is expected to remain.

No attempt has been made to analyze the conductivity results quantitatively. The kinetics of the decay of the conductivity signals were found to be of first or mixed (first and second) order depending on the experimental conditions. So many species (HgCl⁺, H_{aq}⁺, Cl⁻, Hg₂OCl₂, Hg²⁺, HgCl₄²⁻, etc.) formed in various equilibria are present in aqueous solutions of mercuric chloride at concentrations of the same order of magnitude as the products obtained from the single-pulse experiments^{4,5} that it does not appear very meaningful to attribute a rate

constant (within reasonable limits) to a particular neutralization reaction. These considerations also apply to the absolute yields of conductivity changes obtained from the pulse experiments. In addition to the ions resulting from the existing equilibria (eq 1 and 2, and to a minor extent also from others^{4,5}), the reaction products including the Hg_2Cl_2 (the latter according to its solubility prod-

uct) contribute to the final conductivity to an uncalculable extent.

Acknowledgment. The authors are very grateful to Mrs. M. Schöner for experimental assistance. This work has been supported by funds made available from the Verband der Chemischen Industrie.

Electron Spin Resonance Study of Radical Anions from Aromatic Carboxylic Acids¹

P. Neta* and Richard W. Fessenden

Radiation Research Laboratories, Center for Special Studies and Department of Chemistry, Mellon Institute of Science, Carnegie-Mellon University, Pittsburgh, Pennsylvania 15213 (Received September 25, 1972)

Publication costs assisted by the Carnegie-Mellon University and the U.S. Atomic Energy Commission

Radical anions produced by the reaction of hydrated electrons with benzoic, phthalic, isophthalic, terephthalic, trimesic, pyromellitic, mellitic, and biphenyldicarboxylic acids in aqueous solutions have been studied by esr. Solutions containing the aromatic compound together with a scavenger for OH radicals were irradiated by 2.8-MeV electrons while flowing through the esr cavity and the spectra were recorded under steady-state conditions. The acid-base properties of the radicals have been examined and in most cases several different stages of protonation were identified. All protonations of the radical anions were found to take place on the carboxyl groups and not on the ring. The loss of the last dissociable proton from each electron adduct was found to occur at a pH much higher (at least 4 units) than in the case of the parent molecules. The presence of two ortho carboxyl groups was found to result in a strong hydrogen-bonded bridge which, in the case of phthalate, does not dissociate even at pH 14.

Introduction

An electron spin resonance study of radical anions from aromatic carboxylate ions in liquid ammonia has been reported.² The spectra were interpreted in terms of radicals with one more unit of negative charge than in the parent carboxylate ion. These radicals, when produced in aqueous solutions, are expected to protonate at low pH values. In a recent pulse radiolysis study of the radical anion from benzoate it was concluded that two successive protonations take place on the carboxyl group with pK_a values of 5.3 and 12.0.³ An esr study of this radical could reveal additional information on its structure. The present study was undertaken for this reason and was extended to the polycarboxy derivatives.

In recent studies^{4,5} of radical anions from olefinic carboxylate ions a major difference has been found between radicals from maleate and fumarate. The cis isomer forms a strong intramolecular hydrogen bond which resists dissociation even in 1 M base,⁴ whereas the trans isomer is completely dissociated at pH above 11. In parallel with these findings one expects the radical anion from phthalate to form a strong hydrogen bridge between the two carboxyl groups with a high pK_a while lower pK_a values are predicted for the other isomers. These predictions will be examined both in the dicarboxybenzenes and also in pyromellitic and mellitic acids.

Experimental Section

Benzoic acid was a Baker Analyzed Reagent, phthalic and isophthalic acids were obtained from Eastman, the biphenyldicarboxylic acids from Chemicals Procurement Laboratories, and the other acids from Aldrich. All these compounds were of the purest grade commercially available and were used without further purification. *tert*-Butyl alcohol was of Mallinckrodt AR grade. Sodium formate and all the inorganic compounds were Baker Analyzed Reagents. Solutions were prepared in water which was distilled and the vapor passed with oxygen through a silica tube at 600° to destroy all organic impurities. The pH was adjusted using KOH, HClO_4 , $\text{Na}_2\text{B}_4\text{O}_7$, KH_2PO_4 , and K_2HPO_4 , the latter three being used as buffers. Solutions were deoxygenated by bubbling with pure nitrogen and were irradiated with 2.8-MeV electrons directly in the esr cavity. All the other details of the experiment were as described previously.⁶

- (1) Supported in part by the U. S. Atomic Energy Commission.
- (2) A. R. Buick, T. J. Kemp, G. T. Neal, and T. J. Stone, *J. Chem. Soc. A*, 2227 (1970).
- (3) M. Simic and M. Z. Hoffman, *J. Phys. Chem.*, **76**, 1398 (1972).
- (4) P. Neta and R. W. Fessenden, *J. Phys. Chem.*, **76**, 1957 (1972).
- (5) N. H. Anderson, A. J. Dobbs, D. J. Edge, R. O. C. Norman, and P. R. West, *J. Chem. Soc. B*, 1004 (1971).
- (6) K. Eiben and R. W. Fessenden, *J. Phys. Chem.*, **75**, 1186 (1971).

Results and Discussion

Aqueous solutions of the aromatic carboxylate ions (10^{-4} – 10^{-2} *M*), containing an excess (0.1–1 *M*) of an effective scavenger for OH radicals such as formate or *tert*-butyl alcohol, were irradiated and the esr spectra recorded under steady-state conditions. The spectra of the radicals from the OH scavengers have broad lines and are not observed under conditions of low modulation amplitude and low microwave power used for the observation of the narrow lines of the radical anions. (The line of CO_2^- is also masked by the signal from the silica cell.) The quality of the spectra was similar to that in previous studies and none will be shown in the present article. In most cases very intense spectra were recorded as a result of the small number of hyperfine lines and the high steady-state concentration caused by slow radical-radical reaction between multiply charged species.

Benzoic Acid. The spectrum recorded with an irradiated solution of benzoate (10^{-2} *M*) and *tert*-butyl alcohol (1 *M*) at pH 13.0 contains two triplets of 4.18 and 0.83 G and a doublet of 7.58 G. These hyperfine constants can be assigned to the ortho, meta, and para hydrogen atoms, respectively, by analogy to benzyl-type radicals (see, *e.g.*, ref 7–10) and by reference to calculations for this specific radical.² The similarity of anion radicals of the carboxylic acids and the corresponding nitriles can also be used in this connection. The radical structure and the esr parameters are summarized in Table I. The values reported² for the same radical in liquid ammonia are in agreement with the present results except for the *g* factor which was previously reported to be slightly higher.

The spectrum observed at pH 7 has rather similar esr parameters (see Table I) but with an additional 1.08-G doublet. This spectrum is readily assigned to the singly protonated form with the carboxyl proton causing the extra splitting. At pH 11 no spectrum was observed because of line broadening associated with the protonation reaction. The disappearance of the esr spectrum at pH 11 and the existence of different hyperfine constants for the ring protons above and below this pH are in agreement with the $\text{p}K_a$ of 12.0 as determined by pulse radiolysis.³ It was not possible to observe the acid form of this radical (first $\text{p}K_a = 5.3^3$) because of very low esr line intensities. The absence of protonation on the ring is in accord with previous suggestions.³

Phthalic Acid. In this case the same spectrum was observed in the presence of *tert*-butyl alcohol at pH 9, 12, 13, and 14 and also in the presence of formate at pH 12.1 and 13.3. In the latter case some extra lines were also present which are not accounted for. In both cases all lines disappeared with the addition of N_2O which scavenges e_{aq}^- very efficiently but does not react with CO_2^- (see, *e.g.*, ref 4). This result indicates that the radical observed was produced by reaction of e_{aq}^- and that CO_2^- does not transfer an electron efficiently to phthalate. At pH 5.5 a different spectrum was observed and, at the intermediate pH of 6.7, weak lines of both the basic and the acid form of the radical were present. At pH 3.5 the lines became less intense and another splitting seemed to appear but accurate analysis was not possible.

The esr parameters determined from the spectra and the suggested radical structures are given in Table I. The assignment of the hyperfine constants to the specific ring hydrogens of the form observed in basic solutions is made on the basis of the results and spin density calculations for the phthalonitrile anion.^{11,12} The small doublet split-

ting of 0.19 G must be caused by a proton on a carboxyl group and the fact that the ring protons constitute two equivalent pairs indicates that the additional proton must form a bridge between the two carboxyl groups. This proton is undissociated even at 1 *M* base as was found for the maleate radical anion.⁴ A second protonation at the lower pH causes considerable asymmetry and changes the triplet splitting of 3.12 G into two doublets of 1.93 and 4.74 G. The average of these values remains similar to that of the triplet. Only two other splittings of about 0.97 G were observed rather than the four expected. The unresolved splittings were sufficiently large as to cause noticeable line broadening but low signal intensity prevented the use of the low modulation amplitudes necessary for resolving these splittings. Because of the asymmetry evident from the ring proton splittings already mentioned, the protons at the 3 and 6 positions are assigned splittings of 0.97 and ~ 0 G leaving values of 0.97 and ~ 0 G for the two carboxyl protons. A value of 0.97 G for the hyperfine constant of the nonbridged carboxyl proton is in agreement with the values for benzoate, isophthalate, and trimesate. Alternative assignments of the hyperfine constants for this spectrum are also possible.

Isophthalic Acid. The spectrum observed in 10^{-3} – 10^{-2} *M* solutions of isophthalate containing *tert*-butyl alcohol was that of the terephthalate radical anion (see below). This finding suggests that a small amount of terephthalic acid is present in commercial isophthalic acid and that electron transfer from [isophthalate]⁻ to terephthalate takes place. Pulse radiolysis experiments have indeed verified this assumption and allowed measurement of the rate constant for the electron transfer.¹³ Accordingly, when the concentration of isophthalate was lowered to 10^{-4} *M*, the concentration of the terephthalate impurity was not sufficient to react with all the [isophthalate]⁻ and lines of both radical anions were found at comparable intensities.

The hyperfine constants determined from the spectrum recorded at pH 13 (Table I) do not agree with those reported for the same radical in liquid ammonia² and both of these sets of parameters do not resemble those determined for the isophthalonitrile radical anion.¹² In all three studies a 7–8-G triplet was observed but the other two nonequivalent ring protons show very different splittings. The reason for this discrepancy is not clear and it can only be suggested that a large solvent effect on these splittings is present.

The singly protonated form of this radical was observed in neutral solutions. The hyperfine constants (Table I) are similar in magnitude to those for the basic form but the protons at positions 4 and 6 are no longer equivalent. Although it might seem reasonable to assign the splittings of 1.41 and 0.92 G both to the protons at positions 2 and 5 this gives the carboxyl proton a very small splitting which is not in agreement with those for the adducts to benzoate and trimesate. It is for this reason that the assignment shown with a 0.92-G carboxyl splitting is preferred.

Terephthalic Acid. The spectrum recorded at pH 12.2 and 13.3 consisted of a 1.54-G quintet (Table I). This

- (7) H. Fischer, *Z. Naturforsch. A*, **20**, 488 (1965).
- (8) R. Livingston and H. Zeldes, *J. Chem. Phys.*, **44**, 1245 (1966).
- (9) P. Neta, M. Z. Hoffman, and M. Simic, *J. Phys. Chem.*, **76**, 847 (1972).
- (10) A. Carrington and I. C. P. Smith, *Mol. Phys.*, **9**, 137 (1965).
- (11) P. H. Rieger and G. K. Fraenkel, *J. Chem. Phys.*, **37**, 2795 (1962).
- (12) P. H. Rieger, I. Bernal, W. H. Reinmuth, and G. K. Fraenkel, *J. Amer. Chem. Soc.*, **85**, 683 (1963).
- (13) L. K. Patterson and P. Neta, to be submitted for publication.

TABLE I: ESR Parameters of Radicals Produced by Reaction of e_{aq}^- with Aromatic Carboxylic Acids

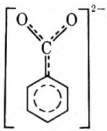
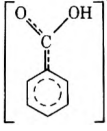
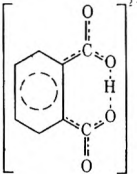
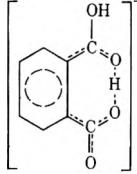
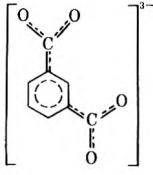
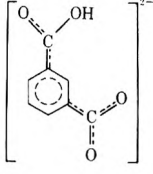
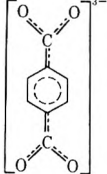
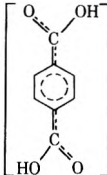
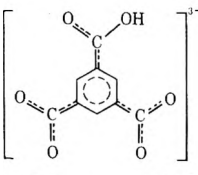
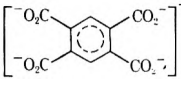
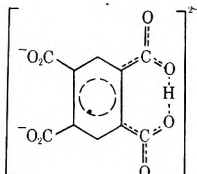
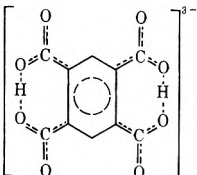
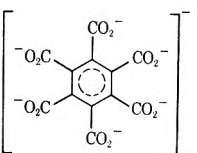
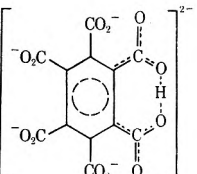
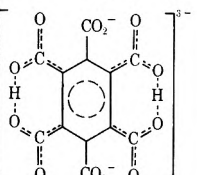
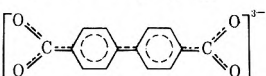
Irradiated solution ^d	Radical	<i>g</i> factor ^b	Hyperfine constants ^c
Benzoate pH 13.0		2.00306	$a_o^H = 4.18$ (2) $a_m^H = 0.83$ (2) $a_p^H = 7.58$
Benzoate pH 7.0		2.00302	$a_o^H = 4.82$ (2) $a_m^H = 1.33$ (2) $a_p^H = 7.26$ $a_{COOH}^H = 1.08$
Phthalate pH 9, 12, 13, 14		2.00321	$a_{3,6}^H = 0.05$ (2) $a_{4,5}^H = 3.12$ (2) $a_{COOH}^H = 0.19$
Phthalate pH 5.5		2.00319	$a_{3,6}^H = 0.97$; $\sim 0^d$ $a_{4,5}^H = 1.93$; 4.74 $a_{COOH}^H = 0.97$; $\sim 0^d$
Isophthalate pH 13.0		2.00305	$a_{4,6}^H = 7.42$ (2) $a_{2,5}^H = 1.34$; 1.32
Isophthalate pH 7.2		2.00304	$a_{4,6}^H = 9.34$; 7.75 $a_{2,5}^H = 1.41$; 0.12 $a_{COOH}^H = 0.92^e$
Terephthalate pH 12.2, 13.3		2.00328	$a^H = 1.54$ (4)
Terephthalate pH 4.5, 5.2, 6.1		2.00330	$a^H = 1.56$ (4) $a_{COOH}^H = 0.25$ (2)
Trimesate pH 7.0		2.00305	$a_{2,6}^H = 4.56$; 4.65 $a_4^H = 8.31$ $a_{COOH}^H = 0.81$
Pyromellitate pH 13.7, 14		2.00352	$a^H = 0.31$ (2)

TABLE I (Continued)

Irradiated solution ^a	Radical	<i>g</i> factor ^b	Hyperfine constants ^c
Pyromellitate pH 12.2		2.00340	$a^H = 0.53$ (2) $a_{\text{COOH}}^H = 0.12$
Pyromellitate pH 5.5, 7.2, 9.0		2.00347	$a^H = 1.08$ (2) $a_{\text{COOH}}^H = 0.28$ (2)
Mellitate pH 13.5		2.00369	
Mellitate pH 11.5		2.00352	$a_{\text{COOH}}^H = 0.69$
Mellitate pH 9.2		2.00352	$a_{\text{COOH}}^H = 0.35$ (2)
4-4'-Biphenyl- dicarboxylate pH 11.3, 12		2.00300	$a_{2,2}^H = 1.63$ (4) $a_{3,3}^H = 0.40$ (4)

^a All solutions contained either *tert*-butyl alcohol or formate as a scavenger for OH. ^b Determined by comparison to the peak from the silica cell and accurate to ± 0.00005 . ^c Given in Gauss and accurate to ± 0.03 G. The number of protons displaying the splitting is given in parentheses. ^d The two splittings of 0.97 G are slightly different in magnitude as shown by the reduced intensity of the central line of these triplets. Alternative assignments which correlate both 0.97-G splittings with either the two carboxyl protons or those at the 3 and 6 positions are possible. ^e This assignment is made by analogy to the results for benzoate and trimesate but the alternative assignment of the 0.12-G splitting to the COOH proton cannot be ruled out completely.

splitting is similar to that observed with liquid ammonia as solvent² and also to that for the terephthalonitrile radical anion.¹² A similar spectrum was observed at pH 9.6 but the lines were less intense and probably broader. At pH 8-9 no lines were observed because of considerable broadening. At pH 4.5, 5.2, and 6.1 the spectrum contained an additional triplet splitting of 0.25 G with little change in the main splitting and in the *g* factor. Clearly two successive protonations on the carboxyl groups take place in the pH region of 7-10. The singly protonated radical was not observed probably because of overlapping proton exchange regions. The last pK_a of the terephthalate radical anion has been recently determined by pulse conductivity and found to be 10.1.¹⁴

Trimesic Acid. The spectrum observed at pH 7.0, 7.5, and 8.6 showed four different proton hyperfine constants (Table I). By comparison with the parameters for the benzoate radical anion the smallest value is assigned to a carboxyl proton, the two very similar splittings of about 4.5 G are assigned to the ortho positions, and the larger split-

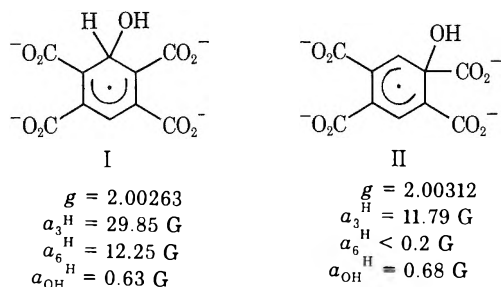
ting is assigned to the para. At pH 4 the spectrum was not observed because further protonations take place. In the alkaline region one expects an intense spectrum for the fully dissociated form with splittings by three equivalent protons but under no conditions was such a spectrum observed.

Pyromellitic Acid. The radical structures and their esr parameters are shown in Table I. At pH 13.7 and 14 only the splitting by the two ring hydrogens is observed. The first protonation takes place around pH 13 and an intramolecular hydrogen bridge is formed leaving the two ring hydrogens equivalent. The doubly protonated radical observed at pH 9, 7.2, and 5.5 must contain two bridge structures because the spectrum consists of two triplet splittings indicating two equivalent pairs of protons. The smaller splitting is assigned to the carboxyl protons to give the closest agreement with the assignment for the

(14) J. Lilie and R. W. Fessenden, *J. Phys. Chem.*, in press.

singly protonated form. Line broadening occurs at pH 4.8 and 4.0 and no spectrum was found at pH 3.3.

With pyromellitic acid at pH 12.2 we also observed two OH adducts and we wish only to present the esr parameters determined and the suggested assignments as shown in structures I and II. The splitting of 0.68 G is assigned to the OH proton by comparison with the value found for the preceding radical. These two radicals were present at comparable concentrations and the spectra of both of them disappeared with the addition of formate.

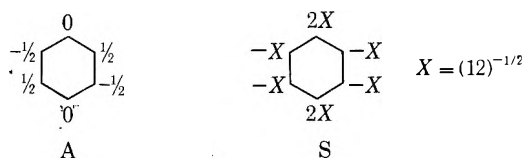


Mellitic Acid. A single line was observed at pH 13.5 as no hydrogen atoms are present in the radical. At pH 12.7 two broad lines were seen and at pH 11.5 the lines had narrowed to a 0.69-G doublet. A triplet appropriate to two equivalent protons was observed at pH 9.2 indicating a symmetrical structure with two hydrogen bridges (Table I). No analyzable spectra were obtained at pH <8 probably because of the many possible protonations in overlapping pH ranges.

Biphenyldicarboxylic Acids. The spectrum observed with irradiated solutions of 4,4'-biphenyldicarboxylic acid at pH 11–12 in the presence or absence of formate was analyzed in terms of two sets of four equivalent protons (Table I) showing a complete delocalization of the electron over the whole molecule. The assignment of the splittings to the protons at the two different types of positions is made by analogy to the biphenyl anion.^{12,15} The addition of N₂O caused the disappearance of the spectrum both in presence and absence of formate. This fact indicates that CO₂⁻ did not transfer electron to the biphenic acid. In neutral solution the spectrum was not sufficiently intense to allow analysis. With 2,2'-biphenyldicarboxylic acid at pH 12.4 only a few lines of low intensity were observed and no analysis could be made.

Magnitudes of the Hyperfine Constants. The relationship of the anion radicals studied here to benzyl-type radicals is noted by considering the sequence C₆H₅CH₂,^{7,10} C₆H₅CHO⁻,⁹ and C₆H₅CO₂⁻. Although the ring proton splittings are similar for all three radicals, calculations² place only 26% of the spin density in the latter on the CO₂⁻ group as compared with 60–70% on the -CH₂ group in benzyl.¹⁰ The difference arises mainly because a positive spin density is calculated for the substituted ring carbon in the former while in benzyl a negative spin density is predicted. The radical C₆H₅CHO⁻ is expected to be intermediate between the other two.

A rather large variation is seen in the hyperfine constants of the ring protons in the various radicals studied here. Because of the similarity of these radicals to those derived from the corresponding nitriles these variations should be understandable in a similar way. The hyperfine constants for aromatic radical anions are customarily understood in terms of the symmetric and antisymmetric orbitals¹⁶ (orbitals S and A, respectively, where the numbers give the amplitude of the wave function at that car-



bon atom). Thus for phthalate the orbital A is of lowest energy and the small splittings of 0.05 G belong to the protons attached to the carbons with near zero spin density. The hyperfine constants of the carboxyl protons vary also considerably and seem to be influenced by similar factors. The hyperfine splitting of about 1 G in the anion radicals of benzoate, isophthalate, and trimesate appears to be the value appropriate to a carboxyl proton in a group attached at a ring position of high spin density. The very much smaller values in the radicals derived from phthalate, pyromellitate, and mellitate are all for protons which bridge between carboxyl groups attached at adjacent positions with opposite signs for the wave function (see orbital A). Thus the proton is in the nodal plane of the orbital and little splitting is to be expected. The singly protonated radical from mellitate has a somewhat larger splitting (0.69 G) than the others in this group but here the symmetric orbital may be more significant. The only other value that seems to depart from this overall pattern is that for terephthalate where the protons in the doubly protonated form have splittings of 0.25 G in contrast to the 1 G expected for them.

We should note finally that the fully dissociated radicals from trimesate and mellitate have, on paper at least, a threefold symmetry and so might show the increased line width generally associated with the orbital degeneracy in such radicals (e.g., C₆H₆⁻).¹⁷ The single line from mellitate seems to have no excessive width but in fact no spectrum was detected for the fully dissociated form of the radical from trimesate. This may be the result of the symmetry or of chemical complications related to the lower stability of this radical. (Note that considerable difficulty was experienced in preparing the radical from isophthalate.)

Discussion of Acid-Base Equilibria. Although accurate dissociation constants for the acid-base equilibria of the electron adducts have not been measured, the nature of the equilibria and the pH region at which they take place have been determined in most cases. Previous pulse radiolysis experiments³ have shown that the pK_a values for the benzoic acid electron adduct are 5.3 and 12.0. The first value is not greatly different than the pK_a (4.17) for benzoic acid itself but the high value for the second dissociation shows the large effect of the additional negative charge.

For terephthalic acid the pK_a values are 3.51 and 4.82. The first pK_a of the radical is also ~4, but the other two dissociations occur at pH ~8 and 10.1.¹⁴ The effect of the negative charge on the pK_a values of the electron adduct is smaller in terephthalate than in benzoate apparently because the additional charge is spread over the two carboxyl groups.

The pK_a values for phthalic acid are 2.98 and 5.28 and are somewhat different from those for terephthalic acid as

- (15) F. C. Adam and C. R. Kepford, *Can. J. Chem.*, **49**, 3529 (1971).
- (16) See the discussion given by J. E. Wertz and J. R. Bolton, "Electron Spin Resonance," McGraw-Hill, New York, N. Y., 1972, p 99 ff.
- (17) See the discussion of relaxation in such radicals by R. G. Kooser, W. V. Volland, and J. H. Freed, *J. Chem. Phys.*, **50**, 5243 (1969); M. R. Das, S. B. Wagner, and J. H. Freed, *ibid.*, **52**, 5404 (1970).

a result of the possible hydrogen bridge between the two carboxyl groups. The first two pK_a values for the phthalic acid electron adduct are in the regions of 3-4 and 6-7, again with little change from those of the parent compound. However, the extra charge associated with the unpaired electron, located in part on the two carboxyl groups, greatly strengthens the hydrogen bond between these two groups and raises the last pK_a to over 14.

All the pK_a values for pyromellitic acid are between 2 and 5.6. The first three pK 's of the electron adduct are below 4 and were not observed. The last two protons were found to involve two intramolecular hydrogen bridges in a symmetric structure and their pK_a values are ~ 10 and ~ 13 . These values are high but not as high as that found for the hydrogen bonded phthalate radical. The difference is most probably due to the distribution of negative charge over all the carboxyl groups which results in a weaker effect on the particular positions. Similarly, the last two pK_a values for the mellitic acid electron adduct are ~ 10 and ~ 12.5 , thus the increased charge delocalization seems to result in a decreased effect on the pK_a .

The observations reported here provide in certain cases qualitative information on the kinetics of the proton exchange associated with the acid-base equilibria. For "nor-

mal" dissociable protons the rate constant for the forward reaction of the equilibrium $\text{ROH} + \text{OH}^- \rightleftharpoons \text{RO}^- + \text{H}_2\text{O}$ should be $\sim 10^{10} \text{ M}^{-1} \text{ sec}^{-1}$ so that line broadening in any spectrum which shows a splitting by this proton will begin at pH 10-11 ($k[\text{OH}^-] \sim 10^6\text{-}10^7 \text{ sec}^{-1}$).¹⁸ Depending on the magnitude of the splitting, the lines of the spectrum should become narrow above about pH 12. This result is obtained for the e_{aq}^- adduct to benzoate in that the spectrum disappears at pH 11. The radicals with intramolecular hydrogen bonds do not behave in this normal fashion. The radical anion obtained from phthalate shows no evidence of exchange even at pH 14 and so it must be concluded that the forward reaction rate constant is less than $\sim 10^6 \text{ M}^{-1} \text{ sec}^{-1}$. A similar conclusion must be reached for the anion radicals produced from o-nitrophenol⁶ and maleate⁴ which also show no exchange of the bridge hydrogen in 1 M base. The radicals from pyromellitic and mellitic acids show intermediate behavior in that dissociation occurs at pH ~ 13 with line broadening starting around pH 12.5. In this case the forward rate constant must be $10^7\text{-}10^8 \text{ M}^{-1} \text{ sec}^{-1}$.

(18) See the discussion in G. P. Laroff and R. W. Fessenden, to be published. Also G. P. Laroff, Ph.D. Thesis, Carnegie-Mellon University, 1972.

Electron Spin Resonance Studies of Heisenberg Spin Exchange. The Effect of Macrocyclic Polyethers on the Spin Exchange Rate for Ion Pairs

M. T. Watts, Ming Liang Lu, and M. P. Eastman*

The University of Texas at El Paso, El Paso, Texas 79968 (Received November 10, 1972)

Publication costs assisted by The University of Texas at El Paso

Heisenberg spin exchange in dimethoxyethane (DME) solutions of potassium tetracyanoethanide (KTCNE) was studied by esr in the absence and presence of the macrocyclic polyether dibenzo-18-crown-6 (DBC). Results indicate that at concentrations of $\sim 10^{-3} \text{ M}$ KTCNE exists primarily as an ion pair in DME. Measurements of line width for a $1.9 \times 10^{-3} \text{ M}$ solution of KTCNE in DME as a function of DBC concentration lead to the conclusion that DBC forms a 1:1 complex with the K^+ in the ion pair and that the equilibrium constant for the complexation reaction is about $4 \times 10^3 \text{ M}^{-1}$ at 15° . The second-order rate constant for spin exchange for the complexed ion pair is $(1.5 \pm 0.3) \times 10^9 \text{ M}^{-1} \text{ sec}^{-1}$ at 15° ; that of the uncomplexed ion pair has previously been shown to be $(4.1 \pm 0.6) \times 10^9 \text{ M}^{-1} \text{ sec}^{-1}$. The rate constant for spin exchange between the complexed and uncomplexed ion pairs is determined to be $(3.0 \pm 0.5) \times 10^9 \text{ M}^{-1} \text{ sec}^{-1}$ at 15° . Studies of line width *vs.* T/η indicate but do not prove that the complexed form of the ion pair undergoes strong exchange in the temperature range $0\text{-}40^\circ$.

I. Introduction

Previous studies of Heisenberg spin exchange have demonstrated that the Heisenberg spin exchange rate (ω_{HE}) for free radicals in solution can be expressed as

$$\omega_{\text{HE}} = [1/(\tau_2)] [(J^2\tau_1^2)/(1 + J^2\tau_1^2)] \quad (1)$$

where τ_2 is the mean time between radical-radical collisions, τ_1 the mean lifetime of a collision pair, and J is minus two times the exchange integral for the radicals in the collision pair.¹⁻⁵

For the case of simple Brownian diffusion of uncharged free radicals⁶

$$\begin{aligned} \tau_2^{-1} &= 4\pi dDN \\ \tau_1^{-1} &= (6D/d^2) \end{aligned} \quad (2)$$

Here d is the "interaction distance" for exchange and N is

- (1) G. E. Pake and T. R. Tuttle, Jr., *Phys. Rev. Lett.*, **3**, 423 (1959).
- (2) D. Kivelson, *J. Chem. Phys.*, **33**, 1094 (1960).
- (3) J. D. Currin, *Phys. Rev.*, **126**, 1995 (1962).
- (4) C. S. Johnson, *Mol. Phys.*, **12**, 25 (1967).
- (5) M. P. Eastman, R. G. Kooser, M. R. Das, and J. H. Freed, *J. Chem. Phys.*, **51**, 2690 (1969).

the number density of radicals. The Stokes-Einstein diffusion coefficient D is given by

$$D = kT/6\pi a\eta \quad (3)$$

where η is the viscosity and a the molecular radius. For the case of like charged free radicals τ_2^{-1} will be decreased from the value calculated on the basis of eq 2 and τ_1^{-1} will be increased.^{7,8}

The line widths measured in an esr experiment are related to ω_{HE} by the expression⁵

$$\omega_{HE} = f_M(1.52 \times 10^7)[\Gamma_M - \Gamma_M(0)] \quad (4)$$

Here \bar{M} is the spectral index of the line being measured,⁹ Γ_M is the line width in the presence of exchange, and $\Gamma_M(0)$ is the line width in the absence of exchange. The statistical factor f_M compensates for the lack of observable line-broadening effects in exchange between radicals with the same nuclear spin configuration.

It has been shown that potassium tetracyanoethanide (KTCNE) undergoes strong exchange ($J^2\tau_1^2 \gg 1$) in dimethoxyethane (DME).⁵ The second-order rate constant for this process is $(4.1 \pm 0.6) \times 10^9 M^{-1} \text{sec}^{-1}$ at 15°. The experimental evidence indicated that the radical exists primarily in the form of an ion pair in the concentration range 10^{-3} – $10^{-4} M$. This conclusion is supported by the work of Szwarc, *et al.*, which showed that a reasonable estimate of the dissociation constant for an ion pair in DME would be $\sim 10^{-6}$.¹⁰

Recently considerable work has been carried out on the class of compounds known as macrocyclic polyethers or crown ethers.^{11–13} These compounds have exhibited the ability to complex a wide variety of cations. In particular the work of Smid, *et al.*,^{14–17} has shown that crown ethers strongly complex the alkali and alkaline earth salts of fluorenyl. In ethereal solvents the salt crown complexes exist in the form of ion pairs which can have two isomeric forms. In general the stoichiometry and nature of cyclic polyether complexes depend on the size of the "hole" in the polyether ring, the size of the cation being complexed, and the nature of the medium in which the reaction takes place.

It would be anticipated that if the potassium ion in the K^+TCNE^- ion pair were complexed by a crown ether the Heisenberg spin exchange rate for the radical ion pair would be considerably altered. This could arise because of an increase in τ_2 due to the increased size of the radical ion pair, because polyether complexation led to an increase in the charge separation in the ion pair and thus to electrostatic radical-radical repulsion, or because the bulky polyether prevented strong overlap of the wave functions for the unpaired electron on the radicals involved in a collision pair. A possible consequence of the latter condition would be that $J^2\tau_1^2 \sim 1$. It has been shown that in the case of the di-*tert*-butyl nitroxide radical $J^2\tau_1^2 \sim 1$; apparently the bulky tertiary butyl groups lead to weak unpaired electron wave junction overlap in radical-radical collision pairs.^{5,18,19}

II. Experimental Section

The synthesis of KTCNE was carried out under vacuum according to the procedure described by Webster, Mahler, and Benson.²⁰ Dibenzo-18-crown-6 (DBC) was purchased from the Aldrich Chemical Co. and was purified by recrystallizing twice from toluene and drying under vacuum. The melting point of the purified material was 163–164°.

Esr samples of KTCNE in DME were prepared in a manner previously described.⁵ The concentration of radicals was determined from the line width of the sample at 15° using the rate constant for spin exchange at 15° ($(4.1 \pm 0.6) \times 10^9 M^{-1} \text{sec}^{-1}$) and the experimental line width. For the T/η vs. line width plots the DBC was added to the sample by means of a break seal after the line width measurements had been made on the solution of KTCNE in DME.

The viscosity values used were those of pure DME.²¹ The line widths were corrected for changes in radical concentration due to changes in sample temperature by means of the published density values for pure DME.²¹

The titration curve in Figure 1 was obtained using a $1.9 \times 10^{-3} M$ sample of KTCNE in DME. A measured volume of a $4.4 \times 10^{-3} M$ solution of DBC in DME was added to the KTCNE solution through a Fisher-Porter Model 795-500 Teflon needle valve and the DME used to carry the DBC was then distilled away. Thus the radical concentration remained constant throughout the titration.

The sample tube employed in the optical work had a Pyrocell No. 6008 quartz optical cell (1 mm path length) side arm. After the optical spectrum of KTCNE in DME was determined a measured amount of DBC was added to the solution through a break seal. All optical studies were made on a Cary-14 spectrophotometer at room temperature.

Esr measurements were made on a Varian V-4500-10 spectrometer employing a V-3900 12-in. magnet. Temperature was controlled by means of a Varian V-4557 variable temperature controller. For samples having line widths greater than 100 mG, 100-KHz field modulation was employed. Small corrections for modulation frequency broadening were made for lines narrower than 200 mG.^{5,22} For narrow line samples (20–40 mG), 400-Hz field modulation was employed. At all modulation frequencies the modulation amplitude was kept to 1/10 or less of the first derivative line width. In all the experiments reported here the overlap of hyperfine lines can be neglected because $\omega_{ex}/a < 0.3$.^{5,19} Here a is the ^{14}N hyperfine splitting constant for the TCNE⁻ radical.

- (6) S. Chandrasekhar, *Rev. Mod. Phys.*, **15**, 1 (1943).
- (7) M. Eigen, *Z. Phys. Chem. (Frankfurt am Main)*, **1**, 176 (1954).
- (8) P. Debye, *Trans. Electrochem. Soc.*, **82**, 265 (1942).
- (9) J. Gendell, J. H. Freed, and G. K. Fraenkel, *J. Chem. Phys.*, **41**, 949 (1964).
- (10) P. Chang, R. V. Slates, and M. Szwarc, *J. Phys. Chem.*, **70**, 3180 (1966).
- (11) C. J. Pedersen, *J. Amer. Chem. Soc.*, **89**, 7017 (1967).
- (12) C. J. Pedersen and H. K. Frensdorff, *Angew. Chem., Int. Ed. Engl.*, **11**, 16 (1972).
- (13) J. J. Christensen, J. O. Hill, and R. M. Izatt, *Science*, **174**, 459 (1971).
- (14) T. E. Hogan Esch and J. Smid, *J. Amer. Chem. Soc.*, **91**, 458 (1969).
- (15) K. H. Wong, G. Konizer, and J. Smid, *J. Amer. Chem. Soc.*, **92**, 666 (1970).
- (16) U. Takaki, T. E. Hogan Esch, and J. Smid, *J. Amer. Chem. Soc.*, **93**, 6760 (1971).
- (17) U. Takaki, T. E. Hogan Esch, and J. Smid, *J. Phys. Chem.*, **76**, 2152 (1972).
- (18) N. Edelstein, A. Kwok, and A. H. Maki, *J. Chem. Phys.*, **41**, 3473 (1964).
- (19) W. Plachy and D. Kivelson, *J. Chem. Phys.*, **47**, 3312 (1967).
- (20) O. W. Webster, W. Mahler, and R. E. Benson, *J. Amer. Chem. Soc.*, **84**, 3678 (1962).
- (21) C. Carvajal, K. J. Tolle, J. Smid, and M. Szwarc, *J. Amer. Chem. Soc.*, **87**, 5548 (1965).
- (22) R. G. Kooser, W. V. Volland, and J. H. Freed, *J. Chem. Phys.*, **50**, 5243 (1969).

III. Results and Discussion

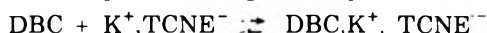
The optical spectrum of DBC in DME consists of an unresolved absorption band with a maximum at 277 nm and shoulders at 273 and 283 nm. In the presence of the K^+ ion the DBC spectrum consisted of two peaks, one at 273 nm and one at 279 nm. The spectrum of $TCNE^-$ which has been described^{20,23} was not measurably affected by the presence of DBC. The optical spectra indicated, as expected on the basis of earlier studies,¹¹ that DBC formed a 1:1 complex with the K^+ ion, but they did not indicate whether or not the complex existed as an ion pair with $TCNE^-$.

Figure 1 shows the effect on the width of the $\bar{M} = 0$ line of adding DBC to a $1.9 \times 10^{-3} M$ solution of KTCNE in DME at 15° . Qualitatively it is seen that the addition of polyether leads to a line width decrease until $[DBC]_0/[KTCNE]_0 \sim 1$. Here $[DBC]_0$ is the total polyether concentration and $[KTCNE]_0$ is the total radical concentration. From this point on the line width is essentially unchanged out to the last experimental point.

The esr line shapes for all the points on Figure 1 were shown to be Lorentzian within experimental error out to at least five first derivative half-widths from the first derivative zero.

There were no indications that the resonance conditions changed as the polyether was added. Thus, in the absence of detailed g value studies it is assumed that the g values for the $TCNE^-$ radical depend little or not at all on the presence of DBC.

Since the optical spectra indicate a 1:1 complex between K^+ and DBC, while the esr line width studies indicate a reduction in the Heisenberg spin exchange rate for the $TCNE^-$ radical upon the addition of DBC, it seems reasonable to conclude that DBC is complexing the K^+ in the KTCNE ion pair according to the equilibrium



Based on studies of crown ether complexes of fluorenyl alkali metal ion pairs¹⁶ and on studies of ion pair dissociation constants in DME¹⁰ the dissociation constant for $DBC, K^+, TCNE^-$ would be expected to be of about the same order as predicted for the KTCNE ion pair, *i.e.*, 10^{-6} . Thus, at the radical and crown ether concentrations used in this study dissociation into free ions is not expected to be important.

Figure 2 shows plots of line width *vs.* T/η for a $2.2 \times 10^{-3} M$ solution of KTCNE in DME and for the same solution in the presence of $4.5 \times 10^{-3} M$ DBC. Solubility studies showed that the solution containing DBC was saturated with DBC in the temperature range $8-10^\circ$ and that it was relatively easy to prepare supersaturated solutions. In Figure 2 the point at $T/\eta = 4.6 \times 10^2 K/cP$ was obtained from a supersaturated solution.

The observation that the line width for the sample containing DBC is linear with T/η indicates that over the temperature range investigated the complexed ion pairs undergo strong exchange. However, because of solubility problems on the one hand and shifting of the complexation equilibrium with temperature on the other, a wide temperature range could not be reliably investigated.

A least-squares fit to the points for the solution containing only KTCNE yields a least-squares slope of $(7.7 \pm 0.2) \times 10^{-4} G cP/^\circ K$ and an intercept of $10 \pm 4 mG$. These results agree within experimental error with those previously reported.⁵ For the complexed ion pairs the slope is

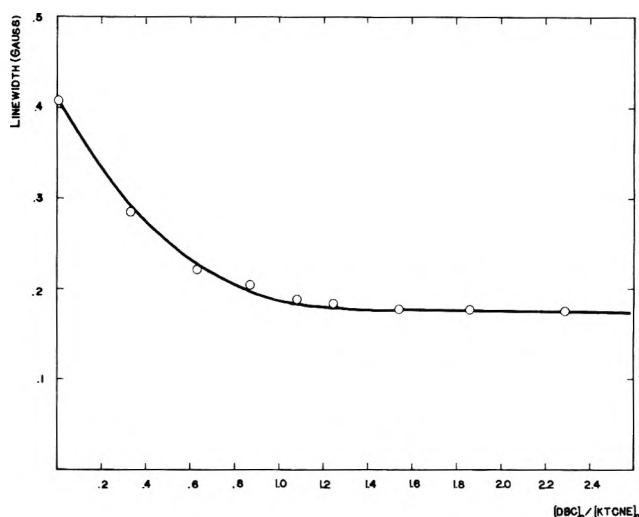


Figure 1. Width of the $\bar{M} = 0$ line for $1.9 \times 10^{-3} M$ KTCNE in DME as a function of $[DBC]_0/[KTCNE]_0$ at 15° . The solid line represents the least-squares fit to the experimental line widths.

$3.9 \times 10^{-4} G cP/^\circ K$. Due to the narrow range of T/η values studied, this value must be regarded as approximate.

A $5 \times 10^{-5} M$ solution of KTCNE in DME yielded a line width of 25 mG at 15° . The addition of DBC ($5 \times 10^{-3} M$) increased the line width to 33 mG. The observation that the line width increased by 30% when the crown ether was added indicated that a substantial portion of the radical was in the form of the $DBC, K^+, TCNE^-$ ion pair. This would be expected if the dissociation constant for the $DBC, K^+, TCNE^-$ ion pair was, as was previously estimated, about 10^{-6} . After correcting for slight spin exchange effects the line width for the DBC complexed ion pair in the absence of exchange at 15° is estimated to be $28 \pm 4 mG$. The line width for KTCNE in DME in the absence of exchange is reported to be 16 mG at 15° .⁵

The ^{14}N hyperfine splitting for radical was measured before and after the addition of DBC in the above experiments. These measurements indicated that the splitting for the complexed ion pair did not differ by more than 1% from the value reported for KTCNE in DME ($1.59 \pm 0.02 G$).⁵

The rate of complexation of DBC with Na^+ ions in dimethylformamide has been determined to be $6 \times 10^7 M^{-1} sec^{-1}$ while the rate of the decomplexation reaction was determined to be about $10^5 sec^{-1}$.²⁴ In tetrahydropyran the rate of complexation of tetraglyme with Na^+ in a sodium naphthalene ion pair is about $10^8 M^{-1} sec^{-1}$ while the decomplexation rate is on the order of $10^6 sec^{-1}$.²⁵ Presumably the forward and reverse rate constants in the above equilibrium are of similar magnitude. Because the ^{14}N hyperfine splitting constants for $TCNE^-$ are not affected by complexation, and because our experiments indicate little or no difference in g value for the complexed and uncomplexed forms, it is assumed that the observed esr lines represent the fast exchange average of lines arising from the two forms of the ion pair.²⁶ As expected for

(23) M. Itoh, *J. Amer. Chem. Soc.*, **92**, 886 (1970).

(24) E. Shchori, J. Jagur-Grodzinski, Z. Luz, and M. Shporer, *J. Amer. Chem. Soc.*, **93**, 7133 (1971).

(25) K. Hofelmann, J. Jagur-Grodzinski, and M. Szwarc, *J. Amer. Chem. Soc.*, **91**, 4645 (1969).

(26) A. Carrington and A. D. McLachlan, "Introduction to Magnetic Resonance," Harper and Row, New York, N. Y., 1967.

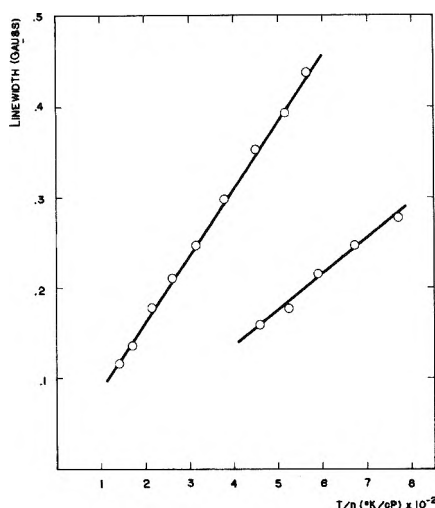


Figure 2. Width of the $\bar{M} = 0$ line for $2.2 \times 10^{-3} M$ KTCNE in DME as a function of T/η : top line in the absence of DBC; bottom line in the presence of $4.5 \times 10^{-3} M$ DBC.

fast exchange the observed lines all have a Lorentzian line shape.

On the basis of the above, the experimentally observed line width may be related to the line width for the complexed and uncomplexed forms of the ion pair by the modified Bloch equation for fast exchange

$$\Gamma = X_c(\Gamma_c) + X_u(\Gamma_u) \quad (5)$$

Here X_c and X_u represent the fractions of ion pairs which are complexed and uncomplexed, respectively. From eq 4 it is seen that Γ_c and Γ_u depend on the exchange rate and the line width in the absence of exchange.

In the system under consideration there are three possible spin exchange reactions which can take place and contribute to the total line width. These are exchange between uncomplexed ion pairs, described by rate constant k_{uu} , exchange between complexed ion pairs, described by rate constant k_{cc} , and mixed spin exchange described by rate constant k_{cu} . Expressions for the exchange frequencies of the complexed and uncomplexed forms ($\omega_{ex,c}$ and $\omega_{ex,u}$, respectively) in terms of these rate constants can be written as

$$\begin{aligned} \omega_{ex,u} &= k_{uu}(u) + \frac{1}{2}k_{uc}(c) \\ \omega_{ex,c} &= k_{cc}(c) + \frac{1}{2}k_{uc}(u) \end{aligned} \quad (6)$$

where (c) and (u) refer to the concentrations of complexed and uncomplexed ion pairs. The factor of $\frac{1}{2}$ in front of k_{uc} in eq 6 reflects the fact that only one-half of the members of a mixed collision pair are of a given type.

The data in Figure 1 show that for $[DBC]_0/[KTCNE]_0 \gtrsim 2$ the line width approaches a value of about 175 mG. Using the value of ω_{ex} calculated from eq 4, where $\Gamma_0(0)$

= 28 mG, and the relation

$$k_{cc} = \omega_{ex}/[KTCNE]_0 \quad (7)$$

the value of k_{cc} is determined to be $(1.5 \pm 0.3) \times 10^9 M^{-1} \text{sec}^{-1}$ at 15° . The value calculated by means of eq 4 and 7 from the data in Figure 2 ($1.6 \times 10^9 M^{-1} \text{sec}^{-1}$) agrees with this value within experimental error.

The equilibrium constant for the complexation reaction, K , can be expressed as

$$K = (C)/([DBC]_0 - (C))([KTCNE]_0 - (C)) \quad (8)$$

Here the concentration of complex is given by (C). By means of eq 4-6 the experimental line widths can be related to the rate constants for the spin exchange reactions. The values of X_c and X_u in eq 6 can be expressed in terms of K , $[DBC]_0$, and $[KTCNE]_0$. Using the following values $k_{uu} = 4.1 \times 10^9 M^{-1} \text{sec}^{-1}$, $k_{cc} = 1.5 \times 10^9 M^{-1} \text{sec}^{-1}$, $\Gamma_0(0)_c = 28 \text{ mG}$, and $\Gamma_0(0)_u = 16 \text{ mG}$, the least-squares fit to the experimental line widths yield $K = 4.3 \times 10^3 M^{-1}$ and $k_{uc} = 3.0 \times 10^9 M^{-1} \text{sec}^{-1}$. As expected on the basis of the simple Brownian diffusion model⁶

$$k_{uc} \sim \frac{1}{2}(k_{uu} + k_{cc})$$

The principle source of error in this experiment is in determining an accurate value for $[KTCNE]_0$. In the experimental work summarized in Figure 1 the value of $[KTCNE]_0$ determined from the line width agreed with the value determined on the basis of the weight of KTCNE and the volume of solvent in the sample within experimental error or about 5%. Calculating the error in K resulting from a 5% error in $[KTCNE]_0$ leads to $K = (4 \pm 1) \times 10^3 M^{-1}$.

Studies in tetrahydrofuran (THF) of the complexation of the K^+ ion in the fluorenyl potassium contact and solvent separated ion pairs by 4-methylbenzo-18-crown-6 have yielded a complexation constant 10^4 - $10^5 M^{-1}$. Presumably the complexation constant for these ion pairs with DBC in THF would be about the same order of magnitude. Clearly the value of K determined in this experiment with KTCNE and DBC in DME is substantially smaller. It is difficult to attribute this to a single factor since the value of K depends both on the ions involved in the ion pair and on the solvents employed. In THF KTCNE ion pairs have been shown to form a diamagnetic dimer.²⁷ Experiments indicate that the addition of DBC to solutions of KTCNE in THF inhibits or prevents the formation of the diamagnetic dimer and that the value of K for the complexation reaction in THF is larger than in DME.²⁸

Acknowledgment. This work was supported by the Robert A. Welch Foundation.

(27) R. Chang, *J. Phys. Chem.*, **74**, 2029 (1970).

(28) Ming Liang Lu, M. T. Watts, and M. P. Eastman, unpublished results.

Electron–Electron Double Resonance of Irradiated Single Crystals of Zinc Acetate and Malonic Acid. The Influence of Nuclear Spin Exchange¹

Lowell D. Kispert,* Kichoon Chang, and Carolyn M. Bogan²

Department of Chemistry, The University of Alabama, Tuscaloosa, Alabama 35486 (Received November 18, 1972)

Publication costs assisted by The University of Alabama

Electron–electron double resonance (eldor) spectra of the $\dot{\text{C}}\text{H}_2\text{COO}^-$ radical in irradiated single crystals of zinc acetate and the $\dot{\text{C}}\text{H}_2\text{COOH}$ radical in irradiated malonic acid were obtained over a temperature range from -100 to $+50^\circ$. A maximum in the eldor intensity of the allowed lines was observed at -70° for $\dot{\text{C}}\text{H}_2\text{COO}^-$ and at 0° for $\dot{\text{C}}\text{H}_2\text{COOH}$. A maximum in the intensity of the forbidden eldor lines was observed approximately 50° below the maximum intensity of the allowed lines. The qualitative aspects of the temperature dependence of the eldor spectra of $\dot{\text{C}}\text{H}_2\text{COO}^-$ and $\dot{\text{C}}\text{H}_2\text{COOH}$ can be explained in terms of the correlation times of the nonadiabatic spin exchange process.

Introduction

The temperature dependence of the esr spectra of $\dot{\text{C}}\text{H}_2\text{COO}^-$ or $\dot{\text{C}}\text{H}_2\text{COOH}$, found in irradiated crystals of malonic acid,³ glycine,^{4,5} sodium acetate trihydrate,^{6,7} and zinc acetate dihydrate,^{8,9} has been the subject of much interest. Marked temperature dependence of the proton coupling constants has been reported in addition to the coalescence of the inner peaks^{6,8,9} at high temperature, and the shifting of the outer peaks toward the center of the spectrum.^{8,10} Despite these changes with temperature, the g values remain constant⁶ and the direction of the carbon p orbital remains quenched in space.⁶

Recently, Hayes, *et al.*,¹⁰ proposed that a nonadiabatic spin exchange is responsible for the observed temperature dependence of $\dot{\text{C}}\text{H}_2\text{COO}^-$ and were able to reproduce many of the features of the spectrum using this model.

Electron–electron double resonance (eldor) has been quite successful in probing intra- and intermolecular relaxation processes.^{11–17} It has been possible in several cases to correlate the magnitude of the various eldor R values with the correlation times of the intramolecular motion.

Kispert, *et al.*,¹² proposed that the eldor signals observed above 10° in $(\text{CH}_3)_2\dot{\text{C}}\text{COOH}$ were dependent on the magnitude of the correlation times of the dynamic process which made the two methyl groups appear equivalent in the esr spectrum.

The nonadiabatic spin exchange proposed by Hayes, *et al.*,¹⁰ for $\dot{\text{C}}\text{H}_2\text{COO}^-$ is also expected to have some effects on the relaxation processes responsible for the observation of an eldor spectrum. It is of interest then to examine the temperature dependence of the eldor spectrum of $\dot{\text{C}}\text{H}_2\text{COO}^-$ in the hope that more can be learned about the origin of the temperature dependence of the esr spectra.¹⁸

Experimental Section

All spectra were run on a standard Varian E-800 eldor accessory coupled to a Varian E-12 esr spectrometer. The magnetic field was measured by a tracking nmr system. Single crystals of malonic acid and zinc acetate were grown from aqueous solution by slow evaporation. The crystals were X-irradiated at room temperature and subsequently investigated by esr over a range of tempera-

tures. The crystals were aged a few days to eliminate any unstable radicals initially present at room temperature. The eldor spectra of $\dot{\text{C}}\text{H}_2\text{COOH}$ in irradiated triclinic malonic acid crystals were taken in the ab plane, nearly parallel to the b axis where a four-line (equally intense) esr

- (1) This research was supported by the Atomic Energy Commission under Contract No. AT-(40-1)-4062 and this is AEC Document No. ORO-4062-8.
- (2) AAUW Fellowship holder 1970–1971.
- (3) A. Horsfield, J. R. Morton, and D. H. Whiffen, *Mol. Phys.*, **4**, 327 (1961).
- (4) J. R. Morton, *J. Amer. Chem. Soc.*, **86**, 2325 (1964).
- (5) R. F. Weiner and W. S. Koski, *J. Amer. Chem. Soc.*, **85**, 873 (1963); H. C. Box, H. G. Freund, and E. E. Budzinski, *ibid.*, **88**, 658 (1966).
- (6) M. Fujimoto and J. Janecka, *J. Chem. Phys.*, **55**, 5 (1971).
- (7) M. T. Rogers and L. D. Kispert, *Advan. Chem. Ser.*, **No. 82**, 327 (1968).
- (8) W. M. Tolles, L. P. Crawford, and J. L. Valenti, *J. Chem. Phys.*, **49**, 4745 (1968).
- (9) H. Ohigashi and Y. Kurita, *Bull. Chem. Soc. Jap.*, **41**, 275 (1968).
- (10) R. G. Hayes, D. J. Steible, W. M. Tolles, and J. W. Hunt, *J. Chem. Phys.*, **53**, 4466 (1970).
- (11) J. S. Hyde, J. C. W. Chien, and J. H. Freed, *J. Chem. Phys.*, **48**, 4211 (1968). References to earlier work cited: J. S. Hyde, L. D. Kispert, R. C. Sneed, and J. C. W. Chien, *J. Chem. Phys.*, **48**, 3824 (1968); J. S. Hyde, R. C. Sneed, Jr., and G. H. Rist, *ibid.*, **51**, 1404 (1969); V. A. Benderskii, L. A. Blumenfeld, P. A. Stunkas, and E. A. Sokalov, *Nature (London)*, **220**, 365 (1968); P. A. Stunkas, V. A. Benderskii, L. A. Blumenfeld, and E. A. Sokalov, *Opt. Spektrosk.*, **28**, 278 (1970); P. A. Stunkas, V. A. Benderskii, and E. A. Sokalov, *ibid.*, **28**, 487 (1970); P. A. Stunkas and V. A. Benderskii, *ibid.*, **30**, 559 (1971); M. P. Eastman, G. V. Bruno, and J. H. Freed, *J. Chem. Phys.*, **52**, 321 (1970); M. Nechtschein and J. S. Hyde, *Phys. Rev. Lett.*, **24**, 672 (1970); V. A. Benderskii, P. A. Stunkas, and A. I. Rakoed, *Mol. Phys.*, **24**, 449 (1972). Eldor results reported by L. D. Kispert, C. M. Bogan, and K. Chang at the Varian EPR Double-Resonance Workshop, Jan. 26–28, 1972, Palo Alto, Calif., and the 23rd Southwestern Regional Meeting of the American Chemical Society, Nashville, Tenn., Nov. 4–5, 1971, Abstract No. 54; H. M. Vieth, H. Brunner, and K. H. Hausser, *Z. Naturforsch. A*, **26**, 167 (1971); T. S. Kuau, D. S. Tinti, and M. A. El-Sayed, *Chem. Phys. Lett.*, **4**, 507 (1970); M. Leung and M. A. El-Sayed, *ibid.*, **16**, 454 (1972).
- (12) L. D. Kispert, K. Chang, and C. M. Bogan, *J. Chem. Phys.*, in press (1973); results given at the 24th Southeastern Regional Meeting of the American Chemical Society, Nov. 2–4, 1972, Physical Chemistry Abstract No. 75, and at the SE Magnetic Resonance Conference held at Athens, Ga., Oct. 12–13, 1972.
- (13) L. D. Kispert, K. Chang, and C. M. Bogan, *Chem. Phys. Lett.*, **17**, 592 (1972); L. D. Kispert and M. T. Rogers, *J. Chem. Phys.*, in press. The effect of chlorine quadrupole relaxation.
- (14) G. Rist and J. H. Freed, personal communication; eldor investigations of $\cdot\text{CH}(\text{COOH})_2$.
- (15) J. H. Freed, D. S. Leniart, and H. C. Connor, *J. Chem. Phys.*, in press.
- (16) Results reported by K. Chang and L. D. Kispert at the 24th Southeastern Regional Meeting of the American Chemical Society, Nov. 2–4, 1972, Physical Chemistry Abstract No. 76. The effect of p orbital anisotropy.

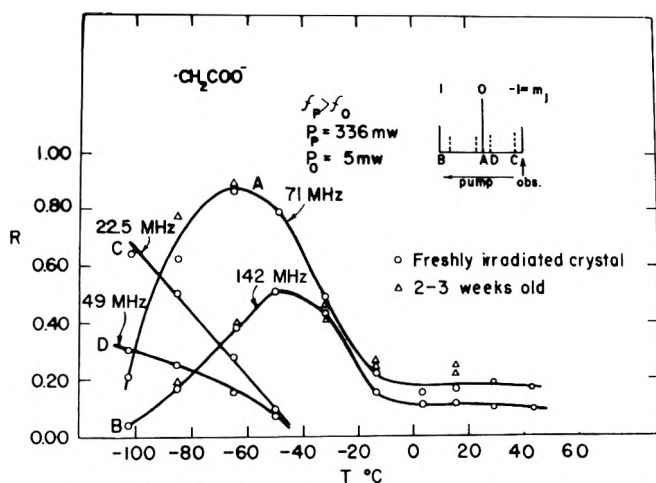


Figure 1. Eldor reduction factors for CH_2COO^- (in zinc acetate) vs. temperature. A and B are the "allowed" eldor lines; both the observing and the pumping esr transitions are allowed with $\Delta M_J = 0$. C and D are the "forbidden" eldor lines; the observing esr transition is allowed but the pumped esr line is forbidden with $\Delta M_J = 1$. For all curves, the $M_J = -1$ esr line is the observing esr line. R_{expt} = eldor line height/esr line height. No corrections were made for the difference in the eldor (5.0 MHz) and esr (6.5 MHz) line widths. The $M_J = -1$ esr and eldor line widths did not vary significantly ($< 10\%$) with temperature.

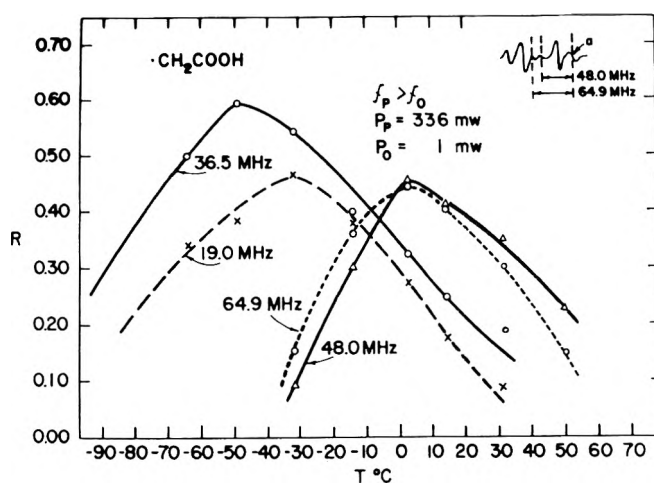


Figure 2. Eldor reduction factors for CH_2COOH (in malonic acid) vs. temperature. Only the allowed eldor lines observed at 64.9 (O) and 48.0 MHz (Δ) and the forbidden eldor lines observed at 36.5 (O) and 19.0 MHz (X) were plotted. A maximum occurs at approximately 0° for the allowed eldor lines and from -50 to -30° for the forbidden eldor lines. R_{expt} was calculated in the same manner as in Figure 1. The eldor (4.5 MHz) and esr (8.5 MHz) line widths did not vary with temperature. The observing field is set at position a.

pattern occurred at temperatures below 50° . On the other hand, the CH_2COO^- radical in monoclinic zinc acetate crystals was investigated at varying crystal angles. However, the temperature dependence of the eldor intensity did not depend on the hfs anisotropy of the crystal position. The results reported here are primarily those observed for the magnetic field parallel to a crystal direction 21° from the a^* axis. In this direction, a 1:2:1 esr triplet was observed at all temperatures between -100 and 50° . All listed R values have been calculated with the observing field positioned at the center of the first derivative esr line (modulation amplitude < 0.7 G).

All eldor spectra were taken with the power of the observing klystron set to less than one-fourth of the power required for maximum esr signal (typically 0.5–2 mW). A very small ($< 10\%$) dependence of the eldor reduction factor on observing microwave power was noted. However, since the reproducibility of measuring the reduction factor was of the same magnitude, this observing power dependence was ignored. All microwave power readings were taken with a Hewlett-Packard 432A temperature-compensated power meter. Full microwave power of the pumping klystron equalled 336 mW at the input flange to the cavity and whenever not stated, a pump power of 336 mW was used. The loaded Q 's of the pumping and observing cavities were approximately 1000 and 2500, respectively.

Results

A plot of reduction factors vs. temperature is given in Figure 1 for the CH_2COO^- radical in single crystals of zinc acetate when the observing field is positioned at the high-field esr line of a 1:2:1 triplet. The eldor reduction factors (R) for the allowed-allowed lines A and B in Figure 1 show a maximum from -70 to -50° . Clearly, line A has a different maximum than line B. The forbidden lines, C and D, have near zero R values at -50° . Upon lowering the temperature, the R values of the lines D and C increased while the R values of the allowed lines A and B decreased. It is to be noted that the maximum R value

of the allowed line A occurs (at -70°) when the correlation time for the spin exchange determined by Hayes, *et al.*,¹⁰ equalled 0.2×10^{-6} sec.

A similar dependence was also observed for the CH_2COOH radical in malonic acid. The observed reduction factors (R) vs. temperature (when observing a four-line esr pattern) are plotted in Figure 2 for the allowed eldor lines at 64.9 and 48.0 MHz and the forbidden lines at 36.5 and 19.0 MHz. The maximum R value for both allowed lines (analogous to line A, Figure 1) occurred at approximately 0° while the maximum R values for the forbidden lines occurred from -30 to -50° . At 50° , the central two lines of the four-line esr pattern began to noticeably collapse to a single line as evidenced by a change in separation of the two central lines from 5.5 G at 0° to 2.5 G at 50° . In fact, the change in the esr hyperfine pattern from 0 to 50° appeared to be similar to the change in the four-line pattern shown for CH_2COO^- in Figures 1a (-70°) and 1b (-31°) of ref 10 where the correlation time was calculated to change from 0.2×10^{-6} to 0.3×10^{-7} sec. The only difference between Figures 1 and 2 appears to be the temperature at which the maximum is observed. From the similarity in the two figures, it is suggested that an intensity maximum occurs for the eldor reduction factors whenever an intramolecular motion is present with a spin exchange correlation time equal to approximately 0.2×10^{-6} sec.

Some Approximate Calculations

Since the relationship between the eldor intensity and the spin exchange correlation time appears to be so apparent, it was hoped that a simple calculation would give more insight into the mechanism responsible.

- (17) L. R. Dalton and W. L. Gamble, *Bull. Amer. Phys. Soc.*, **17**, 1182 (1972); L. R. Dalton, A. L. Kwiram, and J. A. Cowen, *Chem. Phys. Lett.*, **14**, 77 (1972); H. Yoshida, D. Feng, and L. Kevan, *J. Amer. Chem. Soc.*, **94**, 8922 (1972). The effect of intermolecular cross relaxation. These effects were not included in the present study.
- (18) Preliminary eldor results for CCH_2COOH were reported by L. D. Kispert, K. Chang, and C. M. Bogan at the 164th National Meeting of the American Chemical Society, New York, N. Y., Aug 1972, Physical Chemistry Abstract No. 76.

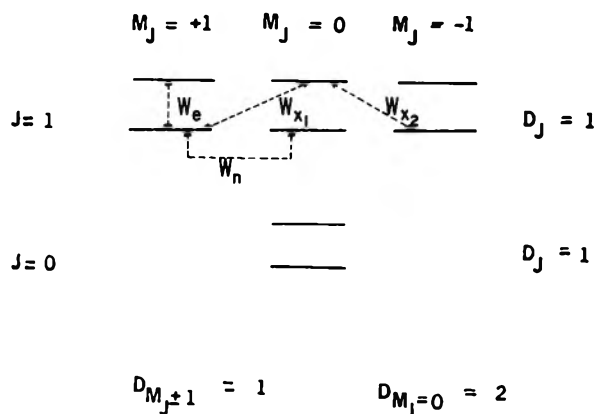


Figure 3. J manifolds for two completely equivalent protons.

The first approach tried was to assume that the two protons could be treated as completely equivalent protons. It is then possible to calculate R from a transition probability matrix using Freed's general theory of double resonance.¹⁹ If only END (electron-nuclear dipolar) interactions are considered, only the $J = 1$ manifold (Figure 3) will be eldor-active and assuming generalized nonsaturation conditions¹⁹ and that $\Delta\omega_o = \Delta\omega_p = 0$, the reduction factor can be written

$$R = \Omega_{op}/\Omega_p = (D_p/D_o)^{1/2}(\Omega_{op}^{J=1}/\Omega_p^{J=1}) \quad (1)$$

where D_p and D_o are the degeneracies of the pumped and observed esr lines, respectively, and $\Omega_{op}^{J=1}$ and $\Omega_p^{J=1}$ are derived from the appropriate double cofactors of the W matrix.¹⁹

The results for different values of b ($\equiv W_n/W_e$), $X1 \equiv W_{X1}/W_e$, and $X2$ ($\equiv W_{X2}/W_e$) are shown in Figures 4 and 5. (W_n is the pure nuclear spin flip transition probability, W_e is the pure electron spin flip transition probability, and W_{X1} and W_{X2} are cross-relaxation probabilities).

Qualitative agreement for the allowed lines A and B (Figure 1) can be obtained if b increases with temperature (from -100 to -70°) and in the region around -70° , the cross-relaxation terms become competitive and reduce the values of R .²⁰

Two definite problems are noted with this treatment. The experimental curves for A and B vs. T do not have their maxima at the same temperature (Figure 1) while the calculated curves have maxima at the same values of b , $X1$, and $X2$. When cross-relaxation terms are added (for constant b) B decreases faster than A. Experimentally, A falls off faster than B.

These are not the only eldor lines observed when observing the $M_J = -1$ line. The lines labeled C and D in Figure 1 are "forbidden lines" since the nuclear spin functions are different in the two energy levels which contribute to the particular esr line.

These forbidden lines have not been explicitly included in the esr theory of saturation of Freed.¹⁹ However, a simple extension of the double cofactor method can be used. The results of such a calculation are shown in Figure 4 for varying b . The intensity of the forbidden line is always greater than that of the closest allowed eldor line. This was also calculated when the cross-relaxation parameters were included in the W matrix (Figure 5).

Experimentally, the intensity of the forbidden lines was greater than the allowed lines at very low temperatures

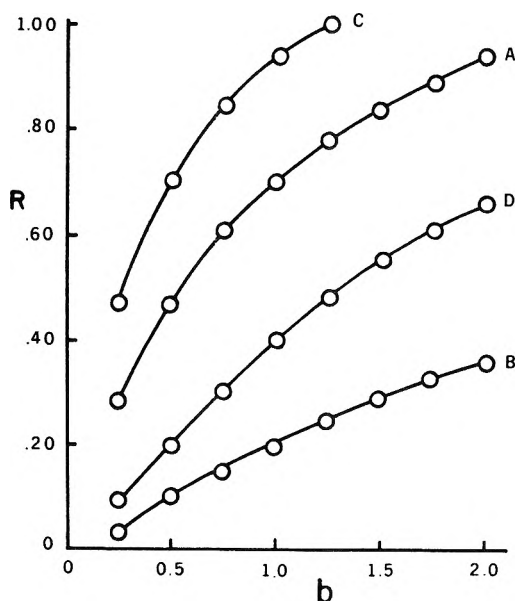


Figure 4. Calculated eldor reduction factors vs. b for two completely equivalent protons, assuming that cross relaxation is negligible. A, B, C, and D refer to the eldor lines as in Figure 1.

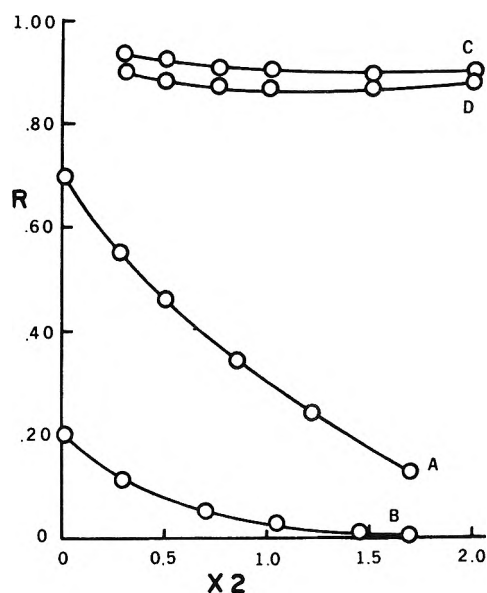


Figure 5. Calculated eldor reduction factors vs. $X2$ ($\equiv W_{X2}/W_e$) for two completely equivalent protons with $b = 1.0$ and $X1 = X2/6.0$. A, B, C, and D refer to the eldor lines as in Figure 1.

and decreased to about zero in the region where the R 's for the allowed lines were a maximum. This type of behavior was never calculable for the forbidden transitions when the calculation of the allowed eldor transitions agreed with the experimentally observed R values.

Calculation of the Eldor Reduction Factors for Two Symmetrically Equivalent Protons

The reduction factors for the allowed eldor lines begin to decrease at about the same temperature region where

(19) J. H. Freed, *J. Chem. Phys.*, **43**, 2312 (1965).

(20) The reduction factors calculated for two completely equivalent protons using the "average eldor" approximations¹⁵ are qualitatively the same as those obtained from eq 1. However, "average eldor" is restricted to temperatures where $b \ll 1$.

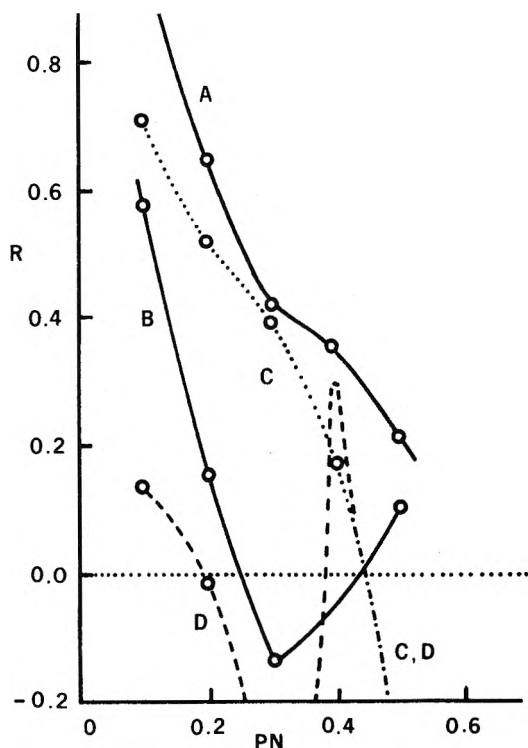
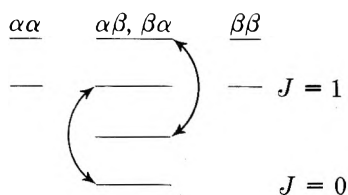


Figure 6. Calculated eldor reduction factors vs. PN (a pseudonuclear spin-flip transition probability) for two symmetrically equivalent protons, with $b = 0.5$, $X_1 = X_2 = PEE = 0$; $PX_2 = 0.5$, $PX_1 = PX_2/6.0$, and $PE = 0.33$. PEE is a pseudoelectron spin-flip probability between off-diagonal density matrix elements, PX_2 and PX_1 are pseudocross relaxation transition probabilities, and PE is a pseudoelectron spin-flip transition probability. A, B, C, and D refer to the eldor lines as in Figure 1.

the outer peaks begin to shift toward the center of the esr spectra due to nonadiabatic spin exchange effects.⁸

The nonadiabatic spin exchange which affects the esr involves an $\alpha_1\beta_2 \leftrightarrow \beta_1\alpha_2$ exchange. In terms of J manifolds this could be pictured as



where the arrows indicate the states which are exchanging. This would lead to a coupling of the J manifolds and indicates that the assumption of only intra J processes is not valid. The selection rule of $\Delta J = 0$ arose from the assumption of completely equivalent nuclei. It is obvious from the esr spectra that this is not the case.

An assumption of two symmetrically equivalent protons would allow coupling of the J manifolds and may give better agreement than the calculations of the previous section. If two protons are symmetrically equivalent, a complete \bar{W} matrix must be used to include inter J coupling. Freed¹⁹ has developed the theory for \bar{W} in connection with a dilute solution esr saturation study.

The reason for using a \bar{W} matrix when the nuclei are not completely equivalent is that pseudotransition probabilities can become important and make important contributions to the spin relaxation processes. The construction of the \bar{W} matrix is discussed in detail by Freed.¹⁹

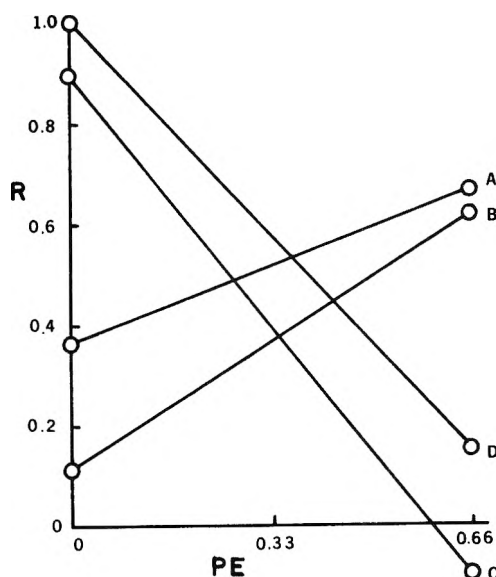


Figure 7. Calculated eldor reduction factors vs. PE (a pseudoelectron spin-flip transition probability) for two symmetrically equivalent protons with $b = 0.5$, $X_1 = 0.667$, $X_2 = 0.4$, $PN = 0.1$, $PX_1 = 0.167$, $PX_2 = 1.0$, and $PEE = 0.66$. A, B, C, and D refer to the eldor lines as in Figure 1. The notation has been defined in the caption to Figure 6.

As can be seen from ref 19, Appendix A, this inclusion of pseudotransition probabilities has increased the number of parameters significantly. As these are not known for CH_2COO^- from the esr spectrum or from theoretical calculations, they have to be varied until some agreement between the experimental and calculated R is noted. The results of several calculations are given in Figures 6 and 7. Only a limited number of calculations were done because of the number of parameters and because preliminary calculations indicate that the same R 's (within experimental errors) can be calculated with several different sets of parameter values. In the absence of some independent determination of at least a few of the parameters, a unique fit cannot be obtained.

However, the trends seem to indicate that the addition of the pseudotransition probabilities changes some of the qualitative aspects from those obtained when two completely equivalent nuclei are assumed.

Three of the major failings of the calculation which assumed complete equivalence can be remedied by the addition of pseudotransition probabilities. The magnitude of the difference between A and B can be varied; A and B can reach a maximum at different temperatures and the intensity of the forbidden lines can be less than that of the allowed by the inclusion of pseudotransition probabilities.

When complete equivalence was assumed, the behavior of A always mimicked that of B, (Figures 4 and 5). The addition of PE, a pseudoelectron spin-flip transition probability (X in eq A2 of Freed¹⁹), and PN (eq A5) can change this drastically.

The experimentally observed A and B maxima occur at different temperatures. It appears that by adding a suitable combination of PN, the pseudonuclear spin-flip probability, and PE, the observed behavior can be calculated.

The calculated difference between A and B is always fairly large (Figures 4 and 5) when A is greater than 0.20 for complete equivalence. The addition of PN, PE, and

PEE (a pseudoelectron spin-flip probability between off-diagonal density matrix elements, included in X in eq A2 of Freed¹⁹) can reduce this difference to about 0.03 which is the order of the experimental difference between A and B in zinc acetate between -30 and 20° . The temperature dependence of the eldor spectrum of CH_2COOH in malonic acid is qualitatively the same as that of CH_2COO^- in zinc acetate. However, the magnitudes of the reduction factor for the allowed lines A and B (Figure 2) are fairly similar over the entire temperature range. Both reduction factors reach a maximum at the same temperature (280°K). These features can be accounted for by varying the magnitudes of the pseudotransition probabilities at different temperatures.

In malonic acid, the radical begins to decay soon after the onset of nonadiabatic shifts in the esr peak positions which occurs at 60 – 70° higher than in zinc acetate.

Discussion

Exact values of b , PN, etc., are not necessary to gain a qualitative understanding of the dominant relaxation processes in CH_2COO^- and CH_2COOH . The important features can be understood from these limited calculations. The fact that the maximum eldor reduction factor occurs in the same temperature range as the nonadiabatic spin exchange effects are evident in the esr spectrum is not really surprising if the spin exchange process can be related to the relaxation processes.

The eldor intensity is directly related to the magnitude of b which is proportional to the nuclear spin-flip probability. The esr effects arise from an $\alpha_1\beta_2 \leftrightarrow \beta_1\alpha_2$ exchange which is really nothing more than the simultaneous flipping of two nuclear spins. As the rate of flipping increases, the flipping becomes "easier" and, correspondingly, the relaxation paths arising from this same flipping become very effective. The nuclear spin-flip probability increases, causing R to increase. When the exchange becomes fast enough to compete with the esr line widths ($\sim 10^7 \text{ sec}^{-1}$) (which depend on relaxation), the exchange should be "opening a new path for the transfer of saturation" which is competitive with other relaxation paths in the spin system. R for the allowed lines should then be a maximum. When the exchange rate becomes much faster than the esr line width (10^7 sec^{-1}), the cross relaxation mechanisms become competitive¹² and reduce the magnitude of R . The corresponding decrease in intensity of the forbidden eldor lines can be correlated with the increasingly important role of the pseudotransition probabilities. Below the coalescence temperature, the protons are not equivalent at all crystal orientations but above this temperature, the protons can be viewed as symmetrically equivalent along all orientations. In constructing the relaxation matrix for two symmetrically equivalent protons, Freed²¹ has shown that, in the limit of uncorrelated

nuclei, the pseudotransition probabilities are zero and in the limit of complete equivalence, the spectral densities for the pseudotransition probabilities become equivalent to those for the transition probabilities. The calculations of the previous section have indicated that in order for the intensity of the forbidden lines to be comparable to or less than that of the allowed lines, the pseudotransition probabilities must be nonnegligible. This is in agreement with the postulate that the protons are becoming more equivalent and the pseudotransitions become more important as the temperature is raised.

In the particular case of CH_2COO^- , in which extensive internal motion has been ruled out as a cause of the temperature dependence,⁶ a correlation between the spin exchange and the pseudonuclear spin-flip probability (PN) has been deduced. Without PN, the forbidden lines are always more intense. As PN increases, the forbidden lines decrease in intensity and the allowed eldor lines become more intense. Experimentally, the forbidden lines decrease in intensity as the rate of the nonadiabatic spin exchange increases. Since this spin exchange involves transitions between degenerate states ($\alpha_1\beta_2 \leftrightarrow \beta_1\alpha_2$) and it involves pseudonuclear spin flips, it is quite reasonable to expect PN to increase as the exchange rate increases.

Conclusion

Spin exchange is a dynamic process which has quite a large eldor effect. The magnitude of the eldor effect is frequency dependent and thus very temperature dependent. An analysis of the temperature dependence of the eldor spectra of CH_2COO^- and CH_2COOH has resulted in some understanding of the role of nonadiabatic spin exchange effects in relaxation processes.

The correlation between the esr-observed non-adiabatic spin-exchange effects and the eldor intensities is quite striking. The outer esr peaks begin to shift inward (-70°) in CH_2COO^- at approximately the same temperature at which the allowed eldor lines show maximum intensity (from -70 to -50°) in CH_2COO^- and the intensity of the forbidden eldor approaches zero. In both CH_2COOH and CH_2COO^- , a maximum reduction factor occurs when the correlation time of the intramolecular motions equals approximately $0.2 \times 10^{-6} \text{ sec}$. As the temperature increases, and presumably the correlation time shortens, cross exchange increases, resulting in a decrease in the observed R factor.

Acknowledgment. We wish to thank the physics department at the University of Alabama for use of the X-ray equipment. A generous amount of computer time was provided by the University of Alabama Computer Center. H. Moore and R. Sneed provided invaluable assistance with the instrumentation.

(21) J. H. Freed and G. K. Fraenkel, *J. Chem. Phys.*, **39**, 326 (1963).

Nitrogen-14 Contact Shifts and Line Broadening Studies for Acetonitrile Complexes of Copper(II), Nickel(II), Cobalt(II), and Titanium(III)

V. K. Kapur and B. B. Wayland*

Department of Chemistry and Laboratory for Research on the Structure of Matter, University of Pennsylvania, Philadelphia, Pennsylvania 19104 (Received September 28, 1972)

Publication costs assisted by The University of Pennsylvania

Nitrogen-14 contact shifts and line broadening studies are reported for acetonitrile complexes of Cu(II), Ni(II), Co(II), and Ti(III). Acetonitrile nitrogen-14 hyperfine coupling constants for the series of metal ion complexes are Cu(II) (30.0 ± 2.0 MHz), Ni(II) (27.0 ± 2.00 MHz), Co(II) (9.5 ± 1.0 MHz), and Ti(III) (negative). Opposite signs for the ^{14}N coupling constant when the spin density is exclusively in the σ orbitals (Cu(II) and Ni(II)) or exclusively in π orbitals, Ti(III), provide direct evidence for positive and negative contributions from σ and π ligand spin density, respectively. Opposing contributions from σ and π spin density result in the small ^{14}N coupling constants observed for Co(II)-, Fe(II)-, Mn(II)-acetonitrile complexes. Kinetic data for pseudo-first-order ligand exchange for the Ni(II) and Co(II) complexes are evaluated from ^{14}N line width studies.

Introduction

Contact shifts of ligand nuclei are widely used to deduce the mechanism and magnitude of spin delocalization in paramagnetic metal ion complexes.¹ The preponderance of these studies have utilized proton nmr.² Conclusions drawn from proton contact shifts are necessarily indirect for the protons are not the ligand donor atoms. As part of a general investigation of the ^{14}N contact shifts of nitrogen bound ligands, this paper reports on the ^{14}N contact shifts and line broadening for acetonitrile complexes of Cu(II), Ni(II), Co(II), and Ti(III).

Experimental Section

Materials. Eastman acetonitrile was used for the preparation of complexes. It was dehydrated and purified by triple distillation over BaO, P₂O₅, and CaH₂, respectively. The complexes of Cu²⁺, Ni²⁺, and Co²⁺ were prepared by Wickenden and Krause³ method, from the hydrated perchlorate salts obtained from the G. Fredrick Smith Chemical Co. Solutions for titanium(III) studies were prepared by dissolving anhydrous TiCl₃ in acetonitrile.

Sample Preparation. The samples for nmr were prepared such that the weight of each constituent (complex and acetonitrile solvent) and the total volume were known. All sample preparation and manipulations were carried out in a drybox under dry nitrogen or on a vacuum line. Solutions of complexes were further analyzed for the metal ion concentration, as an independent check on the solution composition. Solutions of metal complexes were degassed and sealed in 5-mm o.d. thin-walled tubes along with a sealed degassed capillary tube of CH₃NO₂ as external standard. Sample tubes were sealed as close to the solution as possible while still permitting adequate expansion for higher temperature studies. A sample containing pure acetonitrile and a capillary of nitromethane was prepared as a reference and the nmr spectra were recorded at every temperature at which samples of metal complexes were studied. Several metal ion concentrations were studied for each complex.

Apparatus. All ^{14}N spectra were run on a Varian HA-100 spectrometer using the HR mode, at 7.22 MHz and using

^{14}N probe No. V-4333A. Variable temperature controller No. V-4341 was used to maintain constant temperature. The temperature was measured using a copper-constantan thermocouple and was found to be constant within $\pm 0.5^\circ$ throughout most of the temperature range.

The shifts were measured relative to nitromethane as an external standard.⁴ The spectra were recorded by sweeping both from high to low field and the reverse. Line width and contact shift values are averages of at least three runs at each temperature. Spectra were recorded with the spectrometer in the HR and side-band modes. The rf power was kept much below the saturation level. The calibration of the spectra was done by side-band technique. To expand the scale, the modulation frequency was changed from 2.5 to 1.5 kHz, which was accomplished by disconnecting the 2.5-kHz oscillator at V-201 (in integrator decoupler unit) and connecting an external oscillator with adjustable frequencies at V-405 in the same box (V-3521A).

Analysis of Data. The basic equations for calculating the coupling constants and kinetics parameters are⁵ as follows

$$\Delta\omega_m/\omega = -A_n g_e \beta_e S(S+1)h/g_n \beta_n 3kT$$

where A_n is the hyperfine coupling constant in Hz.

$$\Delta\omega_{\text{obsd}} = P_m \Delta\omega_m / [(\tau_m/T_{2m} + 1)^2 + \tau_m^2 \Delta\omega_m^2]$$

where P_m = concentration of coordinated ligand vs. total ligand concentration

$$\frac{1}{T_2} - \frac{1}{T_{2A}} =$$

$$\frac{P_m}{\tau_m} \left\{ \left(\frac{1}{T_{2m}^2} + \frac{1}{T_{2m}\tau_m} + \Delta\omega_m^2 \right) \left[\left(\frac{1}{T_{2m}} + \frac{1}{\tau_m} \right)^2 + \Delta\omega_m^2 \right] \right\}$$

where $T_2 = (\pi\Delta\nu)^{-1}$, T_{2A} is transverse relaxation time of

(1) G. A. Webb, *Annu. Rep. NMR (Nucl. Magn. Resonance) Spectrosc.* **3**, 211 (1970).

(2) W. D. Horrocks, Jr., and D. L. Johnston, *Inorg. Chem.*, **10**, 1835 (1971).

(3) A. E. Wickenden and R. A. Krause, *Inorg. Chem.*, **4**, 404 (1965).

(4) M. Witanowski and H. Januszewski, *J. Chem. Soc. B*, 1062 (1967).

(5) T. J. Swift and R. E. Connick, *J. Chem. Phys.*, **37**, 307 (1962).

TABLE I: Representative Data of Contact Shifts and Line Widths vs. Temperature for Cu(II), Ni(II), and Co(II) Complexes

$10^3/T, ^\circ\text{K}^{-1}$	$[\text{Cu}(\text{CH}_3\text{CN})_6](\text{ClO}_4)_2^a$			$[\text{Ni}(\text{CH}_3\text{CN})_6](\text{ClO}_4)_2$			$10^3/T, ^\circ\text{K}^{-1}$	$[\text{Co}(\text{CH}_3\text{CN})_6](\text{ClO}_4)_2$		
	$10^4 P_m$	$-\Delta\omega/2\pi, \text{Hz}$	$10^3/T, ^\circ\text{K}^{-1}$	$10^4 P_m$	$-\Delta\omega/2\pi, \text{Hz}$	$\Delta\nu, ^\circ\text{Hz}$		$10^4 P_m$	$-\Delta\omega/2\pi, \text{Hz}$	$\Delta\nu, \text{Hz}$
3.32	10.62	102	2.08	4.398		34	2.42	19.91	212	
3.23	7.152	65	2.13	4.398	57	37	2.59	19.91	241	
3.23	7.127	63	2.18	4.398	63	41	2.69	19.91	251	
3.02	7.152	61	2.23	4.398	58	44	2.73	9.499		17
2.82	10.62	77	2.28	4.398		47	2.73	6.638	90	
2.82	7.127	50	2.28	8.797	106		2.82	4.691		15
2.65	10.62	72	2.34	4.398	46	54	2.82	6.638	96	
2.65	7.152	47	2.40	4.398	34	56	2.915	9.499	136	47
			2.46	8.797	69		3.02	4.691	68	35
			2.46	4.398		54	3.12	9.499	98	89
			2.59	4.398	26	47	3.23	4.691	34	47
			2.59	8.797	43		3.32	9.499	42	80
			2.69	8.797		89	3.41	4.691	13	
			2.73	8.797	16	59	3.47	4.691		23
			2.82	8.797	9	40	3.50	9.499		56
			2.91	4.398		13	3.59	4.691		17
			3.02	8.797		16	3.64	9.499		28
			3.31	8.797		9				

^a No line width data were collected for Cu(II). ^b $-\Delta\omega/2\pi$ is the observed shift in Hz downfield from pure acetonitrile. ^c $\Delta\nu$ is full line width at half-height.

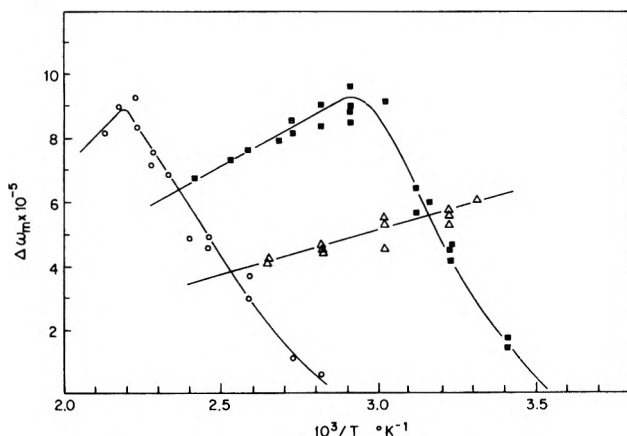


Figure 1. Contact shifts in radians per second normalized to $P_m = 1$, for the solutions of acetonitrile complexes of Cu(II), Ni(II) and Co(II) plotted against $1/T$. O, Ni(II) ($P_m = 4.398 \times 10^{-4}$ and 8.797×10^{-4}); Δ , Cu(II) ($P_m = 7.127 \times 10^{-4}$, 7.157×10^{-4} , and 10.62×10^{-4}); \square , Co(II) ($P_m = 4.691 \times 10^{-4}$, 9.499×10^{-4} , and 19.91×10^{-4}).

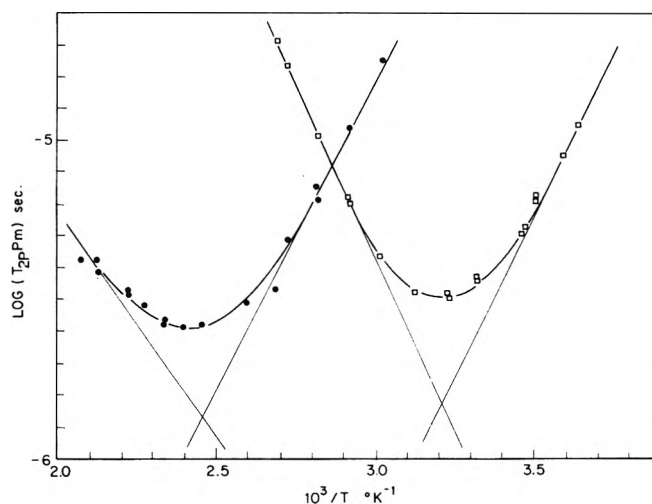


Figure 2. Log of transverse relaxation time normalized to $P_m = 1$ for the solutions of acetonitrile complexes of Ni(II) and Co(II) plotted against $1/T$: O, Ni(II) ($P_m = 4.398 \times 10^{-4}$ and 8.797×10^{-4}); \square Co(II) ($P_m = 4.691 \times 10^{-4}$ and 9.499×10^{-4}).

the pure solvent and $\Delta\nu$ is the observed full line width at half-height. The effect of temperature on τ_m and thus on T_2 is given by

$$\tau_m = (h/kT) \exp[(\Delta H^\ddagger/RT) - (\Delta S^\ddagger/R)]$$

where ΔH^\ddagger and ΔS^\ddagger are the enthalpy and entropy of activation.

Results

Cu(II) Complex. Nitrogen-14 contact shifts for $[\text{Cu}(\text{CH}_3\text{CN})_6](\text{ClO}_4)_2$ in neat acetonitrile are downfield relative to pure acetonitrile (Table I) which corresponds to a positive ^{14}N coupling constant ($+30 \pm 2$ MHz). The contact shifts are found to be inversely dependent on temperature which demonstrates that the observed shifts are authentic contact shifts. The limiting fast exchange region is obtained for the entire temperature range of our studies and therefore kinetic parameters were inaccessible from line broadening data.

Ni(II) Complex. Temperature dependence data for the ^{14}N contact shifts and line widths for solutions of $[\text{Ni}(\text{CH}_3\text{CN})_6](\text{ClO}_4)_2$ in neat acetonitrile are found in Table I. Temperature dependence of the contact shifts and the line widths are plotted in Figures 1 and 2, respectively. Nitrogen-14 contact shifts for Ni(II) solutions are downfield relative to free acetonitrile. The kinetics parameters from the line broadening are given in Table II. The ^{14}N coupling constant from line width data (25 ± 2 MHz) is in satisfactory agreement with the value obtained directly from the contact shifts (27 ± 2 MHz).

Co(II) Complex. Nitrogen-14 contact shifts and line broadening data for solutions of $[\text{Co}(\text{CH}_3\text{CN})_6](\text{ClO}_4)_2$ in acetonitrile are found in Table I. Temperature dependence of the contact shifts and the line widths are plotted in Figures 1 and 2, respectively. Temperature dependent effects are found to be completely reversible. The ^{14}N coupling constant evaluated from line broadening data is

TABLE II

	Ni(CH ₃ CN) ₆ ²⁺	Co(CH ₃ CN) ₆ ²⁺
ΔH^\ddagger , kcal	9.44	8.79
ΔS^\ddagger , eu	-7.8	-4.2
k (25°), sec ⁻¹	1.45×10^4	2.7×10^5
A_n , MHz	27.0	9.5

found to vary with temperature from 7 to 10 MHz. The origin of this discrepancy in the analysis of the data is not yet clear. The ¹⁴N coupling constant obtained directly from contact shift measurements is 9.5 ± 1 MHz. Kinetic parameters for ligand exchange of [Co(CH₃CN)₆](ClO₄)₂ with bulk CH₃CN are given in Table II.

Ti(III) Complexes. Studies of TiCl₃ in acetonitrile were limited to a relative small temperature range because these solutions undergo an irreversible chemical change above 90°. The observed nitrogen-14 shifts for solutions of TiCl₃ in acetonitrile are upfield relative to free acetonitrile, which is opposite to that observed for Cu(II), Ni(II), and Co(II) solutions. The ¹⁴N coupling constant could not be obtained from this study because the experiments could not be carried to sufficiently high temperatures to reach the limiting fast-exchange region. The increasing positive value of the shift (Table III) with increasing temperature does, however, indicate that the ¹⁴N coupling constant is negative ($|A(^{14}\text{N})| \gg 5$ MHz).

Discussion

The reported proton coupling constants for [M(CH₃CN)₆](ClO₄)₂ (M = Ni(II) and Co(II))⁶ in acetonitrile, decrease by an order of magnitude in going from Ni(II) to Co(II). Octahedral Ni(II) complexes $t_{2g}^6e_g^2$ have two unpaired electrons in the d molecular orbitals which can transfer spin density to the σ orbitals of the ligand. While octahedral Co(II) complexes $t_{2g}^5e_g^2$ have unpaired electrons both in the $t_{2g}(\pi)$ and $e_g(\sigma)$ orbitals, so that spin density can directly reach both the σ and π ligand orbitals. The very much smaller proton coupling constant for the Co(II) complex has been proposed⁶ to result from competitive spin delocalization mechanisms. Spin density in the σ orbitals giving a negative coupling constant for methyl protons and π spin density giving a positive contribution to A(H). The net negative A(H) value for σ spin density was proposed to result from σ - π correlation (negative contribution to A(H)). Spin delocalization in π ligand molecular orbital gives a positive coupling constant by directly placing spin density in the methyl hydrogen 1s orbitals which make a substantial contribution to the π orbitals.

Nitrogen-14 coupling constants for [Ni(CH₃CN)₆](ClO₄)₂ and [Cu(CH₃CN)₆](ClO₄)₂ are positive. The direct delocalization of positive spin density to the acetonitrile σ molecular orbitals and thus to the nitrogen 2s atomic orbital results from molecular orbital formation with the metal e_g orbitals which contain the unpaired electrons. A ¹⁴N coupling constant of +30 MHz for the Cu(II) complex corresponds to a N_{2s} spin density of +0.019. In calculating the 2s spin density, we have used the relation $f_s = (2s)A_n/A_{2s}$ and the value of atomic hyperfine coupling constant used for N_{2s} is 1545 MHz.⁷ Both the Ni(II) $t_{2g}^6e_g^2$ and Cu(II) $t_{2g}^6e_g^3$ complexes have unpaired electrons exclusively in the $\sigma(e_g)$ d orbitals. The mechanism of spin delocalization to the CH₃CN is therefore expected to be the same in both complexes, which requires that the ratio

TABLE III: TiCl₃ in CH₃CN Contact Shifts vs. Temperature^a

$10^3/T_n$, °K ⁻¹	$\Delta\nu_1$, ^b Hz	$\Delta\nu_2$, ^c Hz	Shift ($\Delta\nu_2 - \Delta\nu_1$)
3.32	986	999	+13
2.92	970	1007	+37
2.53	960	1013	+53

^a Molality = 5.0429×10^{-2} . ^b ¹⁴N shift of pure CH₃CN relative to nitromethane. ^c ¹⁴N shift of Ti³⁺-acetonitrile solution relative to nitromethane.

of $A(^{14}\text{N})/A(^1\text{H})$ be approximately constant. In satisfactory agreement with this expectation, the $A(^{14}\text{N})/A(^1\text{H})$ ratio is 72 and 80 for the Cu(II) and Ni(II) complexes, respectively.

Proton coupling constants used in this comparison of ratios were determined on the same solutions used in the ¹⁴N studies: Cu(II) A(H) = 4.7×10^5 Hz and Ni(II) A(H) = 3.34×10^5 Hz.

The nitrogen-14 coupling constant for [Co(CH₃CN)₆](ClO₄)₂ (9.5 MHz) in acetonitrile is substantially smaller than those for Cu(II) (30.0 MHz) and Ni(II) (27.0 MHz) complexes. Octahedral cobalt(II) ($t_{2g}^5e_g^2$) can directly delocalize spin in both the σ and π ligand orbitals. The reduced $A(^{14}\text{N})$ could result from a positive contribution from σ spin density and negative contribution from the π spin density. The ratio $A(^{14}\text{N})/A(^1\text{H})$ for the Co(II) complex is 332, which is distinctly different from the ratio characteristic of σ delocalization and supports the presence of competitive (both σ and π) mechanisms. The still smaller values of ¹⁴N coupling constant (5.0 MHz) for Fe(II)-⁸ and (3.2 MHz) for Mn(II)-acetonitrile⁹ complexes also support the presence of competitive mechanisms.

In order to obtain direct evidence for the sign of the contribution to the $A(^{14}\text{N})$ from π spin density, solutions of TiCl₃ in acetonitrile were studied. The Ti(III) complex is found to be in the slow ligand exchange region at 30° and elevated temperatures were required to observe significant ¹⁴N shifts of the bulk CH₃CN. The observed shifts and line widths are reversible up to ~80°. Above 90° Ti(III) probably disproportionates to Ti(II) and Ti(IV) and irreversible changes occur. The data observed were insufficient to determine the value for $A(^{14}\text{N})$; however, the upfield ¹⁴N contact shifts corresponds to a negative $A(^{14}\text{N})$ coupling constant ($|A(^{14}\text{N})| \gg 5.00$ MHz).

The observed negative ¹⁴N coupling constant for the Ti(III)-acetonitrile solutions, where the metal has only unpaired d_π electron density, corroborates the contention that spin density transferred from the metal to the ligand in the π orbitals results in a negative contribution to $A(^{14}\text{N})$. The observed $A(^{14}\text{N})$ for Co(II)-, Mn(II)-, and Fe(II)-acetonitrile complexes thus result from opposing σ and π spin density contributions to $A(^{14}\text{N})$. The negative contribution to $A(^{14}\text{N})$ from π spin density could result from either positive or negative spin density on the ligand with different mechanisms for transferring the effects to the ¹⁴N nucleus. Proton hyperfine coupling is important in deciding this issue. Proton contact shifts in the Ti(III) complex are downfield¹⁰ relative to free acetonitrile corre-

- (6) N. A. Matwiyoff and S. V. Hooker, *Inorg. Chem.*, **6**, 1127 (1967).
- (7) D. R. Hartree, W. Hartree, and B. Swirles, *Phil. Trans. Roy. Soc. London. Ser. A*, **238**, 229 (1940); D. R. Hartree and W. Hartree, *Proc. Roy. Soc., Ser. A*, **156**, 45 (1936).
- (8) R. J. West and S. F. Lincoln, *Aust. J. Chem.*, **24**, 1169 (1971).
- (9) W. L. Purcell and R. S. Marianelli, *Inorg. Chem.*, **9**, 1724 (1970).
- (10) C. C. Hinckley, *Inorg. Chem.*, **7**, 396 (1968).

sponding to a positive spin density in the ligand π orbitals. The negative $A(^{14}\text{N})$ from positive π spin density must result from π - σ spin correlation inducing negative spin density at the ^{14}N nucleus.

To our knowledge this is the first reported negative ^{14}N coupling constant. The reported ^{14}N coupling constant in NH_3^+ and nitrogen containing free radicals are all positive.¹¹ Spin correlation in NH_3^+ places positive spin density in the N_{2s} and negative in the N_{1s} with the positive N_{2s} spin density dominating the coupling constant. In the $\text{Ti}(\text{III})$ -acetonitrile system either both N_{1s} and N_{2s} contain negative spin density or the N_{1s} spin density dominates. Further theoretical work is needed to fully understand the origin of this negative ^{14}N coupling constant.

It is of interest to note that similar trends have been observed in the ^{17}O coupling constant for aquo complexes.

In aquo complexes, the coupling constant changes sign from negative values of -5.5×10^7 for $\text{Cu}(\text{II})^{12}$ and -3.0×10^7 for $\text{Ni}(\text{II})^{13}$ to a positive value of 4.4×10^6 for $\text{Ti}(\text{III})$ complex.¹⁴ The signs of the ^{17}O coupling constants are reverse from that of ^{14}N , because the gyromagnetic ratio of ^{17}O is negative.

Acknowledgment. The authors acknowledge the support of the National Science Foundation through Grant No. GH-33633 and GP-28402.

- (11) T. Cole, *J. Chem. Phys.*, **35**, 1169 (1961).
- (12) W. B. Lewis, M. Alei, Jr., and L. O. Morgan, *J. Chem. Phys.*, **44**, 2409 (1966).
- (13) R. E. Connick and D. Fiat, *J. Chem. Phys.*, **44**, 4103 (1966).
- (14) A. M. Chmelnick and D. Fiat, *J. Chem. Phys.*, **51**, 4238 (1969).

Outer Sphere Complex between Trisethylenediaminecobalt(III) and Phosphate

Thomas H. Martin and B. M. Fung*¹

Department of Chemistry, Tufts University, Medford, Massachusetts 02155 (Received September 14, 1972)

Publications costs assisted by the National Science Foundation

^{59}Co resonance of $\text{Co}(\text{en})_3^{3+}$ (en = ethylenediamine) in the presence of phosphate and ^{31}P resonance of phosphate in the presence of $\text{Co}(\text{en})_3^{3+}$ were studied at different salt concentrations and pH's. The equilibrium quotient for the formation of outer sphere complex was calculated from the ^{59}Co chemical shift data and was found to be $12.0 \pm 2.0 M^{-1}$ at ionic strengths around one. This value fits the ^{31}P chemical shift data very well. The pH dependence of the ^{59}Co shift is also studied.

Nuclear magnetic resonance (nmr) is a useful method for the study of the second coordination sphere of transition metal complexes. A number of reports on that subject has appeared in recent years.²⁻⁹ The formation of an outer sphere complex usually occurs between a transition metal complex and a solvent molecule or another anion. The outer sphere complex between $\text{Co}(\text{en})_3^{3+}$ (en = ethylenediamine) and PO_4^{3-} is of particular interest because of its possible stereo specificity due to hydrogen bonding¹⁰ and its effect on the conformation of the chelate rings in $\text{Co}(\text{en})_3^{3+}$.^{5,6} Its formation has been studied by circular dichroism¹⁰⁻¹² and proton nmr.⁴⁻⁶ However, to our knowledge, the equilibrium constant has not been determined, although that between $\text{Co}(\text{en})_3^{3+}$ and other anions has been reported.^{11,13,14} In this paper we report the study of outer sphere complex between $\text{Co}(\text{en})_3^{3+}$ and PO_4^{3-} by ^{59}Co and ^{31}P nmr with the determination of the equilibrium quotient.

The choice of ^{59}Co and ^{31}P as the probing nuclei in the nmr study is based upon the sensitivity of their chemical shifts to a change in the environment. It is well known that diamagnetic $\text{Co}(\text{III})$ complexes show extremely large ^{59}Co shifts due to the existence of low-lying excited electronic states.¹⁵ Very small changes, such as the solvent composition in trisacetylacetonatocobalt(III)⁹ and isotope substitution in $\text{Co}(\text{en})_3^{3+}$,⁵ cause appreciable variation in

the ^{59}Co chemical shift. The magnitude of the change of ^{31}P chemical shift with the environment is much smaller but can be measured more accurately because ^{31}P is a spin 1/2 nucleus, and therefore has much sharper nmr lines. The change of ^{31}P resonance in phosphate and polyphosphate ions due to ion-pair formation with alkali metal cations has been reported.¹⁶ The proton resonance of the

- (1) Present address: Department of Chemistry, University of Oklahoma, Norman, Okla. 73069.
- (2) B. M. Fung, *J. Amer. Chem. Soc.*, **89**, 5788 (1967).
- (3) B. M. Fung and I. H. Warg, *Inorg. Chem.*, **8**, 1967 (1969).
- (4) J. L. Sudmeier and G. L. Blackmer, *J. Amer. Chem. Soc.*, **92**, 5238 (1970).
- (5) J. L. Sudmeier, G. L. Blackmer, C. H. Bradley, and F. A. L. Anet, *J. Amer. Chem. Soc.*, **94**, 757 (1972).
- (6) L. R. Froebe and B. E. Douglas, *Inorg. Chem.*, **9**, 1513 (1970).
- (7) D. R. Caton, *Can. J. Chem.*, **47**, 2645 (1969).
- (8) L. S. Frankel, *J. Phys. Chem.*, **73**, 3897 (1969).
- (9) L. S. Frankel, C. H. Langford, and T. R. Stengle, *J. Phys. Chem.*, **74**, 1376 (1970).
- (10) S. F. Masson and B. J. Norman, *Proc. Chem. Soc., London*, 339 (1964); *J. Chem. Soc. A*, 307 (1966).
- (11) R. Larsson, S. F. Masson, and B. J. Norman, *J. Chem. Soc. A*, 301 (1966).
- (12) H. L. Smith and B. E. Douglas, *Inorg. Chem.*, **5**, 784 (1966).
- (13) F. A. Posey and H. Taube, *J. Amer. Chem. Soc.*, **78**, 15 (1956).
- (14) M. G. Evans and G. N. Nancollas, *Trans. Faraday Soc.*, **49**, 363 (1953).
- (15) J. W. Emsley, J. Feeney, and L. H. Sutcliffe, "High Resolution Nuclear Magnetic Resonance Spectroscopy," Pergamon Press, Oxford, 1966, p 1178 ff.
- (16) M. M. Crutchfield and R. R. Irani, *J. Amer. Chem. Soc.*, **87**, 2815 (1965).

ligands in Co(III) complexes is also affected by the formation of the second coordination sphere. However, the chemical shifts change appreciably only with a change in the acidity of the solvent^{2,3} and are not suitable for the study of phosphate in basic medium. The resolution of the splittings due to indirect spin-spin coupling improves in the presence of phosphate,⁴⁻⁶ but the change is not large enough for quantitative study. It was therefore expected that ⁵⁹Co and ³¹P nmr would be the most useful tool in the study of the outer sphere complex between Co(en)₃³⁺ and PO₄³⁻.

Experimental Section

[Co(en)₃]Cl₃ was prepared by standard methods¹⁷ and recrystallized from aqueous ethanol. Tetramethylammonium phosphate (TMAP) stock solution was prepared by adding tetramethylammonium hydroxide to concentrated phosphoric acid until a pH of 13.5 was reached.

⁵⁹Co nmr spectra were taken on a Varian VF-16 spectrometer at 8.0 MHz, using concentrated [Co(NH₃)₆]Cl₃ as external standard in a coaxial tube. ³¹P spectra were taken on a Varian HA-100 spectrometer at 40.48 MHz in the field-sweep mode, with a capillary containing 75% H₃PO₄ as an external reference. The chemical shift of each sample was determined from the average of at least four different recordings. Corrections in magnetic susceptibility were not made because they were small for diamagnetic solutions, and would be within the experimental error (5%). All measurements were made at room temperature.

Results and Discussion

The ⁵⁹Co chemical shift of [Co(en)₃]Cl₃ in aqueous solution moves upfield upon the addition of TMAP while the pH was kept constant at 13.5 (Figure 1). In the absence of phosphate, the ⁵⁹Co chemical shift is slightly dependent upon the concentration of the complex, showing a small interaction between Co(en)₃³⁺ and Cl⁻. The signal appears at a lower field for a more concentrated solution, indicating that Cl⁻ and PO₄³⁻ shift the ⁵⁹Co resonance in opposite directions. This was verified by the fact that stepwise addition of tetramethylammonium chloride caused the ⁵⁹Co signal to move gradually downfield, but much less pronounced than the upfield shift caused by TMAP. Because of the complexity of the cause for ⁵⁹Co shifts,¹⁵ we do not attempt to rationalize the opposite effect of chloride and phosphate on the direction of the ⁵⁹Co shift in Co(en)₃³⁺. An attempt was made to minimize the outer sphere complex formation in the absence of phosphate by using the perchlorate salt instead of chloride; however, the perchlorate is much less soluble, especially at high pH and upon the addition of TMAP. Therefore the chloride had to be used and corrections in the calculation of the equilibrium quotient were made. The use of tetramethylammonium instead of alkali metal phosphate would reduce the ion pairing to a minimum although not completely eliminate it.¹⁶

At pH >12.7, phosphate exists mainly as an equilibrium mixture between HPO₄²⁻ and PO₄³⁻. Since HPO₄²⁻ may have a smaller equilibrium constant for the outer sphere complex formation with Co(en)₃³⁺, it is expected that the ⁵⁹Co chemical shift is pH dependent. This was indeed observed, and the data in Figure 2 show that raising the pH causes larger upfield shift for the ⁵⁹Co peak. At

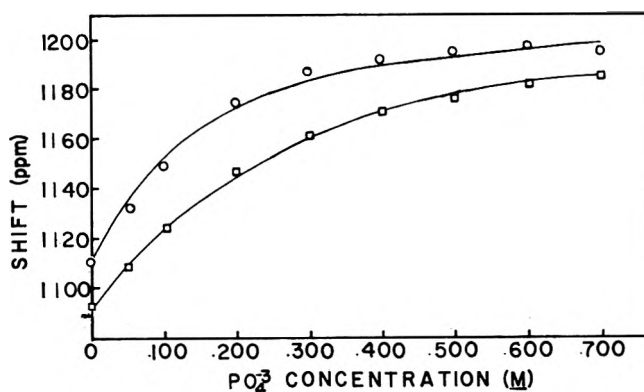


Figure 1. ⁵⁹Co chemical shift of Co(en)₃³⁺ from saturated [Co(NH₃)₆]Cl₃ as a function of phosphate concentration at pH 13.5: O, 0.100 M [Co(en)₃]Cl₃; □, 0.300 M [Co(en)₃]Cl₃. The solid curves are calculated from $K = 12 M^{-1}$.

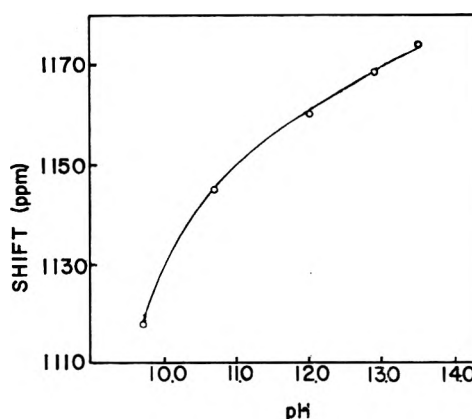
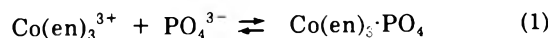


Figure 2. ⁵⁹Co chemical shift of a solution with 0.100 M [Co(en)₃]Cl₃ and 0.300 M [(CH₃)₄N]₃PO₄ as a function of pH.

pH 13.5 and 25°, about 93% of phosphate present would be in the form of PO₄³⁻. Precipitates formed at higher pH's.

In order to obtain the equilibrium quotient for



from the ⁵⁹Co chemical shift data, the following assumptions were made: (1) only a 1:1 outer sphere complex is formed; (2) if the different conformers of Co(en)₃³⁺ do not have the same equilibrium constant, the observed value should be a weighted average between all species; (3) the equilibrium quotient is expressed in terms of concentrations instead of activities and is applicable only in a small range of ionic strength; (4) at pH 13.5 only equilibrium 1 is considered; (5) the effect of chloride is constant at all phosphate concentrations. Data from works on circular dichroism^{10,11} have demonstrated that for Co(en)₃³⁺ and phosphate (but not all anions) the formation of outer sphere complex is not important beyond the ion ratios 1:1. Assumptions 4 and 5 are certainly inaccurate but the resulting errors are probably no larger than the uncertainty in the chemical shift data (±5%). At pH 13.5 and 25°, about 7% of the phosphate present is in the form of HPO₄²⁻, the equilibrium constant of which differs from that of PO₄³⁻; however, the existence of about 7% of

(17) J. B. Work, *Inorg. Syn.*, 2, 221 (1946).

TABLE I: Comparison of the Observed and the Calculated ^{59}Co Chemical Shifts (ppm)

PO_4^{3-} conc. <i>M</i>	0.100 <i>M</i> $\text{Co}(\text{en})_3^{3+}$		0.300 <i>M</i> $\text{Co}(\text{en})_3^{3+}$	
	Exptl	Calcd	Exptl	Calcd
0.050	1129	1125	1106	1109
0.100	1146	1152	1125	1122
0.200	1176	1172	1149	1143
0.300	1189	1182	1160	1159
0.400	1192	1188	1169	1170
0.500	1192	1192	1174	1177
0.600	1198	1195	1185	1182
0.700	1196	1197		1186

HPO_4^{2-} does not introduce a large error in the equilibrium constant because the pH dependence of the ^{59}Co shift is less pronounced when the pH approaches 14 (Figure 2). The last assumption leads to a correction in the chemical shift which will be discussed later.

If *C* is the initial concentration of $\text{Co}(\text{en})_3^{3+}$, *A* is the initial concentration of phosphate, and *x* is the concentration of the outer sphere complex formed, then the equilibrium quotient of 1 is

$$K = \frac{[\text{Co}(\text{en})_3 \cdot \text{PO}_4]}{[\text{Co}(\text{en})_3^{3+}][\text{PO}_4^{3-}]} = \frac{x}{(C-x)(A-x)} \quad (2)$$

The observed ^{59}Co chemical shift (δ_o) is a weighted average of the shift for the first coordination complex (δ_f) and the shift for the outer sphere complex (δ_s)

$$\delta_o = \frac{C-x}{C} \delta_f + \frac{x}{C} \delta_s \quad (3)$$

Equation 3 can be rewritten in a simpler form

$$\delta_o' = (x/C) \delta_s' \quad (4)$$

where $\delta_o' = \delta_o - \delta_f$ and $\delta_s' = \delta_s - \delta_f$. By eliminating *x* from (2) and (4) we obtain

$$K = \frac{\delta_o' \delta_s'}{C \delta_o'^2 + A \delta_s'^2 - (A+C) \delta_o' \delta_s'} \quad (5)$$

As a first approximation, the ^{59}Co chemical shift in the absence of phosphate can be taken as δ , and the asymptotic shift at very large phosphate concentration can be taken as δ_s . Then, *K* for each measured value of δ_o can be calculated from (5). The average value of *K* was subsequently used to recalculate the chemical shifts from (2) and (3), and was then varied slightly to obtain the best fit with the experimental data. The equilibrium constant obtained for (1) is $K = 12.0 \pm 2.0 M^{-1}$ and the calculated chemical shifts are listed in Table I and shown as the smooth curves in Figure 1. The fairly large limits of error are set to allow for the change in ionic strength, as discussed later. In the absence of other interactions, δ_s' (the shift between the first sphere and the second sphere complexes) should be constant. However, the effect of chloride cannot be neglected, as discussed above. The correction appears in the value of δ_s' , the best fit of which was 97 ± 3 ppm for 0.100 *M* $\text{Co}(\text{en})_3^{3+}$ and 107 ± 3 ppm for 0.300 *M* $\text{Co}(\text{en})_3^{3+}$.

To verify the equilibrium quotient obtained we have also studied the ^{31}P chemical shifts of phosphate solutions with constant phosphate concentration and pH. The addition of $\text{Co}(\text{en})_3^{3+}$ causes the ^{31}P peak to move downfield (Figure 3), which is similar to the effect of alkali metal ions. Since the observed ^{31}P resonance is a weighted aver-

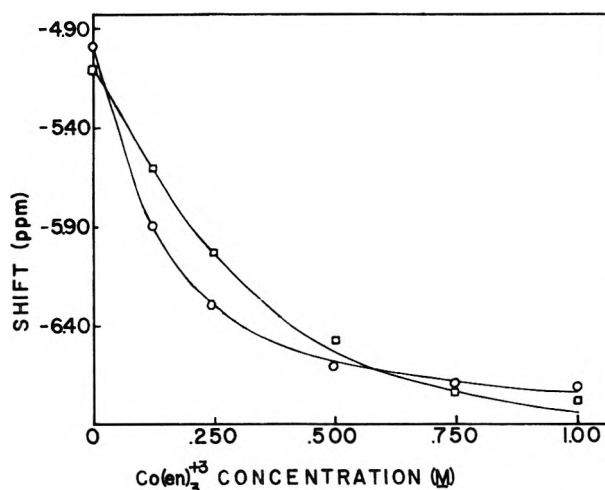


Figure 3. ^{31}P chemical shift of phosphate from 75% H_3PO_4 as a function of $[\text{Co}(\text{en})_3]\text{Cl}_3$ concentration at pH 13.5: O, 0.100 *M* $[(\text{CH}_3)_4\text{N}]_3\text{PO}_4$; □, 0.300 *M* $[(\text{CH}_3)_4\text{N}]_3\text{PO}_4$. The solid curves are calculated from $K = 12 M^{-1}$.

TABLE II: Comparison of the Observed and the Calculated ^{31}P Chemical Shifts (ppm)

$\text{Co}(\text{en})_3^{3+}$ conc. <i>M</i>	0.100 <i>M</i> PO_4^{3-}		0.300 <i>M</i> PO_4^{3-}	
	Exptl	Calcd	Exptl	Calcd
0.125	-5.88	-5.90	-5.60	-5.62
0.250	-6.28	-6.29	-6.08	-6.08
0.500	-6.51	-6.59	-6.54	-6.56
0.750	-6.66	-6.68	-6.71	-6.74
1.000	-6.86	-6.74	-6.76	-6.83

age between all phosphate ions, the lowering of pH causes the peak to shift upfield regardless of the existence of outer sphere complex. The ^{31}P chemical shift can be calculated from (2) and (3) except that *C* is replaced by *A* in (3). Using the value of $K = 12 M^{-1}$ determined from the ^{59}Co data, the ^{31}P chemical shifts were calculated and shown in Table II and as the smooth curves in Figure 3. Since the effect of the bulky tetramethylammonium ion is small, we found that δ_s' has the same value of 1.98 ppm for both 0.100 and 0.300 *M* phosphate.

Sudmeier and coworkers have shown that the resolution of the proton resonance of the CH_2 group in $\text{Co}(\text{en})_3^{3+}$ improves markedly upon the addition of potassium phosphate.^{4,5} We have tested the pH dependence of the CH_2 absorption and found that the resolution at 100 MHz for a D_2O solution with 0.100 *M* $\text{Co}(\text{en})_3^{3+}$ and 0.300 *M* phosphate did not change significantly when the pH of the solution changed from 12.0 to 13.5. Therefore, proton resonance is not sensitive enough for quantitative measurement of the equilibrium between $\text{Co}(\text{en})_3^{3+}$ and PO_4^{3-} .

An attempt was made to study the equilibrium between $\text{Co}(\text{NH}_6)^{3+}$ and PO_4^{3-} . However, hexaminecobalt(III) salts are not very soluble and the phosphate readily precipitates. Therefore quantitative measurements could not be made.

The shortcoming of the nmr method in determining the equilibrium constant is that a series of solutions of relatively high ionic strengths (μ) must be used. In our work $\mu^{1/2}$ varies from 0.32 to 2.8, and it is for this reason we must report an equilibrium quotient instead of a true constant. As a matter of fact, Posey and Taube¹³ showed that the equilibrium quotients for the outer sphere complexes

of $[\text{Co}(\text{NH}_3)_6]^{3+}$ and $[\text{Co}(\text{NH}_3)_5\text{H}_2\text{O}]^{3+}$ with SO_4^{2-} are dependent upon $\mu^{1/2}$. They become quite large in dilute solutions, but their changes at high ionic strengths are much less. The equilibrium quotient for $[\text{Co}(\text{NH}_3)_5\text{H}_2\text{O}]^{3+}$ with SO_4^{2-} is 10.1 at $\mu = 1.05$ and 25° , and the value for $[\text{Co}(\text{NH}_3)_6]^{3+}$ is similar. Evans and Nancolas reported that the equilibrium quotients for the outer sphere complexes between $[\text{Co}(\text{en})_3]^{3+}$ and halides at $\mu = 0.30$ are of the order of 10–20, and would be smaller at higher ionic strengths. Our measurements were limited to solutions of moderately high concentrations. It was difficult to keep the ionic strength constant because of limited solubility for perchlorate in the presence of $[\text{Co}(\text{en})_3]^{3+}$, and the use of other salts for the adjustment of ionic strengths are not suitable. Posey and Taube showed that at higher concentrations the change of the equilibrium quotient with $\mu^{1/2}$ is not large. Moreover, in our results the effect of chloride on the ^{59}Co chemical shift is reflected by the difference in δ_s' in eq 5, and δ_s' for ^{31}P is not affected by the concentration of tetramethylammonium

phosphate. In fact, the reasonable agreement between the experimental results and the data calculated from a single equilibrium quotient for both the ^{59}Co and ^{31}P resonance at different concentrations indicates the validity of our assumptions. The variation of the equilibrium quotient with the ionic strength studied is likely to be within the error limits¹³ allowed for the calculated value, $12.0 \pm 2.0 M^{-1}$, and the value of 12.0 can be regarded as a median one at μ around unity. The fact that $K \approx 12 M^{-1}$ implies that the outer sphere complex between $[\text{Co}(\text{en})_3]^{3+}$ and PO_4^{3-} is a weak one at moderate ionic strengths. The interaction is probably electrostatic in nature but may also involve hydrogen bonding between the NH proton and oxygen. The pH dependence of the ^{59}Co shift and the much smaller effect of Cl^- compared to an equal amount of PO_4^{3-} are consistent with both kinds of interaction.

Acknowledgment. This work was supported by the National Science Foundation.

Raman Studies of Molten Salt Hydrates. The Magnesium Chlorate–Water System

D. J. Gardiner,* R. B. Girling, and R. E. Hester

Department of Chemistry, University of York, York, England (Received May 24, 1972)

The magnesium chlorate–water system has been investigated by Raman spectroscopy. Spectra of solids from the anhydrous salt through to the crystalline hexahydrate are compared with spectra obtained from simple aqueous solutions of $\text{Mg}(\text{ClO}_3)_2$ over the concentration range from dilute to saturated solution and through a series of molten salt hydrates to the composition $\text{Mg}(\text{ClO}_3)_2 \cdot 2.8\text{H}_2\text{O}$. The solution and melt data have been analyzed in three main composition regions: dilute solution to hexahydrate; hexahydrate to tetrahydrate; and the region of lower hydration numbers. Perturbations of the simple C_{3v} ClO_3^- ion spectrum are interpreted as arising from hydrogen bonding with water in the first solution region; from formation of $\text{Mg}^{2+}\text{--ClO}_3^-$ contact ion pairs in the intermediate region, with continuing $\text{ClO}_3^- \text{--H}_2\text{O}$ interactions; and, in part, from more extensive quasilattice interactions in the final region of lowest water content.

Introduction

It is well established that Raman spectroscopic studies can provide significant structural information on aqueous electrolyte solutions and on molten salts.¹ In particular, much use has been made of the characteristics of oxy-anion spectra and their sensitivity to changing environment in the liquid state for the purpose of probing structural relationships that exist in concentrated aqueous solutions and molten salts. Spectroscopic criteria for distinguishing between the formation of direct, or contact, ion pairs and solvent-separated ion pairs have been established with metal nitrate solutions,^{2,3} and it was one of the purposes of the present work to determine the extent to which similar effects could be observed with ClO_3^- as the structural "probe."

Previous work by Oliver and Janz⁴ has shown the ClO_3^- ion spectrum to be sensitive to the nature of ion hydration and interionic interactions in the $\text{LiClO}_3\text{--H}_2\text{O}$ system.

The suitability of the magnesium salt for the purpose at hand was suggested by the recent detailed study by Peleg⁵ of the corresponding nitrate system where formation of contact ion pairs was indicated only on reduction of the water content to below that of the hexahydrate, and by the high aqueous solubility of magnesium chlorate. Both H_2O and the Mg^{2+} ion are known to interact more strongly with O than with Cl atoms, so that it could be anticipated that any such asymmetric interactions with ClO_3^- would lead to loss of degeneracy of the E type vibrational modes of this ion, thus providing a sensitive indication of local structure in the liquid.

- (1) R. E. Hester, *Annu. Rep. Chem. Soc.*, **6**, 79 (1970).
- (2) D. E. Irish and A. R. Davis, *Can. J. Chem.*, **46**, 943 (1968).
- (3) D. E. Irish, A. R. Davis, and R. A. Plane, *J. Chem. Phys.*, **50**, 2262 (1969).
- (4) B. G. Oliver and G. J. Janz, *J. Phys. Chem.*, **75**, 2948 (1971).
- (5) M. Peleg, *J. Phys. Chem.*, **76**, 1019 (1972).

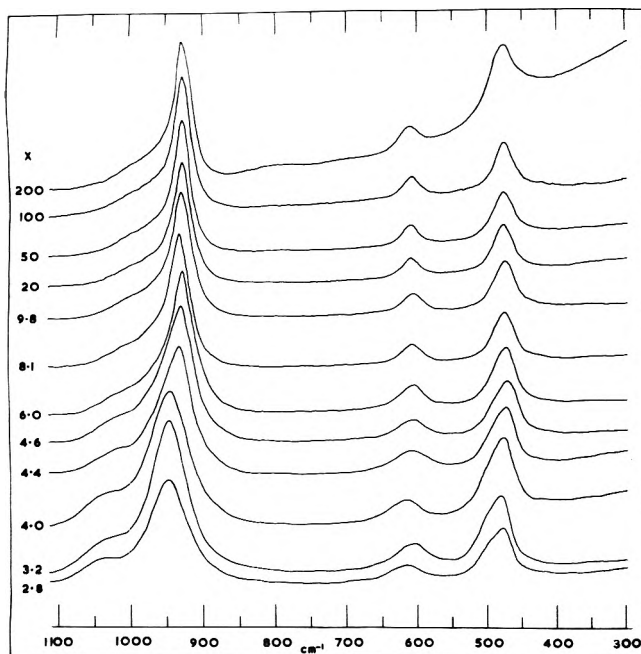


Figure 1. Raman spectra of molten hydrates and solutions of composition $\text{MgClO}_3 \cdot x\text{H}_2\text{O}$ using vertically polarized light.

Experimental Section

Raman spectra were recorded on an instrument comprising a Hilger and Watts D330/331 double monochromator and a Brookdeal ac amplification/phase-sensitive detection system tuned to 800 Hz, the frequency at which a Coherent Radiation Model 52A argon ion laser beam (used at 5145 Å) was chopped. Right angle scattering was used throughout. The system was calibrated with hexane and the curve-resolved band positions are believed to be accurate to $\pm 5 \text{ cm}^{-1}$. The sample holder and furnace have been described elsewhere.⁶ The temperatures required to melt the range of hydrates studied varied from ambient for the higher hydrates and solutions to 120° for $\text{Mg}(\text{ClO}_3)_2 \cdot 2.8\text{H}_2\text{O}$. This composition was found to be the limit of the stable melt range; at lower water contents the salts decomposed on heating without melting.

Reagent grade $\text{Mg}(\text{ClO}_3)_2 \cdot 6\text{H}_2\text{O}$ (BDH) was used without further purification. Anhydrous $\text{Mg}(\text{ClO}_3)_2$ was prepared from this by heating in a vacuum oven at 100° for 72 hr. The various hydrates were then prepared by addition of calculated amounts of water to the anhydrous salt. Magnesium chlorate was always handled in a drybag as it is extremely hygroscopic. Compositions were checked by analysis for Mg^{2+} (EDTA), ClO_3^- (iodimetry), and H_2O (nmr and elemental analysis on a Perkin-Elmer Model 240 CHN analyzer).

Raman spectra of the solid hydrates were obtained by allowing an anhydrous sample to pick up water slowly from the atmosphere, spectra being obtained at the beginning and at intervals during the hydration to the hexahydrate.

Considerable band overlap was found to be a characteristic of all the spectra obtained, so that it was necessary to adopt standard curve-resolving procedures to facilitate analysis of the spectra. A Du Pont Model 310 curve resolver was used for this purpose, with care being taken to avoid generating more bands than were needed to give a close fit to the experimental profiles. A 50/50 Gaussian/Lorentzian product function gave a fit with a physically

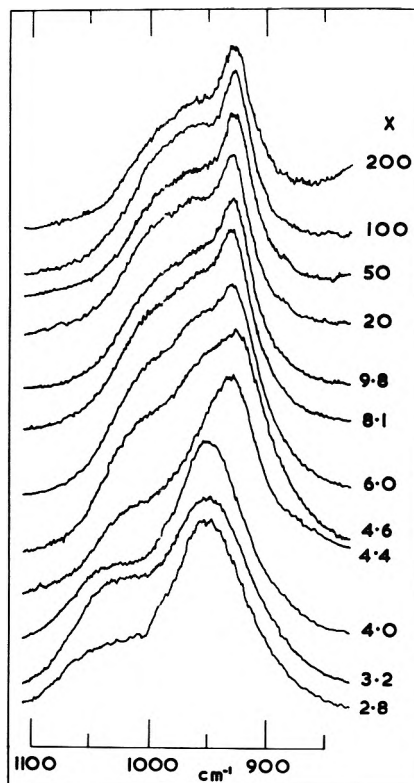


Figure 2. High-frequency region of the Raman spectra of molten hydrates and solutions of composition $\text{MgClO}_3 \cdot x\text{H}_2\text{O}$ using horizontally polarized light.

reasonable number of bands, the residuals in all cases being less than 10% of the total band area. Greatest difficulty was encountered in curve fitting in the wings of sharp bands, and the procedure was adopted of accumulating the errors in curve fitting to a single residual as shown in Figures 3 and 4 by a broken line. No physical significance is to be attached to these residuals.

In order to test the ability of a simple polarization perturbation model to predict changes in the ClO_3^- ion spectrum, due to association with Mg^{2+} or H_2O , calculations were made of the effects of adjusting Cl-O bond force constants such that as one decreased the other two increased so as to maintain a constant sum of the three. This polarization simulation was performed in a manner analogous to earlier work with other oxyanions.^{7,8}

Results

Raman spectra of the molten hydrates and aqueous solutions of $\text{Mg}(\text{ClO}_3)_2$, obtained with parallel plane polarized laser light, are shown in Figure 1. Figure 2 shows the high-frequency region using perpendicular plane polarized light which, due to the polarized nature of the lowest frequency component, renders the multiplet structure more readily resolvable. Typical results of the curve resolution procedure are shown in Figures 3 and 4, taken from three different composition regions. The experimentally observed variation of band frequencies with composition is shown graphically in Figure 5, water content of the system being expressed as percentage by weight in order to show detail in the low water content region. The measured frequencies are listed in Table I.

(6) J. H. R. Clarke and R. E. Hester, *J. Chem. Phys.*, **50**, 3106 (1969).

(7) H. Brintzinger and R. E. Hester, *Inorg. Chem.*, **5**, 980 (1966).

(8) R. E. Hester and W. E. L. Grossman, *Inorg. Chem.*, **5**, 1308 (1966).

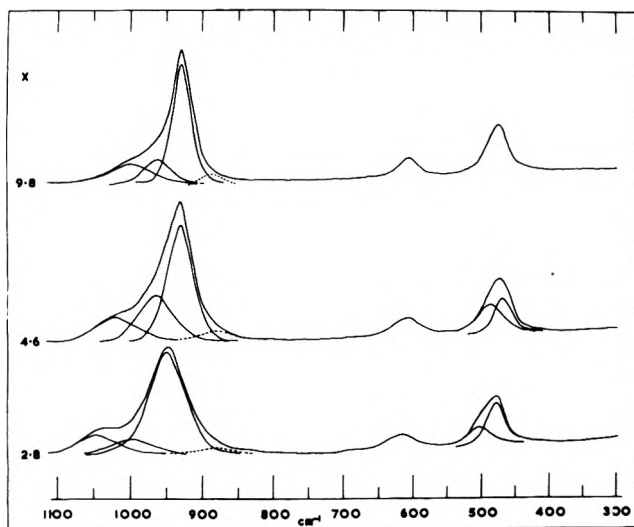


Figure 3. Typical curve resolution results on three Raman spectra of Figure 1 taken from three different composition regions, $\text{MgClO}_3 \cdot x\text{H}_2\text{O}$.

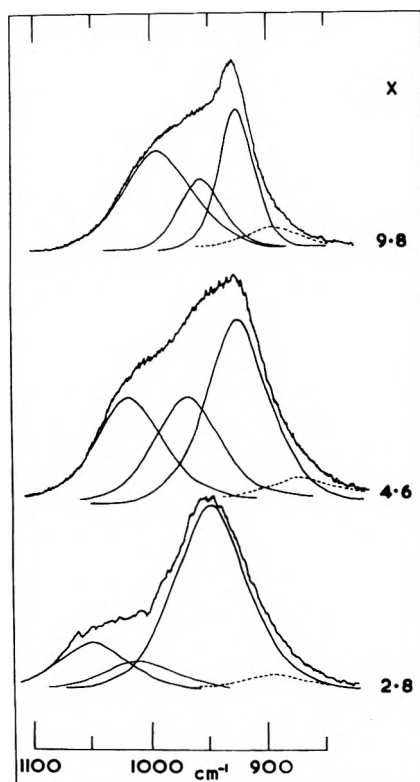


Figure 4. Typical curve resolution results on three Raman spectra of Figure 2 taken from three different composition regions, $\text{MgClO}_3 \cdot x\text{H}_2\text{O}$.

In a separate series of experiments with several of the systems of different composition the effects of varying temperature over the range 20–120° were examined. Within the limits of uncertainty involved in the curve resolution procedure, the temperature effects were found to be insignificant throughout.

The series of Raman spectra of solids, from anhydrous $\text{Mg}(\text{ClO}_3)_2$ through to $\text{Mg}(\text{ClO}_3)_2 \cdot 6\text{H}_2\text{O}$, are shown in Figure 6. Table II lists the observed frequencies of the anhydrous solid and the hexahydrate.

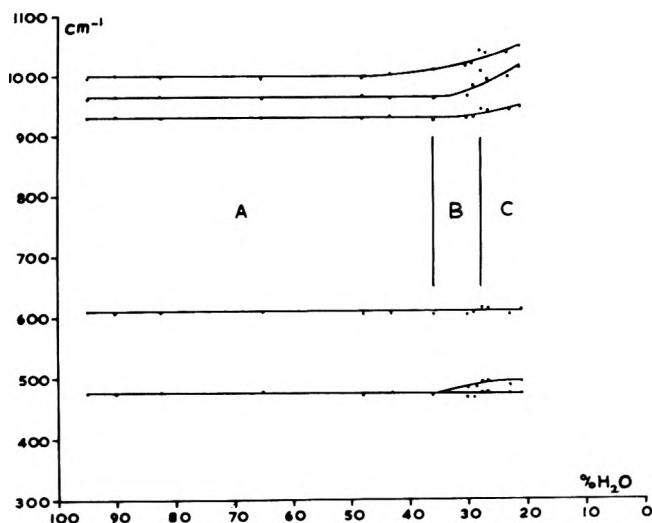


Figure 5. The experimentally observed variation of band frequencies with percentage by weight of water content of $\text{MgClO}_3 \cdot x\text{H}_2\text{O}$. The three composition regions A, B, and C are indicated.

TABLE I: Observed Raman Frequencies of Molten $\text{Mg}(\text{ClO}_3)_2 \cdot x\text{H}_2\text{O}$

x	Frequencies, cm^{-1}					
200	475	608	930	961	996	
100	474	606	929	963	1000	
50	476	608	930	965	998	
20	477	607	930	962	994	
9.8	474	605	930	968	997	
8.1	476	607	932	964	1002	
6.0	473	604	928	965	1012	
4.6	467	484	605	930	967	1017
4.4	467	487	608	932	986	1022
4.0	474	495	616	946	1009	1044
3.8	474	493	614	941	995	1039
3.2	473	489	603	947	999	1041
2.8	474	496	612	949	1015	1052

Figure 7 shows the results of the ClO_3^- ion polarization calculations described in the previous section, with the various band frequencies being plotted as a function of the polarization distortion of the Cl-O bond force constants, ΔF .

Discussion

The unperturbed ClO_3^- ion belongs to the C_{3v} symmetry point group and has a vibrational representation $\Gamma = 2A_1 + 2E$, giving rise to four fundamental modes, all of which are active in both Raman and infrared spectra. Our previous work⁹ established the full vibrational assignment and force constants for ClO_3^- .

It is convenient to consider the data obtained in the following three composition regions: (A) dilute $\text{Mg}(\text{ClO}_3)_2$ solution in water to the molten salt hydrate of composition $\text{Mg}(\text{ClO}_3)_2 \cdot 6\text{H}_2\text{O}$; (B) liquids $\text{Mg}(\text{ClO}_3)_2 \cdot 6\text{H}_2\text{O}$ to $\text{Mg}(\text{ClO}_3)_2 \cdot 4\text{H}_2\text{O}$; (C) liquids $\text{Mg}(\text{ClO}_3)_2 \cdot 4\text{H}_2\text{O}$ to $\text{Mg}(\text{ClO}_3)_2 \cdot 2.8\text{H}_2\text{O}$. Although the full liquid composition range examined was attainable only by varying temperature over the range from room temperature to 120°, it has been established that the spectra under discussion are essentially invariant over this range. The trends in the data presented in Table I and Figure 5 therefore reflect the changing structural features of the liquids through the dif-

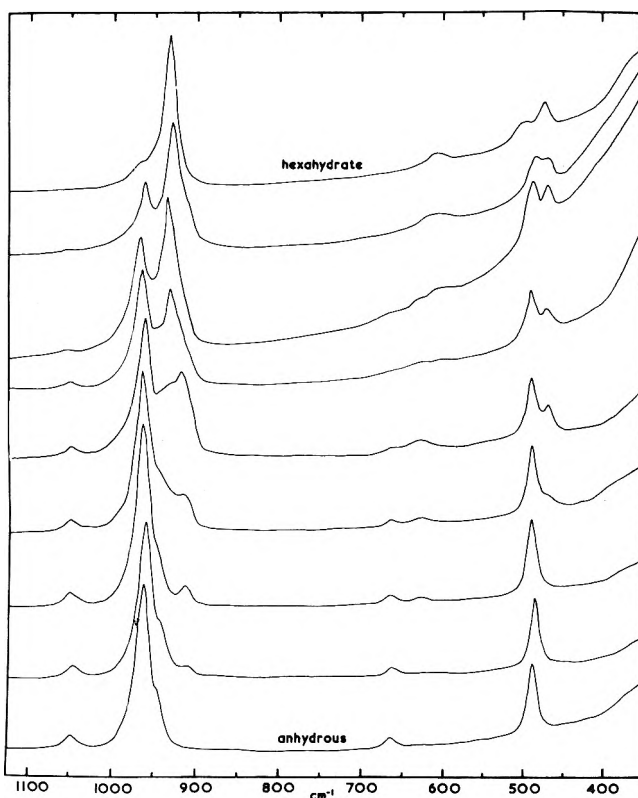


Figure 6. Series of Raman spectra of solids from anhydrous MgClO_3 to $\text{MgClO}_3 \cdot 6\text{H}_2\text{O}$.

TABLE II: Observed Raman Frequencies of Solid Anhydrous $\text{Mg}(\text{ClO}_3)_2$ and $\text{Mg}(\text{ClO}_3)_2 \cdot 6\text{H}_2\text{O}$

	Frequencies, cm^{-1}				
$\text{Mg}(\text{ClO}_3)_2 \cdot 6\text{H}_2\text{O}$	470	494	600	935	970
$\text{Mg}(\text{ClO}_3)_2$	485		660	949(sh)	966 1054

ferent composition regions. Although no sharp divisions exist between the regions A, B, and C, there are sufficient differences in the overall patterns of the spectra to justify separate consideration of these regions.

Throughout region A the Raman band frequencies remain essentially constant and may be assigned to internal modes of the ClO_3^- ion as follows⁹

475 cm^{-1}	$\nu_4(\text{E})$ asymmetric	O-Cl-O deformation
605 cm^{-1}	$\nu_2(\text{A}_1)$ symmetric	O-Cl-O deformation
930 cm^{-1}	$\nu_1(\text{A}_1)$ symmetric	Cl-O stretch
965 cm^{-1}	$\nu_3^{\text{a}}(\text{E})$ asymmetric	Cl-O stretch
997 cm^{-1}	$\nu_3^{\text{b}}(\text{E})$ asymmetric	Cl-O stretch

This assignment is based on the C_{3v} model, but is modified in recognition of the observed ν_3 band splitting to cover the evident loss of degeneracy from this E mode. By analogy with the nitrate analyses of Devlin and coworkers,^{10,11} this ν_3 splitting might be attributed to LO-TO phonons in a liquid quasilattice, although this interpretation might more appropriately be applied to the most concentrated systems. Alternatively, a perturbation of ClO_3^- arising from a specific interaction with water molecules may be invoked. Throughout composition region A the chlorate ions may be assumed to have a water environment, and the invariance of the spectra through this region implies that the ClO_3^- ion probe is insufficiently

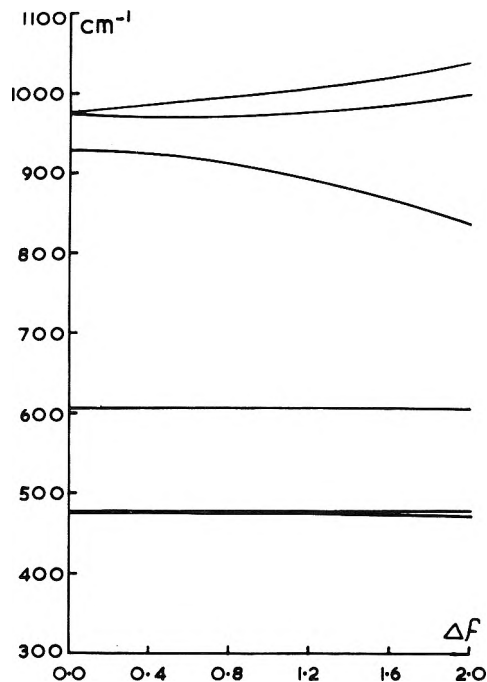


Figure 7. A plot of calculated frequencies against polarization distortion ΔF for the ClO_3^- ion.

sensitive to distinguish "free" water environment from the cation hydration water environment which must exist at the upper concentration limit of this region. That this $\nu_3(\text{E})$ band splitting is the most sensitive spectroscopic feature available is apparent from the results presented here, and also is consistent with expectations based on ion polarization force constant calculations (Figure 7) of the type which have proved useful in analyses of nitrate spectra.^{7,8} In region A it is not proposed that Mg^{2+} ions are effective in polarizing ClO_3^- , but that the dipolar H_2O molecule, either electrostatically or through hydrogen bonding, could have a similar, but weaker, effect.

Our composition region B corresponds with what Braunstein¹² has called "hydrate melts," and it is useful to examine spectral data for this region for evidence of the coexistence of various hydrated magnesium ions, ranging from $\text{Mg}(\text{H}_2\text{O})_6^{2+}$ to $\text{Mg}(\text{H}_2\text{O})_4^{2+}$, the ClO_3^- ions occupying outersphere sites around the metal ions. In this region we note (Table I and Figure 5) the onset of a distinct upward trend in the frequencies of the split $\nu_3(\text{E})$ band components, while ν_1 remains essentially constant and ν_4 also splits into two components. This latter splitting is substantial, reaching $\text{ca. } 20 \text{ cm}^{-1}$, necessitating more than $2 \text{ mdyn } \text{\AA}^{-1}$ change in the relative values of the Cl-O bonds if the ClO_3^- ion polarization model is to explain the effect (see Figure 7). This change is unreasonably large, implying a corresponding $\text{ca. } 50\%$ change in the Cl-O bond order. The model predictions also fail to reproduce the behavior of ν_1 (compare Figures 5 and 7). Analogous splitting of the ν_4 deformation band of NO_3^- in concentrated aqueous solutions has been interpreted as indicative of formation of contact ion pairs.^{2,3} However, although the loss of H_2O from $\text{Mg}(\text{H}_2\text{O})_6^{2+}$ does leave in-

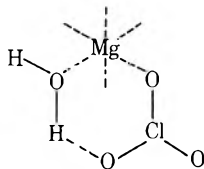
(9) D. J. Gardiner, R. B. Girling, and R. E. Hester, *J. Mol. Struct.*, **13**, 105 (1972).

(10) J. P. Devlin, D. W. James, and R. Frech, *J. Chem. Phys.*, **53**, 4394 (1970).

(11) J. P. Devlin, P. C. Li, and G. Pollard, *J. Chem. Phys.*, **52**, 2267 (1970).

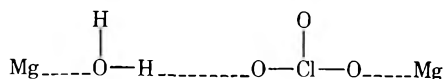
(12) J. Braunstein, *Ionic Interactions*, **1**, 179 (1971).

nersphere coordination sites available for ClO_3^- ion occupancy, it seems likely that interactions between H_2O and ClO_3^- simultaneously coordinated to Mg^{2+} are responsible for differences observed between nitrate and chlorate systems. In composition region B we propose the formation of mixed aquo-chlorate complexes with ligand interactions, which may be represented in the following schematic way, to account for the observed spectra.



Plots were made of trends in intensities and half-widths of bands in region B. However, these were largely unsuccessful due to the accumulation of errors in the curve resolution procedures and no structural conclusions were made on the basis of these data.

In the concentration region C, extending from $\text{Mg}(\text{ClO}_3)_2 \cdot 4\text{H}_2\text{O}$ to $\text{Mg}(\text{ClO}_3)_2 \cdot 2.8\text{H}_2\text{O}$, the several changes in the spectral features recorded for region B are seen to be further extended (Table I and Figure 5). The splitting of the two components of $\nu_3(\text{E})$ does not vary significantly from 40 cm^{-1} throughout the region, but the upward trend in the frequencies of both components is more marked. Unless an increased Cl-O bond order is proposed, this upward trend implies an external restriction on Cl-O bond stretching, which also is reflected in the upward trend of the $\nu_1(\text{A}_1)$ frequency through this region C. In the molecular deformation region, however, the changes are smaller. $\nu_2(\text{A}_1)$ remains virtually constant, while the components of $\nu_4(\text{E})$ remain separated by *ca.* 20 cm^{-1} , both shifting to slightly higher frequencies than observed for region B. This behavior is in general accord with the predictions of the polarization calculations (Figure 7), with the notable exception of the $\nu_1(\text{A}_1)$ frequency. More extensive interactions between Mg^{2+} - H_2O - ClO_3^- mixed ligand complexes are probable in this region, the order and cohesion of the liquid quasilattice so formed being due in part to intermolecular H bonding between mixed H_2O - ClO_3^- complexes of magnesium, *viz.*



The general broadening of the bands in the low water region C (Figures 3 and 4) could be interpreted in terms of disorder in the extended quasilattice. In this situation Devlin's TO-LO component interpretation of the $\nu_3(\text{E})$ mode splitting may be applicable. Alternatively, an interpretation in terms of a multispecies equilibrium, involving species of which the ion pair is merely one simple form,

might be entertained. Attributing the band at 930 cm^{-1} to the essentially "free" ClO_3^- species, the broadening and shift to higher frequencies observed with increasing salt concentration may be attributed to the growth of a band (bands) at *ca.* 945 cm^{-1} characteristic of ion-pair or ion-cluster species.

The solid-state spectra, given in Figure 6, may profitably be compared with those obtained from the liquids of corresponding composition in regions B and C (molten salt hydrates). There are clearly marked differences between the two states throughout the composition range, perhaps the most significant being the apparent lack of splitting of the $\text{ClO}_3^- \nu_3(\text{E})$ band, which occurs at 970 cm^{-1} in the solid hexahydrate. The corresponding band in the anhydrous salt occurs at 1054 cm^{-1} . This lack of splitting may be used as evidence of symmetric ClO_3^- in the anhydrous solid lattice, but the splitting of $\nu_4(\text{E})$ in the solid hexahydrate excludes this conclusion in this case. The high-frequency shifts noted in the liquid spectra as water was removed also are apparent in the solid spectra, though in the solids $\nu_2(\text{A}_1)$ also is strongly affected by dehydration. Spectra of solids of intermediate composition appear in the main to be weighted superpositions of the hexahydrate and anhydrous salt spectra, though additional features in the regions 900 – 930 and *ca.* 630 cm^{-1} are apparent in some of the traces and perhaps arise from distinct hydrate species containing fewer than six H_2O . However, the situation is still more complex for the liquids. The shoulder at 949 cm^{-1} in the spectrum of the anhydrous solid may be assigned to a ^{37}Cl isotope component, by comparison with KClO_3 spectra,¹³ though the absence of this feature from anhydrous LiClO_3 spectra¹⁴ suggests an alternative assignment, perhaps in terms of factor group splittings which are absent from the LiClO_3 case.

In conclusion, these results favor the following structural features for the $\text{Mg}(\text{ClO}_3)_2$ - H_2O systems. With excess water, the Mg^{2+} ions are fully hydrated and exert little influence on the spectrum (molecular symmetry and electronic distribution) of ClO_3^- . ClO_3^- is, however, perturbed by interaction with H_2O , either in bulk water or in the Mg^{2+} hydration sheaths. At water levels less than the hexahydrate ClO_3^- occupies innersphere, or contact, coordination sites around Mg^{2+} , thereby undergoing polarization distortion in addition to local interactions with hydrate water molecules. There is no evidence for discrete $\text{Mg}(\text{H}_2\text{O})_n^{2+}$ species with $n < 6$, but extended lattice-like interactions appear likely in melts of low water content.

Acknowledgment. We thank Dr. A. Covington of Newcastle University for allowing us use of his Du Pont curve resolver.

(13) J. B. Bates, *J. Chem. Phys.*, **55**, 494 (1971).

(14) We thank a reviewer for this datum.

Conformational Effects on the Nitrogen-Hydrogen Stretching Frequencies of Lactams

Charles A. Swenson* and Catherine Y. S. Chen

Department of Biochemistry, University of Iowa, Iowa City, Iowa 52240 (Received June 13, 1972)

Publication costs assisted by the National Science Foundation

The N-H stretching vibrations of lactams with ring sizes greater than seven ($n = 7$) have been studied in the fundamental infrared region in benzene, carbon disulfide, carbon tetrachloride, and other halocarbon solvents. Doubling of the N-H absorptions, which was observed in all the weakly interacting solvents, was interpreted as being due to the existence of two preferred conformations, both of which interact with solvent. Temperature and solvent composition had little effect on the percentages of the conformers.

Introduction

Lactams of varying sizes have been useful as models for studying properties of peptide linkages, particularly with regards to the properties of cis and trans isomers.¹⁻⁵ Ring sizes (n) less than 9 have a cis peptide linkage and those greater than 9 have a trans peptide linkage with the $n = 9$ lactam being a mixture of cis and trans forms.^{6,7} These forms are readily distinguished from their infrared spectrum in the fundamental N-H stretching region where the trans form absorbs at approximately 3450 cm^{-1} and the cis form absorbs at 3410 cm^{-1} . In general the cis forms absorb at lower energies than the trans forms, except for ring sizes of $n = 5$ or less; these lactams have strained rings and the N-H absorptions occur at the same frequency as the trans forms or even higher.¹

The possible existence of an equilibrium between cis and trans conformations for the $n = 9$ lactam suggested it as a model for environmental effects on cis-trans interconversions for peptides and/or proteins. In an earlier study⁸ several solvents were used but little or no interconversion was detected for this lactam or those of any other ring size. Furthermore, there was little effect of temperature on the cis-trans absorption ratios in carbon tetrachloride solution. In summary, neither solvent nor temperature affected the cis-trans ratio. When measuring the spectrum for the above studies an interesting observation was noted, namely, that monomeric lactams in carbon tetrachloride show a doubling of the N-H absorption for ring sizes greater than 7. That is two cis or two trans absorptions were observed, whereas one was expected. In this report we discuss experiments which were performed in order to explain the spectral observations.

Experimental Section

Materials and Methods. Lactam samples were synthesized and purified as previously described.^{1,8} Solvents were from Fisher Scientific Co. and Eastman Organic Chemicals and were used without purification if they were certified, spectral, or reagent grade. Other solvents from the same sources of lower grade were distilled prior to use. Deuterium oxide (99.5%) was obtained from Stohler Isotope Chemicals, Inc.

A Perkin-Elmer Model 521 infrared spectrometer was used for all the measurements. The solution spectra were measured at a spectral slit of about $1\text{--}2\text{ cm}^{-1}$ in cells which ranged from 0.1 mm to 2.5 cm in path length. Infrasil quartz was the window material for the 1- and 2.5-

cm cells and calcium fluoride was used for the shorter path lengths. Solvent compensation was used for all measurements and the gain was adjusted to give the proper pen response.

Preparation of most of the solutions was performed in a drybox to exclude water. Concentrations ranged from 0.001 to 0.1 *M*; most were run at the higher concentrations in the short path length cells.

Temperature was controlled in the sample and reference compartments by variable temperature chambers from Barnes Engineering Co.

Results and Discussion

Infrared spectra of the N-H stretching region for the four lactams in carbon tetrachloride are shown in Figure 1. For both cis and trans forms two N-H absorptions are observed. The difference between the absorption frequencies is smallest for the $n = 8$ lactam ($<10\text{ cm}^{-1}$), is a maximum for $n = 9$ (17 cm^{-1} cis, 20 cm^{-1} trans), and decreases from $n = 9$ to $n = 13$ (14 cm^{-1}). Asymmetry in the N-H absorption band of the $n = 8$ lactam hints at its being split. Two possible explanations for such doubling are (1) a spectroscopic splitting such as Fermi resonance and (2) the existence of two conformers possibly in equilibrium in the solution. In order to investigate the first possibility the peptide hydrogen of the $n = 9$ lactam was replaced with deuterium and the spectrum run. The absorption pattern was the same except for the isotope frequency shift and thus clearly shows the splitting not to be a Fermi resonance interaction as it would have been expected to disappear or at least change markedly upon isotope substitution. Thus it seems likely that the doubling is due to the presence of some conformational equilibria. Using this concept as the "model," the observed spectra suggest that there are *two* highly preferred conformations. This seems difficult to accept since in going from $n = 9$ to 13 the number of conformational variables must increase exponentially. Although it need not be the case, it is

- (1) M. Tsuboi, *Bull. Chem. Soc. Jap.*, **22**, 855 (1949).
- (2) R. C. Lord and T. J. Porro, *Z. Elektrochem.*, **64**, 672 (1960).
- (3) H. Susi, S. N. Timasheff, and J. S. Ard, *J. Biol. Chem.*, **239**, 3051 (1964).
- (4) H. Susi, *J. Phys. Chem.*, **69**, 2799 (1965).
- (5) C. Y. S. Chen and C. A. Swenson, *J. Phys. Chem.*, **73**, 2999 (1969).
- (6) R. Huisgen and H. Walz, *Chem. Ber.*, **89**, 2616 (1956).
- (7) R. Huisgen, H. Brade, H. Walz, and I. Glogger, *Chem. Ber.*, **90**, 1437 (1957).
- (8) C. Y. S. Chen, Ph.D. Thesis, University of Iowa, Iowa City, Iowa, 1968.

TABLE I: Free N-H Stretching Vibrations of $n = 8$ Lactam in Various Solvents^a

Solvent	Frequency, cm^{-1}					
	Trans		$\Delta\nu_T$	Cis		$\Delta\nu_C$
Carbon tetrachloride	3462 \pm 2	3442 \pm 1	20 \pm 3	3415 \pm 1	3398 \pm 1	17 \pm 2
Cyclohexane	3463 \pm 2	3442 \pm 1	21 \pm 3	3419 \pm 1	3396 \pm 1	23 \pm 2
Tetrachloroethylene	3460 \pm 2	3440 \pm 1	20 \pm 3	3414 \pm 1	3392 \pm 1	22 \pm 2
<i>trans</i> -1,2-Dichloroethylene	3460 \pm 2	3438 \pm 1	22 \pm 3	3408 \pm 1	3392 \pm 1	16 \pm 2
<i>cis</i> -1,2-Dichloroethylene	3455 \pm 2	3435 \pm 1	20 \pm 3	3406 \pm 1	3392 \pm 1	14 \pm 2
1,1,2-Trichloroethylene	3460 \pm 2	3440 \pm 1	20 \pm 3	3410 \pm 1	3395 \pm 1	15 \pm 2
1,1,1-Trichloroethane	3460 \pm 2	3440 \pm 1	20 \pm 3	3412 \pm 1	3391 \pm 1	21 \pm 2
Carbon disulfide	3453 \pm 2	3434 \pm 1	19 \pm 3	3406 \pm 1	3387 \pm 1	19 \pm 2
Chloroform	3457 \pm 2	3440 \pm 1	17 \pm 3	3406 \pm 1	3393 \pm 1	13 \pm 2
Methylene chloride	(3455)	3435 \pm 1	20 \pm 5	3405 \pm 1	3395 \pm 1	10 \pm 2
<i>s</i> -Tetrachloroethane	(3458)	3436 \pm 1	22 \pm 5	3405 \pm 1	3395 \pm 1	10 \pm 2
1,2-Dichloroethane		3438 \pm 1			3400 \pm 1	
Benzene (benzene- d_6)		3423 \pm 1			3387 \pm 1	
Methylene iodide		3409 \pm 1			3375 \pm 1	

^a Values in parentheses indicate a shoulder rather than a distinct maximum.

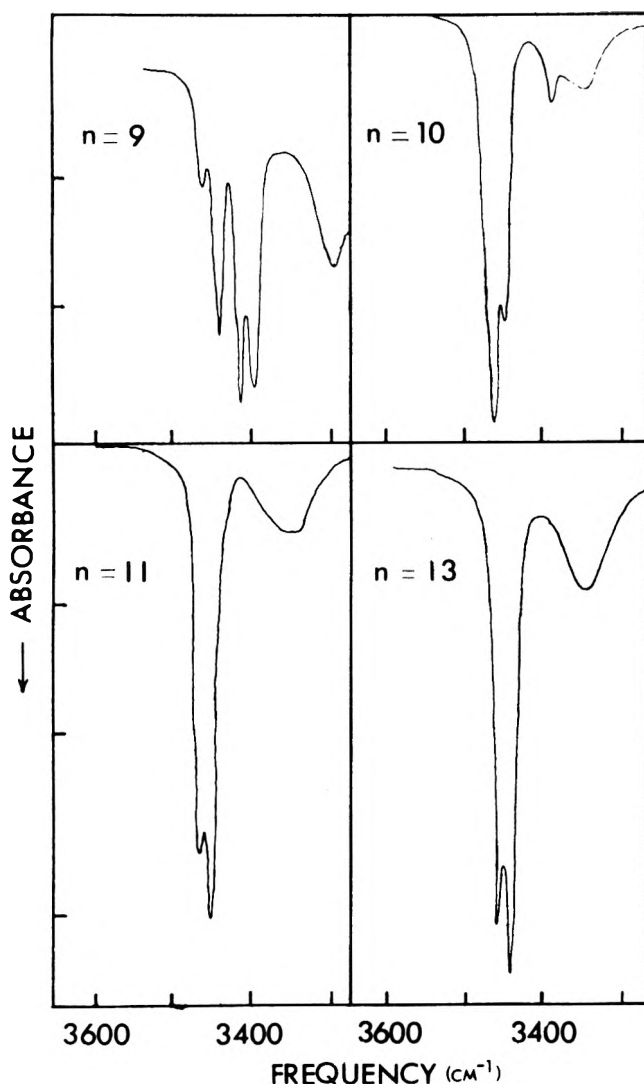


Figure 1. Infrared spectra of monomeric lactams in carbon tetrachloride.

tempting to suggest, since the peptide group is the most likely to interact with solvent, that in solution there is an equilibrium between conformations which have the pep-

ptide group in a *more or less* favorable position for solvent interaction. A similar suggestion was made by Luck⁹ from near-infrared data. In order to test this idea we have studied the magnitude of the splittings and the relative intensities of the components as a function of temperature and solvents.

The effect of temperature on the observed spectra was studied extensively for the $n = 9$ and 13 lactams in carbon tetrachloride solution. The results can be summarized as follows. The bands broaden slightly (less than 10% increase in half-width) and the maximum shifts less than 2 cm^{-1} in the temperature range from 2 to 50°. When the concentration used for the temperature study allowed small amounts of self-association by hydrogen bonding, the temperature effects were dominated by these intensity changes; *i.e.*, production of more free lactam as the temperature increased more than overcame the density correction. Furthermore, it was noted that the *cis* lactam dimer is the predominant dimer species in solution for the $n = 9$ lactam.¹ Intensity changes as a function of temperature indicate that *cis*-*trans* interconversion does not occur as noted earlier. Further, there was no alteration of the intensity of the split *cis* and *trans* components which indicates that there is little interconversion between structures giving rise to them and that neither structure is preferentially involved in self-association by hydrogen bonding. Similar temperature effects were observed with all the other lactams.

Halocarbon solvents were used with the exception of benzene, cyclohexane, and carbon disulfide. Several criteria were used in choosing the solvents: (1) they should interact weakly with the peptide group, (2) they should have negligible absorption from 3350 to 3500 cm^{-1} , (3) they should represent a range of refractive indices and dipole moments. Strongly interacting solvents, such as ketones, show only a broad hydrogen-bonded N-H absorption which would mask any effects observed for the monomer.

Data for the $n = 9$ lactam in the various solvents are presented in Table I. The frequency difference for the *trans* components, $\Delta\nu_T$, for the various weakly interacting solvents is constant to within experimental error for most solvents. For the strongly interacting solvents, 1,2-dichlo-

(9) W. Luck, *Naturwissenschaften*, 52, 25 (1965).

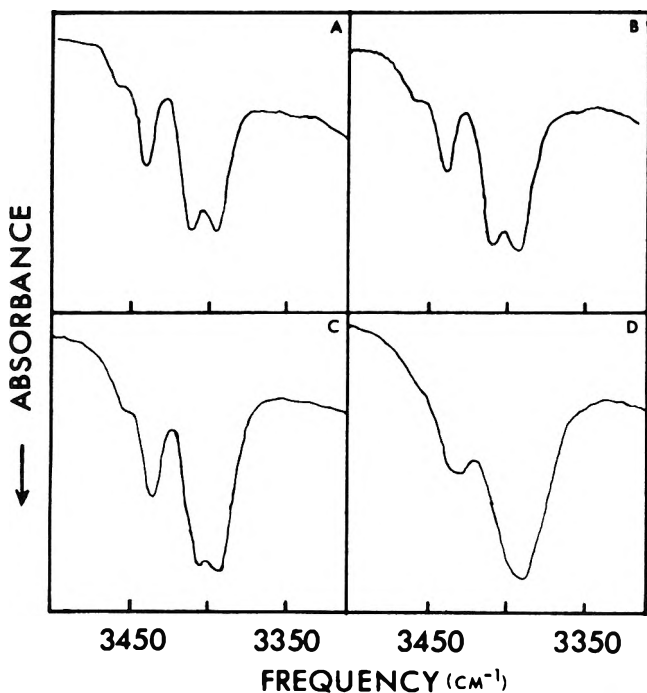


Figure 2. Effect of solvent on the N-H stretching region of $n = 9$ lactam: (A) trichloroethylene, (B) *trans*-1,2-dichloroethylene, (C) *cis*-1,2-dichloroethylene, and (D) 1,2-dichloroethane.

roethane, benzene, and methyl iodide, only one broad component is observed. This peak is at a lower frequency than the low-frequency component of the *trans* doublet in weakly interacting solvents. Most likely the stronger interaction leads to a broadening which obscures the weaker component in the *trans* doublet, although a shift in conformer equilibria could occur. Resolution of the absorption into four Gaussian peaks on a Du Pont 310 curve resolver indicates the former to be likely. Similar arguments could be made for the *cis* components concerning broadening of the absorptions although in this case the observed maxima is an average for the two *cis* components interacting with solvents since they are nearly of equal intensity. The frequency difference, $\Delta\nu_C$, for the two *cis* components shows a variation which is outside of the experimental error. More strongly interacting solvents compared to carbon tetrachloride, such as chloroform or methylene chloride, tend to decrease the splitting in the *cis* components. There appears to be a correlation between dielectric constant and/or refractive index and frequency of absorption of both of the *cis* and *trans* components in the nonpolar solvents carbon tetrachloride and carbon disulfide which suggests that a linear Kirkwood-Bauer plot would result.¹⁰ Solute-solvent interactions are then the likely cause for the poor correlation of the more polar solvents.

Slight intensity variations are observed for the *cis* and *trans* components but are difficult to measure with an accuracy that would allow interpretation after correcting for field effects.¹¹ Intensity ratios as noted in Figure 2 are consistently observed in all the solvents although the pattern does appear different due to the changes in bandwidth. In general the lower frequency components are broader and more intense for both *cis* and *trans* forms as would be expected if these are the absorptions due to the forms which are in more intimate contact with the solvent.

Mixed solvents were used to follow the behavior of the *cis* and *trans* components of the $n = 9$ lactam as the sol-

vent was changed from carbon tetrachloride to 1,2-dichloroethane or benzene. For these solutions the maximum for most of the components are quite easy to discern to a mole fraction of 0.9. For 1,2-dichloroethane-carbon tetrachloride solutions the single *cis* and *trans* components are intermediate in frequency to an extrapolation of the two components for each in the mixed solvent. This likely results from a broadening of the components of the *cis* and *trans* doublets by increased interaction with the added solvent components over that with carbon tetrachloride. Similar broadening is responsible for the single component of the two doublets in benzene although the broadening is more pronounced than with 1,2-dichloroethane; also for the benzene-carbon tetrachloride mixed solvent there is an increase in intensity as the mixed solvent becomes benzene rich.

It is impossible to be specific about the interactions between solvent and the conformers which give rise to the spectral doublet; however, some general comments are useful in light of the assumed model. We consider the most strongly interacting solvents first: benzene, 1,2-dichloroethane, and methyl iodide. All cause a collapse of the band structure of an *apparent* single *cis* and single *trans* component. Benzene is in a class by itself as has been discussed by Hatton and Richards.¹² They suggested a structure from their nmr data which makes apparent the special structural requirements for the interaction (a coplanar arrangement of the benzene ring and the peptide bond). Thus the conformers for which this is sterically possible would interact strongly. Methyl iodide and 1,2-dichloroethane both have dipole moments, 1.6 and 1.9 D, respectively, and can interact with the peptide *via* a dipolar interaction, and/or a hydrogen bond with the carbonyl *via* their acidic hydrogens. Steric effects due to the halogens would be expected to be minimal in both cases. There may be a shift in the conformer equilibria in all the strongly interacting solvents, but it is impossible to detect in the spectra. Methylene chloride (1.54 D) also causes broadening of the bands though not as pronounced as methylene iodide. Steric effects are likely the primary reason why *s*-tetrachloroethane does not interact as strongly as 1,2-dichloroethane since its dipolar moment is larger (1.36 D). Chloroform (1.02 D) causes a slight broadening which is possibly due to a hydrogen bonding interaction of its acidic hydrogen with the carbonyl group of the peptide linkage. *cis*-1,2-Dichloroethylene also causes a slight broadening. The other solvents give frequency and intensity patterns which are similar to carbon tetrachloride. Carbon disulfide is an example which shows the same intensity pattern but with all peaks shifted to a lower frequency. This is likely to be a field effect as noted previously.

In summary, the spectral observations suggest that the observed doubling of N-H absorptions arises from two preferred conformations of the peptide group that are present in the solution for these lactams. Both conformations seem to interact with solvent. For the solvents studied, all of which are thought to be weakly interacting except for benzene, 1,2-dichloroethane, and methyl iodide, no measureable effect was noted on the relative amounts of the conformations. Intensity changes could, however, be

(10) W. West, Ed., "Techniques of Organic Chemistry," Vol. IX, Interscience, New York, N. Y., 1956, p 306.

(11) S. R. Polo and M. K. Wilson, *J. Chem. Phys.*, **23**, 2376 (1955).

(12) (a) J. V. Hatton and R. E. Richards, *Mol. Phys.*, **3**, 253 (1960); (b) J. V. Hatton and R. E. Richards, *ibid.*, **5**, 139 (1960).

interpreted as a shift in the equilibrium in favor of the forms which interact best with solvent. Temperature had no effect on the relative amounts. The solvents do interact differently with the peptide linkage causing frequency shifts in both components and for the more strongly interacting ones intensity changes and band broadening occur as well. The low-frequency components for the cis and trans forms likely arise from the conformers which interact more strongly with solvent as they are broadened and

show intensity increases to a greater degree than the high-frequency components.

Acknowledgment. This work was supported in part by a grant (No. GB 18017) from the Division of Molecular Biology, National Science Foundation, and a Public Health Service Research Career Development Award to C. A. S. (No. GM 42,384) from the Institute of General Medical Sciences.

Hydrophobic Fluorescence Probe Studies with Poly-L-lysine

Gisela Witz and Benjamin L. Van Duuren*

Laboratory of Organic Chemistry and Carcinogenesis, Institute of Environmental Medicine, New York University Medical Center, New York, New York 10016 (Received May 4, 1972)

Publication costs assisted by The National Institutes of Health

The interaction between 2-*p*-toluidinylnaphthalene-6-sulfonate (TNS), a hydrophobic fluorescent probe, and poly-L-lysine was examined by fluorescence and ultraviolet spectroscopy. Poly-L-lysines with degrees of polymerization (DP) 35, 210, and 445 were converted to the random coil, α -helix and β -sheet conformations. Fluorescence titrations of TNS with β -sheet poly-L-lysine were performed in order to determine the effect of polymer chain length and concentration on β -sheet structure. The data indicate that TNS binds specifically to β -sheet poly-L-lysine and to the same kind of hydrophobic sites regardless of polymer chain length or concentration. The fluorescence titration curves for TNS bound to β -sheet poly-L-lysine, DP 210 and DP 445, were identical. Moreover, this curve shows a break at 0.67×10^{-2} g of polypeptide/100 ml. The fluorescence titration curve for TNS bound to β -sheet poly-L-lysine, DP 35, has no break and shows a smaller degree of fluorescence enhancement compared to the high molecular weight polymer titration curves. The isotherm constructed from the titration curves indicates that the enhanced fluorescence intensity of TNS bound to high molecular weight β -sheet poly-L-lysine at initial concentrations less than 0.67×10^{-2} g of polypeptide/100 ml is not due to a change in the quantum yield of bound TNS. These fluorimetric studies indicate that the structure of β -sheet poly-L-lysine varies both with the initial concentration and the chain length of the polymer used.

Introduction

Many reports have appeared concerning the binding of hydrophobic fluorescent probes to proteins.¹⁻³ Since these probes reflect the nature of their environment through characteristic features of their fluorescence spectra, they have been employed in the study of conformational states of proteins,⁴ lipid-protein interactions in membranes,⁵ and rapid structural changes accompanying biological processes.⁶

Previous studies have shown that the conformation of poly-L-lysine in aqueous solution depends upon the extent of ionization of the terminal amino group of the polymer.⁷ Although the β structures of several synthetic polypeptides have been prepared in the laboratory and β -sheet regions have been detected in a number of naturally occurring proteins,⁸⁻¹⁰ the exact nature of the β -sheet conformation is still a matter of dispute.

A previous report by Lynn and Fasman¹¹ indicated that TNS binds specifically to β -sheet poly-L-lysine. In the present work, the interaction between TNS and poly-L-lysine of different molecular weights was examined by flu-

orescence and ultraviolet spectroscopy; the poly-L-lysines were converted to the β sheet, random coil, and α helix for these studies.

Materials and Methods

2-*p*-Toluidinylnaphthalene-6-sulfonate, TNS (Sigma Chemical Co., St. Louis, Mo.), was recrystallized twice

- (1) W. O. McClure and G. M. Edelman, *Biochemistry*, **5**, 1908 (1966).
- (2) S. Ainsworth and M. T. Flanagan, *Biochim. Biophys. Acta*, **194**, 213 (1969).
- (3) H. Takashina, *Biochim. Biophys. Acta*, **200**, 319 (1970).
- (4) W. O. McClure and G. M. Edelman, *Biochemistry*, **6**, 567 (1967).
- (5) D. F. H. Wallach, E. Ferber, D. Selin, E. Weidekamm, and H. Fischer, *Biochim. Biophys. Acta*, **203**, 67 (1970).
- (6) A. Azzi, B. Chance, G. K. Radda, and C. P. Lee, *Proc. Nat. Acad. Sci. U.S.*, **62**, 612 (1969).
- (7) B. Davidson and G. H. Fasman, *Biochemistry*, **6**, 1616 (1967).
- (8) C. C. F. Blake, D. F. Koenig, G. A. Mair, A. C. T. North, D. C. Phillips, and V. R. Sarma, *Nature (London)*, **206**, 757 (1965).
- (9) G. M. Reeke, J. A. Hartsuck, M. L. Ludwig, F. A. Quijcho, T. A. Steitz, and W. N. Lipscomb, *Proc. Nat. Acad. Sci. U.S.*, **58**, 2220 (1967).
- (10) H. W. Wyckoff, K. D. Hardman, N. M. Allewell, T. Inagami, L. N. Johnson, and F. M. Richards, *J. Biol. Chem.*, **242**, 3984 (1967).
- (11) J. Lynn and G. D. Fasman, *Biochem. Biophys. Res. Commun.*, **33**, 327 (1968).

from 2% aqueous potassium hydroxide and dried in a high vacuum for 4 hr at room temperature; the salt showed a single spot on a thin-layer chromatogram, silica gel, with isopropyl alcohol as solvent, $R_f=0.26$.

Anal. Calcd for $C_{17}H_{14}KNO_3S$: C, 58.07; H, 4.01; K, 11.12; N, 3.99. Found: C, 57.96; H, 4.22; K, 11.34; N, 4.27.

Poly-L-lysine hydrobromide (Miles Laboratories, Elkhart, Ind.), mol wt 7315, 43,870, and 97,500, was dried in a high vacuum at room temperature for 4 hr.

Anal. Calcd for $(C_6H_{13}N_2OBr \cdot H_2O)_n$: Br, 35.21 N, 12.34. Found: Br, 34.79; N, 12.80 (mol wt 7315); Br, 35.70; N, 12.65 (mol wt 43,870); Br, 34.29; N, 12.48 (mol wt 97,500).

Quinine bisulfate (K & K Laboratories, Inc., Plainview, N. Y.) was recrystallized from 0.1 *N* H_2SO_4 .

Anal. Calcd for $C_{20}H_{24}N_2O_2 \cdot H_2SO_4 \cdot H_2O$: C, 54.53; H, 6.41; N, 6.36; S, 7.29. Found: C, 54.33; H, 6.26; N, 6.33; S, 7.29.

Instrumentation. All ultraviolet absorption spectra were measured on a Cary, Model 14, spectrophotometer (Applied Physics Corporation, Monrovia, Calif.). All Fluorescence spectra were measured on a custom-designed multipurpose luminescence spectrophotometer (Farrand Optical Co., New York).¹² With this instrument corrected excitation and emission spectra are recorded automatically in energy units; fluorescence emission spectra were also recorded in quantum units for measuring quantum efficiencies. Slits 5 $m\mu$ wide were used.

Titration of TNS with β -Sheet Poly-L-lysine. All solutions were prepared using pure distilled water; TNS solutions were stored in amber flasks at 4°. A typical titration of 10^{-5} *M* TNS with β -sheet poly-L-lysine for a 1:1 solution of TNS:polypeptide, mol wt 7315, is as follows: 1 ml of 0.15 *M* NaCl plus 0.01 *M* NaOH, 6.5 ml of 0.15 *M* NaCl, and 1 ml of 10^{-4} *M* poly-L-lysine hydrobromide in 0.15 *M* NaCl were mixed; a corresponding protein blank was also prepared. Both solutions were heated for 10 min at 50° and cooled to room temperature. All heating volumes were kept constant, *i.e.* 8.5 and 4.25 ml for protein solutions in 10- and 5-ml volumetric flasks, respectively. After cooling, 1 ml of 10^{-4} *M* TNS in 0.15 *M* NaCl was pipetted into the 10-ml volumetric, and both solutions were diluted up to final volume with 0.15 *M* NaCl. All fluorescence and ultraviolet absorption spectra were measured at 24–26° on freshly prepared solutions only. In the case of fluorescence, corrected emission spectra of the TNS-protein solutions were recorded in quantum units using 350 $m\mu$ as the excitation wavelength. After each TNS-protein emission measurement two quinine bisulfate emission spectra were measured under the same optical conditions but at two sensitivity settings. The ultraviolet absorption spectra of the TNS-polypeptide solutions were measured against the corresponding protein β -sheet blank immediately after both solutions had been made up.

α Helix. The procedure used for preparing poly-L-lysine in the α -helical conformation differed from that for the β -sheet conformation only in that the protein solutions were not preheated.

Random Coil. Solutions of poly-L-lysine in the random coil conformation were prepared exactly like those of poly-L-lysine in the α -helical conformation, except that 0.15 *M* NaCl was substituted for 0.15 *M* NaCl plus 0.10 *N* NaOH.

pH Measurements. Nonirradiated solutions had the following pH's: TNS-7315 mol wt polypeptide, β sheet, 11.05–11.24; α helix, 11.08–11.19; random coil, 6.2; TNS-

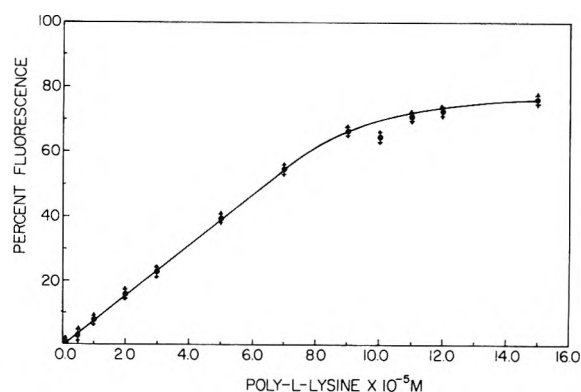


Figure 1. Fluorescence titration of TNS with β -sheet poly-L-lysine, mol wt 7315. TNS, 10^{-5} *M*, was titrated with β -sheet poly-L-lysine as described in Materials and Methods. Per cent fluorescence refers to emission relative to that of a 10^{-5} *M* quinine bisulfate solution.

43,870 mol wt polypeptide, β sheet, 11.15–11.26; α helix, 11.16; random coil, 6.5–6.7; TNS-97,500 mol wt polypeptide, β sheet, 11.6–11.9. The corresponding irradiated solutions had pH's which generally were 0.1 to 0.2 units higher.

Results

β -Sheet Poly-L-lysine, mol wt 7315, and TNS. TNS, 10^{-5} *M*, in 0.15 *M* NaCl, 0.01 *N* NaOH, and β -sheet poly-L-lysine, 0.5×10^{-5} *M*, showed no detectable fluorescence; there was a slight background emission at 397 $m\mu$ ascribed to the aqueous solution of NaCl-NaOH.

The results for the titration of 10^{-5} *M* TNS with 10^{-5} *M* β -sheet poly-L-lysine, mol wt 7315, are shown in Figure 1. A ratio of 1:1 TNS: β -sheet poly-L-lysine in this case corresponds to 10^{-5} *M* TNS and 10^{-5} *M* poly-L-lysine. β -Sheet poly-L-lysine, mol wt 7315, was soluble at all concentrations used and no precipitate or opacity was observed. The bound TNS showed an emission maximum at 428 $m\mu$ which does not shift regardless of TNS:poly-L-lysine ratio. The excitation spectra of the various TNS- β -sheet solutions have maxima at 355, 320, 274, and 228 $m\mu$. These maxima remain constant throughout the titration but they vary in relative intensities.

The absorption spectrum of TNS, 10^{-5} *M*, in 0.15 *M* NaCl and 0.01 *N* NaOH shows maxima at 351, 315.3, 262, and 223 $m\mu$. In the presence of β -sheet poly-L-lysine, the 262- $m\mu$ absorption peak is progressively red shifted with increasing amounts of β sheet. At a ratio of 1:12 TNS: β -sheet polypeptide, where most of the available TNS is bound to the polymer, the red shift is ~ 11 $m\mu$. The 315.3- $m\mu$ absorption peak is also progressively red shifted in the presence of increasing amounts of β sheet. However, even at the highest β -sheet concentration, 15×10^{-5} *M*, the red shift amounts only to ~ 3 $m\mu$. Absorption at 223 and 351.5 $m\mu$ remains relatively unchanged as more TNS binds. TNS in ethanol has absorption maxima at 274 ($\epsilon 3.79 \times 10^4$), 318 ($\epsilon 3.15 \times 10^4$), and 353 $m\mu$ ($\epsilon 8.5 \times 10^3$). As more TNS binds to β -sheet poly-L-lysine, absorption maxima characteristic of TNS in ethanol are obtained.

Conversion of excitation spectra from energy units to quantum units allows comparison with their respective absorption spectra.¹² At high β -sheet concentrations,

(12) S. Cravitt and B. L. Van Duuren, *Chem. Instrum.*, 1, 71 (1968).

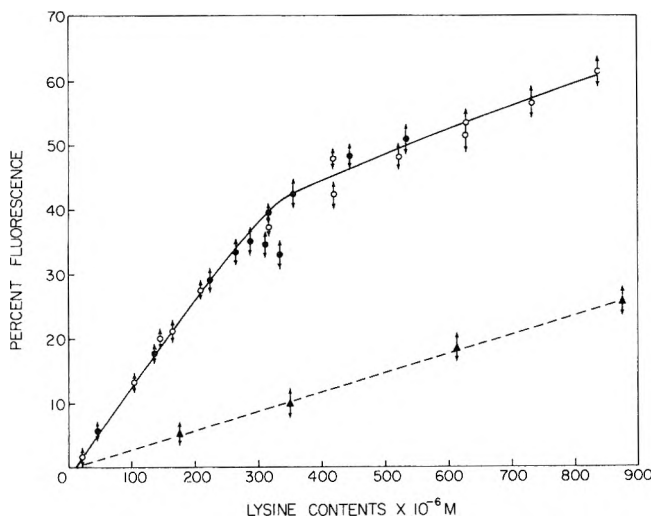


Figure 2. Fluorescence titration of TNS with β -sheet poly-L-lysine. TNS, $10^{-6} M$, was titrated with β -sheet poly-L-lysine, mol wt 7315, 43,870, and 97,500, as described in Materials and Methods. Per cent emission (λ_{exc} 350 $m\mu$) relative to $10^{-6} M$ quinine bisulfate in 0.1 N H_2SO_4 was calculated from the respective areas under the emission curves. The polypeptide concentrations, M , were converted to moles of lysine residue per liter: (\blacktriangle) TNS: β -sheet poly-L-lysine, mol wt 7315; (O) TNS: β -sheet poly-L-lysine, mol wt 43,870; (\bullet) TNS: β -sheet poly-L-lysine, mol wt 97,500.

there is a close correspondence between the maxima of the ultraviolet absorption spectra and the converted excitation spectra. On the other hand, at low β -sheet concentrations, there are real differences. The 1:0.5 solution, for example, has absorption maxima at 262.5 and 316 $m\mu$. The corresponding converted excitation maxima, however, occur at 274 and 319 $m\mu$. Thus, the quantum excitation maxima are red shifted by 11.5 and 3 $m\mu$ compared to their corresponding absorption maxima.

The fluorescence of $10^{-6} M$ TNS was also examined for several β -sheet concentrations. The per cent fluorescence, relative to that of a $10^{-6} M$ quinine bisulfate solution, is shown in Figure 2, together with the same titrations for the higher molecular weight polymers.

β -Sheet Poly-L-lysine, mol wt 43,870 and 97,500, and TNS. Because of the limited solubility of the β sheets formed from poly-L-lysine mol wt 43,870 and 97,500 compared to poly-L-lysine mol wt 7315, lower concentrations of both TNS and β sheets were chosen for the titration procedure. A 1:1 solution in these titrations corresponds to $10^{-6} M$ TNS and $10^{-6} M$ polypeptide. A plot of relative fluorescence vs. β -sheet concentration in lysine units, Figure 2, shows that the fluorescence increases linearly up to $\sim 300 \times 10^{-6} M$ lysine residues ($1 \times 10^{-6} M$ in terms of poly-L-lysine). At higher polypeptide concentrations, TNS fluorescence is enhanced to a lesser extent. On the basis of equal lysine contents, TNS bound to the β sheets of the 7315 mol wt polypeptide shows a decreased fluorescence intensity compared to the 43,870 and 97,500 mol wt polymers. At $300 \times 10^{-6} M$ lysine, TNS bound to the β -sheet polypeptides of the high molecular weight polymers has a fluorescence intensity three times higher than TNS bound to the β sheets of the lowest molecular weight poly-L-lysine. Figure 2 also indicates that at equal lysine contents, β sheets of the 43,870 mol wt polypeptide bind the same amount of TNS as β sheets of the 97,500 mol wt polypeptide, since the per cent fluorescence is identical.

The fluorescence and absorption characteristics of TNS bound to high molecular weight poly-L-lysine are identical with those of TNS bound to β sheet poly-L-lysine, mol wt 7315. Emission of bound TNS occurs at 428 $m\mu$ upon excitation of 350 and 325 $m\mu$. Excitation maxima are identical with those of TNS bound to β -sheet poly-L-lysine mol wt 7315. The ultraviolet spectra of TNS: β -sheet solutions show the same progressive red shift of the 262 and 315 $m\mu$ absorption peaks with increasing β sheet concentration. Conversion of the energy excitation spectra to quantum spectra reveals a close correspondence between the ultraviolet absorption maxima and the converted excitation spectra only at high β -sheet concentrations.

α -Helix and Random Coil Poly-L-lysine, mol wt 7315 and 43,870, and TNS. Neither the 1:1 nor 1:5 solution of TNS: α helix or TNS:random coil poly-L-lysine shows any real TNS fluorescence emission and the ultraviolet absorption spectra of these solutions are characteristic of TNS in aqueous alkaline sodium chloride.

Discussion

The results obtained in this study indicate that TNS binds specifically to β -sheet poly-L-lysine, and not to α -helical or random coil poly-L-lysine which is in agreement with the findings by Lynn and Fasman.¹¹ However, our work indicates that TNS bound to β -sheet poly-L-lysine has a corrected emission maximum at 428 $m\mu$, compared to the uncorrected maximum at 440 $m\mu$ reported by these authors.

Previous studies by McClure and Edelman¹ have established that TNS exhibits a blue shift in the emission and an increased quantum yield when the solvent polarity is decreased. The observed 428- $m\mu$ emission maximum of bound TNS is therefore indicative of TNS binding to a region of low polarity. The similarity of the ultraviolet spectra of TNS bound to β sheet and TNS in ethanol compared to TNS in aqueous solution also supports TNS binding to low-polarity regions. The discrepancies between the absorption spectra and converted excitation spectra (in quantum units) of TNS at low β -sheet concentration result from the type of process measured. Since excitation spectra are characteristic only of bound TNS, and ultraviolet spectra measure absorption both of bound and free TNS, a close correspondence between absorption and excitation spectra is expected only for solutions in which most or all of the TNS is bound.

Experimental conditions were varied in order to establish whether sites of higher or lower polarity than that indicated by emission at 428 $m\mu$ would become available. Addition of TNS to the polypeptide solution before conversion to the β sheet, length of heating time and effect of pH were investigated with the 43,870 mol wt polypeptide and no changes in fluorescence were detected. Thus TNS binds to more or less the same kind of hydrophobic regions of the β sheets of these polypeptides.

The titration curves, Figure 2, show that the fluorescence intensity for TNS bound to low molecular weight β -sheet poly-L-lysine is decreased compared to TNS bound to high molecular weight β -sheet polypeptide, at equal TNS and lysine contents. A double-reciprocal plot of the titration data, Figure 3, shows a break at $\sim 300 \times 10^{-6} M$ lysine residues ($\sim 0.67 \times 10^{-2} g$ of polypeptide/100 ml); this corresponds with the data shown in Figure 2. There is no break in the titration curve of the low molecular weight poly-L-lysine. Extrapolation of the low concen-

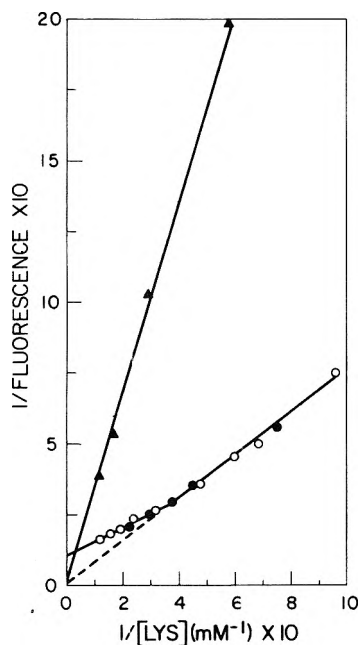


Figure 3. Double-reciprocal plot of TNS bound to β -sheet poly-L-lysine (from the data of Figure 2): (\blacktriangle) TNS: β -sheet poly-L-lysine mol wt 7315; (\circ) TNS: β -sheet poly-L-lysine, mol wt 43,870; (\bullet) TNS: β -sheet poly-L-lysine, mol wt 97,500.

tration region of the high molecular weight curve to infinite concentration results in a y intercept identical with that for poly-L-lysine, mol wt 7315. Thus the enhanced fluorescence intensity of TNS bound to high molecular weight β -sheet poly-L-lysine results from an increase in the number of bound TNS molecules at low polypeptide concentrations; *i.e.*, this enhanced fluorescence is not due to increased quantum efficiencies. Since saturation curves were not obtained for TNS binding, it is not possible at present to determine whether the increase in the number of bound TNS molecules is due to binding at new sites, or tighter binding.¹³ Extrapolation of the high molecular weight poly-L-lysine curve (Figure 3) at high polypeptide concentrations to infinite concentration results in a y intercept different from that of the curve for poly-L-lysine

degree of polymerization (DP) 35. These data indicate a decrease in quantum yield for TNS bound to high molecular weight β sheet formed at high initial polypeptide concentrations. This decrease in quantum yield of bound TNS is not accompanied by a red shift of the emission maximum, as is usually the case for hydrophobic fluorescent probes.¹ These results may point to differences in rigidity of the β -sheet structures of the high molecular weight polypeptides depending on initial polymer concentration.

The data plotted in Figure 3 show that the isotherms for TNS bound to β -sheet poly-L-lysine, DP 210 and 445, are identical. These β sheets, although formed from polypeptides of greatly different chain length, bind the same number of TNS molecules.

Recently, Wooley and Holzwarth¹⁴ determined first-order rate constants for β -sheet formation of polylysines of different chain lengths at different initial concentrations. These data were interpreted in terms of intra- and intermolecular β -sheet formation. The present fluorimetric studies could be interpreted similarly, since the two regions of the high molecular weight titration curve (Figure 2) correspond closely to the concentration regions for which intermolecular ($>300 \times 10^{-6}$ M lysine residues) and intramolecular ($<300 \times 10^{-6}$ M lysine residues) β sheets have been proposed. Similarly the titration curve for poly-L-lysine, DP 35, may represent binding of TNS to intermolecular β sheets. This interpretation leads to the conclusion that intramolecular β sheets bind more TNS than intermolecular β sheets.

In conclusion, these spectroscopic studies point to structural differences in β sheets of poly-L-lysine depending on polymer chain length and initial concentration.

Acknowledgments. Supported by U. S. Public Health Service Grants No. CA-08580 and ES-00260. The authors are indebted to Mr. Sam Cravitt (Farrand Optical Co.) for advice and suggestions in the operation of the spectrofluorimeter and to Miss Tatiana Blazej for technical cooperation.

(13) J. R. Brocklehurst, R. B. Freedman, D. J. Hancock, and G. K. Radda, *Biochem. J.*, **116**, 721 (1970).

(14) Su-Yun C. Wooley and G. Holzwarth, *Biochemistry*, **9**, 3604 (1970).

Location of Nickel Ions in Y Zeolites. I. Influence of Thermal Treatment and Exchange Level on Nickel Positions

P. Gallezot and B. Imelik*

Institut de Recherches sur la Catalyse-CNRS, 69-Villeurbanne, France (Received August 31, 1972)

Publication costs assisted by the Centre National de la Recherche Scientifique

The crystal structure of three nickel-exchanged Y zeolites were studied using X-ray diffraction in order to determine the location and the population of the different cation sites as a function of both exchange and dehydration level. On progressive removal of water molecules nickel ions enter the hexagonal prisms but their population is limited to 12 Ni²⁺ per unit cell. The nickel to framework oxygen distances vary with the number of nickel in S_I sites and with the total number of nickel ions. A chart, which enables us to obtain the population of S_I sites as a function of the cubic unit cell constant and of the total number of nickel ions, is proposed.

Introduction

It can be inferred from the available data on zeolite structures that the positions of exchangeable cations in the porous framework depend upon the nature of both cations and adsorbed molecules. Hence in a previous X-ray diffraction study¹ of a copper-exchanged Y zeolite it was shown that copper ions occupy S_I sites on total removal of water molecules and can move back toward the supercages when various reagents are added. Because of their great stabilization energy in an octahedral ligand field, nickel ions should exhibit a different behavior and one may expect that on total dehydration they fill up S_I sites. However, Olson's results² on a Ni faujasite indicate that even if nickel ions have a preference for S_I sites they are still distributed on various sites. As any discussion concerning the catalytic activity of exchanged zeolites needs information about reagent accessibility to cations (or cations accessibility to reagents) an extensive study was planned about nickel ions properties in Y zeolites. The first part of this work deals with the crystal structure determination of Ni NaY zeolites evacuated at different temperatures. It was undertaken in order to locate nickel ions as a function of both exchange and dehydration level.

Experimental Section

Linde NaY zeolites without binder were ion exchanged in Ni(NO₃)₂ aqueous solutions stirred at room temperature for 24 hr. Large volumes of diluted solution (<0.05 N) were used in order to avoid any pH increase and precipitation of basic nickel salts. Low exchange levels were obtained by allowing the zeolite to exchange with the calculated amounts of nickel ions introduced in the solution. Several subsequent fresh solution must be used to obtain the exchange levels greater than 50%. The composition of washed and dried samples were determined by chemical analysis of nickel and sodium.

Thermal treatments were made in Pyrex or quartz vessel connected to a vacuum line free of grease, then the zeolite was transferred under vacuum in Lindemann glass capillary (0.2 mm diameter) sealed for X-ray investigation. In order to burn possibly adsorbed hydrocarbons standard treatment includes an overnight heating in air, followed by a 6-hr evacuation (10⁻⁵ Torr) at the same temperature. Unit cell composition and treatment condi-

tions for the selected samples are given in Table I.

The crystal structure of the samples was determined from powder data according to the experimental techniques and resolution methods described in previous papers.¹⁻³ Atomic parameters were refined with 232 structure factors corresponding to all reflections with $h^2 + k^2 + l^2 \leq 395$ except 111 line.

TABLE I: Composition and Treatment Conditions of the Samples

Sample	Unit cell composition ^a	Heat treatment, °C
A ₁₄₀	Ni ₁₄ Na ₂₃ H ₅ Y ^b	140
A ₂₀₀	Ni ₁₄ Na ₂₃ H ₅ Y	200
A ₂₈₀	Ni ₁₄ Na ₂₃ H ₅ Y	280
A ₃₀₀	Ni ₁₄ Na ₂₃ H ₅ Y	300
A ₆₀₀	Ni ₁₄ Na ₂₃ H ₅ Y	600
B ₂₀₀	Ni ₁₀ Na ₃₁ H ₅ Y	200
B ₆₀₀	Ni ₁₀ Na ₃₁ H ₅ Y	600
C ₂₀₀	Ni ₁₉ Na ₁₅ H ₃ Y	200
C ₆₀₀	Ni ₁₉ Na ₁₅ H ₃ Y	600

^a After calcination of the sample. ^b Y = Al₅₆Si₁₃₆O₃₈₄.

Results

No attempt has been made to locate extra-framework species which would eventually occupy positions outside the symmetry axes. The cation to framework oxygen distances and the evolution of sites occupancy under the dehydration process were taken as the two main criteria to distinguish nickel from sodium and water molecules. On these bases, electronic density appearing on sites S_I and S_{II}⁴ was readily attributed to nickel and sodium, respectively. Scattering matter was also found in most of the investigated samples at $x = y = z = 0.05; 0.08; 0.16; 0.21$. The double peaks on sites S_I and S_{II} are similar to those encountered by Olson.² Taking in account the results of Olson and from the criteria stated above, the S_I (0.05) sites were ascribed to nickel ions only bonded to the

(1) P. Gallezot, Y. Ben Taarit, and B. Imelik, *J. Catal.*, **26**, 295 (1972).

(2) D. H. Olson, *J. Phys. Chem.*, **72**, 4366 (1968).

(3) P. Gallezot and B. Imelik, *J. Chim. Phys.*, **68**, 34 (1971).

(4) Cation sites nomenclature: J. V. Smith, *Advan. Chem. Ser.*, **No. 101**, 171 (1971).

TABLE II: Tabulated Data for the Number of Species per Unit Cell, Assignment of Species Type, and Its $x = y = z$ Coordinates^a

Sample	Final R index ^b	Unit cell constant, Å (± 0.01)	S_I	$S_{I'}$	$S_{I''}$	$S_{II'}$	$S_{II''}$	S_{III}
A ₁₄₀	0.078	24.625	3.5(2) Ni 0.0	2.5(6) Ni 0.058(3)	3.5(4) Ni 0.078(2)	12.5(1.5) Ow 0.167(2)	1.9(4) Ni 0.196(3)	23.6(1.5) Na 0.236(1)
A ₂₀₀	0.063	24.615	4.1(2) Ni 0.0	3.6(4) Ni 0.055(1)	2.9(4) Ni 0.076(2)	9.5(1.0) Ow 0.166(2)	2.1(2) Ni 0.209(2)	20.0(1.5) Na 0.237(1)
A ₂₈₀	0.066	24.565	6.9(2) Ni 0.0	3.3(2) Ni 0.053(1)	2.5(2) Ni 0.078(2)	5.0(1.0) Ow 0.176(3)	1.5(2) Ni 0.208(3)	20.0(1.2) Na 0.236(1)
A ₃₀₀	0.059	24.51	10.0(2) Ni 0.0	1.5(6) Ni 0.055(1)	1.3(6) Ni 0.073(6)			23.2(1.0) Na 0.234(1)
A ₆₀₀	0.066	24.47	11.7(2) Ni 0.0	1.1(2) Ni 0.065(3)				21.3(1.0) Na 0.235(1)
B ₂₀₀	0.074	24.67	4.4(2) Ni 0.0	3.6(4) Ni 0.055(2)	2.1(4) Ni 0.076(3)	7.5(1.5) Ow 0.169(2)		25.9(1.5) Na 0.236(1)
B ₆₀₀	0.064	24.59	8.8(2) Ni 0.0	1.7(2) Ni 0.052(2)				27.2(1.0) Na 0.235(1)
C ₂₀₀	0.059	24.555	3.6(2) Ni 0.0	3.1(2) Ni 0.051(1)	5.2(2) Ni 0.076(1)	12.0(1.0) Ow 0.167(1)	4.2(2) Ni 0.211(1)	12.1(1.0) Na 0.237(1)
C ₆₀₀	0.069	24.40	11.3(2) Ni 0.0	1.9(2) Ni 0.047(2)				20.2(1.1) Na 0.236(1)

^a Estimated standard errors (in parentheses) may in some case be greatly underestimated especially for atoms with low occupancy factors. ^b $R = \Sigma|F_o - KF_c|/\Sigma|F_o|$.

framework and the $S_{I'}$ (0.08) sites to nickel ions carrying in addition water molecules or hydroxyl groups occupying $S_{II'}$ (0.16) sites. Finally S_{III} (0.21) sites were ascribed to nickel ions bonded to oxygen atoms of the sodalite to supercage aperture. Cubic unit cell constants a , final R indexes ($R = \Sigma|F_o - KF_c|/\Sigma|F_o|$), and population of extra-framework sites are given in Table II. Atomic parameters and structure factors listings are given in the microfilm edition.⁵ Interatomic distances and angles computed with the ORFFE program⁶ can be found in Table III.

For the discussion of the results, one has to bear in mind the two following points. An absolute distinction between extra-framework atoms can never be exactly done, *i.e.*, one or two sodium ions, for instance, may well be mixed with nickel on a definite site although the reported results indicate no sodium on this position. Moreover, some deficiency appears in the count of localized nickel. Cations are generally bonded to framework oxygen atoms inside the hexagonal prism (hp) and on symmetry axes near the centers of the various six-membered rings of tetrahedra; whenever they are out of these special positions they cannot be located with certainty. This is especially true when nickel ions are still solvated by water molecules in zeolite cages, but this also happen for highly exchanged zeolite evacuated at high temperature. Hence, there are only 13 out of 19 Ni^{2+} found in sample C₆₀₀ and even if one argues that about two Ni^{2+} are mixed with Na^+ on S_{II} sites (considering that sodium S_{II} population is far too high compared to C₂₀₀ one) there are nevertheless four missing Ni^{2+} . These nickel ions are out of the special positions mentioned above and probably attached to the cage walls.

Discussion

Table II summarizes the distribution of extra-framework atoms. The discussion will deal first with the analysis of nickel displacement occurring on water removal, then with the special features of nickel ions in each zeolite site.

Nickel Ions Shifts during Dehydration Process. The occupancy of S_I sites by nickel ions increases as the water

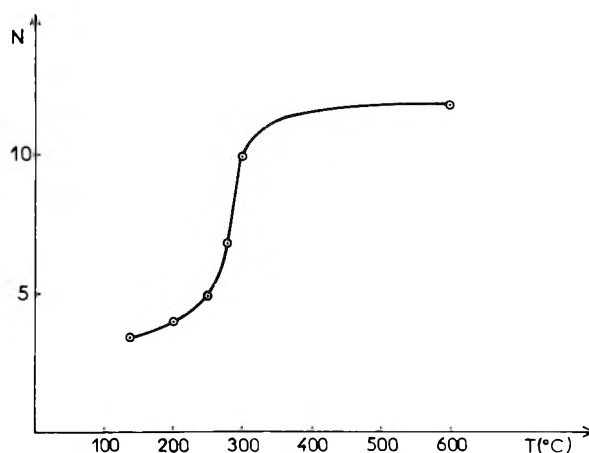


Figure 1. Number N of Ni^{2+} ions in hexagonal prisms vs. the heating temperature of the A samples. The N value for sample heated at 250° was derived from the Figure 2 diagram after measurement of its unit cell constant.

molecules attached to the cations are removed. The number N of nickel ions occupying the hp (Figure 1) sharply increases between 250 and 300° but this temperature range may change under the influence of factors such as residual gas pressure or thickness of the zeolite bed. Table IV gives the variations of some site populations for a number of heating temperature intervals.

The increase of N first occurs (A₁₄₀-A₂₀₀) at the expense of the nonlocalized nickel ions which probably still are fully coordinated by water molecules; the occupancy of $S_{I'}$ (0.05) also increases substantially. In the next step

- (5) Listings of structure factors, atomic coordinates, temperature factors, and occupancy factors will appear following these pages in the microfilm edition of this volume of the journal. Single copies may be obtained from the Business Operations Office, Books and Journals Division, American Chemical Society, 1155 Sixteenth St., N.W., Washington, D. C. 20036. Remit check or money order for \$4.00 for photocopy or \$2.00 for microfiche, referring to code number JPC-73-652.
- (6) W. R. Busing, K. O. Martin, and H. A. Levy, ORFFE, Oak Ridge National Laboratory, Oak Ridge, Tenn., 1964.

TABLE III: Interatomic Distances (Å) and Bond Angles (degrees)

	A ₁₄₀	A ₂₀₀	A ₂₈₀
T-O(1)	1.671(5)	1.657(5)	1.652(5)
T-O(2)	1.628(5)	1.613(4)	1.635(4)
T-O(3)	1.680(7)	1.652(5)	1.649(5)
T-O(4)	1.611(5)	1.635(4)	1.602(4)
M	1.647	1.639	1.634
O(1)-O(2)	2.690(10)	2.703(8)	2.676(8)
O(1)-O(3)	2.761(12)	2.710(10)	2.669(10)
O(1)-O(4)	2.670(5)	2.670(5)	2.693(4)
O(2)-O(3)	2.607(8)	2.650(7)	2.687(7)
O(2)-O(4)	2.633(9)	2.641(8)	2.602(7)
O(3)-O(4)	2.774(13)	2.689(12)	2.687(10)
M	2.689	2.677	2.669
Ni(1)-O(2)	3.50(1)	3.55(1)	3.57(1)
Ni(1)-O(3)	2.52(1)	2.60(1)	2.52(1)
Ni(1')-O(2)	2.98(2)	2.99(1)	3.02(1)
Ni(1')-O(3)	2.15(5)	2.18(2)	2.14(2)
Ni(1')-Ow(11')	2.82(9)	2.91(5)	3.11(6)
Ni(1')*-O(3) ^a	2.61(6)	2.61(5)	2.70(4)
Ni(1')*-Ow(11') ^a	2.20(6)	2.24(6)	2.40(8)
Ni(11')-O(2)	2.41(5)	2.22(2)	2.24(2)
Ni(11')-Ow(11')	1.2(2)	1.9(1)	1.4(2)
Na(11)-O(2)	2.39(1)	2.36(1)	2.32(1)
Na(11)-O(4)	2.93(1)	2.98(1)	2.95(1)
O(3)-Ni(1)-O(3)	84.5(4)	86.1(3)	87.4(3)
O(3)-Ni(1')-O(3)	103.9(3.1)	108.1(1.4)	108.4(1.1)
Ow(11')-Ni(1')-Ow(11')	64.7(2.7)	61.5(1.8)	70.0(3.0)
O(3)-Ni(1')*-O(3) ^a	81.0(2.2)	85.4(2.0)	80.4(1.4)
Ow(11')-Ni(1')*-Ow(11')	83.5(3.7)	79.1(3.3)	94.5(3.6)
O(2)-Ni(11')-O(2)	110.6(2.4)	116(1)	114.5(1.5)

^a (1')* means site Sr... with x = y = z ≈ 0.08

A ₃₀₀	A ₆₀₀	B ₂₀₀	B ₆₀₀	C ₂₀₀	C ₆₀₀
1.656(5)	1.657(5)	1.669(5)	1.646(5)	1.647(4)	1.643(5)
1.633(4)	1.616(4)	1.655(5)	1.633(4)	1.631(4)	1.611(5)
1.656(5)	1.662(6)	1.632(5)	1.674(5)	1.656(4)	1.693(6)
1.605(4)	1.609(4)	1.613(5)	1.620(4)	1.629(4)	1.616(4)
1.637	1.641	1.642	1.643	1.641	1.641
2.693(8)	2.687(9)	2.711(9)	2.700(8)	2.729(7)	2.680(9)
2.661(9)	2.680(10)	2.691(11)	2.652(9)	2.651(9)	2.648(11)
2.669(4)	2.673(5)	2.685(5)	2.681(4)	2.655(4)	2.672(5)
2.683(7)	2.650(8)	2.698(8)	2.671(7)	2.669(6)	2.676(8)
2.628(7)	2.642(8)	2.621(8)	2.654(7)	2.638(7)	2.660(8)
2.710(10)	2.743(11)	2.685(11)	2.739(10)	2.680(9)	2.734(11)
2.674	2.679	2.682	2.687	2.678	2.678
3.56(1)	3.51(1)	3.59(1)	3.54(1)	3.59(1)	3.54(1)
2.47(1)	2.37(1)	2.59(1)	2.43(1)	2.57(1)	2.32(1)
3.02(3)	3.07(4)	3.04(1)	2.98(1)	2.98(1)	2.98(1)
2.19(9)	2.37(8)	2.22(3)	2.15(3)	2.10(1)	2.01(3)
		2.95(6)		3.06(4)	
		2.68(8)		2.59(2)	
		2.31(9)		2.28(3)	
				2.14(1)	
				1.90(5)	
2.29(1)	2.33(1)	2.32(1)	2.34(1)	2.30(1)	2.31(1)
2.97(1)	2.99(1)	2.96(1)	3.01(1)	3.02(1)	3.05(1)
89.0(3)	89.3(3)	87.8(3)	90.1(3)	85.7(3)	90.0(3)
03(1)	90.1(3.0)	106.8(1.8)	105.2(1.7)	111.7(1.0)	108.7(1.7)
		65.8(2.7)		60.3(1.1)	
83.1(6)		83.9(3.2)		85.0(1.0)	
		85.3(5.0)		80.6(1.7)	
		109(1.0)		116.6(3)	

(A₂₀₀-A₂₈₀) the increase of N is balanced by the diminution of the other site populations, all nickel ions being localized. In the following steps more nickel ions migrate toward S_I but it appears that only 12 out of the 14 nickel enter the hp. The nickel ions migration in B and C samples seems to be similar, although the intermediate steps have not been investigated.

It can be noticed that especially in samples treated at low temperatures nickel ions may be found simultaneously in different kind of sites with specific coordination. For example, fully dehydrated, partly dehydrated, and solvated nickel are observed together in sample A₁₄₀. This may be due to an heterogeneous desorption; the cations do not lose their water molecules or hydroxyl groups at the same time in all the cages. This temperature or time-spreading effect is probably the consequence of factors like zeolite crystallite size or sample bed thickness.

S_{II'} (0.21) and S_{I'} (0.05) Nickel Ions. The S_{I'} (0.05) and S_{II'} (0.21) sites are both located inside the sodalite cages and close to an hexagonal aperture. Nickel ions on S_{I'} (0.05) are bonded to three O(3) of the hp, with a Ni-O distance of about 2.15 Å. In the same way nickel ions on S_{II'} (0.21) are bonded to three O(2) of the sodalite to supercage aperture.

Since S_{II'} (0.21) nickel are only present in moderately heated samples they probably still are bonded to extra-framework oxygen so that these nickel should be hexacoordinated. However, the corresponding water molecules or hydroxyl groups cannot be detected because their occupancy factor is too low. According to Olson² each S_{II'} (0.21) nickel may well be coordinated in addition to three O(2), by one water molecule occupying S_{II'} (0.16) sites.

A similar problem arises for S_{I'} (0.05) nickel ions. The reported results do not allow us to conclude that these cations are only bonded to three framework oxygens. The presence in some samples of spurious peaks on difference Fourier synthesis at $x = y = z = 0.105$ may even indicate that one oxygen atom is still attached to each nickel and this would complete a tetrahedral coordination.

However, results about cations having low occupancy factors (or with stronger reasons, about extra-framework species attached to these cations) must be regarded with caution; results about sample C₂₀₀ in which S_{I'} and S_{II'} sites populations are relatively higher are more realistic.

S_{I'} (0.08) Nickel Ions. Nickel ions occupying S_{I'} (0.08) sites are bonded to three S_{II'} (0.16) water molecules at about 2.25 Å. The ratio between water molecules and nickel population is 3:1, discrepancies being within the standard deviations. On the other hand S_{I'} nickel ions are bonded to three O(3) framework oxygen at 2.60 Å. The Ni(I')-O(3) and Ni(I')-Ow(II') bond lengths certainly reflect the differences in the nature of these two ligands; however, nickel ions tend to maintain very similar values for O(3)-Ni(I')-O(3) and Ow-Ni(I')-Ow angles (83 and 84.6°, respectively, as mean value calculated on five samples).

S_I Nickel Ions. Fully dehydrated nickel ions enter the hp and get a near perfect octahedral coordination with the six O(3) oxygens of the double six-membered ring. Precise Ni(I)-O(3) distances cannot be reached because X-ray diffraction gives an information averaged on occupied and empty hp. The given distances undergo two kind of variation.

(i) The Ni(I)-O(3) distances decrease when the S_I site population increases (the discrepancy observed for the A₁₄₀ sample may be due to its high residual water con-

TABLE IV: Variation of the Nickel Site Population for the A Samples

Structures compared	S _I	S _{I'} (0.05)	S _{I'} (0.08)	S _{II'} (0.21)	Un-located
A ₁₄₀ -A ₂₀₀	+0.6	+1.1	-0.6	+0.2	-1.3
A ₂₀₀ -A ₂₈₀	+2.8	-0.3	-0.4	-0.6	-1.3
A ₂₈₀ -A ₃₀₀	+3.1	-1.8	-1.2	-1.5	+1.2
A ₃₀₀ -A ₆₀₀	+1.7	-0.4	-1.3	0	0

tent). This diminution is readily explained because nickel ions involved in the hp attract their six O(3) ligands so that the observed average distance decreases as the hp are progressively filled.

(ii) For a same nickel S_I population, this distance decreases as a function of the zeolite nickel content. Thus 2.37 Å is observed in sample A₆₀₀ (14 Ni²⁺/unit cell), 2.32 Å in C₆₀₀ (19.5 Ni²⁺/unit cell), and 2.29 Å in Olson's sample (27 Ni²⁺/unit cell). For all samples the population of hexagonal prism is very similar: 11.7, 11.3, 10.6 Ni²⁺, respectively. The following interpretation is tentatively proposed. Substitution of monovalent by multivalent cations results in a wrong balancing of framework charges. On the other hand nickel ions occupying hp are associated with twelve tetrahedra *via* six O(3) oxygen atoms so that they are very efficient in neutralizing the charges. It may then be supposed that the specific charge carried by O(3) oxygens increases in relation with the zeolite nickel content; stronger nickel-oxygen interactions produce a shortening of the Ni(I)-O(3) bond length.

One can wonder why S_I population is limited to about 12 Ni/unit cell whereas hp can accommodate 16. A comprehensive interpretation was given by Dempsey and Olson⁷ who were the first to show the reason of this limit from an acute analysis of a set of data. Moreover the relation $N_I = (24 - N_{I'})/2$ that they have proposed (N_I and $N_{I'}$ being the population of S_I and S_{I'} sites, respectively) holds with an excellent agreement for A₆₀₀ and C₆₀₀ samples.

Finally a special comment has to be made about the particular ligand field which is applied to nickel ions occupying hp. Even if the effect of the six O(2) of the double six-membered ring is neglected, the field due to the six O(3) is nevertheless unusual although they are arranged in a near perfect octahedron. This is mostly due to the fact that the six O(3) cannot approach nickel ions at usual Ni-O bond length in spite of an important elongation of T-O(3) bonds and displacement toward the center of hp of the two six-membered rings of tetrahedra. It should be mentioned that crystal field calculations performed in this laboratory on the basis of present results allowed us to find with a good approximation the values of electron transition energy observed in the uv spectra of Ni NaY samples.⁸

Correlation between Nickel S_I Sites Population, Zeolite Unit Cell Constant, and Total Nickel Content. A previous note⁹ reported that a linear relationship exists between N and the zeolite unit cell constant a for a given sample (Ni₁₄Na₂₃H₅Y). This result has now been extended to other nickel-exchanged Y zeolites. In Figure 2 the N values for the investigated samples have been plotted as a function of a . The two straight lines drawn from B₂₀₀ to

(7) E. Dempsey and D. H. Olson, *J. Phys. Chem.*, **74**, 305, (1970).

(8) H. Garboski, Y. Kodratoff, M. V. Mathieu, and B. Imelik, *J. Chim. Phys.*, **69**, 1386 (1972).

(9) P. Gallezot, Y. Ben Taarit, and B. Imelik, *J. Catal.*, **26**, 481 (1972).

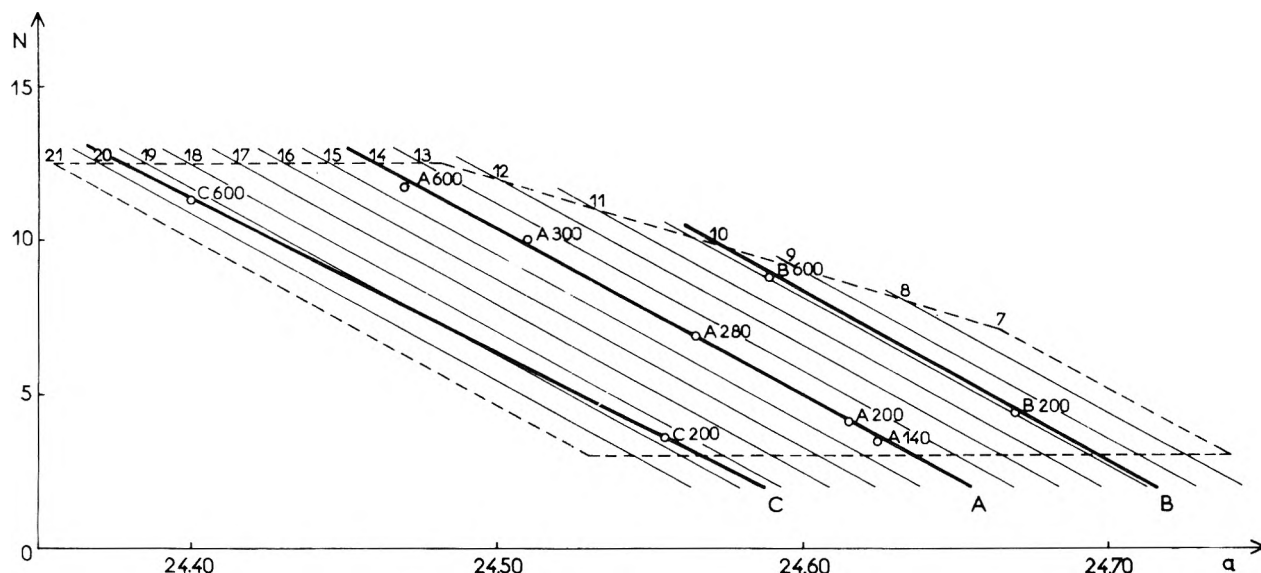


Figure 2. Chart giving N (number of Ni^{2+} ions in hexagonal prisms) vs. the cubic unit cell constant a (\AA) for any sample: heavy lines, plot of N for the A, B, and C samples; light lines, set of equidistant parallel lines drawn for each N_T value which enables us to obtain N as a function of a ; dashed lines, proposed limits of the chart best validity domain.

B_{600} and from C_{200} to C_{600} are nearly parallel to the well-defined A samples line (previously determined with 11 points). Furthermore it may be noticed that for a given ordinate N , Δa is proportional to ΔN_T , N_T being the total number of nickel ions per unit cell (for $N = 10$, $\Delta a/\Delta N_T = 0.015$). A family of straight lines was drawn parallel to the A line at 0.015-\AA absciss intervals; this set of lines gives a graphical solution to estimate N in a Ni NaY zeolite each time N_T and a values are available. The analytical expression

$$N = 1368 - 54.945a - 0.808N_T$$

may also be used for the same purpose. These graphical and analytical solution are only valid in a definite range of hp population and of zeolite nickel content. Within the domain restricted to $3 < N < 12$ and $7 < N_T < 20$, one expects that N is obtained with an accuracy of ± 1 nickel ion.

The variations of unit cell parameter are related to the variations of Ni(I)-O(3) distances discussed above. However, zeolite unit cell constants may be influenced by other factors such as chemisorption of certain molecules which may share or even exchange electrons or protons with the zeolite framework. Hence the relations given above can be used to determine N in a simply activated Ni NaY zeolite but, in other respect, must be used with caution according to the nature of adsorbed molecules.

Conclusion

The conspicuous feature which comes out of these results is the raising of nickel population in hexagonal prisms on progressive dehydration of the zeolite. This situation is entirely different from that encountered for copper ions located in the same conditions essentially in S_1 sites. One may expect that nickel ions in hexagonal prism get a rather stable coordination so they can neither move easily toward the supercages to react with adsorbed molecules nor be reachable by these molecules. Thus, these cations should be inactive in many catalytic processes unlike S_1 copper ions which can migrate out of the sodalite cages. As soon as the exchange level rises above 12 Ni/unit cell the Ni NaY zeolite should exhibit a greater catalytic activity (unless other factors prevent it) because additional ions are then outside the hp and may be involved in the catalytic process. However, even in the low level exchanged samples, there may be Ni ions available outside the hp so that some activity may always occur.

This study has also shown some interesting results on structural chemistry of nickel ions in the zeolite sites, especially inside hexagonal prisms, in which Ni(I)-O(3) distances vary as a function of both S_1 population and zeolite exchange level. A graphical and analytical solution was established in order to determine the number of nickel ions caged in hexagonal prisms each time unit cell constant and total nickel content are known.

Calculated Potential Energies for the Adsorption of Rare Gases on Graphite¹

C. Pisani, F. Ricca,* and C. Roetti

Università di Torino, Cattedra di Chimica Teorica, 10125 Torino, Italy (Received June 20, 1972)

Publication costs assisted by The University of Turin

Two- and three-parameter potential laws are considered for the interaction between nonbonded carbon atoms in graphite. Only the latter can be adapted to fit interlayer spacing, compressibility, and cohesion energy of graphite crystals, in the additive pairwise approximation. Potential energies of adsorption for rare gas atoms on graphite have been calculated using three-parameter potential laws derived from independently determined self-interaction potentials for the gas and for the solid atoms. A satisfactory agreement with experimental data cannot be automatically obtained from self-interaction empirical parameters, even using anisotropic potentials.

Introduction

Due to the homotactic character of its surface, graphite and graphitized carbon black appear ideally suited for experimentally testing the theories about physical adsorption. A number of studies (see, for instance, ref 2 and 3) have then been devoted to comparison of experimental data to theoretical calculations in the simple case of rare gas adsorption. Theoretical calculations are all based on the following simplified assumptions: (1) the adsorbed atom can be considered as a distinct system moving in the field produced by the solid; (2) the potential field can be evaluated in the additive pairwise approximation. Different potential laws have been used in such approximate evaluation, which sometimes render quite difficult a comprehensive discussion, but the essentially empirical approach used by Crowell^{4,5} is generally accepted. This requires the availability of (1) a self-interaction potential for the rare gas being considered, (2) a self-interaction potential for the nonbonded carbon atoms in graphite, and (3) a combination rule to define the potential law for the corresponding unlike pair.

As far as rare gas atoms are concerned, very good potential laws are available, which are derived in essentially a phenomenological way from experimental data referring to both the gaseous and the solid state of rare gases; the same, however, is not true for carbon atoms in graphite. If the phenomenological approach is to be maintained, potential laws for the van der Waals interactions between nonbonded carbon atoms in graphite must be derived from those physical properties of graphite which may be thought of as due to its molecular-solid nature (each layer as a molecule). The model of graphite as planes of hexagonal carbon networks held together by van der Waals' forces is, of course, an oversimplification but this approximation seems to be necessary in order to obtain the potential energy expressions which are used to study gas adsorption on graphite that are compatible with the properties of graphite.

Observational Equations for Graphite

Different experimental data are available to characterize the "intermolecular" interactions in graphite. Of these, three have been taken into account in previous works concerning the potentials to be used for adsorption studies: (1) the equilibrium interlayer distance in the lat-

tice, (2) the compressibility of the crystal in a direction normal to the basal plane, and (3) the energy of cohesion. Further qualitative information arises from the relative stabilities of the three different lattices that could be obtained by the three stacking sequences XYXY, XYZXYZ, and XXX of the parallel layers, where the planes denoted by the same letter are in exact register, while the other planes are rotated by 60°. The XYXY sequence is the most stable one and gives the actual hexagonal lattice of graphite. The XYZXYZ sequence gives the less stable rhombohedral lattice, which appears only at high temperatures, in association with the hexagonal one. Finally, no "in registry" lattices have been found experimentally in graphite, corresponding to the stacking sequence XXX.

The interlayer spacing $d = 3.354 \text{ \AA}$ is known with great accuracy from X-ray measurements,⁶ and a suitable observational equation may put in the form

$$(\partial \phi / \partial h)_{h=d} = 0 \quad (1)$$

where h is the interlayer spacing and ϕ is given by

$$\phi(h) = (1/S) \sum_{m=1}^{\infty} \sum_{i(m)} \{ \epsilon[\mathbf{R}_{A,i}(h)] + \epsilon[\mathbf{R}_{B,i}(h)] \} = \sum_m \varphi_m(h) \quad (2)$$

Here $S = 5.202 \text{ \AA}^2$ is the surface area of the elementary cell in the basal plane. This elementary cell contains one A atom (with two nearest neighbors in the two adjacent planes at a distance $d = 3.354 \text{ \AA}$) and one B atom (with twelve nearest neighbors in the same two planes at a distance $d' = 3.640 \text{ \AA}$). The expression $\epsilon(\mathbf{R})$ gives the potential energy of interaction for a single pair of carbon atoms lying on two different planes, whose relative position is given by \mathbf{R} ; $\mathbf{R}_{A,i}$ and $\mathbf{R}_{B,i}$ are the vectors joining the i th atom in the m th plane to the A and B atom, respectively, in the elementary cell at the plane considered. The sum $\sum_{i(m)}$ extends to all the atoms belonging to the m th plane at a distance mh and the sum \sum_m extends from 1 to ∞ . It turns out that $\varphi_m(h)$ gives the interaction energy between

- (1) This work has been partially supported by the Italian Council of Research (CNR).
- (2) (a) M. Bretz and J. G. Desh, *Phys. Rev. Lett.*, **26**, 963 (1971); (b) D. E. Hagen, A. D. Novaco, and F. J. Milford, "Adsorption-Desorption Phenomena," F. Ricca, Ed., Academic Press, London, 1972.
- (3) J. S. Brown, *Surface Sci.*, **19**, 259 (1970).
- (4) A. D. Crowell, *J. Chem. Phys.*, **29**, 446 (1958).
- (5) A. D. Crowell and C. Ok Chang, *J. Chem. Phys.*, **38**, 2584 (1963).
- (6) W. N. Reynolds, "Physical Properties of Graphite," Elsevier, Amsterdam, 1968.

the unit area of a layer and the whole parallel layer at a distance mh , while $\phi(h)$ gives half the potential energy per unit area of a single basal plane in an infinite graphite crystal, thus giving a direct measure of the crystal lattice energy.

The compressibility of the graphite crystal can be expressed in terms of the previously defined $\phi(h)$, if reference is made to the corresponding Young's modulus in a direction normal to the basal plane $1/s_{33}$ (s_{ij} being the compliance moduli). The observational equation is

$$d_x(\partial^2\phi/\partial h^2)_{h=d} = 1/s_{33} \quad (3)$$

where $s_{33} = (2.75 \pm 0.10) \times 10^{-12} \text{ cm}^2 \text{ dyn}^{-1}$, as found in the complete set of elastic constants given by Reynolds.⁶

In a similar treatment, Girifalco and Lad⁷ assumed s_{33} to be equal to the volume compressibility β , which amounts to the assumption that the total volume change under hydrostatic pressure is only due to the change in the interlayer spacing. In such an approximation they used $\beta = 2.97 \times 10^{-12} \text{ cm}^2 \text{ dyn}^{-1}$, which was extrapolated to atmospheric pressure by Brennan⁸ from the original Bridgman⁹ data. More recently Brown³ used, in a similar approach, $\beta = 2.60 \times 10^{-12} \text{ cm}^2 \text{ dyn}^{-1}$, as extrapolated from Lynch and Drickamer compressibility data.¹⁰

The cohesion energy for graphite may be expressed in terms of φ_m 's so that the following equation must be obeyed

$$\sum_{m=1}^{\infty} m\varphi_m(d) = (\Delta E)_c \quad (4)$$

where $(\Delta E)_c = -238 \text{ erg cm}^{-2}$ is the average value of the cohesion energy, as estimated by Good, *et al.*,¹¹ from a critical review of the available heat of immersion data, with an error which may be evaluated to be about 10%.

Equation 4 disregards the contribution from relaxation energy, which can be calculated only after the interatomic potential has been determined. However, since the relaxation energy is of the order of 0.1 erg cm^{-2} , while the uncertainty in the experimental data is about 25 erg cm^{-2} , this contribution may be dropped without any appreciable consequence.

In order to solve equations such as 1, 3, and 4, with respect to the parameters involved in potential laws, it is expedient to rewrite such potential laws, by explicitly separating the linear from the nonlinear parameters

$$\epsilon(\mathbf{R}, \gamma_\nu, \delta_\mu) = \sum_\nu \gamma_\nu f_\nu(\mathbf{R}, \delta_\mu) \quad (5)$$

where γ_ν and δ_μ are general terms for the two sets of parameters. The linear operators which occur in eq 1, 3, and 4 leave the linear dependence unchanged, so that, from these equations one immediately obtains

$$0 = \sum_\nu \gamma_\nu F_\nu[\mathbf{R}(d), \delta_\mu] \quad (6)$$

$$1/s_{33} = \sum_\nu \gamma_\nu G_\nu[\mathbf{R}(d), \delta_\mu] \quad (7)$$

$$(\Delta E)_c = \sum_\nu \gamma_\nu H_\nu[\mathbf{R}(d), \delta_\mu] \quad (8)$$

where F , G , and H are defined by

$$F_\nu = \left(\partial \sum_m \varphi_{m,\nu} / \partial h \right)_{h=d} \quad (9)$$

$$G_\nu = d \left(\partial^2 \sum_m \varphi_{m,\nu} / \partial h^2 \right)_{h=d} \quad (10)$$

$$H_\nu = \sum_m m\varphi_{m,\nu} \quad (11)$$

with

$$\varphi_{m,\nu} = (1/S) \sum_{i(m)} \{ f_{\nu A}[\mathbf{R}_{A,i}(h), \delta_\mu] + f_{\nu B}[\mathbf{R}_{B,i}(h), \delta_\mu] \} \quad (12)$$

Expressions 9-11, which depend only on the nonlinear parameters and on the crystal lattice, can be evaluated separately, while the linear parameters may be easily obtained by solving equations 6-8. Since the aim is to apply the potential laws to defining a topographically detailed potential energy in the adsorption of gases on the surface layer of graphite, it is a matter of logical consistency and of uniform computational technique to use direct summations instead of approximating integrals in evaluating all such quantities.

Central Potential Laws

Let the interaction potential between two carbon atoms have the form of a Lennard-Jones 12-6 potential

potential Ia

$$\epsilon(R) = (A/R^6) + (B/R^{12}) \quad (13)$$

In this case only the modulus of the vector \mathbf{R} is involved (central potential) and only two linear γ parameters have to be determined, so that eq 5 can be written as

$$\epsilon(R, \gamma_1, \gamma_2 = \gamma_1 f_1(R) + \gamma_2 f_2(R) \quad (14)$$

where $\gamma_1 = A$, $\gamma_2 = B$, $f_1 = R^{-6}$, and $f_2 = R^{-12}$. Equations 6-8 give

$$B/A = -F_1/F_2 \quad (15)$$

$$A = F_2/s_{33} (F_2 G_1 - F_1 G_2) \quad (16)$$

$$A = F_2(\Delta E)_c / (F_2 H_1 - F_1 H_2) \quad (16')$$

where F_1 , G_1 , H_1 , F_2 , G_2 , and H_2 are still defined by equations 9-11. These quantities have been evaluated by direct summation over all the atoms in the underlying layers at a distance $R_i < \rho = 20 \text{ \AA}$ from the A or the B atom in the unit cell considered. For atoms at distances greater than ρ , Crowell's approximation¹² was used. The equilibrium interlayer spacing univocally determines the ratio B/A (eq 15). However, different values for the single constants A and B are obtained depending on their derivation from the compliance modulus ($s_{33} = 2.75 \times 10^{-12} \text{ cm}^2 \text{ dyn}^{-1}$ gives $A = -2.612 \times 10^{-11} \text{ erg \AA}^6$; $B = 4.072 \times 10^{-8} \text{ erg \AA}^{12}$) or from the cohesion energy ($(\Delta E)_c = -238 \text{ erg cm}^{-2}$ gives $A = -1.694 \times 10^{-11} \text{ erg \AA}^6$; $B = 2.640 \times 10^{-8} \text{ erg \AA}^{12}$). The disagreement existing between the two sets cannot be reduced within the limits of the experimental errors affecting s_{33} and $(\Delta E)_c$. In fact the Lennard-Jones potential derived from the experimental compressibility would lead to a cohesion energy value of -367 erg cm^{-2} , while if the cohesion energy is taken as input data a value of $s_{33} = 4.24 \times 10^{-12} \text{ cm}^2 \text{ dyn}^{-1}$ would be obtained.

Let us now write the interaction potential between two carbon atoms in the form of an exp 6 potential

(7) L. A. Girifalco and R. A. Lad, *J. Chem. Phys.*, **25**, 693 (1956).

(8) R. O. Brennan, *J. Chem. Phys.*, **20**, 40 (1952).

(9) P. W. Bridgman, *Proc. Amer. Acad. Arts Sci.*, **76**, 9 (1945).

(10) R. W. Lynch and H. G. Drickamer, *J. Chem. Phys.*, **44**, 181 (1966).

(11) R. J. Good, L. A. Girifalco, and G. Kraus, *J. Phys. Chem.*, **62**, 1418 (1958).

(12) A. D. Crowell, *J. Chem. Phys.*, **22**, 1397 (1954).

potential Ib

$$\epsilon(R) = (A/R^6) + B \exp(-CR) \quad (17)$$

This is still a central potential (only the modulus of the vector R is of interest), but three parameters have to be determined, one of which is a nonlinear δ parameter. Equation 17 can be written as

$$\epsilon(R_1, \gamma_1, \gamma_2, \delta) = \gamma_1 f_1(R) + \gamma_2 f_2(R, \delta) \quad (18)$$

with $\gamma_1 = A$, $\gamma_2 = E$, $\delta = C$, $f_1 = R^{-6}$, and $f_2 = \exp(-CR)$. Equations 15-16' hold true also in this case, where, however, F_2 , G_2 , and H_2 are all functions of the parameter δ . Dividing (16) by (16') the following equation is obtained

$$\frac{F_1 H_2(C) - F_2(C) H_1}{F_1 G_2(C) - F_2(C) G_1} = (\Delta E)_c s_{33} \quad (19)$$

which enable us to evaluate C from the experimental data from both compressibility and cohesion energy. Such an equation has been solved numerically. F_1 , G_1 , and H_1 are the same as in the previous case, while the evaluation of F_2 , G_2 , and H_2 must be carried out for each assigned value of C .

For $s_{33} = 2.75 \times 10^{-12} \text{ cm}^2 \text{ dyn}^{-1}$ and $(\Delta E)_c = -238 \text{ erg cm}^{-2}$ a value $C = 5.139 \text{ \AA}^{-1}$ has been found; $A = 1.387 \times 10^{-11} \text{ erg \AA}^6$ and $B = 3.332 \times 10^{-7} \text{ erg}$ have then been obtained. The resulting potential law is illustrated in Figure 1, together with the two Lennard-Jones potentials previously defined. Since all three observational equations have been employed in defining the three parameters, the adequacy of such a potential cannot be tested through the experimental data considered here for graphite. One can merely say that the exp 6 potential does not present the inner contradictions which were previously found for the 12-6 potential.

As far as the relative stabilities of different lattices are concerned, the situation is illustrated in Table I, where the lattice energies per unit volume $\Psi = \phi/d$ and the equilibrium interlayer spacing d are given, as calculated for the hexagonal, rhombohedral, and in registry packing of graphite layers. No matter which potential is considered, the in registry lattice appears to be less stable than the rhombohedral and hexagonal lattices, which are characterized by the same calculated stability.

One should conclude that central potential laws are not able to justify the greater stability of the hexagonal with respect to the rhombohedral lattice, even if they explain the lower stability of the hypothetical XXX structure.

Anisotropic Potential Laws

The inverse sixth power law used for the attractive term in the previous potentials is generally interpreted as due to the dispersion forces arising from dipole-dipole interactions. The polarizability of the involved atoms plays a fundamental role in current expressions for the dispersion forces, and an attractive potential which is simply proportional to R^{-6} is justified only when such polarizabilities are isotropic. Meyer and Deitz¹³⁻¹⁶ first pointed out that the anisotropic nature of carbon atom polarizability in graphite can markedly affect the dispersion energies, since the attraction should be limited by the restricted electronic oscillation perpendicular to the graphite layers. Searching for an explanation of the heterogeneities connected to the edge effects in the adsorption of gases on graphite, they used the treatment given by de Boer and

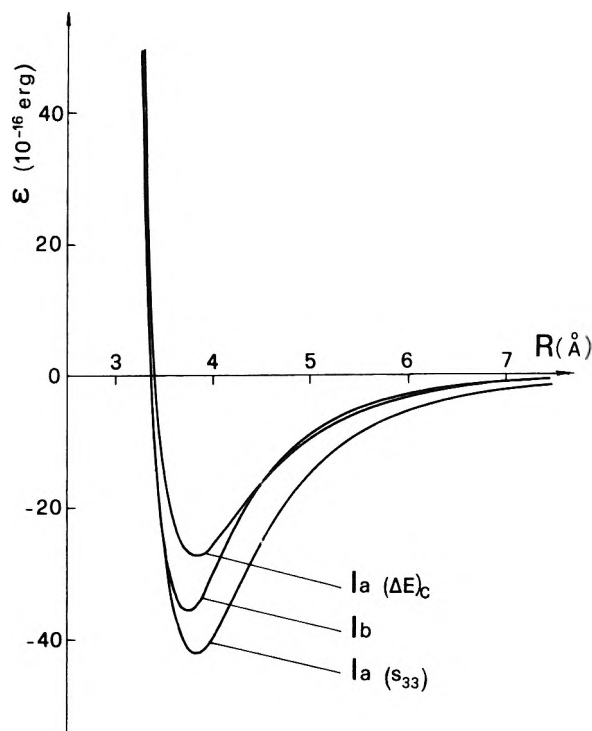


Figure 1. Potential laws for the van der Waals' interaction between carbon atoms in graphite. Ia $(\Delta E)_c$ and Ia (s_{33}) are the Lennard-Jones potentials derived from cohesion energy and compressibility, respectively; Ib is the modified Buckingham exp 6 potential.

TABLE I: Lattice Energy per Unit Volume ψ (10^8 erg cm^{-3}) and Equilibrium Interlayer Spacing d (\AA) for the Actual Hexagonal, the Nonequilibrium Rhombohedral, and the Hypothetical in Registry Lattice as Evaluated from Different Potential Laws^{a,b}

Potential law	XXXX		XYZXYZ		XXX	
	ψ	d	ψ	d	ψ	d
Ia $(\Delta E)_c$	60.041	(3.354)	60.041	3.354	58.463	3.380
Ia (s_{33})	92.264	(3.354)	92.264	3.354	90.188	3.380
Ib	61.914	(3.354)	61.914	3.354	59.471	3.389
IIa $(\Delta E)_c$	60.371	(3.354)	60.371	3.354	60.908	3.356
IIa (s_{33})	92.706	(3.354)	92.706	3.354	93.352	3.356
IIb	66.528	(3.354)	66.528	3.354	65.340	3.376
IIc $(\Delta E)_c$	60.412	(3.354)	60.412	3.354	60.110	3.365
IIc (s_{33})	92.656	(3.354)	92.656	3.354	92.194	3.365

^a For potentials IIc a polarizability ratio $D = 0.1$ has been used. ^b The value $d = 3.354 \text{ \AA}$ for the equilibrium spacing in hexagonal graphite has been used in the evaluation of the parameters for all potential laws.

Heller,¹⁷ which is an extension to the case of anisotropy of London's representation of interacting atoms as harmonic oscillators. Furthermore, they assumed, by referring to the work of Lippincott and Stutman,¹⁸ that the component of the polarizability perpendicular to the basal plane in graphite is zero, while the polarizability is isotropic in that plane. Finally they assumed that repulsive forces are isotropic, so that the repulsive term can be treated as a

- (13) E. F. Meyer and V. R. Deitz, *J. Phys. Chem.*, **71**, 1521 (1967).
 (14) E. F. Meyer, *J. Phys. Chem.*, **71**, 4416 (1967).
 (15) E. F. Meyer, *J. Chem. Phys.*, **48**, 5284 (1968).
 (16) E. F. Meyer, N. R. L. Report No. 6547, Washington, D. C., 1967.
 (17) J. H. de Boer and G. Heller, *Physica*, **4**, 1405 (1937).
 (18) E. R. Lippincott and J. M. Stutman, *J. Phys. Chem.*, **68**, 2926 (1964).

central one. These assumptions that, as far as we are aware, were not directly tested by Meyer and Deitz against the properties of graphite crystals, will be adopted to define non-isotropic self-interaction potentials for carbon atoms in graphite, in a way which strictly parallels that followed in the preceding section for central potentials. The interaction potential proposed by Meyer¹⁵ for carbon atoms in graphite

potential IIa

$$\epsilon(\mathbf{R}) = \frac{A}{R^6} \left(2 - \frac{6r^2}{R^2} + \frac{9r^4}{R^4} \right) + \frac{B}{R^{12}} \quad (20)$$

and the corresponding three-parameter potential

potential IIb

$$\epsilon(\mathbf{R}) = \frac{A}{R^6} \left(2 - \frac{6r^2}{R^2} + \frac{9r^4}{R^4} \right) + B \exp(-CR) \quad (21)$$

can be treated in a way strictly similar to that employed for the 12-6 and the exp 6 potentials. Here r is the projection of \mathbf{R} on the basal plane.

For potential IIa, the observational equations are again the eq 15-16' of the preceding section, obviously with different values of F_1 , G_1 , and H_1 still defined by eq 9-11.

As in the case of the Lennard-Jones potential, while the ratio B/A is univocally determined, the single A and B values depend on their derivation from the compliance modulus ($A = -1.748 \times 10^{-11}$ erg \AA^6 ; $B = 4.035 \times 10^{-8}$ erg \AA^{12}) or from the cohesion energy ($A = -1.139 \times 10^{-11}$ erg \AA^6 ; $B = 2.628 \times 10^{-8}$ erg \AA^{12}). Again, such a disagreement cannot be reduced to the experimental errors in the determination of s_{33} or $(\Delta E)_c$. This should not be considered too surprising since, as was already pointed out by Meyer,¹⁶ potential IIa gives, in Crowell's approximation, the same results as the Lennard-Jones potential, and it is well known that Crowell's approximation is quite satisfactory for graphite.

It can be concluded that the anisotropy of polarizability, as considered in the model by Meyer and Deitz, is not able to take into account the essential features of the van der Waals' interaction in graphite.

For potential IIb, which introduces a nonlinear δ parameter ($\delta = C$), this again can be derived from the experimental data for both compressibility and cohesion energy, by numerically solving an equation of the same form as eq 19 in the preceding section. The sums F_2 , G_2 , and H_2 must be evaluated for each assigned value of C . For the same s_{33} and $(\Delta E)_c$ values used above, $C = 5.123 \text{ \AA}^{-1}$ has been found. The values calculated for the remaining parameters are $A = -9.354 \times 10^{-12}$ erg \AA^6 and $B = 3.167 \times 10^{-7}$ erg. The angular dependence of the corresponding potential is illustrated in Figure 2. This potential law, which has been defined to fit the three chosen observational equations, does not present the intrinsic contradiction previously shown by potential IIa. The same situation as in the case of spherically symmetric laws is found also for the anisotropic polarizability treatment; only the three-parameter potential is compatible with the "molecular" properties of graphite which have been taken into account. This does not mean, however, that such a potential is effective in describing interactions between unlike pairs or in foreseeing adsorption heats or different graphite properties. In particular, the angular dependence of the carbon-carbon interaction, which is shown in Figure 2, is quite unacceptable. This exaggerated variation with ϑ does not produce untreatable results just because,

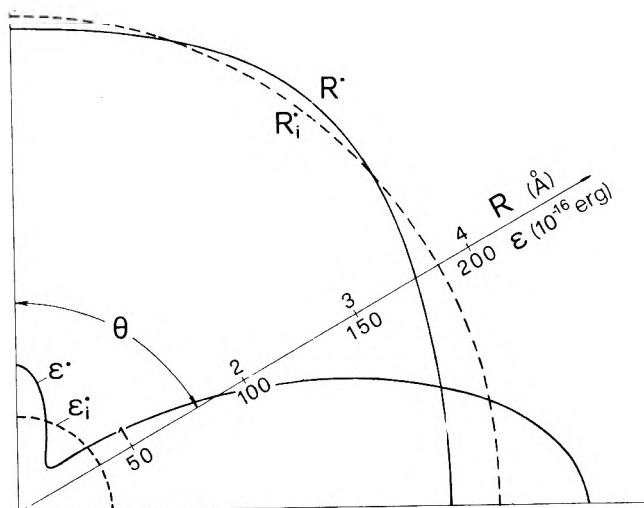


Figure 2. Polar diagram of minimum potential energy of interaction ϵ^* and corresponding equilibrium distance R^* as a function of the angle ϑ (potential IIb). The minimum energy ϵ_i^* and the equilibrium distance R_i^* for the isotropic exp 6 potential lb are also given for comparison.

as a consequence of the crystal structure of graphite, those carbon atoms whose relative position is characterized by high ϑ values are too removed from each other to heavily interact.

As far as the relative stabilities for different graphite lattices are concerned, Table I presents the lattice energies and the equilibrium interlayer spacings that can be calculated for the XYXY, XYZXYZ, and XXX packing of the graphite layers. The striking result for the potential IIa is that the in registry XXX packing appears to be energetically preferred, against any experimental evidence. So the Meyer and Deitz model, which does not enable us to overcome the difficulties encountered with the Lennard-Jones potential, introduces a further paradox from the point of view of lattice stabilities. This paradox, which is avoided with potential IIb, deserves further attention and leads to criticize the way in which the anisotropy has been introduced.

Of course the first criticism concerns the unrealistic assumption that the polarizability in a direction normal to the basal plane is zero.

Following the treatment of anisotropic polarizability that was given by de Boer and Heller, the expression for the attractive dispersion interaction between two atoms is

$$\epsilon_{\text{attr}} = - \frac{h}{4} \sum_{i,k=1}^3 c_{ik}^2 \frac{\nu_i \nu_k'}{\nu_i + \nu_k'} \alpha_i \alpha_k' \quad (22)$$

where the α 's are the components of the polarizabilities and the ν 's are the corresponding characteristic frequencies; c_{ik} is the interaction energy of two unit dipoles oriented in the directions defined by the corresponding unit vectors i and k

$$c_{ik} = (1/R^3)[i \cdot k - (3/R^2)(i \cdot R)(k \cdot R)] \quad (23)$$

Using a model which maintains the isotropy of the carbon atom polarizability in the plane parallel to the graphite layers corresponds to the assumption

$$\begin{aligned} \alpha_i &= \alpha_j = \alpha_i' = \alpha_j' = \alpha^{\parallel} \\ \alpha_k &= \alpha_k' = \alpha^{\perp} \\ \nu_i &= \nu_j = \nu_i' = \nu_j' = \nu^{\parallel} \\ \nu_k &= \nu_k' = \nu^{\perp} \end{aligned} \quad (24)$$

which gives

$$\epsilon(\mathbf{R})_{\text{attr}} = -\frac{\hbar}{4} \frac{1}{R^6} \left\{ \frac{1}{2} \nu^{\parallel} \alpha^{\parallel 2} \left(2 - \frac{6r^2}{R^2} + \frac{9r^4}{R^4} \right) + \frac{\nu^{\parallel} \nu^{\perp}}{\nu^{\parallel} + \nu^{\perp}} \alpha^{\parallel} \alpha^{\perp} \frac{18r^2 z^2}{R^4} + \frac{1}{2} \nu^{\perp} \alpha^{\perp 2} \left(1 - \frac{6z^2}{R^2} + \frac{9z^4}{R^4} \right) \right\} \quad (25)$$

where r is the projection of \mathbf{R} on the basal plane and z is the distance between the planes. This expression suggests a way for writing an interaction potential taking into account the anisotropy of polarizability according to the model illustrated above

potential IIc

$$\epsilon(\mathbf{R}) = \frac{A}{R^6} \left\{ \left(2 - \frac{6r^2}{R^2} + \frac{9r^4}{R^4} \right) + D \frac{18r^2 z^2}{R^4} + D^2 \left(1 - \frac{6z^2}{R^2} + \frac{9z^4}{R^4} \right) \right\} + \frac{B}{R^{12}} \quad (26)$$

Such a potential can be formally derived by associating the attractive term with an inverse twelfth-power repulsive term (as in the potential of Meyer and Deitz), by assuming $\nu^{\parallel} = \nu^{\perp} = \nu$, and by setting $A = -(h\nu\alpha^2)/8$ and $D = \alpha^{\perp}/\alpha^{\parallel}$. This expression defines a reasonable three-parameter potential law with a D parameter directly related to the polarizability ratio $\alpha^{\perp}/\alpha^{\parallel}$. For $\alpha^{\perp} = \alpha^{\parallel}$ it immediately reduces to a simple term in R^{-6} , while for $\alpha^{\perp} = 0$ it reduces to the attractive term proposed by Meyer¹⁵ for carbon atoms in graphite.

Exact determination of the three parameters A , B , and D from the observational equations is not possible, since experimental data for graphite bring us to a quadratic equation in D having imaginary roots. We can, however, assume any arbitrary D value intermediate between the two extreme values $D = 0$ and $D = 1$ (implicitly involved in the Meyer and Deitz and in the Lennard-Jones potential, respectively) and determine the other two parameters by proceeding in the usual way. It is found that lattice energies calculated in this way vary regularly with D ; a value as low as 0.1 is sufficient to produce the inversion in the relative stabilities of the hexagonal and in registry lattice, as shown in Table I. So it appears that the above paradox was not related to the physically obvious strong anisotropy of graphite, but strictly to the crude assumption $\alpha^{\perp} = 0$. On the other hand, one finds that potential IIc results unable, in the same measure as the two-parameter potentials Ia and IIa, to justify both the experimental data for compressibility and cohesion energy, irrespective of the value which is assigned to D .

One can finally observe that, as for the central potentials of preceding section, the anisotropic potential laws examined here fail to explain the higher stability shown by the normal hexagonal lattice with respect to the high-temperature rhombohedral lattice.

Adsorption Potential Energies for Rare Gases on Graphite

The adsorption energies which can be calculated in the additive pairwise approximation for the interaction of rare gases with a graphite surface were thoroughly discussed by Sams¹⁹ some years ago. In that work, the Lennard-Jones potential was employed, and attention was primarily given to the effect of using different sets of self-interaction parameters for the various rare gases, and different combination rules for obtaining unlike pair potentials. It

was apparent that the choice of rare gas parameters is not a critical one; while large differences are introduced by different combination rules.

The potential adsorption energies will now be discussed which can be calculated by using potential laws arising from suitable combinations of independently determined self-interaction potentials for the solid and the gas.

In the preceding sections two different potentials Ib and IIb have been selected for the self-interaction of carbon atoms in graphite, which are compatible with the physical properties of the graphite crystal.

Since both are three-parameter potentials, a three-parameter exp 6 potential must be used also for the self-interaction of rare gas atoms. The parameters employed for different rare gases are those proposed by Srivastava²⁰ which are essentially the same as used by Mason and Rice²¹ with the exception of Kr. In any case it was previously said that their choice was not a critical one in the evaluation of the adsorption energies. As far as the combination rules are concerned, different situations arise in the isotropic and anisotropic case.

For the exp 6 potentials, the Srivastava's combination rules may be adopted, which proved useful in studying unlike pair interactions in rare gases. They can easily be used to numerically evaluate the corresponding A , B , and C parameters in the expression 17 of the exp 6 potential.

On the other hand, the model of Meyer and Deitz¹³ involved in defining the attractive term in potential IIb, also defines in a rather rigid way the combination rule for the attractive term for the unlike pair. By applying the formulas of de Boer and Heller¹⁷ to the attractive interaction between an isotropic rare gas atom and a carbon atom in graphite (as treated in the anisotropic model of Meyer and Deitz), the following expression is obtained

$$\epsilon_{\text{attr}}(\mathbf{R}) = -\frac{h\nu_G \nu_C^{\parallel} \alpha_G \alpha_C^{\parallel}}{4(\nu_G + \nu_C^{\parallel})} \left(\frac{2}{R^6} + \frac{3r^2}{R^8} \right) = A_{CG'} \left(\frac{2}{R^6} + \frac{3r^2}{R^8} \right) \quad (27)$$

where α , ν , α^{\parallel} , and ν^{\parallel} have the same meaning as in the preceding section and indices G and C are for the gas atom and the carbon atom, respectively. The isotropic polarizabilities α_G for different rare gases are given by Hollis-Hallett²² and the anisotropic α_C for the carbon atom in graphite was determined in a semiempirical way by Lippincott and Stutman.¹⁸ Using these polarizabilities, the corresponding characteristic frequencies can be obtained from the attractive constants in the self-interaction potentials and the new attractive constants $A_{CG'}$ can be calculated. The remaining B and C parameters in the repulsive term have then been assumed to be given by the geometric and arithmetic mean, respectively, of the corresponding parameters in the self-interaction potentials. Such simple combination rules have been used, for instance, in the Williams' studies on the carbon-hydrogen interaction in hydrocarbons.²³

The procedure used for the anisotropic case suggests that similar combination rules (corresponding, for the attractive part to the London combination rules) may be used also in obtaining the exp 6 potential law for the

(19) J. R. Sams, Jr., *Trans. Faraday Soc.*, **60**, 149 (1964).

(20) K. P. Srivastava, *J. Chem. Phys.*, **28**, 543 (1958).

(21) E. A. Mason and W. E. Rice, *J. Chem. Phys.*, **22**, 843 (1954).

(22) A. C. Hollis-Hallett, "Argon, Helium, and the Rare Gases," Interscience, New York, N. Y., 1961.

(23) D. E. Williams, *J. Chem. Phys.*, **45**, 3770 (1966).

TABLE II: Values of Parameters for the Interaction between Rare Gases and Graphite^a

Combination rules	Parameters	Interacting atoms				
		He-C	Ne-C	Ar-C	Kr-C	Xe-C
Potential Law Ib						
Srivastava	A	-5.685	-11.00	-37.21	-56.65	-80.00
	B	81.21	441.8	774.1	696.1	925.8
	C	4.547	4.873	4.380	4.078	4.030
London	A	-4.169	-8.027	-30.86	-46.84	-71.09
	B	98.06	495.3	715.9	508.2	635.9
	C	4.547	4.873	4.380	4.078	4.030
Potential Law IIb						
de Boer-Heller	A	-1.662	-3.203	-11.79	-17.92	-26.26
	B	95.48	48.22	697.0	494.7	619.1
	C	4.539	4.865	4.372	4.070	4.022

^a A is in units of 10^{-12} erg \AA^{-6} ; B in units of 10^{-10} erg; C in \AA^{-1} .

isotropic case by employing, for the carbon atom in graphite, the calculated mean value $\bar{\alpha}_C$, corresponding to a hypothetical isotropic polarizability, also given by Lippincott and Stutman.¹⁸ Comparison of the results obtained by using the two different exp 6 potentials so obtained, should enable us to evaluate how far the combination rules affect the calculated potential energies of adsorption.

The evaluated parameters corresponding to the three different potential laws are given in Table II for all the unlike pairs here considered.

For each of the proposed potential laws, the local potential energy for a single rare gas atom adsorbed on the basal plane of a semi-infinite graphite crystal has to be calculated.

The asymmetric field near the surface of a crystal introduces a relaxation in its upper layers, which may be of importance in adsorption studies. The surface relaxation in graphite has been assumed to involve changes solely in the interlayer distances, and has been evaluated for a semi-infinite graphite crystal by minimizing the lattice energies with respect to the spacings. In practice only the spacing between the surface layer and the second layer undergoes an appreciable change (by +0.36%) on relaxation. The relaxation energy corresponds to only 0.06 and 0.05 erg cm^{-2} for potentials Ib and IIb, respectively. The potential energy of the adsorbed atom on the relaxed graphite crystal has then been calculated with reference to a Cartesian system, the x and y axes lying on the surface plane and the z axis pointing upward. The potential $V(x,y,z)$ has been calculated at each point by directly summing up the single-pair interactions for all the atoms of the solid within a sphere of radius 20 \AA centered at that point and by adding the contribution from outer atoms as evaluated in Crowell's approximation. The minimum of V with respect to z gives the potential energy of adsorption $V^0(x,y)$.

Three points of particular interest may be identified: the center of the hexagon where the minimum of V^0 occurs and which therefore corresponds to the preferential adsorption site; surface atoms corresponding to maxima of V^0 , no appreciable difference existing between the two topologically different types of surface carbon atoms; and saddle points at the middle between two nearest carbon atoms. In Table III values of V^0 are given at these points for all the rare gases and for the three different potential laws adopted.

TABLE III: Values of the Potential Energy of Adsorption at Site (V_s^0), Saddle (V_{sp}^0), and Atom (V_a^0) for Rare Gases on Graphite as Compared with Adsorption Potentials (V_e^0) from Experimental Data^a

Adsorbed gas	Potential energy of adsorption	Potential law and combination rules			V_e^0
		Ib Srivastava	Ib London	IIb deBoer-Heller	
He	V_s^0	-306.3	-181.3	-235.8	-337
	V_{sp}^0	-285.2	-171.8	-218.7	
	V_a^0	-282.7	-170.7	-216.8	
Ne	V_s^0	-607.5	-375.4	-485.2	-512
	V_{sp}^0	-560.9	-350.9	-444.9	
	V_a^0	-555.4	-348.1	-440.5	
Ar	V_s^0	-1342	-1067	-1291	-1474
	V_{sp}^0	-1285	-1024	-1226	
	V_a^0	-1279	-1019	-1219	
Kr	V_s^0	-1602	-1392	-1689	-1946
	V_{sp}^0	-1559	-1351	-1625	
	V_a^0	-1553	-1346	-1619	
Xe	V_s^0	-2152	-2119	-2449	-2565
	V_{sp}^0	-2098	-2057	-2360	
	V_a^0	-2091	-2050	-2350	

^a Energies are in units of 10^{-16} erg.

In the same table the data V_e^0 of adsorption potential deduced from experimental data are also given for comparison; they are those proposed by Yang, *et al.*,²⁴ for helium and by Olivier and Ross²⁵ for the other gases. All these data were calculated starting from experimental adsorption isotherms of rare gases on graphitized carbon black at different temperatures in the range of validity of Henry's law.²⁶⁻²⁹ Steele³⁰ recently discussed the possible ways of deducing the adsorption potentials from experi-

- (24) K. Yang, P. L. Gant, and D. E. Cooper, *J. Phys. Chem.*, **69**, 1768 (1968).
- (25) S. Ross and J. P. Olivier, "On Physical Adsorption," Interscience, New York, N. Y., 1964.
- (26) G. Constabaris and G. D. Halsey, Jr., *J. Chem. Phys.*, **27**, 1433 (1957).
- (27) G. Constabaris, J. H. Singleton, and G. D. Halsey, Jr., *J. Phys. Chem.*, **63**, 1350 (1959).
- (28) J. R. Sams, Jr., G. Constabaris, and G. D. Halsey, Jr., *J. Phys. Chem.*, **64**, 1689 (1960).
- (29) W. A. Steele and G. D. Halsey, Jr., *J. Phys. Chem.*, **59**, 181 (1955).
- (30) W. A. Steele, *J. Low Temp. Phys.*, **3**, 257 (1970).

mental data in the case of He on graphite, and a substantial agreement is found starting from different approaches.

The results given in Table III show a marked disagreement of the potential energies as calculated through the different potential laws with the values obtained from experimental adsorption data. Such a disagreement is higher than found by Sams¹⁹ using a Lennard-Jones 12-6 potential law, even if the Lennard-Jones potential proved to be inconsistent with the physical properties of the graphite crystal.

Conclusions

The Lennard-Jones 12-6 potential and the two-parameter potential proposed by Meyer were not found to fit the experimental data as far as spacing in the lattice, compressibility in a direction normal to the basal plane, and cohesion energy are concerned. The two potentials must then be excluded if potential laws, which are adequate to study the adsorption of rare gases on graphite in the additive pairwise approximation, have to be obtained by suitably combining empirical self-interaction potentials independently defined for each interacting species. The modified Buckingham exp 6 potential and the anisotropic three-parameter potential that can be obtained by combining an attractive term owing the model of Meyer and Deitz with an exponential repulsive term obviously can be adapted to fit the three observational equations considered here for graphite. These two potential laws succeed in assigning the correct relative stabilities to the

hexagonal (XYXY) and in registry (XXX) stacking, but are not able to introduce any difference between the hexagonal and the rhombohedral (XYZXYZ) stacking. Their suitability in giving useful interaction potentials for unlike pairs must then be judged from the results they are able to give for the potential energies of adsorption of different rare gases. As was seen in Table III such results are not very satisfactory.

This perhaps could indicate that it is not possible to obtain adequate potential laws for the physical adsorption of rare gases on graphite by rigorously applying the criterion of combining empirical self-interaction potentials independently defined. The fundamental reason should probably be found in the inadequacy of the additive pairwise approximation to describe van der Waals' interactions in graphite.

Another possible reason, however, can certainly be found in the rather arbitrary nature of combination laws. To this purpose, one must take into account that greater discrepancies are introduced by using different combination rules in the exp 6 potential, than by changing from the exp 6 potential to the modified Meyer and Deitz potential (*i.e.*, by passing from isotropic to anisotropic description of dispersion forces in graphite).

Finally one must consider that the uncertainty in many of the experimental data (both for graphite properties and for adsorption energies) are of the order of some per cent, and that a much better agreement with calculated energies either reflects a preoriented selection of the possible potential laws, or represents a lucky and fortuitous goal.

Adsorption of Ammonia in Copper(II) Y Zeolites

Yun-yang Huang* and E. F. Vansant¹

Department of Chemistry, Texas A & M University, College Station, Texas 77843 (Received October 13, 1972)

Adsorption and desorption of ammonia in Cu(II)Y zeolites were measured gravimetrically. In comparison with NaY, CaY, and decationated Y zeolites, the large ammonia uptakes in Cu(II)Y samples were attributed to the formation of copper(II)-ammine complexes, which were mainly in the form of $\text{Cu}(\text{NH}_3)_4^{2+}$. Desorption study showed that both the decationated Y and Cu(II)Y zeolites had stronger adsorption sites than other cation forms. No specific interaction between carbon monoxide and Cu(II)Y was observed, suggesting that Cu^{2+} ions were not exposed to the supercages. Adsorption of ammonia, however, would pull most Cu^{2+} ions out of the small cavities to form copper(II)-ammine complexes. Preadsorbed ammonia enhanced the reduction by carbon monoxide of cupric ions to cuprous ions.

Introduction

Ammonia is a small polar molecule. It has been used as a probe to study the gas-zeolite interaction, especially in terms of electrostatic energies. In particular, the adsorption of ammonia on X type zeolites exchanged with alkali metal and alkaline earth metal ions was investigated by Barrer and Gibbons.^{2a} They concluded that the electrostatic components, *i.e.*, the polarization energy and the field-dipole energy, were important contributions to the

initial heat of adsorption. A sequence of increasing heat with increasing polarizing power of the cation was clearly indicated. The heats of adsorption are in general between 10 and 20 kcal/mol, but are as high as 26 kcal/mol in the

- (1) On leave from the Laboratorium voor Oppervlaktescheikunde, Heverlee, Belgium.
- (2) (a) R. M. Barrer and R. M. Gibbons, *Trans. Faraday Soc.*, **59**, 2569 (1963); (b) J. E. Benson, K. Ushiba, and M. Boudart, *J. Catal.*, **9**, 91 (1967).

TABLE I: Adsorption-Desorption Measurement of Ammonia in Y Zeolites

Zeolite	CuY(75%)	CuY(48%)	CuY(13%)	CaY(77%)	NaY	Decationated Y
Cation content						
in mmol/g	1.60(Cu ²⁺)	1.12(Cu ²⁺)	0.27(Cu ²⁺)	1.66(Ca ²⁺)	4.40(Na ⁺)	3.92(H ⁺)
in cations/unit cell	21(Cu ²⁺)	14.5(Cu ²⁺)	3.5(Cu ²⁺)	21(Ca ²⁺)	56(Na ⁺)	46(H ⁺)
NH ₃ adsorption at 23° and 20 Torr, mmol/g	12.25	10.23	7.60	7.50	6.95	11.00
NH ₃ remaining after evacuation at 25°, mmol/g	3.98		1.57	2.24	1.16	4.38
NH ₃ remaining after evacuation at 100°, mmol/g	2.47		0.56	1.25	0.15	2.70

case of Ca²⁺ and Sr²⁺ forms at very low surface coverages.

Because of its strong basicity, ammonia has also been widely used to investigate the acidic sites on the surface of catalysts. For instance, Benson, Ushiba, and Boudart^{2b} studied the adsorption of ammonia on a decationated Y zeolite. Isothermic heat of adsorption was determined to characterize the binding force between ammonia and the acidic sites on the catalytically superactive material. At high surface coverages, the heat is only 10 kcal/mol, but increases to about 40 kcal/mol at very low coverages. This shows that on few acidic sites, ammonia is bound more strongly than on cation sites. In fact, calorimetric measurement on Y type zeolites³ indicated that the heats of ammonia adsorption at coverages below one NH₃ per cavity were above 20 kcal/mol for HY, CaY, and LaY samples, but not for NaY. The authors attributed the high initial values to the interaction of ammonia with proton centers, which would be present only in decationated and multivalent Y zeolites.

It is well known that ammonia forms complexes with transition metal ions in solutions. The nature of this coordination is different from those just mentioned due to the role which d electrons play in transition metal ions. By analogy, complex formation would be expected in zeolite cavities in which transition metal ions are present. This has indeed been observed. Much work has been devoted to study the copper(II)-ammine complexes in zeolites by electron spin resonance (esr) spectroscopy. Recently, Vansant and Lunsford⁴ reported that the Cu(NH₃)₄²⁺ complex in Y zeolite had a square planar symmetry and that desorption of ammonia at 100° gave an esr spectrum corresponding to a distorted tetrahedral symmetry with one ammonia per Cu²⁺ ion. ESR studies of complex formation in CuY zeolites prior to their work were properly surveyed and listed in the reference of their paper.

In spite of the extensive work which has been done in this area, all the esr investigations were limited to samples with low copper contents only, in order to avoid the spin exchange interaction between neighboring copper ions occurring at higher concentrations. Yet, it is conceivable that high exchanged zeolites might have adsorption properties and catalytic activities different from those of the low exchanged ones. We thus decided to study the complex formation of ammonia in high exchanged CuY zeolites by gravimetric adsorption-desorption measurement. The method would provide more quantitative information about the copper(II)-ammine complexes in zeolites, which would not be directly available from esr spectroscopy alone. Since ammonia would adsorb on acidic and cation sites, NaY, CaY, and decationated Y zeolites

were also studied in addition to CuY samples with various copper contents so that we could ensure the specific complex formation due to copper ions.

Experimental Procedure

Various cation-exchanged Y zeolites were prepared from Linde NaY zeolite by a conventional ion-exchange procedure. The high exchanged samples were obtained by treating the zeolite several times with the respective salt solutions. The contents of exchanged cations are given in Table I.

Anhydrous ammonia, 99.99% purity, supplied from Matheson Gas Products, was used for the adsorption study without further purification. Carbon monoxide, CP grade with 99.5% purity, also from Matheson, was passed slowly through a liquid nitrogen cold trap before use. Commercial oxygen, 99.5% purity, supplied from Airco Inc., was condensed in a liquid nitrogen cold trap and then distilled into a gas storage bulb for the pretreatment of CuY samples.

The adsorption-desorption experiment was carried out by a Cahn recording electrobalance, Model RG 2002, Ventron Instruments Corp. The apparatus of the gravimetric adsorption system in connection with a vacuum system was similar to that described by Huang, Benson, and Boudart.⁵

Zeolite samples were evacuated overnight at room temperature before heating up slowly at an increment of 100°/hr to 400°. The evacuation was continued at the final temperature for at least 3 hr. The CuY samples were then treated with 150 Torr of oxygen at 400° for 6 hr, followed by evacuation for 1 hr. The dehydrated samples showed a light green color.

Ammonia was adsorbed on dehydrated samples at room temperature and at pressures up to 70 Torr. A deep blue color developed in Cu(II)Y samples. Desorption points of the isotherms were then taken down to 5 Torr before the samples were evacuated. In the desorption runs, the samples were evacuated at room temperature for 9 hr, at 100° for 7 hr, at 200° for 6 hr, and then finally at 400° for at least 1 hr. The ultimate vacuum was 10⁻³ Torr at room temperature, but was 10⁻⁴ Torr or lower above 100°. The weight of the sample in each desorption step was recorded. For all zeolites, about 0.1 g of the dehydrated sample was used. The experimental precision of the weight measurement was less than 0.01 mmol/g. Reversibility of the

(3) B. V. Romanovskii, K. V. Topchieva, L. V. Stolyarova, and A. M. Alekseev, *Kinet. Catal.*, **12**, 890 (1971).

(4) E. F. Vansant and J. H. Lunsford, *J. Phys. Chem.*, **76**, 2860 (1972).

(5) Y. Y. Huang, J. E. Benson, and M. Boudart, *Ind. Eng. Chem., Fundam.*, **8**, 346 (1969).

adsorption isotherms could be assured above 1 Torr of pressure. Desorption measurement was also found to be reproducible.

To examine the effect of the reduction of copper(II) ions, the higher exchanged Cu(II)Y sample was treated with 120 Torr of carbon monoxide at 400° for 28 hr. The sample turned white after this treatment. Adsorption of ammonia at room temperature was then measured. No change of color was observed.

Adsorption of carbon monoxide on Cu(II)Y and CaY samples at 0° was carried out in order to probe the accessibility of bivalent cations to the supercages. This method has been used by Egerton and Stone.⁶

The electron spin resonance measurements were made by a Varian (V4502) spectrometer, with a TE₁₀₂ mode microwave cavity. The instrument was operated in the X-band region at 9.3 GHz. The *g* values were measured by comparison with a 2,2-diphenyl-1-picrylhydrazyl (DPPH) sample (*g* = 2.0036) attached to the outside of the sample tube.

Results and Discussion

Adsorption isotherms at 23° of ammonia in various Y zeolites are shown in Figure 1. Obviously, more ammonia was adsorbed on CuY samples even at pressures as low as a few Torrs, and the amount increased with increasing copper contents. For the CuY(13%) sample, which was used by Vansant and Lunsford⁴ in their esr study, the adsorption was close to NaY and CaY zeolites. Because of its low copper content, the specific interaction of ammonia was hardly noticeable from adsorption measurements. In the case of CuY(48%) and CuY(75%) samples, however, the adsorption was remarkably different from other cation forms. The uptake at 50 Torr for the CuY(75%) sample reached a value of 12.7 mmol/g, which corresponds to 167 NH₃ molecules per unit cell. This is very close to the saturation capacity of 170 NH₃ molecules per unit cell at 30° for NaX zeolite, as was reported by Barrer and Gibbons.^{2a} But before assessing the copper(II)-ammine complexes, let us consider the adsorption of ammonia on other surface sites.

The large ammonia adsorption on decationated Y zeolite is expected since it has more acidic sites than other cation forms. By means of deuterium exchange, Uytterhoeven, Christner, and Hall⁷ found that the hydrogen contents in the Na⁺ and Ca²⁺ forms were much lower than in the decationated zeolites, although that in the Ca²⁺ form, they were several times higher than the Na⁺ form. With the adsorption of pyridine, Ward investigated by infrared spectroscopy the proton acidity of various cation-exchanged zeolites.⁸⁻¹⁰ Both the Cu²⁺ and Ca²⁺ forms were found to have much fewer acidic sites than the decationated form. Hence, to account for the adsorption on acidic sites, CuY must be compared with NaY or CaY, but not with the decationated Y zeolite. The role of cation sites other than Cu²⁺ ions is less pronounced, as is indicated by the small difference in adsorption at 23° between NaY and CaY samples. Therefore, the high uptake of ammonia in CuY zeolites must mainly be due to the formation of copper(II)-ammine complexes.

Adsorption isotherms indicate that the formation of complexes was probably completed at pressures less than 20 Torr. Further increase of pressure to 70 Torr only increased slightly the amount of adsorption, especially in the CuY(75%) sample. If the uptake at 20 Torr is plotted against the copper content in zeolite samples, a fairly

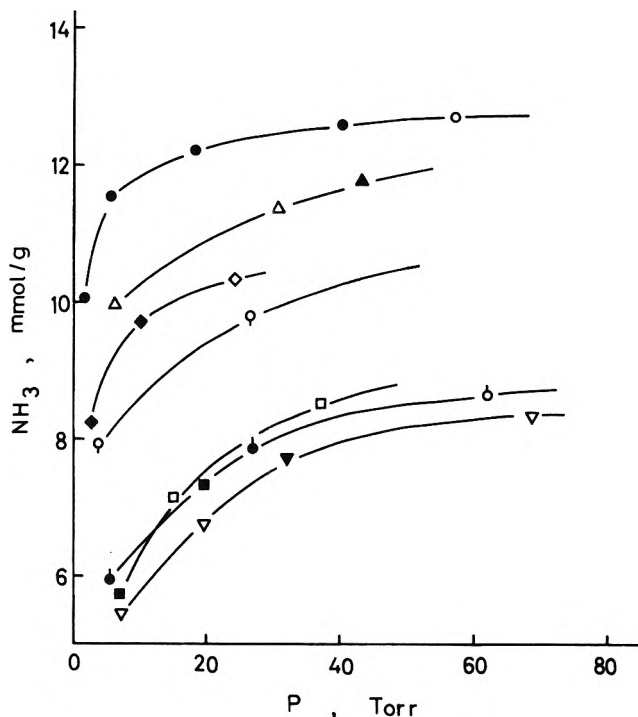


Figure 1. Adsorption isotherms at 23° of ammonia in Y zeolites (open symbols, adsorption; solid symbols, desorption): O, CuY(75%); \diamond , CuY(48%); \circ , CuY(13%); Δ , decationated Y; \square , CaY; ∇ , NaY; ϕ , CO-reduced CuY(75%).

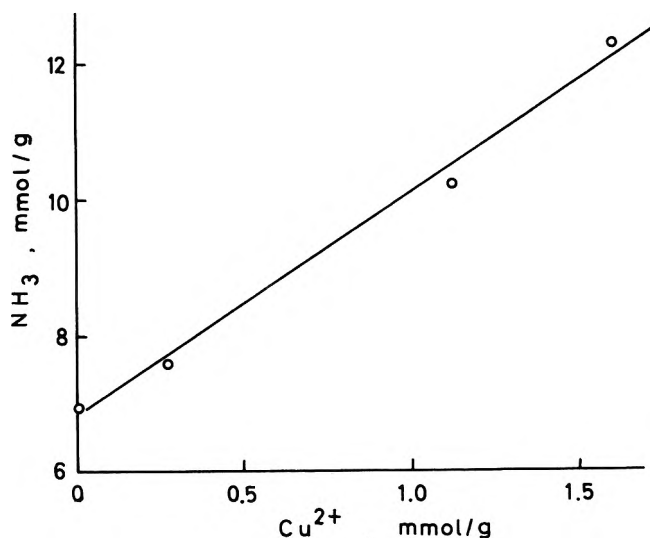


Figure 2. Ammonia adsorption in relation to the copper content in Y zeolites ($T = 23^\circ$, $P = 20$ Torr).

good correlation line is shown in Figure 2, with a slope corresponding to 3.3 NH₃/Cu²⁺. It is quite likely that in samples with higher copper contents, not all the Cu²⁺ ions were involved in the complex formation. The ammonia to copper ratio of the complexes would be slightly greater than this value; it would probably be very close to four. We conclude that the major portion of the ammine

(6) T. A. Egerton and F. S. Stone, *Trans. Faraday Soc.*, **66**, 2364 (1970).

(7) J. B. Uytterhoeven, L. G. Christner, and W. K. Hall, *J. Phys. Chem.*, **69**, 2117 (1965).

(8) J. W. Ward, *J. Catal.*, **22**, 237 (1971).

(9) J. W. Ward, *J. Catal.*, **10**, 34 (1968).

(10) J. W. Ward, *J. Catal.*, **13**, 364 (1969).

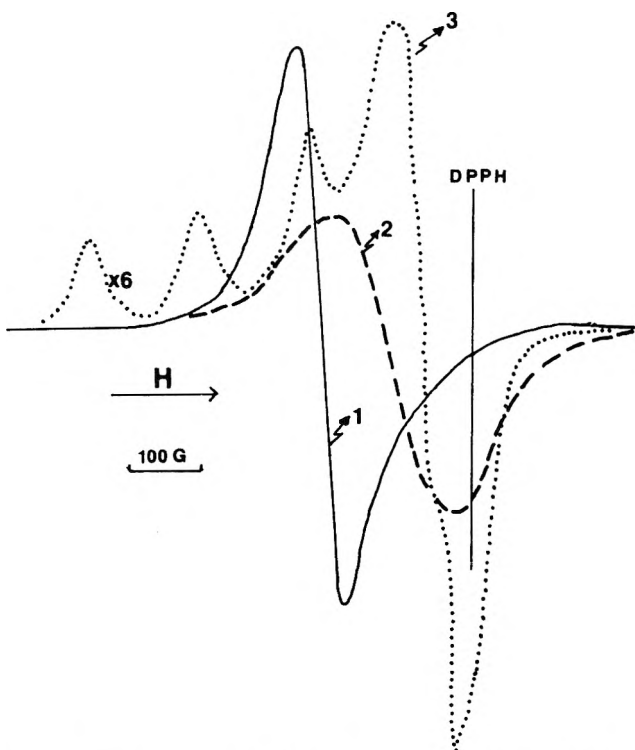


Figure 3. ESR spectra of CuY zeolites recorded at -196° : (1) dehydrated CuY(75%); (2) ammonia adsorbed in CuY(75%); (3) ammonia adsorbed in CuY(13%).⁴

complexes in zeolites, even with high copper contents, was in the form of $\text{Cu}(\text{NH}_3)_4^{2+}$.

In the CuY(13%) sample, there were only 3.5 Cu^{2+} ions per unit cell. Because of the low copper content, it is most likely that only one $\text{Cu}(\text{NH}_3)_4^{2+}$ would be formed in a supercage. The well-resolved hyperfine structure of the esr spectrum did indicate so.⁴ In CuY(48%) and CuY(75%) samples, there were 14.5 and 21 Cu^{2+} ions per unit cell, respectively. If all the Cu^{2+} ions were involved in the formation of complexes, then, there would be about two and three copper(II)-ammine complexes, respectively, in a supercage of approximately 13 Å in diameter. The complexes would be so close together and the distance between two neighboring Cu^{2+} ions would be so small that the spin exchange interaction would occur.¹¹ Indeed, this was revealed from the esr spectrum of the copper(II)-ammine complexes in the CuY(75%) zeolite (Figure 3). Only a broad symmetric line with $g_{\text{iso}} = 2.089$ was observed. Before the adsorption of ammonia, the dehydrated sample also gave a symmetric spectrum, but with $g_{\text{iso}} = 2.170$, due to the copper pair formation inside the sodalite cages, as was pointed out by Chao and Lunsford.¹²

Adsorption of carbon monoxide showed that, in dehydrated CuY zeolites, high or low exchanged, a negligibly small number of Cu^{2+} ions were exposed to the supercages (Figure 4). X-Ray diffraction study by Gallezot, Ben Taarit, and Imelik¹³ indicated that Cu^{2+} ions prefer S_1 sites in the sodalite cages. In contrast, about 25% of the exchanged Ca^{2+} ions in CaY(77%) was interacting with carbon monoxide. According to Egerton and Stone,⁶ the calcium ions occupy preferentially the hexagonal prisms (site I), the remainder will be in site II positions so that, on these sites, each calcium ion would adsorb specifically one CO molecule. Since Cu^{2+} ions occupied site I and I' positions,¹³ they were not accessible to carbon monoxide. However, adsorption of ammonia would pull Cu^{2+} ions

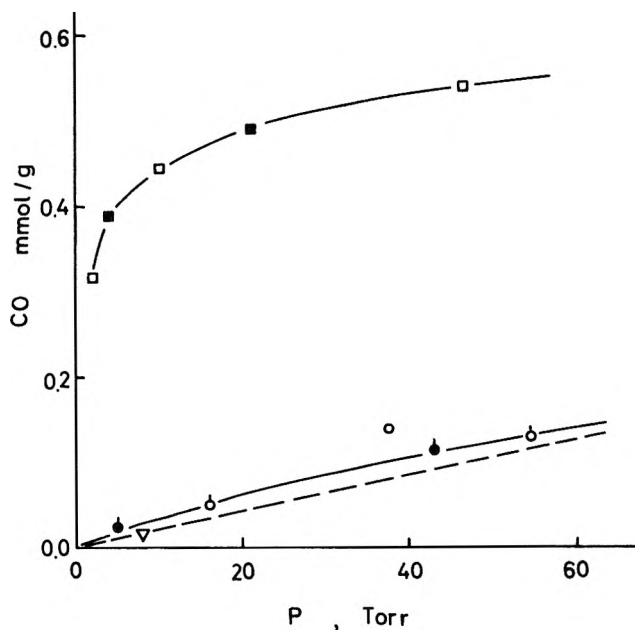


Figure 4. Adsorption isotherms at 0° of carbon monoxide in Y zeolites (open symbols, adsorption; solid symbols, desorption): O, CuY(75%); \circ , CuY(13%); \square , CaY(77%); ∇ , NaY.⁶

out of the small cavities and form copper(II)-ammine complexes in the supercages. The migration of Cu^{2+} ions upon the adsorption of ammonia in low exchanged CuY has been reported by esr studies.⁴ It is interesting that, even in high exchanged samples, most Cu^{2+} ions migrated out of the small cavities to form complexes.

Adsorption isotherms at higher temperatures for CuY zeolites were not measured because of the possible reduction of Cu^{2+} ions by ammonia above 100° , according to Krüerke and Jung.¹⁴ The isosteric heat of adsorption on CuY, especially at very low surface coverages, cannot be reliably determined. Nevertheless, the affinity of ammonia interaction with various cation-exchanged Y zeolites may be inferred by comparing adsorption isotherms at room temperature and also from the results of desorption measurements. The extent of desorption during a period of pumping would depend on the heat of adsorption; it is harder to desorb molecules held on stronger adsorption sites. After several hours of evacuation at room temperature and at 100° , the amount of ammonia remaining in zeolite samples, as indicated in Table I, had the following order: decationated Y > CuY(75%) > CaY > CuY(13%) > NaY. Apparently, at surface coverages less than 4 mmol/g or about 6 NH_3/cage , ammonia was adsorbed more strongly on the CuY(75%) and decationated Y zeolites than on others. Desorption at room temperature and at 100° also revealed that CuY(75%) did not have stronger adsorption sites than the decationated Y sample.

Desorption measurements of CuY(13%) zeolite at room temperature and at 100° showed that the $\text{NH}_3/\text{Cu}^{2+}$ ratio was 1.5.⁴ This was based on the difference in the amount of ammonia remaining between CuY(13%) and NaY samples. Similarly, the ratios were calculated for CuY(75%) sample, based on the amount in excess of NaY or CaY (Table II). The latter would be more suitable if the contribution from acidic sites is considered. The $\text{NH}_3/\text{Cu}^{2+}$

(11) J. H. Lunsford, *Advan. Catal.*, **22**, 265 (1972).

(12) C. C. Chao and J. H. Lunsford, *J. Chem. Phys.*, **57**, 2890 (1972).

(13) P. Gallezot, Y. Ben Taarit, and B. Imelik, *J. Catal.*, **26**, 295 (1972).

(14) U. Krüerke and P. Jung, *Z. Phys. Chem.*, **58**, 53 (1968).

TABLE II: Ammonia to Copper(II) Ratios from Desorption Measurements

Desorption Temp	CuY(75%)		CuY(13%)
Room temperature	1.76 ^a	1.09 ^b	1.52 ^a
100°	1.45 ^a	0.76 ^b	1.52 ^a

^a Ratio based on NaY. ^b Ratio based on CaY.

ratio was close to one when evacuated at room temperature, but less than one after desorption at 100°. In other words, more Cu²⁺ ions were detached from ammonia in the latter. The esr spectrum showed a symmetric line with $g_{iso} = 2.170$, but was broader than that of the dehydrated sample.

The effect of the reduction of cupric ions on the adsorption of ammonia must also be mentioned. From Figure 1, we see that much less ammonia was adsorbed on the CO-reduced CuY(75%) sample, the difference being about 1.8 NH₃ molecules per Cu²⁺ ion present in the Cu(II)Y zeolite. Naccache and Ben Taarit¹⁵ have pointed out that cupric ions were reduced to cuprous ions during the CO

treatment. Consequently, less ammonia would be adsorbed since the common cuprous-ammine complex in solution is known to be Cu(NH₃)₂⁺. In the course of this study, we also discovered that the reduction of cupric ions in Cu(II)Y zeolite was much easier when a small amount of ammonia was introduced before the CO treatment. Due to the complex formation, Cu²⁺ ions were pulled out of the small cavities and could easily be reduced by carbon monoxide. The reduction was completed within 3 hr at 100°; no esr signal of Cu²⁺ ions was observed. Without preadsorbed ammonia, the sample must be treated with carbon monoxide at temperatures higher than 400° for a much longer period.

In conclusion, the adsorption-desorption measurement on Cu(II)Y zeolites, in comparison with other cation forms, indicated that a considerable amount of ammonia was specifically coordinated to copper(II) ions. The ammine complexes were mainly Cu(NH₃)₄²⁺. Migration of Cu²⁺ ions from the sodalite cages to the supercages, when ammonia was adsorbed, was observed by esr spectroscopy incorporation with the CO adsorption measurement.

(15) C. M. Naccache and Y. Ben Taarit, *J. Catal.*, **22**, 171 (1972).

Viscous Liquids and the Glass Transition. IV. Thermodynamic Equations and the Transition¹

Martin Goldstein

Beller Graduate School of Science, Yeshiva University, New York, New York and Department of Mechanics, Technion—Israel Institute of Technology (Received June 30, 1972)

Earlier studies of the application of thermodynamics to the glass transition appeared to show that $dT_g/dP \simeq TV\Delta\alpha/\Delta C_p < \Delta\beta/\Delta\alpha$. These results gave support to an entropy or energy theory of the transition over free volume theory. Recently it has been proposed that the experimental definitions of certain quantities in the above relations have been at fault, and new definitions have been suggested that give $dT_g/dP = \Delta\beta/\Delta\alpha$ in agreement with free volume theory. The physical meanings of the various experimental parameters are examined in this paper and it is concluded that the original definitions are the appropriate ones to use in the thermodynamic analysis and that the original conclusion is correct. It is pointed out that the success or failure of the thermodynamic equations is equivalent to the question of whether glasses prepared by cooling under different pressures do or do not have the same free volume or the same configurational entropy or energy.

I. Introduction

Davies and Jones,^{2a} extending an equation of irreversible thermodynamics derived by Prigogine and Defay,^{2b} proposed that if certain conditions are met the following equations would apply to glass transition phenomena (see sections III and IV below for definitions of these quantities)

$$dT_g/dP = \Delta\beta/\Delta\alpha \quad (1)$$

$$\Delta\beta/\Delta\alpha = TV\Delta\alpha/\Delta C_p \quad (2)$$

Examination of experimental data by various authors³⁻⁷ appeared to show that

$$dT_g/dP = TV\Delta\alpha/\Delta C_p < \Delta\beta/\Delta\alpha \quad (3)$$

The conditions for validity of (1) and (2) are therefore not met.

- (1) Previous papers in this series: M. Goldstein, *J. Chem. Phys.*, **51**, 3728 (1969); G. P. Johari and M. Goldstein, *ibid.*, **53**, 2372 (1970); G. P. Johari and M. Goldstein, *ibid.*, **55**, 4245 (1971).
- (2) (a) R. O. Davies and G. O. Jones, *Advan. Phys.*, **2**, 370 (1953); (b) I. Prigogine and R. Defay, "Chemical Thermodynamics," Longmans, Green and Co., London, 1954.
- (3) R. D. Maurer, *J. Amer. Ceram. Soc.*, **40**, 211 (1957).
- (4) F. Bueche, *J. Chem. Phys.*, **36**, 2940 (1962).
- (5) J. M. O'Reilly, *J. Polym. Sci.*, **57**, 429 (1962).
- (6) M. Goldstein, *J. Chem. Phys.*, **39**, 3369 (1963); **43**, 1852 (1965).
- (7) G. Gee, *Polymer*, **7**, 177 (1966); *Contemp. Phys.*, **11**, 313 (1970).

The conclusion was drawn that the glass transition, rather than being determined by free volume,⁸ was determined by configurational entropy, as proposed in a theory of Gibbs.^{9,10}

However, the question was reopened in a series of publications by Bianchi,^{11,12} Kovacs,¹³ Ferry,¹⁴ and Quach and Simha¹⁵ in this journal and elsewhere, who proposed alternate experimental definitions of the observables dT_g/dP and $\Delta\beta$, which when substituted in eq 1 satisfy the equation. This of course gives new support to the free volume approach to the glass transition.

This paper attempts a reexamination of the definitions of dT_g/dP and $\Delta\beta$. The problem of concern may seem purely semantic, but it is carried out in the belief that good definitions permit asking good scientific questions and getting sensible answers. The thesis presented here is that the old definitions are best, and the failure of the quantities so defined to satisfy (1) is a true weakness of the free volume theory.

II. The Definition of Configurational Properties

I will begin by assuming that no apology is needed for applying thermodynamics to the glassy state well below T_g where the properties are reproducible and time independent, nor to the supercooled metastable liquid.

The starting point for a thermodynamics of the glass transition is the possibility of performing "fast" experiments which still maintain thermodynamic equilibrium and during which therefore such thermodynamic properties as entropy, free energy, and temperature are unambiguously defined. Whether the quantities measured in such an experiment are truly thermodynamic is determined by whether the "fast" experiment is done reversibly or not. The reader should remember that a reversible process is defined as one in which the work done on the system in going in one direction is completely recovered in going in the reverse direction. This definition is an experimental one, and it does not presuppose any knowledge of the thermodynamic stability of the system studied.

In a practical sense the kind of experiment we can perform depends on the characteristic relaxation time of the system. In the transition range such fast experiments may be performed isothermally or isobarically if we wish, and T and P are the natural variables. When the structural relaxation time is short, the high frequency of an acoustic wave is needed and the experiment is adiabatic.

A nonthermodynamic but plausible assumption is generally made about fast experiments, at least as performed in the transition region: in such an experiment the "structure" does not change, and the only changes in thermodynamic properties observed are those that result from the changes in population of the vibrational energy levels of the fixed "structure."

The concept of an invariant structure is equivalent to a hypothesis proposed in the first paper of this series:¹⁶ the state point in configurational space (a $3N$ dimensional vector representing the instantaneous atomic configuration) spends most of its time near the bottom of minima of the potential energy U of the whole system, and in a fast experiment remains trapped in one such minimum. Such a hypothesis is necessary if we assert that the only changes in thermodynamic properties are vibrational.

This hypothesis cannot remain valid indefinitely as temperature is raised. In the earlier paper it was suggested on the basis of several different criteria that the range

of validity cannot extend beyond that temperature where the characteristic structural relaxation time τ_v of the liquid is about 10^{-9} sec. This is well above T_g , but usually below the melting point of simple liquids.

It should be noted that high-frequency adiabatic experiments distinguish "fast" and "slow" adiabatic compressibilities in liquids at temperatures well above the temperature for which $\tau_v = 10^{-9}$ sec. What ceases to be valid at this temperature is the concept of a fixed structure in a fast experiment.

We refer now to the transition region, where the separation of thermodynamic contributions at fixed structure or configuration from those arising from the change in configuration is believed to be valid.

The hypothesis of a fixed structure for the liquid at equilibrium at some starting temperature T_1 and pressure P_1 does not of course imply that each atomic position is the same in each sample of the liquid at T_1 and P_1 , but only that there are a large number Ω of structures appropriate to T_1 and P_1 , each one differing in the atomic coordinates and therefore differing to some extent in the vibrational spectrum; however, there will be some ensemble average vibrational partition function for all samples at equilibrium at T_1 and P_1 . The entropy of the liquid will thus be

$$S_{\text{liq},1} = k \ln \Omega_1 + S_{\text{vib},1}$$

where $S_{\text{vib},1}$ is the entropy associated with the ensemble average vibrational partition function. In a fast experiment only this latter changes and

$$dS = C_{p,\text{vib},1} dT/T$$

In a slow experiment a new set of structures, Ω_2 in number, becomes available. These will in general have a different ensemble average vibrational partition function, and the new entropy is

$$S_{\text{liq},2} = k \ln \Omega_2 + S_{\text{vib},2}$$

$$dS = k d \ln \Omega + S_{\text{vib},2} - S_{\text{vib},1}$$

The usual assumption made is that the vibrational spectra are not much altered by structure and that

$$S_{\text{vib},2}(T_2) - S_{\text{vib},1}(T_1) \cong C_{p,\text{vib}} dT/T$$

This is clearly an approximation, as the looser structures that are the equilibrium ones at higher temperature should surely have lower average vibrational frequencies and a higher vibrational entropy even when compared at the same temperature. Fortunately, this is a question that can be answered by experiment. If the differences in entropy between the equilibrium states at two different temperatures were largely vibrational and only marginally due to the change in $k \ln \Omega$, these entropy differences would tend to diminish with temperature and vanish at absolute

- (8) M. L. Williams, R. F. Landel, and J. D. Ferry, *J. Amer. Chem. Soc.*, **77**, 3701 (1955).
- (9) J. H. Gibbs, "Modern Aspects of the Vitreous State," Vol. I, Butterworths, London, 1960, Chapter 7.
- (10) G. Adam and J. H. Gibbs, *J. Chem. Phys.*, **43**, 139 (1965).
- (11) U. Bianchi, *J. Phys. Chem.*, **69**, 1497 (1965).
- (12) U. Bianchi, A. Tuturro, and G. Basile, *J. Phys. Chem.*, **71**, 3555 (1967).
- (13) A. J. Kovacs in "Relaxation Phenomena in Polymers," R. Longworth, Ed., Interscience, New York, N. Y., in press.
- (14) J. D. Ferry, "Viscoelastic Properties of High Polymers," 2nd ed, Wiley, New York, N. Y., 1970.
- (15) A. Quach and R. Simha, *J. Appl. Phys.*, **42**, 4592 (1971); *J. Phys. Chem.*, **76**, 416 (1972).
- (16) M. Goldstein, *J. Chem. Phys.*, **51**, 3728 (1969).

zero. If we compare then two samples of liquid at equilibrium at T_1 and T_2 , respectively, and cool them both in "fast" experiments to absolute zero, the entropy differences observed at T_1 and T_2 would disappear. While the experiment is straightforward, it has not been done often, or with sufficient care. Chang, *et al.*,¹⁷ have reviewed such data as were available to them and concluded that most of the excess entropy at T_g is truly configurational, and in a careful experiment on diethyl phthalate, Bestul and Chang found that 77% of the entropy difference between two samples in effect equilibrated at two different temperatures in the transition region was retained at 4°K.¹⁸ While the evidence is scanty, we will accept as a working hypothesis for the present that the difference in the changes in entropy between a slow and fast experiment thus arises primarily from changes in $k \ln \Omega$.

Other first derivative thermodynamic properties V and E will be assumed to behave similarly. We use the subscript c to denote a change in a configurational property and write

$$dS_c = (\Delta C_p/T)dT - V\Delta\alpha dP \quad (2.a)$$

$$dV_c = V\Delta\alpha dT - V\Delta\beta dP \quad (2.b)$$

where

$$C_{p,c} = \Delta C_p = C_{p,liq} - C_{p,gl} \quad (3.a)$$

$$\alpha_c = \Delta\alpha = \alpha_{liq} - \alpha_{gl} \quad (3.b)$$

$$\beta_c = \Delta\beta = \beta_{liq} - \beta_{gl} \quad (3.c)$$

define the configurational specific heat, thermal expansion, and compressibility, respectively.

The subscript liq in the above denotes the equilibrium properties observed in a slow experiment on a liquid; the subscript gl denotes a glassy property measured in a fast experiment that maintains the sample on which it is performed at constant structure. As will be seen later, other definitions of glass properties such as β_{gl} have been proposed. These, however, are not equivalent to a measurement at fixed structure, and therefore have a different physical significance.

Note that eq 2.a and 2.b define changes dS_c and dV_c , but not total quantities S_c and V_c . These quantities cannot as easily be operationally defined without reference to some molecular theory.

"Free volume" is a concept that has been defined by different workers in many different ways. In the original formulation of the well-known WLF free volume equation for viscosity or relaxation time, what I have called the configurational volume V_c was used.⁸ The free volume fraction f is thus given by

$$df = V_c/\bar{v} \quad (4)$$

The concept of free volume has been used by Simha and coworkers to develop a modified cell theory of liquids and polymers.^{15,19,20} The changes in thermodynamic properties arise both from the changes in volume, energy, etc. of the cell with its imprisoned molecule, and from the introduction of vacant cells. This treatment has given a good description of the P - V - T properties of polymers, but has not been extended to nonthermodynamic properties such as viscosity.

A different free volume quantity proposed by Simha and Boyer²¹ is the product $\Delta\alpha \cdot T_g$, which has a surprisingly constant value close to 0.113 for many different

polymers when T_g is measured at atmospheric pressure. The behavior of this product as pressure is varied will be discussed in section VII.

In section IV the glass transition temperature T_g is defined in the conventional way as a relaxational or viscous parameter of a substance. The theories to be considered in this paper are those that attempt a prediction of relaxational behavior. For this reason the definition of free volume of eq 2b and 4 will be given the closest examination.

III. The Criterion of Validity of One-Parameter Theories

We have defined configurational or excess properties operationally near T_g . Statistical mechanical models must provide quantitative predictions of them and from them in turn conditions any model must meet can be inferred. There is a class of theories which introduce a single parameter such as the numbers of holes or of broken bonds, which determine the configurational contributions to the thermodynamic properties. If a hole is assigned a volume and energy, and if the entropy of mixing is random, it is intuitively obvious that if the number of holes is fixed, the configurational volume, energy, and entropy are also.

As is well known, if such a model is valid, the following relation holds

$$\frac{\Delta\beta \cdot \Delta C_p}{TV(\Delta\alpha)^2} = R = 1 \quad (5)$$

R being the Prigogine-Defay ratio.² The above relation is equivalent to the assertion that ΔC_v , the configurational contribution to the specific heat at constant volume, is zero.⁶

If one parameter is not sufficient, considerations of thermodynamic stability ensure

$$R > 1 \quad (6)$$

These relations can also be written

$$\Delta\beta/\Delta\alpha \geq TV\Delta\alpha/\Delta C_p \quad (7)$$

These relations may be derived in a number of equivalent ways. Most usually, an internal ordering parameter Z is postulated, which at equilibrium is a function of P and T . If one is constructing a statistical mechanical model, Z is some parameter defined in the model, such as the number of holes in a hole model, or the number of A-B pairs in a mixing model. The free energy G is calculated as a function of T , P , and Z , and the dependence of Z on P and T at equilibrium is found from setting $\partial G/\partial Z = 0$ at each temperature and pressure. It is further assumed that in a fast experiment, Z is unchanged. From a purely thermodynamic point of view it is not necessary to specify a molecular meaning for Z , but the idea that it is a variable with respect to which G is a minimum at equilibrium, and which remains constant in a fast experiment is still necessary. Some workers applying free volume theory to relaxation below T_g , have assumed that free volume may still change with temperature below T_g , but at a different rate from that observed above T_g .¹⁴

(17) S. S. Chang, A. B. Bestul, and J. A. Horman, *Proc. 7th Int. Congr. Glass, Brussels, 1965*, 26-1.3.1 (1966).

(18) S. S. Chang, J. A. Horman, and A. B. Bestul, *J. Res. Nat. Bur. Stand.*, **71A**, 293 (1967).

(19) R. Simha and T. Somcynsky, *Macromolecules*, **2**, 342 (1969).

(20) T. Somcynsky and R. Simha, *J. Appl. Phys.*, **42**, 4545 (1971).

(21) R. Simha and R. F. Boyer, *J. Chem. Phys.*, **37**, 1003 (1962).

Somcynsky and Simha²⁰ have found that their cell model, which worked well for polymer liquids, did not give a good description of the glassy state. The discrepancy could be explained by assuming that at least some vacancies do not freeze in at T_g but are eliminated as temperature is lowered further. Also, Simha and coworkers have demonstrated that small changes in α_g occur below T_g , at the temperatures where secondary relaxations are known to occur.^{22,23} So far, these changes in thermal expansion have not been incorporated as a correction to the free volume model of viscosity. Without passing on the merits of an attempt to do so, we may state that eq 5 and the subsequent analysis here will not be expected to be relevant.

We note that the Gibbs-diMarzio theory⁹ introduces two internal ordering parameters explicitly: the number of flexed bonds in a polymer chain and the number of unoccupied lattice sites. The configurational energy and entropy will be functions of both parameters, the configurational volume only of the second.

It would be expected, therefore, that if the Gibbs-diMarzio theory is correct, the configurational properties will obey the inequality (6) rather than the equality (5). However, Moacanin and Simha²⁴ and Eisenberg and Saito²⁵ have given evidence for the view that while the Gibbs-diMarzio theory is formally a two-parameter theory, the two parameters it contains are found experimentally not to be independent of each other, but to vary simultaneously in such a way as to reduce effectively to a single one. Their analysis is based on an examination of the values of the parameters found by fitting the theory to experimental data on polymers. Further, the idea that entropy and free volume should vary together is a plausible one, aside from the question of whether the Gibbs-diMarzio theory is right or wrong. The crucial point, however, is that the question of whether one parameter is sufficient or not is one we can and should answer experimentally, by examining whether R of relations (5) and (6) is unity or not. We can do this without committing ourselves in advance to any particular molecular theory.

In earlier papers I and others⁵⁻⁷ reviewed the somewhat scanty experimental data and came to the conclusion that the equality is almost never satisfied. $\Delta\beta/\Delta\alpha$ appeared consistently to be about twice $TV\Delta\alpha/\Delta C_p$. The conclusion was tentative, as $\Delta\beta$ is difficult to measure, and the three second derivative quantities are hardly ever determined in a single laboratory on the same sample.

Recently, Breuer and Rehage²⁶ have claimed that (5) is valid for polystyrene, but Ichihara and coworkers²⁷ find $R = 2.1$, in agreement with the earlier conclusion.

IV. The Definition of T_g and Its Pressure Dependence

There are a number of techniques that have been used to define a glass transition temperature T_g . The usual dilatometric technique is to cool the liquid at a constant rate and extrapolate the linear portions of the volume-temperature relation above and below the transition region to their intersection. The temperature of this intersection is taken as T_g . It is obviously dependent on the cooling rate chosen but for a given cooling rate it is quite reproducible, and because of the marked temperature dependence of relaxation rates near T_g it does not vary that much with experimentally achievable cooling rates. A rate of $1^\circ/\text{min}$ is typical. The rate cannot be so fast that a sample of convenient size is appreciably nonuniform in

temperature. On the other hand, there is nothing to be gained by cooling much more slowly than sufficient to avoid temperature nonuniformity, as thermodynamic equilibrium is not achievable much below T_g on any experimentally accessible time scale.

The kinetics of the volume relaxation process are quite complex.²⁸ Experiments performed under linear conditions usually demonstrate a spectrum of relaxation times, and the dilatometric determination of T_g is invariably performed under nonlinear conditions. Roughly, T_g is the temperature at which some mean structural relaxation time (τ_v) has reached a characteristic value determined by the cooling rate chosen, but there is no precise relationship. The definition of T_g is retained because the experiment is easy to do, because of value of T_g is not very sensitive to cooling rate, and because the resulting T_g is a useful predictor of a variety of other relaxational properties. The statement above about a mean structural relaxation time is phenomenological and does not tell us how in a particular substance the molecular properties determine T_g . There is thus no contradiction between the above statement and the hypothesis that T_g occurs when the free volume fraction drops to some characteristic value.

The view that the liquid at T_g is an "iso-viscous" state with shear viscosity usually being implied is also an attempt at a phenomenological definition. The definition in terms of structural relaxation time is closer to the experimental reality and can be applied equally well to cross-linked polymers which do not possess a finite shear viscosity. However, in molecular liquids structural or volume relaxation times and shear relaxation times are almost equal to each other over wide variations of temperature and pressure;²⁹ also the effect of pressure on T_g , on dielectric relaxation time, or on shear viscosity in liquids in which it can be measured, is about the same. Again the "iso-viscous" definition is not in contradiction to the free volume theory, being a phenomenological rather than a molecular description.

Lately calorimetric methods have also been used for T_g determinations. The phenomenological basis is equivalent and the T_g 's by both methods usually agree.

It is important to keep in mind that T_g as so defined measures a relaxational or kinetic property, not a thermodynamic one. This is independent of the question of whether the glass transition is regarded as having a thermodynamic origin or not. Both the free volume theory⁸ and the entropy theory of Gibbs¹⁰ regard relaxational behavior as being intimately connected with the thermodynamic properties, and of course the use we intend to make of the equations of the paper is to help us decide which of these theories is closer to the truth.

It is also important to keep in mind that if we agree that what we want to measure by our determination of T_g is a relaxational property, the method of extrapolating two

- (22) J. L. Zakim, R. Simha, and H. C. Hershey, *J. Appl. Polym. Sci.*, **10**, 1455 (1966).
- (23) W. J. Schell, R. Simha, and J. J. Aklonis, *J. Macromol. Sci.*, **A3**, 1297 (1969).
- (24) J. Moacanin and R. Simha, *J. Chem. Phys.*, **45**, 964 (1966).
- (25) A. Eisenberg and S. Saito, *J. Chem. Phys.*, **45**, 1673 (1966).
- (26) H. Breuer and G. Rehage, *Kolloid Z. Z. Polym.*, **216-217**, 159 (1967).
- (27) Ichihara, Komatsu, Tsujita, Nose, and Hata, *Polym. J.*, **2**, 530 (1971).
- (28) M. Goldstein, "Modern Aspects of the Vitreous State," Vol. III, Butterworths, London, 1964, Chapter 4.
- (29) K. F. Herzfeld and T. A. Litovitz, "Absorption and Dispersion of Ultrasonic Waves," Academic Press, New York, N. Y., 1959.

straight lines to their intersection is only one way to do it. We could have defined T_g just as well as the point in the V - T curve at fixed cooling rate where d^2V/dT^2 has a maximum. We would have gotten about the same T_g as by the present definition except that it is more troublesome this way and we have not gained anything in return for the extra trouble. However, there is nothing sacrosanct about the intersection of two straight lines. It is the concept the definition attempts to embody that counts, not the definition.

V. Experimental Results for Volume

In Figure 1 we represent schematically the V - T relationships observed in isobaric cooling experiments at various fixed pressures. The decrease in volume in the liquid region observed between the samples under different pressures at a given temperature of course gives us the liquid compressibility. The relation of the difference in volume for the various glass samples to the glass compressibility is a more complicated question, which we hope to clarify in this paper. ABC represents isobaric cooling at atmospheric pressure (essentially zero pressure), and DEF, JKL cooling under successively higher pressures.

Analogous experiments can be done by increasing pressure at a fixed rate isothermally, producing a glass transition at a pressure P_g , which in turn will depend on the temperature of the experiment.¹⁵ We will not discuss them here.

In Figure 2 we represent the volumes at atmospheric pressure of the samples of liquid and glass observed under various pressures in Figure 1. Here the transition region must be excluded from consideration as the volumes are time dependent: the removal of a high pressure may convert a glassy sample into a relaxing liquid. The liquid of course returns on removal of pressure to its equilibrium volume and retains no memory of the high pressure to which it was exposed. ABC is the same as in the previous diagram.

The glasses, however, do retain a memory. Those formed under higher pressure have lower volumes at any given pressure and temperature below the transition range. This is an experimental fact for almost all glasses that have been tested so far, and it is not so far as I know disputed by any of the parties to the controversy over the definition of T_g or β_{g1} . The lines H and M thus represent the volumes at $P = 0$ of samples cooled under high pressures.

Figure 3 shows a three-dimensional representation of the V - P - T behavior of the liquid and of samples of glass prepared by cooling under various fixed pressures. Once the glasses are formed, the transition region is avoided, so that the volume of each sample is a single-valued function of P and T . The isobaric cooling paths ABC, DEF, and JKL are represented in Figure 1, and the zero pressure behavior by ABC and the lines H and M in Figure 2.

For simplicity, both in the figures and in the subsequent discussion, it is assumed that the liquid surface and the various glass surfaces are planes of small slope and that the glass surfaces V_1, V_2, V_3, \dots are parallel. Also, the transition from liquid to glass is shown as a sharp break, instead of a rapid but continuous change in slope. As we noted before, the experimental fact is that the glass surfaces are displaced vertically from each other in this diagram. There is no *a priori* reason why the surfaces could not have coincided, and indeed, if the free volume

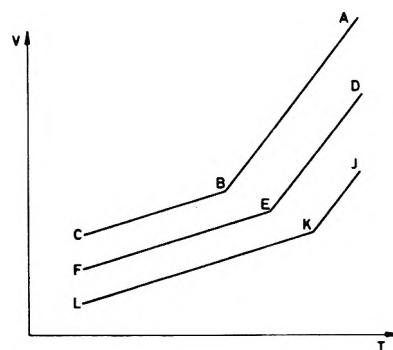


Figure 1. V - T relationship for a liquid cooled under various pressures. ABC represents a cooling curve at $P_1 = 0$. B is the transition, shown here schematically as a sharp break. DEF and JKL represent experiments done under successively higher pressures P_2 and P_3 .

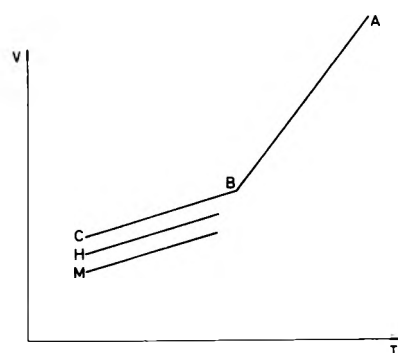


Figure 2. V - T relationship at zero pressure. ABC is the isobaric cooling curve under $P_1 = 0$, H and M representing the volumes at $P = 0$ of glasses cooled through the transition region at P_1 and P_2 .

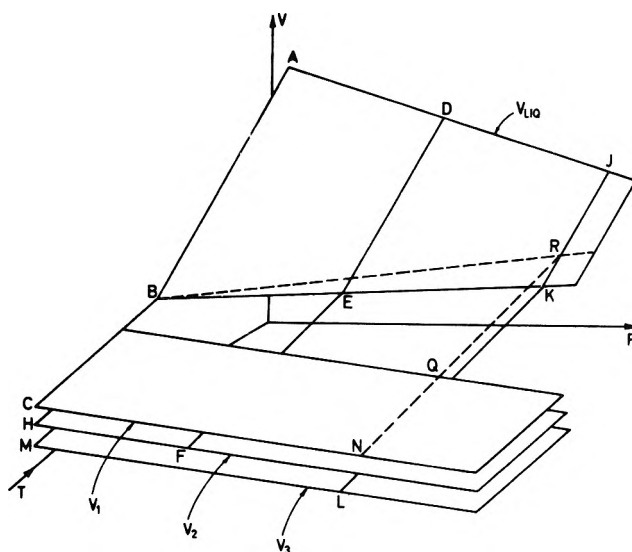


Figure 3. V - T - P relationship of a liquid and the various glasses that can be made from it. ADJ KEB is the V - T - P relationship of the equilibrium liquid (schematically represented as a plane surface). ABC, DEF, JKL are isobaric cooling curves for $P_1 = 0$, $P_2 > P_1$, and $P_3 > P_2$, respectively. These three cooling procedures produce glasses whose V - T - P behavior is represented by the parallel surfaces V_1, V_2 , and V_3 .

frozen in at the glass transition temperature T_g at various pressures were a constant, they would have. The experimental fact that they do not is evidence against the free volume theory.

Let us use the usual definitions of the thermodynamic second derivative properties of the samples of glass. The slope of the V surfaces of the glasses in the direction of increasing T is $V\alpha_{g1}$ and of increasing P is $-V\beta_{g1}$. As we argued before, for testing the correctness of one-parameter thermodynamic theories these are the correct definitions to use.

According to this definition, a change in the free volume fraction df would be given by

$$df = \Delta\alpha dT - \Delta\beta dP \quad (8)$$

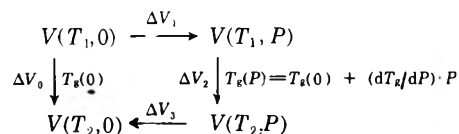
In Figure 3 the glass transition takes place (as we have defined it) along the line BEK. The projection of this line on the P - T plane has the slope dT_g/dP (Figure 4).

If $T_g(P)$ also coincides with constant f , we have

$$dT_g/dP = (\partial T/\partial P)_f = \Delta\beta/\Delta\alpha \quad (9)$$

It is an experimental fact that this equation does not hold, $\Delta\beta/\Delta\alpha$ usually being about 2 or more times greater than dT_g/dP . It was pointed out by Maurer³ and by Bueche⁴ and by Gee⁷ that its failure is equivalent to the observation that glasses prepared by cooling under different pressures have different volumes at a given T and P below the transition range. The proof is simple, upon consideration of Scheme I.

Scheme I



We compare the final volumes of two samples of glass, one which has been cooled at zero pressure from a temperature T_1 in the liquid state to a final temperature T_2 in the glassy state; the second has been compressed as a liquid to a pressure P , cooled under constant pressure to T_2 , undergoing its transition at $T_g(P) = T_g(0) + (dT_g/dP) \cdot P$ and then decompressed at T_2 to $P = 0$.

The volumes of the two samples at T_1 and $P = 0$ are of course equal. The first undergoes a volume change ΔV_0

$$\Delta V_0 = V\alpha_{liq}[T_g(0) - T_1] + V\alpha_{gl}[T_2 - T_g(0)] \quad (9.a)$$

The second undergoes a volume change $\Delta V_p = \Delta V_1 + \Delta V_2 + \Delta V_3$

$$\Delta V_1 = -V\beta_{liq} \cdot P \quad (9.b)$$

$$\Delta V_2 = V\alpha_{liq}[T_g(0) + (dT_g/dP) \cdot P - T_1] + \quad (9.c)$$

$$\begin{aligned} & V\alpha_{gl}[T_2 - T_g(0) - (dT_g/dP) \cdot P] \\ & \Delta V_3 = V\beta_{gl} \cdot P \end{aligned} \quad (9.d)$$

we find

$$(V_0 - \Delta V_p)/V = [\Delta\beta - \Delta\alpha(dT_g/dP)P] \quad (10)$$

which vanishes only if $\Delta\beta/\Delta\alpha = dT_g/dP$. Experimentally $\Delta\beta/\Delta\alpha$ is greater than dT_g/dP , implying that glasses prepared under high pressures have lower volumes.

The free volume theory has had some success in describing the temperature dependence of viscosity and other relaxation phenomena and besides has the merit of considerable intuitive plausibility in a field where rigorous molecular theories are unlikely to appear for some time. Those who accept it have quite reasonably been led to a

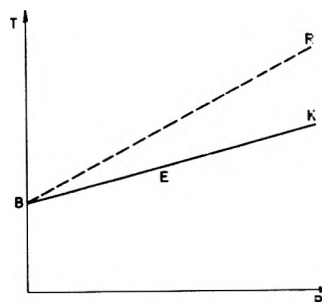


Figure 4. Projection onto the P - T plane of the transition lines $T_g(P)$ (BEK) and $T_g^*(P)$ (BR).

reexamination of the experimental quantities in eq 1 to see if alternate definitions can enable the equation to hold.

Some of these attempts have basically treated $\Delta\beta$ or $\Delta\alpha$ as adjustable parameters and have of course succeeded. Others have not been so arbitrary and require more serious analysis.¹¹⁻¹⁵

It has been proposed that T_g under a pressure P not be defined by dilatometric isobaric cooling curves, but rather by mathematically extrapolating the glass surface along a line of constant P to its intersection with the liquid surface. In Figure 3, line NQ is extrapolated to its intersection with the plane V_{liq} at point R; the locus of such intersections of V_1 with V_{liq} is shown as line BR. It should be noted that point B is T_g at $P = 0$, the pressure the sample was formed. However, at higher pressure the temperatures of intersection differ from $T_g(P)$ as measured by isobaric cooling. Let us call these temperatures $T_g^*(P)$. The projection of $T_g^*(P)$ on the P , T plane is a line with slope dT_g^*/dP , which coincides with T_g as ordinarily defined only at $P = 0$ (Figure 4). It has been noted that this definition of T_g leads to

$$dT_g^*/dP = \Delta\beta/\Delta\alpha \quad (11)$$

being satisfied.

However, it has not been generally realized that the "experimental" result is exact because it is a tautology. It is a purely geometric consequence of the hypothesis that the two planes V_1 and V_{liq} intersect, and contains no new information not already implied by the definition of $T_g^*(P)$ as the intersection of the planes. The proof of this will be given below.

While this is a matter of definition, it should be clear that the T_g^* so defined tells us nothing whatever about the effect of pressure on relaxation. It should be obvious that in the procedure proposed for defining it, a relaxational property has been measured only at $P = 0$, not at any other pressure.

In fact experimentally if glass V_1 is heated under a high pressure P at a fixed rate, it begins to relax at lower temperatures than T_g^* , as noted by Bianchi, *et al.*,¹² who therefore required that T_g be obtained by extrapolating across the transition region from low temperatures rather than by direct measurement. The definition proposed by Bianchi thus retains the intersection of two straight lines but drops the relationship to structural relaxation.

A second proposal is as follows. Consider a plane V^* that contains the lines BC, EF, KL, that represent the V - T relationship in the glassy state for isobaric cooling. While this plane does not represent the volume of any single chemical substance, but rather is the envelope of the

isobaric cooling lines of an infinite series of glasses which differ in their volumes at any P and T , it does indeed possess derivatives with respect to P and T .

$dV^*/dT = V\alpha_{g1}$ as before but $dV^*/dP \neq -V\beta_{g1}$ as previously defined. Define β_{g1}^* by $dV^*/dP = -V\beta_{g1}^*$ and $\Delta\beta^*$ as $\beta_{liq} - \beta_{g1}^*$. V^* , if extrapolated to its intersection with V_{liq} , intersects along the transition line $T_g(P)$ as it is defined dilatometrically. Using this definition we find

$$dT_g/dP = \Delta\beta^*/\Delta\alpha \quad (12)$$

is satisfied. Again this is a tautology.

We have defined $\Delta\alpha$ by assuming the liquid and glassy states are represented by two intersecting plane surfaces. The tautological character of this equation was pointed out by Passaglia and Martin.³⁰ A simple proof adapted from their paper applicable both to eq 11 and 12 is as follows. Consider the planes $z_1(x,y)$ and $z_2(x,y)$ known to intersect at x_0, y_0 . What is the equation of their line of intersection? Let x_0, y_0 be the coordinates of a point where the surfaces are known to intersect. Then

$$z_1(x_0, y_0) = z_2(x_0, y_0)$$

$$dz_1 = (\partial z_1/\partial x)dx - (\partial z_1/\partial y)dy$$

$$dz_2 = (\partial z_2/\partial x)dx + (\partial z_2/\partial y)dy$$

Along the intersection $dz_1 = dz_2$.

The relationship between x and y along the intersection is thus

$$dx/dy = -\frac{\left(\frac{\partial z_2}{\partial y}\right) - \left(\frac{\partial z_1}{\partial y}\right)}{\left(\frac{\partial z_2}{\partial x}\right) - \left(\frac{\partial z_1}{\partial x}\right)} \quad (13)$$

On setting $x = T$, $y = P$, $z_2 = V_{liq}$, $z_1 = V^*$, eq 12 results.

A similar analysis applies if dx/dy is set equal to dT_g^*/dP . "Experimental" comparisons of dT_g^*/dP with $\Delta\beta/\Delta\alpha$ or of dT_g/dP with $\Delta\beta^*/\Delta\alpha$ will of course not necessarily give exact numerical equality, as a result of rounding-off errors, estimation of derivatives by finite differences, etc.

To summarize: the failure of eq 1 to hold is equivalent to the fact that there is not a single glass surface but a family of parallel surfaces. If it had happened that there were a single surface V_{g1} for all glasses, lines BEK and BR would coincide and eq 1 would hold.

The failure of eq 9 to hold has been sometimes reconciled with free volume theory by suggesting that along the transition line $T_g(P)$ the order parameter Z , here being equivalent to free volume, is not remaining constant. Bianchi¹¹ and Quach and Simha¹⁵ have proposed a correction term dV_f/dT along the transition line, which eliminates the discrepancy. In my view, this evades the question. The great strength of the free volume theory lay in its apparent success in explaining T_g as a point of constant free volume. If this is taken away, what is left?

VI. Experimental Results for Entropy

A similar analysis can be applied to the entropy surfaces S . The slopes of these surfaces in the T and P directions are C_p/T and $-V\alpha$, respectively. Most glasses that have been examined obey the equation analogous to (1)

$$dT_g/dP = TV\Delta\alpha/\Delta C_p \quad (14)$$

This may not be general: Angell has found that $ZnCl_2$ glass does not obey it³¹ and Breuer disputes it for polysty-

rene²⁶ although he is again contradicted by Ichihara.²⁷ If, however, it is generally true, it in turn implies that glasses prepared under different pressures all have the same entropy at a given T and P below the transition range, or in other words that there is a single surface S_{g1} and not a set of parallel surfaces.

Again, that this is the experimental situation for most glass formers that have been studied is not disputed. Further, that this is so can hardly be irrelevant to the relative merits of free volume theory and the entropy theory of Gibbs.

If the classic definitions are used, as has been proposed here, the experimental situation is summarized by

$$dT_g/dP \cong TV\Delta\alpha/\Delta C_p < \Delta\beta/\Delta\alpha \quad (15)$$

While we may redefine some of the above quantities to satisfy an equation similar in appearance to (1), we will be concealing from ourselves an important aspect of reality.

VII. The Simha-Boyer Relation

If it is assumed that the Simha-Boyer product $\Delta\alpha \cdot T_g$ should be constant for a single substance as pressure is varied, a prediction of dT_g/dP is readily obtained

$$dT_g/dP = - (T_g/\Delta\alpha)d\Delta\alpha/dP \quad (16)$$

Recent very careful measurements by McKinney³² on polyvinyl acetate permit a test of this relation. His results show that at low pressures $\Delta\alpha = 4.3 \times 10^{-4}/^\circ K$, $d\Delta\alpha/dP = 1.0 \times 10^{-4}/^\circ K\text{-kbar}$, and $T_g = 304^\circ K$. dT_g/dP is thus predicted to be $70^\circ K/\text{kbar}$. $\Delta\beta/\Delta\alpha$ was found to be $48^\circ K/\text{kbar}$. McKinney's measured value for dT_g/P is $26.6^\circ K/\text{kbar}$. Specific heat data on McKinney's sample of polyvinyl acetate were not available. O'Reilly, in his paper first pointing out the approximate validity of eq 14, gave $22^\circ K/\text{kbar}$ for dT_g/dP and $25^\circ K/\text{kbar}$ for $TV\Delta\alpha/\Delta C_p$. He determined dT_g/dP by dielectric relaxation and he used literature values for $\Delta\alpha$ and ΔC_p .

VIII. Energy Considerations

We close by noting that eq 14 is also consistent with an energy model of the transition. Let us represent the energy E as a function of the variables P , T . We have

$$(\partial E/\partial T)_P = [\partial(H - PV)/\partial T]_P = C_p - PV\alpha \quad (17)$$

$$(\partial E/\partial P)_T = (\partial E/\partial V)_T(\partial V/\partial P)_T = VT\alpha + PV\beta \quad (18)$$

In the limit of low pressures, and for condensed phases, the quantities $PV\alpha$ and $PV\beta$ are negligible, and eq 14 would imply that glasses prepared under various pressures have the same energy as well as the same entropy. It would take more careful experiments over a wider range of P and T than have so far been performed to distinguish between an entropy and an energy description of the glass transition.

Acknowledgment. Support by the Owens-Illinois Foundation and the hospitality of the Department of Mechanics of the Technion—Israel Institute of Technology are gratefully acknowledged.

(30) E. Passaglia and G. M. Martin, *J. Res. Nat. Bur. Stand.*, **68A**, 273 (1964).

(31) C. A. Angell, personal communication.

(32) J. E. McKinney, unpublished data.

An Alternating Current Conductivity Method for Studies of Pulse Radiolysis in Aqueous Solutions. Determination of the State of Ionization of Several e_{aq}^- Adducts^{1a}

J. Lilie and Richard W. Fessenden*^{1b}

Radiation Research Laboratories, Center for Special Studies, and Department of Chemistry, Mellon Institute of Science, Carnegie-Mellon University, Pittsburgh, Pennsylvania 15213 and Hahn-Meitner Institut für Kernforschung Berlin GmbH, Sektor Strahlenchemie, 1 Berlin 39, Germany (Received October 12, 1972)

Publication costs assisted by The Carnegie-Mellon University and the U. S. Atomic Energy Commission

An ac method for detecting conductivity changes in aqueous solution produced by pulse radiolysis is described. This method is applicable with constant sensitivity to solutions of up to 10^{-2} M of ionic solute and hence can be used in the range pH 2-12. The sensitivity corresponds to a signal-to-noise ratio of 10 for a product H^+ ion concentration of 10^{-6} M. The response time is $<2 \mu\text{sec}$. Initial applications described here are to the radicals formed by scavenging of e_{aq}^- by the pairs of compounds *o*- and *p*-nitrophenol, maleate-fumarate, and phthalate-terephthalate. In each case it is demonstrated that the e_{aq}^- adduct of the first member of the pair retains an otherwise dissociable proton at pH >11 while the radical formed from the second member of the pair is essentially fully dissociated at pH 11. In the cases of fumarate and terephthalate a decrease in the conductivity change is found at lower pH which can be interpreted in terms of the equilibrium for dissociation of the final proton to give the trianion. The pK values are 10.7 and 10.1, respectively. The results are in agreement with esr data on these systems and demonstrate the unusual stability of the proton in those radicals which can form an intramolecular hydrogen bond.

Introduction

Conductivity changes in aqueous solutions have provided a method of investigating the reactions in pulse irradiated solutions which is often complementary to optical detection techniques.^{2,3} The method is specific for the state of ionization of the transient species so that the extra information provided is of great value when combined with optical results. Often the combination can provide essentially complete identification of the transient species where the optical results alone are not unambiguous. Much of the work which has been reported is based on conductivity as sensed by dc currents. The main limitation of this approach is that ionic solutes above $\sim 10^{-4}$ M cannot be studied conveniently because of the high conductivity of the solution before irradiation. Even at this level only small percentage changes in cell resistance occur and the sensing current is likely to cause electrolysis of the sample solution.

These limitations are particularly evident in a study of the dissociation of the e_{aq}^- adducts the three isomeric nitrophenols.⁴ In that paper, Grünbein and Henglein found conductivity changes in the region pH 9-10 (*i.e.*, near the upper pH limit) which were interpreted in terms of the equilibrium for dissociation of the phenolic proton of the radicals and pK values were assigned on this basis. Subsequent esr investigations⁵ have shown very clearly that while the para and meta isomers are dissociated in basic solution the ortho isomer remains undissociated to pH 14. As a result considerable doubt exists as to the correctness of results obtained by this method near the ends of its useful pH range. The conclusion makes clear the value of a conductivity method which is valid in solutions contain-

ing a high background concentration of ionic solute. The purpose of the present paper is to describe an ac conductivity detection system which can be applied to solutions of up to 10^{-2} M of ionic solute and to demonstrate the method in the cases of the two nitrophenols and several related systems.

Experimental Section

The approach used here is derived from an application of 10-MHz conductivity to detect a moving boundary in studies of transference.⁶ In that work contact with the solution was avoided by use of capacitance coupling to the solution from electrodes on the outside of the glass cell. Initial attempts in the present work to use that type of cell were not very satisfactory because the series combination of electrode-solution capacitance and solution resistance did not allow sufficient voltage drop across the solution resistance and seriously lowered the sensitivity. This problem was overcome by reverting to a cell with internal parallel electrodes. To maintain a constant sensitivity up to high electrolyte concentrations it was necessary to use electrodes with a small surface area. The design finally adopted has parallel electrodes of 0.5-mm platinum wire 1 cm long and 2 cm apart and gives a resistance of $\sim 100 \Omega$

- (1) (a) Supported in part by the U. S. Atomic Energy Commission. (b) Address correspondence concerning this work to Carnegie-Mellon University, Pittsburgh, Pa. 15213.
- (2) G. Beck, *Int. J. Radiat. Phys. Chem.*, **1**, 361 (1969).
- (3) See, *e.g.*, K.-D. Asmus, *Int. J. Radiat. Phys. Chem.*, **4**, 417 (1972).
- (4) W. Grünbein and A. Henglein, *Ber. Bunsenges. Phys. Chem.*, **73**, 376 (1969).
- (5) K. Eiben and R. W. Fessenden, *J. Phys. Chem.*, **75**, 1186 (1971).
- (6) K. S. Pribadi, Ph.D. Dissertation, Carnegie-Mellon University, 1971; *J. Solution Chem.*, **1**, 455 (1972).

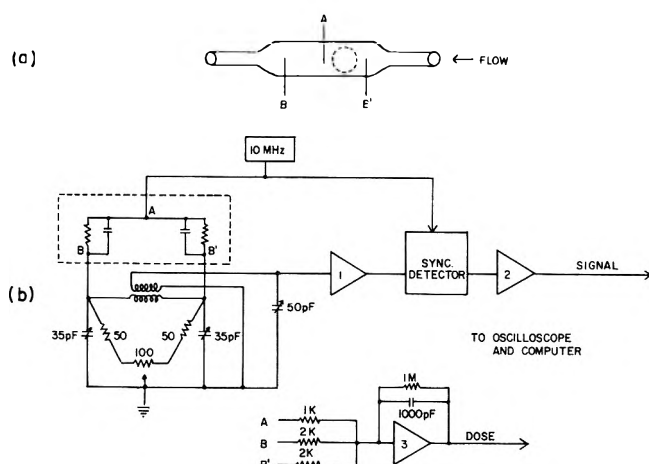


Figure 1. (a) Conductivity cell showing the two sections (AB and AB'). The approximate size and location of the irradiation zone are shown by the dashed circle. The cell was fabricated from 1-cm square tubing and the electrodes are separated by 2 cm so little or no electron beam is incident on the electrodes. (b) Schematic representation of the conductivity circuit. The 10-MHz bridge is at the left with the equivalent circuit of the cell enclosed in a dashed line. The dose measuring circuit is connected to the bridge at the three points indicated. The amplifiers, 1, 2, and 3 are Motorola MC1510G, MC1439G, and Fairchild Controls ADO-84/10 (FET input), respectively. The synchronous detector is a Motorola MC1596G.

at 10^{-1} M KOH. The cell has two approximately matched sections as shown in Figure 1a. The center electrode is used as for the 10-MHz input and the two sections are connected in a bridge as in Figure 1b. Irradiation is in only one of the two sections. This overall changes in sample affect both arms of the bridge in the same way and are largely balanced out while changes produced in the pulse radiolysis occur in one arm only.

Operation at 10 MHz was considered a convenient compromise between circuit design (easier for lower frequencies) and the need for a sufficiently high frequency to allow response in the $1\text{-}\mu\text{sec}$ region. The detection circuit used is shown in Figure 1b. It consists of an input transformer, amplifier, and balanced mixer to provide phase-sensitive detection. This form of detection provides a signal with a sign which depends on the direction of imbalance of the bridge and responds only to changes in cell resistance. Because only dc amplification is provided after the phase-sensitive detector it is possible to monitor conductivity changes occurring at times of up to seconds after the pulse.

Radiolysis was with a pulse of 2.8-MeV electrons from a Van de Graaff accelerator. The usual pulse length was 0.5 μsec . The absorbed dose given the sample was monitored by integrating the instantaneous voltage produced by the electron beam current which appears across resistors in the ground return of the bridge. It was found that the collected charge depended slightly on the conductivity of the solution so all solutions contained 10^{-4} M NaClO₄ or Na₂SO₄ if they were not otherwise conducting. For the work described here a continuous flow of solution was maintained through the cell at $0.5\text{--}1\text{ cm}^3\text{ sec}^{-1}$.

The output of the conductivity detector and the beam current monitor are processed by a Digital Equipment Corp. PDP-8 computer in a fashion very much like that used for the polarography work reported earlier.⁷ The output, which is proportional to conductivity change, is sampled⁸ at 20 equally spaced time intervals and the values

stored digitally. A base-line reading before the irradiation pulse is also provided. The change in voltage of the beam current monitor is also read before and after the pulse. The measured conductivity voltage is divided by the output corresponding to the integrated electron beam current and scaled by the expected radiation chemical yield and a further calibration factor to provide direct values of equivalent conductance. This calibration factor is chosen from the results on a system of known chemistry such as the reaction of e_{aq}^- with methyl chloride.⁹ The approximate constancy of this factor from day to day showed that variations in cell positioning under the beam port do not greatly affect the results. Provision exists for averaging the results of a number of experiments on the same sample for improvement of signal-to-noise ratio. Output from the computer is provided both to an oscilloscope display and to an X-Y recorder.

Typical doses corresponded to the formation of $\sim 5 \times 10^{-6}$ M of product with $G = 3$. For a system such as CH₃Cl in acid solution, which has a large conductivity change ($\Delta\Lambda = 425$), the signal-to-noise ratio was 10 for 1×10^{-6} M of product. The sensitivity seems to be about a factor of 10 less than obtainable with the dc method. In the present work most curves of conductivity change were averaged four times for some improvement in signal-to-noise ratio before being plotted.

The experiments were carried out at 25°. Chemicals were of the purest grade commonly obtainable and were used without further purification. Most were the same as had been used in the esr experiments. The water was doubly distilled. Solutions were deoxygenated by bubbling with Baker ultra pure nitrogen or, for the calibration runs, with CH₃Cl (Matheson Co.). The pH was adjusted with HClO₄ or NaOH.

Results and Discussion

The reaction



was used as a calibration and to verify the behavior as a function of pH. In acid solution the conductance change for each electron scavenged should correspond to an equivalent conductance of $\Delta\Lambda = 425 \Omega^{-2} \text{ cm}^2 \text{ equiv}^{-1}$ ¹⁰ for the net formation of $\text{H}^+ + \text{Cl}^-$. The yield for this reaction is taken⁹ as $G = 3.1$ because of the high concentration of methyl chloride in a saturated solution (0.1 M). Data for CH₃Cl at pH ~ 6 with 10^{-4} M NaClO₄ are shown in Figure 2 with an interpoint spacing of 5 μsec . From the fact that the first point has reached $>90\%$ of the final value it is clear that the response half-time is $<2 \mu\text{sec}$. The average deviation is ~ 10 units with a maximum deviation of about 20 units so that relative measurements appear to be reliable at the several per cent level. In basic solution the conductance change corresponds to production of Cl^- and removal of OH^- and should give $\Delta\Lambda = -125$. Data for CH₃Cl in basic solution show conductivity changes of -160 , -170 , and -140 units for pH 10.2, 11.7,

(7) J. Lillie, *J. Phys. Chem.*, **76**, 1487 (1972).

(8) J. M. Warman, R. W. Fessenden, and G. Bakale, *J. Chem. Phys.*, **57**, 2702 (1972).

(9) T. I. Balkas, J. H. Fendler, and R. H. Schuler, *J. Phys. Chem.*, **74**, 4497 (1970).

(10) Values for equivalent conductance at 25° tabulated in the "Handbook of Chemistry and Physics," Chemical Rubber Publishing Co., Cleveland, Ohio, 1966–1967, p D89, are H^+ , 350; OH^- , 192; Cl^- , 75 ($\Omega^{-1} \text{ cm}^2 \text{ equiv}^{-1}$). The value for $\text{C}_6\text{H}_5\text{NO}_2^-$ is 403 and is typical of that of large anions.

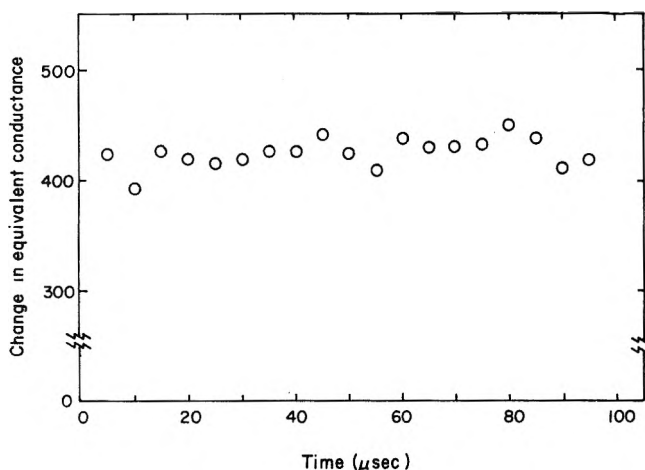
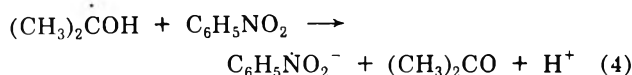
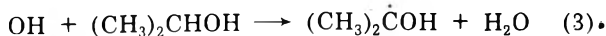
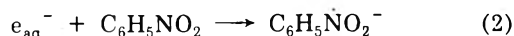


Figure 2. Voltage change from the conductivity detector following pulse radiolysis of a saturated aqueous solution of CH_3Cl containing $10^{-4} M$ NaClO_4 ($\text{pH} \sim 6$). The curve represents the average obtained with four pulses as accumulated by the computer. The yield for $e_{\text{aq}}^- + \text{CH}_3\text{Cl}$ is taken as 3.1 and the calibration factor adjusted to give $\Delta\Lambda = 425$.

and 12.1, respectively. In this case no further adjustment of the calibration was made so a direct comparison between basic and acid solution is possible. The conductivity change (-160) is somewhat higher than the expected -125 . The values are quite constant and only a moderate decrease is observed at $\text{pH} 12.1$. A decrease in response is expected under these conditions because here the cell resistance becomes comparable to that of the other arms of the bridge.

As a test of the system for basic solutions an experiment was carried out with nitrobenzene ($\sim 10^{-3} M$) in the presence of isopropyl alcohol ($0.1 M$). The reactions here are³



so that the yields of both e_{aq}^- and OH lead to production of $\text{H}^+ + \text{C}_6\text{H}_5\text{NO}_2^-$ with a total yield of 6. The data from this experiment ($\text{pH} 10$) are shown in Figure 3 and give a conductivity change of $-170 (\pm 10)$. The expected value is -160 showing excellent agreement.

All of the systems to be studied involved e_{aq}^- adducts so that experiments were done with $0.1 M$ *tert*-butyl alcohol present to avoid complications from OH reaction products. Appropriate blank experiments were carried out with only $0.1 M$ *tert*-butyl alcohol and a typical result is shown in Figure 3. The curve ($\text{pH} 11$) shows an initial change of -30 and values of -15 for times from 20 – $100 \mu\text{sec}$ after the pulse. The amplitude of this change was reproducible and approximately constant with dose so it contributed less at higher doses.

The problems which were selected for further investigation were suggested by the disagreement between esr and dc conductivity results mentioned above for *o*-nitrophenol and all involved the question of the state of ionization of the e_{aq}^- adduct. Thus data were sought on the isomeric pairs maleate–fumarate^{11,12} and phthalate–terephthalate¹³ which have also been studied by esr. Under the pH conditions used, the reactions in the case of the nitrophen-

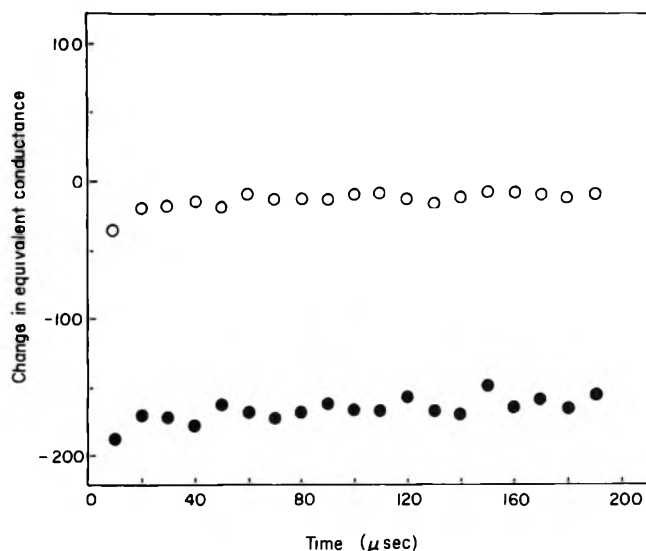
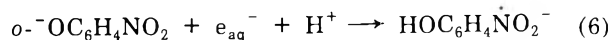
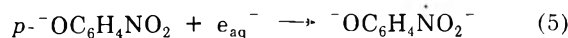


Figure 3. Conductivity changes produced in solutions of $0.1 M$ *tert*-butyl alcohol at $\text{pH} 10.8$ (O) and $\sim 2 \times 10^{-3} M$ nitrobenzene containing $0.1 M$ 2-propanol at $\text{pH} 10.0$ (●). Curves are averages of four runs and the doses are similar. The amplitude of the upper curve is scaled for $G = 2.80$ while that for nitrobenzene (lower) is for $G = 6.0$.

nols should be



The data of Table I show complete agreement with this expectation. The behavior of the para isomer is like that of nitrobenzene itself in showing a decrease of conductivity corresponding to removal of OH^- by H^+ . In the case of the ortho isomer the H^+ is incorporated into the radical product and essentially no net change is observed. The behavior of the pairs maleate–fumarate and phthalate–terephthalate should be similar on the basis of the esr results which show in each case a hyperfine splitting by an acid proton for the e_{aq}^- adduct to the first member of the pair. The data of Table I support this conclusion fully. It is worthwhile noting that a sequence of reactions is involved in the case of the undissociated species such as with *o*-nitrophenoxide. On the $1\text{-}\mu\text{sec}$ time scale one has the e_{aq}^- scavenging and $\text{H}^+ + \text{OH}^-$ reactions and subsequently the protonation of the phenoxide anion radical by water. From the fact that no large conductivity change is observed for times 5 – $10 \mu\text{sec}$ after the pulse it must be concluded that this protonation is completed in very short times.

While the results for fumarate and terephthalate in Table I show essentially the full change expected at high pH , a lower change is found at $\text{pH} \sim 10$. More complete data taken at a number of pH values are shown in Figure 4.¹⁴ These curves can be interpreted in terms of the equilibrium associated with the dissociation of the last readily dissociable proton to give the trianion radical ($-\text{O}_2\text{C}-\text{CHCHCO}_2^-$). The pK values are found from the curves to be 10.7 for fumarate and 10.1 for terephthalate. These values are consistent with esr data in that for fumarate a

(11) P. Neta, *J. Phys. Chem.*, **75**, 2570 (1971).

(12) P. Neta and R. W. Fessenden, *J. Phys. Chem.*, **76**, 1957 (1972).

(13) P. Neta and R. W. Fessenden, *J. Phys. Chem.*, **77**, 620 (1973).

(14) These data were taken on another version of the apparatus constructed at the Hahn-Meitner Institut für Kernforschung, Berlin, West Germany.

TABLE I: Conductivity Changes Following Pulse Radiolysis^a

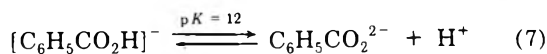
Compound ^b	pH	$\Delta\Lambda^c$
<i>p</i> -OC ₆ H ₄ NO ₂	10.9	-170
	11.9	-160
<i>o</i> -OC ₆ H ₄ NO ₂	10.7	-18
	11.5	-20
Fumarate	10.0	-60
	10.6	-120
	11.0	-100
	11.2	-160
Maleate	10.5	-12
	11.5	-16
Phthalate	11.0	-11
	11.6	-24
Terephthalate	10.3	-50
	10.7	-110
	11.2	-140
Benzoate	10.0	-30
	10.7	-50
	11.1	-120

^a Values pertain to the approximate time period 30–100 μ sec after the pulse and were obtained by averaging the data of four runs. Correction was made for the change of -15 units observed with *tert*-butyl alcohol alone. ^b Concentration $1-2 \times 10^{-3}$ M. Solutions also contained 0.1 M *tert*-butyl alcohol. ^c In units of $\Omega^{-1} \text{cm}^2 \text{equiv}^{-1}$.

change in the spectrum is observed over the region pH 10–11.¹⁵ Similarly, the esr data for terephthalate¹³ show a change in the spectrum around pH 9–10.

Experiments were also carried out with maleic and fumaric acids in acid solution. In each case 2×10^{-3} M acid was half-neutralized by addition of an equal concentration of NaOH. The results at pH 3.0 and 3.6, respectively, show a significant decrease in conductivity by 100–160 units. A quantitative interpretation of the decrease is difficult because of the buffering action of the acids but the fact that a decrease is observed shows that the net reaction involves some take-up of H⁺ in addition to incorporation of the radiolytically produced $e_{aq}^- + H^+$. The radicals should exist, therefore, as partially dissociated for the first dissociation. This result is consistent with the esr results¹⁶ which show spectra clearly attributable to the singly charged radicals at pH 4–5 and changes in the spectra between this region and more strongly acid solutions.

Benzoate was studied as a final example. Here optical pulse radiolysis data¹⁷ show the second p*K* of the e_{aq}^- adduct to be near 12



The conductivity results in Table I are consistent with this interpretation in that no conductivity change is observed in the region pH 9–10 indicating incorporation of both e_{aq}^- and an equivalent amount of H⁺ into the radical. The existence of a larger change at pH 11.1 suggests the shift of equilibrium 3 to the right in agreement with the optical data. The change is occurring at a somewhat lower pH than expected, however.

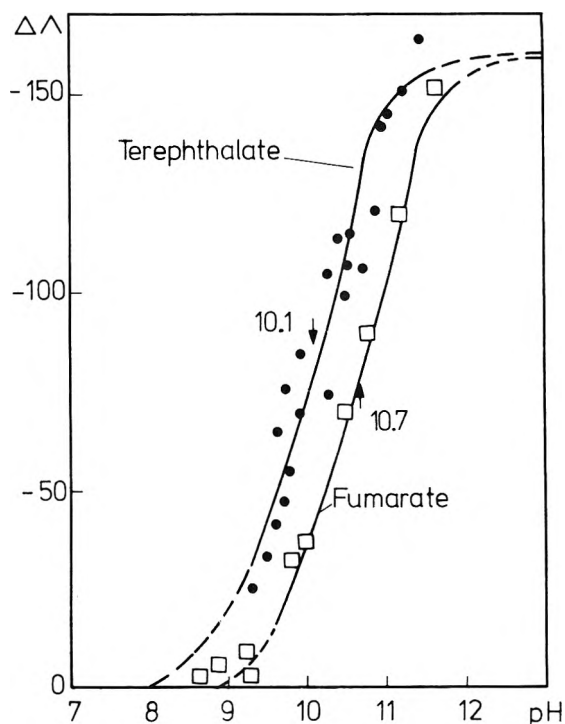


Figure 4. Changes in equivalent conductance produced by pulse irradiation of solutions of fumarate and terephthalate. The p*K* values at the midpoints of these curves are indicated by the arrows.

Conclusion

The preceding results show very clearly that high-frequency ac conductivity methods are applicable for studying conductivity changes following pulse radiolysis and can significantly extend the region available for study to pH 2–12. Although some loss of sensitivity over the dc method occurs, the sensitivity is still adequate for most purposes and does not require an excessive radiation dose per pulse. The response time of this detection system has not been investigated in detail but it is estimated to be <2 μ sec and may be slightly superior to that of the dc method. Because of the 10-MHz carrier frequency there is also less potential for interference produced by direct collection of the electron pulse. The dc coupling after the phase-sensitive detector makes it possible to monitor conductivity changes at long times after the pulse. This feature may be of use in certain special instances.

The chemical results obtained clearly show that while the e_{aq}^- adducts of *o*-nitrophenol, maleate, and phthalate contain a potentially dissociable proton, this proton in fact does not dissociate up to pH 12. These results are in agreement with esr results which show no dissociation to pH 14. The special stability of these radicals toward dissociation appears to be the result of the intramolecular hydrogen bond.

(15) A previous study¹¹ reported the esr spectrum of the e_{aq}^- adduct to be the same over the pH range 7–14. More recent work (O. P. Chawla, unpublished results) shows that a spectrum is found in the pH region 9–10 which is clearly assignable to the singly protonated radical.

(16) N. H. Anderson, A. J. Dobbs, D. J. Edge, R. O. C. Norman, and P. R. West, *J. Chem. Soc. B*, 1004 (1971).

(17) M. Simic and M. Z. Hoffman, *J. Phys. Chem.*, **76**, 1398 (1972).

Effect of Water on the Titanium Complexes in Methanolic Solutions Containing Hydrogen Chloride

E. P. Parry,* I. B. Goldberg,* D. H. Hern, and W. F. Goepfinger

North American Rockwell Science Center, Thousand Oaks, California 91360 (Received October 16, 1972)
Publication costs assisted by the North American Rockwell Corp.

The electrochemical behavior of the Ti(III)|Ti(IV) couple was investigated in methanol solutions containing 0.02–0.22 *M* chloride ion and 0.02–7.0 *M* water. The presence of two electrochemically distinct Ti(III) complexes was observed and the mechanism of the electrode processes was shown to consist of the reactions $e^- + \text{Ti(IV)} \rightleftharpoons \text{Ti(III)(a)}$ ($E_{1/2} \sim -0.4$ V); $\text{Ti(III)(a)} + \text{H}_2\text{O} \rightleftharpoons \text{Ti(III)(b)} + \text{Cl}^-$ (K); $\text{Ti(III)(b)} \rightleftharpoons \text{Ti(IV)} + e^-$ ($E_{1/2} \sim 0.1$ V). The equilibrium constant *K* was evaluated from pulse polarographic and cyclic voltammetric data to be 0.029 ± 0.006 . The reaction rates have been calculated from the kinetic contribution to the kinetic polarographic current, and the parameters k_s and α of the first electron transfer reaction were estimated from pulse polarographic data. Combining these results with electron spin resonance measurements, the species Ti(III)(a) comprised $[\text{TiCl}_2(\text{CH}_3\text{OH})_4]^+$ and $[\text{TiCl}(\text{CH}_3\text{OH})_5]^{2+}$. These two species equilibrate rapidly on an electrochemical time scale. Ti(III)(b) was assigned the structure $[\text{TiCl}(\text{CH}_3\text{OH})_4\text{H}_2\text{O}]^{2+}$. In addition, the Ti(IV) in methanol containing more than 0.3 *M* H₂O contains at least one more water ligand than the Ti(III), based on the negative shift of the half-wave potential with the concentration of water.

Introduction

A recent paper from this laboratory reported the oxidation state of titanium after electrochemical dissolution in methanol–HCl solutions.¹ Some evidence was given in this work to suggest that in the presence of more than 0.5% water Ti(III) gave two electrochemically distinguishable complex species. Electron spin resonance (esr) results, which have recently been obtained in this laboratory,² have indicated that in dilute solutions of TiCl₃ in anhydrous methanol, two distinct Ti(III) complexes are distinguishable at low temperatures.

Other electrochemical studies of the Ti(III)|Ti(IV) couple in nonaqueous solvents^{3–5} have been reported. This couple has also been studied by polarography in acetonitrile⁶ and methanol⁷ containing small amounts of water. A study of methoxide complexes of Ti(IV) in neutral and basic solutions was also reported.⁸ Some studies have been reported in which esr has been used to elucidate the structure of the Ti(III) species in solution. Various titanium(III) chelates⁹ in aqueous media, fluoride and methoxide complexes in methanol,^{10a} and the complexes in a 20% *tert*-butyl alcohol–water mixture^{10b} have been studied.

In this work the combination of normal and pulse polarography, linear sweep voltammetry, and esr spectroscopy has been employed to investigate the nature of titanium complexes in HCl–methanol solutions containing various amounts of H₂O. Values of the equilibrium constants between different chloride complexes of Ti(III) and the rates of conversion between the complexes have been estimated, structures of complexes have been postulated, and the heterogeneous rate constants for the Ti(IV)–Ti(III) electron transfer process have been estimated.

Experimental Section

Anhydrous methanol solutions containing HCl were prepared by adding gaseous HCl to Mallinkrodt Nanograde absolute methanol (H₂O content $\sim 0.02\%$) to make a stock solution which was standardized by acid–base titra-

tion. The approximate water content of these solutions was 0.05–0.06% as determined by coulometric Karl Fischer titration. Subsequent solutions were made by taking suitable aliquots of this stock solution. The stock solutions were prepared weekly since HCl reacts slowly with methanol to give methyl chloride and water. A stock solution of Ti(IV) in methanol was made by adding a known amount of reagent grade TiCl₄ to a measured volume of Baker Nanograde methanol and calculating the concentration. Previous work¹ showed that the calculated value agreed with the value obtained by complexometric titration to within 5%.

For some experiments, Ti(III) was required. This was prepared by complete reduction of a given concentration of Ti(IV) in the supporting electrolyte of interest at a large mercury pool or was prepared from TiCl₃ powder (Alfa Chemical Co.). The latter material was analyzed by titration with dichromate and found to be 99.4% TiCl₃.

A multipurpose electrochemical instrument and a previously described pulse polarograph built in this laborato-

- (1) E. P. Parry and D. H. Hern, *J. Electrochem. Soc.*, **119**, 1141 (1972).
- (2) I. B. Goldberg and W. F. Goepfinger, *Inorg. Chem.*, **11**, 3129 (1972).
- (3) I. M. Kolthoff and F. G. Thomas, *J. Electrochem. Soc.*, **111**, 1065 (1964).
- (4) V. Gutmann and M. Michlmayr, *Monatsh. Chem.*, **99**, 316 (1968); V. Gutmann, M. Kogelnig, and M. Michlmayr, *ibid.*, **99**, 707 (1968); V. Gutmann and E. Nedbalek, *ibid.*, **88**, 320 (1957); V. Gutmann and G. Schober, *ibid.*, **88**, 206 (1957); **93**, 1353 (1962); G. Schober, V. Gutmann, and E. Nedbalek, *Z. Anal. Chem.*, **186**, 115 (1962).
- (5) H. G. Brown and Hsiao-shu Hsiung, *J. Electrochem. Soc.*, **110**, 1085 (1963).
- (6) P. J. Shirvington, *Aust. J. Chem.*, **20**, 447 (1967).
- (7) P. Desideri and F. Patami, *Ric. Sci.*, **30**, 125, 233 (1966).
- (8) R. Gut, E. Schmid, and J. Serrallach, *Helv. Chim. Acta.*, **54**, 593, 609 (1971).
- (9) S. Fujiwara and M. Codell, *Bull. Chem. Soc. Jap.*, **37**, 49 (1964); S. Fujiwara, K. Nagashima, and M. Codell, *ibid.*, **37**, 773 (1964); T. Watanabe and S. Fujiwara, *J. Magn. Resonance*, **2**, 103 (1970).
- (10) (a) E. L. Waters and A. H. Maki, *Phys. Rev.*, **125**, 233 (1962); (b) R. Johnson, P. Wormington Murchison, and J. R. Bolton, *J. Amer. Chem. Soc.*, **92**, 6354 (1970).

TABLE I: Effect of Water on the Normal Polarographic and Pulse Polarographic Reduction Waves of Ti(IV) in HCl-Methanol Solutions^a

[H ₂ O], M	E _{1/2} (normal pol.), V	E _{1/2} (normal pulse), V	ΔE _{1/2} ^a	Derivative peak half-width, V	i ₁ cathodic (pulse), μA	i _d (Normal), μA	i _p (derivative), μA
0.04	-0.360	-0.398	-0.038	0.123	27.6	4.27	1.6
0.13	-0.374	-0.413	-0.039	0.120	28.5	4.49	2.2
0.39	-0.390	-0.435	-0.045	0.107	28.8	4.31	2.2
0.71	-0.408	-0.455	-0.047	0.115	29.6	4.20	2.0
1.41	-0.424	-0.479	-0.055	0.114	28.4	4.22	1.8

^a Methanol, 0.02 M HCl, 1 × 10⁻³ M Ti(IV). ^b Difference between half-wave potentials measured by normal pulse polarography and normal polarography.

ry¹ were used for the electrochemical measurements and for the large-scale reduction. The water was determined using a Photovolt Model II Aquatest coulometric water titrator.

Electron spin resonance spectra were obtained on a modified Varian V-4502 spectrometer equipped with a Hewlett-Packard X532B wavemeter, dual cavity, and Magnion 15-in. magnet. The titanium sample was monitored with 100-kHz field modulation, and the DPPH (diphenyl picryl hydrazyl) reference with 18-kHz field modulation. The experimental procedure is described elsewhere.² To improve resolution D₂O, DCl in D₂O, and CH₃OD, obtained from Bio-rad Laboratories, were used as the solvent system for measurements of hyperfine splittings and *g* factors. The CH₃OD was found to contain 0.04% D₂O.

Results

Polarography. The cathodic scan normal pulse polarogram for the reduction of Ti(IV) in 0.02 M HCl in methanol gives a well-defined wave. The half-wave potential shifts to more negative potentials with increasing amounts of water (Table I), but the single wave remains well defined. The plots of log [(i_d - i)/i] vs. *E* for the normal pulse polarograms deviate from linearity at *i* > 3/4*i*_d indicating irreversible behavior, although similar plots for polarographic waves are linear. The effect of various amounts of water on the half-wave potential and limiting current for both the polarographic and pulse polarographic reduction wave of Ti(IV) in methanol-0.02 M HCl is shown in Table I. The derivative pulse polarographic data were obtained with a pulse amplitude of 10 mV. Both the polarographic and pulse polarographic waves shift about the same amount with increasing water content. The normal polarographic wave appears reversible even in 1.4 M water as indicated by the slope of the plot of log [(i_d - i)/i] vs. *E*¹¹ and by the equivalence of the half-wave potentials for oxidation of Ti(III) and reduction of Ti(IV). This shows at least quasireversible behavior. The difference between the normal and pulse polarograms results from the different time scales of these measurements. A plot of the polarographic E_{1/2} vs. log [H₂O] is shown in Figure 1. The slope of the upper linear portion of the plot is 60 mV per decade.

In anodic pulse polarography, the initial potential is set on the cathodic diffusion plateau (e.g., -0.7 V) so that during most of the drop life Ti(IV) is reduced to Ti(III). For each drop successively more anodic potentials are then applied near the end of the drop life in order to reoxidize the Ti(III). Polarograms recorded in this manner exhibit two waves when sufficient water is present (Figure 2). This suggests that there is either a transient Ti(III) species formed upon reduction of Ti(IV), or there is an

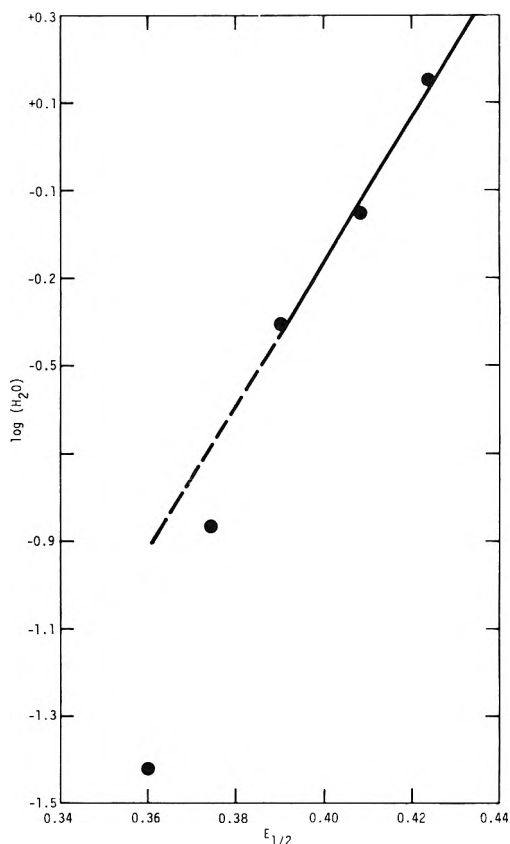


Figure 1. Log [H₂O] vs. half-wave potential for the polarographic reduction of 1 mM Ti(IV) in methanol containing 0.02 M HCl.

equilibrium between two Ti(III) species which are oxidized at different potentials. In 0.24 M H₂O the half-wave potential of the first anodic wave was -0.37 V (as compared to -0.41 V for the cathodic wave) and that of the second wave was -0.11 V. The total anodic wave height in methanol containing up to about 1.5 M H₂O was constant, and was also approximately the same height as that of the cathodic wave. The relative heights of each of the oxidation waves to the total wave height and the half-wave potentials as a function of water content are given in Table II. The relative wave height ratios were also found to be a function of chloride ion concentration as shown in Table III. Moreover in the pulse polarographic anodic scan in

(11) A plot of log [(i_d - i)/i] vs. *E* for the pulse polarographic wave as well as tables of results for cyclic voltammetry, measured values of the equilibrium constant, and kinetic currents will appear following these pages in the microfilm edition of this volume of the journal. Single copies may be obtained from the Business Operations Office, Books and Journals Division, American Chemical Society, 1155 Sixteenth St., N. W., Washington, D. C. 20036. Remit check or money order for \$3.00 for photocopy or \$2.00 for microfiche, referring to code number JPC-73-678.

TABLE II: Effect of Variation of Water Content on Normal Pulse Scan for $1 \times 10^{-3} M$ Ti(IV) in Methanol Containing 0.02 M HCl

Water concn, M	Oxidation ^c				Reduction ^d	
	$E_{1/2}(1)^a$	$i_1(i_1), \mu A^a$	$E_{1/2}(2)^b$	$i_2(i_2), \mu A^b$	$E_{1/2}$	i_1
0.038	-0.398	27.6	No second wave		-0.398	27.6
0.133	-0.373	23.3	-0.093	5.4	-0.413	28.4
0.392	-0.402	19.5	-0.110	10.0	-0.435	28.8
0.705	-0.428	15.7	-0.116	15.0	-0.455	29.6
1.41	-0.455	11.9	-0.140	17.8	-0.479	28.4

^a First oxidation wave of Ti(III). ^b Second oxidation wave of Ti(III). ^c Starting potential $-0.7 V$; anodic scan. ^d Starting potential $-0.0 V$; cathodic scan.

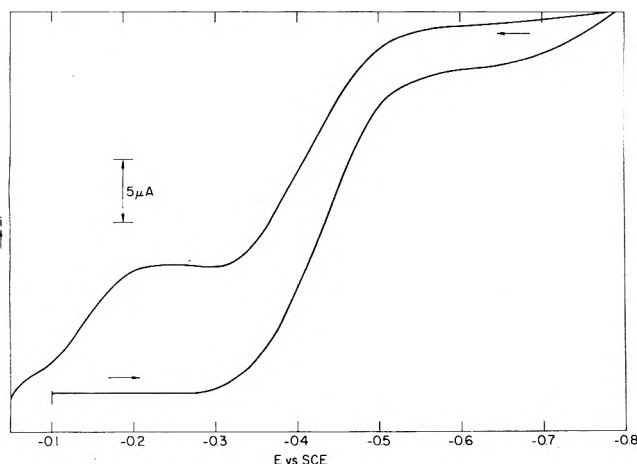


Figure 2. Anodic and cathodic pulse polarograms of the Ti(III)/Ti(IV) couple in methanol containing 0.02 M HCl and 0.24 M H₂O.

TABLE III: Effect of Lithium Chloride on the Relative Wave Heights for Anodic Pulse Polarographic Scan at 1.1 M Water Content^a

LiCl concn Added, M	Relative height of wave at $-0.35 V$	Relative height of wave at $\sim -0.1 V$
0.0	0.54	0.46
0.067	0.79	0.21
0.10	0.83	0.17
0.10	0.82	0.18
0.20	0.88	0.12
0.20	0.89	0.11

^a $[Ti(IV)] = 1 \times 10^{-3} M$. $[HCl] = 0.02 M$.

methanol solutions containing up to 1.5 M H₂O, the limiting current for both waves is diffusion controlled as indicated by the constancy of the product of the current and the square root of the measuring time. In a similar manner the pulse polarographic limiting current for the reduction of Ti(IV) was shown to be diffusion controlled.

In order to study the oxidation process of Ti(III) independently, solutions of Ti(IV) were reduced at a large mercury electrode at constant potential until the current decayed to less than 1% of the initial value, and an anodic pulse polarogram was recorded. Such an experiment would indicate whether the two Ti(III) species noted in the anodic pulse polarogram were in equilibrium or one was a transient species. It was observed that the pulse polarogram obtained with the Ti(III) from bulk reduction was identical with the above anodic waves. It was also found that the wave heights were independent of whether the addition of up to 1 M deaerated water was made before or after reduction of Ti(IV). Moreover, pulse polaro-

grams recorded on methanol-water solutions in which TiCl₃ was added directly to the electrochemical cell gave equivalent results to both of the other experiments. These results thus suggest two electrochemically distinguishable species of Ti(III) in equilibrium in the methanol-water system. Since the pulse polarographic waves are diffusion controlled, the equilibrium concentrations of the two species can be determined from the pulse polarographic wave heights.

Normal polarograms of Ti(III) solutions prepared as described above also exhibit two waves. The relative heights of the first oxidation wave to the second oxidation wave are considerably greater than those recorded by pulse polarography. Measurements of the dependence of the current on the mercury height show that the current increases more slowly than the expected proportionality to the $1/2$ power of the mercury height. The data therefore suggest that there is a kinetic contribution to the first polarographic wave. In solutions containing 7 M H₂O, where the first wave is considerably smaller than the second, a plot of $\log [(i_d - i)/i]$ vs. E for the second wave is linear with a slope of 0.059 V. At this water concentration the half-wave potential is $-0.022 V$.

Cyclic Voltammetry. Cyclic voltammetric studies of the Ti(III)-Ti(IV) systems were carried out at sweep rates between 50 and 400 mV/sec. Several typical results are shown in Figure 3. A negative shift of the Ti(IV) reduction potential at maximum current ($E(p_c)$) with water is found to be similar to that of the polarographic measurements. Only one cathodic peak is observed throughout the range of water concentrations studied. One reoxidation wave is observed at about $-0.3 V$ in solutions with less than 0.1 M H₂O. However, at 0.2 M H₂O, a shoulder on the positive side of the oxidation wave can be observed. At concentrations of water greater than 0.5 M, a second oxidation peak at about $-0.1 V$ becomes evident (Figure 3a). The height of the peak ($i(p_a)^1$) at $-0.3 V$ decreases with water content (Figure 3b) and sweep rate (Figure 3c) while the height of the peak at $-0.1 V$ ($i(p_a)^2$) increases. At 5 M H₂O, the peak near $-0.3 V$ is barely visible. These results also suggest an equilibrium between two different Ti(III) species where the rate of conversion from one complex to the other is significant at the slower sweep rates and higher water concentrations.

Esr Studies. Spectra of Ti(III) produced by controlled potential electrolysis of TiCl₄ in HCl-H₂O-CH₃OH media were obtained and were identical with those obtained from solutions prepared directly from TiCl₃. Since it has been shown that there is significant unresolved hyperfine interaction with the protons of the solvent,¹² better resolution is obtained if deuterated solvents are used.^{10b} Re-

(12) A. M. Chmelnick and D. Fiat, *J. Chem. Phys.*, **51**, 4238 (1969).

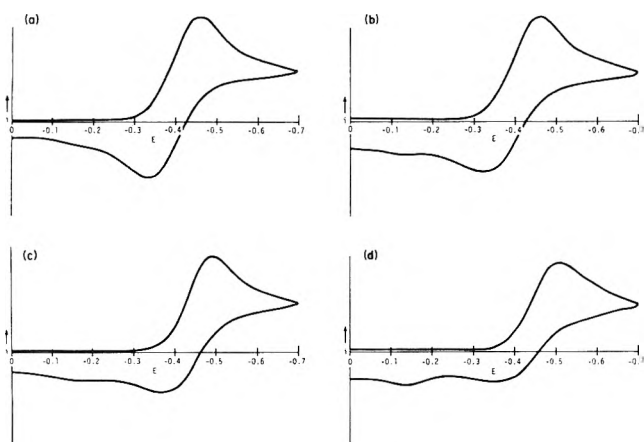


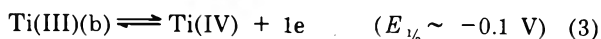
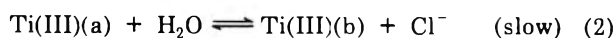
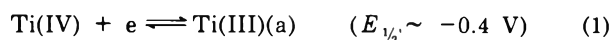
Figure 3. Cyclic voltammetry of 1 mM Ti(IV) in methanol containing 0.02 M HCl and water: (a) 50 mV/sec, 0.5 M H₂O; (b) 200 mV/sec, 0.5 M H₂O; (c) 50 mV/sec, 2 M H₂O; (d) 200 mV/sec, 2 M H₂O.

sults obtained using CH₃OD as the solvent are reported here.

Figure 4 shows typical esr spectra obtained from solutions of TiCl₃ in CH₃OD at -10°. In each spectrum a low-field (l) and high-field (h) absorption can be observed. When the concentration of TiCl₃ is decreased from 7.8 (Figure 4) to 3.1 mM (Figure 4b), the amplitude of h decreases relative to l. The addition of 0.064 M LiCl to 7.0 mM TiCl₃ decreases l relative to h, whereas the addition of 0.4 M D₂O increases l relative to h.

Discussion

Equilibrium. The results from the electrochemical measurements suggest that the following reactions and equilibria are important in the titanium-HCl-methanol system in the presence of water



where Ti(III)(a) and Ti(III)(b) are two different complexes of Ti(III) which are electrochemically distinguishable. Reactions 1 and 3 appear reversible by normal polarography but kinetically controlled by pulse polarography whereby it is possible to evaluate the kinetic parameters of the electron transfer (see below). The conversion from Ti(III)(a) to Ti(III)(b) is slow and thus allows both species to be observed electrochemically.

In solutions of low water content, a Ti(IV) complex containing no water is reduced to a Ti(III) complex which also contains no water and the polarographic half-wave potential is independent of water. As more water is added and a significant amount of aquated complex is formed, the half-wave potential shifts to reflect an elimination of one water molecule per ion of Ti(IV) reduced (*i.e.*, a slope of 60 mV/decade, see Figure 1). Since the exchange between methanol and water is rapid in Ti(IV),¹³ only one reduction wave is observed.

The esr data definitely indicate two different species at low temperature. In anhydrous methanol, absorption l (see Figure 4) has been attributed to [TiCl(MeOD)₅]²⁺ and absorption h to [TiCl₂(MeOD)₄]⁺.² This was based on the following: (1) Chmelnick and Fiat found that in con-

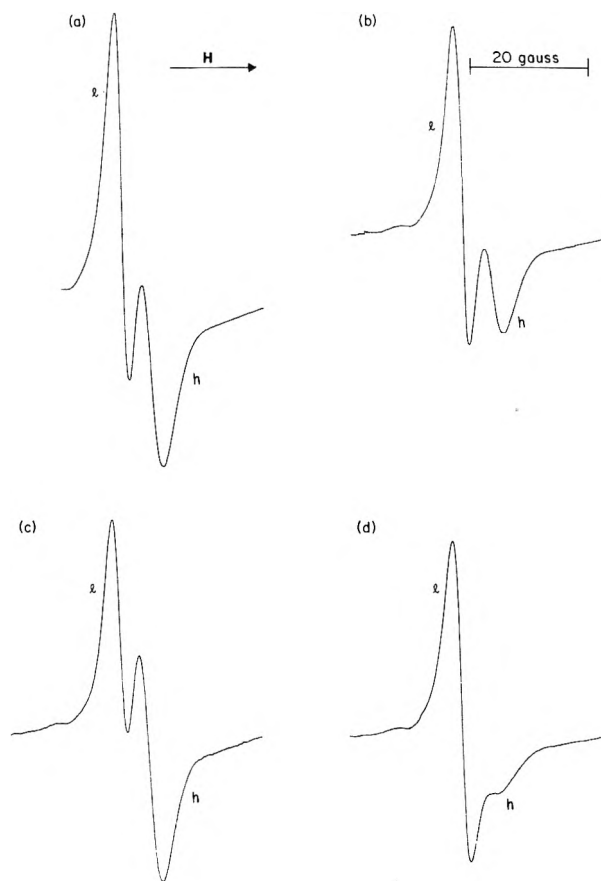


Figure 4. ESR spectra of TiCl₃ in CH₃OD at -10°. Solutions contain (a) 7.1 mM TiCl₃, (b) 3.1 mM TiCl₃, (c) 7.0 mM TiCl₃ and 65 mM LiCl, and (d) 7.2 mM TiCl₃ and 0.5 M D₂O.

centrated solutions of TiCl₃, the Ti(III) ion is solvated by four methanol ligands;¹² and (2) [Ti(MeOH)₆]³⁺ would exhibit a very broad line and would be difficult to observe above liquid nitrogen temperatures in dilute solutions. It was further observed that at room temperature, absorptions l and h begin to broaden which suggests that there is an exchange between ligands of each complex in solution. For this reason the complexes containing only methanol and chloride ligands would not be expected to be distinguishable by electrochemical measurements. As a result, the species labeled Ti(III)(a) in eq 1 and 2 is a combination of chloro and dichloro complexes, which do not contain water. The following reaction, eq 4, therefore, must be added to eq 1-3



Since the amplitude of l increases and that of h decreases with the addition of D₂O, a complex containing water must contribute to l. Because water and methanol exhibit similar crystal field effects on titanium ions,¹⁴ the complexes containing different ratios of water to methanol would be expected to give nearly the same esr absorption. Thus, the esr spectrum of [TiCl(D₂O)(CH₃OD)₄]²⁺ would be expected to be almost identical with the spectrum of [TiCl(CH₃OD)₅]²⁺.

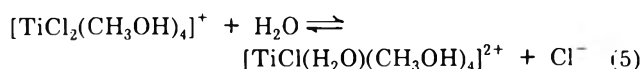
Esr measurements of solutions of TiCl₃ at 25° which were equivalent to those used in the electrochemical ex-

(13) A. Fratiello, R. E. Lee, D. P. Miller, and V. M. Nishida, *Mol. Phys.*, **13**, 349 (1967).

(14) R. J. H. Clark, "The Chemistry of Titanium and Vanadium," Elsevier, Amsterdam, 1968, Chapter 6.

periments, except that deuterated solvents were used, show that the contribution of the dichloro complex to the amplitude of the spectrum is in the order of 10% when 0.5 M D₂O and 0.02 M DCl is present. At D₂O concentrations of about 1 M only a relatively small contribution to the spectrum can be seen. This appears as a high-field broadening of the line rather than a second absorption. When H₂O and CH₃OH are used as the solvents, the distinction between two complexes is more difficult because the spectra appear to be high-field broadened. This broadening had previously been attributed by other authors both to slow rotation time of the Ti(III) in methanol and to vibrational interactions.¹⁵

Combining these observations with the results of the electrochemical measurements, we can define in greater detail the nature of the Ti(III)(a) and Ti(III)(b) species. As indicated above, [TiCl₂(CH₃OH)₄]⁺ and [TiCl(CH₃OH)₅]²⁺ are indistinguishable electrochemically, so this combination represents Ti(III)(a). The equilibrium of eq 2, therefore, is better given by eq 4 and



where Ti(III)(b) is the complex [TiCl(H₂O)(CH₃OH)₄]²⁺. Ti(III)(a) oxidation gives rise to the first polarographic wave (-0.3 V) and Ti(III)(b) oxidation to the second wave (-0.1 V). The fact that certain complexes which are indistinguishable by electrochemical measurements can be defined by esr (and *vice versa*) illustrates the power of the combined technique for studies of transition metal complexes.

As the results have indicated, the rate of conversion of b to a is on the same time scale as that for normal polarography so the wave for the oxidation of a (first wave) has a kinetic contribution. However, because there is a difference of 150-fold in the current measurement time scale between normal polarography and pulse polarography (*i.e.*, 3 vs. 0.02 sec), the pulse polarographic waves are diffusion controlled and thus give the equilibrium concentrations. With known concentrations of water and chloride ion, the equilibrium constant *K* for eq 2 can be calculated. The equilibrium expression, neglecting activity coefficients, is given by

$$K = [\text{Cl}^-][\text{Ti(III)(b)}]/[\text{H}_2\text{O}][\text{Ti(III)(a)}] \quad (6)$$

Values of *K* were calculated for variation of both the water content between 0.1 and 7.0 M at constant chloride ion concentration and for variation of the chloride ion concentration between 0.02 and 0.22 M at constant water. The average value for *K* was found to be 0.029 with a standard deviation of ±0.006.

Even though no corrections were made for ionic strength effects or for changes in the solvent activity, the values were reasonably constant. It was assumed that HCl and LiCl are completely dissociated. The value for the dissociation constant of HCl in anhydrous methanol is reported to be 6 × 10⁻².¹⁶ Thus, 0.02 M HCl would be about 75% dissociated. In methanol containing about 2.4 M water, however, the dissociation constant increases by about threefold.¹⁶ Thus, in the range of water content covered by these experiments, the dissociation of HCl may actually increase to about 90 or 95%. No dissociation constant for LiCl in methanol has been reported,¹⁷ but at concentrations as high as 0.2 M, it would be expected to be partially associated.

The effect of the two methanol-chloride species which comprise Ti(III)(a) can also be considered. For simplicity we can represent [TiCl(CH₃OH)₅]²⁺ by TiCl²⁺ and [TiCl₂(CH₃OH)₄]⁺ by TiCl₂⁺. Assuming constant activity of methanol and neglecting activity coefficients, the equilibrium constant *K*₂ for these complexes is

$$[\text{TiCl}^{2+}][\text{Cl}^-]/[\text{TiCl}_2^+] = K_2 \quad (7)$$

Since Ti(III)(a) is the sum of two complexes given by

$$[\text{Ti(III)(a)}] = [\text{TiCl}^{2+}] + [\text{TiCl}_2^+] = [\text{TiCl}_2^+]\{1 + (K_2/[\text{Cl}^-])\} \quad (8)$$

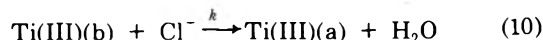
the equilibrium expression for *K* becomes

$$K = [\text{Cl}^-][\text{Ti(III)(b)}]/[\text{H}_2\text{O}][\text{Ti(III)(a)}]\{1 + (K_2/[\text{Cl}^-])\} \quad (9)$$

If *K*₂ is small, or the equilibrium is shifted toward the dichloro species, then the measured values of *K* would be approximately constant. However, in more dilute chloride media, deviations of *K* calculated from eq 6 might be observed. The most likely source of deviation in the values of *K*, however, appears to arise from measurements of the diffusion currents from the incompletely separated polarographic waves.

If we assume that a 20% deviation from the value of *K* = 0.029 for a tenfold change in chloride can be observed, then an upper limit for *K*₂ is estimated to be about 5 × 10⁻³ M. Thus, at a concentration of 0.02 M HCl and 0.001 M TiCl₃ in methanol in the absence of added water about 20% of the Ti(III)(a) could be in the TiCl²⁺ form.

Rate of Conversion of Ti(III)(b) to Ti(III)(a). In normal polarography the oxidation wave of Ti(III)(a) is larger than that observed in pulse polarography. During the time of the polarographic measurement, the reverse reaction of eq 2 contributes to the amount of Ti(III)(a) at the electrode surface, and the amount oxidized is greater than would be predicted from the equilibrium concentrations. From this kinetic contribution to the polarographic wave, the rate constant for the conversion of Ti(III)(b) to Ti(III)(a), eq 10, can be calculated.



If the concentrations of Cl⁻ and H₂O are sufficiently greater than the concentrations of the titanium complexes, the reaction is pseudo first order, and first-order reaction rate expressions, eq 11, can be used, where *k*' is the pseudo-first-order reaction rate constant.

$$-d[\text{Ti(III)(b)}]/dt = k[\text{Ti(III)(b)}][\text{Cl}^-] = k'[\text{Ti(III)(b)}] \quad (11)$$

After Brdicka and Wiesner,¹⁸ we can write

$$i_k = nF10^3 A \mu k' [\text{Ti(III)(b)}]_0 \quad (12)$$

where *i*_k is the kinetic current, *n* the number of electrons transferred, *F* the Faraday, *A* the electrode area, *μ* the

- (15) N. F. Garif'yanov, E. I. Semenova, N. F. Usacheva, *Zh. Strukt. Khim.*, **3**, 596 (1969); *J. Strukt. Chem.*, **3**, 570 (1962); N. S. Garif'yanov and E. I. Semenova, *Dokl. Akad. Nauk SSSR*, **140**, 157 (1961); *Dokl. Phys. Chem.*, **140**, 568 (1961); A. V. I. Aurakova, N. S. Garif'yanov, and E. I. Semenova, *Sov. Phys. JETP*, **12**, 847 (1961); **14**, 243 (1962); N. S. Garif'yanov, A. V. Danilova, and R. R. Shagidvlin, *Opt. Spectrosc.*, **13**, 116 (1962).
 (16) T. Shedlovsky and R. L. Kay, *J. Phys. Chem.*, **60**, 151 (1956).
 (17) G. Charlot and B. Tremillon, "Chemical Reactions in Solvents and Melts," Pergamon Press, New York, N. Y., 1969, p 276.
 (18) R. Brdicka and K. Wiesner, *Collect. Czech. Chem. Commun.*, **12**, 138 (1947); see also I. M. Kolthoff and J. J. Lingane, "Polarography," 2nd ed, Interscience, New York, N. Y., 1952, pp 269-273.

TABLE IV: Values of the Rate Constant for Conversion of Ti(III)(b) to Ti(III)(a)^a

Water concn, <i>M</i>	<i>i</i> _d (total), μA	<i>i</i> _d (Ti(III)(a) equil), μA	<i>i</i> _d (Ti(III)(b) equil), μA	Kinetic current, μA	<i>k</i> ' , sec^{-1}	<i>k</i> , $M^{-1} \text{sec}^{-1}$
0.5	4.19	2.17	2.12	1.7	4.3	231
1.0	4.0	1.47	2.53	1.8	2.0	100
2.0	3.6	0.88	2.74	1.9	3.3	167
5.0	2.6	0.31	2.3	1.4	4.0	198

^a Chloride ion concentration constant at 0.02 *M*.Av 174 $\sigma = 55$

thickness of the reaction layer, and $[\text{Ti(III)(b)}]_0$ is the concentration of the species at the electrode surface. We also have the relation

$$i_k = \chi \{ [\text{Ti(III)(b)}]_{\infty} - [\text{Ti(III)(b)}]_0 \} \quad (13)$$

where $[\text{Ti(III)(b)}]_{\infty}$ is the concentration of these species in the solution bulk, and χ is $706 \times 10^3 n D^{1/2} m^{2/3} t^{1/6}$ when the maximum current is taken. Equation 12 can be rewritten as

$$i_k = i_d(\text{Ti(III)(b)}) - \chi [\text{Ti(III)(b)}]_0 \quad (14)$$

where $i_d(\text{Ti(III)(b)})$ would be the diffusion current of Ti(III)(b) if no reaction occurred. Koutecky and Brdicka¹⁹ have derived an expression for the thickness of the reaction layer

$$\mu = \sqrt{D\tau} \quad (15)$$

where τ is the mean life time of the depolarizer. The mean life time of a first-order reaction is the reciprocal of the rate constant. Using pseudo-first-order rate constants for the forward and reverse reactions, it can easily be shown that the thickness of the reaction layer is given by

$$\mu = \sqrt{\frac{D}{k'k([\text{H}_2\text{O}]/[\text{Cl}^-])}} \quad (16)$$

where K is the equilibrium constant of eq 2, k' is the pseudo-first-order rate constant of eq 10, and D is the diffusion coefficient of the Ti(III)(a) complex. If we assume that the diffusion coefficients of both titanium complexes are equal, we can combine eq 13, 14, and 16 to obtain the expression

$$k'^{1/2} = \frac{\sqrt{K([\text{H}_2\text{O}]/[\text{Cl}^-])706m^{2/3}t^{1/6}}}{FA} \frac{i_k}{i_{d(\text{Ti(III)(b)})} - i_k} \quad (17)$$

Values of k' and k for eq 10 calculated from eq 17 are given in Table IV. For these conditions $m^{2/3}t^{1/6}$ and A were $2.30 \text{ mg}^{2/3}\text{sec}^{1/6}$ and 0.036 cm^2 , respectively. The data for the equilibrium values of $i_d(\text{Ti(III)(a)})$ and $i_d(\text{Ti(III)(b)})$ were obtained by multiplying the appropriate fraction of the total current as determined by the ratio of wave heights of the pulse polarograms by the total current of the polarogram. Considering that no corrections have been made for double layer and activity effects and possible changes in ionization, we consider the agreement very good.

It is evident from Table IV that the value of i_d decreases significantly at water concentrations greater than 2 *M*. Since Ti(IV) is easily hydrolyzed, as shown by Shirvington for TiCl_4 in acetonitrile containing 0.03 *M* water,⁶ it seems likely that at high water contents in methanol even in 0.02 *M* HCl, some hydrolysis can occur. This product may be electroinactive at the low values of the negative potentials which can be reached in acidic metha-

nol. The additional possibility that an electroinactive product of Ti(III) is formed must also be considered, but this appears less likely. These questions are under current investigation.

To verify the magnitude of the rate constants obtained by the above calculations, digital simulations²⁰ of the cyclic voltammetry were carried out. Although many parameters could be varied in the simulation process to find the optimized results, only the equilibrium constant and rate constant were varied. The electron transfer was treated as Nernstian, and the rate constants were again pseudo first order. Linear diffusion was also assumed. The best values of the equilibrium constant obtained here based on superposition of the simulated and actual current voltage plots was 0.03 ± 0.01 for K and $1.6 \pm 0.3 \text{ sec}^{-1}$ for the pseudo-first-order rate constant k' . This corresponds to a value of about $80 M^{-1} \text{ sec}^{-1}$ for the value of k . These results agree well with the values obtained from polarographic data, especially considering the assumptions made in the digital simulations as well as the method for calculation of k' from the kinetic current.

Heterogeneous Kinetics. The reversibility of the normal polarographic wave for the Ti(IV)|Ti(III) couple in methanol with and without water present is evident from the data. Plots of E vs. $\log [(i_d - i)/i]$ are linear with a slope of 0.059 V, and the oxidation of Ti(III) and reduction of Ti(IV) have the same half-wave potentials. However, the electrode reaction is not fast enough for the pulse polarographic wave to be diffusion controlled. The heterogeneous rate constant for the electrode reaction and the transfer coefficient can be estimated from the normal and derivative pulse data of Table II. It is acknowledged that these values will also reflect the presence of homogeneous chemical reactions, and possible uncompensated iR .

Using a small pulse amplitude ($\sim 10 \text{ mV}$), the width at half height of the derivative pulse polarogram ($W_{1/2}$) can be used to obtain a value of $n\alpha$ for the electrode reaction. The equation for this calculation²¹ is given by

$$n\alpha = (0.0835 / W_{1/2}) V \quad (18)$$

Since the half-width does not change significantly with water content, the value of α is not markedly affected by addition of water.

In a previous paper,²¹ it was shown that the electrochemical rate constants can be determined from the normal pulse polarographic wave from a simple algebraic expression rather than from graphical or tabular interpolation. A

- (19) J. Koutecky and R. Brdicka, *Collect. Czech. Chem. Commun.*, **12**, 337 (1947); see also J. Heyrovsky and J. Kuta, "Principles of Polarography," Academic Press, New York, N. Y., 1966, p 346.
 (20) S. W. Feldberg, "Electroanalytical Chemistry," Vol. 3, A. J. Bard, Ed., Marcel Dekker, New York, N. Y., 1969, p 299 ff, S. W. Feldberg, *J. Phys. Chem.*, **75**, 2377 (1971).
 (21) K. B. Oldham and E. P. Parry, *Anal. Chem.*, **40**, 65 (1968).

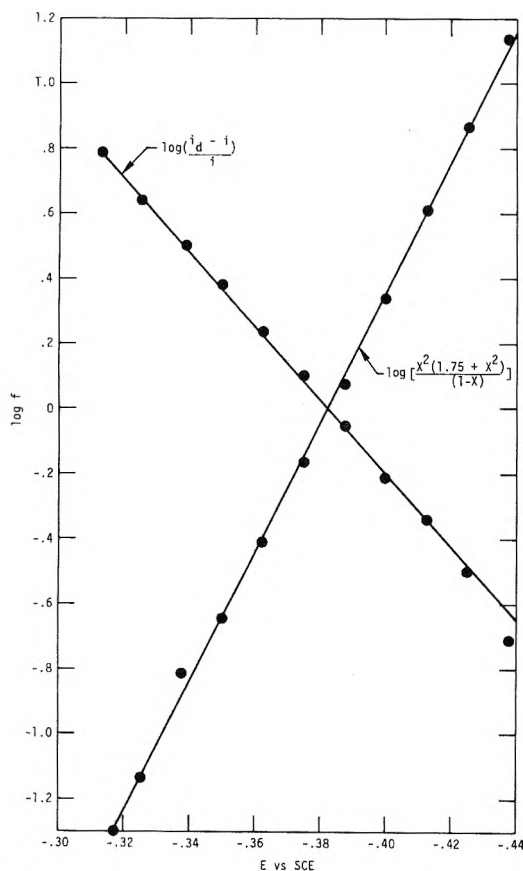


Figure 5. Plots of $\log [(i_d - i)/i]$ and $\log [X^2(1.75 + X^2)/(1 - X)]$ where $X = i/i_d$ vs. E for the pulse polarographic reduction of 1 mM TiCl_4 in methanol containing 0.02 M HCl.

plot of $\log [X^2(1.75 + X^2)/(1 - X)]$ vs. E where $X = i/i_d$ for a pulse polarographic wave will yield a straight line for an irreversible reaction with a slope of $n\alpha/0.059 \text{ V}^{-1}$ and an intercept $E_{1/2}$. The $E_{1/2}$ value is related to the electrochemical rate constant by the expression

$$E_{1/2} = E_s + (0.0592/n\alpha) \log \{2.31 k_s(t/D)^{1/2}\} \quad (19)$$

where E_s is the standard potential of the system, k_s is the rate constant, t is the time of measurement after pulse application, and D is the diffusion coefficient which was found to be $1.0 \pm 0.1 \times 10^{-5} \text{ cm}^2 \text{ sec}^{-1}$. A plot of $\log [(i_d - i)/i]$ vs. E for an irreversible pulse polarographic wave has been shown to be nonlinear.²¹ Figure 5 shows a plot of $\log [X^2(1.75 + X^2)/(1 - X)]$ vs. E , and the corresponding plot of $\log [(i_d - i)/i]$ vs. E . The value of $n\alpha$ obtained from the slope of the line is 0.06, while eq 18 gives a value of 0.68. By assuming that the normal polarographic wave is reversible and using this half-wave potential for the value of E_s , the value of the electrochemical rate constant can be calculated from eq 19. The values of k and α are given in Table V as a function of water content.

TABLE V: Electrochemical (Heterogeneous) Rate Constant and Transfer Coefficient for Ti(IV) Reduction in Methanol-HCl as Function of Water Content^a

Water concn, M	$\Delta E_{1/2}$, V	$W_{1/2}$, V	αn	$10^3 k_s$, cm sec^{-1}
0.038	-0.038	0.123	0.68	3.5
0.133	-0.039	0.120	0.70	3.5
0.392	-0.045	0.117	0.71	3.0
0.705	-0.047	0.115	0.73	2.8
1.41	-0.055	0.114	0.73	2.3

^a 1 mM Ti(IV), 0.02 M HCl.

The maximum variation of α over the range of water concentration is about 7% which is well within the accuracy of the method, especially considering the agreement (see above) between the value of α obtained from the half-width of the derivative pulse polarogram compared to that obtained from the slope of the log plot. For this reason the value of α was taken as 0.65 ± 0.07 for all values of water concentration.

Previous work has indicated that the upper limit of applicability for the determination of k_s using normal pulse polarography is about $2 \times 10^{-2} \text{ cm sec}^{-1}$ for values of D and t of $10^{-5} \text{ cm}^2 \text{ sec}$ and 20 msec, respectively. It is, therefore, expected that for values of k_s in the order of $10^{-3} \text{ cm sec}^{-1}$ the precision of the measurement would not be high. The experimental techniques used did not optimize the accurate measurement of these small differences in half-wave potential. Therefore, when the uncertainty of the measurement of α is considered, the values of rate constant should be considered only as an approximation, and no real difference in the value of k_s with varying water content can be suggested by these data. The value of the heterogeneous rate constant for the reduction of titanium(IV) in methanol-0.02 M HCl calculated here is approximately $3 \times 10^{-3} \text{ cm sec}^{-1}$ with an uncertainty of at least $\pm 50\%$. This rate is fast enough to appear reversible in normal polarography.

Possible reasons for the apparently slow electron transfer step may be the result of changes in the geometry or coordination between the electroactive reactant and product. It could be expected from the dependence on water of the normal polarographic $E_{1/2}$ values that at high water concentrations Ti(IV) loses one H_2O ligand during reduction to Ti(III). This could account for some degree of irreversibility. The effect of the homogeneous reaction (eq 2) on these measurements should be fairly small during the time scale of the pulse polarographic measurements.

Acknowledgments. The authors thank Dr. R. Lee Myers, Dr. Leo Topol, Dr. George Lauer, and W. M. Moore for many helpful discussions concerning these experiments.

Self-Diffusion in Normal and Heavy Water in the Range 1–45°

R. Mills

Diffusion Research Unit, Research School of Physical Sciences, Australian National University, Canberra, A.C.T., Australia
(Received November 7, 1972)

Self-diffusion coefficients of tritiated water in normal (H_2O) and heavy water (D_2O) have been measured over the temperature range 1–45°. The diaphragm-cell technique was used and the results are considered to be probably accurate to $\pm 0.2\%$. The data of Longworth^{1,2} for HDO diffusion in both H_2O and D_2O in conjunction with the tritiated water values measured here have been used to calculate the self-diffusion coefficients of pure normal water (H_2O – H_2O) and pure heavy water (D_2O – D_2O). These coefficients have been tabulated and compared with molecular dynamics and nmr data.

Introduction

One hesitates to report yet another set of data for self-diffusion in liquid water. The fact remains that present values for tritiated water (HTO) in normal water (H_2O) over a temperature range are sparse and inaccurate and even at 25° vary from 2.2 to $2.6 \times 10^{-9} \text{ m}^2 \text{ sec}^{-1}$. There are similar variations in respect to HDO, H_2^{18}O and also to pure H_2O self-diffusion as determined by nmr methods. The serious discrepancies between these various sets of data have been discussed extensively in recent reviews.^{3–5} In the last of these,⁵ it was pointed out that probably the only reliable data of good precision were those of Longworth² for HDO in H_2O and D_2O . However, two sets of values, both by capillary methods, for tritiated water in normal water at 25° those of Devell³ and Jones, Monk, and Rowlands⁶ were considered to be reliable within their limits of error, each of $\sim 2\%$. It was considered necessary therefore to confirm the value at 25° to better precision using diaphragm cells and to extend the measurements over the temperature range 1–45°.

Measurements have also been made of the self-diffusion of tritiated water in pure D_2O . The motivation here was to try and gain more insight into the mass dependence of the self-diffusion rates of the various isotopic forms of water. In particular, in order to compare isotopic diffusion data with those determined by the nmr spin echo method, one needs to extrapolate from isotopic data to the value for pure water.⁷ The availability of Longworth's accurate optical data² of the mutual diffusion of light and heavy water allows such an estimate to be made. Finally, it is hoped that the extrapolated values for pure water reported here will provide calibration points for the nmr method and so bring self-diffusion data obtained by this technique into better agreement with those from isotopic work.

Experimental Section

The normal water used in these experiments was distilled and passed through an ion-exchange column at a fast rate. It was then heated to boiling and vigorously degassed on a water pump. The specific conductance measured with a Jones-Dike bridge was $0.85 \times 10^{-6} \text{ ohm}^{-1} \text{ cm}^{-1}$. Heavy water (99.7 atom % D) was obtained from Merck Sharp and Dohme, Canada, and tritiated water from the Radiochemical Centre, Amersham, England. Both of these were used without further purification.

The magnetically stirred diaphragm cell method as developed originally by Stokes⁸ was used in these determinations. The solvent-filled technique in which tracer is added to the top compartment was used throughout. Details of the apparatus and general procedure are given in a recent publication.⁹ Additional precautions arising from work with organic solvents,¹⁰ in particular the thermostating of the cells during sampling, were also incorporated. The counting techniques were based on the method outlined in ref 9. It was found that the usual dioxane-based scintillator solutions were not stable enough to give the precision required for these studies. A solution containing 750 ml of toluene, 300 ml of ethanol, and 9 g of butyl-BPD scintillator gave excellent results, however.

Analysis of Errors

As the isotopic extrapolations used later in this paper involve the use of small differences between diffusion coefficient values, a discussion of error limits is necessary.

The diaphragm cell was calibrated using the system 0.5 M KCl diffusing into water for which accurate Gouy data are available.⁹ The cell compartment concentrations were determined by measuring their conductance with a Jones-Dike bridge which gives analyses accurate to $\pm 0.01\%$. Duplicate calibration runs usually agreed to 0.05%. As the cell had a platinum sinter and Teflon-coated stirrers no correction for a wear factor was necessary.

- (1) L. G. Longworth, *J. Phys. Chem.*, **58**, 770 (1954).
- (2) L. G. Longworth, *J. Phys. Chem.*, **64**, 1914 (1960).
- (3) L. Devell, *Acta Chem. Scand.*, **16**, 2177 (1962).
- (4) H. R. Pruppacher, *J. Chem. Phys.*, **56**, 101 (1972).
- (5) R. Mills, *Ber. Bunsenges Phys. Chem.*, **75**, 195 (1971).
- (6) J. R. Jones, D. L. G. Rowlands, and C. B. Monk, *Trans. Faraday Soc.*, **61**, 1384 (1965).
- (7) Some explanation is needed as to what is meant by "the self-diffusion coefficient for pure water." A diffusion coefficient is defined relative to a gradient of some kind. In a tracer experiment it would be a gradient of radioactivity but in the absence of a tracer it becomes a little more difficult. In an assemblage of identical molecules one can, however, conceptually identify a certain number of them and then a gradient of identified molecules exists. The essential point is that the process of identification must not change any of the chemical or physical properties of the molecules. In practice a molecular dynamics "experiment" does this insofar as the momentum and space coordinates of all the molecules are known at any time. It is also very closely approached in an nmr experiment where the only gradient present is related to the phase of nuclear magnetic moments present in the molecules which will not sensibly affect their rate of diffusion.
- (8) R. H. Stokes, *J. Amer. Chem. Soc.*, **72**, 763 (1950).
- (9) R. Mills and L. A. Woolf, "The Diaphragm Cell," DRU Report RR1, A.N.U. Press, Canberra, 1968.
- (10) A. F. Collings and R. Mills, *Trans. Faraday Soc.*, **66**, 2761 (1970).

When tracers are used analytical errors are somewhat greater. The liquid-scintillation counting apparatus has been described in detail in ref 9. All samples for counting are prepared by accurate weight dilution. Each sample is counted simultaneously by two independent counter systems and any appreciable difference between the two results gives an indication of malfunction in one of the electronic components. Normally agreement between the two counters is $\pm 0.1\%$. More than 10^6 counts are recorded on all samples so that statistical counting error is expected to be $< \pm 0.1\%$. The top compartment solution is diluted by weight to give the same counting rate as the bottom to avoid coincidence errors. Other procedures automatically correct for drift in the photomultipliers and amplifiers in the time between analyses of the two compartments. Overall reproducibility between tracer runs is $\pm 0.2\%$.

One serious source of error was found, however, in relation to the radioactive tritiated water. In the first 20 or so runs, at several temperatures, the measured diffusion coefficients showed a slight linear increase with time. This effect appears to be due to the high specific activity of the tracer. Tritiated water is readily available at very high specific activities and there is a natural tendency to use high counting rates with consequent low backgrounds. When the specific activity used in the above runs was reduced by a factor of 30, the time variation disappeared and the reproducibility was excellent. It is well known that the recoils of disintegrating tritium atoms can affect molecules in their vicinity and this effect is in fact the basis of the Wilzbach method of tritium labeling. It would appear in the diffusion case that high activities cause some alteration to the water structure although more work needs to be done to specify this more closely. The effect may have contributed to previous anomalous results for tritiated water.

The cells were immersed in a well stirred water thermostat, and temperature fluctuations were measured continuously for all runs with a recording platinum resistance thermometer. In the range $1-35^\circ$ these fluctuations were not greater than $\pm 0.002^\circ$ and at 45° not greater than $\pm 0.01^\circ$. Absolute temperatures as measured with calibrated calorimeter thermometers and the platinum resistance thermometer are probably correct to $\pm 0.005^\circ$.

At a given temperature runs were repeated at least three times for normal water runs and twice for all heavy water runs. The overall reproducibility as shown in Table I was at least of order $\pm 0.2\%$. There always remains of course the possibility of some unrecognized systematic error.

Results

In Table I are listed the self-diffusion coefficients measured in this work together with Longworth's extrapolated values for HDO in both normal and heavy water. An asterisk denotes that the species is present effectively in trace amounts.

Before discussing the data in more detail a few comments should be made as to the tracer species present in these experiments. It is obvious that due to the ionization of water there will be rapid exchange between hydrogen, deuterium, and tritium ions. Thus if a small amount of D_2O is introduced into a large volume of H_2O , the only two species virtually present will be HDO and H_2O and similarly for other combinations. In Longworth's mutual diffusion work on H_2O-D_2O mixtures the limiting mutual

diffusion coefficients (obtained by extrapolation) refer to the diffusion of vanishingly small amounts of HDO in H_2O and D_2O at each end of the concentration scale. This fact does not seem to have been appreciated by some authors (see, e.g., Eisenberg and Kauzmann,¹¹ pp 218-219). Theory indicates^{12,13} that these limiting mutual coefficients should be identical with the tracer or self-diffusion coefficients of HDO in these solvents and this equivalence has been borne out by experiment for similar systems. For this reason our tracer coefficients obtained with HTO are directly comparable with Longworth's data. Another important consequence of this exchange process is that when tritiated water is added to D_2O , the effective tracer species is DTO*. It should be added that tritiated water is not obtained in a pure state but is in trace quantities in normal water. However, the amount of normal water accompanying the tritiated water which is added to the D_2O in the diffusion cell is very small (< 0.02 mol %) and has a negligible effect. For a 50 mol % H_2O-D_2O solution, the tracer is an equimolar mixture of DTO* and HTO*.

Comparison with all previous results for tritiated water would serve no useful purpose. However, it may be noted that the two values previously considered most reliable by Mills⁵ for HTO in H_2O at 25° were those of Devell³ (2.25) and Jones, Rowlands, and Monk⁶ (2.22) and the average of these is practically the same as the value shown in Table I. Their combined error limits of $\pm 3\%$ obviously lessen the significance of this agreement. The value of 2.029 in the last column is for an equimolar HTO*-DTO* mixture diffusing in a 50/50 mol % H_2O-D_2O solution. This value is almost half-way between the corresponding tracer values for pure H_2O and D_2O and supports Longworth's conclusion² that there are no unusual properties connected with solutions of this composition. It will be observed in Table I that, as might have been expected from mass considerations, the HTO values in H_2O and the DTO values in D_2O are consistently lower than the corresponding HDO ones. These systematic differences are tabulated as percentages in Table II. In all cases the data for HDO are from Longworth.² The parentheses enclose solvents; tracer species either have an asterisk or are subscripted.

Column 2 presents the differences observed when changing from H_2O to D_2O as solvent for the tritiated species used in this work whereas column 3 differences are for the same solvent change but for Longworth's HDO values. The parallelism between the two sets of data over the three temperatures is quite remarkable. It is even better than it seems because the tritiated tracer changes from HTO to DTO when in D_2O and the mass increase of one unit would slightly increase the differences in column 2. In columns 4 and 5, the differences in diffusion rate between HTO* and HDO* in H_2O and between HDO* and DTO* in D_2O are tabulated and again considering the small differences involved, the data are very consistent.

An analysis of the information contained in Table II now allows calculation of the self-diffusion coefficients of pure normal water⁷ (H_2O in H_2O) and also of pure heavy water (D_2O in D_2O). In the first place it can be deduced from columns 2 and 3 that over the range 5 to 45° , HDO and HTO react similarly in changing from one solvent

(11) D. Eisenberg and W. Kauzmann, "The Structure and Properties of Water," Clarendon Press, Oxford, 1969, pp 218-219.

(12) R. J. Bearman, *J. Phys. Chem.*, **65**, 1961 (1961).

(13) D. W. McCall and D. C. Douglass, *J. Phys. Chem.*, **71**, 987 (1967).

TABLE I: Self-Diffusion of Isotopic Species of Water

Temp. °C	HTO*–H ₂ O	HDO*–H ₂ O ^a	DTO*–D ₂ O	HDO*–D ₂ O ^a	HTO* } / 50 mol % DTO* } / D ₂ O–H ₂ O
	$D^* \times 10^9 \text{ m}^2 \text{ sec}^{-1}$				
1	1.113 ± 0.002	1.128			
4	1.236 ± 0.003				
5	1.272 ± 0.002	1.295	1.001 ± 0.001	1.034	
15	1.724 ± 0.003				
25	2.236 ± 0.004	2.272	1.849 ± 0.001	1.902	2.029
35	2.838 ± 0.002				
45	3.474 ± 0.003	3.532	2.939 ± 0.005	3.027	

^a Longworth's data^{1,2} (precision ±0.1%).

TABLE II: Differences in Diffusion Rate Due to Isotopic Mass

Temp. °C	$[D^*(\text{H}_2\text{O}) - D^*(\text{D}_2\text{O})] \times 10^2$		$[D^*_{\text{HDO}} - D^*_{\text{HTO}}] \times 10^2$	$[D^*_{\text{HDO}} - D^*_{\text{DTO}}] \times 10^2$
	$D^*(\text{H}_2\text{O})$		D^*_{HDO}	D^*_{HDO}
	H ¹⁸ O* D ¹⁸ O*	HDO*	(H ₂ O)	(D ₂ O)
5	21.4%	20.2%	1.8%	3.2%
25	17.3	16.3	1.6	2.8
45	15.4	14.3	1.6	2.9

TABLE III: Calculated Self-Diffusion Coefficients of H₂O and D₂O

Temp. °C	$D^* \times 10^9 \text{ m}^2 \text{ sec}^{-1}$, H ₂ O–H ₂ O	$D^* \times 10^9 \text{ m}^2 \text{ sec}^{-1}$, D ₂ O–D ₂ O
1	1.149	
4	1.276	
5	1.313	1.015
15	1.777	
25	2.299	1.872
35	2.919	
45	3.575	2.979

(H₂O) to another (D₂O) and the mass effects are carried over in almost exact proportion. Therefore it is reasonable to assume that changes in diffusion rate arising from mass differences between isotopic species in solvent D₂O should be equally applicable to the change in solvent H₂O. In column 5 of Table II, there is tabulated the percentage change in diffusion rate in the solvent D₂O between molecules of mass 21 (DTO) and mass 19 (HDO), a difference of 2 mass units. Now for the solvent H₂O, we have measured diffusion coefficients for molecules of mass 20 (HTO) and what we are trying to calculate are values for molecules of mass 18 (H₂O), again a difference of 2 mass units. Therefore increasing our measured values for HTO by the percentages given in column 5 should give the corresponding values for self-diffusion in pure water, (H₂O in H₂O). Similarly self-diffusion in pure heavy water (D₂O in D₂O) can be obtained by decreasing Longworth's HDO in D₂O values by the percentages given in column 4 which correspond to a mass change of one unit in H₂O. The coefficients so obtained should be accurate to a few tenths of a per cent and are listed in Table III. For values other than 5, 25, and 45°, averaged percentages have been used.

An Arrhenius plot ($\log D$ vs. $1/T$) for both sets of data is given in Figure 1. If activation energy theories are applicable to diffusion in liquids one would expect a linear relation among the points; instead there is a gentle curvature in both sets. However, without implying that the ac-

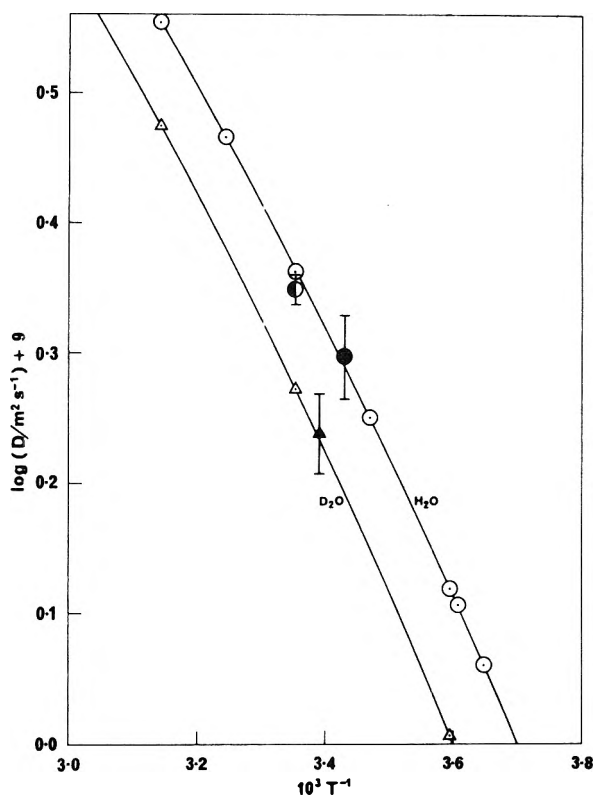


Figure 1. Arrhenius plot of $\log D$ vs. $1/T$ of the self-diffusion coefficients of pure H₂O (O) and pure D₂O (Δ): (●, \blacktriangle), nmr values of Murday and Cotts;¹⁵ (○, \triangle), nmr value of O'Reilly and Peterson.¹⁶

tivation approach is valid one can give experimental activation energies for the temperature regions 1–15° and 15–45° as these data are useful to workers in the biological sciences and other areas. For H₂O, $E_A = 4.7$ kcal/mol (1–15°) and 4.2 kcal/mol (15–45°) and for D₂O, $E_A = 5.0$ kcal/mol (1–15°) and 4.5 kcal/mol (15–45°).

The only comparisons that can be made with the data in Table III are as has been implied earlier, with molecular dynamics and nmr results where the identification process has virtually no effect on physical or chemical properties. A molecular dynamics study of liquid water has recently been reported by Rahman and Stillinger.¹⁴ At a temperature of 34.3° they obtain a figure of $4.2 \times 10^{-9} \text{ m}^2 \text{ sec}^{-1}$ for the self-diffusion coefficient of water which can be compared with our value at that temperature of 2.84. Although the discrepancy is large, the technique of computer simulation of the properties of complex liquids such as water is in its infancy. It might be hoped indeed that feedback from our results into the calculations may eventually help to refine the simulation techniques.

In nmr studies, up until a year or two ago, there was a wide scatter of results for the self-diffusion of liquid water at 25°. These values ranged from 2.13 to $2.51 \times 10^{-9} \text{ m}^2 \text{ sec}^{-1}$ (see, e.g., ref 5). More recently, Murday and Cotts¹⁵ have reported a value of $1.98 \pm 0.14 \times 10^{-9} \text{ m}^2 \text{ sec}^{-1}$ at 18.4° and O'Reilly and Peterson¹⁶ $2.23 \pm 0.06 \times 10^{-9} \text{ m}^2 \text{ sec}^{-1}$ at 25.0°. For D₂O, Murday and Cotts¹⁵ have determined also a value of $1.73 \pm 0.12 \times 10^{-9} \text{ m}^2 \text{ sec}^{-1}$ at 21.7°. These values have been included in our Figure 1

and it is seen that within their limits of error there is satisfactory agreement. The actual reproducibility of nmr results can be of the order of $\pm 0.5\%$ and the large errors quoted in nmr data therefore appear to be due to uncertainties in the machine calibration factor. It might be more practical now to obtain this calibration factor by direct comparison with the data presented in Table III.

So far in this discussion we have been using experimental considerations only to obtain these self-diffusion coefficients. It will be realized that for both H₂O and D₂O, we now have original and derived experimental data for the diffusion of three isotopic forms of water over a considerable temperature range. There is the possibility therefore that the functional form of the mass dependence can be determined. This functional relationship does not appear to be a simple square root of the mass dependence and it seems probable that the differing interaction potentials of the various isotopic species are also involved. This problem is undergoing further study.

(14) A. Rahman and F. H. Stillinger, *J. Chem. Phys.*, **55**, 3336 (1971).

(15) J. S. Murday and R. M. Cotts, *J. Chem. Phys.*, **53**, 4724 (1970).

(16) D. E. O'Reilly and E. M. Peterson, *J. Chem. Phys.*, **55**, 2155 (1971).

The Limiting Equivalent Conductance of Perchloric Acid in 0.9914 Mole Fraction *N*-Methylacetamide (NMA) at 40°

Jerry F. Casteel and Edward S. Amis*

Department of Chemistry, University of Arkansas, Fayetteville, Arkansas 72701 (Received October 30, 1972)

At 40.00° and in 0.9914 mole fraction NMA, Λ values for perchloric acid were determined over a range of concentrations of the acid. Λ_0 was obtained from the Λ values using the methods of Kohlrausch, Fuoss and Kraus, and Shedlovsky. The Λ_0 values obtained by the three methods were in excellent agreement and, if the limiting equivalent ionic conductances recorded in the literature are applicable to anhydrous NMA, indicate little or no Grothuss conductance in NMA, and no formation of hydrated entities with ions of perchloric acid which were of different mobilities than the ion entities existing in pure NMA.

Shedlovsky¹ noted in his studies of hydrochloric acid in the water-methanol system that a remarkable drop occurred in the equivalent conductance at infinite dilution when trace amounts of water were added to the pure methanol solvent. Similar decreases were found by Goldenberg and Amis^{2,3} for perchloric acid in water-ethanol and water-methanol solvents. The reasons for such sharp decreases are usually ascribed to a breaking up of the Grothuss conduction chains in the alcohols and the formation of H₃O⁺ and H₉O₄⁺ which move as entities through the solution. The highly hydrogen bonded nature of *N*-methylacetamide suggests that it could be a good solvent to test whether a proton jump mechanism is general for strong acids in hydrogen bonded solvents rather than just for water or low molecular weight alkyl alcohols.

Dawson, Newell, and McCreary⁴ have suggested that the proton does not move by a unique method in formamide.

Experimental Section

The conductance measurements were made at 0.5, 1.0, 2.0, 5.0, and 10.0 kHz and extrapolated to infinite frequency. The conductance apparatus and methods were

(1) T. Shedlovsky, "The Structure of Electrolytic Solutions," W. J. Hamer, Ed., Wiley, New York, N. Y., 1959.

(2) N. Goldenberg and E. S. Amis, *Z. Phys. Chem. (Frankfurt am Main)*, **30**, 65 (1961).

(3) N. Goldenberg and E. S. Amis, *Z. Phys. Chem. (Frankfurt am Main)*, **31**, 145 (1962).

(4) L. R. Dawson, T. M. Newell, and W. J. McCreary, *J. Amer. Chem. Soc.*, **76**, 6024 (1954).

TABLE I: Equivalent Conductances and Limiting Equivalent Conductances at Infinite Frequency of Perchloric Acid in 0.9914 Mole Fraction at 40.00°

10°C	Λ_{∞}	10°C	Λ_{∞}
315.41	23.38	51.31	25.00
204.21	23.92	30.60	25.24
128.88	24.37	19.01	25.44
78.38	24.75	6.642	25.62
$\Lambda_0(\lambda(\text{H}^+) + \lambda(\text{ClO}_4^-))$	$\Lambda_0(\text{Kohlrausch})$	$\Lambda_0(\text{Fuoss-Kraus})$	$\Lambda_0(\text{Shedlovsky})$
25.9	26.06	26.02	26.02

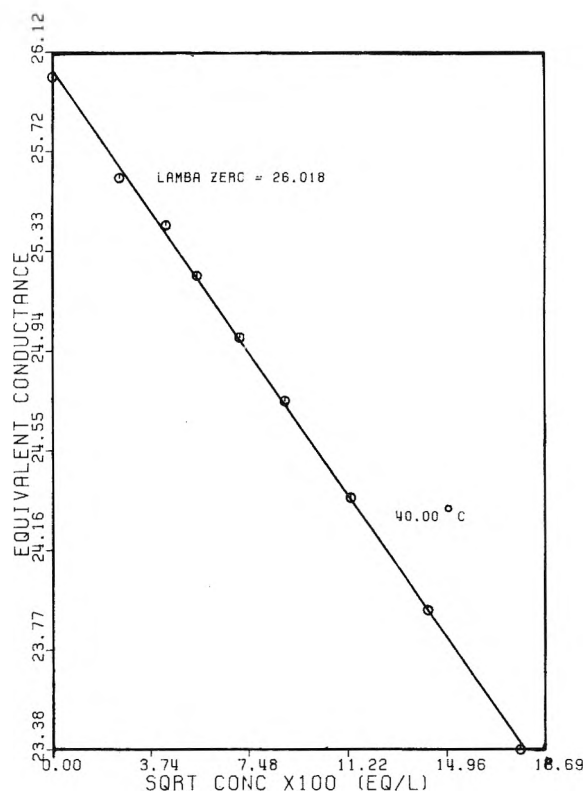
described previously.^{5,6} Reagent grade perchloric acid was standardized against sodium hydroxide which was previously standardized with potassium acid phthalate. The *N*-methylacetamide was distilled and then fractionally crystallized repeatedly until a melting point of 30.28° was obtained.^{7,8} Analyses by Karl Fischer reagent and gas-phase chromatography showed a purity of 99.998 wt % or greater.

Results

Table I gives the values of the equivalent conductance of perchloric acid at infinite frequency in 0.9914 mole fraction *N*-methylacetamide at 40.00°. Figure 1 shows a Kohlrausch type⁹ plot of the data. The value of Λ_0 in pure *N*-methylacetamide was found by adding the limiting ionic conductances of the perchlorate ion and hydrogen ion given by Dawson, Wilhoit, Holmes, and Sears.¹⁰ $\lambda_0(\text{H}^+) = 9.1$; $\lambda_0(\text{ClO}_4^-) = 16.8$. These values give $\Lambda_0(\text{HClO}_4) = 25.9$.

The values of Λ_0 in 0.9914 mole fraction *N*-methylacetamide were obtained by the methods of Kohlrausch,⁹ Fuoss and Kraus,¹¹ and Shedlovsky.¹² The values are also shown in Table I.

If the limiting ionic conductances of ref 10 are applicable to anhydrous NMA, the very small difference in the calculated Λ_0 in pure NMA and in 0.9914 mole fraction NMA implies that there is little if any Grothuss type conduction of the hydrogen ion in this solvent. At least a small amount of water did not reduce the limiting equivalent conductance of HClO_4 in NMA, thus apparently not

**Figure 1.** Perchloric acid in 0.9914 mole fraction NMA at 40°.

breaking down Grothuss conductance chains, and also not forming hydrated entities with ions of perchloric acid which were of different mobilities than the ion entities existing in pure NMA.

- (5) J. F. Casteel and E. S. Amis, *J. Electrochem. Soc.*, **117**, 213 (1970).
- (6) J. F. Casteel and E. S. Amis, *J. Chem. Eng. Data*, **17**, 55 (1972).
- (7) L. R. Dawson, J. W. Vaughn, M. E. Pruitt, and H. C. Eckstrom, *J. Phys. Chem.*, **66**, 2684 (1962).
- (8) L. R. Dawson, J. W. Vaughn, G. R. Lester, M. E. Pruitt, and P. G. Sears, *J. Phys. Chem.*, **67**, 278 (1963).
- (9) F. Kohlrausch and L. Holczron, "Das Leitvermögen der Electrolyte," Teubner, Leipzig and Berlin, 1916.
- (10) L. R. Dawson, E. D. Wilhoit, R. R. Holmes, and P. G. Sears, *J. Amer. Chem. Soc.*, **79**, 3004 (1957).
- (11) R. M. Fuoss and C. A. Kraus, *J. Amer. Chem. Soc.*, **55**, 476 (1933).
- (12) T. Shedlovsky, *J. Amer. Chem. Soc.*, **54**, 1405 (1932).

High-Temperature Kinetics of Pyrolytic Graphite Gasification by Fluorine Atoms and Molecules¹

Daniel E. Rosner*² and Joseph P. Strakey

Department of Engineering and Applied Science, Yale University, New Haven, Connecticut 06520 (Received August 17, 1972)

Publication costs assisted by the U.S. Army Research Office—Durham

Kinetic data for basal and edge plane pyrolytic graphite gasification in atomic and diatomic fluorine are reported in the surface temperature range 1036–1715°K, and at fluorine pressures from 3×10^{-3} to 0.6×10^{-1} Torr. Inferred carbon atom removal probabilities, ϵ , for the F atom attack of either basal or edge plane graphite reveal a sharp maximum at intermediate temperature ($\approx 1122^\circ\text{K}$), with $\epsilon_{\text{max}} \approx 1/4$. Under these conditions it appears that each incident F atom chemisorbs and is ultimately used in the production–desorption of one $\text{CF}_4(\text{g})$ molecule. In contrast, C atom removal probabilities observed in F_2 are much lower above 1050°K, show a much shallower ϵ_{max} at noticeably higher surface temperature (near 1280°K), and exhibit great sensitivity to crystallographic orientation of the surface. It is concluded that F_2 has difficulty chemisorbing, especially on the predominantly basal plane, whereas F atoms chemisorb with nearly unit probability on either face provided the adsorbed F atom population sufficiently low. Despite the thermodynamic stability of the reaction product CF_4 over the entire surface temperature range examined here, the decrease in ϵ observed at high temperatures is attributed to the thermal desorption of F adatoms which have not been able to find reactive sites by the process of surface diffusion. At the lower temperatures investigated here, both kinetic and electron micrograph evidence for the formation of carbon subfluoride reaction product layers is presented. Instructive comparisons are made between this system, and the gasification kinetics of graphite in oxygen and hydrogen atom-containing gas streams.

1. Introduction

In ref 3 it was demonstrated that the kinetics of reactions of F atoms and F_2 molecules with refractory solids forming volatile fluorides can be studied in the absence of the intervention of physical phenomena at temperatures up to the onset of substrate sublimation or melting. In the present paper we document our application of these experimental techniques to the important and interesting refractory solid, pyrolytic graphite (PG), in the surface temperature range 1036–1715°K. Our choice of PG stems from a number of diverse considerations, not the least of which is its widespread use as a high-temperature containment material in rocket motors employing fluorine-containing oxidizers. In addition, pyrolytic graphites now commercially available (i) offer the possibility of studying the “structure sensitivity” of gasification rates in atomic and diatomic fluorine since both the “basal” plane and “edge” (prismatic) plane (see Figures 1 and 2) can be independently investigated in the same experiment, (ii) come sufficiently close to the theoretical density of single crystal graphite to eliminate the kinetic complications of pore diffusion and crystallite removal (“ablation”) commonly encountered in oxidation studies of lower density polycrystalline graphites, (iii) can be cut into strips easily heated resistively to temperatures which are not only in the range of interest but also remarkably uniform in the span-wise direction (owing to the high thermal conductivity of PG in the ab direction, and (iv) could probably be used in research applications as a thermal (oven) source of atomic fluorine⁴ for atomic beam experiments at sufficiently high oven temperatures (see section 4).

In view of the above, one might expect that the high-temperature fluorination kinetics of pyrolytic graphite, or fluorine chemisorption on “clean” single crystal graphite (Figure 1)⁵ would have been extensively studied before

this, however, this turns out to be far from the case. Moreover, while several investigators have studied the reaction of $\text{F}_2(\text{g})$ with “isotropic” (randomly oriented, polycrystalline) graphites at temperature corresponding to the volatilization of simple fluorocarbon gases (predominantly carbon tetrafluoride ($\text{CF}_4(\text{g})$),⁶ none of these experiments was carried out under reactor conditions such that the observed reaction rates were free of the influence of gas-phase transport limitations. Hence, previously available data are difficult to generalize, and unsuitable as a starting point for instructive mechanistic inferences. As noted in ref 7–11, these difficulties can be circumvented, even for reactions which are “successful” upon nearly every reactant gas collision with the surface, only by combining the experimental conditions of small specimen size, low total pressure and high gas flow rate over the specimen (section 2). As will be seen (section 4) these reactor

- (1) This research was supported by the U. S. Army Research Office, Durham, N. C., under Contract No. DAH CO4-C-0027.
- (2) Associate Professor, Chemical Engineering Group, Mason Laboratory; to whom inquiries concerning this manuscript should be sent.
- (3) D. E. Rosner and H. D. Allendorf, *J. Phys. Chem.*, **75**, 308 (1971).
- (4) Until now, only isotropic graphites have been used for this purpose.
- (5) In pyrolytically deposited graphites an oriented, hexagonal net, lamellar structure is obtained, however, carbon atom stacking in the c direction is imperfect (randomly shifted) with respect to the positions shown in Figure 1.
- (6) See, e.g., A. K. Kuriakose and J. L. Margrave, *J. Phys. Chem.*, **69**, 2772 (1965), and the background references cited therein.
- (7) D. E. Rosner, *Symp. (Int.) Combust.*, [Proc.], 11th, 1966, 181 (1967).
- (8) D. E. Rosner and H. D. Allendorf, “Heterogeneous Kinetics at Elevated Temperatures,” Plenum Press, New York, N. Y., 1970, pp 231–251.
- (9) D. E. Rosner, “Annual Review of Materials Science,” Vol. 2, Annual Reviews Inc., Palo Alto, Calif., pp 573–606.
- (10) D. E. Rosner and H. D. Allendorf, *J. Electrochem. Soc.*, **114**, 305 (1967).
- (11) D. E. Rosner, NATO Advisory Group for Aerospace Research and Development, Conference Proceedings on High-Temperature Corrosion of Aerospace Alloys, in press.

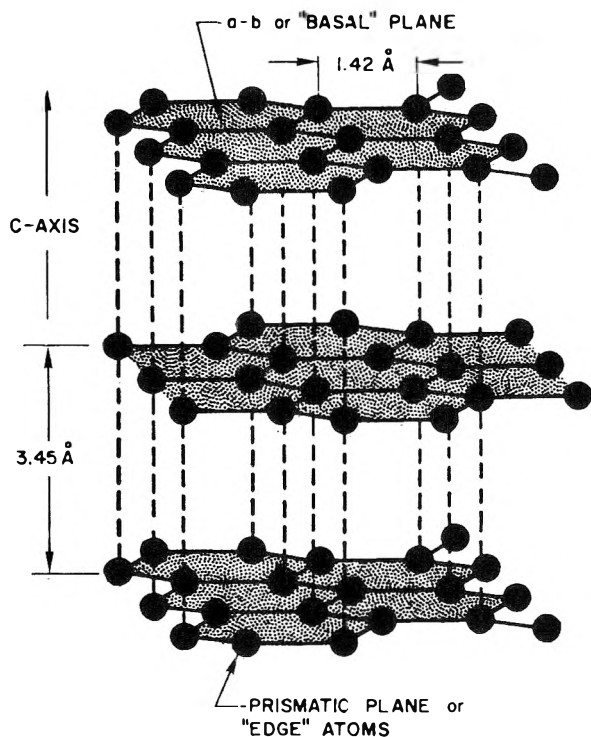


Figure 1. Graphite crystal structure/nomenclature.

conditions are particularly important for investigations of dissociated gas–solid interactions when *reaction* (in this case C atom transfer) rather than surface-catalyzed atom *recombination* is the favored “path,”^{8,12} (and the reaction probability is large). Indeed, our preliminary F atom data on an isotropic graphite³ suggested that when $T \approx 1110^\circ\text{K}$ at $p_F \approx 10^{-2}$ Torr every F atom encounter leads to chemisorption and the ultimate formation and desorption of a $\text{CF}_4(\text{g})$ molecule.

In what follows, our approach is to focus attention on the probability, ϵ , that an F atom or F_2 molecule incident upon the surface will lead to the removal (*via* fluorocarbon desorption) of a carbon atom originally bound in the solid. Apart from practical interest in this carbon loss (“gasification”), it will be seen (section 4) that insight into the reaction mechanism can be obtained by systematically studying the dependence of ϵ on the (i) chemical state of the attacking gas (ground-state atoms or molecules), (ii) crystallographic structure of the solid surface (basal or edge plane), (iii) surface temperature, T , and (iv) reactant gas arrival rate corresponding to the prevailing fluorine partial pressure. Additionally, scanning electron microscope (sem) pictures have been taken of the PG specimen surfaces before and after fluorination; some of these photographs are included and discussed in section 3.

In view of the rich possibilities inherent in fluorocarbon chemistry,¹³ direct sampling and mass spectrometric identification of the vapor-phase reaction products would certainly be of added interest. While this has not been attempted in the present exploratory investigations, reasonable estimates of the likely reaction products can be derived from our observed carbon atom removal probabilities when suitably combined with quasiequilibrium concepts, and previous data on the analogous H/graphite reaction. We will return to these kinetic and thermodynamic considerations in section 4, following a description

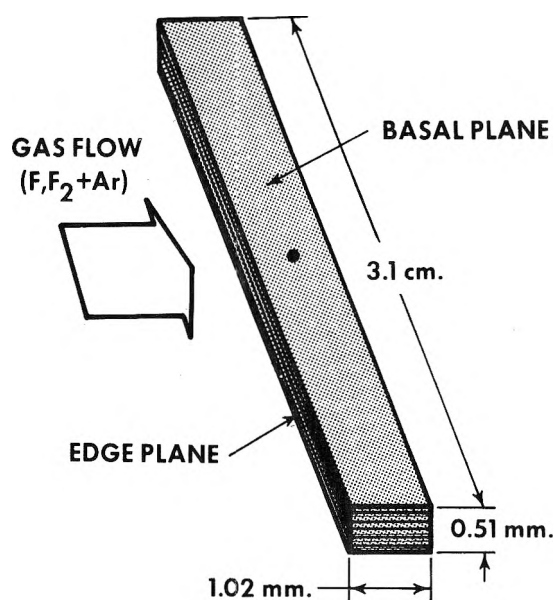


Figure 2. PG specimen configuration for atom flow reactor gasification kinetic studies.

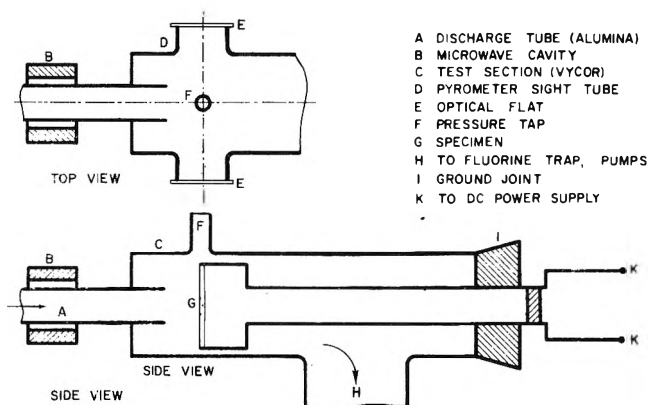


Figure 3. Specimen fluorination apparatus (schematic).

of our experimental techniques (section 2), and principal experimental results (section 3).

2. Experimental Section

Fluorination Apparatus. The fluorination apparatus, shown schematically in Figure 3, is a modification of that previously used by Rosner and Allendorf³ to study the fluorination kinetics of tungsten and molybdenum. Gas mixtures of 0.2–5 vol % diatomic fluorine in argon were passed through a 0.95 cm i.d. \times 45 cm long dense alumina tube (A, Coors AD-998) at about 1.1 Torr pressure and 1300 standard cc/min. The corresponding average gas velocity was about 2.3×10^4 cm/sec. As discussed in ref 3, under these conditions extensive dissociation of F_2 occurs

- (12) Owing to the low bond energy, D_0° , for $\text{F}_2(\text{g})$. (ca. 37 kcal mol⁻¹) associative desorption of $\text{F}_2(\text{g})$ from the graphite surface can be shown to be thermodynamically unlikely at all surface temperatures in the range experimentally studied herein ($T > 1000^\circ\text{K}$), at the prevailing fluorine pressures.
- (13) As is now well known, the family of fluorocarbons is architecturally and stoichiometrically similar to their hydrocarbon analogs, having the same C atom skeletal structure. Thus, one has saturated and unsaturated fluorocarbons, straight chain, branched chain, and cyclic (ring) fluorocarbons, as well as fluorocarbon polymers. However, owing primarily to the greater strength of the C–F bond, the analog of dehydrogenation is thermodynamically unfavorable with respect to C–C bond cleavage.

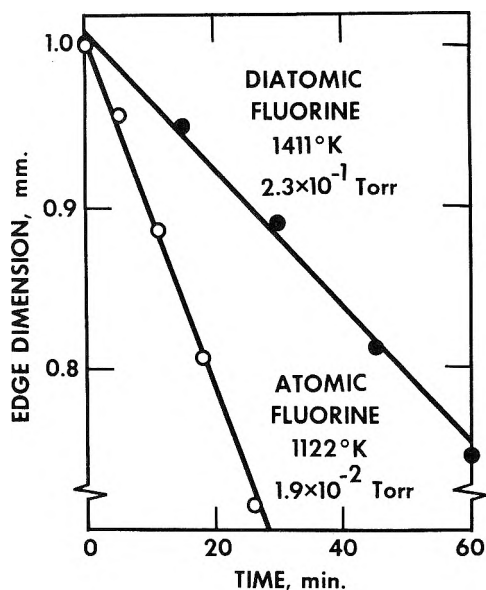


Figure 4. Fluorination rate as determined by transverse specimen dimension as a function of time: edge plane recession in atomic and diatomic fluorine.

as the gas mixture passes through a modified Evenson-type microwave discharge cavity¹⁴ (B) surrounding the alumina discharge tube approximately 28-cm upstream of the reacting PG specimen. Microwave power (2450 MHz) was supplied to this cavity from a Scintillonics, Inc., 120-W power supply operated at an output power level of 92 W. The discharge products entered the 4.8 cm i.d. Pyrex test section (C) through a Teflon-lined aluminum "header" (not shown in Figure 3) with provision for two additional discharge tubes to be used for subsequent experiments on PG reactivity in mixed atomic gases. Seals to the Pyrex test section and discharge tubes were made with Viton O rings.

The PG specimen (G) was supported on a two-pronged monel probe inserted *via* a ground joint (I) in the rear. Downstream of the test section the gas mixture (comprised of fluorine, reaction products, and argon) passed through a large radial-flow packed bed (not shown in Figure 3) of 8-14 Tyler mesh activated alumina within which the fluorine is removed *via* an oxygen displacement reaction. The resulting gas mixture then passed on to a large (130 CFM) Kinney KDH-130 mechanical vacuum pump. Gaseous diatomic fluorine was supplied from a barricaded cylinder in accord with Matheson Co. recommendations. Any HF contained in the cylinder gas was removed by a NaF-packed bed trap operating at room temperature in the fluorine supply line. Aluminum and Teflon tubing with Al-Si bronze valves and a Matheson Model B15F-679K regulator were used upstream of the test section, and copper and brass parts were used downstream. Fluorinated hydrocarbon stopcock greases and manometer oils (supplied by Halocarbon Products Corp.) were used where necessary. Occasional ignition of the stopcock grease exposed to pure fluorine necessitated vigilance on the part of the experimenter. As a precautionary measure a high-capacity aluminum ventilating hood was installed over the entire apparatus and frequent leak testing of the fluorine supply system and reactor was performed.

Argon and fluorine were metered separately with the aid of critical flow orifices¹⁵ and fluorocarbon oil-filled burets, respectively. The two gases were then mixed just up-

stream of the entrance to the discharge tube. The gas mixture static pressure level in the test section was controlled at about 1.1 Torr by bleeding air into the high-capacity pump downstream of the fluorine trap.

Specimen Preparation. The specimens were cut from commercially available thin plates of pyrolytic graphite (Union Carbide Corp., Carbon Products Div., New York, N. Y., grade HPG). This graphite is formed by high-temperature vapor deposition and is free-standing (no substrate), quite strong, and free of voids, with a density (2.18 g/cc) approaching the theoretical single crystal graphite density. The $1.5 \times 1.0 \times 0.020$ in. "as received" PG plates were first fastened to a flat carbon block using a small amount of plastic cement applied to the ends of the plate. The block was then mounted in a milling machine and a thin circular metal saw which cut through into the carbon block was used to slice the plate into specimens suitable for resistive heating. The nominal dimensions of the resulting specimens were $0.051 \times 0.102 \times 3.8$ cm with the basal plane being the largest face. They were mechanically secured to the monel specimen holder (using small stainless steel washers and screws)¹⁶ with the basal planes parallel to the gas flow direction and the prism planes perpendicular, as shown in Figure 2.

Reaction Rate Measurements. In almost all cases the PG specimens were reacted in fluorine-argon mixtures for a time sufficient to remove about 0.25 mm from the edge plane. However, at high temperatures, this was not always possible since a higher reaction rate prevailed near the cooler regions of the specimen (see section 3) where localized burn out often terminated the run. The transverse dimensions for both planes were measured using an optical microscope before and after reaction of measured duration. A small shallow pit drilled into the basal plane was used to locate the span-wise point at which the specimen size measurements were made. During an experiment, the optical pyrometer used for temperature control was sighted on the basal plane in the area around this pit. Time independence of the reaction rate, expected for gas/solid reactions forming volatile or "nonprotective" products, was verified for the edge plane at temperature levels corresponding to maximum fluorination rate by measuring this dimension at several successive exposure times. The inferred reaction rate was found to be quite constant for both F and F₂ attack, as shown in Figure 4.

Pyrometry. The direct heating current passing through the specimen was manually adjusted to maintain a constant apparent ("brightness") temperature, T_{λ} , as observed with a vanishing-filament micro-optical pyrometer (Pyro Instrument Co., Bergenfield, N. J.). The brightness temperature of the basal plane in the presence of a low concentration¹⁷ of F₂ was related to the true PG-specimen temperature, T_w , by determination of the apparent melting points of gold, silver, and nickel in intimate contact with the specimen. Thus, small chips of these metals were forced into a small hole drilled into the basal plane of the

(14) The modification used, described by McCarroll (*Rev. Sci. Instrum.*, **41**, 279 (1970)) was obtained from Ophthos Instrument Co., Rockville, Md. While it did not appear to significantly increase the fraction dissociated, it was much easier to "tune" (*i.e.*, to minimize the reflected microwave power).

(15) D. E. Rosner, *J. Basic Eng.*, **84**, 459 (1962).

(16) Constancy of the observed reaction rate (regardless of time at temperature) and the absence of enhanced reactivity in the immediate vicinity of the specimen supports at midpoint temperatures less than 1100°K suggest the absence of specimen contamination due to this cause.

(17) The presence of F₂ altered the observed brightness temperature less than 2°K.

specimen, and the specimen temperature was gradually increased until the melting point of the metal was attained, at which a "collapse" of the metal chip could be observed. This was straightforward and repeatable for gold, but somewhat more difficult for the other metals. The normal spectral emittance of the basal plane at 0.65μ calculated from these observed reference temperatures is shown in Table I.¹⁸ Window-loss corrections have already been applied to the observed specimen brightness temperatures.¹⁹ True specimen temperatures used in reporting the reaction rate behavior below were calculated from a calibration curve passing through the basal plane data of Table I. During each experiment it was accordingly assumed that both planes were at the same temperature, *i.e.*, transverse temperature gradients *within* the PG specimen at mid-span were neglected.

Reactant Arrival Rate. To infer the C atom removal probability, ϵ , from a knowledge of the measured reaction rate (*via* dimension change) it is necessary to (a) convert the observed recession rate to C atom flux, $\epsilon_{(C)}$, *via* the known density of the specimen and atomic mass, m_C , of carbon, and (b) calculate the arrival (impingement) rate Z of F or F_2 with the surface at the prevailing flow rate and reactant partial pressures. Then, regardless of the stoichiometry of the reaction products, we define

$$\epsilon \equiv \epsilon_{(C)}/Z \quad (1)$$

Provided the fluorine plus argon gas mixture flow rate is sufficiently large, and the specimen size and total pressure level are sufficiently small, reactant partial pressure gradients *normal* to the specimen surfaces can be suppressed,⁷⁻¹¹ thereby simplifying the inference of Z if the ambient reactant partial pressure is known, together with the mixture pressure distribution around the specimen cross section. Thus, for reactant species i ($i = F$ or F_2) the Hertz-Knudsen equation provides

$$Z_i = [p_i/(kT)][kT_{i,w}/(2\pi m_i)]^{1/2} \quad (2)$$

where p_i is the average prevailing reactant partial pressure at the specimen surface in question, $T_{i,w}$ is the translational temperature of species i one mean-free-path from the surface, k is the Boltzmann constant, and Z_i has the units molecule $\text{cm}^{-2} \text{sec}^{-1}$. Since the ambient mean-free-path at the free stream static pressure of 1.1 Torr is less than one-tenth of the smallest specimen transverse dimension, we tentatively estimate $T_{i,w} \approx T_w$, *i.e.*, incident fluorine atoms or molecules²⁰ are raised to near the surface temperature (by collisions with argon) prior to impacting on the surface. Estimating the value of p_{F_2} clearly presents a simple problem than that of p_F since the value of p_{F_2} in the feed stream is known from the total pressure and relative flow rates of Ar and F_2 . However, for either F_2 or F it is necessary to correct for the fact that, at the gas flow rates required to suppress external diffusional limitations, the local pressures on the specimen surfaces can depart noticeably from the free stream static pressure. Since the overriding effect here is the increased ("stagnation" or "impact") pressure on the leading surface of the specimen, a flat-faced cylindrical Pitot (impact pressure) probe, comprised of a 0.508 mm circular opening in a 2.54 mm o.d. cylinder facing upstream, was introduced to measure the impact pressure at a flow rate of 1300 cc/min. The result was found to be a factor of 1.94 larger than the ambient steam pressure, in approximate accord with

TABLE I: Normal Spectral Emittance^a of Pyrolytic Graphite^b

Face	$T, ^\circ\text{K}$	Emittance ^a
Basal	1234 (Ag)	0.697
Basal	1336 (Au)	0.669
Basal	1726 (Ni)	0.613
Edge	1336 (Au)	0.834

^a Spectral emittance at 0.65μ . ^b Union Carbide Grade HPG.

that expected by isentropically stagnating the discharge tube gas flow.²¹ Peripheral pressure distribution measurement on an unheated cylinder in crossflow made in our laboratory, and by others,²² suggests smaller departures from the steam pressure at other locations on the specimen, especially in the rear stagnation region.²³ In the absence of more direct experimental pressure distribution data on rectangular cross section objects in the Reynolds number, Mach number, and surface temperature range encountered in our fluorination experiments, in what follows we have therefore estimated arrival rates based on an average²⁴ pressure on the edge planes (forward plus rear facing; *cf.* Figure 2) of 1.47 times ambient, and an average pressure on the basal planes of approximately the ambient value. All values of ϵ reported herein incorporate eq 2 for Z , with these pressure correction factors applied to the edge and basal plane rate data.

If a reliable and convenient absolute F atom detection scheme were available (*e.g.*, based on a chemiluminescent titration reaction, or the energy released upon surface-catalyzed F atom recombination; *cf.* ref 3) then the arrival rate for F atoms could be calculated as above, in terms of the measured F atom partial pressure, p_F , at the specimen location downstream of the microwave electrical discharge. Pending the development of satisfactory F atom detection methods, we have adopted an alternative approach based on maximum inferred ϵ values for the fluorination of molybdenum, titanium, boron, and graphite in the present apparatus. As reported in ref 3, we have found that in the latter three cases (Ti, B, and C) the *maximum* gasification rates observed all correspond to an F atom arrival rate of about 4.6×10^{18} atom $\text{cm}^{-2} \text{sec}^{-1}$ at 1.1 Torr if it is assumed that *every* incident F atom leads respectively to the production of TiF(g), BF(g), and CF₄(g). Since this also proved to be true for our present results on edge plane pyrolytic graphite, this in effect validates the

- (18) For comparison, a similar procedure was used to determine the spectral emittance of the edge plane at 1336°K. This value is also included in Table I.
- (19) To calculate the specimen brightness temperature in the absence of an intervening window it was assumed that the reduction in transmitted intensity at 0.65μ is due to reflection at the two gas/glass interfaces. In that case the intensity ratio at normal incidence would be $(1 - \rho)^2$ where $\rho = [(n - 1)/(n + 1)]^2$ and n is the refractive index of the glass. The brightness temperature difference corresponding to this intensity ratio at 0.65μ was then calculated from Wein's law.
- (20) The procedure ultimately adopted for estimating the F atom arrival rate (see below) is insensitive to this specific assumption, however, F_2 arrival rates were calculated on this basis.
- (21) A. H. Shapiro, "The Dynamics and Thermodynamics of Compressible Fluid Flow," Vol. 1, Ronald Press, New York, N. Y., 1953.
- (22) See, *e.g.*, the review of G. K. Batchelor, "An Introduction to Fluid Mechanics," Cambridge University Press, New York, N. Y., 1967, Section 4.12.
- (23) The perimeter-averaged static pressure on a 2.54-mm o.d. cylinder under these conditions (1300 cc/min, 1.1 Torr) was 1.12 times the free stream static pressure.
- (24) Edge-plane surface-recession measurements were based on an average of both forward-facing and rear-facing surfaces (Figure 2). Hence, the average overpressure used in estimating ϵ for the edge planes was $(\frac{1}{2})(1.94 + 1.00)$ times ambient.

procedure of ref 3, and permits the calculation of all ϵ values for PG based on setting $\epsilon_{\max} = \frac{1}{4}$ for the edge plane. At other surface temperatures it was assumed that (a) the F atom arrival rate varied as $T_w^{-1/2}$ (cf. eq 2) and (b) the F₂ contribution to the observed C atom removal rate in partially dissociated fluorine is estimable using $\epsilon(T)$ for the F₂ contribution as determined in our experiments with undissociated fluorine. In effect, this latter procedure treats the F and F₂ contributions to the gasification rate as additive, and assumes that the F₂ reaction is nearly first order in p_{F_2} . But since even for the edge plane the F₂ correction never amounted to more than about 11%, and was negligible near ϵ_{\max} , this data reduction procedure was deemed adequate for PG fluorination experiments carried out in highly dissociated F plus F₂ mixtures, as obtained using the present microwave discharge technique.²⁵

An interesting question arises as to whether the reaction rates we report in "undissociated" fluorine are influenced by thermal dissociation in the vicinity of the 1000–1800°K PG specimens. This possibility was quantitatively considered in ref 3, dealing with the fluorination kinetics of tungsten and molybdenum under similar conditions but at filament temperatures up to 3000°K. There, it was concluded that the F₂ residence time in the vicinity of the specimen is quite inadequate to permit any appreciable thermal dissociation. However, this does not preclude the surface-catalyzed dissociation of F₂ molecules that may suffer multiple encounters on the microscopically rough specimen surfaces. The extent of this latter effect is difficult to assess, and, if present, it would cause our reported ϵ for F₂ to differ from the true (usually lower) *single-encounter* reaction probability for F₂.

3. Experimental Results

Using the definition of the carbon atom removal probability, eq 1, and estimates of the F and F₂ arrival rates as outlined in section 2, our data for the temperature dependence of the specimen recession rates can be cast in the Arrhenius form shown in Figure 5. Examination of these experimental results reveals the following noteworthy features. (i) The maximum C atom removal probability for F atom attack of edge plane PG is about $\frac{1}{4}$, and occurs at about 1120°K; at this rather well-defined temperature the reaction probability for atom attack of the basal plane is only slightly lower than that corresponding to the edge plane. (ii) In contrast, there is a much more marked effect of orientation on the fluorination probabilities with F₂, with basal plane values being lower than those for the edge plane by some five-tenfold over a considerable temperature range on either side of the more shallow F₂ rate maxima. (iii) Above about 1030°K, dissociation of fluorine causes a dramatic increase in the C atom removal probability on basal plane graphite, with rate enhancements near ϵ_{\max} of about 45-fold. While significant, the rate enhancement caused by dissociation is considerably smaller on the edge plane, amounting to about eightfold near ϵ_{\max} . Interestingly enough, for both planes, the rate enhancement due to dissociation seems to disappear at sufficiently high surface temperatures. Moreover, at sufficiently low surface temperatures, and on both the basal and edge planes, C atom removal probabilities associated with F atom attack will evidently drop below the corresponding F₂ values. In this "low-temperature" regime the F atom reaction is significantly more temperature sensitive than the corresponding F₂ reaction, the latter exhibiting a tem-

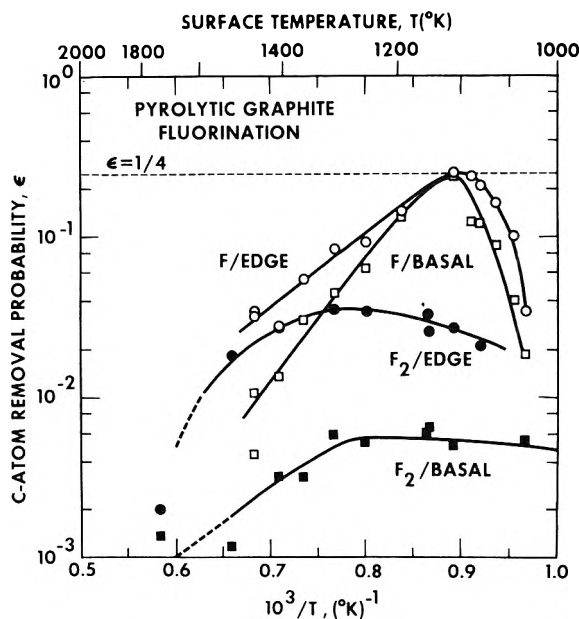


Figure 5. Carbon atom removal probabilities vs. temperature for the attack of pyrolytic graphite by atomic and diatomic fluorine: O, F/edge at $p_F = 1.9 \times 10^{-2}$ Torr; \square , F/basal at $p_F = 1.3 \times 10^{-2}$ Torr; \bullet , F₂/edge at $p_{F_2} = 0.84 \times 10^{-1}$ Torr, \square , F₂/basal at $p_{F_2} = 0.57 \times 10^{-1}$ Torr.

perature dependence equivalent to an overall activation energy of only some 4.4 kcal mol⁻¹. (iv) All C atom removal probabilities above about 1800°K at the prevailing fluorine pressures are less than 10⁻³ regardless of graphite face or fluorine dissociation. (v) The F atom attack of both planes of graphite peaks at a temperature which is noticeably lower (ca. 100°K) than the corresponding attack of graphite by F₂. Even the *maximum* C atom removal probability for F₂ on basal plane is less than 10⁻². It is appropriate to remark here that our experimental results for a more isotropic, commercially available grade of polycrystalline graphite (Speer 580, data not shown)⁹ exhibit many features similar to those shown in Figure 5, with the notable exceptions that (i) the maximum F₂ reaction probability was somewhat higher than the edge plane value shown in Figure 5, resulting in a maximum enhancement in C atom removal probability due to dissociation that never exceeded about threefold and (ii) the F atom rate data did not peak at a noticeably lower surface temperature than that of the corresponding F₂ reaction.

Two types of experiments were performed to investigate the dependence of the C atom probability on fluorine atom pressure. First, the temperature dependence of the F/edge and F/basal-plane reactions was studied at F atom pressures nominally double those shown in Figure 5. Values of ϵ calculated based on the reasonable assumption that the dissociation efficiency of the electrical discharge is constant in this (low) range of initial F₂ mole fractions, are shown in Figure 6. While the qualitative behavior is

(25) When due account is taken of the impact pressure effect, the inferred F atom arrival rate corresponds to an ambient F atom pressure of about 1.3×10^{-2} Torr for most of the Arrhenius data reported here (see Figure 5), or the dissociation of about 57% of the F₂ molecules passing through a microwave discharged 1% F₂ plus Ar mixtures. For investigating the F atom pressure dependence of the gas-solid reactions it is further assumed that the discharge efficiency for F atom production is insensitive to the mole fraction of F₂ in the electrically discharged gas mixture. This assumption is defensible for the dilute F₂ plus Ar mixtures investigated herein ($\leq 5\%$ F₂), but would certainly fail for discharges through nearly pure fluorine.

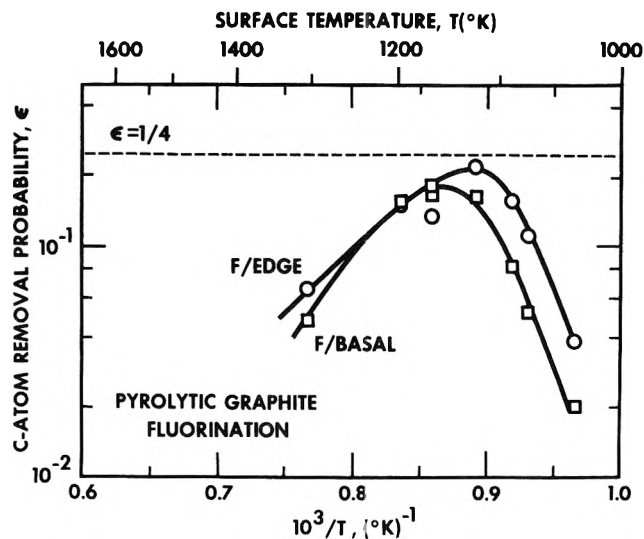


Figure 6. Carbon atom removal probabilities vs. temperature for the attack of pyrolytic graphite by atomic fluorine: O, F/edge at $p_F = 3.7 \times 10^{-2}$ Torr; □, F/basal at $p_F = 2.5 \times 10^{-2}$ Torr.

identical with that shown in Figure 5, detailed comparison of Figures 5 and 6 reveals that the increased F atom pressure has had the effects of (i) slightly lowering ϵ_{\max} , and (ii) shifting $T_{\max \epsilon}$ to higher temperature, especially for the basal plane. To explore a wider range of F atom pressures, additional experiments were performed at a fixed graphite temperature of 1122°K (*i.e.*, $T_{\max \epsilon}$ for the conditions of Figure 5). As shown in Figure 7 these results indicate virtually constant value of ϵ near $1/4$ for both basal and edge-plane graphite at F atom pressures up to about 2×10^{-2} or 3×10^{-2} Torr, respectively. Above these "threshold" pressures ϵ sharply decreases, with a slope revealing an insensitivity of the absolute C atom removal rate to p_F in this range of pressures. This reduction in ϵ is a kinetic consequence of high F atom pressure and is not due to atom loss *via* homogeneous recombination or a decrease in atom production efficiency in the discharge since our previous work on the F/Mo and F/W reactions in this same p_F range exhibited no such drop off above 2×10^{-2} Torr. Cooled-down PG specimens exposed to these high F atom pressures exhibited a surface coating readily visible under an optical microscope. Subsequent examination of this surface *via* scanning electron microscopy (sem) indicated the presence of rough fluorocarbon product layers on these surfaces (Figure 8f and the discussion below). These layers were absent at $p_F \leq 2 \times 10^{-2}$ Torr (Figure 8d).

Since the unaided eye is not a reliable indicator of the presence or absence of significant topographical changes on the specimen surface, a series of sem photographs of PG specimens was taken over a range of conditions representative of the reaction rate data shown in Figures 5-7. Photographs at 100×, 1000×, and 10,000× were taken using a Jeolco JSM-U3 instrument²⁶ on a series of PG specimens whose basal and edge-plane surfaces were mounted at 45° to the electron beam with the downstream edge plane (see Figure 2) and/or the basal plane surface (opposite the alignment pit) "illuminated" by the electron beam. The specimen orientation for the photographs is evident from the low magnification (100×) photograph of the as-received diagonally cut specimen shown in Figure 8a. This photograph, incidentally, illustrates the lamellar nature of the as-received (deposited) PG basal plane surface, and the presence of abrupt, ledge-like de-

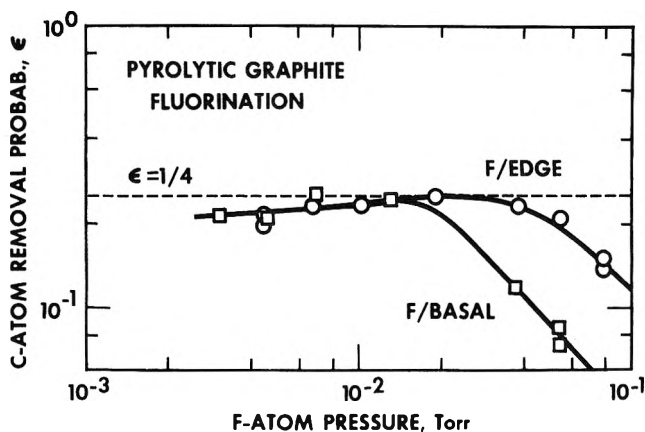


Figure 7. Carbon atom removal probabilities vs. fluorine atom pressure at 1122°K.

fects on this "basal" plane surface. Extensive localized damage to the edge plane associated with the PG plate cutting operation (section 2, Specimen Preparation) was readily apparent at 10,000×, however, all evidence of the cut-off operation was removed upon exposure to F atoms or F_2 molecules at sufficiently high temperature (*cf.* Figure 8h, which reveals the orientation of the individual columnar grains comprising the specimen). Perhaps the most interesting aspect of the sem photographs are what appear to be complex reaction product overlayers²⁷ observed if the fluorine pressure is sufficiently large at the prevailing specimen temperature. Figures 8b and 8c compare the rather different product layers observed at 1036°K for an F atom pressure of 2.7×10^{-2} Torr. One notes a rather isotropic "moss-like" overlayer on the basal surface and a vine-like (oriented) overlayer on the edge surface. Neither of these structures was apparent to the unaided eye. Rough product layers are also observed in F_2 if the pressure is sufficiently large. An interesting example is shown at 1000× in Figure 8i, for the edge surface of a 1715°K specimen exposed to $p_{F_2} = 6 \times 10^{-2}$ Torr. To the naked eye this surface looked like it was covered with black soot. It is interesting to compare these product-covered surfaces to the corresponding product-free surfaces at somewhat lower fluorine pressures. Two examples at 1000× near their respective $T_{\max \epsilon}$ are shown in Figures 8d and 8e for the basal plane exposed to F atoms (1.3×10^{-2} Torr) and F_2 (5.5×10^{-2} Torr). Figure 8e also shows the "developed" appearance of the surface obtained by exposing the basal plane to F_2 molecules under conditions for which the edge/basal ϵ ratio is greatest. Any suggestion that the basal surface is nearly defect free (*cf.* Figure 1) in the absence of a product layer, or nearly identical with

(26) Selected specimens were supplied to Structure Probe Inc. (West Chester, Pa.) where they were treated with a vacuum-deposited Au-Pd alloy prior to sem examination. We are indebted to Dr. C. A. Garber for his cooperation in preparing these specimens and supplying the photographs included here.

(27) While these layers have not been subjected to further analysis, their white color at high fluorine pressures and available evidence in the literature indicates they are of the polymeric carbon subfluoride form, $(CF_x)_n$, as opposed to restructured carbon. For example, nonprotective, solid polycarbon subfluorides ($0.65 \leq x \leq 0.8$) were observed below 920°K by Kuriakose and Margrave⁶ in their studies of graphite fluorination at $p_{F_2} = 1.32 \times 10^1 - 0.747 \times 10^2$ Torr. It is interesting to note that $(CF_x)_n$ powders ($0.7 \leq x \leq 1.12$) are useful as solid lubricants in high-temperature corrosive environments (marketed by Air Products and Chemicals Inc.) and electrode materials for non-aqueous high-energy batteries (see *Chem. Eng. News*, **78**, 26 (1971)).

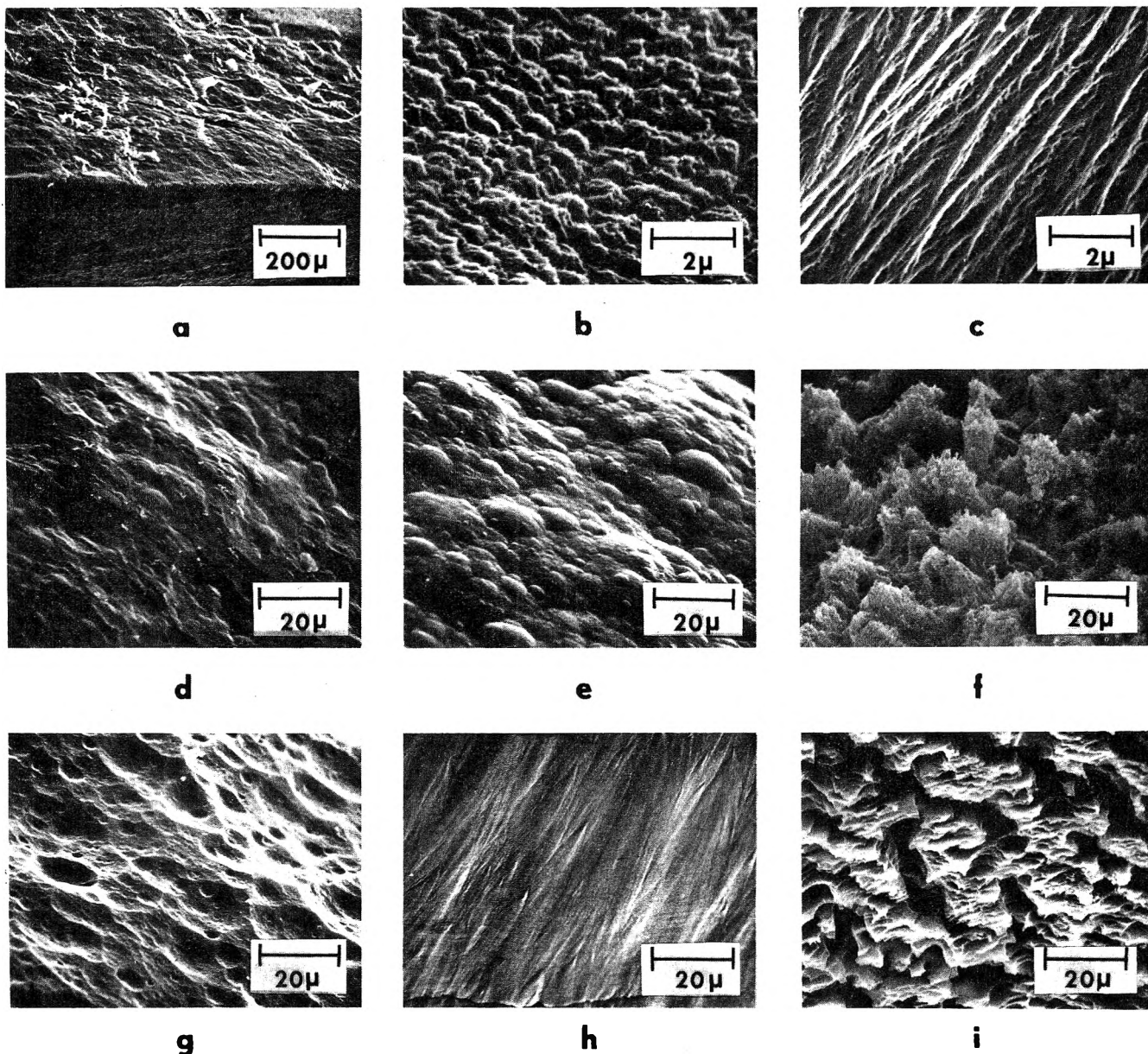


Figure 8. Scanning electron micrographs of pyrolytic graphite specimens: (a) as received and cut, basal and edge plane, 100X; (b) F/basal at $p_F = 2.7 \times 10^{-2}$ Torr, $T = 1036^\circ\text{K}$, 10,000X; (c) F/edge at $p_F = 2.7 \times 10^{-2}$ Torr, $T = 1036^\circ\text{K}$, 10,000X; (d) F/basal at $p_F = 1.3 \times 10^{-2}$ Torr, $T = 1122^\circ\text{K}$, 1000X; (e) F_2 /basal at $p_{\text{F}_2} = 0.55 \times 10^{-1}$ Torr, $T = 1303^\circ\text{K}$, 1000X; (f) F/basal at $p_F = 0.53 \times 10^{-1}$ Torr, $T = 1122^\circ\text{K}$, 1000X; (g) F/basal at $p_F = 1.3 \times 10^{-2}$ Torr, $T = 1465^\circ\text{K}$, 1000X; (h) F/edge at $p_F = 1.3 \times 10^{-2}$ Torr, $T = 1465^\circ\text{K}$, 1000X; (i) F_2 /edge at $p_{\text{F}_2} = 0.6 \times 10^{-1}$ Torr, $T = 1715^\circ\text{K}$, 1000X.

the as-received surface (Figure 8a) is dispelled upon studying Figures 8d and 8g which pertain to F atom exposures (1.3×10^{-2} Torr) at temperatures 1112 and 1465°K, respectively. The heavily "cratered" appearance shown in Figure 8g indicates that edge (prismatic plane) C atoms are in abundance even on the "basal" plane during F atom reaction.

4. Discussion and Conclusions

Besides providing direct information on pyrolytic graphite gasification rates in fluorine-containing environments likely to be encountered in engineering practice, our present data contain valuable clues concerning the reaction mechanism, especially when viewed against the background of available thermodynamic and kinetic data for this, and related gas/solid systems. Thus, despite (a) the evident complexity in our ϵ trends (Figures 5-7) and scan-

ning electron micrographs (Figure 8) and (b) the inevitable need for additional measurements using independent and perhaps more "atomistic" experimental methods, we would be remiss in not seeking potentially instructive or useful regularities in presently available data, or extracting the maximum possible amount of information from them. At the very least such discussion and speculation can provide guidance for extrapolating our results to other combinations of fluorine pressure and temperature of possible future interest. But equally important, we would hope to pinpoint significant chemical implications of these results both as an aid to our ultimate understanding of gas/solid chemical reactions, and as a guide to fruitful future experiments.

A clearer picture of the processes underlying the overall rate parameter ϵ reported in section 3 can be derived from F element balances which must be satisfied regardless of

the detailed reaction mechanism. Thus, in the steady state the rate of fluorine element chemisorption on the PG surface must be equal to the rate at which F atoms leave either as elemental fluorine (F, F₂) or in the form of volatile fluorocarbon products (e.g., CF_n, n = 1,2,3,4; C₂F_m, m = 2,4,6, etc.) If we provisionally neglect the presence of two-carbon (and higher) products then the F element balance can be expressed

$$\nu s Z = \epsilon_{\text{F}} + 2\epsilon_{\text{F}_2} + \sum_{n=1}^4 n \epsilon_n \quad (3)$$

where s is the chemisorption probability, ν is the number of fluorine atoms per incident reactant "molecule" ($\nu = 1$ for F atoms, 2 for F₂), ϵ_{F} and ϵ_{F_2} are respectively the evaporation rates of F and F₂ from the graphite surface, and ϵ_n represents the evaporation rate of CF_n(g). If eq 3 is combined with the definition of ϵ , and use is made of the fact that the total carbon element flux will be given by²⁸

$$\epsilon_{(\text{C})} = \sum_{n=0}^4 \epsilon_n \quad (4)$$

then we find

$$\epsilon = \nu s \left[\sum_{n=0}^4 \epsilon_n / \left(\epsilon_{\text{F}} + 2\epsilon_{\text{F}_2} + \sum_{n=0}^4 n \epsilon_n \right) \right] \quad (5)$$

In this form we note that when carbon vapor sublimation is negligible the C atom removal probability, ϵ , cannot exceed νs , where s is the chemisorption probability. Moreover, it is clear that the desorption rate of "unreacted" fluorine (i.e. $\epsilon_{\text{F}} + 2\epsilon_{\text{F}_2}$ and the product distribution determine the amount by which ϵ falls beneath νs . For reasons which will become clear below, it is interesting to consider the special cases (a) $2\epsilon_{\text{F}_2} \ll \epsilon_{\text{F}}$ and (b) predominance of one reaction product (with evaporation rate ϵ_n). Then eq 5 specializes to

$$\epsilon = (\nu s/n) / [1 + (\epsilon_{\text{F}}/n\epsilon_n)] \quad (6)$$

Thus, in the absence of F atom desorption, ϵ cannot exceed $\nu s/n$, or $s/4$ if, say, $\nu = 1$ (F atom impingement) and $n = 4$ (carbon tetrafluoride product). We have already remarked (section 3) that ϵ_{max} for the F atom attack of basal or edge PG was observed to be about $1/4$. Comparison with eq 6 reveals that this can come about if²⁹ $s = 1$ and $n = 4$, i.e., every incident F atom chemisorbs, and ultimately leaves in the form of a carbon tetrafluoride molecule.³⁰ For F₂ attack with CF₄ as the dominant product eq 6 reveals that ϵ can be as large as $s/2$. The fact that ϵ_{max} for F₂ attack of either the basal or edge plane was observed to be much lower than $1/2$ (cf. Figure 5) suggests that the chemisorption probability for F₂ on these surfaces is always much less than unity (e.g., about 1.2×10^{-3} for "basal" plane PG near 1250°K). This large disparity in the chemisorption probability for F and F₂ on the prevailing basal plane of PG is of considerable fundamental interest, and reminiscent of recently reported disparities in the chemisorption probability of atomic and diatomic hydrogen on ordinary graphite at low coverage.³¹

Perhaps the most striking feature of our Arrhenius data is the phenomenon of the maximum in ϵ at some intermediate surface temperature, $T_{\text{max } \epsilon}$. While observed here for the first time for the fluorine/pyrolytic graphite reactions, qualitatively similar maxima have been reported for the oxygen/graphite reaction,³²⁻³⁵ as well as for the low-pressure oxidation of metals forming volatile oxides^{10,36} or

halides.^{3,37} Of interest here is the question of whether the cause of ϵ_{max} is the same in these diverse chemical systems. Inspection of eq 5 and its counterpart for the O/C, O₂/C, O/Re, and O₂/Re systems reveals that there are two distinct possibilities to consider. The first, invoked by Strickland-Constable and Walls³² and Olander, *et al.*,³⁵ to account for ϵ_{max} and reaction rate "hysteresis" in the O₂/PG reaction, is the reduction in the adsorption probability, s , at high temperature due to the thermal destruction of adsorption sites.³⁸ The second alternative, apparently operative for the oxidation or halogenation of refractory metals,^{3,36,37} is the reduction in ϵ at high temperature associated with the desorption of "unreacted" gas atoms/molecules while s increases or plateaus at the bare surface value s_{max} . Further discussion of these alternatives is best postponed until after a brief consideration of the thermodynamics of the F/C system, however, it is interesting to observe here that the thermal destruction of adsorption or reaction sites, and the possible generation or interconversion of types of adsorption or reaction sites are common postulates in describing reactions on graphitic materials.^{32,35} While invoked to explain the complex temperature and pressure dependence of these reactions, it is sobering to note that the details and uniqueness of such variable site type-variable site number-variable reactant coverage schemes remain questionable even when the basic kinetic data include the dynamic response of the reaction to changing (modulated) reactant pressure, surface temperature, and mass spectrometric sampling of reaction products.³⁵

Since it is now known that many features of the product distribution for high-temperature gas-metal reactions (e.g. O₂/W, O₂/Mo) are in accord with the notion of quasiequilibrium (QE) among all desorbing reaction products,³⁹ it is interesting to inquire into the consequences of this postulate for the F₂/PG reaction. For this purpose a series of computer calculations was made in which we assumed thermochemical equilibrium between a selected set of eligible reaction products and constrained the quantity ϵ to take on the experimentally observed values. The output of each such calculation was then a predicted product distribution and an effective adsorption (or "equilibra-

- (28) Here ϵ_0 , by definition, represents the total flux of elemental carbon vapor, regardless of its detailed state of polymerization (i.e., C, C₂, C₃, ...). Based on available equilibrium vapor pressure data for pure graphite, it is readily shown that ϵ_0 is negligible compared to Z even at the maximum temperatures ($\approx 1715^\circ\text{K}$) studied herein. Thus, the sublimation contribution to the inferred C atom removal probability defined by eq 1 is disregarded in the following discussion.
- (29) Of course, it is also possible that $s = 1/2$ and $n = 2$, i.e., only half of the incident F atoms chemisorb, ultimately to leave in CF₂ radicals, etc. However, as shown below, CF₄ is the most thermodynamically favored reaction product under the experimental conditions explored here.
- (30) Obviously such a reaction would reveal a p_{F} independent C atom removal probability, as observed here below $p_{\text{F}} = 2 \times 10^{-2}$ Torr (see Figure 7).
- (31) G. A. Beitel, *J. Vac. Sci. Tech.*, **6**, 224 (1969).
- (32) J. R. Walls and R. F. Strickland-Constable, *Carbon*, **1**, 333 (1964).
- (33) D. E. Rosner and H. D. Allendorf, *AIAA J.*, **6**, 515 (1969).
- (34) D. E. Rosner and H. D. Allendorf, *Carbon*, **7**, 515 (1969).
- (35) D. R. Olander, W. Siekhaus, R. Jones, and J. A. Schwarz, *J. Chem. Phys.*, **57**, 408 (1972).
- (36) D. E. Rosner and H. D. Allendorf, *J. Chem. Phys.*, **49**, 5553 (1968).
- (37) D. E. Rosner and H. D. Allendorf, *J. Phys. Chem.*, **69**, 4290 (1965).
- (38) In principle, s could decrease due to a decrease in any one of the following factors: (a) surface concentration of adsorption sites, (b) cross sectional area/site, (c) intrinsic adsorption probability for molecules incident upon a bare site, and (d) fraction of sites unoccupied by fluorine adatoms. Here, attention is focused on contribution a. The existence of hysteresis (double-valued high-temperature ϵ behavior observed in the O₂/PG reaction) could not be conveniently studied for F₂/PG using the present techniques.
- (39) J. C. Batty and R. Stickney, *J. Chem. Phys.*, **51**, 4475 (1970).

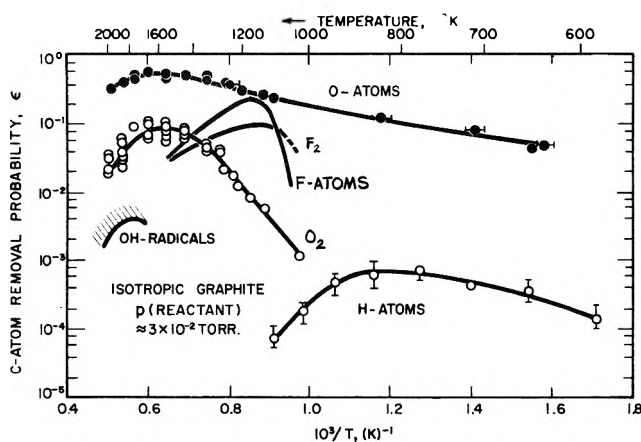


Figure 9. C atom removal probabilities for the attack of an isotropic polycrystalline graphite ($\rho = 1.73 \text{ g cm}^{-3}$) by O, O₂, OH, F, F₂, and H; ref 9.

tion”) probability, s_{QE} . Calculations using JANAF thermochemical data⁴⁰ and made “allowing” only the six product species F, F₂, and CF_n ($n = 1-4$) revealed (a) CF₄ to be the dominant species desorbed under all conditions investigated here,⁴¹ with F and CF₃ (the only competitors) being negligible even at 1420°K, and (b) the reduction in ϵ at $T > T_{max}$ is formally associated with a reduction in s_{QE} rather than the onset of appreciable F atom desorption. When these calculations were repeated allowing in addition the equilibrium desorption of C₂F₂(g), C₂F₄(g), and C₂F₆(g), similar results were obtained, except the product C₂F₂(g) became important at the highest temperatures investigated. Thus, if the quasiequilibrium model were valid CF₄ should be the dominant reaction product near ϵ_{max} and, in contrast to previous work on gas-metal reactions, the reduction of ϵ at higher temperatures would *not* be attributed to the desorption of atomic fluorine from the graphite surface. However, each of these conclusions must be critically examined in the light of the implicit assumptions underlying the quasiequilibrium postulate, since it is questionable that QE applies to each overall consequence of the actual fluorine-graphite reaction mechanism. In particular, it is interesting to inquire whether the prediction of negligible ϵ_F for $T > T_{max}$ is compatible with what is known about the binding energy of foreign adatoms on crystalline graphite. In this connection the semiempirical molecular orbital (MO) calculations of Bennett, McCarroll, and Messmer^{42,43} for the chemisorption behavior of H, C, N, O, and F on a simulated basal (0001) graphite surface are of interest. At low coverages these authors concluded that (a) the adsorbates H, F, and O are most tightly bound (most stable) above the center of each bond connecting nearest neighbor carbons, (b) the sequence of binding strengths, E_{bind} , increases in the order $H < F < O < N < C$, and (c) a single adatom (e.g., H(ads)) binds much more strongly to an edge carbon than to the periodic basal plane C atoms (≈ 3.5 times for H(ads)). While the MO methods used are presently not capable of predicting absolute values for E_{bind} , it would appear from the calculated and experimental values quoted in ref 42 and 43 that E_{bind} for F(ads) on a defect-free basal plane should be in the vicinity of 50 kcal mol⁻¹. If this were the case, the adatom thermal desorption rate, ϵ_F , from such binding sites could be estimated from an absolute rate theory expression which takes advantage of the absence of an apprecia-

ble activation entropy term for simple bond cleavage, *i.e.*

$$\epsilon_F = N_s \theta \left\{ (kT/h) \exp[-E_{bind}/(RT)] \right\} \quad (7)$$

(where N_s is the total adsorption site density,⁴⁴ θ is the fraction of these sites occupied by F(ads), k is the Boltzmann constant, h is Planck’s constant, and R the universal gas constant). Inserting $N_s \approx 5.7 \times 10^{15}$, $\theta \approx 1$, $E_{bind} \approx 50 \text{ kcal mole}^{-1}$ we find that ϵ_F can indeed become comparable to the arrival rate Z at temperatures near T_{max} , for the F atom/PG reaction. Thus, in contrast to the QE expectation, it appears that the cause of the drop in ϵ beyond T_{max} could indeed be the thermal desorption of F(ads) prior to their finding a reactive (edge atom or defect) site by the random process of surface diffusion along C-C bonds on the (0001) surface.⁴⁵

Another argument against adsorption site annealing as the “universal” cause of ϵ_{max} for gas atom reactions with graphite is provided by inspection of our pooled data⁹ for the gasification kinetics of an isotropic graphite in atomic oxygen, fluorine, and hydrogen, shown in Figure 9. The large disparity in T_{max} for these systems, and their sequence (*cf.* the E_{bind} sequence) makes it unlikely that thermal destruction of adsorption or reaction sites accounts for ϵ_{max} in each case. Especially for the H/C and F/C reactions, it appears more likely that ϵ decreases above T_{max} owing to the thermal desorption of H₂ and F, respectively. Another interesting pattern, which emerges upon studying the *magnitudes* of ϵ_{max} in Figure 9, is that ϵ_{max} appears to be large for those systems (O/C, F/C) in which product formation is more exothermic than surface-catalyzed recombination, and small for those systems where atom recombination is energetically more favorable (H/C, Cl/C, N/C; the latter two not being shown).⁹

It thus appears that the C atom removal probability, ϵ , for the fluorine-PG reaction drops to low values ($< 10^{-2}$) at surface temperatures above about 1600–1700°K for kinetic reasons. Advantage could be taken of this in the design of a “clean,” thermal F atom source using a PG oven into which F₂ is directed, however, the average dissociation probability for incident F₂ is not yet known on such a surface, and might be quite low in comparison to that on refractory metals.⁴⁶

It is now interesting to consider the possible cause of the fact that ϵ_{max} evidently occurs at lower temperatures for the F atom/PG reactions than for the corresponding F₂/PG reactions (see Figure 5). This can be explained by recalling that if incident F atoms can adsorb and bind anywhere, but must surface diffuse to widely separated reactive positions where CF₄ is constituted, then thermal

(40) D. R. Stull and H. Prophet, “JANAF Thermochemical Tables,” 2nd ed, National Standard Reference System, NBS Publication No. 37, U. S. Government Printing Office, Washington, D. C., June 1971.

(41) It is interesting to note that CH₄ has been found to be the dominant C-containing reaction product in the H atom reaction with carbon films (from 365 to 500°K; A. B. King and H. Wise, *J. Phys. Chem.*, **67**, 1163 (1963)) and graphite (from 500 to 1250°K, R. K. Gould, Ph.D. Dissertation, University of Wisconsin, 1969).

(42) A. J. Bennett, B. McCarroll, and R. P. Messmer, *Surface Sci.*, **24**, 191 (1971).

(43) A. J. Bennett, B. McCarroll, and R. P. Messmer, *Phys. Rev. B*, **3**, No. 4, 1397 (1971).

(44) It is readily shown from the geometry of Figure 1 that there are 5.7×10^{15} such binding sites per square centimeter of the basal plane (0001) graphite surface.

(45) Of course we do not rule out the possible contribution to CF₄ formation-desorption due to the occasional direct F atom impact at a reaction site.

(46) Our preliminary work on the fluorination kinetics of Pt and, especially, Ir suggests that these metals would make vastly improved F atom oven sources.

desorption should cause ϵ to diminish when the average surface diffusion range becomes shorter than the mean separation of reactive sites.⁴⁷ However, if incident F_2 can only chemisorb "at" such sites then the effects of thermal desorption for the F_2 /PG reaction would not be expected to set in until much higher temperatures are achieved. In these terms the disparity between the F_2 /edge and F_2 /basal rates shown in Figure 5 is largely due to the increased concentration of adsorption-reaction sites on the prevailing "edge" plane surface.⁴⁸ The fact that our previous data for $T_{\max \epsilon}$ for gas-metal reactions is about the same for either atom or molecule attack is compatible with this picture since, in contrast to (0001) graphite, clean metal surfaces offer abundant adsorption sites even for diatomic molecules.⁴⁹

It remains for us to consider the observed ϵ behavior at temperatures lower than $T_{\max \epsilon}$, and the remarkable fact (suggested in Figure 5 and shown in Figure 9 for an isotropic graphite) that ϵ for F atom attack of PG can be lower than that in undissociated fluorine. It is reasonable to attribute this "reversal" behavior to the formation of nonvolatile carbon subfluoride films in the presence of atomic fluorine; indeed, qualitatively similar kinetic behavior was observed by us in the oxidation of silicon carbide by O and O_2 at temperatures such that $SiO_2(c)$ was stable on the reacting surface.⁵⁰ Of course carbon subfluoride films also form in F_2 at sufficiently low temperatures, however, our sem photographs indicate their macroscopic structure is very different from these shown in Figures 8b and 8c.⁵¹ At somewhat higher temperatures, but below $T_{\max \epsilon}$, the steady-state surfaces are probably partially covered with $F(ads)$, causing the adsorption probabilities to be less than the bare surface values achieved near $T_{\max \epsilon}$. Thus, referring again to eq 5 and 6, we expect that ϵ decreases for $T < T_{\max \epsilon}$ because s decreases on a "crowded" surface, not because F or F_2 desorption remains important. At sufficiently high steady state $F(ads)$ concentrations it is not surprising that macroscopic subfluoride "patches" would nucleate, and ultimately appear under sem examination at 10,000 \times . In the light of these results it would be interesting to extend the present rate measurements below 1050°K, correlating these results with both the morphology and stoichiometry of the resulting reaction product films. However, even in the absence of these measurements, it is clear that the remarkable differences in low-temperature reaction rate behavior between the F/C system (Figures 5, 6, and 9), and the O/C and H/C systems (see Figure 9) must be attributed to the blockage effect of nonvolatile product layers in the fluorine/graphite reaction.

This concludes our initial survey high-temperature kinetics of the fluorine/graphite reaction, with emphasis on

the effects of fluorine dissociation, and graphite surface orientation. While the present experimental methods should be supplemented in the future to more directly verify several of the inferences made herein, their simplicity has enabled a wide range of new conditions to be conveniently explored, thereby establishing the magnitudes of the important C atom removal probability for F and F_2 attack of basal and edge-plane pyrolytic graphite. We hope that these experimental measurements, and the accompanying discussion, will both stimulate and help direct further research on this important class of relatively unexplored gas/solid reactions.

Acknowledgments. It is a pleasure to acknowledge the helpful suggestions and data provided by our colleague Dr. Paul Nordine, especially with regard to the effects of high gas flow rate on the reactant arrival rate distribution around resistively heated specimens of circular cross section. We are also indebted to Dr. H. M. Davis, Director of the Metallurgy and Ceramics Division of the U. S. Army Research Office, without whose confidence and encouragement this halogen atom/solid kinetics program would have been impossible.

- (47) Moreover, for $T > T_{\max \epsilon}$, this decrease should be more severe on the prevailing "basal" surface than on the "edge" plane surface (on which the reactive sites are far more abundant). This is consistent with the F atom data shown in Figure 5.
- (48) Recall W. H. Horton's inference (for the O_2 /PG reaction) that relative measurements in the two principal directions of PG are not indicative of the relative rates of edge atoms and atoms in perfect basal planes, but rather relative rates of attack of the same kind of C atoms present in different surface concentrations on each face (W. S. Horton, *NBS J. Res.*, **74A**, No. 3, 325 (1970)).
- (49) This difference in $T_{\max \epsilon}$ is masked for the F, F_2 /isotropic graphite reaction (Figure 9) and did not show up in our previous investigation of the O, O_2 /basal plane PG reaction.³³ However, for this latter reaction the recent molecular beam work of Olander, *et al.*,³⁵ suggests the absence of appreciable oxygen desorption (ξ_0, ξ_{O_2}) i.e., ϵ_{\max} is attributed to the thermal destruction of adsorption-reaction sites at high temperatures.
- (50) D. E. Rosner and H. D. Allendorf, *J. Phys. Chem.*, **74**, 1829 (1970).
- (51) Recall that, as shown in Figure 8, there are also marked differences in the nature of the carbon subfluoride overlayer on the basal and edge planes in either F or F_2 . Additionally, Badachhape and Margrave have reported that a white, solid carbon subfluoride forms on diamond exposed to 2×10^1 Torr at 1073°K. In contrast to the product layer formed on graphite, this film impedes the diamond fluorination reaction at lower pressures. Carbon subfluoride nucleation and growth kinetics on the edge plane graphite surface would be of particular interest in view of the well-known ability of graphite to form *intercalation* compounds via halogen atom penetration of the interlayer spaces in graphite. For example, isotherm studies in the Br/C system reveal that compounds of successively lower adduct/C ratios are found at higher temperatures, each compound corresponding to an increase in the c direction lattice spacing (cf. Figure 1), specimen weight, and electrical resistance. However, our recession rate vs. time data near $T_{\max \epsilon}$ (see Figure 4), and the superficial nature of carbon subfluoride formation observed at 1036°K (Figure 8b,c) preclude the possible importance of extensive F atom penetration of our reacting specimens under conditions of the present experiments.

Dissociation Energies and Heats of Formation of the Gaseous Eu_2 and EuAg Molecules

J. Kordis and K. A. Gingerich*

Department of Chemistry, Texas A & M University, College Station, Texas 77843 (Received August 7, 1972)

Publication costs assisted by the Robert A. Welch Foundation

Mass spectroscopic investigation of the vapor above the EuN-Ag system led to the derivation of the dissociation energy (D_0° , kcal mol⁻¹) and heat of formation ($\Delta H_f, 298^\circ$, kcal mol⁻¹), respectively, of $\text{Eu}_2(\text{g})$ (11.4 ± 4.0 , 71.9 ± 4.4) and $\text{EuAg}(\text{g})$ (30.5 ± 3.0 , 78.8 ± 3.4) from a consideration of the enthalpy changes (ΔH_0° , kcal) of the following reactions: $\text{Eu}_2(\text{g}) = 2\text{Eu}(\text{g})$ (11.4 ± 4.0), $\text{Eu}_2(\text{g}) + 2\text{Ag}(\text{g}) = 2\text{Eu}(\text{g}) + \text{Ag}_2(\text{g})$ (-26.3 ± 3.0), $\text{EuAg}(\text{g}) = \text{Eu}(\text{g}) + \text{Ag}(\text{g})$ (30.9 ± 2.5), and $\text{EuAg}(\text{g}) + \text{Ag}(\text{g}) = \text{Eu}(\text{g}) + \text{Ag}_2(\text{g})$ (-7.7 ± 3.3). These thermodynamic properties permit the application and a first test of the Pauling model of a polar bond to europium compounds. A method of estimating the heats of formation of yet unknown diatomic lanthanides is also suggested.

Introduction

Dissociation energies of numerous diatomic homo- and heteronuclear gaseous metallic molecules have been reported.¹⁻³ Of the homonuclear diatomic lanthanides only the dissociation energies of $\text{Ce}_2(\text{g})$,³ $\text{Ho}_2(\text{g})$,⁴ $\text{Tb}_2(\text{g})$,⁵ and $\text{Lu}_2(\text{g})$ ⁶ are presently known. It was the intent of the present study to add another member of the lanthanides to this list and eventually, as opportunity arises, to complete the series entirely. The choice of $\text{Eu}_2(\text{g})$ is particularly significant insofar as europium with its six 4f electrons lies adjacent to the half-filled 4f shell that is customarily associated with perturbations in the normal progression of the thermodynamic properties of the lanthanide series. Similar considerations prompted us to investigate the dissociation energy of $\text{EuAg}(\text{g})$. The only previous gaseous diatomic lanthanide-silver compound investigated in this way is $\text{HoAg}(\text{g})$,⁴ whereas with the corresponding lanthanide-gold compounds considerably more has already been accomplished.³⁻⁶ The knowledge of the bond energy of $\text{Eu}_2(\text{g})$ permits the application of the Pauling model of a polar single bond⁷ to gaseous europium compounds. The determination of the dissociation energy of the molecule EuAg permits a first test of this model for an intermetallic europium compound.

Experimental Section

The mass spectrometer and the experimental procedures used for this work have been described previously.^{4,8} The mass spectrometer operations were standardized for the measurement of the metallic ion species at 2-mA emission current, 12-eV electron voltage, and 4.5-kV accelerating voltage. The ionic species were characterized by their mass to charge ratios, normal shutter profiles, appearance potentials, and isotopic abundances. A molybdenum Knudsen cell with a 0.010-in. orifice was employed. The sample charge consisted primarily of EuN with a minor component of silver. Temperatures were measured by focusing a calibrated optical pyrometer on a blackbody hole at the base of the Knudsen cell. All necessary window and prism reflector corrections were applied to the temperature readings.

Results and Discussion

The relevant ion intensities are shown in Table I. Frequently, measurements were made on all the isotopic species, but those listed in Table I are the ones of highest abundance and these are the ones from which the thermodynamic data were computed after adjustments for isotopic abundance.

The partial pressures were obtained from the corresponding intensities by the standard relationship $P_i = k_j I_j + T$, where P_j was expressed in atmospheres, T in K, I_j in amperes and whence k_j follows in atm A⁻¹ K⁻¹ units. The pressure constant, k_i , was itself derived from $k_i = k_{\text{Ag}}(\sigma_{\text{Ag}}\gamma_{\text{Ag}})/(\sigma_i\gamma_i)$, where the σ 's and γ 's are the ionization cross sections and multiplier gains of secondary electrons, respectively. The primary calibration constant, k_{Ag} , was obtained from the equilibrium dissociation of $\text{Ag}_2(\text{g}) = 2\text{Ag}(\text{g})$,⁴ where the enthalpy change for this reaction was taken to be $\Delta H_0^\circ = 38.0 \pm 1.5$ kcal.³ The multiplier gains of Ag^+ (3.76×10^5) and Eu^+ (3.23×10^5) were obtained experimentally, those of Ag_2^+ and Eu_2^+ were assumed to be the same as of the respective monatomic species, and that of EuAg^+ (3.50×10^5) was assumed to be the mean of those of Eu^+ and Ag^+ . The maximum ionization cross sections of the singly ionized atomic species were obtained from the tables of Mann.⁹ The ionization cross sections of Ag_2^+ and Eu_2^+ were taken to be 1.5 times that of the respective monatomic species,¹⁰ and similarly that of EuAg^+ was assumed to be 0.75 times that of the sum of those of Ag^+ and Eu^+ . In all cases, the

- (1) B. Siegel, *Quart. Rev., Chem. Soc.*, **19**, 77 (1965).
- (2) J. Drowart, "Phase Stability in Metals and Alloys" P. S. Rudman, J. Stringer, and R. I. Jaffee, Ed., McGraw-Hill, New York, N. Y., 1967.
- (3) K. A. Gingerich, *J. Cryst. Growth*, **9**, 31 (1971).
- (4) D. L. Cocke and K. A. Gingerich, *J. Phys. Chem.*, **75**, 3264 (1971).
- (5) J. Kordis, K. A. Gingerich, and R. J. Seyse, submitted for publication.
- (6) K. A. Gingerich, *Chem. Phys. Lett.*, **13**, 262 (1972).
- (7) L. Pauling, "The Nature of the Chemical Bond," 3rd ed, Cornell University Press, Ithaca, N. Y., 1960.
- (8) K. A. Gingerich, *J. Chem. Phys.*, **49**, 14 (1968).
- (9) J. B. Mann, Recent Develop. Mass Spectrom., *Proc. Int. Conf. Mass Spectrosc.*, 1970, 814 (1970).
- (10) J. Drowart and P. Goldfinger, *Angew. Chem.*, **79**, 589 (1967).

TABLE I: Observed Intensities at 12 eV

T, °K	I × 10 ¹² , A				
	¹⁵³ Eu ⁺	³⁰⁴ Eu ₂ ⁺	¹⁰⁷ Ag ⁺	²¹⁶ Ag ₂ ⁺	²⁶⁰ EuAg ⁺
1406	41,700	0.145			
1426	42,500	0.175			
1474	62,130	0.30	300	0.125	4.8
1464	38,800	0.14			
1430	27,200	0.075			
1375	9,450		42.0		0.27
1358	7,800		33.5		0.20
1333	6,100		30.0		0.15
1285	3,400		15.0		0.08
1299	4,900		23.0		0.125
1376	16,650		75.5		0.60
1407	25,800		166		1.23
1450	47,220	0.16	255	0.09	4.0
1471	36,800	0.08	189	0.12	1.4
1499	61,130	0.18	243	0.14	3.0
1460	43,000	0.15	218	0.13	2.5
1479	55,900	0.13	310	0.15	3.8
1517	36,300		171	0.15	1.05
1548	24,300		114		0.69
1572	30,000		144		0.57
1606	8,400		910	0.48	1.08
1646	6,400		1380	0.99	0.90
1685	8,400		2130	4.0	1.55

intensities had to be adjusted by an empirical factor, I_{\max}/I , to bring them in line with the maximum cross sections given by Mann. The I_{\max}/I factor as obtained from the ionization efficiency curves was 1.14, 1.10, 1.22, 1.17, and 1.12 for Ag⁺, Ag₂⁺, Eu⁺, Eu₂⁺, and EuAg⁺, respectively. Concurrently, the ionization efficiency curves yielded (by the linear extrapolation method) the appearance potentials (in eV) of the new species, Eu₂(g) (6.3 ± 1.0) and EuAg(g) (6.1 ± 0.5), relative to Ag(g) (7.574)¹¹ as the standard. Insofar as Eu₂(g) is concerned, it can be further stated that in the temperature range where this molecule was studied (1406–1499°K), no oxides of europium were observed, so that there can be no question of any fragment contribution to the Eu₂⁺ intensities from this source.

In the single instance of the reaction of EuAg(g) = Eu(g) + Ag(g), where a second-law evaluation of the enthalpy change was justified by the extent of the temperature range, this was done according to $\log K = -\Delta H^\circ/4.576T + \Delta S^\circ/4.576$. For the third-law evaluation, $\Delta H_0^\circ/T = -4.576 \log K - \Delta G_T^\circ - H_0^\circ/T$. The free energy functions, $-(G_T^\circ - H_0^\circ)/T$, of Ag(g) and Eu(g) were taken from Hultgren, *et al.*,¹² those of Ag₂(g)⁴ were calculated from known molecular parameters,¹³ and those of Eu₂(g) and EuAg(g) from estimated parameters by means of the rigid-rotator, harmonic oscillator approximation. The equilibrium internuclear distances of Eu₂(g) ($r_e = 3.700$ Å) and EuAg(g) ($r_e = 2.885$ Å) were calculated from the sum of the Pauling single bond metallic radii,⁷ with corrections for bond shortening in EuAg(g) in the same proportions as observed in MgAu(g) and AlAu(g), respectively.¹³ No corresponding correction was made for Eu₂(g) in view of the very small observed bond shortening in Al₂(g),¹⁴ a molecule with a larger bond energy than has been found for Eu₂(g) in this investigation. In fact, the sum of the metallic single bond radii may well be too low a value for the internuclear distance in Eu₂(g). The vibra-

tional frequencies of Eu₂(g) ($\omega_e = 110.6$ cm⁻¹) and EuAg(g) ($\omega_e = 193.0$ cm⁻¹) were obtained from the Guggenheimer relationships¹⁵ by taking z values of 3 and 5 for Ag and Eu, respectively. The resultant free energy functions, $-(G_T^\circ - H_0^\circ)/T$, with an arbitrary addition of 3 entropy units for the electronic contributions, are (60.23, 59.02), (71.31, 70.85), (72.67, 72.19), (74.85, 73.36), and (76.37, 74.40) at 298, 1200, 1400, 1600, and 1800°K for Eu₂(g) and EuAg(g), respectively. The ($H_{298} - H_0$) values came to 2.43 kcal for EuAg(g) and 2.52 kcal for Eu₂(g).

The equilibrium constants and third-law enthalpy changes for the reactions investigated are shown in Table II. Error limits in the enthalpy changes refer to standard deviations only. The enthalpy change of the direct dissociation of Eu₂(g) = 2Eu(g), $\Delta H_0^\circ = 11.4 \pm 0.5$ kcal is in good agreement with the value $\Delta H_0^\circ = 11.7 \pm 2.9$ kcal, obtained from a combination of the enthalpy change of the pressure-independent reaction, Eu₂(g) + 2Ag(g) = 2Eu(g) + Ag₂(g), $\Delta H_0^\circ = -26.3 \pm 1.3$ kcal, and the enthalpy change of Ag₂(g) = 2Ag(g), $\Delta H_0^\circ = 38.0 \pm 1.5$ kcal.³ This agreement is, however, only independent to the extent to which different data sets have been used in the reactions evaluated.

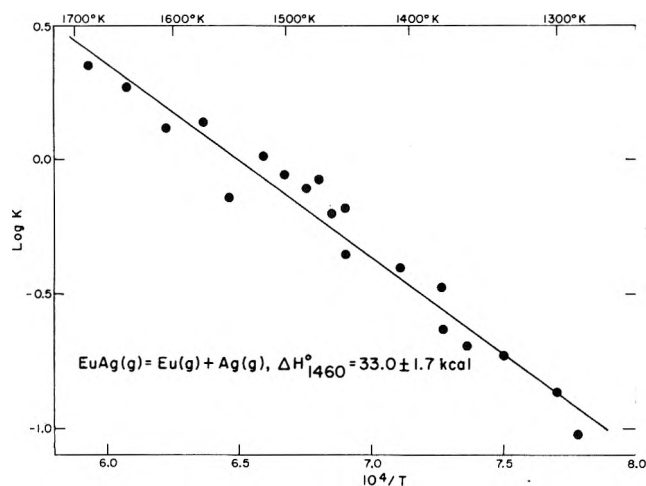
The use of an auxiliary pressure-independent reaction, such as the one above, provides a suitable cross check on the reaction of our main interest since the reference constant, in this case k_{Ag} , cancels out and hence also any error that might be associated with it. However, the further frequently employed simplification of mutual cancellation of cross sections and multiplier gains would lead to a considerably different value for the enthalpy change, $\Delta H_0^\circ = -30.1 \pm 1.4$ kcal, for the reaction Eu₂(g) + 2Ag(g) = 2Eu(g) + Ag₂(g) than obtained previously. This is primarily due to the almost threefold larger ionization cross section of Eu(g) as compared to Ag(g)⁹ that finds no appropriate compensation in the multiplier gains. The present severe case of imbalance in the ionization cross sections emphasizes the desirability of avoiding, whenever possible, the simplifying assumption of mutual cancellation of cross sections and multiplier gains.

The final enthalpy change values for the reactions Eu₂(g) = 2Eu(g) and Eu₂(g) + 2Ag(g) = 2Eu(g) + Ag₂(g) are chosen as $\Delta H_0^\circ = 11.4 \pm 4.0$ kcal (47.7 ± 17 kJ), or $\Delta H_{298}^\circ = 11.9 \pm 4.0$ kcal (49.8 ± 17 kJ) and $\Delta H_0^\circ = -26.3 \pm 3.0$ kcal, respectively, after inclusion of all possible sources of error. The enthalpy change for the dissociation of Eu₂(g) as obtained from the latter reaction in conjunction with the dissociation enthalpy of Ag₂(g) was given no weight because it results in considerably wider error limits. Thus we select $D_0^\circ(\text{Eu}_2) = 11.4 \pm 4.0$ kcal mol⁻¹ or 47.7 ± 17 kJ mol⁻¹, or $D_{298}^\circ(\text{Eu}_2) = 11.9 \pm 4.0$ kcal mol⁻¹ or 49.8 ± 17 kJ mol⁻¹. The standard heat of formation of Eu₂(g) comes to $\Delta H_{f,298}^\circ = 71.9 \pm 4.4$ kcal mol⁻¹ (300.8 ± 18.4 kJ mol⁻¹) when the heat of sublimation of europium ($\Delta H_{v,298}^\circ = 41.9 \pm 0.2$ kcal mol⁻¹)¹² is combined with the presently derived heat of atomization of Eu₂(g).

- (11) R. W. Kiser, "Introduction to Mass Spectrometry and its Applications," Prentice-Hall, Englewood Cliffs, N. J., 1964.
- (12) R. Hultgren, R. L. Orr, and K. K. Kelley, "Supplement to Selected Values of Thermodynamic Properties of Metals and Alloys," University of California, Berkeley, Calif., 1968.
- (13) C. J. Cheatham and R. F. Barrow, *Advan. High Temp. Chem.*, **1**, 7 (1967).
- (14) D. S. Ginter, M. M. Ginter, and K. K. Innes, *Astrophys. J.*, **139**, 365 (1964).
- (15) K. M. Guggenheimer, *Proc. Phys. Soc.*, **58**, 456 (1946).

TABLE II: Equilibrium Constants and Third-Law Enthalpy Changes for Various Reactions of Europium

T, °K	Eu ₂ (g) = 2Eu(g)		Eu ₂ (g) + 2Ag(g) = 2Eu(g) + Ag ₂ (g)		EuAg(g) = Eu(g) + Ag(g)		EuAg(g) + Ag(g) = Eu(g) + Ag ₂ (g)	
	Log K	ΔH ₀ ^o , kcal	Log K	-ΔH ₀ ^o , kcal	-Log K	ΔH ₀ ^o , kcal	Log K	-ΔH ₀ ^o , kcal
1406	3.04	11.4						
1426	2.98	11.9						
1474	3.09	11.6	3.75	24.8	0.179	30.3	0.47	6.1
1464	3.01	12.1						
1430	3.00	12.1						
1375					0.630	31.0		
1358					0.687	30.9		
1333					0.725	30.5		
1285					1.023	31.1		
1299					0.867	30.6		
1376					0.475	30.0		
1407					0.402	30.3		
1450	3.12	11.2	3.89	25.3	0.351	30.9	0.42	5.6
1471	3.21	10.8	4.25	28.1	0.0725	29.5	0.97	9.4
1499	3.31	10.4	4.19	27.4	0.0657	30.0	0.81	8.5
1460	3.07	11.7	3.91	25.6	0.198	30.1	0.64	7.1
1479	3.20	10.9	3.91	25.9	0.107	29.9	0.60	6.9
1517					-0.0164	29.9	1.22	11.5
1548					0.143	31.6		
1572					-0.140	30.1		
1606					-0.119	31.0	0.36	5.8
1646					-0.272	30.6	0.45	6.6
1685					-0.353	30.8	0.75	9.1
		ΔH ₀ ^o = 11.4 ± 0.5		ΔH ₀ ^o = -26.3 ± 1.3		ΔH ₀ ^o = 30.5 ± 0.5		ΔH ₀ ^o = -7.7 ± 1.8

Figure 1. Second-law plot for the reaction $\text{EuAg(g)} = \text{Eu(g)} + \text{Ag(g)}$.

Of the lanthanide homonuclear gaseous diatomic species thus far reported,³⁻⁵ the dissociation energy of $\text{Eu}_2(\text{g})$ is clearly the lowest. In ascending order the other dissociation energies (D_0° , kcal mol⁻¹) are $\text{Ho}_2(\text{g})$ (19 ± 4),⁴ $\text{Tb}_2(\text{g})$ (30.5 ± 4.0),⁵ $\text{Lu}_2(\text{g})$ (33, preliminary value),⁶ $\text{Ce}_2(\text{g})$ (57.0 ± 5.0),³ and for the other rare earths,³ $\text{Y}_2(\text{g})$ (37.3 ± 5.0), $\text{Sc}_2(\text{g})$ (38.0 ± 5.0), La_2 (57.6 ± 5.0). The accuracy of these data do not allow for any specific correlation among the dissociation energies of $\text{Ln}_2(\text{g})$ species but it is quite evident that the dissociation energies follow the trend of the heats of sublimation of the corresponding lanthanide elements. Thus, the heat of sublimation of europium also has the lowest value among the elements of the $\text{Ln}_2(\text{g})$ species examined. The best that can be said at present is that the ratio $\Delta H_{f,0}^\circ/\Delta H_{v,0}^\circ$ where $\Delta H_{f,0}^\circ$ is the

standard heat formation of $\text{Ln}_2(\text{g})$, and $\Delta H_{v,0}^\circ$ the heat of sublimation of Ln(s) , falls between 1.44 and 1.74. This ratio is also applicable in regard to $\text{Sc}_2(\text{g})$, $\text{Y}_2(\text{g})$, and $\text{La}_2(\text{g})$. It might be regarded as a useful guide in establishing favorable experimental conditions for the measurement of the dissociation energies of the remaining $\text{Ln}_2(\text{g})$ species. A similar approach, namely, the assumption of a constant value for $\Delta H_{v,0}^\circ[\text{Ln(s)}]/D_0^\circ(\text{Ln}_2)$, had previously been used to predict the dissociation energies of the yet unknown diatomic lanthanides.¹⁶ The predictions had been somewhat higher for Ho_2 , Tb_2 , Lu_2 , and Eu_2 than the experimental values found later, but they gave the correct trend. Thus the predicted value $D_0^\circ(\text{Eu}_2) = 18$ kcal mol⁻¹ compares with 11.4 ± 4.0 kcal mol⁻¹ found in this investigation.

As shown in Figure 1 and Table II, the second- and third-law enthalpy changes, respectively, for the reaction $\text{EuAg(g)} = \text{Eu(g)} + \text{Ag(g)}$ are in good agreement. The second-law enthalpy change at temperature, $\Delta H_{1460}^\circ = 33.0 \pm 1.7$ kcal, reduces to $\Delta H_0^\circ = 31.3 \pm 1.7$ kcal, as compared to the third-law value, $\Delta H_0^\circ = 30.5 \pm 0.5$ kcal. The agreement between second-law and third-law enthalpy changes, $\Delta S_{1460}^\circ = 21.4 \pm 1.1$ eu and $\Delta S_{1460}^\circ = 20.9$ eu, respectively, is also satisfactory. In view of the fact that the total pressure in the Knudsen cell might be considered to approach non-Knudsen conditions at the higher temperatures, full weight is given to the third-law enthalpy change.

The third-law enthalpy change for the dissociation of EuAg(g) is also well supported by the subsidiary pressure-independent reaction, $\text{EuAg(g)} + \text{Ag(g)} = \text{Eu(g)} + \text{Ag}_2(\text{g})$, whose enthalpy change $\Delta H_0^\circ = -7.7 \pm 1.8$ kcal (Table II), and as corrected for all possible errors, $\Delta H_0^\circ =$

(16) K. A. Gingerich, *Chem. Commun.*, 9 (1969); K. A. Gingerich and H. C. Finkbeiner, *ibid.*, 901 (1969).

-7.7 ± 3.3 kcal, yields in conjunction with the dissociation energy of $\text{Ag}_2(\text{g})$ a value of $\Delta H_0^\circ = 30.3 \pm 4.8$ kcal for the dissociation in $\text{EuAg}(\text{g})$. As in the previous case of the pressure-independent reaction involving $\text{Eu}_2(\text{g})$, the simplifying assumption of mutual cancellation of cross sections and multiplier gains would yield, for similar reasons, a significantly different value of $\Delta H_0^\circ = -9.7 \pm 1.8$ kcal.

The final value of the dissociation energy of $\text{EuAg}(\text{g})$ is chosen to be $D_0^\circ = 30.5 \pm 3.0$ kcal mol⁻¹ (127.6 ± 12.6 kJ mol⁻¹) or $D_{298^\circ} = 31.0 \pm 3.0$ kcal mol⁻¹ (129.7 ± 12.6 kJ mol⁻¹), from which follows that with the inclusion of the heats of sublimation of europium and silver,¹² the standard heat of formation of $\text{EuAg}(\text{g})$, $\Delta H_{f,298^\circ} = 78.8 \pm 3.4$ kcal mol⁻¹ (329.7 ± 14.2 kJ mol⁻¹).

The dissociation energy of the only other $\text{LnAg}(\text{g})$ species reported thus far, $\text{HoAg}(\text{g})$, has a somewhat similar value, $\Delta D_0^\circ = 28.6 \pm 4$ kcal mol⁻¹,⁴ to the one above for $\text{EuAg}(\text{g})$. However, the Pauling model of a polar bond⁷

yields, with an electronegativity value of 1.3 for Eu and Ho, and of 1.9 for Ag, $D_0^\circ = 36.6$ kcal mol⁻¹⁴ for the dissociation energy of $\text{HoAg}(\text{g})$, and $D_0^\circ = 33.4$ kcal mol⁻¹ for that of $\text{EuAg}(\text{g})$. Thus it appears that the better agreement between the experimental and Pauling model dissociation energies in the case of $\text{EuAg}(\text{g})$ means an appreciably larger ionic contribution to bonding in this molecule relative to that of $\text{HoAg}(\text{g})$. It will be most instructive to see how the series progresses as data on other $\text{LnAg}(\text{g})$ molecules become available, and to what extent they conform to the Pauling model of a polar bond, as evidently is by and large the case for the corresponding $\text{LnAu}(\text{g})$ molecules.

Acknowledgment. The authors wish to acknowledge the continued support of the Robert A. Welch Foundation under Grant No. A-387.

Binary Diffusion Coefficients for the System Helium-Chlorotrifluoromethane at 300 K and 1 Atmosphere. A Test of the Chapman-Enskog Theory

M. A. Yabsley, P. J. Carson, and Peter J. Dunlop*

Department of Physical and Inorganic Chemistry, University of Adelaide, Adelaide, South Australia 5001
(Received October 20, 1972)

Binary diffusion coefficients, D_{12} , are reported as a function of concentration for the system He-CClF_3 at 300 K and 1 atm pressure. The data agree, within the estimated experimental error of approximately 0.1%, with the Kihara second approximation of the Chapman-Enskog theory, and permit calculation of potential parameters.

The Kihara second approximation for the Chapman-Enskog theory¹ predicts an expression for the concentration dependence of the binary diffusion coefficient, D_{12} , at constant temperature and pressure. According to this theory, the graph of D_{12} vs. the mole fraction, x_2 , of the heavy component is sensitive to the ratio of the molecular masses of the two components and to the magnitude of their potential energy of interaction. The purpose of this paper is to report data for the concentration dependence of the binary diffusion coefficient of the system He-CClF_3 and, using these results, to test the Chapman-Enskog theory. It was hoped that, since the theory should only be valid for atoms, the values of D_{12} might show an unusual concentration dependence. However, no unusual behavior was observed.

Experimental Section

The details of the method used to measure the binary diffusion coefficients have been described previously.² It is suggested that that paper be read in conjunction with this article. As before, all experiments were performed in a water bath controlled at 300 K to better than 0.001°. The

purities of the He and CClF_3 were stated by the manufacturers to be better than 99.99 and 99.0%, respectively.

We have now shown that two small corrections must be made to diffusion data obtained with the present apparatus.² The first is an end correction of +0.3% due to the presence of the jets and the Nupro bellows valves in each end of the cell, and the second correction is due to the "heat-of-mixing" which varies from experiment to experiment. The maximum correction in the present experiments was +0.1%. These corrections were investigated in a Loschmidt type cell^{3,4} and will be described in detail in a future publication.

Results

Table I summarizes the diffusion coefficients, D_{12}^{exptl} , which were measured at a series of mole fractions of CClF_3 , x_2 . Each coefficient was measured at approximate-

- (1) E. A. Mason, *J. Chem. Phys.*, **27**, 75 (1957).
- (2) P. J. Carson, T. N. Bell, and P. J. Dunlop, *J. Chem. Phys.*, **56**, 531 (1972).
- (3) L. E. Boardman and N. E. Wild, *Proc. Roy. Soc., Ser. A*, **162**, 511 (1937).
- (4) R. A. Strehlow, *J. Chem. Phys.*, **21**, 2101 (1953).

TABLE I: Binary Diffusion Coefficients for the System He-CClF₃ at 300 K and 1 Atm

x_2	P , atm	D_{12} , cm ² sec ⁻¹	
		Exptl	Corrected to 1 atm
0.0499	0.5662	0.7407	0.4194
0.0518	0.5819	0.7192	0.4185
0.0547	0.5809	0.7215	0.4191
0.0793	0.5750	0.7280	0.4186
0.1305	0.5808	0.7266	0.4220
0.1956	0.6243	0.6790	0.4239
0.2910	0.5808	0.7328	0.4256
0.3975	0.5836	0.7308	0.4265
0.5052	0.6283	0.6802	0.4274
0.5385	0.6736	0.6355	0.4281
0.5996	0.5811	0.7384	0.4291
0.6468	0.6281	0.6848	0.4301
0.8996	0.5809	0.7414	0.4307
0.9495	0.5669	0.7604	0.4311
0.9754	0.5513	0.7807	0.4304

ly 0.6 atm pressure and then corrected to a pressure of unity to give, D_{12} . The corrected data can be represented by the equation

$$D_{12} = 0.4161 + [0.05959x_2/(1 + 2.985x_2)] \quad (1)$$

with a standard error of 0.15%. We have shown that this type of equation, first suggested by Amdur and Schatzki⁵ and later by Mason and Marrero,⁶ reproduces with extremely accuracy concentration dependences generated by Kihara's second approximation to the Chapman-Enskog theory.

An iterative procedure and values of D_{12} calculated from eq 1 for the lowest and for the highest concentration in Table I were used to determine intermolecular parameters for the Lennard-Jones 12-6 potential from the Kihara second approximation and quantum collision integrals.⁷ Errors in these parameters were calculated from the standard error of eq 1. This procedure, which has previously been shown⁸ to yield parameters of somewhat similar pre-

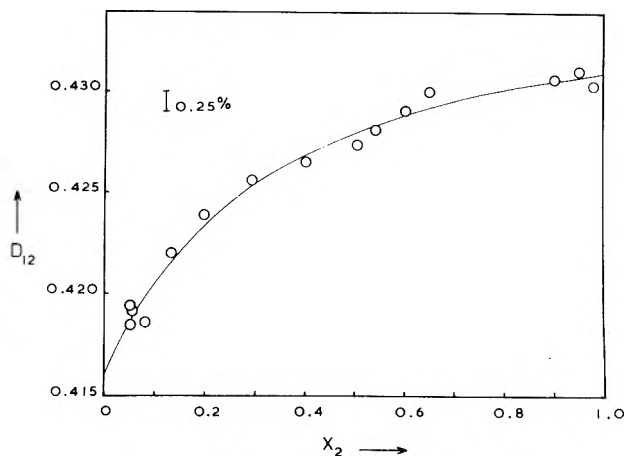


Figure 1. Test of the Chapman-Enskog theory for He-CClF₃ at 1 atm and 300 K: O, experimental points; —, eq 1 and the Kihara second approximation using $\epsilon_{12}/k = 48.1$ and $\sigma_{12} = 3.83$ for the Lennard-Jones 12-6 potential.

cision to that obtained from temperature dependence studies gave $\epsilon_{12}/k = 48.1 \pm 12.4$ K and $\sigma_{12} = 3.83 \pm 0.10$ Å (95% fiducial limits) for this system. Figure 1 compares the experimental data with the concentration dependence of D_{12} predicted by theory and these parameters. The difference between values of D_{12} generated by eq 1 and by the theory is approximately 0.01%, and therefore we have used the single smooth curve in Figure 1 to represent both the theoretical and experimental concentration dependences. We were unable to find similar data in the literature for comparison with this work.

Acknowledgment. This work was supported in part by a grant from the Australian Research Grants Committee.

- (5) I. Amdur and T. F. Schatzki, *J. Chem. Phys.*, **29**, 1 (1958).
- (6) T. R. Marrero and E. A. Mason, *J. Phys. Chem. Ref. Data*, **1**, 3 (1972).
- (7) R. J. Munn, F. J. Smith, E. A. Mason, and L. Monchick, *J. Chem. Phys.*, **42**, 537 (1965).
- (8) P. J. Carson and P. J. Dunlop, *Chem. Phys. Lett.*, **14**, 377 (1972).

Relative Bond Dissociation Energies of Silicon-Hydrogen Bonds in Methylsilanes as Estimated from Recoil Tritium Abstraction Yields¹

Akio Hosaka and F. S. Rowland*

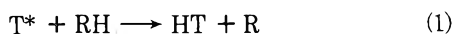
Department of Chemistry, University of California, Irvine, California 92664 (Received October 18, 1972)

Publication costs assisted by the Division of Research, U. S. Atomic Energy Commission

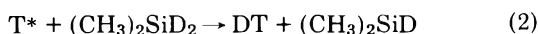
The relative DT yields per Si-D bond for the abstraction of D by recoil tritium atoms have been measured as 4360 for (CH₃)₃SiD, 3790 for (CH₃)₂SiD₂, and 3680 for CH₃SiD₃, as compared with yields per C-D bond of 2380 for (CH₃)₃CD and 1190 for CH₃CD₃. The substantially higher yields from Si-D bonds than from C-D bonds suggest that all Si-D bond dissociation energies are appreciably less than 90 kcal/mol. The Si-D bond dissociation energies in CH₃SiD₃ and (CH₃)₂SiD₂ are each estimated to be approximately 2-3 kcal/mol higher than that in (CH₃)₃SiD. These differences are substantially smaller than those found with the corresponding C-D bonds in alkanes.

Introduction

Energetic tritium atoms are capable of abstracting hydrogen atoms from all carbon-hydrogen positions, as in (1), and the yields of these reactions with alkanes and cycloalkanes correlate quite well with the accepted bond dissociation energies of the corresponding C-H bonds.^{2,3} Measurements with several amines have also shown a similar correlation for N-H bonds.⁴ While studies with CHF₃ and CH₃CD=CD₂ have indicated that important deviations from the C-H correlation are found in comparisons involving rather dissimilar residual R radicals,^{5,6} comparison of the HT yields from molecules with similar residual radicals permits estimation of the relative bond dissociation energies involved. In connection with studies of all of the reactions of recoil tritium atoms with methylsilanes,^{7,8} we have measured the abstraction yields from several kinds of silicon-hydrogen bonds. For more accurate comparative measurements, we have now carried out abstraction experiments in the presence of excess moderators, using both C₂H₄ and N₂ in this role.



The abstraction contributions from carbon-hydrogen and silicon-hydrogen bonds in the methylsilanes have been separated through the utilization as substrates of the partially deuterated compounds (CH₃)₃SiD, (CH₃)₂SiD₂, and CH₃SiD₃, and measurement of the yield of DT, as illustrated for (CH₃)₂SiD₂ in reaction 2. These measurements confirm that abstraction from silicon-hydrogen bonds occurs in higher yields than from most hydrocarbon C-H bonds. If the plausible assumption is made that abstraction from silicon-hydrogen and carbon-hydrogen positions occurs by similar mechanisms, the higher yields suggest that the silicon-hydrogen bonds are normally weaker than carbon-hydrogen bonds. However, much less variation in DT yield, and therefore in apparent bond strength, is observed among the primary, secondary, and tertiary silicon-hydrogen bonds than among the corresponding carbon-hydrogen bonds.



Experimental Section

Chemicals. The three partially deuterated methylsilanes were synthesized by the reaction of LiAlD₄ with the corresponding methylsilyl chlorides.^{9,10} The LiAlD₄ was obtained from Merck Sharpe and Dohme and had a stated isotopic purity of ≥99% D; the isotopic purity of the Si-D positions was not checked. Each of the methylsilanes was purified by preparative gas chromatography using silicone oil columns.

Preparation and Irradiation of Samples. The samples were filled following the standard techniques used in our laboratories for gas-phase recoil tritium experiments, relying on neutron irradiation of ³He for the formation of the energetic tritium atoms.²⁻⁸ Each sample bulb was about 12 ml in volume, and contained 10-18 Torr of ³He, 8-22 Torr of O₂, about 50 Torr of methylsilane, and about 700 Torr of C₂H₄ or N₂. Groups of samples were irradiated simultaneously in the rotating specimen rack of a Triga nuclear reactor for about 12 min in a flux of 10¹² n/cm²/sec. Complete details are given in ref 8.

Radio Gas Chromatography. The isotopic hydrogen molecules were separated with a 12-ft activated alumina-Chromosorb P column operated at -196°, and assayed by routine proportional counting procedures.^{11,12} The macro-

- (1) This research was supported by A.E.C. Contract No. AT(04-3)-34, Agreement No. 126, and constituted part of the work submitted by A. Hosaka in partial fulfillment of the requirements for the Ph.D. degree at the University of California, Irvine.
- (2) J. W. Root, W. Breckenridge, and F. S. Rowland, *J. Chem. Phys.*, **43**, 3694 (1965).
- (3) E. Tachikawa and F. S. Rowland, *J. Amer. Chem. Soc.*, **90**, 4767 (1968).
- (4) T. Tominaga and F. S. Rowland, *J. Phys. Chem.*, **72**, 1399 (1968).
- (5) E. Tachikawa, Y.-N. Tang, and F. S. Rowland, *J. Amer. Chem. Soc.*, **90**, 3584 (1968).
- (6) E. Tachikawa and F. S. Rowland, *J. Amer. Chem. Soc.*, **91**, 559 (1969).
- (7) T. Tominaga, A. Hosaka, and F. S. Rowland, *J. Phys. Chem.*, **73**, 465 (1969).
- (8) A. Hosaka, Ph.D. Thesis, University of California, Irvine, 1971.
- (9) A. E. Finholt, A. G. Bond, K. E. Wilzbach, and H. I. Schlesinger, *J. Amer. Chem. Soc.*, **69**, 2692 (1947).
- (10) C. Eaborn, "Organosilicon Compounds," Academic Press, New York, N. Y., 1960.
- (11) J. K. Lee, E. K. C. Lee, B. Musgrave, Y.-N. Tang, J. W. Root, and F. S. Rowland, *Anal. Chem.*, **34**, 741 (1962).
- (12) E. Tachikawa, Ph.D. Thesis, University of California, Irvine, 1967.

scopic content of ^3He was measured for each sample through the difference in thermal conductivity between ^3He and the ^4He of the flow gas. The yields of HT and DT have all been normalized per unit amount of ^3He , and are thus based on sequential thermal conductivity and radioactivity measurements on the same gaseous aliquot of each sample.

Results and Discussion

DT Yields in Excess C_2H_4 . Since the absolute yields of hot reactions are dependent upon both the reactivity of the particular bond involved and upon the specific energy loss processes in each individual molecular system, we have followed our standard procedure of making these comparisons in the presence of a large excess of some moderator-scavenger molecule combination.²⁻⁶ The data for DT yields from the methylsilanes are given in Table I for systems in which C_2H_4 is the moderator, and for which both C_2H_4 and O_2 serve as scavenger molecules for removing thermal atoms and radicals. Although HT was also routinely measured, its primary source in these mixtures lies in abstraction from C_2H_4 and the yield for abstraction from the CH_3 groups in the methylsilanes represents a small, very imprecisely measured increment to the HT formed by reaction with the moderator. For two of the methylsilane samples, the O_2 concentration was reduced by about a factor of 2, with a measurable increase in the observed DT yield as a result. This sensitivity of yield to the precise O_2 scavenger concentration is typical of very weak bonds from which abstraction occurs quite readily. In the comparisons made in Table I and Figure 1, these low O_2 concentration experiments have been excluded.

TABLE I: Specific Yields of DT from Recoil Tritium Reactions with Partially Deuterated Methylsilanes in Excess C_2H_4

Substrate ^a	Specific DT activity		Average yield per Si-D bond
	Per molecule	Per bond	
$(\text{CH}_3)_3\text{SiD}$	$4,290 \pm 70$	4290 ± 70	4360 ± 80
	$4,430 \pm 80$	4430 ± 80	
$(\text{CH}_3)_2\text{SiD}_2$	$8,090 \pm 80^b$	4050 ± 40	3790 ± 30
	$7,580 \pm 60$	3790 ± 30	
CH_3SiD_3	$11,700 \pm 90^b$	3900 ± 30	3680 ± 40
	$11,130 \pm 90$	3710 ± 30	
	$10,820 \pm 80$	3610 ± 30	
	$11,210 \pm 110$	3730 ± 40	
$(\text{CH}_3)_3\text{CD}$	$2,410 \pm 90$	2410 ± 90	2380 ± 90
	$2,350 \pm 80$	2350 ± 80	
$\text{c-C}_4\text{D}_8$	$12,530 \pm 90$	1570 ± 20	1570 ± 20
CH_3CD_3	$3,580 \pm 60$	1190 ± 20	1190 ± 20

^a Standard sample pressures (Torr): ^3He , 18; O_2 , 15; RH, 50; C_2H_4 , 700. ^b These samples contained only 8 Torr of O_2 and are not included in the averages.

Normalization points were measured for several deuterated hydrocarbons, irradiated simultaneously and measured under closely normalized conditions: CH_3CD_3 for primary C-D; $\text{c-C}_4\text{D}_8$ for secondary C-D; and $(\text{CH}_3)_3\text{CD}$ for tertiary C-D. The relative yields of DT per bond summarized in Table I show that the DT yields per bond from Si-D bonds are all much higher than from any of the C-D positions. Further, the relative increase in DT yield from progressively more substituted central silicon atoms is

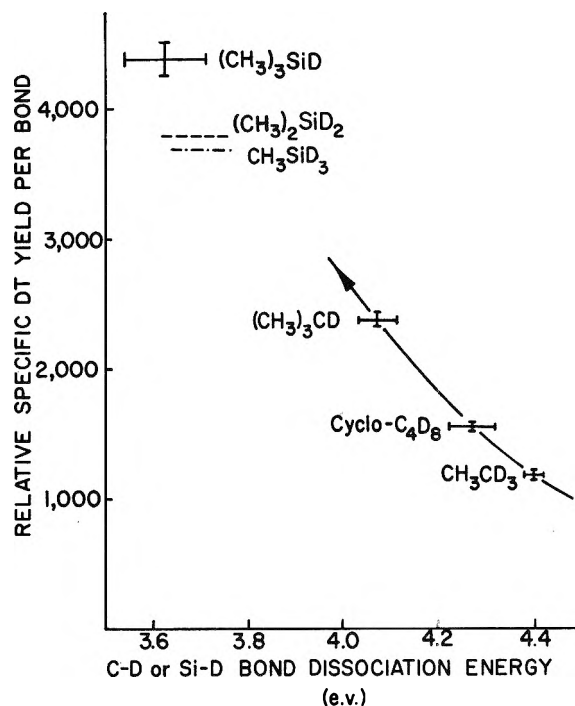


Figure 1. Relative specific DT yields per bond vs. C-D or Si-D bond dissociation energy. All deuterated bond dissociation energies assumed as 0.12 eV higher than the corresponding Si-H or C-H bond dissociation energies. Si-D in $(\text{CH}_3)_3\text{SiD}$ from ref 16. Measured DT yields are indicated for $(\text{CH}_3)_2\text{SiD}_2$ and CH_3SiD_3 for which no bond dissociation energy values are available.

markedly less than for the comparison hydrocarbons (even the absolute increments in yield are less for Si-D than for C-D).

Previous experiments have established a correlation curve between HT yields for abstraction from RH in C_2D_4 , as well as the fact that deuterated positions routinely give lower yields for abstraction than the corresponding protonated positions (e.g., HT/DT from $\text{CH}_2\text{D}_2 = 1.32 \pm 0.01$).¹³ Under our standard conditions, the DT yields from C-D positions show essentially the same correlation found in the RH- C_2D_4 systems but shifted to higher energies as shown in Figure 1.

The data of Table I have been graphed vs. the bond dissociation energies of the individual C-D and Si-D bonds in Figure 1. Very few C-D bond dissociation energies have actually been measured, so that data have been plotted vs. the accepted bond dissociation energies, with an estimated correction for deuteration.^{14,15} The bond dissociation energies of DCl, DBr, and DI are 0.137, 0.126, and 0.108 eV higher than those for the respective protonated halides, and the few hydrocarbon values seem consistent with a spread of this magnitude. Accordingly, we have adopted 0.12 eV (2.8 kcal/mol) as an approximate added correction for calculation of the bond dissociation energies of the deuterated hydrocarbons from the best estimates for the corresponding protonated species. It should be noted that the yields for abstraction from C-D bonds fit rather well to the curve established for abstraction from C-H bonds (lower DT yields and higher bond dissociation

(13) J. W. Root and F. S. Rowland, *J. Amer. Chem. Soc.*, **85**, 1021 (1963).

(14) J. A. Kerr, *Chem. Rev.*, **66**, 465 (1966).

(15) See J. W. Root, Ph.D. Thesis, University of Kansas, 1964.

energies). The implication is that there is very little isotopic influence on the mechanistic process of abstraction other than those differences already reflected in the increased bond dissociation energies of the deuterated species.

Substantial disagreement exists concerning the bond dissociation energies of Si-H (and Si-D) bonds, with values for Si-H in $(\text{CH}_3)_3\text{SiH}$ ranging from 81 ± 2 ¹⁶ to 88 ¹⁷ kcal/mol, while the more recent values for Si-H in SiH_4 are 94 ± 3 ¹⁸ and 95 ¹⁹ kcal/mol. The concave upward curve through the hydrocarbon data in Figure 1 would fit smoothly through a value of about 87–88 kcal/mol for Si-D in $(\text{CH}_3)_3\text{SiD}$, corresponding to about 85 kcal/mol for Si-H in $(\text{CH}_3)_3\text{SiH}$ (a value midway between the two discrepant literature numbers for the Si-H bond). However, no information exists concerning the relative yields of DT to be expected from (hypothetical) C-D, Si-D, N-D, or O-D bonds of the same bond dissociation energies. Therefore, we do not know how to extend a hydrocarbon curve to fit silicon-hydrogen bond yield data, and can make no legitimate estimate of the *absolute* bond dissociation energies of these Si-D bonds.

Estimates of *relative* bond dissociation energies can be obtained by assuming that the slope of the yield *vs.* bond dissociation energy curve for Si-D will be similar to that for C-D bonds. The general uncertainty in this slope leads to the estimate that the Si-D bonds in $(\text{CH}_3)_2\text{SiD}_2$ and CH_3SiD_3 are 1.5–2.0 and 1.8–2.4 kcal/mol stronger, respectively, than in $(\text{CH}_3)_3\text{SiD}$. The total spread in Si-D bond dissociation energies from tertiary to primary is indicated as <3 kcal/mol, substantially less than the 7 kcal/mol difference between the tertiary C-H in isobutane and the primary C-H in ethane.¹⁴

DT Yields in Excess N₂. When N₂ is used as the moderator, together with O₂ as the scavenger molecule, a much larger fraction of the tritium atoms reacts by abstraction of H or D from the substrate molecule. Data for the three deuteriomethylsilanes is given in Table II for N₂-moderated experiments. The DT yields *per bond* increase from primary to tertiary Si-D more strikingly here than in C₂H₄ moderator systems because there is far less competition for the low-energy tritium atoms in the N₂ system. The absolute DT yields in comparable samples are more than ten times larger in N₂ than in C₂H₄; in C₂H₄, these "extra" tritium atoms do not find the substrate molecule at low energy because they have been removed in prior collisions at higher energies by abstraction or addition reactions with the olefin itself.

The sums of the HT plus DT observed yields in Table II are roughly constant, indicating that approximately the same fraction of the total tritium atoms (~30–40%) reacts by abstraction with each of the methylsilane substrates. In each case, the *per bond* specific yield is far greater for Si-D bonds than for C-H, since the Si-D bonds are competitive with the reaction of T + O₂ to much lower tritium atom kinetic energies. The absolute observed yields of DT increase steadily from $(\text{CH}_3)_3\text{SiD}$ to CH_3SiD_3 , demonstrating that three Si-D bonds scavenge low-energy tritium more efficiently than one Si-D bond for equal numbers of substrate molecules. On the other hand, the one Si-D bond in $(\text{CH}_3)_3\text{SiD}$ is more efficient than each of the three Si-D bonds in CH_3SiD_3 taken individually, as the latter are all in competition with one another as well as with the O₂ for the low-energy tritium atoms. In the N₂

TABLE II: Specific Yields of HT and DT from Recoil Tritium Reactions with Partially Deuterated Methylsilanes in Excess Nitrogen

Substrate ^a	Observed yields ^b		Specific yields per bond ^c	
	HT	DT	HT	DT
$(\text{CH}_3)_3\text{SiD}$	3480	5320	4990 ± 20	68,620 ± 230
$(\text{CH}_3)_2\text{SiD}_2$	2270	6830	5280 ± 40	47,570 ± 180
CH_3SiD_3	1630	9980	6800 ± 50	41,540 ± 120
$(\text{CH}_3)_4\text{C}$	4590		4790 ± 50	

^a Standard sample pressures (Torr); ³He, 10; O₂, 22; RH, 50; N₂, 700. ^b HT and DT yields per unit amount of ³He, in arbitrary units. ^c After correction for chromatographic flow rates, and small variations in actual composition.

moderator system, then, the spectrum of recoil tritium atoms available to each substrate molecule is dependent in part upon the characteristics of the substrate itself, making comparisons less significant, especially for those reactions which can be initiated by relatively low-energy tritium atoms.

The observed HT yields furnish an upper limit to the HT yields from the CH₃ positions in partially deuterated methylsilanes, and would lead to good estimates of the bond dissociation energies in each molecule, were it not for the isotopic impurity Si-H in the nominally fully deuterated Si-D positions. The data are not available for accurate corrections in N₂ moderator systems since we have no measure of either the per cent H impurity in Si-D bonds or the HT/DT ratio to be expected from such weak bonds under N₂ moderator conditions. While the HT yield of 6800 from CH_3SiD_3 is suggestive of a weaker C-H bond than, for example, in neopentane, an accurate experiment would best be done through observation of the DT yield from the oppositely deuterated CD_3SiH_3 , for which isotopic impurity C-H in the methyl groups would cause only a minor effect.

Mechanism of the Abstraction Reaction. Two general mechanistic arguments have been presented in explanation of the clear dependence of the measured abstraction yields upon the bond dissociation energies of the attacked C-H bonds in alkanes and cyclanes.^{2-8,20} Our own preferred explanation is that most of these abstraction reactions occur at relatively low tritium atom energies (a few electron volts or less), and that the higher yields from weaker bonds are a natural consequence of the lower activation energies for those abstraction processes.²⁻⁸ The alternate proposal is that the H or D atoms are "stripped" off at relatively high energies (generally 10 eV or more), and that weaker bonds permit such stripping to occur in higher yield.²⁰

The current experiments were not designed with any intention to provide information about the relative merits of these two mechanistic proposals. Nevertheless, we believe that the tenfold higher yields of D from Si-D than of H from C-H in Table II, and the general sensitivity of the

- (16) S. J. Band, I. M. T. Davidson, C. A. Lambert, and I. L. Stephenson, *Chem. Commun.*, 723 (1967).
- (17) G. G. Hess, F. W. Lampe, and L. H. Sommer, *J. Amer. Chem. Soc.*, **87**, 5329 (1965).
- (18) F. F. Saalfeld and H. J. Svec, *Inorg. Chem.*, **3**, 1442 (1964).
- (19) W. C. Steele, L. D. Nichols, and F. G. A. Stone, *J. Amer. Chem. Soc.*, **84**, 4441 (1962).
- (20) For a review of the proposed stripping mechanism, see R. Wolfgang, *Progr. React. Kinet.*, **3**, 97 (1965).

yields from Si-D bonds to the concentration of O₂ present, are both completely consistent with our low-energy model. On the other hand, abstraction with 30–40% yields in moderator systems in which the relatively few collisions in the 10–50-eV range are mostly with N₂ seems to us to make the stripping mechanism an increasingly implausi-

ble explanation except for a negligibly small fraction of all of the observed events. In any event, the postulate of a correlation between DT yields and Si-D bond dissociation energies is not mechanism dependent, and the conclusions about relative Si-D bond energies are valid whatever the mechanistic details of the abstraction process itself.

Electron Paramagnetic Resonance Studies of the Kinetics of the Intramolecular Cation Migration Process in Alkali Metal Anthraquinone¹

Kuang S. Chen, Takuo Takeshita, Kazuo Nakamura, and Noboru Hirota*

Department of Chemistry, State University of New York at Stony Brook, Stony Brook, New York 11790 (Received June 12, 1972)

Detailed epr studies of the kinetics of the intramolecular cation migration processes in alkali metal anthraquinone are reported. The analysis of the epr spectra and the determination of the rate constants, activation energies, and entropies of activation were made by using the relaxation matrix theory and the computer-simulated spectra obtained by the steady-state solutions of the modified Bloch equations. The obtained rate parameters were explained in terms of the suggested model of the cation migration process.

1. Introduction

Since de Boer and Mackor discovered the line width alternation due to intramolecular cation migration between two equivalent sites in anion radicals,² numerous epr investigations of such processes have been reported.³ Quantitative measurements of migration rates have been made in several systems.^{4–11} Nevertheless, there remain several questions concerning the migration process.

First, agreements among the values of rate constants, activation energies, and entropies of activation reported by different workers on the same system are rather poor. Consequently some of the reported values are not very reliable. Second, although it appears that the entropy of activation (ΔS^\ddagger) is important in determining the migration rate and solvation is largely responsible for it, two different views on the major factors contributing to ΔS^\ddagger have been given.^{10,11} Third, ΔS^\ddagger appears to vary considerably depending on the system, but it is not completely clear how ΔS^\ddagger depends on the type of system.

In the course of our studies on the spin distributions in anthraquinone ion pair systems¹² we noted that potassium and sodium anthraquinones undergo cation migration (Figure 1) with rates suitable for epr studies. It was thought that the detailed investigations of the cation migration rates in this system may be helpful in clarifying the uncertainties associated with the migration processes and in obtaining information about the factors controlling the rates. Accordingly, we have made detailed investigations of the migration processes in ethereal solvents and in a mixture of THF and DMF.

The epr spectra of ion pairs of anthraquinone are rather complex and the accurate determination of the rate pa-

rameters are often not trivial. In order to analyze the spectra we used Freed-Fraenkel relaxation matrix theory¹³ in the rapid migration region whenever it was applicable, but in most cases we analyzed the observed spectra over wider ranges of migration rates with the help of the computer-simulated spectra obtained by solving the modified Bloch equation.¹⁴

While our work was in progress two papers concerning the anthraquinone anion appeared in the literature.^{15,16} However, no detailed studies on the kinetics of the cation migration have been reported so far.

- (1) This work was supported by a Grant from the National Science Foundation.
- (2) E. deBoer and E. L. Mackor, *J. Amer. Chem. Soc.*, **86**, 1513 (1964).
- (3) Numerous examples of line width alternation in the epr spectra due to intramolecular cation transfer are given in a review article by P. D. Sullivan and J. R. Bolton, *Advan. Magn. Resonance*, **4**, 39 (1970).
- (4) (a) N. M. Atherton and A. E. Goggins, *Trans. Faraday Soc.*, **61**, 1399 (1965); (b) J. C. Chippendale and E. Warhurst, *ibid.*, **64**, 2332 (1968).
- (5) A. F. Neiva Correia, Thesis, University of Amsterdam, 1968.
- (6) K. Nakamura, *Bull. Chem. Soc. Jap.*, **40**, 1019 (1967).
- (7) P. S. Gill and T. E. Gough, *Trans. Faraday Soc.*, **64**, 1997 (1968).
- (8) B. S. Prabhananda, M. P. Khakhar, and M. R. Das, *J. Ind. Chem. Soc.*, **46**, 659 (1969).
- (9) J. Oakes and M. C. R. Symons, *Trans. Faraday Soc.*, **66**, 10 (1970).
- (10) E. Warhurst and A. M. Wilde, *Trans. Faraday Soc.*, **67**, 605 (1971).
- (11) T. E. Gough and P. R. Hindle, *Can. J. Chem.*, **49**, 2412 (1971).
- (12) T. Takeshita and N. Hirota, *J. Amer. Chem. Soc.*, **93**, 6421 (1971).
- (13) J. H. Freed and G. K. Fraenkel, *J. Chem. Phys.*, **39**, 326 (1963).
- (14) (a) H. S. Gutowsky, D. W. McCall, and C. P. Slichter, *J. Chem. Phys.*, **21**, 279 (1953); (b) H. S. Gutowsky and C. H. Holm, *ibid.*, **25**, 1288 (1956).
- (15) A. W. Rutter and E. Warhurst, *Trans. Faraday Soc.*, **64**, 2338 (1968).
- (16) T. E. Gough and P. R. Hindle, *Trans. Faraday Soc.*, **66**, 2420 (1970).

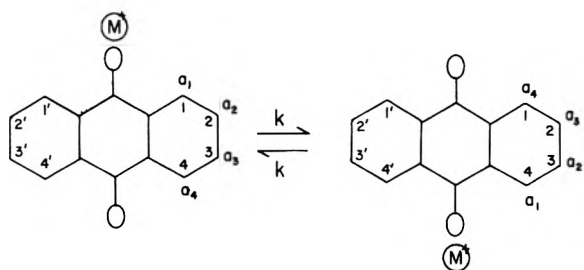


Figure 1. Scheme for cation migration and the numbering of protons and splittings.

2. Experimental Section

The preparation of most of the samples and the epr measurements were made in the usual manner using an alkali metal mirror.¹⁷ The Li anthraquinone samples were reduced by Li-Hg amalgam. Pink colored solutions of anthraquinone anions were easily obtained, but they were converted easily into blue-green solutions of dinegative ions when they were in contact with metal for long periods of time.

Good concentrations of radical anion can be obtained by adding a small amount of neutral molecule to the solution of dinegative ions. In order to render the solution free of any small particles of precipitate, the radical anion solutions were filtered through fritted glass.

The preparation of the sample in the mixture of THF and DMF was made by adding a small amount of DMF to the sample cell through a vacuum line. Epr measurements were made on a Varian V-4502 spectrometer according to the procedure already described elsewhere.¹⁷

3. Results and Discussions

3.1. Epr Spectra. Most spectra are interpreted as those of ion pairs. However the spectra of dissociated ions are often observed, particularly at low temperature. The extent of the mixing of free ion spectra increases as the size of counter ion increases. In Figures 2-5 some representative epr spectra are shown together with the computer-simulated spectra obtained with appropriate rate constants. The values of hyperfine splittings were reported in a previous paper.¹² Both proton and alkali metal splittings are very sensitive to temperature. The temperature dependence of these splittings is shown in Figures 6 and 7. A few comments on the characteristics of the individual systems are given below.

A. Li-Anthraquinone (Li^+A^-). Over the entire temperature range the spectrum of Li-anthraquinone was found to be in the slow-limit region ($k \ll \Delta\omega_i$, where $\Delta\omega_i$ is the difference in the hyperfine splitting in the i th proton in the structure A and B). Only in the mixture of THF and DMF at higher temperature Li^+A^- goes into the intermediate migration region ($k \sim \Delta\omega_i$). No free ion spectra were detected in this system. No kinetic studies were made in this system.

B. Na-Anthraquinone (Na^+A^-). In THF and DME most epr lines are in the slow limit at low temperatures (-30° and lower). At higher temperatures some lines are in the intermediate to the fast migration limits.

C. K-Anthraquinone in THF and DME (K^+A^-). At room temperature many epr lines are in the intermediate region, but at higher temperature they go to the fast limit. Lines due to the free ion are very strong at low temperature, particularly in DME. This is clearly seen in the spectrum shown in Figure 4.

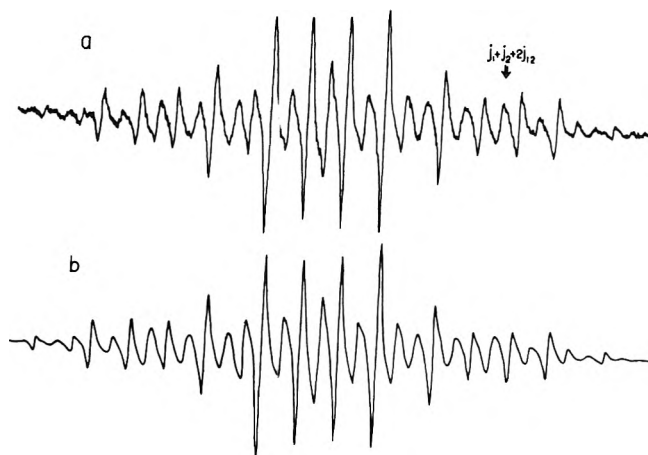


Figure 2. Na-anthraquinone in THF at 14.4° : (a) experimental spectrum, peak indicated by \rightarrow is modulated by $J_1 + J_2 + 2J_{12}$ and is most sensitive to temperature changes; (b) computer-simulated spectrum with $k = 1.11 \times 10^6 \text{ sec}^{-1}$.



Figure 3. Na-anthraquinone in THF at 44.6° : (a) experimental spectrum; (b) computer-simulated spectrum with $k = 2.09 \times 10^6 \text{ sec}^{-1}$.

D. Cs-Anthraquinone in THF (Cs^+A^-). This spectrum can be explained by assuming the fast migration limit. No kinetic studies were made in this system.

3.2. Structure of Ion Pairs. Temperature dependence of the alkali metal splittings is shown in Figure 6. It is seen that the magnitudes and the temperature dependence of the alkali metal splittings of anthraquinone systems are very similar to those observed in fluorenone ketyls. Therefore the discussion made concerning the ion pair structures of fluorenone ketyls¹⁸ should be applicable to the anthraquinone anion case. A MO calculation based on the structure shown in Figure 1 can explain the proton hyperfine splittings and g values reasonably well. As in the case of fluorenone ketyls¹⁸ cations are located in the vicinity of oxygen, but not on the the $C=O$ group.

The position of the cation in the ion pairs of small cations is considered to be close to the plane of molecule, but deviating toward an on-plane position as the size of cation increases and as the temperature is raised.

3.3. Bases of Analysis. In order to analyze the observed spectra we have used two methods: (1) comparison of the experimental spectra with the computer-simulated spectra obtained by the solution of the modified Bloch equation¹⁴ with appropriate migration rates and (2) use of the Freed-Fraenkel relaxation matrix theory¹³ whenever cer-

(7) N. Hirota, *J. Amer. Chem. Soc.*, **89**, 37 (1967).

(8) K. S. Chen, S. W. Mao, K. Nakamura, and N. Hirota, *J. Amer. Chem. Soc.*, **93**, 6004 (1971).

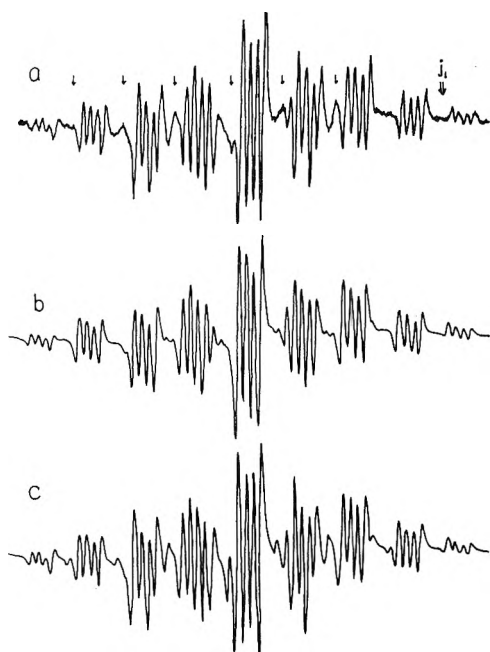


Figure 4. K-antraquinone in THF at 10.5°: (a) experimental spectrum, \rightarrow indicates the peak position for free ion spectrum, \rightarrow indicates the peak with J_1 ; modulation. (b) computer-simulated spectrum for ion pair only ($k = 2.02 \times 10^7 \text{ sec}^{-1}$); (c) computer-simulated spectrum obtained by the superposition of ion pair spectrum with small amount of free ion spectrum.

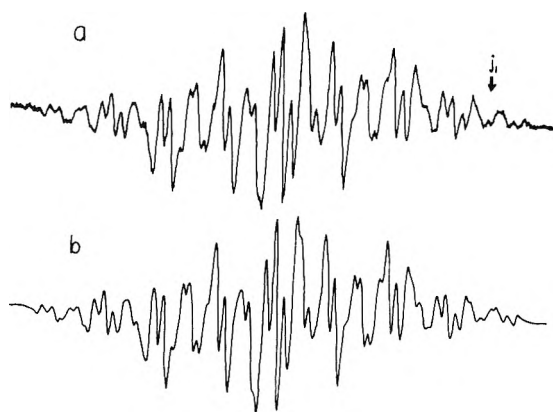


Figure 5. K-antraquinone in THF at 49.1°: (a) experimental spectrum; (b) computer-simulated spectrum with $k = 6.28 \times 10^7 \text{ sec}^{-1}$.

tain well-separated peaks can be treated as being in the fast limit. The bases of these analyses are given below.

(1) *Modified Bloch Equation.*¹⁴ The steady-state solution of the modified Bloch equation for anthraquinone ion pair undergoing cation migration is given by

$$G = G_A + G_B = -\frac{1}{2} \gamma_e H_1 M_0 \tau \frac{(2 + \tau \alpha_A)^{-1} + (2 + \tau \alpha_B)^{-1}}{1 - (2 + \tau \alpha_A)^{-1} - (2 + \tau \alpha_B)^{-1}} \quad (1)$$

Here we follow the standard notations for G , α , and τ .¹⁴ τ is given by $\tau = 1/k$.

The computer program for the solution of this equation was written assuming $T_{2,0}(A) = T_{2,0}(B)$ (T_2 for A and B in the absence of cation migration) and the spectra were simulated for various values of k and the hfs, a_1 , a_2 , a_3 , and a_4 . The computer program used in this work is very similar to that by Sullivan and Bolton,³ but slightly modified to save computing time.

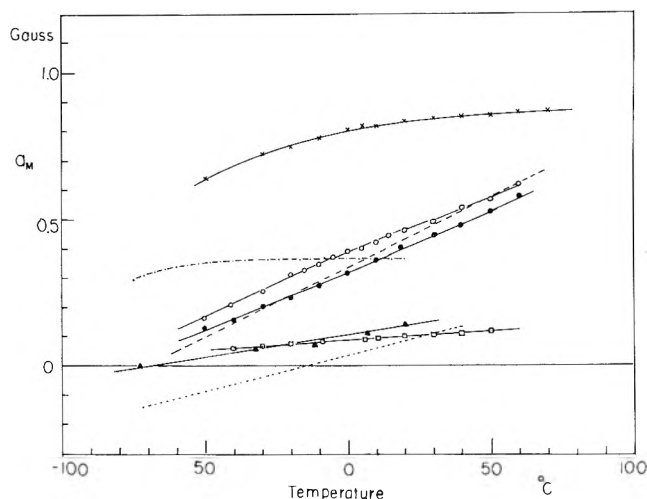


Figure 6. Temperature dependence of alkali metal splittings of anthraquinone (\blacktriangle , Li in THF; \bullet , Na in DME; \circ , Na in THF; \square , K in THF; \times , Cs in THF) and fluorenone (----, Li in THF; - - - - , Na in THF; - · - · - · , Cs in THF).

(2) *Relaxation Matrix Theory.*¹³ The Freed-Fraenkel relaxation matrix theory was applied to the cation jump process. Assuming that the process is two jumps and following the standard procedure of the relaxation matrix theory already described elsewhere,¹³ we obtain the line width formula for the line broadening of the resonance peaks. They are given by

$$\Delta\omega = (1/T_2) - (1/T_{2,0}) = J_1(M_1 - M_4)^2 + J_2(M_2 - M_3)^2 + 2J_{12}(M_1 - M_4)(M_2 - M_3) \quad (2)$$

where

$$J_1 = \frac{1}{8} \gamma_e^2 (a_1 - a_4)^2 \tau$$

$$J_2 = \frac{1}{8} \gamma_e^2 (a_2 - a_3)^2 \tau$$

$$J_{12} = \frac{1}{8} \gamma_e^2 (a_1 - a_4)(a_2 - a_3) \tau$$

and

$$1/T_2 = (1/T_{2,0}) + \frac{1}{8} \gamma_e^2 (1/k) [(a_1 - a_4)^2 (M_1 - M_4)^2 + (a_2 - a_3)^2 (M_2 - M_3)^2 + 2(a_1 - a_4)(a_2 - a_3)(M_1 - M_4)(M_2 - M_3)] \quad (3)$$

Here M_1 , M_2 , M_3 , and M_4 are given by $M_1 = m_1 + m_1'$, $M_2 = m_2 + m_2'$, and so forth. m_1 , m_1' , and others are the magnetic quantum numbers of respective protons. $\Delta\omega$ were calculated from the comparisons of intensities assuming Lorentzian line shape. However, overlapping of lines with different M sometimes takes place. In order to make accurate intensity comparisons, computer-simulated spectra with the trial values of $\Delta\omega$ were compared with the experimental spectra.

For the kinetic studies which overlap least with others and are in the region of appropriate modulation ranges were selectively used. Usually the intensities of these peaks and the one which is not affected by the cation migration were compared. The sets of peaks used for kinetic measurements are tabulated in Table I together with the modulation associated with these peaks.

3.4. *Calculation of Rate Constants.* (1) *Temperature Dependence of the Proton Splittings and the Estimates of a_1 , a_2 , a_3 , and a_4 .* In order to make accurate determinations of the migration rates the proton splittings, a_1 , a_2 , a_3 , and a_4 have to be determined correctly. This, of course, is trivial if all lines are in the slow migration limits, and can be determined directly from epr spectra. At

TABLE I

Systems	Peaks used				Modulation	Temp range of kinetic measurements
	M_1	M_2	M_3	M_4		
A + Na in THF	0	0	-1	-1	$J_1 + J_2 + 2J_{12}$ almost temp independent	+15 ~ +50°
	-1	-1	0	0		
	0	0	1	1		
	1	1	0	0		
A + Na in DME	0	0	-1	-1	$J_1 + J_2 + 2J_{12}$ almost temp independent	-10 ~ -40°
	-1	-1	0	0		
	0	0	1	1		
	1	1	0	0	J_1 strongly temp dependent	+60 ~ +80°
	-1	-1	-1	0		
	0	-1	-1	-1		
	1	1	1	0		
0	1	1	1			
A + Na + 4.79 mol % DMF in THF	-1	-1	-1	0	J_1 strongly temp dependent	+15 ~ +55°
	0	-1	-1	-1		
	1	1	1	0		
	0	1	1	1		
A + K in THF and DME	-1	-1	-1	0	J_1 strongly temp dependent	+10 ~ +50°
	0	-1	-1	-1		
	1	1	1	0		
	0	1	1	1		

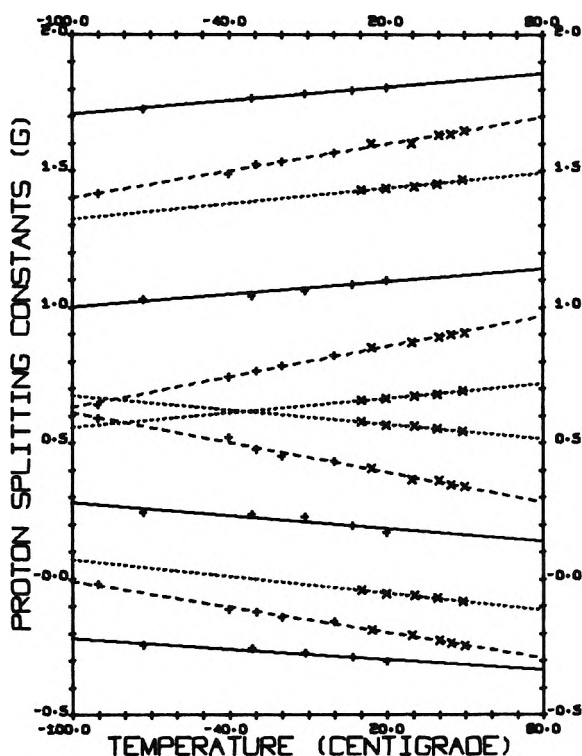


Figure 7. Temperature dependence of proton splittings: —, Li; ----, Na; ·····, K; + indicates the observed splittings; x indicates the splitting obtained by the best fits of the simulated spectra to the experimental spectra.

low temperature in sodium systems these splittings can be determined in this way. However, in other systems spectra are in the intermediate or rapid migration region and these splittings cannot be determined directly. As shown in Figure 7 proton splittings are quite temperature dependent. Therefore the values determined at low temperature cannot be used at higher temperatures.

Proton splittings in Na-anthraquinone system change linearly with temperature over the range from -20 to

-95° as shown in Figure 7. The values at higher temperatures were first estimated by the extrapolation of the low-temperature values and then checked by comparison between the observed spectra and the simulated ones. The values best fit to the observed spectra were used for the calculation of kinetic parameters. In the case of potassium systems, spectra are mostly in the intermediate region except at very low temperatures. Therefore, proton splittings cannot be determined directly from the observed spectra. However, the detailed features of the simulated spectra are very sensitive to the choice of splittings as well as the migration rates. Therefore, splittings for potassium systems were determined from the best fit between the simulated spectra and the experimental spectra. These values are given in Figure 7.

The broadening due to the migration process in the fast exchange region is proportional to terms such as $(a_1 - a_2)^2$, $(a_2 - a_3)^2$, and $(a_1 - a_4)(a_2 - a_3)$. Over the temperature range from -80 to +50°, $(a_1 - a_4)^2$ changes from ~0.5 to ~1.35 G² in the case of sodium system in THF and from ~0.25 to ~0.60 G² in the case of potassium system in THF. Other values change similarly. Therefore, it is very clear that the rates determined without taking into account of the temperature dependence of the proton splittings could be erroneous.

Similar temperature dependence of the proton splittings has been found in other semiquinone systems in recent studies by Gough and Hindle,¹¹ as well as those made in our laboratory.¹⁹ It is our belief that one of the major causes of the discrepancies among the reported values of migration rates is due to failure to recognize the temperature dependence of the modulation amplitude caused by the temperature dependence of the proton splittings.

(2) *Estimates of $1/T_{2,0}$.* $1/T_{2,0}$ was estimated from the measurement of the line width of the peak with $M_1 = 1$, $M_2 = 1$, $M_3 = 1$, and $M_4 = 1$. $1/T_{2,0}$ of this peak is not affected by the cation migration.

(3) *Calculation of Rate Constants.* Whenever possible approximate values of rate constants were first estimated

(19) K. S. Chen and N. Hirota, *J. Amer. Chem. Soc.*, **94**, 5550 (1972).

TABLE II: Rate Parameters for the Intramolecular Cation Migration in Anthraquinone Ions

Data	System				
	Na ⁺ A ⁻ THF	Na ⁺ A ⁻ DME	Na ⁺ A ⁻ 4.79 mol % DMF in THF	K ⁺ A ⁻ THF	K ⁺ A ⁻ DME
E_a , kcal/mol	4.0 ± 0.3	3.7 ± 0.3	4.7 ± 0.7	5.3 ± 0.7	4.9 ± 0.7
Log A^a	9.1 ± 0.2	9.6 ± 0.2	10.7 ± 0.5	11.4 ± 0.5	11.2 ± 0.5
k_{298} , sec ⁻¹	1.38×10^6	7.80×10^6	1.82×10^7	3.18×10^7	4.54×10^7
ΔS^\ddagger , eu	-18.8 ± 1.0	-16.6 ± 1.0	-11.6 ± 2.0	-8.5 ± 2.0	-9.1 ± 2.0
ΔG^\ddagger , kcal/mol	9.1 ± 0.1	8.0 ± 0.1	7.6 ± 0.1	7.2 ± 0.1	7.0 ± 0.1
ΔH^\ddagger , kcal/mol	3.5 ± 0.3	3.1 ± 0.3	4.1 ± 0.6	4.7 ± 0.6	4.3 ± 0.6

^a A units are in sec⁻¹.

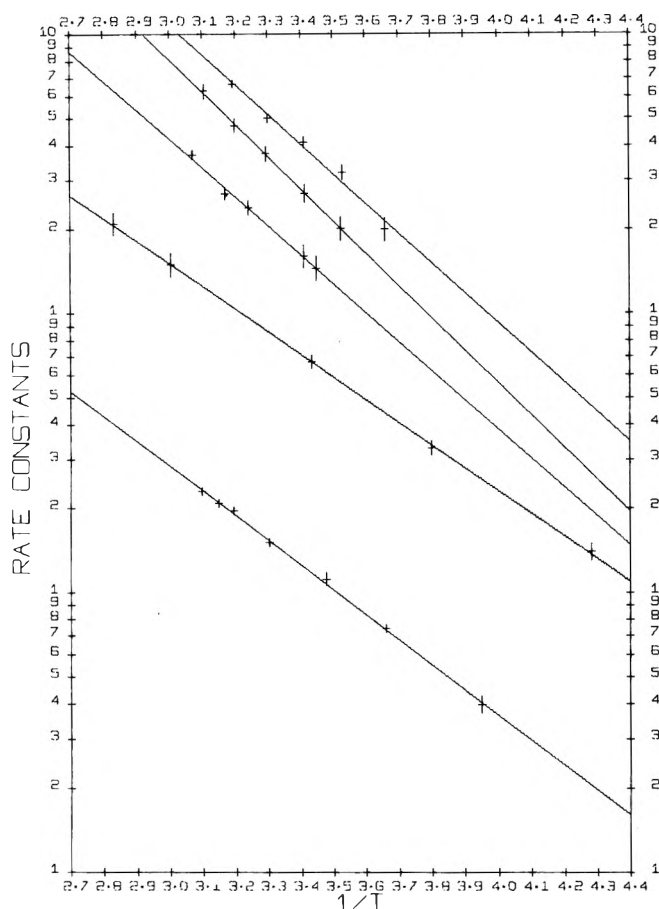


Figure 8. Log k vs. $1/T$ plots for cation migration in anthraquinone (from bottom to top): Na in THF; Na in DME; Na in THF plus 4.79 mol % of DMF; K in THF; K in DME.

by the relaxation matrix method. The estimated rate constants and the splittings were put into simulation program and the entire spectra were compared with the experimental spectra. The rate constants and the splittings were adjusted until the best fit was obtained. Generally the rate constants determined by the relaxation matrix theory agree within 10% with the rate constants which best simulate the experimental spectra.

The overall agreement between the observed spectra and those simulated by the solution of the modified Bloch equation was found to be excellent as shown in Figures 2-5, indicating the appropriateness of the use of the modified Bloch equation in treating this type of problem. The determined rate constants at various temperatures for five

different systems are plotted in Figure 8. As seen from the figure the plots of log k vs. $1/T$ give quite satisfactory straight lines over relatively wide temperature ranges.

The activation energies and preexponential factors were determined from these plots. The values of ΔH^\ddagger , ΔS^\ddagger and ΔG^\ddagger were also determined by using the usual transition state expression.²⁰ These values are tabulated in the Table II. Several noteworthy observations are described below.

A. Pure Solvents. From Table II it is quite clear that ΔS^\ddagger plays an important role in determining the transfer rates. The order of E_a does not follow the order of reaction rates. The values of activation energy (E_a) are relatively small, being 3.7 ~ 5.3 kcal/mol, but smaller E_a were found for the systems with slower migration rates. Quite large negative ΔS^\ddagger were found for the Na systems but ΔS^\ddagger for the K systems are much smaller. Large negative entropy indicates increased solvation in the transition state.

B. Mixed Solvents. It is known from our previous studies¹⁸ that DMF preferably solvates to the cation in the mixtures of ethereal solvents and DMF. In the mixture of 5% DMF about 60% of ion pair is DMF solvated. Thus the mixture of THF and DMF is useful in seeing the effect of solvation of cation on the migration rates. A striking increase of the migration rates was found upon DMF solvation. The conversion rate between DMF solvated and unsolvated ion pairs are faster than the intramolecular migration process. The apparent rate constant k for migration is given by

$$k = k_s f_s + k_u f_u \quad (4)$$

where f_s and f_u are the fractions of DMF solvated pair and unsolvated pair and k_s and k_u are the cation migration rates for each species. The increase of the rate constants in the DMF mixture indicates $k_s \sim 20k_u$. Then the second term in the above expression is negligible and the thermodynamic parameters given in Table II represent those for DMF solvated pairs. It is shown that the decrease in ΔS^\ddagger is primarily responsible for the increase.

3.5 Factors which Control the Migration Rates. The value of ΔS^\ddagger obtained for anthraquinone systems in THF and DME are $-16 \sim -19$ eu for sodium and $-8 \sim -10$ eu for potassium. These values are close to those for duroquinone systems reported by Gough and Hindle very recently.¹¹ For a given solvent the value of E_a (or ΔH^\ddagger) is smaller for sodium systems than for potassium systems, although the migration rates are faster in the potassium systems. The major contributions to ΔS^\ddagger and ΔH^\ddagger may be

(20) I. Amdur and G. G. Hammes, "Chemical Kinetics, Principles, and Selected Topics," McGraw-Hill, New York, N. Y. 1966, p 55.

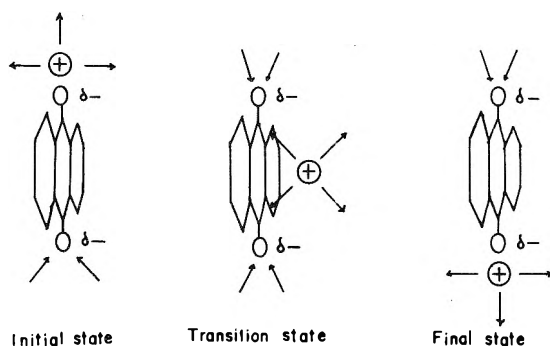


Figure 9. Schematic presentation of the model of cation migration with solvent shared transition state. Arrow indicates solvent dipole.

divided into the following for the purpose of discussion

$$\Delta S^\ddagger \simeq \Delta S_{A-S}^\ddagger + \Delta S_{C-S}^\ddagger$$

$$\Delta H^\ddagger \simeq \Delta H_{C-A}^\ddagger + \Delta H_{C-S}^\ddagger + \Delta H_{A-S}^\ddagger$$

Here the subscripts A-S, C-S, and C-A indicate the contributions from anion solvation, cation solvation, and cation-anion interaction. The negative entropy of activation indicates that the degree of solvation increase at the transition state. This can arise from (1) the increased solvation to anion and (2) the increased solvation of cation. The former was emphasized by Warhurst and Wilde,¹⁰ while the latter was suggested by Gough and Hindle.¹¹ The changes in the solvation are schematically shown in Figure 9.

When the cation moves away from the oxygen, solvation to anion is expected to increase. Our recent MO calculation does indicate that there is significant solvation of the carbonyl oxygen not associated with metal ion by THF.¹⁹ Thus negative ΔS_{A-S}^\ddagger is expected. However, contrary to the suggestions made by Warhurst and Wilde, we think that this contribution does not change much depending on the cation for the following reasons. Warhurst and Wilde suggested that the negative charge density at the oxygen atom not associated with cation changes substantially depending on the size of cation. In order to see whether or not the charge densities on the oxygen are significantly altered by changing the cation from sodium to potassium, we made MO calculations of the charge densities on the oxygen. Our calculation indicated that the difference in charge densities at the oxygen between the potassium and the sodium systems are less than 4% of the total charge density on the oxygen. We think this difference is not sufficient to cause the observed large differences in ΔS^\ddagger in going from the potassium to the sodium systems. Thus the large decrease in ΔS^\ddagger in going from the potassium system to the sodium system is considered to be due to

ΔS_{C-S}^\ddagger . It is well known that the solvation of cation by ethereal solvent strongly depends on the size of cation.²¹ It is also known that large entropy changes (~ -30 eu) are associated with the changes from contact to solvent separated ion pairs in sodium naphthalenides.²² Therefore, a large negative ΔS_{C-S}^\ddagger can accompany the migration process depending on the structure of the transition states.

The ion pair structure of anthraquinone is considered to be the contact type.^{12,18} However, the cations are solvated. If the transition state is the contact type ΔS_{C-S}^\ddagger could be positive because of the less space available for solvation. On the other hand, if the transition state is a solvent shared or solvent separated structure, a negative ΔS_{C-S}^\ddagger is expected for the following reasons. First, more space for solvation is available. Second, when the cation is attached to the oxygen, the negative charge on the oxygen reduces the effective charge and solvation of the cation (in other words, solvents are less tightly bound to cation because of the less effective positive charge). This effect is stronger for cations of smaller size.²³ When the cation is removed from a position near oxygen and forms a solvent shared or separated ion pair, solvation to cation can increase substantially because neighboring negative charge has less effect. We think that the contribution of ΔS_{C-S}^\ddagger is responsible for the large negative ΔS^\ddagger in the sodium system and that the transition state is a solvent shared type as shown in Figure 9.

The above argument is also consistent with the cation dependence of ΔH^\ddagger . ΔH_{C-A}^\ddagger is probably large and positive but ΔH_{A-S}^\ddagger is expected to be negative. ΔH_{C-S}^\ddagger depends on the structure of the transition state, but is expected to be negative if the cation is more solvated at the transition state. Larger negative values of ΔH_{C-S}^\ddagger due to stronger solvation of sodium ion can make ΔH^\ddagger smaller for the sodium system than for the potassium system.

The importance of the cation solvation in determining the migration rates is also clearly demonstrated by the large increase of the migration rates caused by the solvation of sodium ion by DMF. DMF solvation of cation changes the solvation of THF both at the initial and the transition state and reduces $|\Delta S_{C-S}^\ddagger|$.

Acknowledgment. The financial support from the National Science Foundation (Grant No. GP-15365) is greatly appreciated.

- (21) (a) D. N. Bhattacharyya, C. L. Lee, J. Smid, and M. Szwarc, *J. Phys. Chem.*, **69**, 608 (1965); (b) C. Carvajal, K. J. Tölle, J. Smid, and M. Szwarc, *J. Amer. Chem. Soc.*, **87**, 5548 (1965); (c) D. Nicholls, C. Sutphen, and M. Szwarc, *J. Phys. Chem.*, **72**, 1021 (1968).
- (22) (a) N. Hirota, *J. Amer. Chem. Soc.*, **90**, 3104 (1968); (b) N. Hirota, R. Carraway, and W. Schook, *ibid.*, **90**, 3111 (1968).
- (23) It has been shown that the charge on the counter ion affects the solvation very strongly. K. Nakamura, B. Wong, and N. Hirota, to be submitted for publication.

Dielectric Studies. XXXIII. Establishment of Acetyl Group Relaxation in Mono- and Para-Substituted Benzene Compounds

D. B. Farmer, P. F. Mountain, and S. Walker*¹

Lakehead University, Thunder Bay, Ontario, Canada (Received January 28, 1972)

Publication costs assisted by Lakehead University

The dielectric absorption of five or six microwave frequencies of acetophenone, ω,ω,ω -trifluoroacetophenone, and all four *p*-haloacetophenones in cyclohexane solution at 40° has been determined. Acetophenone has also been examined in the same solvent at 25°. For ω,ω,ω -trifluoroacetophenone the predominant process detectable is molecular relaxation while for the *p*-haloacetophenones the identifiable process is largely group relaxation. Acetophenone, however, is a case in which both relaxation processes yield appreciable contributions to the dielectric absorption which is detectable in the microwave region. A procedure is outlined where for para-substituted acetophenones—by the choice of a suitable substituent in that position—the dielectric absorption can be arranged to be principally group relaxation.

Introduction

Several dielectric studies have been made on acetyl group substituted aromatic molecules.^{2,3} One of the first was by Fischer,² on acetophenone at a single wavelength of 4.5 m, who compared the observed relaxation time with that of an estimated molecular relaxation time. Since the observed relaxation time was only slightly shorter, Fischer concluded that there was a slight indication of intramolecular relaxation of the acetyl group. A more rigorous study of acetyl group rotation was made by Fong and Smyth³ who examined the molecules *p*-phenylacetophenone, 2-acetonaphthone, 4-acetyl-*o*-terphenyl, and *p*-diacetylbenzene at three microwave frequencies and three to five temperatures. In each case there was found to be a small contribution (~15%) of the total dielectric absorption from acetyl group rotation. With such a small weight factor on the group relaxation process it must now be considered difficult to be sure whether group relaxation is in fact taking place, especially since there may be a weak contribution to the dielectric absorption at the high-frequency side of the microwave region; this absorption corresponds with the tail end of a broad band exhibited by most (if not all) liquids somewhere in the 5–150-cm⁻¹ region of the far-infrared.⁴ Thus, with the possibility of such a contribution to the dielectric absorption it becomes imperative to establish group relaxation by this approach with great care when the analysis from the Budó equation⁵ yields a small C_2 value. In fact, Klages and Krauss⁶ in a recent study on acetophenone, *p*-chloroacetophenone, and *p*-diacetylbenzene in nonpolar solvents concluded that the acetyl group is rigid. If this conclusion is correct, then it would seem unlikely that acetyl group relaxation would occur in, for example, *p*-phenylacetophenone and 2-acetonaphthone where the conjugation is greater than in acetophenone, and the energy barrier about the C_{aliphatic}-C_{aromatic} bond is likely to be greater and the molecule, consequently, more rigid.

It was the intention of our study to examine molecules where the calculated weight factor (C_2) for acetyl group relaxation is varied from ~0.8 to ~0 by a suitable choice of substituents. The most interesting case is when $C_2 \gg C_1$ since the group relaxation, if it occurs, can then be studied more precisely. By examining a number of such

cases for substituted acetophenones of differing sizes and comparison of their observed relaxation times with the molecular relaxation time of a rigid molecule of corresponding shape and size, it should become feasible to establish whether acetyl group relaxation is taking place.

From bond and group moment calculations of C_2 three systems suitable to this type of study are (i) ω,ω,ω -trifluoroacetophenone ($C_2 \sim 0$), (ii) acetophenone ($C_1 \sim 0.4$), and (iii) *p*-haloacetophenones ($C_2 \sim 1.0$). In addition, this study ought to indicate the adequacy or otherwise of such estimations.

For this investigation cyclohexane was chosen as solvent, since it is one of the most inert, while 40° was preferred to room temperature, since this would tend to lessen any possible dipolar association of the solute molecules. Acetophenone was also examined in this solvent at 25°.

Experimental Methods

Apparatus. The apparatus and techniques employed have been described previously^{7,8} and the errors assessed.⁹ The dielectric constant (ϵ') and loss factor (ϵ'') were determined by a bridge method at some of the following frequencies: 70.0, 35.11, 23.98, 9.313, 16.20, and 6.70 GHz. For *p*-iodoacetophenone the frequency 1.9 GHz was also employed. The static dielectric constant (ϵ_0) was measured with a heterodyne beat apparatus at 2 MHz.

Purification of Materials. With the exception of *p*-iodoacetophenone these commercially available liquids were dried prior to distillation and then distilled by using a (30 theoretical plates) spinning band column, and a small center fraction was collected and then stored over a

- (1) Correspondence should be addressed to 44 Park Town, Oxford, England.
- (2) E. Fischer, *Z. Naturforsch. A*, **9**, 695 (1954).
- (3) (a) F. K. Fong and C. P. Smyth, *J. Amer. Chem. Soc.*, **85**, 548 (1963); (b) F. K. Fong and C. P. Smyth, *ibid.*, **85**, 1565 (1963).
- (4) M. Davies, G. W. F. Pardoe, J. E. Chamberlain, and H. A. Gebbie, *Trans. Faraday Soc.*, **64**, 847 (1968).
- (5) A. Budó, *Phys. Z.*, **39**, 706 (1938).
- (6) G. Klages and G. Krauss, *Z. Naturforsch. A*, **26**, 1272 (1971).
- (7) W. F. Hassell, M. D. Magee, S. W. Tucker, and S. Walker, *Tetrahedron*, **20**, 2137 (1964).
- (8) D. B. Farmer and S. Walker, *Tetrahedron*, **22**, 111 (1966).
- (9) M. D. Magee and S. Walker, *Trans. Faraday Soc.*, **62**, 3093 (1966).

suitable drying agent in darkened glassware. The *p*-iodoacetophenone was vacuum-distilled and recrystallized. The observed boiling and melting points compared well with literature values, and gas-liquid partition chromatography could not then detect impurities in these compounds.

Results

The evaluation of the high-frequency dielectric constant (ϵ_∞), distribution coefficient (α), mean relaxation time (τ_0), discrete relaxation times (τ_1 and τ_2), weight factors (C_1 and C_2), and dipole moment (μ) has been described previously.⁸ The use of Debye distributions to analyze the dielectric data of dilute solutions can be defended empirically and theoretically¹⁰ and has been confirmed by experiment.⁹ If the dielectric data are analyzed into contributions from two relaxation times, τ_1 and τ_2 , then the values of the dielectric constant (ϵ'_{calcd}) and the loss ($\epsilon''_{\text{calcd}}$) calculated from the τ_1 , τ_2 , and C_1 values⁵ have to correspond with the measured values within the limits of the appropriate experimental error.⁹ In fact, for the systems listed in Table I there is, in general, good agreement between the calculated and experimental values within the limits of experimental error. It should be noted that it might prove equally feasible to analyze the results in terms of a mean relaxation time (τ_0) and a distribution parameter (α), where both this approach and the Budó one (*i.e.*, analysis into τ_1 , τ_2 , and C_1) yield calculated values of the dielectric constant and loss which correspond with the observed ones within experimental error. However, the Budó analysis is acceptable only if a plausible physical mechanism can be associated with the evaluated parameters.¹¹

For the computer analysis on the data of acetophenone C_1 was fixed at 0.33, while for the *p*-haloacetophenones a value of 0.25 was employed (see later). The analyses are given in Table II together with the mean relaxation time, weight fraction, dipole moment, static and high frequency dielectric constant, and distribution coefficient.

Discussion

If the mono- and para-substituted acetophenones exhibit two relaxation times τ_1 and τ_2 , the possible candidates for these processes are (i) molecular relaxation for τ_1 and group relaxation for τ_2 and (ii) molecular relaxation about more than one axis. The latter can be ruled out since previous studies have shown that for such small molecules the relaxation data cannot be analyzed into relaxation contributions about different axes.¹² Thus, we shall now consider whether process i is a reasonable candidate for the interpretation of the dielectric data.

If relaxation of the acetyl group is detectable in the frequency range employed, then the weight factors C_1 and C_2 of the molecular and group relaxation times in acetophenone will depend on the angle, θ , that the molecular dipole moment subtends with the long axis of the molecule (between the carbon-1-carbon-4 axis in the benzene ring). If μ is the dipole moment of the molecule, then $\mu_1 = \mu \cos \theta$ and $\mu_2 = \mu \sin \theta$ while $C_1/C_2 = (\mu_1/\mu_2)^2$ and $C_1 + C_2 = 1$.¹³ One way of evaluating θ is from the knowledge of the dipole moment of a para-substituted acetophenone. This will be the resultant of contributions from the group moments of the acetyl group and that of the para-substituent. If the group moment of the para-substituent is in a direction along the long axis of the molecule and away from the molecule, then the resultant dipole mo-

ment is found from the equation

$$\mu(p\text{-X-acetophenone})^2 = [\mu(\text{acetophenone})^2 + \mu(\text{C}_6\text{H}_5\text{X})^2 - 2\mu(\text{acetophenone})\mu(\text{C}_6\text{H}_5\text{X}) \cos \theta]^{1/2}$$

where X is the parasubstituent and θ is the angle that the moment of the acetyl group subtends with the long axis of the molecule. This value of θ may be taken as equal to that in acetophenone if there is but little mesomeric interaction between the acetyl group and the parasubstituent. By taking the moment of 4-bromoacetophenone in *p*-xylene at 15° to be 2.27 D and the moments of acetophenone and bromobenzene¹⁴ under the same conditions to be 2.83 and 1.59 D, respectively, the resulting angle $\theta = 53^\circ 15'$. Similar calculations using 4-chloroacetophenone, 4-acetylpyridine, and 4-nitroacetophenone as the para-substituted compound yield $54^\circ 23'$, $52^\circ 32'$, and 55° . An angle $\theta = 54^\circ$ (the appropriate mean of the above) produces a molecular weighting factor for acetophenone of 0.33. In a similar way the molecular weighting factor for *p*-bromoacetophenone turns out to be zero. This would suggest that the *p*-haloacetophenones are ideal compounds for studying intra-molecular rotation ($C_2 \sim 1$) if it is detectable in the frequency range employed. The above method of determining θ does assume that there is no mesomeric interaction between the acetyl group and the para-substituent. The fairly constant value of θ from the various para-substituents supports such a concept.

The dielectric data of acetophenone were analyzed with a fixed C_1 value of 0.33 to determine whether this yielded a reasonable value for the molecular relaxation time. The values for τ_1 and τ_2 obtained for acetophenone are listed in Table II. A molecular relaxation time of 17×10^{-12} sec for acetophenone in cyclohexane at 25° seems at least of the correct order when compared with the value of 14×10^{-12} sec for anisole in *p*-xylene¹⁵ at the same temperature, since the anisole is a slightly smaller molecule of fairly similar shape.

The C_1 value of acetophenone was also calculated for acetophenone by the bond moment procedure employing data given in Smith,¹⁶ and this yielded a value of 0.51. A number of computer analyses were carried out on the acetophenone data for a number of fixed values of C_1 , and it would seem that $C_1 = 0.42 \pm 0.1$ would provide an acceptable value for the molecular weight factor. This value of C_1 is in agreement with the mean value calculated from bond and group moment data.

To establish the τ_1 of acetophenone more precisely ω, ω, ω -trifluoroacetophenone was examined at the same temperature in the same solvent. Bond and group moment calculations on ω, ω, ω -trifluoroacetophenone indicate that this has a high C_1 value (~ 1) and thus $\tau_1 \rightarrow \tau_0$. This molecule is similar in shape to acetophenone and only slightly larger since the van der Waals radii¹⁷ of fluorine

(10) C. J. F. Bottcher, "Theory of Electric Polarization," Elsevier, Amsterdam, 1952, pp 374-378.

(11) F. K. Fong and C. P. Smyth, *J. Chem. Phys.*, **40**, 2404 (1964).

(12) J. Crossley and S. Walker, *Can. J. Chem.*, **46**, 2369 (1968).

(13) E. L. Grubb and C. P. Smyth, *J. Amer. Chem. Soc.*, **83**, 4873 (1961).

(14) A. L. McClellan, "Tables of Experimental Dipole Moments," W. H. Freeman and Co., San Francisco, Calif., 1963.

(15) D. B. Farmer, Ph.D. Thesis, University of Aston in Birmingham, England, 1967.

(16) J. W. Smith, "Electric Dipole Moments," Butterworths, London, 1955.

(17) L. Pauling, "The Nature of the Chemical Bond," Cornell University Press, Ithaca, N. Y., 1960.

TABLE I: Dielectric Constant and Loss Data for Acetophenone, ω,ω,ω -Trifluoroacetophenone, and p -Haloacetophenones in Cyclohexane Solution at Specified Weight Fractions (w_2)^a

Solute	w_2	$t, ^\circ\text{C}$	Frequency, GHz	ϵ'	ϵ''	ϵ'_{calcd}	$\epsilon''_{\text{calcd}}$
Acetophenone	0.02030	25	70.0	2.04 ₀	0.027 ₅	2.04 ₉	0.025 ₅
			35.11	2.05 ₂	0.037 ₇	2.05 ₅	0.042 ₅
			23.98	2.06 ₆	0.050 ₂	2.07 ₀	0.050 ₄
			16.20	2.09 ₉	0.053 ₂	2.08 ₉	0.053 ₅
			9.313	2.11 ₂	0.047 ₆	2.11 ₅	0.047 ₇
Acetophenone	0.02168	40	70.0	1.99 ₉	0.033 ₁	2.01 ₇	0.031 ₃
			35.11	2.03 ₈	0.046 ₁	2.03 ₇	0.047 ₈
			23.98	2.05 ₁	0.053 ₄	2.05 ₅	0.052 ₆
			16.20	2.07 ₇	0.053 ₆	2.07 ₄	0.051 ₇
			9.313	2.09 ₂	0.044 ₂	2.09 ₇	0.042 ₂
ω,ω,ω -Trifluoroacetophenone	0.02541	40	70.0	1.98 ₅	0.022 ₀	2.00 ₆	0.020 ₀
			35.11	2.01 ₁	0.035 ₇	2.01 ₄	0.036 ₁
			23.98	2.02 ₂	0.046 ₅	2.02 ₅	0.047 ₅
			16.20	2.04 ₄	0.060 ₃	2.04 ₂	0.058 ₉
			9.313	2.06 ₉	0.064 ₀	2.07 ₆	0.064 ₇
p -Fluoroacetophenone	0.03800	40	35.11	2.03 ₆	0.044 ₅	2.03 ₇	0.044 ₁
			23.98	2.04 ₅	0.050 ₇	2.05 ₃	0.051 ₅
			16.20	2.08 ₁	0.052 ₉	2.07 ₃	0.052 ₈
			9.313	2.09 ₈	0.043 ₃	2.09 ₈	0.043 ₃
			6.70	2.10 ₉	0.034 ₇	2.10 ₈	0.034 ₈
p -Chloroacetophenone	0.04400	40	70.0	2.02 ₄	0.025 ₈	2.02 ₁	0.024 ₅
			35.11	2.03 ₃	0.040 ₃	2.03 ₅	0.041 ₉
			23.98	2.05 ₀	0.050 ₂	2.05 ₀	0.050 ₃
			16.20	2.07 ₈	0.054 ₁	2.07 ₀	0.054 ₁
			9.313	2.09 ₆	0.048 ₈	2.09 ₆	0.048 ₃
p -Bromoacetophenone	0.04308	40	70.0	2.25 ₈	0.018 ₀	2.25 ₅	0.018 ₇
			35.11	2.27 ₀	0.034 ₃	2.26 ₄	0.034 ₁
			23.98	2.27 ₅	0.041 ₇	2.27 ₄	0.043 ₆
			16.20	2.29 ₃	0.052 ₂	2.29 ₁	0.051 ₁
			9.313	2.31 ₉	0.050 ₃	2.31 ₉	0.050 ₆
p -Iodoacetophenone	0.03482	40	70.0	2.33 ₇	0.043 ₈	2.33 ₈	0.044 ₃
			35.11	2.01 ₈	0.019 ₃	2.01 ₆	0.019 ₄
			23.98	2.02 ₄	0.023 ₆	2.02 ₃	0.023 ₆
			16.20	2.03 ₈	0.027 ₂	2.03 ₁	0.025 ₆
			9.313	2.04 ₃	0.023 ₈	2.04 ₄	0.023 ₉
			1.9	2.06 ₀	0.011 ₂	2.06 ₂	0.009 ₈

^a ϵ' and ϵ'' are the measured values while ϵ'_{calcd} and $\epsilon''_{\text{calcd}}$ are the values estimated from τ_1 , τ_2 , and C_1 values in Table II.

and hydrogen are 1.35 and 1.2 Å, respectively. The τ_0 value for this molecule in cyclohexane at 40° is 16×10^{-12} sec (see Table II) and may be taken as a good approximation to the molecular relaxation time value. This is to be compared with the value of 14×10^{-12} sec obtained from the analysis of the acetophenone data in cyclohexane at 40°. Thus the observed relaxation time value for ω,ω,ω -trifluoroacetophenone supports our analysis of the acetophenone data as being a reasonable one, providing the true value of C_1 is approximately unity, as both bond and group moment calculations indicate. Fortunately the p -haloacetophenones provide a means of assessing the validity of such calculations for acetophenone and probably for its derivatives.

For all the p -haloacetophenones the C_1 values calculated from group and bond moments are respectively 0 and 0.25. Thus, if C_1 is of this order, then the observed relaxation time would tend to approximate to the value of that for group relaxation (*i.e.*, $\tau_0 \rightarrow \tau_2$) which is roughly the case in Table II for the p -haloacetophenones even when the C_1 value is 0.25 as opposed to zero when $\tau_2 = \tau_0$. In Table II it is striking how similar are the τ_0 values of p -

fluoro-, p -chloro-, p -bromo-, and p -iodoacetophenone in cyclohexane at 40°, the values being respectively, 8.7, 10, 11.4, and 11.4×10^{-12} sec. These values are to be contrasted with the molecular relaxation time values for fluoro-, chloro-, bromo-, and iodobenzene which in p -xylene at 15° are 6.8, 10, 14, and 18×10^{-12} sec.¹⁸ Thus, as the halogen atom increases in size (the van der Waals radii¹⁷ being 1.35, 1.80, 1.95, and 2.15 Å, respectively), the relaxation time exhibits an appreciable increase, altering by more than 100% from the fluorine to the iodine derivatives. In fact, for monohalobenzene compounds the molecular relaxation time is proportional to the cube of half the distance measured across the long axis (between the halogen and C-H group in the para position).¹⁸ Hence variation in the size in the p -haloacetophenones on passing from the fluoro to the iodo derivatives should produce a much greater alteration in the molecular relaxation times than the variation seen in the observed relaxation times. There can be little doubt from the near constancy of the

(18) W. F. Hassell and S. Walker, *Trans. Faraday Soc.*, **62**, 2695 (1966).

TABLE II: Relaxation Times, Distribution Parameter (α), Static Dielectric Constant (ϵ_0), Dielectric Constant at Very High Frequency (ϵ_∞), and Dipole Moment (μ) for Solutions of Weight Fraction w_2 at Temperature t ($^\circ\text{C}$) for Molecules Containing Acetyl Groups or Substituted Acetyl Groups^a

Compound	$t, ^\circ\text{C}$	w_2	τ_0	τ_1	τ_2	C_1	α	ϵ_0	ϵ_∞	μ, D
Acetophenone	25	0.02030	10. ₂	17	7.8	0.33	0.05	2.147	2.03 ₃	2.82
	40	0.02168	8.0	14	6.0	0.33	0.03	2.120	2.00 ₆	2.84
ω, ω, ω -Trifluoroacetophenone ^b	40	0.02541	15. ₆				0.01	2.134	2.00 ₂	3.40
<i>p</i> -Fluoroacetophenone	40	0.03300	8.7	12	7.9	0.25	0.01	2.121	2.01 ₃	2.24
<i>p</i> -Chloroacetophenone	40	0.04400	10	18	8.6	0.25	0.03	2.125	2.01 ₅	2.25
<i>p</i> -Bromoacetophenone	40	0.04308	11. ₄	26	9.3	0.25	0.04	2.097	2.00 ₆	2.31
<i>p</i> -Iodoacetophenone	40	0.03482	11. ₄	35	9.0	0.25	0.09	2.065	2.00 ₇	2.33

^a The solvent in all cases is cyclohexane. Relaxation time values have been multiplied by 10^{12} . ^b The dielectric data of ω, ω, ω -trifluoroacetophenone may be analyzed to give $\tau_1 = 16 \times 10^{-12}$ sec, $\tau_2 = 2.5 \times 10^{-12}$ sec, and $C_1 = 0.98$, but in view of the small C_2 value the analysis is of dubious significance.

observed relaxation times for chloro-, bromo-, and iodoacetophenone that the contribution of the molecular relaxation time to the dielectric absorption is not the major absorption process, that is $C_1 \ll C_2$. Under such circumstances, for these a major contribution to the absorption by the acetyl group is to be inferred.

For the cyclohexane solutions at 40° in Table II it is to be noted that the increase in molecular relaxation from 14×10^{-12} sec for acetophenone to 16×10^{-12} sec for ω, ω, ω -trifluoroacetophenone would seem reasonable, since the van der Waals radius of the fluorine atom is only 0.15 Å greater than that of the hydrogen atom. However, the τ_1 value of *p*-fluoroacetophenone comes out $\sim 15\%$ shorter than that for acetophenone, whereas the reverse order would be expected. For such analyses with a small C_1 of about 0.25 the τ_1 values may well be no more accurate than about $\pm 20\%$. At least the sequence of τ_1 values of the fluoro-, chloro-, bromo-, and iodoacetophenones of 12, 18, 26, and 35×10^{-12} sec is correct. The value for *p*-bromoacetophenone would appear reasonable when compared with the observed relaxation time of *p*-bromoanisole in *p*-xylene at 40° which is 22×10^{-12} sec.¹⁹ For *p*-bromoanisole $C_1 \sim 0.8$, and this corresponds with a molecular relaxation time of 27×10^{-12} sec.¹⁹ Since *p*-bromoanisole is

very similar in size and shape to *p*-bromoacetophenone, the τ_1 value of 26×10^{-12} sec is (within the errors of analysis) in good correspondence.

The τ_2 values, which have a weight factor ~ 0.75 , would be expected to be more accurate, and it is to be noted that for the *p*-haloacetophenones the τ_2 value is 8.6×10^{-12} sec ($\pm 8\%$). This approximate constancy of τ_2 would seem to bear out the dipole moment calculations given earlier which indicate that there are no mutual conjugation effects between the substituents in these para-substituted acetophenones.

The analyses in Table II for the *p*-haloacetophenones are, on the whole, convincing and, further, support the C_2 value calculated from group and bond moments as being of the correct order for the *p*-haloacetophenones. Since these C_2 calculations appear adequate for these molecules, there is no reason to doubt the validity of this approach in the case of acetophenone. Hence, it would seem that our C_1 value of 0.42 ± 0.1 (a mean of the value calculated from group and bond moments) is of the correct order for this molecule and that acetyl group relaxation in acetophenone is to be inferred.

(19) D. B. Farmer and S. Walker, *Can. J. Chem.*, **47**, 4645 (1969).

Conductance of 1-1 Electrolytes in Sulfolane and 3-Methylsulfolane at 30.0°

Arden P. Zipp

Chemistry Department, State University College, Cortland, New York 13045 (Received June 29, 1972)

Conductance measurements have been made for several alkali metal and tetraalkylammonium picrates in 3-methylsulfolane and for $i\text{-Am}_3\text{BuN}^+\text{BPh}_4^-$ in both sulfolane and 3-methylsulfolane. Single ion conductivities were calculated using the Fuoss-Onsager equation and the Fuoss-Coplan split for $i\text{-Am}_3\text{BuN}^+\text{BPh}_4^-$. These values were generally lower in 3-methylsulfolane, in which a greater degree of association was found to occur as well. These results are discussed in terms of the theory of dielectric friction and the differences in the properties of the solvent produced by the change in molecular structure.

Introduction

In recent years much interest has been shown in the solvent properties of sulfolane (tetramethylenesulfone). This study has been due in part to its dielectric constant ($\epsilon = 43.3$) which makes it an important solvent for extending the knowledge about the properties of electrolytes in intermediate dielectric constant solvents, especially with regard to their conductance behavior.¹ In addition, it has received some interest as a solvent for potentiometry² and polarography.³ This high level of interest has prompted an investigation of the closely related solvent, 3-methylsulfolane, in order to determine how the change in molecular structure alters the properties of the solvent, particularly its behavior as a medium for conductance. The results of this investigation are presented here.

Experimental Section

Materials. Sulfolane (S) and 3-methylsulfolane (3-MS) were purified by repeated distillation from sodium hydroxide *in vacuo*⁴ until specific conductivities less than 5×10^{-8} (S) and 2×10^{-8} mhos (3-MS) were obtained. For even the most dilute solutions studied, these values represented less than 0.5% of the solution conductivities and no correction for the solvent conductance was employed. The values for the solvent parameters used in the calculations for S were taken from the literature (density = 1.2618 g/ml,⁵ viscosity = 0.1029 P,^{1a} and dielectric constant = 43.3).⁶ The values used for 3-MS determined in the course of the present investigation (density = 1.1838 g/ml, viscosity = 0.1013 P, and dielectric constant = 29.5) are in excellent agreement with literature values (density = 1.1833 g/ml, viscosity = 0.10137 P, and dielectric constant = 29.2).⁶

Triisooamylbutylammonium iodide, picrate, and tetraphenylborate were prepared and purified according to known methods.⁷ Sodium and potassium picrate were obtained by neutralizing picric acid with the appropriate hydroxide⁷ and the tetraalkylammonium picrates were prepared by reacting picric acid with the tetraalkylammonium hydroxides, which had been made by the reaction of silver oxide with the tetraalkylammonium halide.⁸ After purification, all salts were dried and stored *in vacuo* until needed.

Apparatus and Procedure. Conductances were measured in Kraus-type erlenmeyer cells fitted with platinized platinum electrodes.⁹ The cell constants of 0.1347 and 0.1763 cm^{-1} were determined using two different aqueous KCl

solutions.¹⁰ An atmosphere of dry N_2 was used to protect the solutions from air and moisture during preparation and measurement. All measurements were made at a temperature of $30.00 \pm 0.01^\circ$ which was set with an NBS-calibrated thermometer. A Wayne-Kerr capacitance bridge, Model 221B, was used throughout the investigation, which entailed duplicate runs for each salt.

Solutions in S and 3-MS were prepared by the successive addition of weighed quantities of a stock solution to a known weight of the pure solvent. The stock solutions were prepared by weight and all weights were corrected to vacuum.

Results

The measured equivalent conductances and corresponding electrolyte concentrations have been filed with the ACS Microfilm Depository Service.¹¹ The molarities were calculated from the weights and densities of the various solutions. These densities were determined by using the equation $d = d_0 + Am$, in which d is the solution density, d_0 is the solvent density, A a correction factor, and m the concentration in moles of solute per kilogram of solution. Values of A were obtained from densities measured pycnometrically for the most concentrated solution of each electrolyte.

- (1) (a) R. Fernandez-Prini and J. E. Prue, *Trans. Faraday Soc.*, **62**, 1257 (1966); (b) M. Della Monica, U. Lamanna, and L. Janelli, *Gazz. Chim. Ital.*, **97**, 367 (1967); (c) M. Della Monica, U. Lamanna, and L. Senatore, *J. Phys. Chem.*, **72**, 2124 (1968); (d) M. Della Monica and U. Lamanna, *ibid.*, **72**, 4329 (1968); (e) M. Della Monica, *J. Amer. Chem. Soc.*, **91**, 508 (1969).
- (2) D. H. Morman and G. A. Harlow, *Anal. Chem.*, **39**, 1869 (1967).
- (3) J. F. Coetzee, J. S. Simon, and R. J. Bertozzi, *Anal. Chem.*, **41**, 766 (1969).
- (4) R. L. Burwell and C. H. Langford, *J. Amer. Chem. Soc.*, **81**, 3799 (1959).
- (5) U. Lamanna, O. Scivelli, and L. Janelli, *Gazz. Chim. Ital.*, **94**, 567 (1964).
- (6) J. W. Vaughn and C. F. Hawkins, *J. Chem. Eng. Data*, **9**, 140 (1964).
- (7) M. A. Coplan and R. M. Fuoss, *J. Phys. Chem.*, **68**, 1177 (1964).
- (8) D. F. Evans, C. Zawoyski, and R. L. Kay, *J. Phys. Chem.*, **69**, 3878 (1965).
- (9) H. M. Daggett, E. J. Bair, and C. A. Kraus, *J. Amer. Chem. Soc.*, **73**, 799 (1951).
- (10) J. E. Lind, J. J. Zwolenik, and R. M. Fuoss, *J. Amer. Chem. Soc.*, **81**, 1557 (1959).
- (11) Molar concentrations and equivalent conductivities will appear following these pages in the microfilm edition of this volume of the journal. Single copies may be obtained from the Business Operations Office, Books and Journals Division, American Chemical Society, 1155 Sixteenth St., N.W., Washington, D. C. 20036. Remit check or money order for \$3.00 for photocopy or \$2.00 for microfiche, referring to code number JPC-73-718.

TABLE I: Conductance Parameters for 1-1 Electrolytes in Sulfolane and 3-Methylsulfolane at 30°

Salt	Λ_0	K	J	$\sigma\Lambda$
3-Methylsulfolane				
NaPic	6.823 ± 0.008	174 ± 82	125	0.04
KPic	7.281 ± 0.030	88 ± 39	305	0.02
Me ₄ NPic	7.792 ± 0.003	1.5 ± 1.3	142	0.002
Et ₄ NPic	7.676 ± 0.015	10 ± 7	115	0.01
Pr ₄ NPic	7.321 ± 0.064			0.07
Bu ₄ NPic	6.508 ± 0.028	57 ± 37	307	0.03
<i>i</i> -Am ₃ BuNPic	6.449 ± 0.007	0	98.7	0.009
<i>i</i> -Am ₃ BuNPh ₄	4.617 ± 0.008	0	90.6	0.01
Sulfolane				
<i>i</i> -Am ₃ BuNPic	6.282 ± 0.006	0		0.03
<i>i</i> -Am ₃ BuNI	9.801 ± 0.036	0		0.06
<i>i</i> -Am ₃ BuNBPh ₄	4.900 ± 0.038	0		0.01

The data were analyzed by means of the Fuoss-Onsager equation¹²

$$\Lambda = \Lambda_0 - S(C\gamma)^{1/2} + EC\gamma \log C\gamma + (J - BA_0)C\gamma - KA_0C\gamma\Lambda f^2 \quad (1)$$

employing a computerized least-squares program.¹³ The values of Λ were unweighted and the viscosity correction factor B was set equal to zero. It has been shown¹⁴ that the value of B does not affect the limiting conductance or the association constant of the electrolyte and has only a slight influence on the value of \tilde{d} . At 30° the constants α , β , E_1 , and E_2 are respectively 0.9700, 8.612, 9.470, and 12.313 for 3-MS and 0.5455, 6.9978, 2.9946, and 5.6264 for S.

The conductance parameters obtained for the various electrolytes are listed in Table I. Values for the limiting single ion conductivities were found from the Λ_0 value of the electrolytes by making use of the conductivity equivalence of the *i*-Am₃BuN⁺ and BPh₄⁻ ions which has been demonstrated to apply in many nonaqueous solvents.⁷ The value of λ_0^- found by this method for the iodide ion in sulfolane (7.33 ± 0.04) is in reasonable agreement with that established earlier (7.25 ± 0.02) from transport studies^{1c} and supports the use of *i*-Am₃BuNBPh₄ as a reference electrolyte in these solvents. The limiting single ion conductivities in 3-MS are listed in Table II along with the Walden products where they can be compared with similar data for the same ions in S.

Discussion

Limiting Conductivities. The data in Table I show the conductivities of a given salt to be very similar in S and 3-MS, but much lower than those found in most other solvents even at lower temperatures, e.g., Λ_0 Et₄NPic = 7.68 (3-methylsulfolane), 32.43 (nitrobenzene),¹⁵ and 73.31 (pyridine).¹⁶ That this behavior is due primarily to the high viscosities of the sulfolanes is indicated by the much closer agreement of the $\Lambda_0\eta$ values calculated for the same salt in these solvents, $\Lambda_0\eta = 0.789$ (3-methylsulfolane), 0.647 (pyridine), and 0.587 (nitrobenzene).

The conductivities of specific salts as well as single ion conductivities in S and 3-MS do not show any simple correlation with the solvent viscosities, however. Indeed a comparison of the single ion conductivities (Table II) shows the λ_0 of every ion except picrate to be greater in S than in 3-MS, contrary to expectations based on viscosity

Table II: Single Ion Conductivities and Walden Products in Sulfolane and 3-Methylsulfolane

Cation	λ_0^+	$\lambda_0^+\eta_0$
Sulfolane		
Na ⁺	3.61 ^a	0.372 ^a
K ⁺	4.05 ^a	0.417 ^a
Rb ⁺	4.16 ^a	0.428 ^a
Cs ⁺	4.27 ^a	0.439 ^a
Me ₄ N ⁺	4.31 ^b	0.425 ^b
Et ₄ N ⁺	3.95 ^a	0.390 ^a
Pr ₄ N ⁺	3.23 ^b	0.319 ^b
Bu ₄ N ⁺	2.80 ^b	0.276 ^b
<i>i</i> -Am ₃ BuN ⁺	2.45	0.252
3-Methylsulfolane		
Na ⁺	2.68	0.272
K ⁺	3.14	0.318
Me ₄ N ⁺	3.65	0.370
Et ₄ N ⁺	3.54	0.358
Pr ₄ N ⁺	3.18	0.322
Bu ₄ N ⁺	2.37	0.240
<i>i</i> -Am ₃ BuN ⁺	2.31	0.234
Anion	λ_0^-	$\lambda_0^-\eta_0$
Sulfolane		
Cl ⁻	9.30 ^a	0.957 ^a
Br ⁻	8.92 ^a	0.918 ^a
I ⁻	7.33	0.756
ClO ₄ ⁻	6.68 ^a	0.687 ^a
Pic ⁻	3.83	0.394
BPh ₄ ⁻	2.45	0.252
3-Methylsulfolane		
Pic ⁻	4.14	0.420
BPh ₄ ⁻	2.31	0.234

^a Reference 1c. ^b Reference 1d. The remaining values are from this work.

considerations alone ($\eta_S = 0.1029$, $\eta_{3-MS} = 0.1013$). This apparent difference in mobilities is even more obvious when the $\lambda_0\eta$ products are compared (Table II). Thus, $\lambda_0\eta$ is greater in S than in 3-MS for every ion except picrate and tetrapropylammonium. The lower mobility in the lower dielectric solvent (3-MS) is in accord with the equation¹⁷

$$\lambda_0\eta = |Z_i|eF / \{ [A_V\pi r_i + A_D Z_i^2 \tau e^2 (\epsilon_0 - \epsilon_\infty)] / r_i^3 \eta_0 (2\epsilon_0 + 1) \} \quad (2)$$

which has been proposed to account for specific ion-solvent interactions. In this equation, the parameters A_V and A_D refer to the effects of viscous and dielectric friction on the mobility of the ion, ϵ_0 and ϵ_∞ are the low-frequency and high-frequency dielectric constants, respectively, and the other symbols have their usual meaning. The dependence of the ionic mobility on the solvent dielectric constant can be seen to result primarily from the $(\epsilon_0 - \epsilon_\infty) / \epsilon_0(2\epsilon_0 + 1)$ term which occurs in the denominator, and

- (12) R. M. Fuoss and Accascina, "Electrolytic Conductance," Interscience, New York, N. Y., 1959.
 (13) R. L. Kay, *J. Amer. Chem. Soc.*, **82**, 2099 (1960).
 (14) D. F. Evans and P. Gardam, *J. Phys. Chem.*, **72**, 3281 (1968).
 (15) E. G. Taylor and C. A. Kraus, *J. Phys. Chem.*, **51**, 1731 (1947).
 (16) H. L. Pickering and C. A. Kraus, *J. Phys. Chem.*, **71**, 3288 (1949).
 (17) R. Zwanzig, *J. Chem. Phys.*, **38**, 1603 (1963); **52**, 3625 (1970).

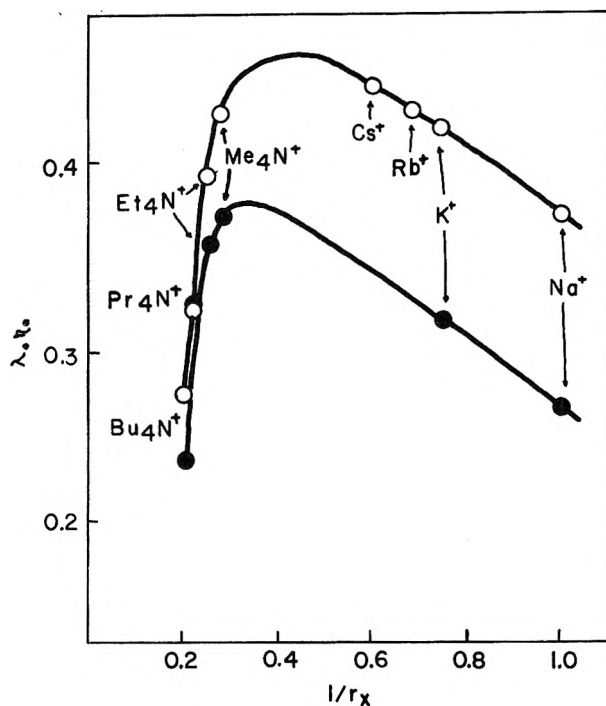


Figure 1. Walden product vs. $1/r_x$ for cations in S (O) and 3-MS (●). (The lines have been drawn to aid the eye and have no theoretical significance.)

leads to a greater $\lambda_0\eta$ value in the higher dielectric medium.

In Figure 1 the $\lambda_0\eta$ products have been plotted against the reciprocals of the crystallographic radii¹⁸ for all the cations studied in S and 3-MS. Several features are apparent from these plots; (1) maxima occur at $1/r_x$ values corresponding to small tetraalkylammonium or large alkali metal ions; (2) $\lambda_0\eta$ differences between ions in the two solvents are greater for alkali metal than for tetraalkylammonium ions; (3) the $\lambda_0\eta$ maximum occurs at a greater $1/r_x$ value in S than in 3-MS.

With regard to 1, the occurrence of maxima in such $\lambda_0\eta$ plots is typical of electrolyte behavior in a wide range of solvents.¹⁹ The rise in the $\lambda_0\eta$ plot found with increasing $1/r_x$ (up to the maximum) is due to the inherent mobilities of the tetraalkylammonium ions alone, since these ions are generally considered to be unsolvated. The decrease in $\lambda_0\eta$ observed with still further increase in $1/r_x$ can be attributed to a lowering of the mobilities of the alkali metal ions due to increasing solvation with decreasing radii.

The greater $\lambda_0\eta$ difference between the two solvents for the alkali metal ions than for the tetraalkylammonium ions is the behavior which would be expected for specific ion-solvent interactions, since small ions would interact more extensively with the solvent than larger ones. It is unclear at this time exactly how this difference in ion-solvent interaction is related to the replacement of a hydrogen atom in S with a methyl group, but the solvent properties which might be expected to be altered by such a substitution are the molecular volume and the dipole moment.

The difference in the sizes of ions solvated by a given number of S or 3-MS molecules might be sufficient to lower the mobilities of the latter species as has been suggested to explain the difference in mobility of various ions in methanol and ethanol,²⁰ and to explain the differences

in the viscosities of electrolytes in a variety of solvents.²¹ While solvent dipole moments have been invoked to explain differences in ionic mobilities (between acetonitrile and methanol),²⁰ the dipole moments of these solvents are quite different (4.0 and 1.7D, respectively²²), whereas those of S and 3-MS are rather similar (4.90 and 4.38D, respectively⁶) so this effect would be expected to be quite small. Of these two parameters, therefore, the molecular volume seems the more important in explaining the differences in ionic mobilities.

Similar comparative data for anions in these solvents are more limited, but those which do exist display a decrease in $\lambda_0\eta$ with an increase in ionic radius. This can be attributed to the greater mobilities of the smaller ions uncomplicated by solvation and supports the view²³ that specific interactions between anions and nonaqueous solvents (including solvation) are generally small, S being comparable to nitromethane²⁴ in this regard.

Finally, the occurrence of the maximum $\lambda_0\eta$ at a greater $1/r_x$ value in S than in 3-MS is in accord with the equation

$$(r)_{\max}^4 = Z_i^2 e^2 (\epsilon_0 - \epsilon_\infty) \tau 3A_D / \epsilon_0 (2\epsilon_0 + 1) \eta \pi A_v \quad (3)$$

as derived in the theory of dielectric friction.¹⁷ The unavailability of values for τ (relaxation time) and ϵ_∞ (high-frequency dielectric constant) for these solvents preclude quantitative comparisons with this theory, but calculations for other aprotic solvents have generally shown very good agreement with experiment.¹⁹ In contrast, protic solvents have been found to agree only qualitatively,²⁵ although they also exhibit a decrease in the maximum value of $1/r_x$ with decreasing dielectric constant.

Association Constants. From the data given in Table I, it can be seen that the picrates of smaller cations show a definite tendency to associate in 3-MS, K_A ranging from 174 for Na^+ to 1.5 for Me_4N^+ . These values are intermediate between those obtained for the same salts in acetone^{26,27} and methanol,²⁸ or acetonitrile,²⁸ as might be expected from the respective dielectric constants; $\epsilon = 20.7$ (acetone), 29.5 (3-MS), 32.6 (methanol), and 36.0 (acetonitrile). The higher dielectric constant for S (43.3) suggests that even less association would be expected in that instance. Although K_A values for picrates have not been measured in S, the low values which have been found for several other alkali metal halides and perchlorates ($K_A < 10$)^{1a} support this view.

When the K_A values for the various salts in 3-MS are examined, two distinct orders can be seen for the relationship between the size of the cation and its association with the picrate ion. The value of K_A decreases in the se-

(18) R. A. Robinson and R. H. Stokes, "Electrolyte Solutions," Butterworths, London, 1968, pp 125 and 461.

(19) R. Fernandez-Prini and G. Atkinson, *J. Phys. Chem.*, **75**, 239 (1971), and references therein.

(20) R. L. Kay, B. J. Hales, and G. P. Cunningham, *J. Phys. Chem.*, **71**, 3925 (1967).

(21) J. P. Bare and J. F. Skinner, *J. Phys. Chem.*, **76**, 434 (1972).

(22) A. L. McClellan, "Tables of Experimental Dipole Moments," W. H. Freeman, San Francisco, Calif., 1963.

(23) A. J. Parker, *Quart. Rev. Chem. Soc.*, **16**, 63 (1962).

(24) U. Mayer and V. Gutmann, *Monatsch. Chem.*, **101**, 912 (1970).

(25) D. F. Evans and P. Gardam, *J. Phys. Chem.*, **73**, 158 (1969).

(26) M. B. Reynolds and C. A. Kraus, *J. Amer. Chem. Soc.*, **70**, 1709 (1948).

(27) M. J. McDowell and C. A. Kraus, *J. Amer. Chem. Soc.*, **73**, 3293 (1951).

(28) R. L. Kay, C. Zawoyki, and D. F. Evans, *J. Phys. Chem.*, **69**, 4208 (1965).

(29) E. C. Evers and A. G. Knox, *J. Amer. Chem. Soc.*, **73**, 1739 (1951).

ries $\text{Na}^+ > \text{K}^+ > \text{Me}_4\text{N}^+$ then increases as $\text{Me}_4\text{N}^+ < \text{Et}_4\text{N}^+ < \text{Bu}_4\text{N}^+$. The former order has been observed in many other studies and is expected from simple electrostatic considerations. In contrast, the increased association with increasing size of the R_4N^+ ions is much less common, although it has been reported in at least one study of these same salts in methanol.²⁹

The association of large ions is usually attributed to their lack of solvation, such solvation decreasing with increasing ionic size. Thus, it may be that the minimum in K_A observed here for the Me_4N^+ ion occurs as the result of two opposing trends; a decrease in electrostatic attraction with increasing ionic size and a consequent decrease in K_A , and a decrease in solvation with increasing ionic size leading to increasing K_A values. A recent report³⁰ suggests that Me_4N^+ exists in a state of partial solvation in contrast to the larger unsolvated R_4N^+ ions. The be-

havior of the Me_4N^+ ion thus may be especially subject to the nature of the solvent.

In conclusion, electrolytes in 3-methylsulfolane exhibit greater association and lower mobilities than in sulfolane itself, presumably due to the lower dielectric constant and the larger molecular volume produced by replacing a hydrogen atom with a methyl group.

Acknowledgment. The author wishes to express his appreciation to Dr. R. L. Kay of Carnegie-Mellon University, Pittsburgh, Pa., for a copy of the Fortran program used to analyze the data and to acknowledge the financial support of the Research Foundation of the State University of New York.

(30) M. Della Monica and L. Senatore, *J. Phys. Chem.*, **74**, 205 (1970).

COMMUNICATIONS TO THE EDITOR

An Interpretation of the $K\beta$ X-Ray Emission Spectra of Dibenzyl Sulfide and S_8 ¹

Sir: Frost, *et al.*,² have interpreted the high-resolution valence photoelectron emission spectra of several aliphatic and aromatic sulfides with the aid of CNDO/2 molecular orbital calculations. It is our intention here to show that X-ray photon emission spectra involving valence electron transitions of similar compounds may also be interpreted using a molecular orbital description of the chemical bonding of divalent sulfur in aliphatic sulfides. We also wish to present an interpretation of the valence electron X-ray photon emission spectra of rhombic sulfur (S_8) based on similar arguments.

Figures 1 and 2 show the high-resolution sulfur $K\beta$ emission spectra of solid dibenzyl sulfide and S_8 obtained with our previously described two-crystal X-ray attachment.³ The S_8 $K\beta$ spectrum shown here agrees with previously reported measurements.⁴⁻⁸ Note that certain similarities occur between the spectra of dibenzyl sulfide and of S_8 , in particular, a high-intensity, high-energy transition, accompanied by several lower-energy, lower-intensity transitions. The high-energy line occurs at the same energy for both compounds, while the lower-energy lines differ in their respective energies.

The bonding of divalent sulfur has been described² in terms of two strong σ bonds involving two of sulfur's 3p orbitals and two lone pairs in the other 3p orbital and the sulfur 3s orbital. These essential ideas can be carried over into a molecular orbital description of dibenzyl sulfide, if one assumes negligible interaction between the sulfur atom and the benzene ring. Such an assumption is not at all unreasonable in light of a comparison of the valence photoelectron spectra of α -toluenethiol and benzenethiol.²

A CNDO/2 calculation⁹ was carried out for dimethyl sulfide as an approximation to a complete molecular orbital description of dibenzyl sulfide. Using the one-center integral intensity approximation¹⁰ and the ionization potentials for dimethyl sulfide,² spectral assignments may be made for dibenzyl sulfide as shown in Figure 1.¹¹

Peak A is shown to originate from the $2b_1$, sulfur 3p lone pair, orbital and the broader peak B from the $4a_1$ and $3b_2$, S 3p-C 2p, σ -bonding orbitals. The next three orbitals ($2b_2$, $1b_1$, and $3a_1$) are primarily methyl group orbitals,² but the CNDO/2 calculation does give them significant intensities which are apparently observed in the spectrum of dibenzyl sulfide (peaks C and D). The $2a_1$, sulfur 3s lone pair, orbital has been shown to occur in the region of peak D,² but is given negligible intensity by the CNDO/2 approximation. Peak E then, may be assigned to the $1b_2$ and $1a_1$, S 3sp-C 2s, σ -bonding orbitals. The nature of the lone pair and bonding orbitals predicted by the CNDO/2 calculation for dimethyl sulfide was further confirmed from an examination of the band shapes in the valence photoelectron spectrum of dimethyl sulfide.² Thus, by analogy to dimethyl sulfide, the essential features of

(1) This research was supported by the National Science Foundation.

(2) D. C. Frost, *et al.*, *J. Phys. Chem.*, **76**, 1030 (1972).

(3) H. C. Whitehead, J. D. Layfield, and G. Andermann, *Rev. Sci. Instrum.*, **43**, 50 (1972).

(4) D. Lundquist, *Kgl. Fysiogr. Sællsk. Lund. Foerh.*, **1**, 12 (1931).

(5) A. Faessler and E. D. Schmid, *Z. Phys.*, **138**, 71 (1954).

(6) I. B. Borovskii and I. A. Ovsyannikova, *J. Exp. Theor. Phys.*, **37**, 1033 (1959).

(7) C. Sugiura, *J. Phys. Soc. Jap.*, **30**, 1766 (1971).

(8) E. K. Kortela, *et al.*, *J. Phys. B. Atom. Mol. Phys.*, in press.

(9) J. A. Pople and D. L. Beveridge, "Approximate Molecular Orbital Theory," McGraw-Hill, New York, N. Y., 1970, Appendix A.

(10) G. Karlsson and R. Manne, *Phys. Scr.*, **4**, 119 (1971).

(11) The relative intensities shown in both Figures 1 and 2 for the ionization potentials of Frost, *et al.* and Chen's calculation are identical with the CNDO/2 results.

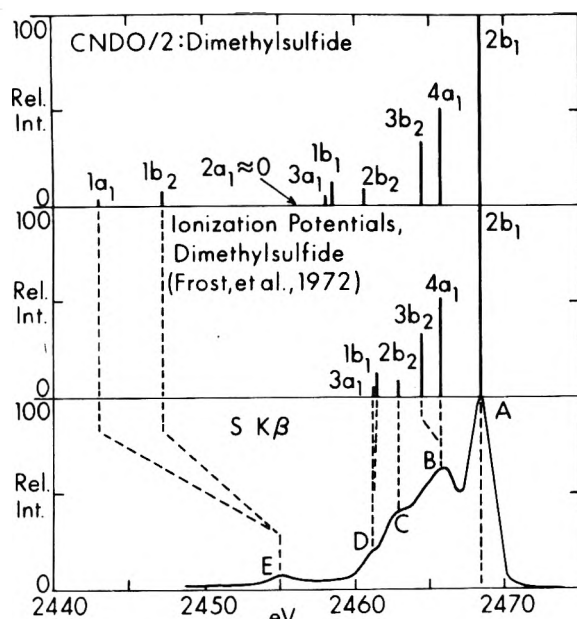


Figure 1. Molecular orbital assignments for the sulfur K β emission spectrum of dibenzyl sulfide based on a CNDO/2 calculation and ionization potentials² for dimethyl sulfide.

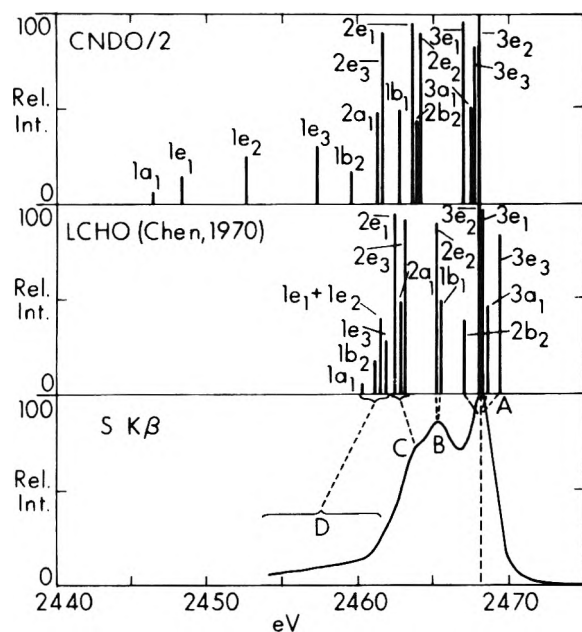


Figure 2. Molecular orbital assignments for the sulfur K β emission spectrum of rhombic sulfur (S_8) based on a CNDO/2 and a linear combination of hybrid orbitals calculations.¹²

the bonding of divalent sulfur have been retained in the assumed molecular orbital description of dibenzyl sulfide.

The CNDO/2 calculation for S_8 compared poorly even with the semiempirical calculation reported by Chen¹² and did not lend itself readily to a thorough interpretation of the S_8 K β spectrum.¹³ The results of the one-center integral approximation for both the CNDO/2 and Chen's calculations are presented in Figure 2. In this case, a detailed valence photoelectron spectrum of S_8 was not available to help indicate which molecular orbitals correspond to lone pair or bonding orbitals, but, in keeping with the bonding scheme assigned to divalent sulfur, we may consider the highest energy peak (A) in the K β spectrum of S_8 to arise from one or more sulfur lone pair orbitals. A

shifting of the sulfur K β lines with oxidation state, or more specifically, with the charge on the sulfur atom, is a well-known phenomenon,¹⁴ and the occurrence of the dibenzyl sulfide lone pair peak coincidental with the S_8 lone pair peak is consistent with Siegbahn's assignment of a zero charge to sulfur in both S_8 and dibenzyl sulfide.¹⁵ Peak B, then, may originate from S 3p-S 3p, σ -bonding orbitals such as 1b₁ and 2e₂, while peak C and the low-energy tailing (D) may be assigned to the remaining orbitals. Again, the sulfur 3s lone pair is not observed in this spectrum. Sugiura⁷ made a similar assignment but not on the basis of the bonding of divalent sulfur, nor did he explicitly consider the intensity pattern shown in Figure 2.

While the interpretations given here for the high-resolution X-ray photon emission spectra of dibenzyl sulfide and S_8 are only tentative, owing to the lack of more rigorous molecular orbital calculations, the application of high-resolution X-ray photon emission spectroscopy as a complementary tool for the study of the valence electronic structure of complex molecules appears to be well illustrated.

- (12) I. Chen, *Phys. Rev. B*, **2**, 1053 (1970).
- (13) After submission of this paper, the authors received a preprint of the interpretation of the S_8 K β spectrum by Kortela, *et al.*⁸ Their CNDO/2 results are identical with ours, but their basis of interpretation differs.
- (14) K. Siegbahn, *et al.*, *Nova Acta Regiae Soc. Sci. Upsal.*, **20** (1967).
- (15) K. Siegbahn, *et al.*, *Nova Acta Regiae Soc. Sci. Upsal.*, **20**, 114 (1967).

Department of Chemistry and
Hawaii Institute of Geophysics
University of Hawaii
Honolulu, Hawaii 96822

H. C. Whitehead
G. Andermann*

Received August 9, 1972

On the Electron Spin Resonance Measurement of Radical Termination Rates

Publication costs assisted by Kanton Zurich

Sir: Recently, several groups have determined absolute rate constants for the termination reactions of transient free radicals in solution using esr spectroscopy.^{1,2} Usually, decays of the esr signal S at a magnetic field value corresponding to a peak in the first-derivative spectrum were measured during the "off" periods of intermittent radical production and analyzed in terms of the second-order rate law

$$S_0/S_t = [R\cdot]_0/[R\cdot]_t = 1 + 2k[R\cdot]_0t$$

where $[R\cdot]_0$ is the radical concentration at the beginning

- (1) For the generation of radicals by electron radiolysis, see the following: (a) R. W. Fessenden, *J. Phys. Chem.*, **68**, 1508 (1964); (b) B. Smaller, J. R. Remko, and E. C. Avery, *J. Chem. Phys.*, **48**, 5174 (1968).
- (2) For the generation of radicals by photolysis, see the following and references therein: (a) E. J. Hamilton, Jr., D. E. Wood, and G. S. Hammond, *Rev. Sci. Instrum.*, **41**, 452 (1970); (b) S. A. Weiner, *J. Amer. Chem. Soc.*, **94**, 581 (1972); (c) G. B. Watts and K. U. Ingold, *ibid.*, **94**, 491 (1972); (d) P. B. Ayscough, R. C. Sealy, and D. E. Woods, *J. Phys. Chem.*, **75**, 3454 (1971); (e) G. S. Hammond, E. J. Hamilton, Jr., S. A. Weiner, H. J. Heffer, and A. Gupta, *Spec. Lect. XXIII Int. Congr. Pure Appl. Chem.*, **4**, 257 (1971).

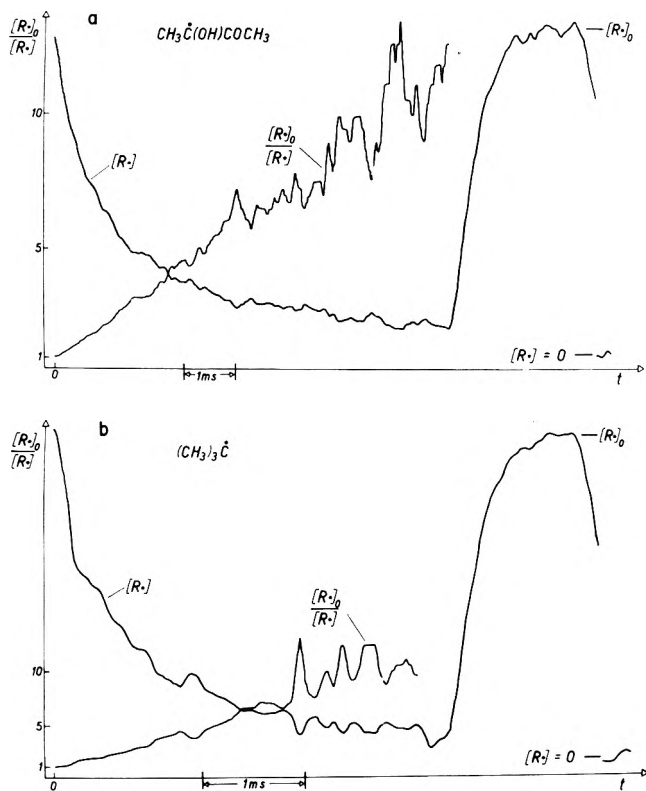


Figure 1. Radical decay-rise curves, baselines, and $[R\cdot]_0/[R\cdot]$ plots for (a) $\text{CH}_3\text{C(OH)COCH}_3$ radical and (b) $(\text{CH}_3)_3\text{C}$ radical. The baselines are shown in the lower right-hand corners.

of the off period ($t = 0$). This analysis requires the knowledge of the signal at zero radical concentration, *i.e.*, the baseline of the spectrometer; this has usually been estimated visually from the behavior of S_t at long times. We report here a modification of the above esr procedure which avoids this estimation by a direct measurement of the baseline and thus increases the certainty with which the rate law may be determined. Rate constants for the termination of two photochemically produced radicals are also reported.

The experiment is computer controlled and proceeds as follows. First, a number of signal decays is taken on-resonance as usual and accumulated in one part of the memory. Then the magnetic field is rapidly shifted to an off-resonance position; here the same number of baseline signals is taken and accumulated in another part of the memory. The field is then rapidly shifted back to the resonance position and further decays are accumulated. This cycle is repeated many times during the experiment to average out low-frequency noise. Finally, the on- and off-resonance data are displayed and processed to give $1/S_t$.³

The apparatus included a Varian E-9 spectrometer with dual cavity and field/frequency (F/F) lock unit, and a Varian 620/i computer plus interfacing to the spectrometer. The light from an Hanovia 977B-1 1-kW Hg-Xe compact arc lamp was focused at a small aperture where it was chopped by a rotating sector which also triggered decay data acquisition; a second lens focused the light at the sample. The quartz flow cell and light filter were as previously described.⁴ Samples were degassed by bubbling He through them before irradiation. The 620/i was programmed in machine language to provide sector speed measurement and time base adjustment; decay data ac-

quisition and averaging; periodic field shifting with baseline data acquisition and averaging; oscilloscope display and recorder output of decay curves; processing of averaged decay curve and baseline to yield $1/S_t$ plot; and parameter input and output through the TTY.

The field shifting was accomplished by changing the scan voltage input to the F/F lock unit (this voltage comes from a potentiometer that is mechanically linked to the recorder X-axis position). First, the voltage from this recorder potentiometer was measured using the computer ADC, and the computer DAC was set equal to the same voltage. Then the F/F input was switched to the DAC line using a fast (<1 msec) relay which was operated by a computer control line. The DAC voltage was then linearly stepped at a rate equivalent to 50 G/sec until the desired field shift was completed. The reverse of the above procedure, including reconnection of the F/F input to the recorder potentiometer, completed the cycle. Control experiments with solutions not containing radicals ascertained that the field shift does not cause changes in the baseline.

An example of an averaged decay curve and baseline is shown in Figure 1a for the $\text{CH}_3\text{C(OH)COCH}_3$ radical produced by irradiation of 5% (v/v) biacetyl in 2-propanol⁵ at $25 \pm 2^\circ$. Analysis of $1/S_t$ vs. time yields the line (slope = $2k[R\cdot]_0 = 1.28 \times 10^3 \text{ sec}^{-1}$) shown in Figure 1a. Within the noise, second-order kinetics are seen to be obeyed over the full range of the decay. Figure 1b shows corresponding data for *tert*-butyl radical produced by irradiation of 10% (v/v) di-*tert*-butyl ketone in benzene⁶ at $19 \pm 2^\circ$. Here second-order kinetics are less well but still reasonably fulfilled. Several determinations gave a value of $2.9 \pm 0.3 \times 10^3 \text{ sec}^{-1}$ for $2k[R\cdot]_0$. In each of these two examples, the steady-state spectrum showed only one radical, and this radical is expected from known photochemistry^{5,6} to undergo only a second-order self-reaction.

Measurement of the steady-state radical concentration, $[R\cdot]_0$, was carried out by determination of the first moment of the sample resonance relative to the first-derivative height of the Varian strong pitch sample which was placed in the rear of the dual cavity as a substandard. Basic standardization was carried out using solutions of DPPH and galvinoxyl in benzene.

The termination rate constant, $2k$, obtained for each radical is shown in Table I,⁷⁻¹¹ together with literature

- (3) Direct measurement of the baseline may also be accomplished by methods which yield the esr signal as a function of time for many magnetic field values in a spectrum. However, these methods require very long measurement times, giving more data than is needed for a single rate constant measurement; further, some of them can yield data which is distorted by low-frequency noise. See ref 1 and the following: (a) E. W. Firth and D. J. E. Ingram, *J. Sci. Instrum.*, **44**, 821 (1967); (b) P. W. Atkins, K. A. McLaughlan, and A. F. Simpson, *Nature (London)*, **219**, 927 (1968); (c) T. J. Bennett, R. C. Smith, and T. H. Wilmshurst, *J. Sci. Instrum.*, **2**, 393 (1969); (d) J. Sohma, T. Komatsu, and Y. Kanda, *Japan. J. Appl. Phys.*, **7**, 298 (1968).
- (4) H. Paul and H. Fischer, *Chem. Commun.*, 1038 (1971).
- (5) For product analysis, see W. H. Urry and D. J. Trecker, *J. Amer. Chem. Soc.*, **84**, 118 (1962); W. G. Bentrude and K. R. Darnall, *Chem. Commun.*, 810 (1968).
- (6) For product analysis in pentane, which is nearly identical with that in benzene (B. Blank, private communication), see N. C. Yang, E. D. Feit, M. H. Hui, N. J. Turro, and J. C. Dalton, *J. Amer. Chem. Soc.*, **92**, 6974 (1970).
- (7) P. B. Ayscough and M. C. Brice, *J. Chem. Soc. B*, 491 (1971).
- (8) S. A. Weiner, E. J. Hamilton, Jr., and B. M. Monroe, *J. Amer. Chem. Soc.*, **91**, 6350 (1969).
- (9) P. B. Ayscough, private communication.
- (10) S. A. Weiner and G. S. Hammond, *J. Amer. Chem. Soc.*, **91**, 986 (1969).
- (11) D. J. Carlsson and K. U. Ingold, *J. Amer. Chem. Soc.*, **90**, 7047 (1968).

TABLE I: Termination Rate Constants^a

Radical	$2k (10^{-9}),$ $M^{-1} \text{ sec}^{-1}$	Solvent	Ref
CH ₃ ĊOHCOCH ₃	0.42	2-Propanol	This work
	0.30	2-Propanol	2d,7
	0.78	2-Propanol	8
	0.70	2-Propanol	9
	5.7(19°)	Benzene	This work
(CH ₃) ₃ Ċ	1.5	Benzene	10
	4.4	Cyclohexane	10
	2.1	Cyclohexane	11
	8.1	Di- <i>tert</i> -butyl peroxide	2c

^a At or near 25° unless otherwise noted.

values. We estimate the absolute error in our values as $\pm 50\%$, primarily due to uncertainty in $[R\cdot]_0$. The data of Table I show a considerable spread. This and the recent

discussions^{2c,e} of rate constants and rate laws of radical termination reactions show the need for data which are as accurate as possible. The procedure applied here avoids some possible error sources. With some modifications it may be used in other than esr techniques.

Acknowledgment. Support by the Swiss National Foundation for Scientific Research is gratefully acknowledged. We are indebted to Mr. J. Henthorne and Dr. J. Hyde of Varian for their suggestions on implementing the field shift, and to Mr. H. Paul of this laboratory for helpful discussions.

Physikalisch-Chemisches Institut
der Universität Zürich
Rämistrasse 76
8001 Zürich, Switzerland

E. J. Hamilton, Jr.
H. Fischer*

Received July 31, 1972

The ADVANCES IN CHEMISTRY Series...

Excellent Reviews in Book Form of Specialized Chemical Topics

For comprehensive reviews of all the important aspects of a chemical subject... read the books in the ADVANCES IN CHEMISTRY Series.

Ranging up to 750 pages in length, ADVANCES volumes include...

- Authoritative, thought-provoking articles by as many as several dozen scientists per volume.
- Carefully compiled collections of data.
- Groups of related papers presented at important national and international symposia.
- Invited reviews of current work written by researchers eminent in the field discussed.

With the ADVANCES you learn about brand-new chemical subjects... and bring yourself up to date on familiar chemical topics. The numerous scientists contributing to each volume provide you with stimulating reading enriched by a variety of viewpoints. And the ADVANCES bring material together under one cover which would otherwise be scattered among many journals... *or not available at all!*

... Put chemical topics of interest to you in proper perspective. Read the ADVANCES IN CHEMISTRY Series.

Listed here are the 26 most recent titles in the ADVANCES IN CHEMISTRY SERIES.

No.	Title	Price	Cost
103	Origin and Refining of Petroleum 230 pp (1971)		\$10.00
102	Molecular Sieve Zeolites--II 459 pp (1971)		\$16.00
101	Molecular Sieve Zeolites--I 526 pp (1971)		\$16.00
101	and 102 ordered together		\$30.00
100	Bioinorganic Chemistry 436 pp (1971)		\$14.00
99	Multicomponent Polymer Systems 598 pp (1971)		\$16.50
98	Platinum Group Metals and Compounds 165 pp		\$9.00
97	Refining Petroleum for Chemicals 293 pp (1970)		\$11.50
96	Engineering Plastics and Their Commercial Development 128 pp (1969)		\$7.50
95	Cellulases and Their Applications 470 pp (1969)		\$14.50
94	Dietary Chemicals vs. Dental Caries 186 pp (1970)		\$9.00
93	Radionuclides in the Environment 529 pp (1970)		\$15.00
92	Epoxy Resins 230 pp (1970)		\$10.50
91	Addition and Condensation Polymerization Processes 767 pp (1969)		\$19.50
90	Fuel Cell Systems--II 446 pp (1969)		\$17.50
89	Isotope Effects in Chemical Processes 278 pp (1969)		\$13.00
88	Propellants Manufacture, Hazards, and Testing 395 pp (1969)		\$12.00
87	Interaction of Liquids at Solid Substrates 212 pp (1968)		\$9.50
86	Pesticidal Formulations Research. Physical and Colloidal Chemical Aspects 212 pp (1969)		\$9.50
85	Stabilization of Polymers and Stabilizer Processes 332 pp (1968)		\$12.00
84	Molecular Association in Biological and Related Systems 308 pp (1968)		\$10.50
83	Chemical Marketing: The Challenges of the Seventies 199 pp (1968)		\$9.50
82	Radiation Chemistry--II 558 pp (1968)		\$16.00
81	Radiation Chemistry--I 616 pp (1968)		\$16.00
81	and 82 ordered together		\$30.00
80	Chemical Reactions in Electrical Discharges 514 pp (1969)		\$15.00

Prices postpaid in U. S. and Canada, plus 35 cents elsewhere. For copies and/or information on these or on 74 other titles in this series, address

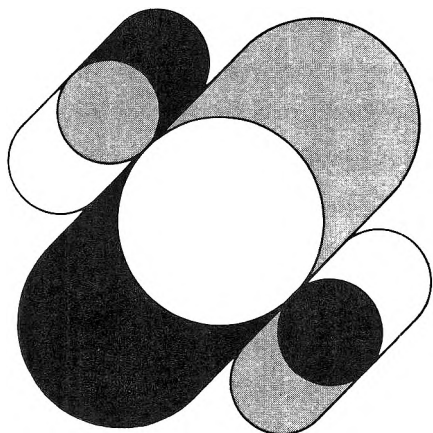
Special Issues Sales, Dept. 201

American Chemical Society
1155 Sixteenth St., N. W.
Washington, D. C. 20036

Nonequilibrium Systems In Natural Water Chemistry

ADVANCES IN CHEMISTRY
SERIES No. 106

Thirteen papers from a symposium by the Division of Water, Air, and Waste Chemistry of the American Chemical Society, chaired by J. D. Hem.



Which is more important: efficient exploitation of our natural resources or a stable ecosystem? What is the relationship between a wide variety of life forms and a healthy environment? What do geology and groundwater flow patterns have to do with the chemical composition of water? How may one predict when a lake will reach equilibrium or tell how long it has supported life?

This volume features:

- principles of water pollution control
- methods of analysis for dissolved chemicals
- mathematical models
- discussion of stratified lakes
- chemical processes in a carbonate aquifer
- decomposition and racemization of amino acids

342 pages with index Cloth (1971) \$11.00
Postpaid in U.S. and Canada; plus 40 cents elsewhere.
Set of L.C. cards with library orders upon request.

Other books in the ADVANCES IN CHEMISTRY SERIES on water chemistry include:

No. 105 Anaerobic Biological Treatment Processes

Nine papers survey the state of the art of this natural process for waste treatment, with three papers on methane fermentation, others on process control and design. Considers volatile acid formation, toxicity, synergism, antagonism, pH control, heavy metals, light metal cations.
196 pages with index Cloth (1971) \$9.00

No. 79 Adsorption from Aqueous Solution

Fifteen papers discuss thermodynamic and kinetic aspects of adsorption phenomena and the results of studies on a variety of adsorbate-adsorbent systems.
212 pages with index Cloth (1968) \$10.00

No. 73 Trace Inorganics in Water

Research reports; analytical developments including atomic absorption, flame emission, and neutron activation; and broad reviews, such as effects of trace inorganics on the ice-water system and the role of hydrous manganese and iron oxides on fixing metals in soils and sediments.
396 pages with index Cloth (1968) \$12.50

No. 67 Equilibrium Concepts in Natural Water Systems

Sixteen papers represent the collaboration of aquatic chemists, analytical chemists, geologists, oceanographers, limnologists, and sanitary engineers, working with simplified models to produce fruitful generalizations and valuable insights into the factors that control the chemistry of natural systems.
344 pages with index Cloth (1967) \$11.00

No. 38 Saline Water Conversion—II

Fourteen papers from two symposia; includes recovery of minerals from sea water, minimizing scale formation, wiped thinfilm distillation, diffusion still, solar flash evaporation, osmosis, electrodialysis (3 paper), research in Israel, hydrate process.
199 pages Paper (1963) \$8.00

No. 27 Saline Water Conversion

Thermodynamics of desalting, solvent extraction, freezing, centrifugal phase barrier recompression distillation, multi-stage flash evaporation, ion exchange, osmosis, and electrochemical demineralization.
246 pages Paper (1960) \$9.00

Order from: **Special Issues Sales, American Chemical Society**
1155 Sixteenth St., N.W., Washington, D.C. 20036

23 W.A. 2518